



**DANIEL P. RAYMER**

**Aircraft Design:  
A Conceptual Approach**



**AIAA**

**Education Series**

J.S. PRITCHARD / SERIES EDITOR-IN-CHIEF

**[www.ASEC.ir](http://www.ASEC.ir)**

# **Aircraft Design: A Conceptual Approach**

**Daniel P. Raymer**

President, Conceptual Research Corporation  
Sylmar, California



## **EDUCATION SERIES**

**J. S. Przemieniecki**

Series Editor-in-Chief

Air Force Institute of Technology

Wright-Patterson Air Force Base, Ohio

Published by

American Institute of Aeronautics and Astronautics, Inc.  
370 L'Enfant Promenade, S.W., Washington, D.C. 20024

## DEDICATION

This book is dedicated to all who taught me, especially Lester Hendrix, Richard Hibma, Louis Hecq, Harry Scott, Richard Child, George Owl, Robert Maier, Ed McGachan, Doug Robinson, Steve White, Harvey Hoge, Michael Robinson, George Palmer, Henry Yang, Robert Swaim, C. T. Sun, Dave Schmidt, Bruce Reese, William Heiser, and Gordon Raymer (test pilot, aeronautical engineer and my father).

Thanks also to Rockwell North American Aircraft Operations for permission to use various illustrations. All other artwork is original, in the public domain, or copyrighted by AIAA.

American Institute of Aeronautics and Astronautics, Inc., Washington, DC

### Library of Congress Cataloging-in-Publication Data

Raymer, Daniel P.

Aircraft design:a conceptual approach/Daniel P. Raymer.

p. cm.—(AIAA education series)

Bibliography: p.

Includes index.

1. Airplanes—Design and construction. I. American Institute of Aeronautics and Astronautics. II. Title. III. Series.

TL671.2.R29 1989 629.134'1—dc20 89-14912 CIP

ISBN 0-930403-51-7

Second Edition, Second Printing

Copyright © 1992 by Daniel P. Raymer. Printed in the United States of America. No part of this publication may be reproduced, distributed, or transmitted in any form or by any means, or stored in a data base or retrieval system, without prior written permission of the publisher.

*DISCLAIMER: The Author and the AIAA do not guarantee the accuracy of the information provided in this book, and it should not be referenced as an authoritative source for aircraft design data or methods.*

### **Texts Published in the AIAA Education Series**

Re-Entry Vehicle Dynamics

Frank J. Regan, 1984

Aerothermodynamics of Gas Turbine and Rocket Propulsion

Gordon C. Oates, 1984

Aerothermodynamics of Aircraft Engine Components

Gordon C. Oates, Editor, 1985

Fundamentals of Aircraft Combat Survivability Analysis and Design

Robert E. Ball, 1985

Intake Aerodynamics

J. Seddon and E. L. Goldsmith, 1985

Composite Materials for Aircraft Structures

Brian C. Hoskins and Alan A. Baker, Editors, 1986

Gasdynamics: Theory and Applications

George Emanuel, 1986

Aircraft Engine Design

Jack D. Mattingly, William Heiser, and Daniel H. Daley, 1987

An Introduction to the Mathematics and Methods of Astrodynamics

Richard H. Battin, 1987

Radar Electronic Warfare

August Golden Jr., 1988

Advanced Classical Thermodynamics

George Emanuel, 1988

Aerothermodynamics of Gas Turbine and Rocket Propulsion,

Revised and Enlarged

Gordon C. Oates, 1988

Re-Entry Aerodynamics

Wilbur L. Hankey, 1988

Mechanical Reliability: Theory, Models and Applications

B. S. Dhillon, 1988

Aircraft Landing Gear Design: Principles and Practices

Norman S. Currey, 1988

Gust Loads on Aircraft: Concepts and Applications

Frederic M. Hoblit, 1988

Aircraft Design: A Conceptual Approach

Daniel P. Raymer, 1989

Boundary Layers

A. D. Young, 1989

Aircraft Propulsion Systems Technology and Design

Gordon C. Oates, Editor, 1989



Basic Helicopter Aerodynamics  
J. Seddon, 1990

Introduction to Mathematical Methods in Defense Analyses  
J. S. Przemieniecki, 1990

Space Vehicle Design  
Michael D. Griffin and James R. French, 1991

Inlets for Supersonic Missiles  
John J. Mahoney, 1991

Defense Analyses Software  
J. S. Przemieniecki, 1991

Critical Technologies for National Defense  
Air Force Institute of Technology, 1991

Orbital Mechanics  
Vladimir A. Chobotov, 1991

Nonlinear Analysis of Shell Structures  
Anthony N. Palazotto and Scott T. Dennis, 1992

Optimization of Observation and Control Processes  
Veniamin V. Malyshev, Mihkail N. Krasilshikov, and Valeri I. Karlov, 1992

Aircraft Design: A Conceptual Approach  
Second Edition  
Daniel P. Raymer, 1992

**Published by**  
**American Institute of Aeronautics and Astronautics, Inc., Washington, DC**

## FOREWORD

As one of its major objectives, the AIAA Education Series is creating a comprehensive library of the established practices in aerospace design. *Aircraft Design: A Conceptual Approach* by Daniel P. Raymer provides an authoritative exposition of aircraft conceptual design. The great demand for the first edition of this new authoritative text on aircraft design has prompted the author to update and enlarge the text content into a second edition. In particular, Chapters 8 (Special Considerations in Configuration Layout), 13 (Propulsion), 17 (Performance and Flight Mechanics), and 21 (Conceptual Design Examples) have been extensively enlarged to cover some of the latest developments. The author's extensive experience with several aircraft companies supports the broad cross section of different views and approaches discussed in this comprehensive volume.

This textbook offers aircraft designers, design managers, and design instructors an industry perspective on the new aircraft concept development process, which basically consists of two major activities: design layout and design analysis. The whole process is described in a very comprehensive manner, tailored to serve as a college design textbook. However, only an elementary knowledge of mathematics is required to make full use of the text, for the book focuses on industry design practice rather than theoretical definitions. A simplified but complete set of first-order analytical methods is presented. The text covers every phase of conceptual design: configuration layout, payload considerations, aerodynamics, propulsion, structure and loads, weights, stability and control, handling qualities, performance, cost analysis, tradeoff analysis, and many other topics.

This latest text in the AIAA Education Series offers students, teachers, and practicing designers a unique source of information on current design practice in the U.S. aircraft industry—its science and art. To write a textbook on aircraft design is indeed a formidable task. Raymer has succeeded in creating a balanced text in which all the necessary topics needed to understand the design process are clearly described.

For many years *Aircraft Design: A Conceptual Approach* will be a valuable textbook for all who struggle with the fundamentals and intricacies of aircraft design.

**J. S. PRZEMIENIECKI**  
Editor-in-Chief  
AIAA Education Series

# TABLE OF CONTENTS

<b>Author's Note</b>	xiii
<b>Chapter 1. Design—A Separate Discipline</b>	
1.1 What Is Design?	1
1.2 Introduction to the Book	1
<b>Chapter 2. Overview of the Design Process</b>	
2.1 Introduction	3
2.2 Phases of Aircraft Design	4
2.3 Aircraft Conceptual Design Process	7
<b>Chapter 3. Sizing from a Conceptual Sketch</b>	
3.1 Introduction	11
3.2 Takeoff-Weight Buildup	11
3.3 Empty-Weight Estimation	12
3.4 Fuel-Fraction Estimation	14
3.5 Takeoff-Weight Calculation	23
3.6 Design Example: ASW Aircraft	24
<b>Chapter 4. Airfoil and Geometry Selection</b>	
4.1 Introduction	33
4.2 Airfoil Selection	33
4.3 Wing Geometry	47
4.4 Biplane Wings	65
4.5 Tail Geometry and Arrangement	67
<b>Chapter 5. Thrust-to-Weight Ratio and Wing Loading</b>	
5.1 Introduction	77
5.2 Thrust-to-Weight Ratio	78
5.3 Wing Loading	84
5.4 Selection of Thrust-to-Weight and Wing Loading	99
<b>Chapter 6. Initial Sizing</b>	
6.1 Introduction	101
6.2 Rubber-Engine Sizing	102
6.3 Fixed-Engine Sizing	108
6.4 Geometry Sizing	109
6.5 Control-Surface Sizing	113
<b>Chapter 7. Configuration Layout and Loft</b>	
7.1 Introduction	117
7.2 End Products of Configuration Layout	117
7.3 Conic Lofting	123
7.4 Conic Fuselage Development	129
7.5 Flat-Wrap Fuselage Lofting	135
7.6 Circle-to-Square Adapter	136
7.7 Fuselage Loft Verification	137
7.8 Wing/Tail Layout and Loft	139
7.9 Aircraft Layout Procedures	149
7.10 Wetted Area Determination	150
7.11 Volume Determination	152

**Chapter 8. Special Considerations in Configuration Layout**

8.1	Introduction	155
8.2	Aerodynamic Considerations	155
8.3	Structural Considerations	158
8.4	Radar Detectability	165
8.5	Infrared Detectability	170
8.6	Visual Detectability	171
8.7	Aural Signature	171
8.8	Vulnerability Considerations	172
8.9	Crashworthiness Considerations	174
8.10	Producibility Considerations	175
8.11	Maintainability Considerations	179

**Chapter 9. Crew Station, Passengers, and Payload**

9.1	Introduction	181
9.2	Crew Station	181
9.3	Passenger Compartment	185
9.4	Cargo Provisions	186
9.5	Weapons Carriage	188
9.6	Gun Installation	191

**Chapter 10. Propulsion and Fuel System Integration**

10.1	Introduction	193
10.2	Propulsion Selection	193
10.3	Jet-Engine Integration	196
10.4	Propeller-Engine Integration	220
10.5	Fuel System	226

**Chapter 11. Landing Gear and Subsystems**

11.1	Introduction	229
11.2	Landing Gear Arrangements	229
11.3	Tire Sizing	233
11.4	Shock Absorbers	239
11.5	Castoring-Wheel Geometry	246
11.6	Gear-Retracton Geometry	247
11.7	Seaplanes	250
11.8	Subsystems	252

**Chapter 12. Aerodynamics**

12.1	Introduction	257
12.2	Aerodynamic Forces	258
12.3	Aerodynamic Coefficients	262
12.4	Lift	263
12.5	Parasite (Zero-Lift) Drag	280
12.6	Drag Due to Lift (Induced Drag)	297
12.7	Aerodynamic Codes and Computational Fluid Dynamics (CFD)	305

**Chapter 13. Propulsion**

13.1	Introduction	313
13.2	Jet-Engine Thrust Considerations	315
13.3	Turbojet Installed Thrust	317
13.4	Thrust-Drag Bookkeeping	317
13.5	Installed-Thrust Methodology	318
13.6	Piston-Engine Performance	325
13.7	Turboprop Performance	331

**Chapter 14. Structures and Loads**

14.1	Introduction	333
14.2	Loads Categories	334
14.3	Air Loads	335
14.4	Inertial Loads	347
14.5	Power-Plant Loads	348
14.6	Landing-Gear Loads	348
14.7	Structures Fundamentals	349
14.8	Material Selection	354
14.9	Material Properties	357
14.10	Structural-Analysis Fundamentals	369
14.11	Finite-Element Structural Analysis	389

**Chapter 15. Weights**

15.1	Introduction	395
15.2	Approximate Group Weights Method	399
15.3	Statistical Group Weights Method	399
15.4	Additional Considerations in Weights Estimation	407

**Chapter 16. Stability, Control, and Handling Qualities**

16.1	Introduction	411
16.2	Coordinate Systems and Definitions	413
16.3	Longitudinal Static Stability and Control	414
16.4	Lateral-Directional Static Stability and Control	433
16.5	Stick-Free Stability	441
16.6	Effects of Flexibility	442
16.7	Dynamic Stability	443
16.8	Quasi-Steady State	446
16.9	Inertia Coupling	448
16.10	Handling Qualities	449

**Chapter 17. Performance and Flight Mechanics**

17.1	Introduction and Equations of Motion	455
17.2	Steady Level Flight	457
17.3	Steady Climbing and Descending Flight	463
17.4	Level Turning Flight	467
17.5	Gliding Flight	471
17.6	Energy-Maneuverability Methods	475
17.7	Operating Envelope	483
17.8	Takeoff Analysis	486
17.9	Landing Analysis	489
17.10	Other Fighter Performance Measures of Merit	491

**Chapter 18. Cost Analysis**

18.1	Introduction	501
18.2	Elements of Life-Cycle Cost	503
18.3	Cost-Estimating Methods	505
18.4	RDT&E and Production Costs	506
18.5	Operations and Maintenance Costs	510
18.6	Cost Measures of Merit (Military)	514
18.7	Airline Economics	514

## Chapter 19. Sizing and Trade Studies

19.1	Introduction	519
19.2	Detailed Sizing Methods	519
19.3	Improved Conceptual Sizing Methods	520
19.4	Sizing Matrix and Carpet Plots	525
19.5	Trade Studies	532

## Chapter 20. VTOL Aircraft Design

20.1	Introduction	537
20.2	VTOL Terminology	538
20.3	Fundamental Problems of VTOL Design	538
20.4	VTOL Jet-Propulsion Options	541
20.5	Vectoring-Nozzle Types	547
20.6	Suckdown and Fountain Lift	551
20.7	Recirculation and Hot-Gas Ingestion	552
20.8	VTOL Footprint	553
20.9	VTOL Control	554
20.10	VTOL Propulsion Considerations	555
20.11	Weight Effects of VTOL	556
20.12	Sizing Effects of VTOL	557

## Chapter 21. Conceptual Design Examples

21.1	Introduction	559
21.2	Single-Seat Aerobatic	559
21.3	Lightweight Supercruise Fighter	603

## Appendix A

A.1	Conversion Tables	658
A.2	Standard Atmosphere and Shock Tables	660
A.3	Airfoil Data	687
A.4	Typical Engine Performance Curves	717
A.5	Design Requirements and Specifications	731

References	735
------------	-----

Subject Index	739
---------------	-----

## AUTHOR'S NOTE

There are two equally important aspects of aircraft design: design layout and design analysis. These very different activities attract different types of people. Some people love playing with numbers and computers, while others can't stop doodling on every piece of paper within reach.

This book was written to fill a perceived need for a textbook in which both aircraft analysis and design layout are covered equally, and the interactions between these two aspects of design are explored in a manner consistent with industry practice.

This book is not intended to be definitive on the subject of aircraft analysis. The analysis techniques presented are simplified to permit the student to experience the whole design process in a single course, including the key concepts of trade studies and aircraft optimization.

No textbook can contain the methods actually used in industry, which tend to be proprietary and highly computerized. When the student goes into an industry or government design job, the more sophisticated methods of his or her chosen specialty will be better understood in the broader context of the whole of design as presented here.

One key area in which this book differs from prior aircraft design books is in the chapters on aircraft configuration layout. The actual development of the aircraft design drawing is not a trivial task of drafting based upon the analysis results, but rather is a key element of the overall design process and ultimately determines the performance, weight, and cost of the aircraft.

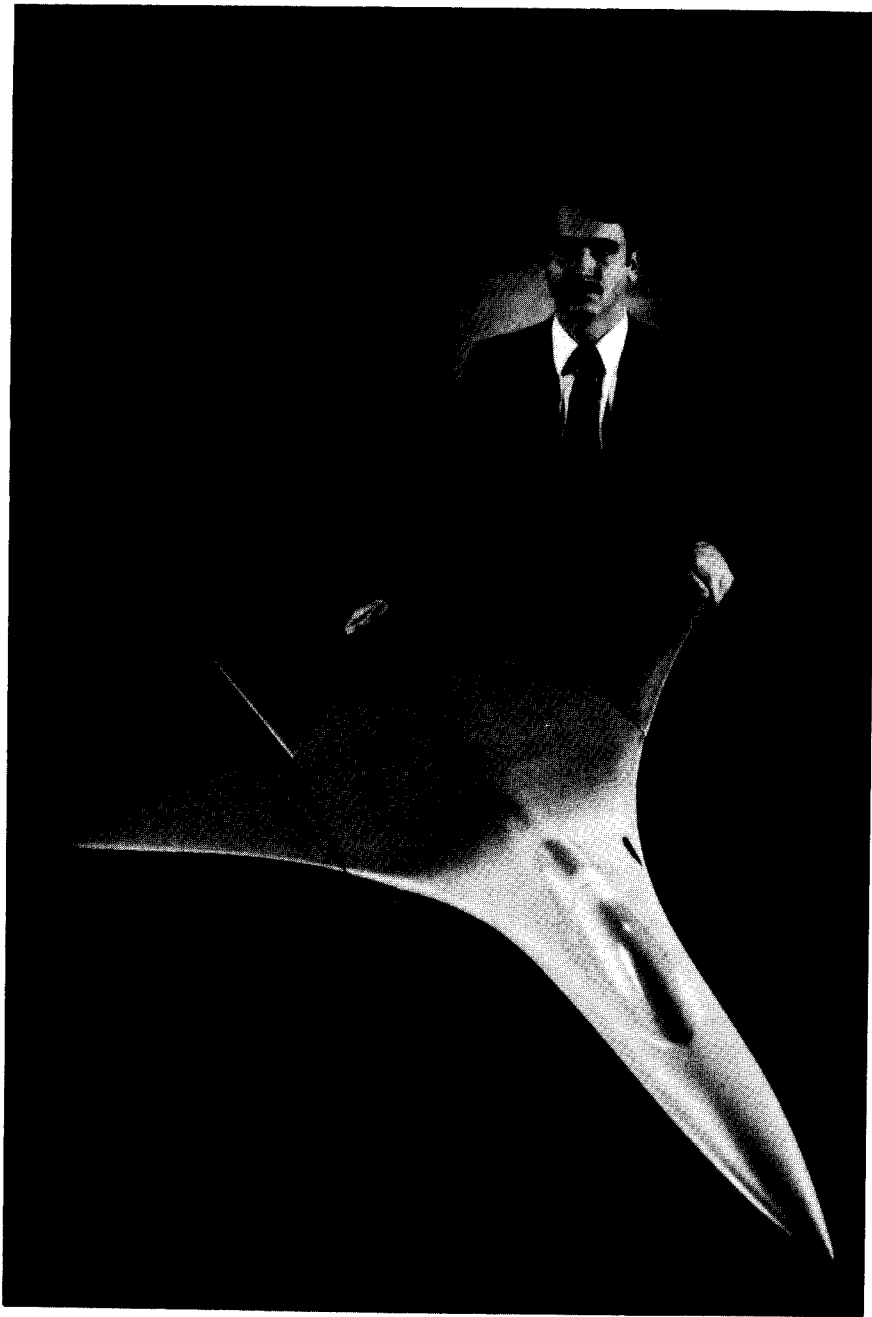
The ability to visualize and draw a new aircraft that has a streamlined aerodynamic shape, an efficient internal layout, yet satisfies an incredible number of real-world constraints and design specifications is a rare talent that takes years to cultivate. While to some extent good designers are "born, not made," a number of concepts and techniques in aircraft configuration layout can be taught, and are covered here.

Writing this book has been an educating and humbling experience. It is my sincere wish that it help aspiring aircraft designers to "learn the ropes" more quickly.

This second edition of *AIRCRAFT DESIGN: A Conceptual Approach* offers several new subjects, including production methods, post-stall maneuver, an update on VSTOL, and a brief introduction to engine cycle analysis. Also, typographical and technical errors from the first edition are corrected.

A key difference in the second edition is Chapter 21, the Conceptual Design Examples. These are reworked to better serve as examples for the chapters of the book. The second example illustrates the use of RDS, a PC-based design, sizing and performance program now available from AIAA. RDS uses the methods in this book, and permits rapid design, analysis, and trade studies.

AIAA and the author would like to thank the many people who have offered constructive suggestions for this second edition, as well as the more than 7000 students and working engineers who made the first edition an AIAA best seller.



Display model of an Advanced Supercruise Fighter Concept (Ref. 13). Photo courtesy of Rockwell International North American Aircraft Operations.

# 1

## DESIGN—A SEPARATE DISCIPLINE

### 1.1 WHAT IS DESIGN?

Aircraft design is a separate discipline of aeronautical engineering—different from the analytical disciplines such as aerodynamics, structures, controls, and propulsion. An aircraft designer needs to be well versed in these and many other specialties, but will actually spend little time performing such analysis in all but the smallest companies. Instead, the designer's time is spent doing something called "design," creating the geometric description of a thing to be built.

To the uninitiated, "design" looks a lot like "drafting" (or in the modern world, "computer-aided drafting"). The designer's product is a drawing, and the designer spends the day hunched over a drafting table or computer terminal. However, the designer's real work is mostly mental.

If the designer is talented, there is a lot more than meets the eye on the drawing. A good aircraft design seems to miraculously glide through subsequent evaluations by specialists without major changes being required. Somehow, the landing gear fits, the fuel tanks are near the center of gravity, the structural members are simple and lightweight, the overall arrangement provides good aerodynamics, the engines install in a simple and clean fashion, and a host of similar detail seems to fall into place.

This is no accident, but rather the product of a lot of knowledge and hard work by the designer. This book was written primarily to provide the basic tools and concepts required to produce good designs which will survive detailed analysis with minimal changes.

Other key players participate in the design process. Design is not just the actual layout, but also the analytical processes used to determine what should be designed and how the design should be modified to better meet the requirements. In a small company, this may be done by the same individuals who do the layout design. In the larger companies, aircraft analysis is done by the sizing and performance specialists with the assistance of experts in aerodynamics, weights, propulsion, stability, and other technical specialties.

In this book, the design layout techniques are discussed primarily in Chapters 4–11, while the analysis and optimization methods are presented in Chapters 12–19.

### 1.2 INTRODUCTION TO THE BOOK

This book describes the process used to develop a credible aircraft conceptual design from a given set of requirements. As a part of the AIAA

Education Series, the book is written primarily for the college student. Every effort has been made to achieve a self-contained book.

In an aircraft company, the designer can ask a functional specialist for a reasonable initial tire size, inlet capture area, weight savings due to the use of composites, or similar estimates. Such specialists are not available at most universities. This book thus gives various "rule-of-thumb" approximations for initial estimation of design parameters.

The book has 21 chapters, and approximately follows the actual design sequence. Chapters 2 and 3 provide an overall introduction to the design process. Chapter 2 discusses how the conceptual design process works, and how it fits into the overall process of aircraft development. Chapter 3 presents a "first-pass" design procedure to familiarize the reader with the essential concepts of design, including design layout, analysis, takeoff-weight estimation, and trade studies.

In Chapters 4–11 the techniques for the development of the initial configuration layout are presented. These include the conceptual sketch, initial sizing, wing geometry selection, lofting, inboard layout, and integration of propulsion, crew station, payload/passenger compartment, fuel system, landing gear, and considerations for observability, producibility, and supportability. While the text implies that the design is done on a drafting board, it should be understood that in major aircraft companies today most aircraft design work is done on a computer-aided design system. However, the same basic design techniques are used whether on a drafting table or computer scope.

Chapters 12–19 address the analysis, sizing, and optimization of the design layout. Various chapters discuss aerodynamics, weights, installed propulsion characteristics, stability and control, performance, cost, and sizing. Optimization based upon design requirements is introduced in a section on trade studies.

These methods are simplified to allow rapid design analysis by students. No college textbook can contain the methods actually used by major aircraft companies, which tend towards highly sophisticated computer programs operated by specialists. Simplified analysis methods allow the student more time to experience the all-important optimization and iteration process.

Chapter 20 presents an overview of VTOL aircraft design. This material builds upon the methods for conventional aircraft design. However, VTOL introduces additional considerations that affect the design layout and analysis.

The last chapter, 21, contains two complete design project examples which use the methods presented in the previous chapters. These are provided instead of numerous example calculations throughout the text to illustrate how the different aspects of design fit together as a whole.

The appendices contain information useful in conceptual design, such as conversion tables, atmosphere and shock tables, and data on airfoils and engines. Also included is a summary of the current civil and military design requirements and specifications, which have been taken primarily from Federal Aviation Regulations (FAR) and Military Specifications (Mil-Specs).

## OVERVIEW OF THE DESIGN PROCESS

### 2.1 INTRODUCTION

Those involved in design can never quite agree as to just where the design process begins. The designer thinks it starts with a new airplane concept. The sizing specialist knows that nothing can begin until an initial estimate of the weight is made. The customer, civilian or military, feels that the design begins with requirements.

They are all correct. Actually, design is an iterative effort, as shown in the "Design Wheel" of Fig. 2.1. Requirements are set by prior design trade studies. Concepts are developed to meet requirements. Design analysis frequently points toward new concepts and technologies, which can initiate a whole new design effort. However a particular design is begun, all of these activities are equally important in producing a good aircraft concept.

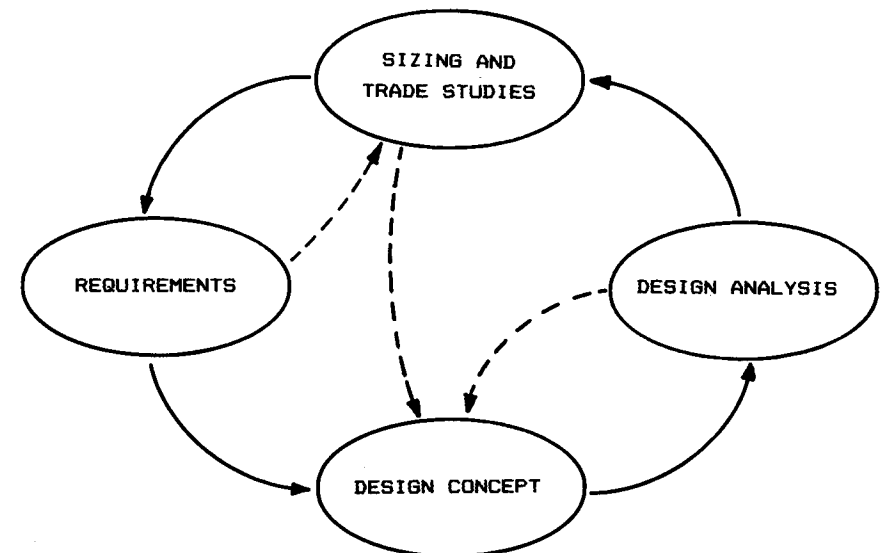


Fig. 2.1 The design wheel.

## 2.2 PHASES OF AIRCRAFT DESIGN

### Conceptual Design

Aircraft design can be broken into three major phases, as depicted in Fig. 2.2. Conceptual design is the primary focus of this book. It is in conceptual design that the basic questions of configuration arrangement, size and weight, and performance are answered.

The first question is, "Can an affordable aircraft be built that meets the requirements?" If not, the customer may wish to relax the requirements.

Conceptual design is a very fluid process. New ideas and problems emerge as a design is investigated in ever-increasing detail. Each time the latest design is analyzed and sized, it must be redrawn to reflect the new gross weight, fuel weight, wing size, engine size, and other changes. Early wind-tunnel tests often reveal problems requiring some changes to the configuration. The steps of conceptual design are described later in more detail.

### Preliminary Design

Preliminary design can be said to begin when the major changes are over. The big questions such as whether to use a canard or an aft tail have been resolved. The configuration arrangement can be expected to remain about as shown on current drawings, although minor revisions may occur. At some point late in preliminary design, even minor changes are stopped when a decision is made to freeze the configuration.

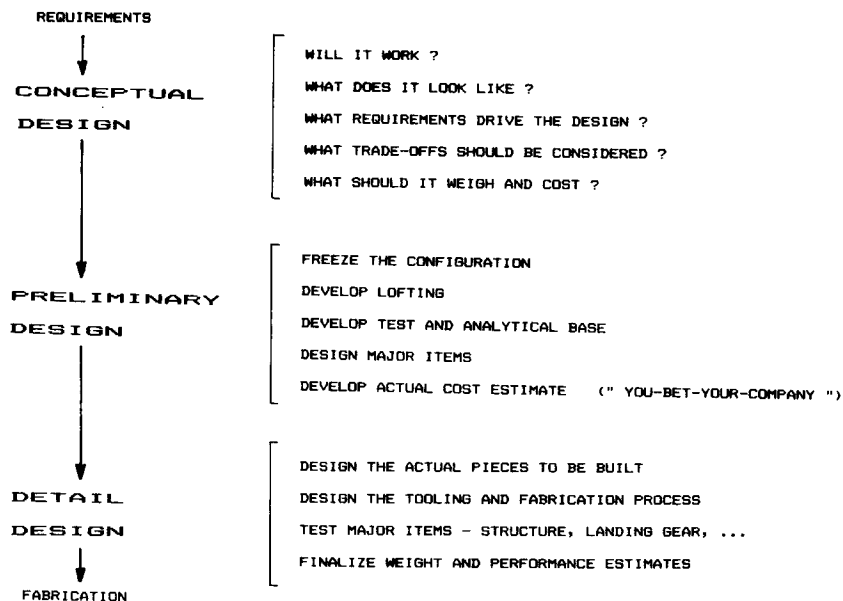


Fig. 2.2 Three phases of aircraft design.

During preliminary design the specialists in areas such as structures, landing gear, and control systems will design and analyze their portion of the aircraft. Testing is initiated in areas such as aerodynamics, propulsion, structures, and stability and control. A mockup may be constructed at this point.

A key activity during preliminary design is "lofting." Lofting is the mathematical modeling of the outside skin of the aircraft with sufficient accuracy to insure proper fit between its different parts, even if they are designed by different designers and possibly fabricated in different locations. Lofting originated in shipyards and was originally done with long flexible rulers called "splines." This work was done in a loft over the shipyard; hence the name.

The ultimate objective during preliminary design is to ready the company for the detail design stage, also called full-scale development. Thus, the end of preliminary design usually involves a full-scale development proposal. In today's environment, this can result in a situation jokingly referred to as "you-bet-your-company." The possible loss on an overrun contract or from lack of sales can exceed the net worth of the company! Preliminary design must establish confidence that the airplane can be built on time and at the estimated cost.

### Detail Design

Assuming a favorable decision for entering full-scale development, the detail design phase begins in which the actual pieces to be fabricated are designed. For example, during conceptual and preliminary design the wing box will be designed and analyzed as a whole. During detail design, that whole will be broken down into individual ribs, spars, and skins, each of which must be separately designed and analyzed.

Another important part of detail design is called production design. Specialists determine how the airplane will be fabricated, starting with the smallest and simplest subassemblies and building up to the final assembly process. Production designers frequently wish to modify the design for ease of manufacture; that can have a major impact on performance or weight. Compromises are inevitable, but the design must still meet the original requirements.

It is interesting to note that in the Soviet Union, the production design is done by a completely different design bureau than the conceptual and preliminary design, resulting in superior producibility at some expense in performance and weight.

During detail design, the testing effort intensifies. Actual structure of the aircraft is fabricated and tested. Control laws for the flight control system are tested on an "iron-bird" simulator, a detailed working model of the actuators and flight control surfaces. Flight simulators are developed and flown by both company and customer test-pilots.

Detail design ends with fabrication of the aircraft. Frequently the fabrication begins on part of the aircraft before the entire detail-design effort is completed. Hopefully, changes to already-fabricated pieces can be avoided.

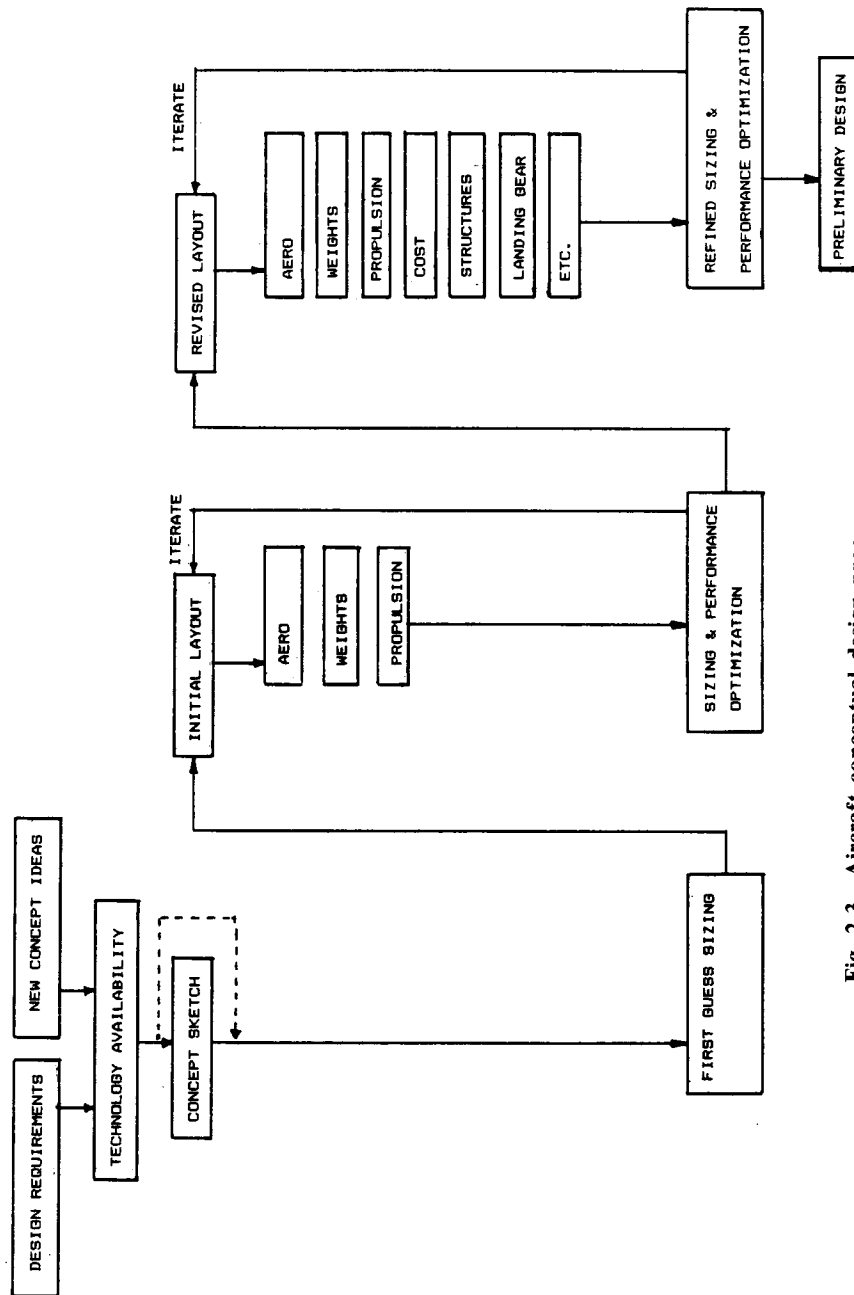


Fig. 2.3 Aircraft conceptual design process.

The further along a design progresses, the more people are involved. In fact, most of the engineers who go to work for a major aerospace company will work in preliminary or detail design.

### 2.3 AIRCRAFT CONCEPTUAL DESIGN PROCESS

Figure 2.3 depicts the conceptual design process in greater detail. Conceptual design will usually begin with either a specific set of design requirements established by the prospective customer or a company-generated guess as to what future customers may need. Design requirements include parameters such as the aircraft range and payload, takeoff and landing distances, and maneuverability and speed requirements.

The design requirements also include a vast set of civil or military design specifications which must be met. These include landing sink-speed, stall speed, structural design limits, pilots' outside vision angles, reserve fuel, and many others.

Sometimes a design will begin as an innovative idea rather than as a response to a given requirement. The flying wings pioneered by John Northrop were not conceived in response to a specific Army Air Corps requirement at that time, but instead were the product of one man's idea of the "better airplane." Northrop pursued this idea for years before building a flying wing to suit a particular military requirement.

Before a design can be started, a decision must be made as to what technologies will be incorporated. If a design is to be built in the near future, it must use only currently-available technologies as well as existing engines and avionics. If it is being designed to be built in the more distant future, then an estimate of the technological state of the art must be made to determine which emerging technologies will be ready for use at that time.

For example, an all-composite fighter has yet to enter high-rate production as of this date (1989), but can confidently be predicted by 1999. On the other hand, active laminar flow control by suction pumps shows great payoff analytically, but would be considered by many to be too risky to incorporate into a new transport jet in the near future.

An optimistic estimate of the technology availability will yield a lighter, cheaper aircraft to perform a given mission, but will also result in a higher development risk.

The actual design effort usually begins with a conceptual sketch (Fig. 2.4). This is the "back of a napkin" drawing of aerospace legend, and gives a rough indication of what the design may look like. A good conceptual sketch will include the approximate wing and tail geometries, the fuselage shape, and the internal locations of the major components such as the engine, cockpit, payload/passenger compartment, landing gear, and perhaps the fuel tanks.

The conceptual sketch can be used to estimate aerodynamics and weight fractions by comparison to previous designs. These estimates are used to make a first estimate of the required total weight and fuel weight to perform the design mission, by a process called "sizing." The conceptual sketch may not be needed for initial sizing if the design resembles previous ones.

The "first-order" sizing provides the information needed to develop an initial design layout (Fig. 2.5). This is a three-view drawing complete with





For example, controls experts will perform a six-degree-of-freedom analysis to ensure that the designer's estimate for the size of the control surfaces is adequate for control under all conditions required by design specifications. If not, they will instruct the designer as to how much each control surface must be expanded. If a larger aileron is required, the designer must ensure that it can be incorporated into the design without adversely affecting something else, such as the flaps or the landing gear.

The end product of all this will be an aircraft design that can be confidently passed to the preliminary design phase, as previously discussed. While further changes should be expected during preliminary design, major revisions will not occur if the conceptual design effort has been successful.

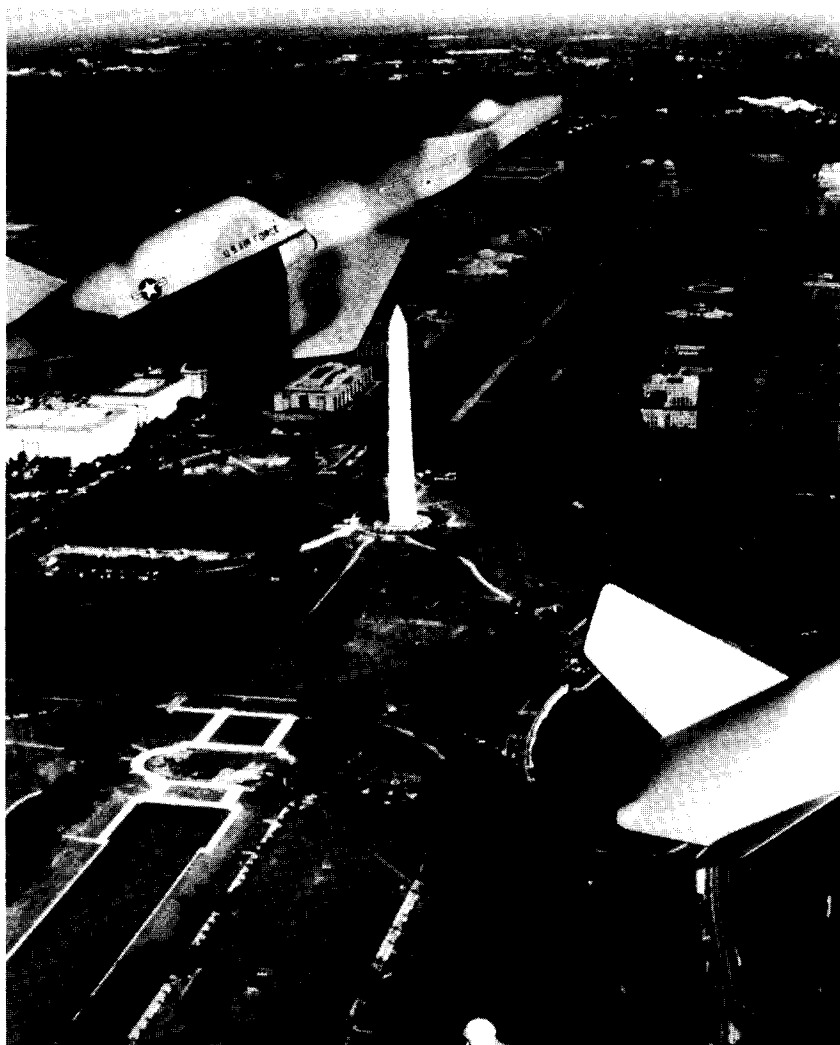


Photo by Bruce Frisch

Reverse Installation Vectored Engine Thrust ("RIVET") Supersonic VSTOL  
Concept Model

## 3 SIZING FROM A CONCEPTUAL SKETCH

### 3.1 INTRODUCTION

There are many levels of design procedure. The simplest level just adopts past history. For example, if you need an immediate estimate of the takeoff weight of an airplane to replace the Air Force F-15 fighter, use 44,500 lb. That is what the F-15 weighs, and is probably a good number to start with.

To get the "right" answer takes several years, many people, and lots of money. Actual design requirements must be evaluated against a number of candidate designs, each of which must be designed, analyzed, sized, optimized, and redesigned any number of times.

Analysis techniques include all manner of computer code as well as correlations to wind-tunnel and other tests. Even with this extreme level of design sophistication, the actual airplane when flown will never exactly match predictions.

In between these extremes of design and analysis procedures lie the methods used for most conceptual design activities. As an introduction to the design process, this chapter presents a quick method of estimating takeoff weight from a conceptual sketch.

The simplified sizing method presented in this chapter can only be used for missions which do not include any combat or payload drops. While admittedly crude, this method introduces all of the essential features of the most sophisticated design by the major aerospace manufacturers. In a later chapter, the concepts introduced here will be expanded to a sizing method capable of handling all types of mission.

### 3.2 TAKEOFF-WEIGHT BUILDUP

"Design takeoff gross weight" is the total weight of the aircraft as it begins the mission for which it was designed. This is not necessarily the same as the "maximum takeoff weight." Many military aircraft can be overloaded beyond design weight but will suffer a reduced maneuverability. Unless specifically mentioned, takeoff gross weight, or " $W_0$ ," is assumed to be the design weight.

Design takeoff gross weight can be broken into crew weight, payload (or passenger) weight, fuel weight, and the remaining (or "empty") weight. The empty weight includes the structure, engines, landing gear, fixed equipment, avionics, and anything else not considered a part of crew, payload, or fuel. Equation (3.1) summarizes the takeoff-weight buildup.

$$W_0 = W_{\text{crew}} + W_{\text{payload}} + W_{\text{fuel}} + W_{\text{empty}} \quad (3.1)$$

The crew and payload weights are both known since they are given in the design requirements. The only unknowns are the fuel weight and empty weight. However, they are both dependent on the total aircraft weight. Thus an iterative process must be used for aircraft sizing.

To simplify the calculation, both fuel and empty weights can be expressed as fractions of the total takeoff weight, i.e.,  $(W_f/W_0)$  and  $(W_e/W_0)$ . Thus Eq. (3.1) becomes:

$$W_0 = W_{\text{crew}} + W_{\text{payload}} + \left(\frac{W_f}{W_0}\right)W_0 + \left(\frac{W_e}{W_0}\right)W_0 \quad (3.2)$$

This can be solved for  $W_0$  as follows:

$$W_0 - \left(\frac{W_f}{W_0}\right)W_0 - \left(\frac{W_e}{W_0}\right)W_0 = W_{\text{crew}} + W_{\text{payload}} \quad (3.3)$$

$$W_0 = \frac{W_{\text{crew}} + W_{\text{payload}}}{1 - (W_f/W_0) - (W_e/W_0)} \quad (3.4)$$

Now  $W_0$  can be determined if  $(W_f/W_0)$  and  $(W_e/W_0)$  can be estimated. These are described below.

### 3.3 EMPTY-WEIGHT ESTIMATION

The empty-weight fraction  $(W_e/W_0)$  can be estimated statistically from historical trends as shown in Fig. 3.1, developed by the author from data taken from Ref. 1 and other sources. Empty-weight fractions vary from about 0.3 to 0.7, and diminish with increasing total aircraft weight.

As can be seen, the type of aircraft also has a strong effect, with flying boats having the highest empty-weight fractions and long-range military aircraft having the lowest. Flying boats are heavy because they need to carry extra weight for what amounts to a boat hull. Notice also that different types of aircraft exhibit different slopes to the trend lines of empty-weight fraction vs takeoff weight.

Table 3.1 presents statistical curve-fit equations for the trends shown in Fig. 3.1. Note that these are all exponential equations based upon takeoff gross weight. The exponents are small negative numbers, which indicates that the empty weight fractions decrease with increasing takeoff weight, as shown by the trend lines in Fig. 3.1. The differences in exponents for different types of aircraft reflect the different slopes to the trend lines, and imply that some types of aircraft are more sensitive in sizing than others.

A variable-sweep wing is heavier than a fixed wing, and is accounted for at this initial stage of design by multiplying the empty-weight fraction as determined from the equations in Table 3.1 by about 1.04.

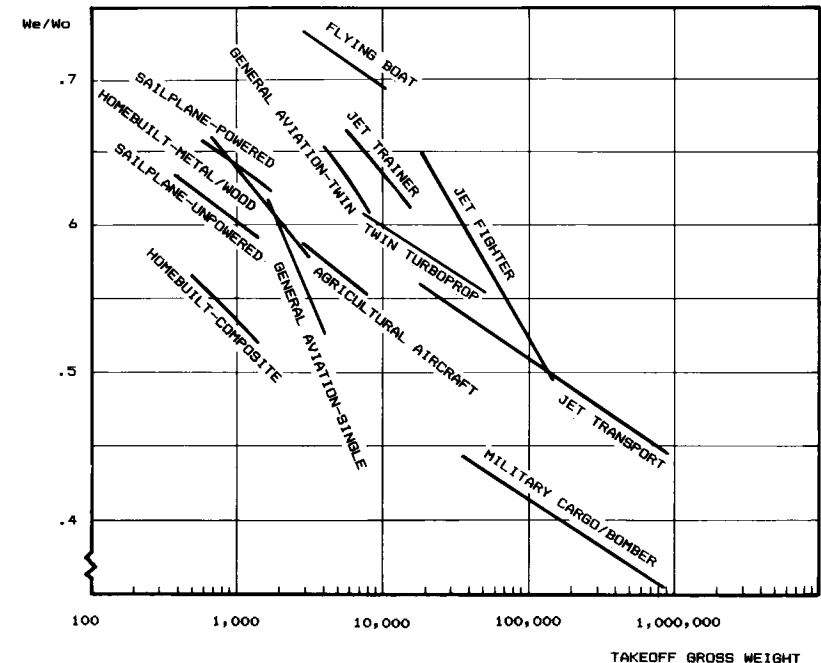


Fig. 3.1 Empty weight fraction trends.

Table 3.1 Empty weight fraction vs  $W_0$

$W_e/W_0 = A W_0^C K_{vs}$	A	C
Sailplane—unpowered	0.86	-0.05
Sailplane—powered	0.91	-0.05
Homebuilt—metal/wood	1.19	-0.09
Homebuilt—composite	0.99	-0.09
General aviation—single engine	2.36	-0.18
General aviation—twin engine	1.51	-0.10
Agricultural aircraft	0.74	-0.03
Twin turboprop	0.96	-0.05
Flying boat	1.09	-0.05
Jet trainer	1.59	-0.10
Jet fighter	2.34	-0.13
Military cargo/bomber	0.93	-0.07
Jet transport	1.02	-0.06

$K_{vs}$  = variable sweep constant = 1.04 if variable sweep  
= 1.00 if fixed sweep

Advanced composite materials such as graphite-epoxy are replacing aluminum in a number of new designs. There have not yet been enough composite aircraft flown to develop statistical equations. Based on a number of design studies, the empty-weight fraction for other types of composite aircraft can be estimated at this stage by multiplying the statistical empty-weight fraction by 0.95.

“Composite” homebuilt aircraft are typically of fiberglass-epoxy construction rather than an advanced composite material. The statistically estimated empty weight fraction for fiberglass-epoxy composite homebuilts is approximately 0.85 times the metal homebuilt empty-weight fraction ( $0.99/1.19 = 0.85$ ). However, this is not due to the material used for construction as much as the different design philosophies concerning ease of manufacture, passenger comfort, maintenance accessibility, and similar factors.

### 3.4 FUEL-FRACTION ESTIMATION

Only part of the aircraft's fuel supply is available for performing the mission (“mission fuel”). The other fuel includes reserve fuel as required by civil or military design specifications, and also includes “trapped fuel,” which is the fuel which cannot be pumped out of the tanks.

The required amount of mission fuel depends upon the mission to be flown, the aerodynamics of the aircraft, and the engine's fuel consumption. The aircraft weight during the mission affects the drag, so the fuel used is a function of the aircraft weight.

As a first approximation, the fuel used can be considered to be proportional to the aircraft weight, so the fuel fraction ( $W_f/W_0$ ) is approximately independent of aircraft weight. Fuel fraction can be estimated based on the mission to be flown using approximations of the fuel consumption and aerodynamics.

#### Mission Profiles

Typical mission profiles for various types of aircraft are shown in Fig. 3.2. The Simple Cruise mission is used for many transport and general-aviation designs, including homebuilts. The aircraft is sized to provide some required cruise range.

For safety you would be wise to carry extra fuel in case your intended airport is closed, so a loiter of typically 20–30 min is added. Alternatively, additional range could be included, representing the distance to the nearest other airport or some fixed number of minutes of flight at cruise speed (the FAA requires 30 min of additional cruise fuel for general-aviation aircraft).

Other missions are more complex. The typical Air Superiority mission includes a cruise out, a combat consisting of either a certain number of turns or a certain number of minutes at maximum power, a weapons drop, a cruise back, and a loiter. The weapons drop refers to the firing of gun and missiles, and is often left out of the sizing analysis to insure that the aircraft has enough fuel to return safely if the weapons aren't used. Note that the second cruise segment is identical to the first, indicating that the aircraft must return to its base at the end of the mission.

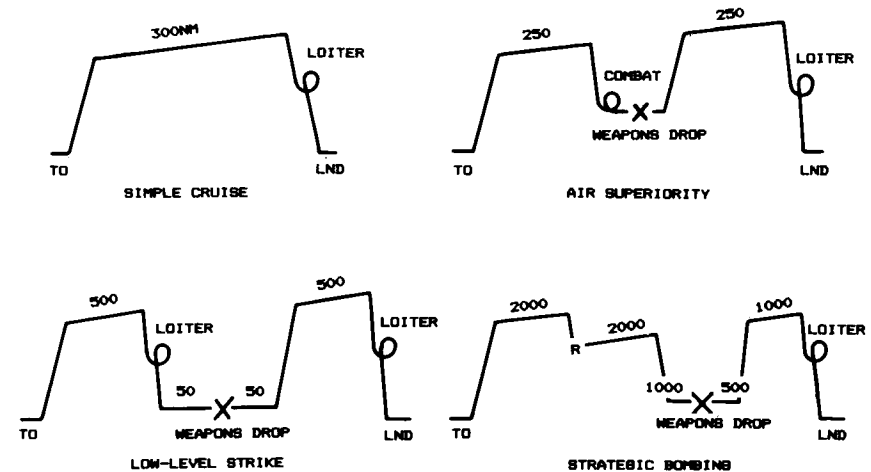


Fig. 3.2 Typical mission profiles for sizing.

The Low-Level Strike mission includes “dash” segments that must be flown at just a few hundred feet off the ground. This is to improve the survivability of the aircraft as it approaches its target. Unfortunately, the aerodynamic efficiency of an aircraft, expressed as “lift-to-drag ratio” ( $L/D$ ), is greatly reduced during low-level, high-speed flight, as is the engine efficiency. The aircraft may burn almost as much fuel during the low-level dash segment as it burns in the much-longer cruise segment.

The Strategic Bombing mission introduces another twist. After the initial cruise, a refueling segment occurs, as indicated by an “R.” Here the aircraft meets up with a tanker aircraft such as an Air Force KC-135 and receives some quantity of fuel. This enables the bomber to achieve far more range, but adds to the overall operating cost because a fleet of tanker aircraft must be dedicated to supporting the bombers.

Also note that the bomber in this typical strategic mission will fly at low level as it nears the target area to improve its chances of survival. Earlier bombers such as the B-52 were originally designed to cruise at high altitudes throughout the mission.

Another difference in this strategic mission is the fact that the return cruise range is far shorter than the outbound range. This is necessary because of the extreme range required. If the aircraft were sized to return to its original base, it would probably weigh several million pounds. Instead, it is assumed that strategic bombers will land on bases in friendly countries for refueling after completion of their mission.

These are merely typical missions, and the ranges shown are just examples. When an aircraft is designed, the actual mission profile and ranges will be provided by the customer or determined by operational analysis methods beyond the scope of this book.

In addition to the mission profile, requirements will be established for a number of performance parameters such as takeoff distance, maneuverabil-

ity, and climb rates. These are ignored in the simplified sizing method of this chapter, but will be discussed in detail later.

### Mission Segment Weight Fractions

For analysis, the various mission segments, or “legs,” are numbered, with zero denoting the start of the mission. Mission leg “one” is usually engine warmup and takeoff for first-order sizing estimation. The remaining legs are sequentially numbered.

For example, in the simple cruise mission the legs could be numbered as (1) warmup and takeoff, (2) climb, (3) cruise, (4) loiter, and (5) land (see the example mission at the end of this chapter).

In a similar fashion, the aircraft weight at each part of the mission can be numbered. Thus,  $W_0$  is the beginning weight (“takeoff gross weight”).

For the simple cruise mission,  $W_1$  would be the weight at the end of the first mission segment, which is the warmup and takeoff.  $W_2$  would be the aircraft weight at the end of the climb.  $W_3$  would be the weight after cruise, and  $W_4$  after loiter. Finally,  $W_5$  would be the weight at the end of the landing segment, which is also the end of the total mission.

During each mission segment, the aircraft loses weight by burning fuel (remember that our simple sizing method doesn’t permit missions involving a payload drop). The aircraft weight at the end of a mission segment divided by its weight at the beginning of that segment is called the “mission segment weight fraction.” This will be the basis for estimating the required fuel fraction for initial sizing.

For any mission segment “ $i$ ,” the mission segment weight fraction can be expressed as  $(W_i/W_{i-1})$ . If these weight fractions can be estimated for all of the mission legs, they can be multiplied together to find the ratio of the aircraft weight at the end of the total mission,  $W_x$  (assuming “ $x$ ” segments altogether) divided by the initial weight,  $W_0$ . This ratio,  $W_x/W_0$ , can then be used to calculate the total fuel fraction required.

These mission segment weight fractions can be estimated by a variety of methods. For our simplified form of initial sizing, the types of mission leg will be limited to warmup and takeoff, climb, cruise, loiter, and land. As previously mentioned, mission legs involving combat, payload drop, and refuel are not permitted in this simplified sizing method but will be discussed in a later chapter.

The warmup, takeoff, and landing weight-fractions can be estimated historically. Table 3.2 gives typical historical values for initial sizing. These

**Table 3.2 Historical mission segment weight fractions**

	$(W_i/W_{i-1})$
Warmup and takeoff	0.970
Climb	0.985
Landing	0.995

values can vary somewhat depending on aircraft type, but the averaged values given in the table are reasonable for initial sizing.

In our simple sizing method we ignore descent, assuming that the cruise ends with a descent and that the distance traveled during descent is part of the cruise range.

Cruise-segment mission weight fractions can be found using the Breguet range equation (derived in Chapter 17):

$$R = \frac{V}{C} \frac{L}{D} \ln \frac{W_{i-1}}{W_i} \quad (3.5)$$

or

$$\frac{W_i}{W_{i-1}} = \exp \frac{-RC}{V(L/D)} \quad (3.6)$$

where

- $R$  = range
- $C$  = specific fuel consumption
- $V$  = velocity
- $L/D$  = lift-to-drag ratio

Loiter weight fractions are found from the endurance equation (also derived in Chapter 17):

$$E = \frac{L/D}{C} \ln \frac{W_{i-1}}{W_i} \quad (3.7)$$

or

$$\frac{W_i}{W_{i-1}} = \exp \frac{-EC}{L/D} \quad (3.8)$$

where  $E$  = endurance or loiter time.

(Note: It is very important to use consistent units! Also note that  $C$  and  $L/D$  vary with speed and altitude. Furthermore,  $C$  varies with throttle setting, and  $L/D$  varies with aircraft weight. These will be discussed in detail in later chapters.)

### Specific Fuel Consumption

Specific fuel consumption (“SFC” or simply “ $C$ ”) is the rate of fuel consumption divided by the resulting thrust. For jet engines, specific fuel consumption is usually measured in pounds of fuel per hour per pound of thrust [(lb/hr)/lb, or 1/hr]. Figure 3.3 shows SFC vs Mach number.

Propeller engine SFC is normally given as  $C_{bhp}$ , the pounds of fuel per hour to produce one horsepower at the propeller shaft (or one “brake horsepower”: bhp = 550 ft-lb/s).

A propeller thrust SFC equivalent to the jet-engine SFC can be calculated. The engine produces thrust via the propeller, which has an efficiency  $\eta_p$

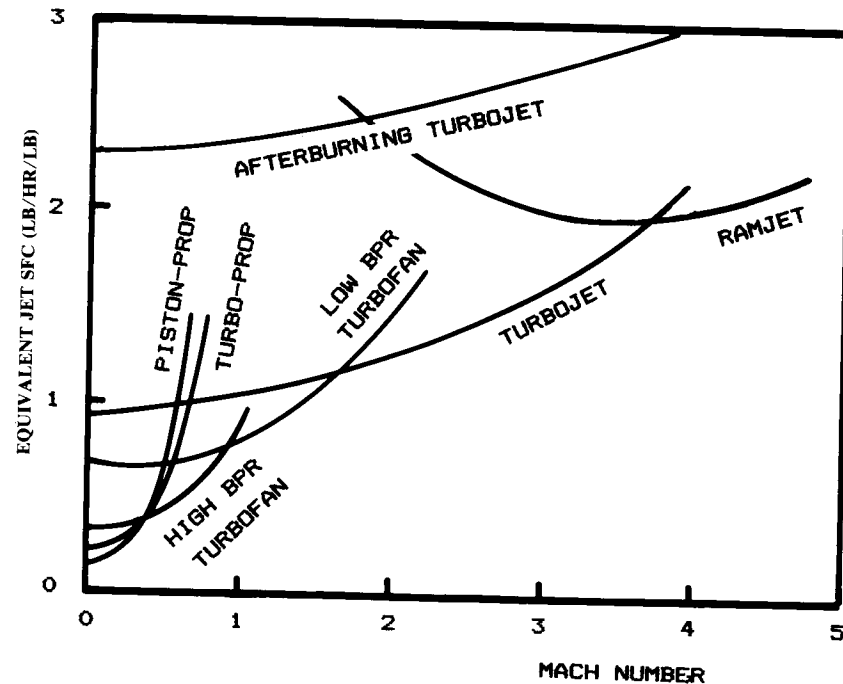


Fig. 3.3 Specific fuel consumption trends.

defined as thrust power output per horsepower input [Eq. (3.9)]. The 550 term assumes that  $V$  is in feet per second.

$$\eta_p = \frac{TV}{550 \text{ hp}} \quad (3.9)$$

Equation (3.10) shows the derivation of the equivalent-thrust SFC for a propeller-driven aircraft. Note that for a propeller aircraft, the thrust and the SFC are a function of the flight velocity. For a typical aircraft with a propeller efficiency of about 0.8, one horsepower equals one pound of thrust at about 440 ft/s, or about 260 knots.

$$C = \frac{W_f/\text{time}}{\text{thrust}} = C_{bhp} \frac{V}{550 \eta_p} \quad (3.10)$$

Table 3.3 provides typical SFC values for jet engines, while Table 3.4 provides typical  $C_{bhp}$  and  $\eta_p$  values for propeller engines. These can be used for rough initial sizing. In later chapters more detailed procedures for calculating these values, which change as a function of altitude, velocity, and power setting, will be presented.

Table 3.3 Specific fuel consumption ( $C$ )

Typical jet SFC's	Cruise	Loiter
Pure turbojet	0.9	0.8
Low-bypass turbofan	0.8	0.7
High-bypass turbofan	0.5	0.4

Table 3.4 Propeller specific fuel consumption ( $C_{bhp}$ )

Propeller: $C = C_{bhp} V / (550 \eta_p)$	Cruise	Loiter
Typical $C_{bhp}$ and $\eta_p$		
Piston-prop (fixed pitch)	0.4/0.8	0.5/0.7
Piston-prop (variable pitch)	0.4/0.8	0.5/0.8
Turboprop	0.5/0.8	0.6/0.8

### L/D Estimation

The remaining unknown in both range and loiter equations is the  $L/D$ , or lift-to-drag ratio, which is a measure of the design's overall aerodynamic efficiency. Unlike the parameters estimated above, the  $L/D$  is highly dependent upon the configuration arrangement. At subsonic speeds  $L/D$  is most directly affected by two aspects of the design: wing span and wetted area.

In level flight, the lift is known. It must equal the aircraft weight. Thus,  $L/D$  is solely dependent upon drag.

The drag at subsonic speeds is composed of two parts. "Induced" drag is the drag caused by the generation of lift. This is primarily a function of the wing span.

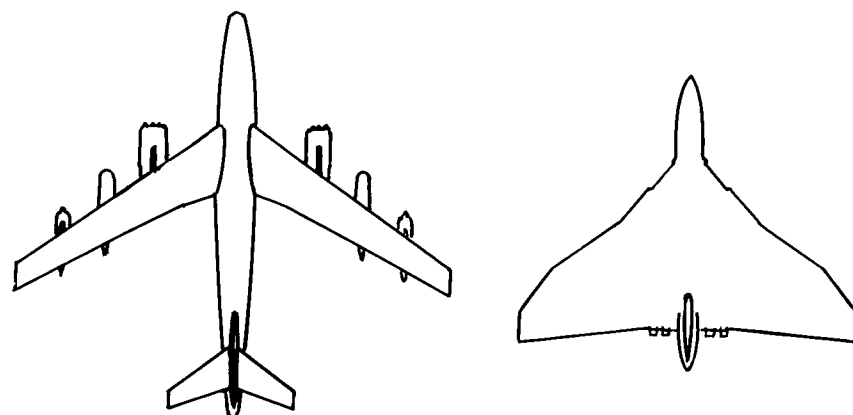
"Zero-lift," or "parasite" drag is the drag which is not related to lift. This is primarily skin-friction drag, and as such is directly proportional to the total surface area of the aircraft exposed ("wetted") to the air.

The "aspect ratio" of the wing has historically been used as the primary indicator of wing efficiency. Aspect ratio is defined as the square of the wing span divided by the wing reference area. For a rectangular wing the aspect ratio is simply the span divided by chord.

Aspect ratios range from under one for re-entry lifting bodies to over thirty for sailplanes. Typical values range between three and eight. For initial design purposes, aspect ratio can be selected from historical data. For final determination of the best aspect ratio, a trade study as discussed in Chapter 19 should be conducted.

Aspect ratio could be used to estimate subsonic  $L/D$ , but for one major problem. The parasite drag is not a function of just the wing area, as expressed by aspect ratio, but also of the aircraft's total wetted area.

Figure 3.4 shows two widely different aircraft concepts, both designed to perform the same mission of strategic bombing. The Boeing B-47 features a conventional approach. With its aspect ratio of over 9, it is not surprising



	B-47	AVRO VULCAN
S reference	1430	3446
S wetted	11300	9600
SPAN	116	90
Swet/Sref	7.9	2.8
ASPECT RATIO	9.4	3.0
WETTED ASPECT RATIO	1.2	1.1
L/D max	17.2	17.0

Fig. 3.4 Does aspect ratio predict drag?

that it attains an  $L/D$  of over 17. On the other hand, the AVRO Vulcan bomber has an aspect ratio of only 3, yet it attains almost exactly the same  $L/D$ .

The explanation for this curious outcome lies in the actual drivers of  $L/D$  as discussed above. Both aircraft have about the same wing span, and both have about the same wetted areas, so both have about the same  $L/D$ . The aspect ratio of the B-47 is higher not because of a greater wing span, but because of a smaller wing area. However, this reduced wing area is offset by the wetted area of the fuselage and tails.

This is illustrated by the ratios of wetted area to wing reference area ( $S_{wet}/S_{ref}$ ). While the AVRO design has a total wetted area of less than three times the wing area, the Boeing design has a wetted area of eight times the wing area.

This wetted-area ratio can be used, along with aspect ratio, as a more reliable early estimate of  $L/D$ . Wetted-area ratio is clearly dependent on the actual configuration layout. Figure 3.5 shows a spectrum of design approaches and the resulting wetted-area ratios.

As stated above,  $L/D$  depends primarily on the wing span and the wetted area. This suggests a new parameter, the "Wetted Aspect Ratio," which is defined as the wing span squared divided by the total aircraft wetted area. This is very similar to the aspect ratio except that it considers total wetted area instead of wing reference area.

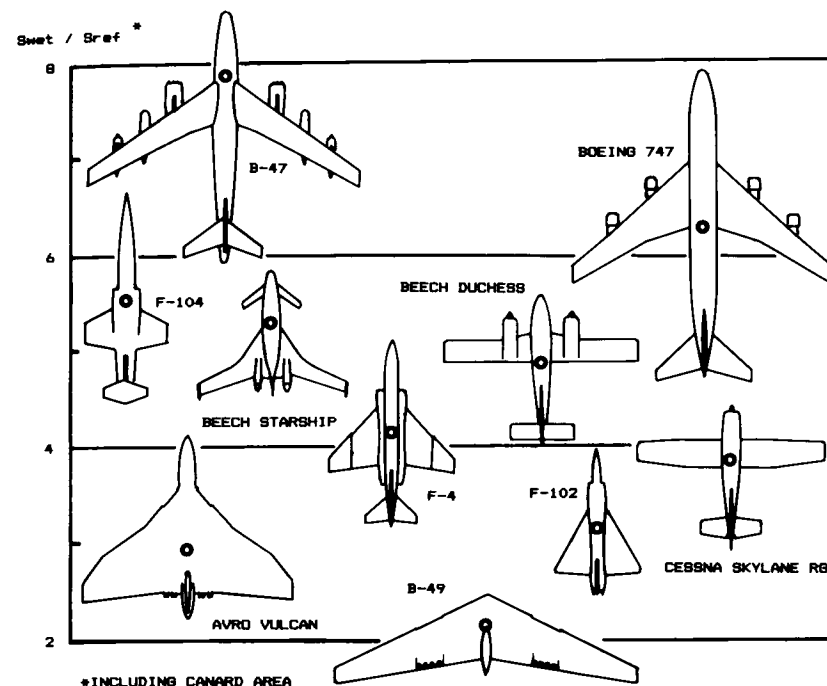


Fig. 3.5 Wetted area ratios.

Figure 3.6 plots maximum  $L/D$  for a number of aircraft vs the wetted aspect ratio, and shows clear trend lines for jet, prop, and fixed-gear prop aircraft. Note that the wetted aspect ratio can be shown to equal the wing geometric aspect ratio divided by the wetted-area ratio,  $S_{wet}/S_{ref}$ .

It should be clear at this point that the designer has control over the  $L/D$ . The designer picks the aspect ratio and determines the configuration arrangement, which in turn determines the wetted-area ratio.

However, the designer must strike a compromise between the desire for a high  $L/D$  and the conflicting desire for low weight. The statistical equations provided above for estimating the empty-weight fraction are based on "normal" designs. If the aspect ratio selected is much higher than that of other aircraft in its class, the empty-weight fraction would be higher than estimated by these simple statistical equations.

$L/D$  can now be estimated from a conceptual sketch. This is the crude, "back of a napkin" drawing mentioned earlier. On the conceptual sketch the designer arranges the major components of the aircraft, including wings, tails, fuselage, engines, payload or passenger compartment, landing gear, fuel tanks, and others as needed.

From the sketch the wetted-area ratio can be "eyeball-estimated" using Fig. 3.5 for guidance. The wetted aspect ratio can then be calculated as the wing aspect ratio divided by the wetted-area ratio. Figure 3.6 can then be used to estimate the maximum  $L/D$ .

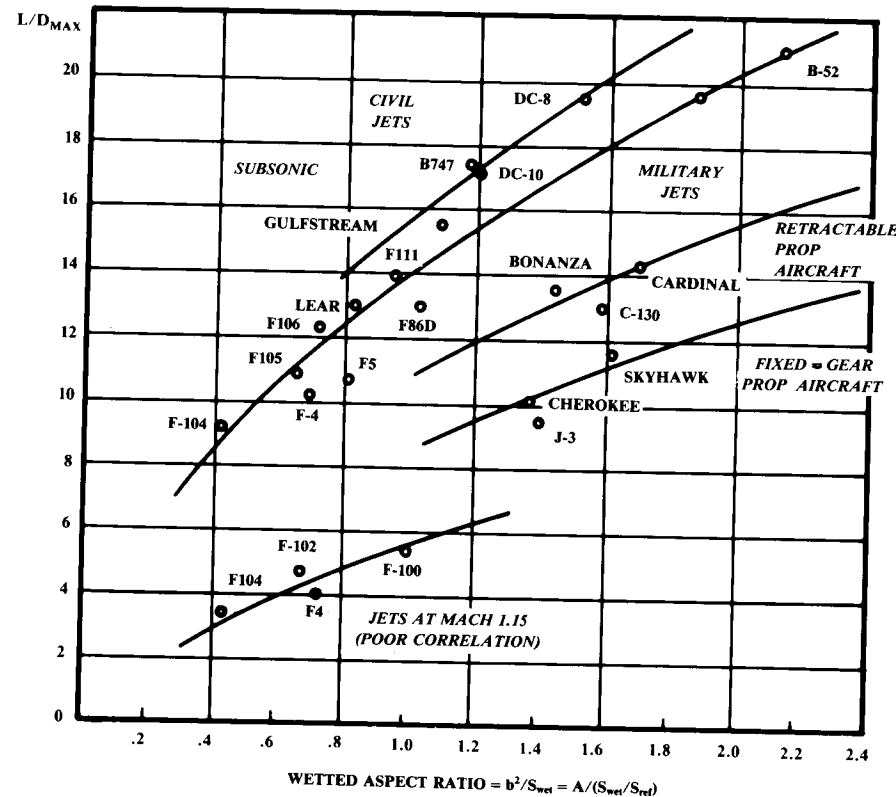


Fig. 3.6 Maximum lift to drag ratio trends.

Note that the  $L/D$  can usually be estimated without a sketch by an experienced designer. The wetted aspect ratio method is provided primarily for the student, but can be useful for quickly evaluating novel concepts.

Drag varies with altitude and velocity. For any altitude there is a velocity which maximizes  $L/D$ . To maximize cruise or loiter efficiency the aircraft should fly at approximately the velocity for maximum  $L/D$ .

For reasons which will be derived later, the most efficient loiter for a jet aircraft occurs exactly at the velocity for maximum  $L/D$ , but the most efficient loiter speed for a propeller aircraft occurs at a slower velocity that yields an  $L/D$  of 86.6% of the maximum  $L/D$ .

Similarly, the most efficient cruise velocity for a propeller aircraft occurs at the velocity yielding maximum  $L/D$ , whereas the most efficient cruise for a jet aircraft occurs at a slightly higher velocity yielding an  $L/D$  of 86.6% of the maximum  $L/D$ .

	Cruise	Loiter
Jet	$0.866 L/D_{\max}$	$L/D_{\max}$
Prop	$L/D_{\max}$	$0.866 L/D_{\max}$

For initial sizing, these percents can be multiplied times the maximum  $L/D$  as estimated using Fig. 3.6 to determine the  $L/D$  for cruise and loiter.

### Fuel-Fraction Estimation

Using historical values from Table 3.2 and the equations for cruise and loiter segments, the mission-segment weight fractions can now be estimated. By multiplying them together, the total mission weight fraction,  $W_x/W_0$ , can be calculated.

Since this simplified sizing method does not allow mission segments involving payload drops, all weight lost during the mission must be due to fuel usage. The mission fuel fraction must therefore be equal to  $(1 - W_x/W_0)$ . If you assume, typically, a 6% allowance for reserve and trapped fuel, the total fuel fraction can be estimated as in Eq. (3.11).

$$\frac{W_f}{W_0} = 1.06 \left( 1 - \frac{W_x}{W_0} \right) \quad (3.11)$$

### 3.5 TAKEOFF-WEIGHT CALCULATION

Using the fuel fraction found with Eq. (3.11) and the statistical empty-weight equation selected from Table 3.1, the takeoff gross weight can be found iteratively from Eq. (3.4). This is done by guessing the takeoff gross weight, calculating the statistical empty-weight fraction, and then calculating the takeoff gross weight. If the result doesn't match the guess value, a value between the two is used as the next guess. This will usually converge in just a few iterations. This first-order sizing process is diagrammed in Fig. 3.7.

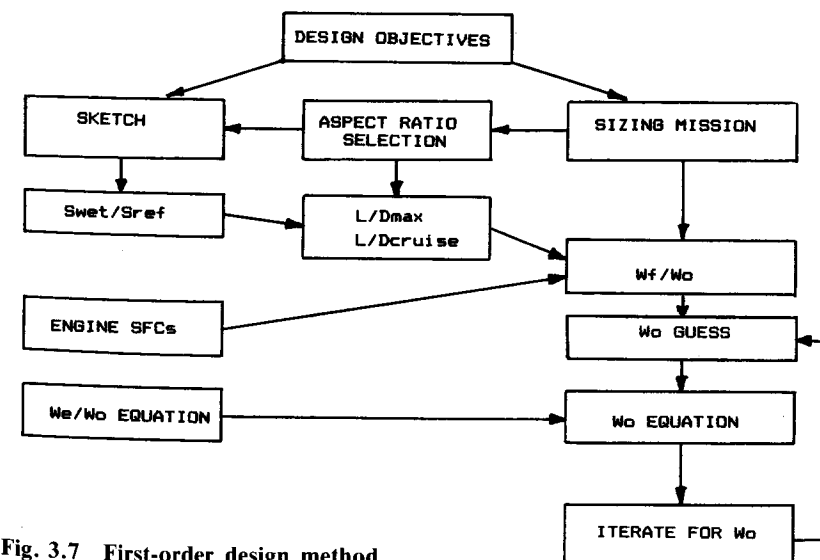


Fig. 3.7 First-order design method.



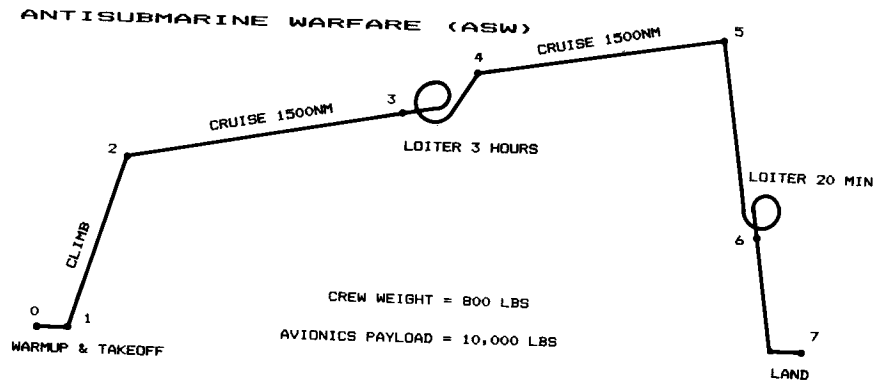


Fig. 3.8 Sample mission profile.

### 3.6 DESIGN EXAMPLE: ASW AIRCRAFT

#### ASW Requirements

Figure 3.8 illustrates the mission requirement for a hypothetical antisubmarine warfare (ASW) aircraft. The key requirement is the ability to loiter for three hours at a distance of 1500 n.mi. from the takeoff point. While loitering on-station, this type of aircraft uses sophisticated electronic equipment to detect and track submarines. For the sizing example, this equipment is assumed to weigh 10,000 lb. Also, a four-man crew is required, totalling 800 lb. The aircraft must cruise at 0.6 Mach number.

#### Conceptual Sketches

Figure 3.9 shows four conceptual approaches considered by the designer in response to these mission requirements. Concept one is the conventional

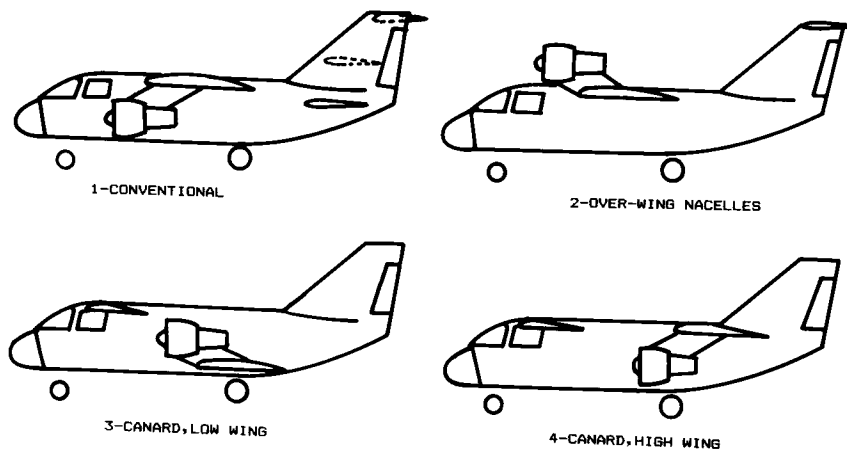


Fig. 3.9 ASW concept sketches.

approach, looking much like the Lockheed S-3A that currently performs a similar mission. The low horizontal tail position shown in solid line would offer the lightest structure, but may place the tail in the exhaust stream of the engines, so other positions for the horizontal tail are shown in dotted lines.

The second concept is much like the first except for the engine location. Here the engines are shown mounted over the wing. This provides extra lift due to the exhaust over the wings, and also provides greater ground clearance for the engines, which reduces the tendency of the jet engines to suck up debris. However, the disadvantage of this concept is the difficulty in reaching the engines for maintenance work.

Concepts three and four explore the canarded approach. Canards offer the potential for reduced trim drag and may provide a wider allowable range for the center of gravity. In concept three, the wing is low and the engines are mounted over the wing as in concept two. This would allow the main landing gear to be stowed in the wing root.

In concept four, the wing is high with the engines mounted below. This last approach offers better access to the engines, and for this reason was selected for further development.

Figure 3.10 is a conceptual sketch prepared, in more detail, for the selected concept. Note the locations indicated for the landing-gear stowage, crew station, and fuel tanks.

This points out a common problem with canard aircraft, the fuel tank locations. The fuel tanks should be placed so that the fuel is evenly dis-

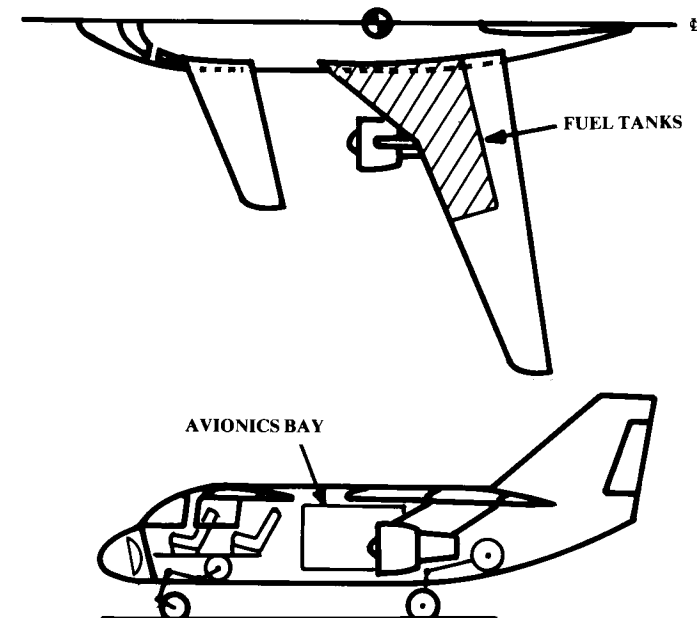


Fig. 3.10 Completed ASW sketch.

tributed about the aircraft center of gravity (estimated location shown by the circle with two quarters shaded). This is necessary so that the aircraft when loaded has nearly the same center of gravity as when its fuel is almost gone. However, the wing is located aft of the center of gravity whenever a canard is used, so the fuel located in the wing is also aft of the center of gravity.

One solution to this problem would be to add fuel tanks in the fuselage, forward of the center of gravity. This would increase the risk of fire in the fuselage during an accident, and is forbidden in commercial aircraft. Although this example is a military aircraft, fire safety should always be considered.

Another solution, shown on the sketch, is to add a wing strake full of fuel. This solution is seen on the Beech Starship among others. The strakes do add to the aircraft wetted area, which reduces cruise aerodynamic efficiency.

This example serves to illustrate an extremely important principle of aircraft design; namely, that there is no such thing as a free lunch! All aircraft design entails a series of trade offs. The canard offers lower trim drag, but in this case may require a higher wetted area. The only true way to determine whether a canard is a good idea for this or any aircraft is to design several aircraft, one with and one without a canard. This type of trade study comprises the majority of the design effort during the conceptual design process.

### L/D Estimation

For initial sizing, a wing aspect ratio of about 11 was selected. With the area of the wing and canard both included, this is equivalent to a combined aspect ratio of about 8.

Comparing the sketch of Fig. 3.10 to the examples of Fig. 3.5, it would appear that the wetted area ratio ( $S_{wet}/S_{ref}$ ) is about 5.5. This yields a wetted aspect ratio of 1.45 (i.e., 8/5.5).

For a wetted aspect ratio of 1.45, Fig. 3.6 indicates that a maximum lift-to-drag ratio of about 17 would be expected. This value, obtained from an initial sketch and the selected aspect ratio, can now be used for initial sizing.

Since this is a jet aircraft, the maximum  $L/D$  is used for loiter calculations. For cruise, a value of 0.866 times the maximum  $L/D$ , or about 15, is used.

### Takeoff-Weight Sizing

From Table 3.3, initial values for SFC are obtained. For a subsonic aircraft the best SFC values are obtained with high-bypass turbofans, which have typical values of about 0.5 for cruise and 0.4 for loiter.

Table 3.1 does not provide an equation for statistically estimating the empty weight fraction of an antisubmarine aircraft. However, such an aircraft is basically designed for subsonic cruise efficiency so the equation for military cargo/bomber can be used. The extensive ASW avionics would not be included in that equation, so it is treated as a separate payload weight.

### Box 3.1 ASW sizing calculations

#### Mission Segment Weight Fractions

1) Warmup and takeoff	$W_1/W_0 = 0.97$	(Table 2)
2) Climb	$W_2/W_1 = 0.985$	(Table 2)
3) Cruise	$R = 1500\text{nm} = 9,114,000 \text{ ft}$ $C = 0.5 \text{ 1/hr} = 0.0001389 \text{ 1/s}$ $V = 0.6\text{M} \times (994.8 \text{ ft/s}) = 569.9 \text{ ft/s}$ $L/D = 16 \times 0.866 = 13.9$ $W_3/W_2 = e^{-(RC/VL/D)} = e^{-0.16} = 0.852$	
4) Loiter	$E = 3 \text{ hours} = 10,800 \text{ s}$ $C = 0.4 \text{ 1/hr} = 0.0001111 \text{ 1/s}$ $L/D = 16$ $W_4/W_3 = e^{-(EC/L/D)} = e^{-0.075} = 0.9277$	
5) Cruise (same as 3)	$W_5/W_4 = 0.852$	
6) Loiter	$E = 1/3 \text{ hours} = 1200 \text{ s}$ $C = 0.0001111 \text{ 1/s}$ $L/D = 16$ $W_6/W_5 = e^{-0.0083} = 0.9917$	
7) Land	$W_7/W_6 = 0.995$	(Table 2)

$$W_7/W_0 = (0.97)(0.985)(0.852)(0.9277)(0.852)(0.9917)(0.995) = 0.635$$

$$W_f/W_0 = 1.06(1 - 0.6505) = 0.387$$

$$W_e/W_0 = 0.93 W_0^{-0.07} \quad (\text{Table 1})$$

$$W_0 = \frac{10,800}{1 - 0.387 - \frac{W_e}{W_0}} = \frac{10,800}{0.613 - 0.93 W_0^{-0.07}}$$

$W_0$ Guess	$W_e/W_0$	$W_0$ Calculated
50,000	0.4361	61,057
60,000	0.4305	59,191
59,200	0.4309	59,328
59,300	0.4309	59,311
59,310	0.4309	59,309.6

Box 3.1 gives the calculations for sizing this example. Note the effort to insure consistent dimensions, including the conversion of cruise velocity (Mach 0.6) to ft/s by assuming a typical cruise altitude of 30,000 ft. At this altitude the speed of sound (see Appendix A.2) is 994.8 ft/s.

The calculations in box 3.1 indicate a takeoff gross weight of 59,310 lb. Although these calculations are based upon crude estimates of aerodynamics, weights, and propulsion parameters, it is interesting to note that the actual takeoff gross weight of the Lockheed S-3A, as quoted in Ref. 1, is 52,539. While strict accuracy should not be expected, this simple sizing method will usually yield an answer in the "right ballpark."

### Trade Studies

An important part of conceptual design is the evaluation and refinement, with the customer, of the design requirements. In the ASW design example, the required range of 1500 n.mi. (each way) is probably less than the customer would really like. A "range trade" can be calculated to determine the increase in design takeoff gross weight if the required range is increased.

**Box 3.2 Range trade**

#### 1000 nm Range

$$W_3/W_2 = W_5/W_4 = e^{-0.1065} = 0.899$$

$$W_7/W_0 = 0.7069$$

$$W_f/W_0 = 1.06(1 - 0.7069) = 0.3107$$

$$W_0 = \frac{10,800}{1 - 0.3107 - \frac{W_e}{W_0}} = \frac{10,800}{0.6893 - 0.93W_0^{-0.07}}$$

$W_0$ Guess	$W_e/W_0$	$W_0$ Calculated
50,000	0.4361	42,657
45,000	0.4393	43,203
43,500	0.4403	43,384
43,400	0.4404	43,396
43,398	0.4404	43,397

#### 2000 nm Range

$$W_3/W_2 = W_5/W_4 = e^{-0.213} = 0.8082$$

$$W_7/W_0 = 0.5713$$

$$W_f/W_0 = 0.4544$$

$$W_0 = \frac{10,800}{1 - 0.4544 - \frac{W_e}{W_0}} = \frac{10,800}{0.5456 - 0.93W_0^{-0.07}}$$

$W_0$ Guess	$W_e/W_0$	$W_0$ Calculated
50,000	0.4361	98,660
80,000	0.4219	87,331
86,000	0.4198	85,889
85,900	0.4199	85,913
85,910	0.4199	85,911

This is done by recalculating the weight fractions for the cruise mission segments, using arbitrarily selected ranges. For example, instead of the required 1500 n.mi., we will calculate the cruise weight fractions using 1000 and 2000 n.mi., and will size the aircraft separately for each of those ranges. These calculations are shown in Box 3.2, and the results are plotted in Fig. 3.11.

In a similar fashion, a "payload trade" can be made. The mission-segment weight fractions and fuel fraction are unchanged but the numerator of the sizing equation, Eq. (3.4), is parametrically varied by assuming different payload weights. The given payload requirement is 10,000 lb of avionics equipment. Box 3.3 shows the sizing calculations assuming payload weights of 5000, 15,000, and 20,000 lb. The results are plotted in Fig. 3.12.

The statistical empty-weight equation used here for sizing was based upon existing military cargo and bomber aircraft, which are all of aluminum construction. The takeoff gross weight calculations above have thus implicitly assumed that the new aircraft would also be built of aluminum.

To determine the effect of building the aircraft out of composite materials, the designer must adjust the empty-weight equation. As previously mentioned, this can be approximated in the early stages of design by taking 95% of the empty-weight fraction obtained for a metal aircraft. The calculations for resizing the aircraft using composite materials are shown in box 3.4.

The use of composite materials reduces the takeoff gross weight from 59,310 lb to only 53,771 lb yet the aircraft can still perform the same

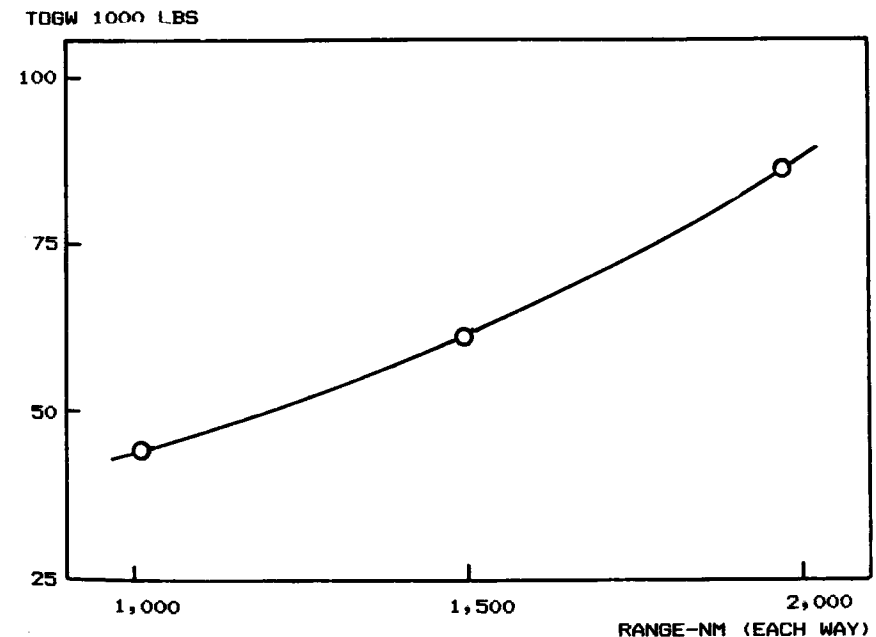


Fig. 3.11 Range trade.

**Box 3.3 Payload trade**

$$\text{Payload} = 5000 \text{ lb} \quad W_0 = \frac{5800}{0.613 - 0.93 W_0^{-0.07}}$$

$W_0$ Guess	$W_e / W_0$	$W_0$ Calculated
50,000	0.4361	32,787
35,000	0.4471	34,960
34,970	0.4471	34,965
34,966	0.4471	34,966

$$\text{Payload} = 15,000 \text{ lb} \quad W_0 = \frac{15,800}{0.613 - 0.93 W_0^{-0.07}}$$

$W_0$ Guess	$W_e / W_0$	$W_0$ Calculated
50,000	0.4362	89,366
85,000	0.4202	81,937
82,000	0.4212	82,389
82,350	0.4211	82,335

$$\text{Payload} = 20,000 \text{ lb} \quad W_0 = \frac{20,800}{0.613 - 0.93 W_0^{-0.07}}$$

$W_0$ Guess	$W_e / W_0$	$W_0$ Calculated
90,000	0.4185	106,941
100,000	0.4154	105,272
105,000	0.4140	104,522
104,600	0.4141	104,581

**Box 3.4 Composite material trade**

$$W_e / W_0 = (0.95)(0.93 W_0^{-0.07}) = 0.8835 W_0^{-0.07}$$

$$W_0 = \frac{10,800}{1 - 0.387 - \frac{W_e}{W_0}} = \frac{10,800}{0.613 - 0.8835 W_0^{-0.07}}$$

$W_0$ Guess	$W_e / W_0$	$W_0$ Calculated
50,000	0.4143	54,344
54,000	0.4120	53,742
53,800	0.4122	53,771

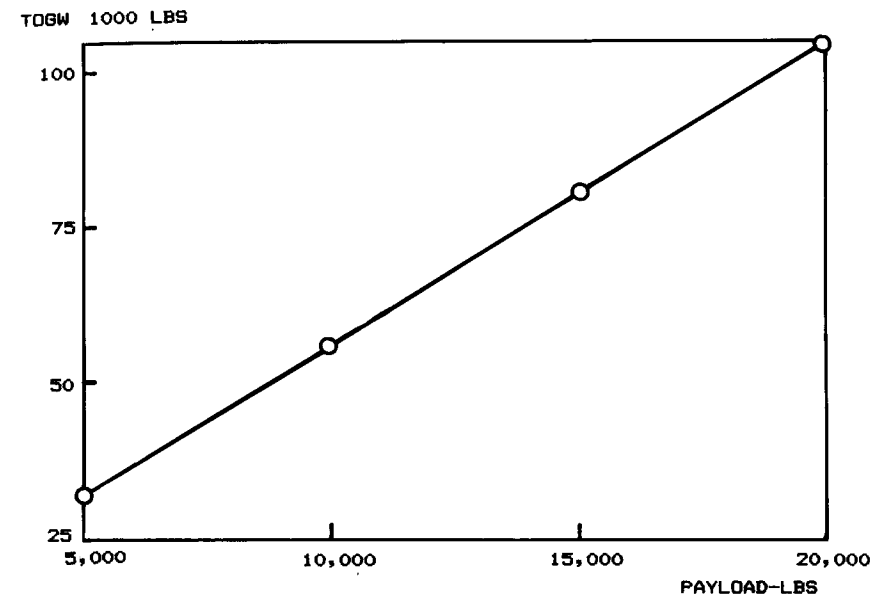


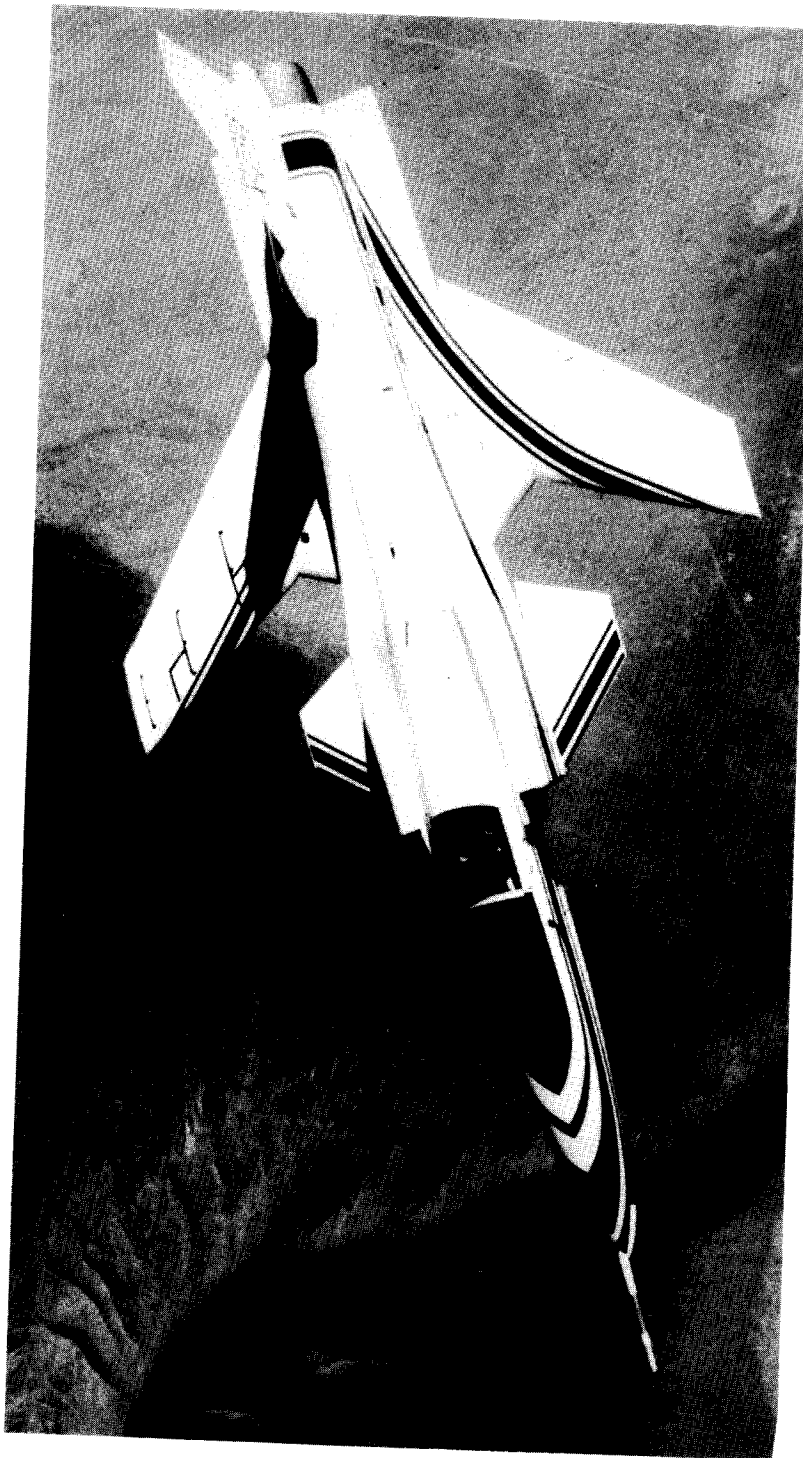
Fig. 3.12 Payload trade.

mission. This is a 9.3% takeoff-weight savings, resulting from only a 5% empty-weight saving.

This result sounds erroneous, but is actually typical of the “leverage” effect of the sizing equation. Unfortunately, this works both ways. If the empty weight creeps up during the detail-design process, it will require a more-than-proportional increase in takeoff gross weight to maintain the capability to perform the sizing mission. Thus it is crucial that realistic estimates of empty weight be used during early conceptual design, and that the weight be strictly controlled during later stages of design.

There are many trade studies which could be conducted other than range, payload, and material. Methods for trade studies are discussed in detail in Chapter 19.

The remainder of the book presents better methods for design, analysis, sizing, and trade studies, building on the concepts just given. In this chapter a conceptual sketch was made, but no guidance was provided as to how to make the sketch or why different features may be good or bad. Following chapters address these issues and illustrate how to develop a complete three-view drawing for analysis. Then more-sophisticated methods of analysis, sizing, and trade studies will be provided.



X-29 Forward-Swept-Wing Demonstrator

## AIRFOIL AND GEOMETRY SELECTION

### 4.1 INTRODUCTION

Before the design layout can be started, values for a number of parameters must be chosen. These include the airfoil(s), the wing and tail geometries, wing loading, thrust-to-weight or horsepower-to-weight ratio, estimated takeoff gross weight and fuel weight, estimated wing, tail, and engine sizes, and the required fuselage size. These are discussed in the next three chapters.

This chapter covers selecting the airfoil and the wing and tail geometry. Chapter 5 addresses estimation of the required wing loading and thrust-to-weight ratio (horsepower-to-weight ratio for a propeller aircraft). Chapter 6 provides a more refined method for initial sizing than the quick method presented in the last chapter, and concludes with the use of the sizing results to calculate the required wing and tail area, engine size, and fuselage volume.

### 4.2 AIRFOIL SELECTION

The airfoil, in many respects, is the heart of the airplane. The airfoil affects the cruise speed, takeoff and landing distances, stall speed, handling qualities (especially near the stall), and overall aerodynamic efficiency during all phases of flight.

Much of the Wright Brothers' success can be traced to their development of airfoils using a wind tunnel of their own design, and the in-flight validation of those airfoils in their glider experiments of 1901-1902. The P-51 was regarded as the finest fighter of World War II in part because of its radical laminar-flow airfoil. Recently, the low-speed airfoils developed by Peter Lissaman contributed to the success of the man-powered Gossamer Condor.

#### **Airfoil Geometry**

Figure 4.1 illustrates the key geometric parameters of an airfoil. The front of the airfoil is defined by a leading-edge radius which is tangent to the upper and lower surfaces. An airfoil designed to operate in supersonic flow will have a sharp or nearly-sharp leading edge to prevent a drag-producing bow shock. (As discussed later, wing sweep may be used instead of a sharp leading edge to reduce the supersonic drag.)

The chord of the airfoil is the straight line from the leading edge to the trailing edge. It is very difficult to build a perfectly sharp trailing edge, so most airfoils have a blunt trailing edge with some small finite thickness.

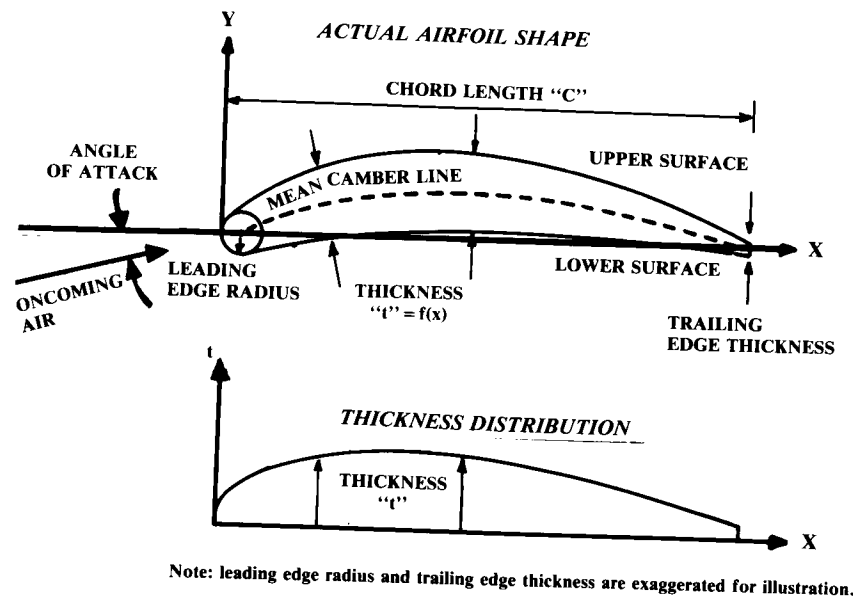


Fig. 4.1 Airfoil geometry.

“Camber” refers to the curvature characteristic of most airfoils. The “mean camber line” is the line equidistant from the upper and lower surfaces. Total airfoil camber is defined as the maximum distance of the mean camber line from the chord line, expressed as a percent of the chord.

In earlier days, most airfoils had flat bottoms, and it was common to refer to the upper surface shape as the “camber.” Later, as airfoils with curved bottoms came into usage, they were known as “double-cambered” airfoils. Also, an airfoil with a concave lower surface was known as an “under-cambered” airfoil. These terms are technically obsolete but are still in common usage.

The thickness distribution of the airfoil is the distance from the upper surface to the lower surface, measured perpendicular to the mean camber line, and is a function of the distance from the leading edge. The “airfoil thickness ratio” ( $t/c$ ) refers to the maximum thickness of the airfoil divided by its chord.

For many aerodynamic calculations, it has been traditional to separate the airfoil into its thickness distribution and a zero-thickness camber line. The former provides the major influence on the profile drag, while the latter provides the major influence upon the lift and the drag due to lift.

When an airfoil is scaled in thickness, the camber line must remain unchanged, so the scaled thickness distribution is added to the original camber line to produce the new, scaled airfoil. In a similar fashion, an airfoil which is to have its camber changed is broken into its camber line and thickness distribution. The camber line is scaled to produce the desired maximum camber; then the original thickness distribution is added to obtain the new

airfoil. In this fashion, the airfoil can be reshaped to change either the profile drag or lift characteristics, without greatly affecting the other.

### Airfoil Lift and Drag

An airfoil generates lift by changing the velocity of the air passing over and under itself. The airfoil angle of attack and/or camber causes the air over the top of the wing to travel faster than the air beneath the wing.

Bernoulli's equation shows that higher velocities produce lower pressures, so the upper surface of the airfoil tends to be pulled upward by lower-than-ambient pressures while the lower surface of the airfoil tends to be pushed upward by higher-than-ambient pressures. The integrated differences in pressure between the top and bottom of the airfoil generate the net lifting force.

Figure 4.2 shows typical pressure distributions for the upper and lower surfaces of a lifting airfoil at subsonic speeds. Note that the upper surface of the wing contributes about two-thirds of the total lift.

Figure 4.3a illustrates the flowfield around a typical airfoil as a number of airflow velocity vectors, with the vector length representing local velocity magnitude. In Fig. 4.3b, the freestream velocity vector is subtracted from each local velocity vector, leaving only the change in velocity vector caused by the presence of the airfoil. It can be seen that the effect of the airfoil is to introduce a change in airflow, which seems to circulate around the airfoil in a clockwise fashion if the airfoil nose is to the left.

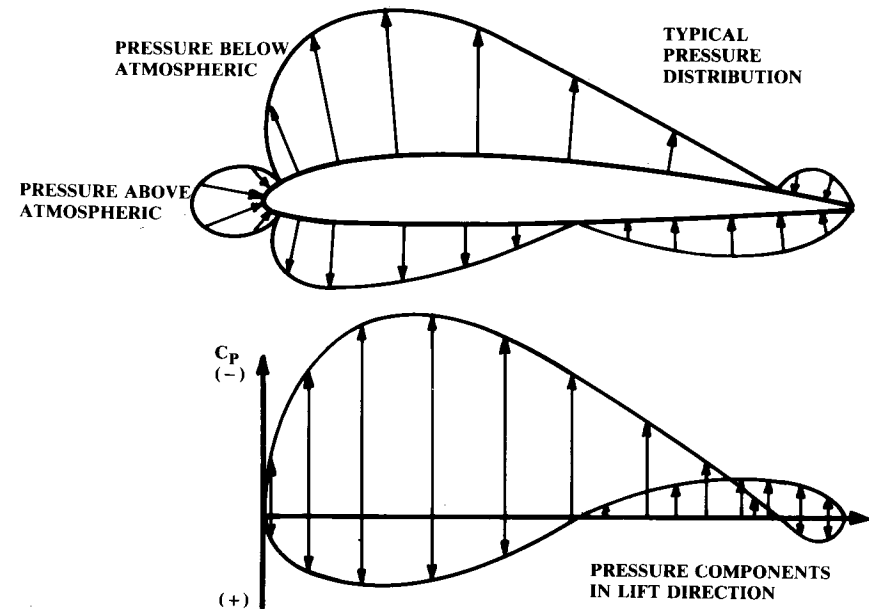


Fig. 4.2 Typical airfoil pressure distribution.

This "circulation" is the theoretical basis for the classical calculation of lift and drag-due-to-lift. The greater the circulation, the greater the lift. Circulation is usually represented by  $\Gamma$  and is shown as a circular flow direction as in Fig. 4.3c.

As a side effect of the generation of lift, the airfoil imparts a downward momentum on the flowfield. The downward force exerted on the air must equal the lift force produced on the airfoil. However, the lift is not "caused" by the downward motion of the air but by the pressure forces the air exerts upon the airfoil.

A flat board at an angle to the oncoming air will produce lift. However, the air going over the top of the flat "airfoil" will tend to separate from the surface, thus disturbing the flow and therefore reducing lift and greatly increasing drag (Fig. 4.4). Curving the airfoil (i.e., camber) allows the air flow to remain attached, thus increasing lift and reducing drag. The camber also increases lift by increasing the circulation of the airflow.

In fact, an airfoil with camber will produce lift even at zero angle between the chord line and the oncoming air ("angle of attack"). For a cambered airfoil there is some negative angle at which no lift is produced, the "angle

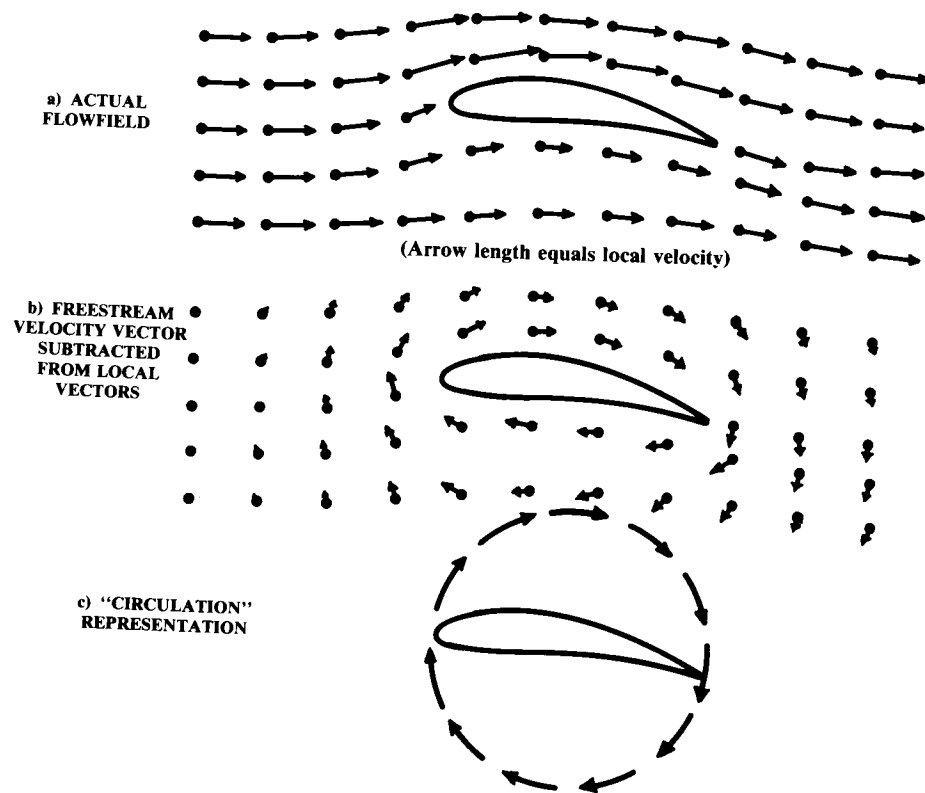


Fig. 4.3 Airfoil flowfield and circulation.

of zero lift." This negative angle is approximately equal (in degrees) to the percent camber of the airfoil.

Odd as it sounds, an airfoil in two-dimensional (2-D) flow does not experience any drag due to the creation of lift. The pressure forces produced in the generation of lift are at right angles to the oncoming air. All two-dimensional airfoil drag is produced by skin friction and pressure effects resulting from flow separation and shocks. It is only in three-dimensional (3-D) flow that drag due to lift is produced.

The airfoil section lift, drag, and pitching moment are defined in non-dimensional form in Eqs. (4.1), (4.2), and (4.3). By definition, the lift force is perpendicular to the flight direction while the drag force is parallel to the flight direction. The pitching moment is usually negative when measured about the aerodynamic center, implying a nose-down moment. Note that 2-D airfoil characteristics are denoted by lowercase subscripts (i.e.,  $C_l$ ) whereas the 3-D wing characteristics are denoted by uppercase subscripts (i.e.,  $C_L$ ).

$$C_l = \frac{\text{section lift}}{qc} \quad (4.1)$$

$$C_d = \frac{\text{section drag}}{qc} \quad (4.2)$$

$$C_m = \frac{\text{section moment}}{qc^2} \quad (4.3)$$

where

$c$  = chord length

$q$  = dynamic pressure =  $\rho V^2/2$

$\alpha$  = angle of attack

$C_{l_\alpha}$  = slope of the lift curve =  $2\pi$  (typically)

The point about which the pitching moment remains constant for any angle of attack is called the "aerodynamic center." The aerodynamic center is not the same as the airfoil's center of pressure (or lift). The center of pressure is usually behind the aerodynamic center. The location of the center of pressure varies with angle of attack for most airfoils.

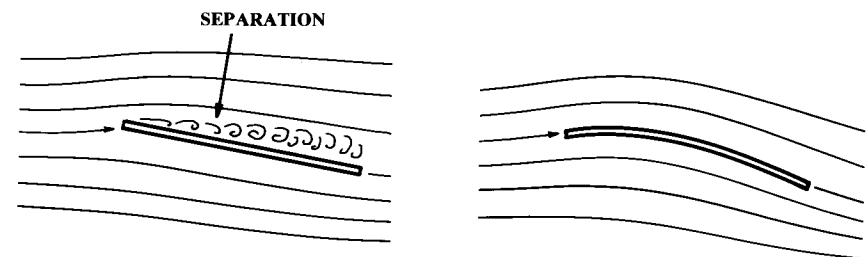


Fig. 4.4 Effect of camber on separation.

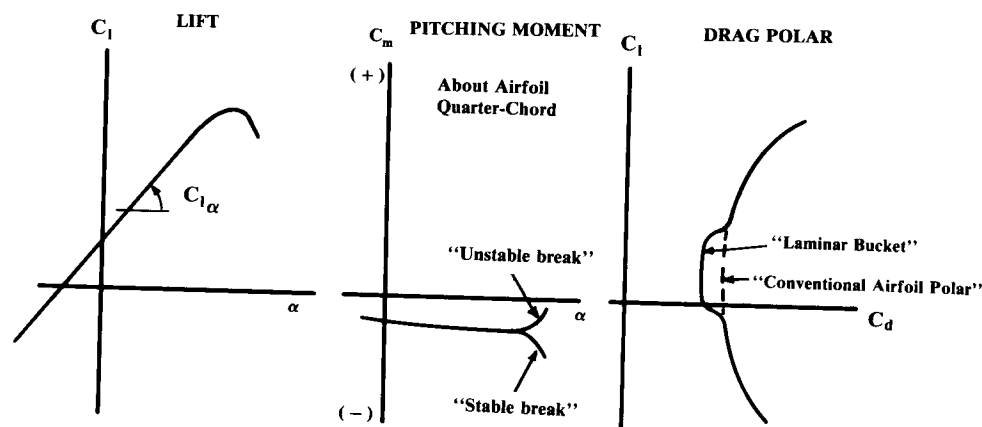


Fig. 4.5 Airfoil lift, drag, and pitching moment.

Pitching moment is measured about some reference point, typically the quarter-chord point (25% of the chord length back from the leading edge). The pitching moment is almost independent of angle of attack about the quarter-chord for most airfoils at subsonic speeds (i.e., the aerodynamic center is usually at the quarter-chord point.)

Lift, drag, and pitching-moment characteristics for a typical airfoil are shown in Fig. 4.5.

Airfoil characteristics are strongly affected by the "Reynolds number" at which they are operating. Reynolds number, the ratio between the dynamic and the viscous forces in a fluid, is equal to  $(\rho V l / \mu)$ , where  $V$  is the velocity,  $l$  the length the fluid has traveled down the surface,  $\rho$  the fluid density, and  $\mu$  the fluid viscosity coefficient. The Reynolds number influences whether the flow will be laminar or turbulent, and whether flow separation will occur. A typical aircraft wing operates at a Reynolds number of about ten million.

Figure 4.5 illustrates the so-called "laminar bucket." For a "laminar" airfoil operating at the design Reynolds number there is a range of lift coefficient for which the flow remains laminar over a substantial part of the airfoil. This causes a significant reduction of drag for a given lift coefficient.

However, this effect is very dependent upon the Reynolds number as well as the actual surface smoothness. For example, dirt, rain, or insect debris on the leading edge may cause the flow to become turbulent, causing an increase in drag to the dotted line shown in Fig. 4.5. This also can change the lift and pitching-moment characteristics.

In several canarded homebuilt designs with laminar airfoils, entering a light rainfall will cause the canard's airflow to become turbulent, reducing canard lift and causing the aircraft to pitch downward. Earlier, nonlaminar airfoils were designed assuming turbulent flow at all times and do not experience this effect.

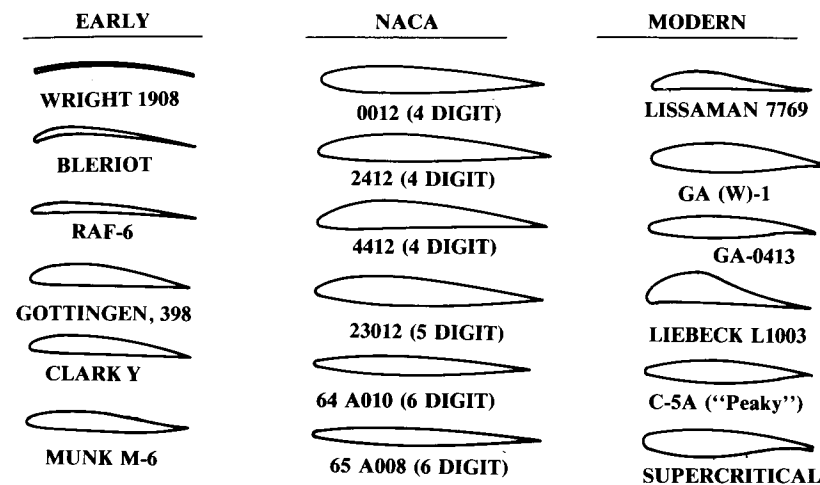


Fig. 4.6 Typical airfoils.

### Airfoil Families

A variety of airfoils is shown in Fig. 4.6. The early airfoils were developed mostly by trial and error. In the 1930's, the NACA developed a widely-used family of mathematically defined airfoils called the "four-digit" airfoils. In these, the first digit defined the percent camber, the second defined the location of the maximum camber, and the last two digits defined the airfoil maximum thickness in percent of chord. While rarely used for wing design today, the uncambered four-digit airfoils are still commonly used for tail surfaces of subsonic aircraft.

The NACA five-digit airfoils were developed to allow shifting the position of maximum camber forward for greater maximum lift. The six-series airfoils were designed for increased laminar flow, and hence reduced drag. Six-series airfoils such as the 64A series are still widely used as a starting point for high-speed-wing design. The Mach 2 F-15 fighter uses the 64A airfoil modified with camber at the leading edge. Geometry and characteristics of these "classical" airfoils are summarized in Ref. 2, a must for every designer's library.

### Airfoil Design

In the past, the designer would select an airfoil (or airfoils) from such a catalog. This selection would consider factors such as the airfoil drag during cruise, stall and pitching-moment characteristics, the thickness available for structure and fuel, and the ease of manufacture. With today's computational airfoil design capabilities, it is becoming common for the airfoil shapes for a wing to be custom-designed.

Modern airfoil design is based upon inverse computational solutions for desired pressure (or velocity) distributions on the airfoil. Methods have been



developed for designing an airfoil such that the pressure differential between the top and bottom of the airfoil quickly reaches a maximum value attainable without airflow separation. Toward the rear of the airfoil, various pressure recovery schemes are employed to prevent separation near the trailing edge.

These airfoil optimization techniques result in airfoils with substantial pressure differentials (lift) over a much greater percent of chord than a classical airfoil. This permits a reduced wing area (and wetted area) for a required amount of lift. Such airfoil design methods go well beyond the scope of this book.

Another consideration in modern airfoil design is the desire to maintain laminar flow over the greatest possible part of the airfoil. Laminar flow can be maintained by providing a negative pressure gradient, i.e., by having the pressure continuously drop from the leading edge to a position close to the trailing edge. This tends to "suck" the flow rearward, promoting laminar flow.

A good laminar-flow airfoil combined with smooth fabrication methods can produce a wing with laminar flow over about 50–70% of the wing. Figure 4.7 shows a typical laminar flow airfoil and its pressure distribution.

As an airfoil generates lift the velocity of the air passing over its upper surface is increased. If the airplane is flying at just under the speed of sound, the faster air traveling over the upper surface will reach supersonic speeds causing a shock to exist on the upper surface, as shown in Fig. 4.8. The speed at which supersonic flow first appears on the airfoil is called the "Critical Mach Number" ( $M_{crit}$ ).

The upper-surface shock creates a large increase in drag, along with a reduction in lift and a change in the pitching moment. The drag increase

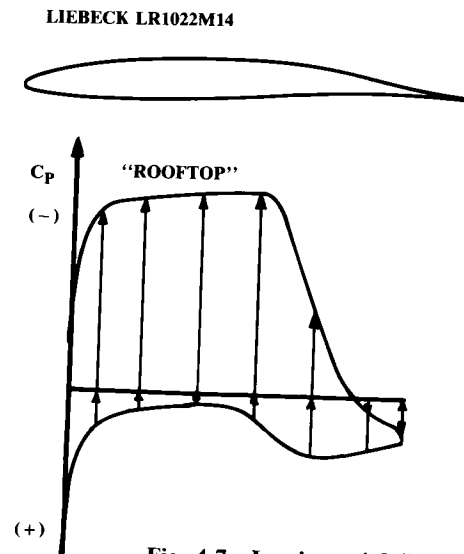


Fig. 4.7 Laminar airfoil.

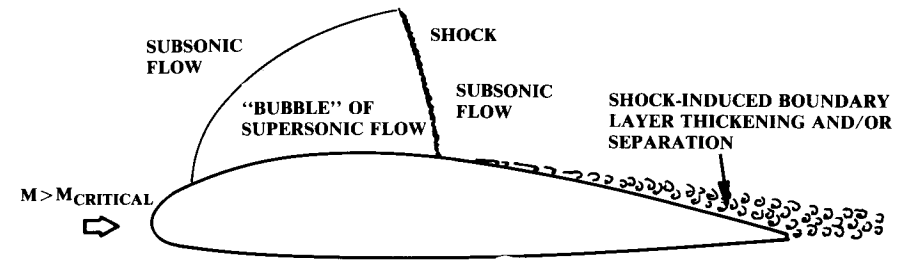


Fig. 4.8 Transonic effects.

comes from the tendency of the rapid pressure rise across the shock to thicken or even separate the boundary layer.

A "supercritical" airfoil is one designed to minimize these effects. Modern computational methods allow design of airfoils in which the upper-surface shock is minimized or even eliminated by spreading the lift in the chordwise direction, thus reducing the upper surface velocity for a required total lift. This increases the Critical Mach Number.

### Design Lift Coefficient

For early conceptual design work, the designer must frequently rely upon existing airfoils. From existing airfoils, the one should be selected that comes closest to having the desired characteristics.

The first consideration in initial airfoil selection is the "design lift coefficient." This is the lift coefficient at which the airfoil has the best  $L/D$  (shown in Fig. 4.9 as the point on the airfoil drag polar that is tangent to a line from the origin and closest to the vertical axis).

In subsonic flight a well-designed airfoil operating at its design lift coefficient has a drag coefficient that is little more than skin-friction drag. The aircraft should be designed so that it flies the design mission at or near the design lift coefficient to maximize the aerodynamic efficiency.

As a first approximation, it can be assumed that the wing lift coefficient,  $C_L$ , equals the airfoil lift coefficient,  $C_l$ . In level flight the lift must equal the weight, so the required design lift coefficient can be found as follows:

$$W = L = qSC_L \cong qSC_l \quad (4.4)$$

$$C_l = \frac{1}{q} \left( \frac{W}{S} \right) \quad (4.5)$$

Dynamic pressure ( $q$ ) is a function of velocity and altitude. By assuming a wing loading ( $W/S$ ) as described later, the design lift coefficient can be calculated for the velocity and altitude of the design mission.

Note that the actual wing loading will decrease during the mission as fuel is burned. Thus, to stay at the design lift coefficient, the dynamic pressure must be steadily reduced during the mission by either slowing down, which

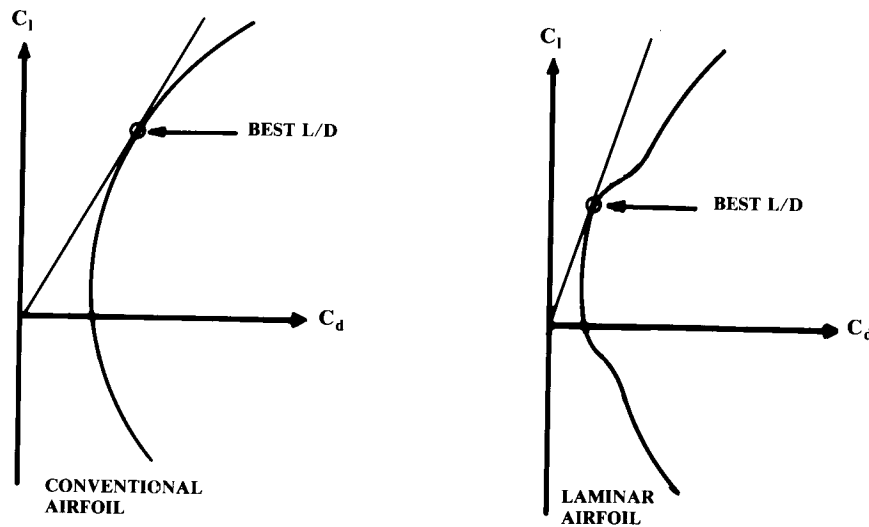


Fig. 4.9 Design lift coefficient.

is undesirable, or climbing to a higher altitude. This explains the “cruise-climb” followed by an aircraft trying to maximize range.

In actual practice, a design lift coefficient usually will be based upon past experience, and for most types of aircraft typically will be around 0.5. In fact, the initial selection of the airfoil is often simply based upon prior experience or copied from some successful design.

### Stall

Stall characteristics play an important role in airfoil selection. Some airfoils exhibit a gradual reduction in lift during a stall, while others show a violent loss of lift, accompanied by a rapid change in pitching moment. This difference reflects the existence of three entirely different types of airfoil stall.

“Fat” airfoils (round leading edge and  $t/c$  greater than about 14%) stall from the trailing edge. The turbulent boundary layer increases with angle of attack. At around 10 deg the boundary layer begins to separate, starting at the trailing edge and moving forward as the angle of attack is further increased. The loss of lift is gradual. The pitching moment changes only a small amount.

Thinner airfoils stall from the leading edge. If the airfoil is of moderate thickness (about 6–14%), the flow separates near the nose at a very small angle of attack, but immediately reattaches itself so that little effect is felt. At some higher angle of attack the flow fails to reattach, which almost immediately stalls the entire airfoil. This causes an abrupt change in lift and pitching moment.

Very thin airfoils exhibit another form of stall. As before, the flow separates from the nose at a small angle of attack and reattaches almost

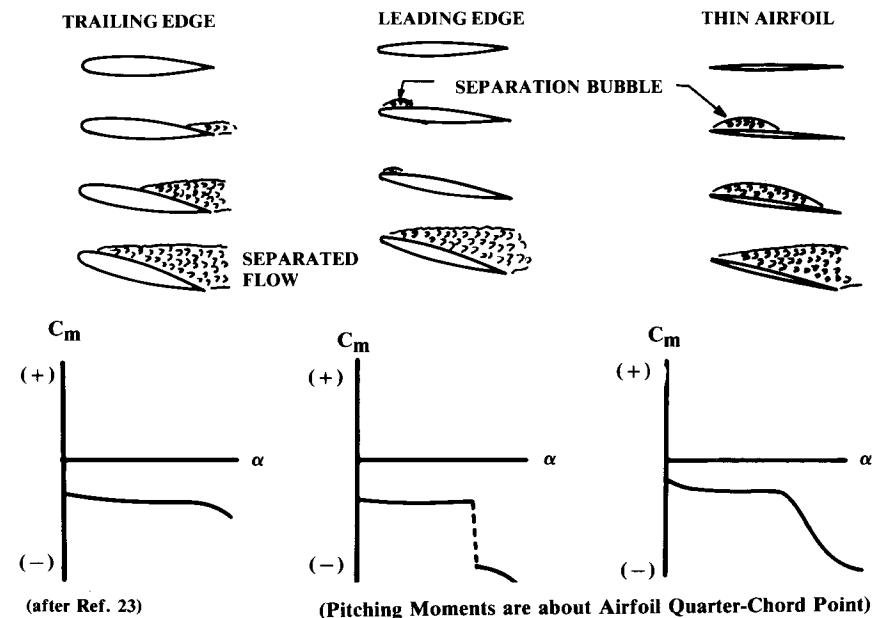


Fig. 4.10 Types of stall.

immediately. However, for a very thin airfoil this “bubble” continues to stretch towards the trailing edge as the angle of attack is increased. At the angle of attack where the bubble stretches all the way to the trailing edge, the airfoil reaches its maximum lift. Beyond that angle of attack, the flow is separated over the whole airfoil, so the stall occurs. The loss of lift is smooth, but large changes in pitching moment are experienced. The three types of stall characteristics are depicted in Fig. 4.10.

Twisting the wing such that the tip airfoils have a reduced angle of attack compared to the root (“washout”) can cause the wing to stall first at the root. This provides a gradual stall even for a wing with a poorly stalling airfoil. Also, the turbulent wake off the stalled wingroot will vibrate the horizontal tail, notifying the pilot that a stall is imminent.

In a similar fashion, the designer may elect to use different airfoils at the root and tip, with a tip airfoil selected which stalls at a higher angle of attack than the root airfoil. This provides good flow over the ailerons for roll control at an angle of attack where the root is stalled.

If different airfoils are used at the root and tip, the designer must develop the intermediate airfoils by interpolation (discussed later). These intermediate airfoils will have section characteristics somewhere between those of the root and tip airfoils, and can also be estimated by interpolation. This interpolation of section characteristics does not work for modern supercritical or laminar-flow airfoils. Estimation of the section characteristics in those cases must be done computationally.

Stall characteristics for thinner airfoils can be improved with various leading-edge devices such as slots, slats, leading-edge flaps, Krueger flaps,

and active methods (e.g., suction or blowing). These are discussed in the Aerodynamics Chapter.

Wing stall is directly related to airfoil stall only for high-aspect-ratio, unswept wings. For lower aspect ratio or highly swept wings the 3-D effects dominate stall characteristics, and airfoil stall characteristics can be essentially ignored in airfoil selection.

Pitching moment must also be considered in airfoil selection. Horizontal tail or canard size is directly affected by the magnitude of the wing pitching moment to be balanced. Some of the supercritical airfoils use what is called "rear-loading" to increase lift without increasing the region of supersonic flow. This produces an excellent  $L/D$ , but can cause a large nose-down pitching moment. If this requires an excessive tail area, the total aircraft drag may be increased, not reduced.

For a stable tailless or flying-wing aircraft, the pitching moment must be near zero. This usually requires an "S"-shaped camber with the characteristic upward reflex at the trailing edge. Reflexed airfoils have poorer  $L/D$  than an airfoil designed without this constraint. This tends to reduce some of the benefit that flying wings experience due to their reduced wetted area. However, a computerized, "active" flight control system can remove the requirement for natural stability, and thus allow a nonreflexed airfoil.

### Airfoil Thickness Ratio

Airfoil thickness ratio has a direct effect on drag, maximum lift, stall characteristics, and structural weight. Figure 4.11 illustrates the effect of thickness ratio on subsonic drag. The drag increases with increasing thickness due to increased separation.

Figure 4.12 shows the impact of thickness ratio on Critical Mach Number, the Mach number at which supersonic flow first appears over the wing. A supercritical airfoil tends to minimize shock formation and can be used to reduce drag for a given thickness ratio or to permit a thicker airfoil at the same drag level.

The thickness ratio affects the maximum lift and stall characteristics primarily by its effect on the nose shape. For a wing of fairly high aspect ratio and moderate sweep, a larger nose radius provides a higher stall angle and a greater maximum lift coefficient, as shown in Fig. 4.13.

The reverse is true for low-aspect-ratio, swept wings, such as a delta wing. Here, a sharper leading edge provides greater maximum lift due to the formation of vortices just behind the leading edge. These leading edge vortices act to delay wing stall. This 3-D effect is discussed in the Aerodynamics Chapter.

Thickness also affects the structural weight of the wing. Statistical equations for wing weight show that the wing structural weight varies approximately inversely with the square root of the thickness ratio. Halving the thickness ratio will increase wing weight by about 41%. The wing is typically about 15% of the total empty weight, so halving the thickness ratio would increase empty weight by about 6%. When applied to the sizing equation, this can have a major impact.

For initial selection of the thickness ratio, the historical trend shown in Fig. 4.14 can be used. Note that a supercritical airfoil would tend to be about 10% thicker (i.e., conventional airfoil thickness ratio times 1.1) than the historical trend.

Frequently the thickness is varied from root to tip. Due to fuselage effects, the root airfoil of a subsonic aircraft can be as much as 20–60% thicker than the tip airfoil without greatly affecting the drag. This is very beneficial, resulting in a structural weight reduction as well as more volume for fuel and landing gear. This thicker root airfoil should extend to no more than about 30% of the span.

### Other Airfoil Considerations

Another important aspect of airfoil selection is the intended Reynolds number. Each airfoil is designed for a certain Reynolds number. Use of an airfoil at a greatly different Reynolds number (half an order of magnitude or so) can produce section characteristics much different from those expected.

This is especially true for the laminar-flow airfoils, and is most crucial when an airfoil is operated at a lower than design Reynolds number. In the past this has been a problem for homebuilt and sailplane designers, but there are now suitable airfoils designed especially for these lower Reynolds number aircraft.

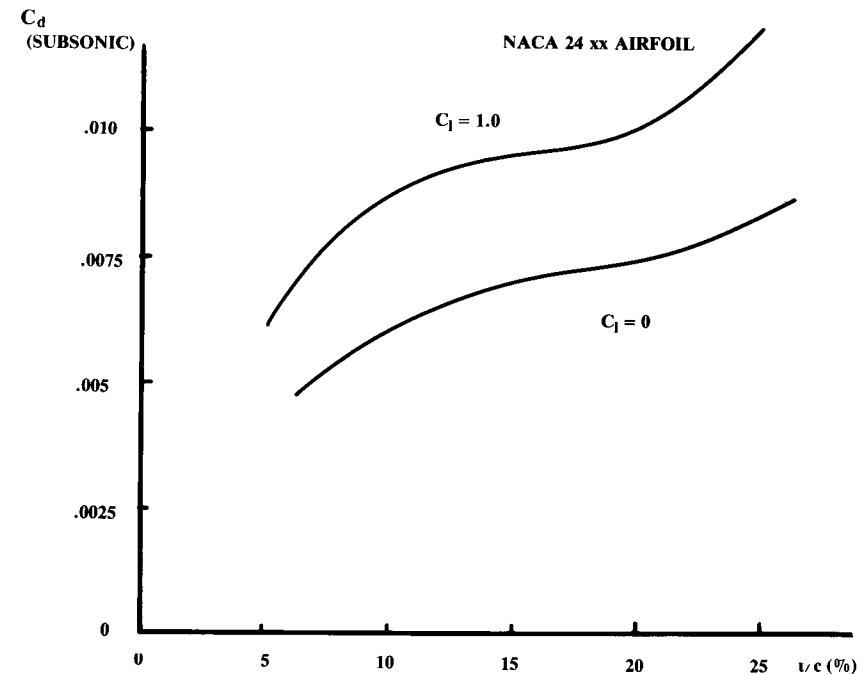


Fig. 4.11 Effects of  $t/c$  on drag.

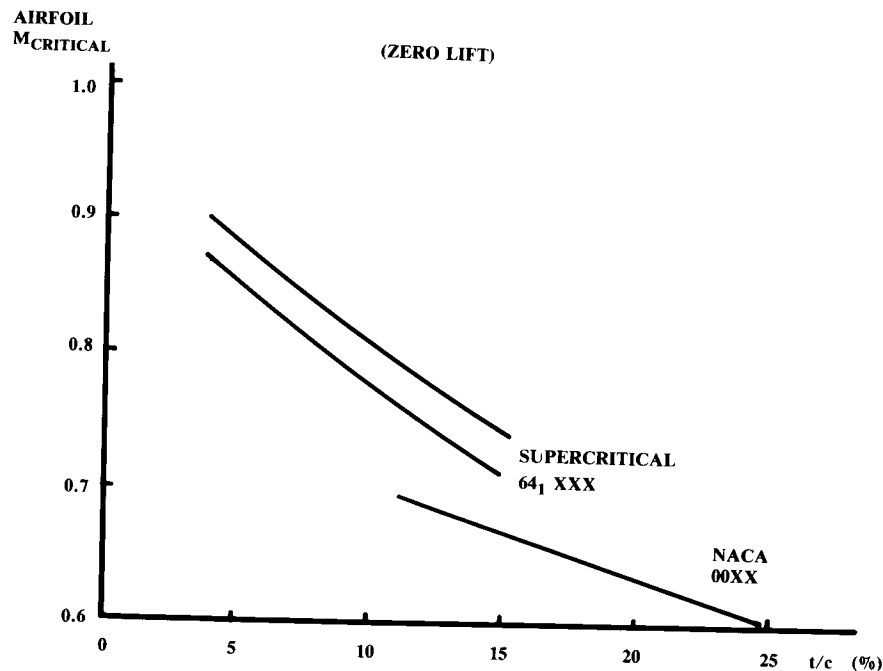
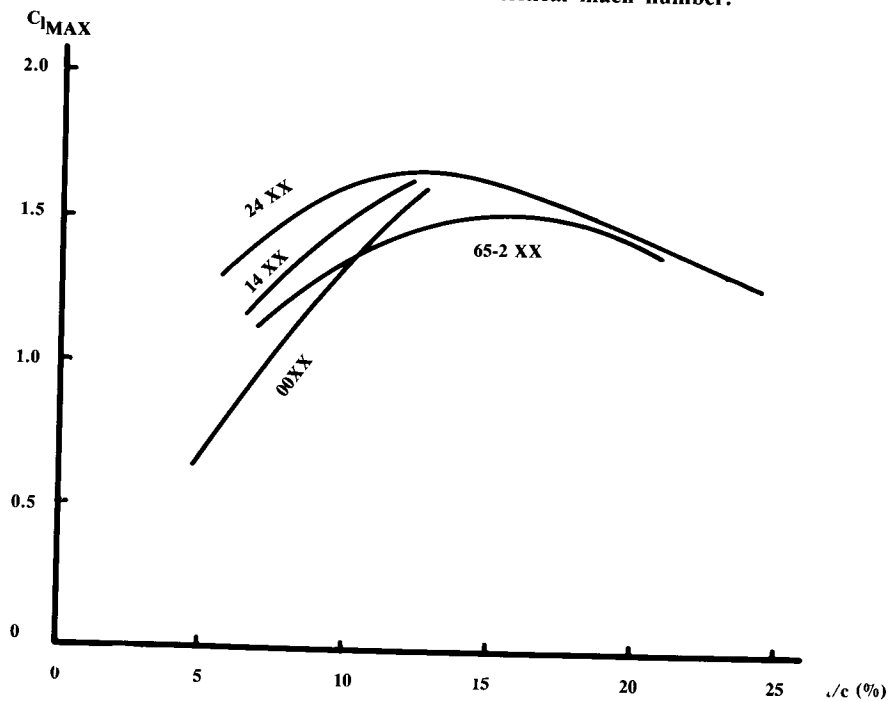
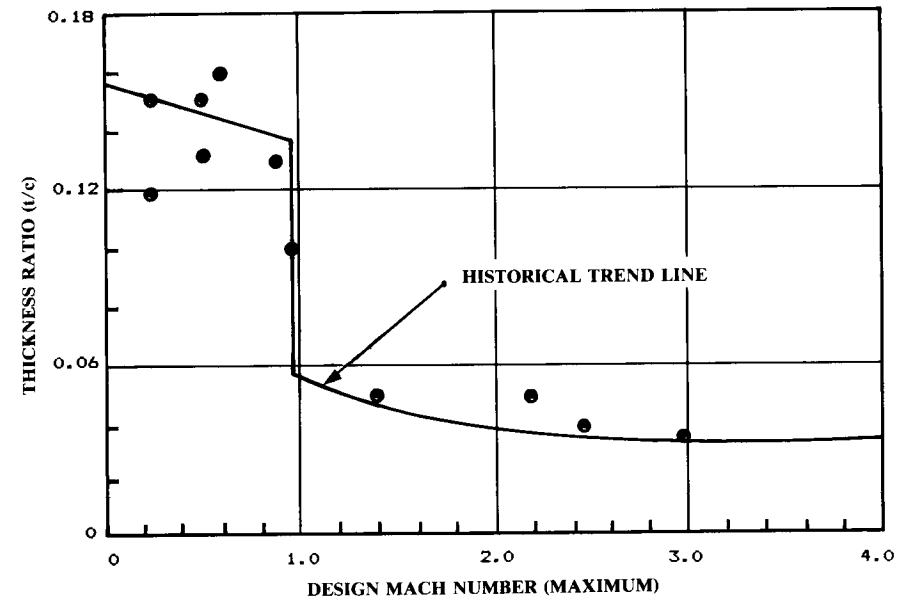
Fig. 4.12 Effect of  $t/c$  on critical mach number.Fig. 4.13 Effect of  $t/c$  on maximum lift.

Fig. 4.14 Thickness ratio historical trend.

The laminar airfoils require extremely smooth skins as well as exact control over the actual, as-manufactured shape. These can drive the cost up significantly. Also, the camouflage paints used on military aircraft are rough compared to bare metal or composite skins. This must be considered before selecting certain airfoils.

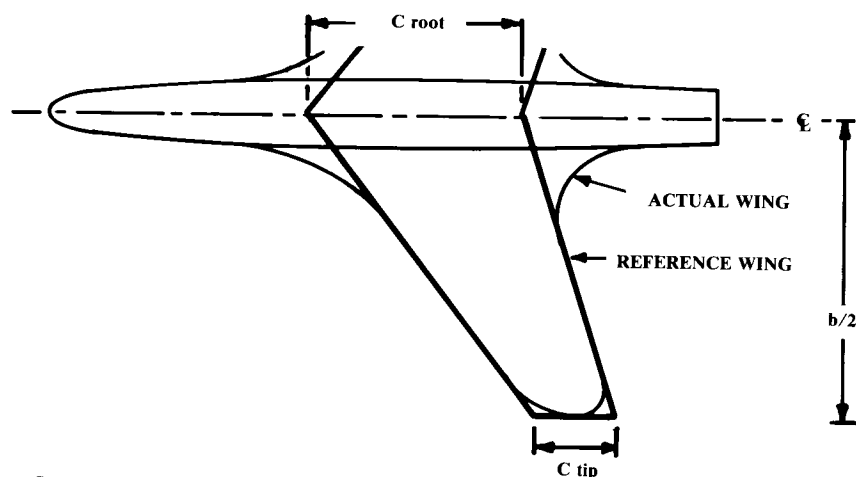
While an understanding of the factors important to airfoil selection is important, an aircraft designer should not spend too much time trying to pick exactly the "right" airfoil in early conceptual design. Later trade studies and analytical design tools will determine the desired airfoil characteristics and geometry. For early conceptual layout, the selected airfoil is important mostly for determining the thickness available for structure, landing gear, and fuel.

Appendix A.3 provides geometry and section characteristics for a few airfoils useful in conceptual design. For swept-wing supersonic aircraft, the NACA 64A and 65A sections are good airfoils for initial design. The appendix describes a supercritical section suitable for transports and other high-subsonic aircraft, along with a typical modern NASA section for general aviation. A few specialized airfoils are provided for other applications.

The airfoils presented in Appendix A.3 are not being recommended as the "best" sections for those applications, but rather as reasonable airfoils with which to start a conceptual design. Again, Ref. 2 is highly recommended.

### 4.3 WING GEOMETRY

The "reference" ("trapezoidal") wing is the basic wing geometry used to begin the layout. Figures 4.15 and 4.16 show the key geometric parameters of the reference wing.

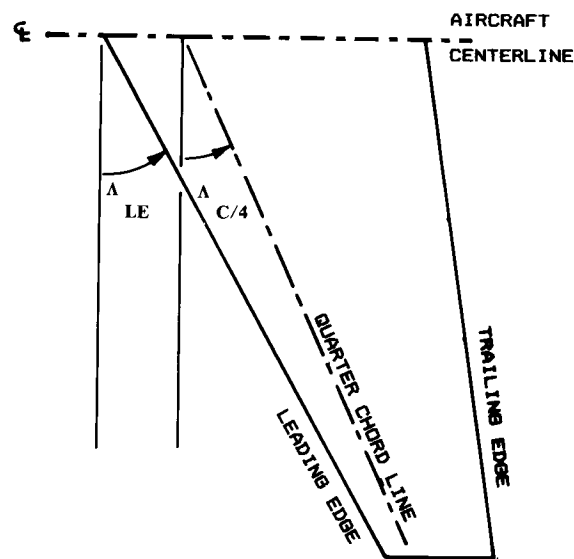


- $S$  = REFERENCE WING AREA  
 $C$  = CHORD (DISTANCE L.E. TO T.E.)  
 $A$  = ASPECT RATIO =  $b^2/S$   
 $t/c$  = AIRFOIL THICKNESS RATIO (MAXIMUM THICKNESS/CHORD)  
 $\lambda$  = TAPER RATIO =  $C_{tip}/C_{root}$   
 $b$  = SPAN

GIVEN:  $W/S$ ,  $A$ ,  $\lambda$

$$S = W/(W/S) \quad b = \sqrt{A \cdot S} \quad C_{root} = 2 \cdot S/[b(1 + \lambda)] \quad C_{tip} = \lambda \cdot C_{root}$$

Fig. 4.15 Wing geometry.



$$\tan \Lambda_{LE} = \tan \Lambda_{C/4} + [(1 - \lambda)/A(1 + \lambda)]$$

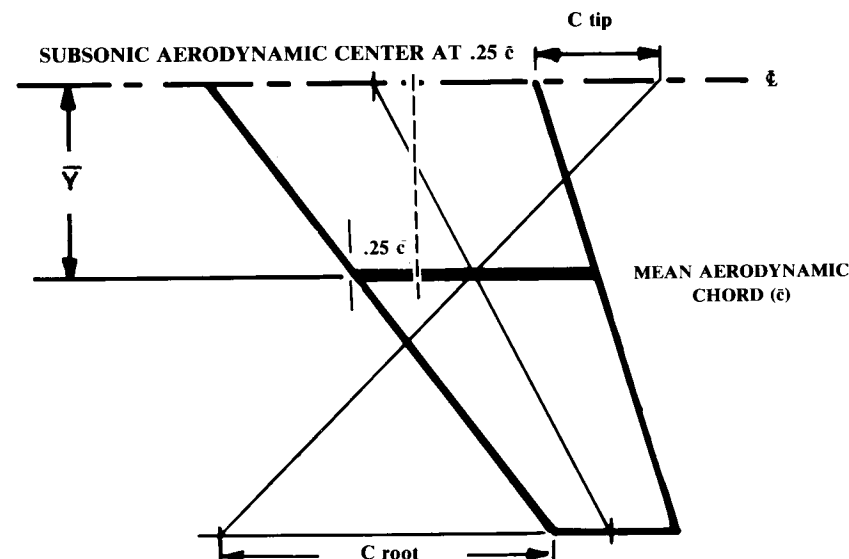
Fig. 4.16 Wing sweep  $\Lambda$ .

Note that the reference wing is fictitious, and extends through the fuselage to the aircraft centerline. Thus the reference wing area includes the part of the reference wing which sticks into the fuselage. For the reference wing, the root airfoil is the airfoil of the trapezoidal reference wing at the centerline of the aircraft, not where the actual wing connects to the fuselage.

There are two key sweep angles, as shown in Fig. 4.16. The leading-edge sweep is the angle of concern in supersonic flight. To reduce drag it is common to sweep the leading edge behind the Mach cone. The sweep of the quarter-chord line is the sweep most related to subsonic flight. It is important to avoid confusing these two sweep angles. The equation at the bottom of Fig. 4.16 allows converting from one sweep angle to the other.

Airfoil pitching moment data in subsonic flow is generally provided about the quarter-chord point, where the airfoil pitching moment is essentially constant with changing angle of attack (i.e., the "aerodynamic center"). In a similar fashion, such a point is defined for the complete trapezoidal wing and is based on the concept of the "mean aerodynamic chord." The mean aerodynamic chord (Fig. 4.17) is the chord " $\bar{c}$ " of an airfoil, located at some distance " $\bar{Y}$ " from the centerline.

The entire wing has its mean aerodynamic center at approximately the same percent location of the mean aerodynamic chord as that of the airfoil



$$\bar{c} = (2/3) C_{root} (1 + \lambda + \lambda^2)/(1 + \lambda)$$

$$\bar{Y} = (b/6)[(1 + 2\lambda)(1 + \lambda)]$$

TYPICAL, WING AERODYNAMIC CENTER =  $.25 \bar{c}$  SUBSONIC  
 =  $.4 \bar{c}$  SUPERSONIC

Fig. 4.17 Mean aerodynamic chord.

alone. In subsonic flow, this is at the quarter-chord point on the mean aerodynamic chord. In supersonic flow, the aerodynamic center moves back to about 40% of the mean aerodynamic chord. The designer uses the mean aerodynamic chord and the resulting aerodynamic center point to position the wing properly. Also, the mean aerodynamic chord will be important to stability calculations. Figure 4.17 illustrates a graphical method for finding the mean aerodynamic chord of a trapezoidal-wing planform.

The required reference wing area ("S") can be determined only after the takeoff gross weight is determined. The shape of the reference wing is determined by its aspect ratio, taper ratio, and sweep.

### Aspect Ratio

The first to investigate aspect ratio in detail were the Wright Brothers, using a wind tunnel they constructed. They found that a long, skinny wing (high aspect ratio) has less drag for a given lift than a short, fat wing (low aspect ratio). This is due to the 3-D effects.

As most early wings were rectangular in shape, the aspect ratio was initially defined as simply the span divided by the chord. For a tapered wing, the aspect ratio is defined as the span squared divided by the area (which defaults to the earlier definition for a wing with no taper).

When a wing is generating lift, it has a reduced pressure on the upper surface and an increased pressure on the lower surface. The air would like to "escape" from the bottom of the wing, moving to the top. This is not possible in 2-D flow unless the airfoil is leaky (a real problem with some fabric wing materials unless properly treated). However, for a real, 3-D wing, the air can escape around the wing tip.

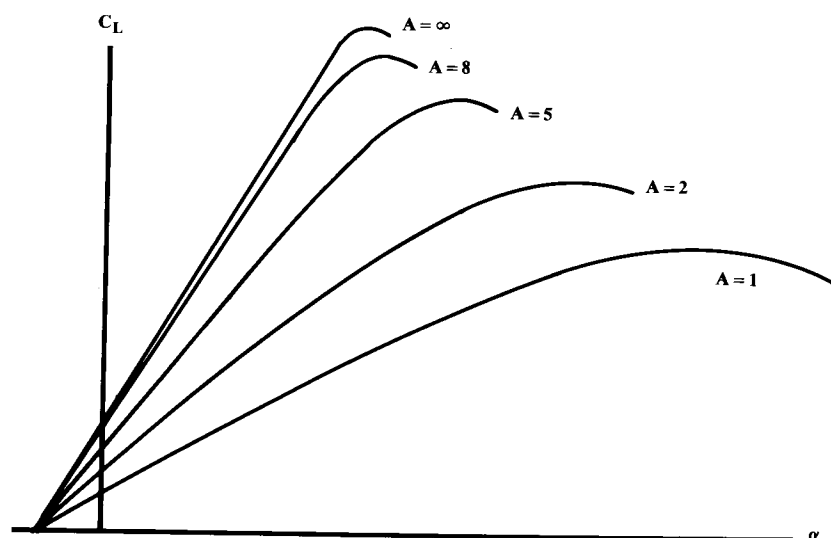


Fig. 4.18 Effect of aspect ratio on lift.

Air escaping around the wing tip lowers the pressure difference between the upper and the lower surfaces. This reduces lift near the tip. Also, the air flowing around the tip flows in a circular path when seen from the front, and in effect pushes down on the wing. Strongest near the tip, this reduces the effective angle of attack of the wing airfoils. This circular, or "vortex" flow pattern continues downstream behind the wing.

A wing with a high aspect ratio has tips farther apart than an equal area wing with a low aspect ratio. Therefore, the amount of the wing affected by the tip vortex is less for a high aspect ratio wing than for a low-aspect-ratio wing, and the strength of the tip vortex is reduced. Thus, the high-aspect-ratio wing does not experience as much of a loss of lift and increase of drag due to tip effects as a low-aspect-ratio wing of equal area.

(It is actually the wing span which determines the drag due to lift. However, wing area is usually held constant unless widely different aircraft concepts are being evaluated. When wing area is held constant, the wing span varies as the square root of the aspect ratio.)

As was shown in Fig. 3.6, the maximum subsonic  $L/D$  of an aircraft increases approximately by the square root of an increase in aspect ratio (when wing area and  $S_{wet}/S_{ref}$  are held constant). On the other hand, the wing weight also increases with increasing aspect ratio, by about the same factor.

Another effect of changing aspect ratio is a change in stalling angle. Due to the reduced effective angle of attack at the tips, a lower-aspect-ratio wing will stall at a higher angle of attack than a higher-aspect-ratio wing (Fig. 4.18). This is one reason why tails tend to be of lower aspect ratio. Delaying tail stall until well after the wing stalls assures adequate control.

Table 4.1 Aspect ratio

Sailplane equivalent* aspect ratio = 4.464 (best $L/D$ ). <sup>69</sup>		
Propeller aircraft	Equivalent aspect ratio	
Homebuilt	6.0	
General aviation—single engine	7.6	
General aviation—twin engine	7.8	
Agricultural aircraft	7.5	
Twin turboprop	9.2	
Flying boat	8.0	
Jet aircraft	Equivalent aspect Ratio = $aM_{max}^C$	
	$a$	$C$
Jet trainer	4.737	− 0.979
Jet fighter (dogfighter)	5.416	− 0.622
Jet fighter (other)	4.110	− 0.622
Military cargo/bomber	5.570	− 1.075
Jet transport	7.50	0

\*Equivalent aspect ratio = wing span squared/(wing and canard areas)

Conversely, a canard can be made to stall before the wing by making it a very high aspect ratio surface. This prevents the pilot from stalling the wing, and is seen in several canarded homebuilt designs.

Later in the design process, the aspect ratio will be determined by a trade study in which the aerodynamic advantages of a higher aspect ratio are balanced against the increased weight. For initial wing layout, the values and equations provided in Table 4.1 can be used. These were determined through statistical analysis of a number of aircraft, using data from Ref. 1.

Sailplane aspect ratio was found to be directly related to the desired glide ratio, which equals the  $L/D$ . Propeller aircraft showed no clear statistical trend, so average values are presented. Jet aircraft evidence a strong trend of aspect ratio decreasing with increasing Mach number evidence due to drag due to lift becoming relatively less important at higher speeds. Designers of high-speed aircraft thus use lower-aspect-ratio wings to save weight.

Note that, for statistical purposes, Table 4.1 uses an equivalent wing area that includes the canard area in defining the aspect ratio of an aircraft with a lifting canard. To determine the actual wing geometric aspect ratio, it is necessary to decide how to split the lifting area between the wing and canard. Typically, the canard will have about 10–25% of the total lifting area, so the wing aspect ratio becomes the statistically determined aspect ratio divided by 0.9–0.75.

### Wing Sweep

Wing sweep is used primarily to reduce the adverse effects of transonic and supersonic flow. Theoretically, shock formation on a swept wing is determined not by the actual velocity of the air passing over the wing, but rather by the air velocity in a direction perpendicular to the leading edge of the wing. This result, first applied by the Germans during World War II, allows an increase in Critical Mach Number by the use of sweep.

At supersonic speeds the loss of lift associated with supersonic flow can be reduced by sweeping the wing leading edge aft of the Mach cone angle [ $\arcsin(1/\text{Mach No.})$ ].

Figure 4.19 shows a historical trend line for wing leading-edge sweep vs Mach number. Note that sweep is defined aft of a line perpendicular to the flight direction, while the Mach angle is defined with respect to the flight direction. Thus, the line labeled “ $90 - \arcsin(1/\text{Mach No.})$ ” is the wing sweep required to place the wing leading edge exactly on the Mach cone.

The historical trend differs from this theoretical result for two reasons. In the high-speed range, it becomes structurally impractical to sweep the wing past the Mach cone. In this speed regime, over about Mach 2.5, it is necessary to use sharp or nearly sharp airfoils.

Selecting the wing sweep to equal the Mach-cone angle would indicate a zero sweep for speeds at or below Mach 1.0. However, in the transonic speed regime (roughly Mach 0.9–1.2) the desire for a high critical Mach number predominates. This requires subsonic airflow velocity over the airfoil (when measured perpendicular to the leading edge), and thus a swept wing.

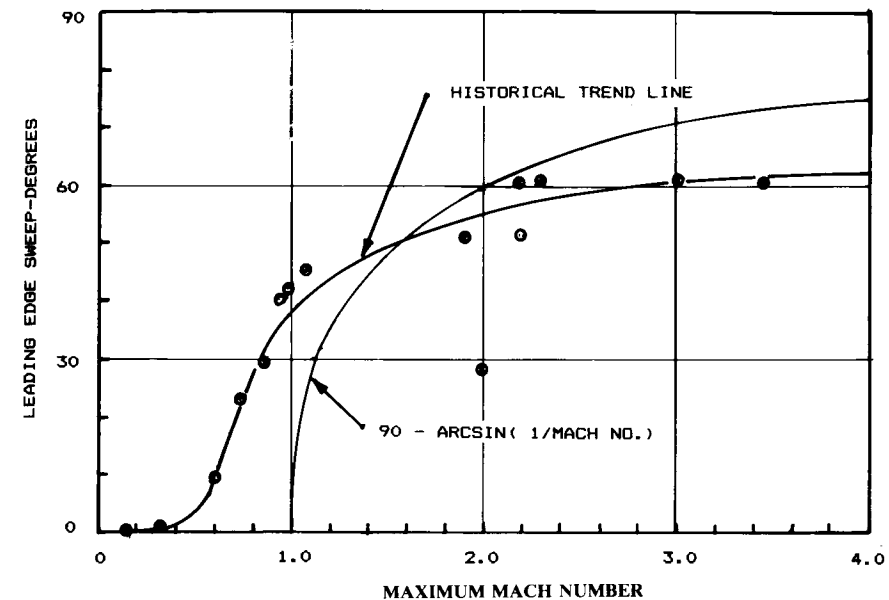


Fig. 4.19 Wing sweep historical trend.

The exact wing sweep required to provide the desired Critical Mach Number depends upon the selected airfoil(s), thickness ratio, taper ratio, and other factors. For initial wing layout the trend line of Fig. 4.19 is reasonable.

There is no theoretical difference between sweeping a wing aft and sweeping it forward. In the past, wings have been swept aft because of the structural divergence problem associated with forward sweep. With the use of composite materials, this can be avoided for a small weight penalty.

Also, there is no reason why one cannot sweep one wing aft and the other wing forward, creating an “oblique wing.” This arrangement produces unusual control responses, but a computerized flight control system can easily provide normal handling qualities. The oblique wing also tends to have lower wave drag.

There are other reasons for sweeping a wing. For example, the fuselage layout may not otherwise allow locating the wing carry-through structure at the correct place for balancing the aircraft. Canarded aircraft with pusher engines are frequently tail-heavy, requiring wing sweep to move the aerodynamic center back far enough for balance. This is why most canard pushers have swept wings.

Wing sweep improves stability. A swept wing has a natural dihedral effect. In fact, it is frequently necessary to use zero or negative dihedral on a swept wing to avoid excessive stability.

If an aircraft has its vertical tails at the wingtips, sweeping the wing will push the tails aft, increasing their effectiveness. This is also seen on many canard pusher aircraft.

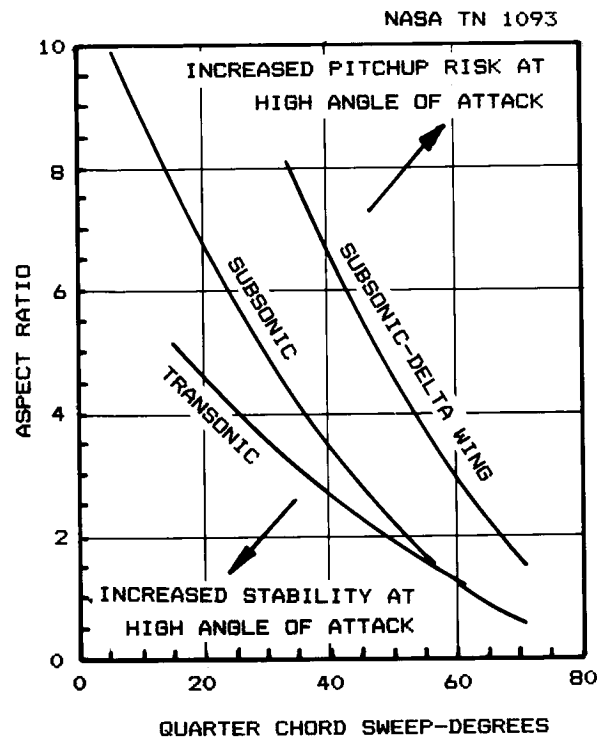


Fig. 4.20 Tail-off pitchup boundaries.

Note on Fig. 4.19 the data point at Mach 2.0 and leading-edge sweep just under 30 deg. This is the Lockheed F-104, which used a different approach for reducing drag at supersonic speeds. The F-104 had a razor-sharp leading edge, so sharp that it was covered on the ground for the safety of line personnel. The F-104 also had a very thin wing, only 3.4% thick.

The wing sweep and aspect ratio together have a strong effect on the wing-alone pitchup characteristics. "Pitchup" is the highly undesirable tendency of some aircraft, upon reaching an angle of attack near stall, to suddenly and uncontrollably increase the angle of attack. The aircraft continues pitching up until it stalls and departs totally out of control. The F-16 fighter requires a computerized angle-of-attack limiter to prevent a severe pitchup problem at about 25-deg angle of attack.

Figure 4.20 describes boundaries for pitchup avoidance for combinations of wing quarter-chord sweep angle and aspect ratio. Pitchup avoidance should be considered for military fighters, aerobatic aircraft, general-aviation aircraft, and trainers.

These boundaries may limit the allowable aspect ratio to a value less than that estimated earlier. However, Fig. 4.20 provides data for the wing alone. If a properly designed horizontal tail is used, the aspect ratio may be higher than that allowed by the graph. This is discussed later. Also, a large, all-

moving canard such as that seen on the Grumman X-29 can be used to control a pitchup tendency. However, this requires a computerized flight control system.

For high-speed flight, a swept wing is desirable. For cruise as well as takeoff and landing, an unswept wing is desirable. A wing of variable sweep would offer the best of both worlds. Variable sweep was first flight-tested in the 1950's, and is now on several operational military aircraft including the F-111, F-14, B-1B, and the European Tornado and Soviet Backfire.

For design purposes, the planform for a variable-sweep aircraft should be developed in the unswept position, and then swept to the desired leading-edge angle for high-speed flight. The pivot position about which the wing is swept must be near the thickest part of the chord, between about the 30- and 40%-chord locations. Also, provisions must be made for smoothly fairing the wing root in both extended and fully-swept positions.

Controlling the balance of a variable sweep aircraft is a major design problem. When the wing swings aft, the aerodynamic center moves with it. The center of gravity also moves due to the wing movement, but not nearly as much as the aerodynamic center. To balance the aircraft, either fuel must be pumped to move the center of gravity, or the tail must provide a tremendous down-load (or both).

Yet another problem with the variable-sweep wing is the weight penalty associated with the pivot mechanism and less-than-optimal load paths. As shown in Table 3.1, variable sweep increases total empty weight roughly 4%. The detailed statistical weight equations of Chapter 15 show a 19% increase in the weight of the wing itself if it has variable sweep.

### Taper Ratio

Wing taper ratio,  $\lambda$ , is the ratio between the tip chord and the centerline root chord. Most wings of low sweep have a taper ratio of about 0.4–0.5. Most swept wings have a taper ratio of about 0.2–0.3.

Taper affects the distribution of lift along the span of the wing. As proven by the Prandtl wing theory early in this century, minimum drag due to lift, or "induced" drag, occurs when the lift is distributed in an elliptical fashion. For an untwisted and unswept wing, this occurs when the wing plan-

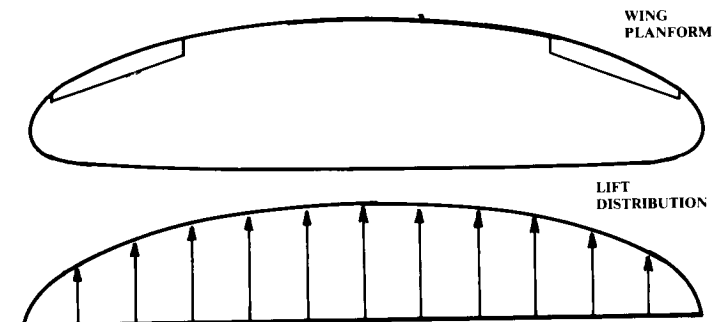


Fig. 4.21 Elliptical wing.



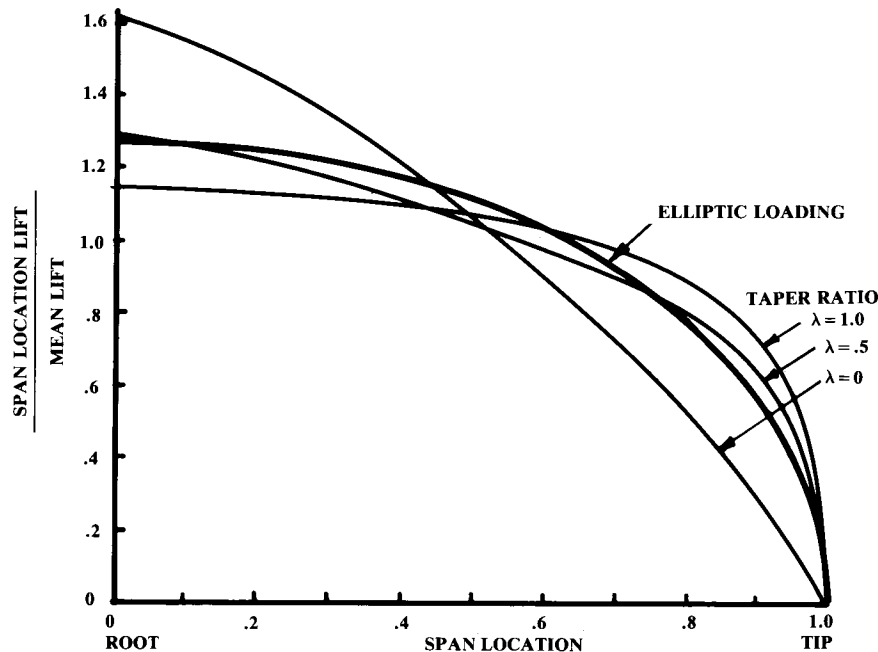


Fig. 4.22 Effect of taper on lift distribution.

form is shaped as an ellipse, as shown in Fig. 4.21. This result was the basis of the graceful wing of the Supermarine Spitfire, a leading British fighter of World War II.

An elliptical wing planform is difficult and expensive to build. The easiest wing to build is the untapered ( $\lambda = 1.0$ ) rectangular wing. However, the untapered wing has constant chord length along the span, and so has excessive chord towards the tip when compared to the ideal elliptical wing. This “loads up” the tip, causing the wing to generate more of its lift toward the tip than is ideal. The end result is that an untwisted rectangular wing has about 7% more drag due to lift than an elliptical wing of the same aspect ratio.

When a rectangular wing is tapered, the tip chords become shorter, alleviating the undesired effects of the constant-chord rectangular wing. In fact, a taper ratio of 0.45 almost completely eliminates those effects for an unswept wing, and produces a lift distribution very close to the elliptical ideal (Fig. 4.22). This results in a drag due to lift less than 1% higher than the ideal, elliptical wing.

A wing swept aft tends to divert the air outboard, towards the tips. This loads up the tips, creating more lift outboard than for an equivalent unswept wing. To return the lift distribution to the desired elliptical lift distribution, it is necessary to increase the amount of taper (i.e., reduce the taper ratio,  $\lambda$ ).

Figure 4.23 illustrates the results of NACA wind tunnel tests to determine the taper ratio required to approximate the elliptical lift distribution for a swept untwisted wing. This figure can be used for a first approximation of the desired taper ratio for a swept wing. However, it should be noted that taper ratios much lower than 0.2 should be avoided for all but delta wings, as a very low taper ratio tends to promote tip stall.

Figure 4.23 also indicates that an untwisted wing with no taper should have a forward sweep of 22 deg to approximate an elliptical lift distribution. This unusual planform was the basis of the design presented in the first section as Fig. 2.5. The intent was to provide an elliptical lift distribution with an easy-to-construct rectangular wing.

However, cost analysis indicated that the total reduction in manufacturing cost was small. Furthermore, the weight increase caused by the lack of wing thickness at the root when compared to a conventional, tapered wing caused this design to cost more than a regular design. (Well, at least it was an interesting trade study!)

### Twist

Wing twist is used to prevent tip stall and to revise the lift distribution to approximate an ellipse. Typically, wings are twisted between zero and five degrees.

“Geometric twist” is the actual change in airfoil angle of incidence, usually measured with respect to the root airfoil. A wing whose tip airfoil

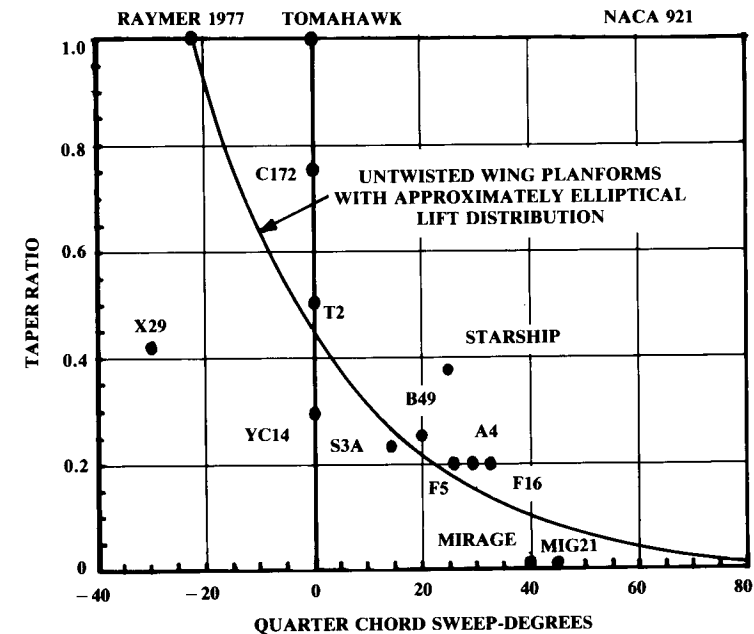


Fig. 4.23 Effect of sweep on desired taper ratio.

is at a negative (nose-down) angle compared to the root airfoil is said to have "wash-out." If a wing has "linear twist," the twist angle changes in proportion to the distance from the root airfoil.

"Aerodynamic twist" is the angle between the zero-lift angle of an airfoil and the zero-lift angle of the root airfoil. If the identical airfoil is used from root to tip, the aerodynamic twist is the same as the geometric twist.

On the other hand, a wing with no geometric twist can have aerodynamic twist if, for example, the root airfoil is symmetric (zero-lift angle is zero) but the tip airfoil is highly cambered (zero-lift angle is nonzero). The total wing aerodynamic twist equals the wing geometric twist plus the root airfoil zero-lift angle, minus the tip airfoil zero-lift angle.

When wing twist is used to reshape the lift distribution, the change in lift at some chord station along the span is proportional to the ratio between the new airfoil angle of attack and the original one. Thus, the effect on lift distribution depends upon the original angle of attack of the wing, which in turn depends upon the lift coefficient at which the wing is flying.

In other words, any attempt to optimize the lift distribution by twisting the wing will be valid only at one lift coefficient. At other lift coefficients, the twisted wing will not get the whole benefit of the twist optimization. The more twist required to produce a good lift distribution at the design lift coefficient, the worse the wing will perform at other lift coefficients. It is for this reason that large amounts of twist (much over 5 deg) should be avoided.

It is very difficult to optimize twist for an arbitrary wing planform. A computerized solution is employed at large companies. For initial design purposes, historical data should be used. Typically, 3 deg of twist provides adequate stall characteristics.

### Wing Incidence

The wing incidence angle is the pitch angle of the wing with respect to the fuselage. If the wing is untwisted, the incidence is simply the angle between the fuselage axis and the wing's airfoil chordlines. If the wing is twisted, the incidence is defined with respect to some arbitrarily chosen spanwise location of the wing, usually the root of the exposed wing where it intersects the fuselage. Frequently the incidence is given at the root and tip, which then defines the twist as the difference between the two.

Wing incidence angle is chosen to minimize drag at some operating condition, usually cruise. The incidence angle is chosen such that when the wing is at the correct angle of attack for the selected design condition, the fuselage is at the angle of attack for minimum drag.

For a typical, circular straight fuselage, this is approximately zero degrees angle of attack. For passenger aircraft, the incidence angle must be carefully chosen to insure that the flight attendants do not have to push the food carts uphill!

Wing incidence angle is ultimately set using wind tunnel data. For most initial design work, it can be assumed that general aviation and homebuilt aircraft will have an incidence of about 2 deg, transport aircraft about 1 deg, and military aircraft approximately zero. Later in the design process, aero-

dynamic calculations can be used to check the actual wing incidence angle required during the design condition.

These values are for untwisted wings. If the wing is twisted, the average incidence should equal these values.

A few aircraft have been built with a variable wing incidence angle. The wing aft-attachment is pivoted, and the forward attachment connects to a powerful actuator which pushes the front of the wing up for landing. This arrangement, seen on the Vought F8U Crusader aircraft, allows a short landing gear because the aircraft does not need to rotate to a high fuselage angle for additional lift during takeoff and landing. However, this arrangement is heavy and complicated, and has not been incorporated in a new design in several decades.

### Dihedral

Wing dihedral is the angle of the wing with respect to the horizontal when seen from the front. Dihedral tends to roll the aircraft level whenever it is banked. This is frequently, and incorrectly, explained as the result of a greater projected area for the wing that is lowered.

Actually, the rolling moment is caused by a sideslip introduced by the bank angle. The aircraft "slides" toward the lowered wing, which increases its angle of attack. The resulting rolling moment is approximately proportional to the dihedral angle.

Wing sweep also produces a rolling moment due to sideslip, caused by the change in relative sweep of the left and right wings. For an aft-swept wing, the rolling moment produced is negative and proportional to the sine of twice the sweep angle. This creates an effective dihedral that adds to any actual geometric dihedral.

Roughly speaking, 10 deg of sweep provides about 1 deg of effective dihedral. For a forward swept wing, the sweep angle produces a negative dihedral effect, requiring an increased geometric dihedral in order to retain natural directional stability.

In addition, the position of the wing on the fuselage has an influence on the effective dihedral, with the greatest effect provided by a high wing. This is frequently, and incorrectly, explained as a pendulum effect.

Actually, the fuselage in sideslip pushes the air over and under itself. If the wing is high-mounted, the air being pushed over the top of the fuselage pushes up on the forward wing, providing an increased dihedral effect. The reverse is true for a low-mounted wing.

Due to the additive effects of sweep and wing position, many high-winged transports such as the Lockheed C-5 actually require a negative geometric dihedral angle to avoid an excess of effective dihedral. Excessive dihedral effect produces "Dutch roll," a repeated side-to-side motion involving yaw and roll. To counter a Dutch roll tendency, the vertical tail area must be increased, which increases weight and drag.

Unfortunately, as yet no simple technique for selecting dihedral angle takes all of these effects into account. Like so many parameters in initial design, the dihedral angle must be estimated from historical data and then revised following analysis of the design layout.

Table 4.2, developed by the author from data taken from Ref. 1, provides initial estimates of dihedral. For a wing in which the center section is flat and the outer sections alone have dihedral, a first approximation of the required dihedral for the outer panels is the one that places the wing tips as high as they would be for a wing with dihedral starting at the root.

### Wing Vertical Location

The wing vertical location with respect to the fuselage is generally set by the real-world environment in which the aircraft will operate. For example, virtually all high-speed commercial transport aircraft are of low-wing design, yet military transport aircraft designed to similar mission profiles and payload weights are all of high-wing design. The reasons for this are discussed later.

The major benefit of a high wing is that it allows placing the fuselage closer to the ground (Fig. 4.24). For military transport aircraft such as the C-5 and C-141, this allows loading and unloading the cargo without special ground handling gear. In fact, these aircraft place the floor of the cargo compartment about 4–5 ft off the ground, which is the height of the cargo area of most trucks. If cargo is needed at a remote field lacking ground-handling gear, the trucks can be backed right up to the aircraft for loading.

With a high wing, jet engines or propellers will have sufficient ground clearance without excessive landing-gear length. Also, the wing tips of a swept high wing are not as likely to strike the ground when in a nose-high, rolled attitude. For these reasons, landing-gear weight is generally reduced for a high-wing aircraft.

Table 4.2 Dihedral guidelines

	Wing position		
	Low	Mid	High
Unswept (civil)	5 to 7	2 to 4	0 to 2
Subsonic swept wing	3 to 7	–2 to 2	–5 to –2
Supersonic swept wing	0 to 5	–5 to 0	–5 to 0

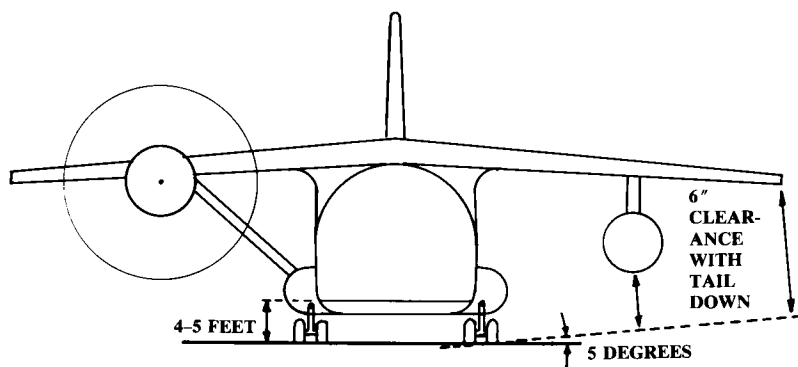


Fig. 4.24 High wing.

For low-speed aircraft, external struts can be used to greatly lower wing weight. However, external struts add substantially to the drag. Since roughly two-thirds of the lift is contributed by the upper surface of the wing, it follows that less drag impact will be seen if the strut disturbs the airflow on the lower surface of the wing than if the strut is above the wing, as would be necessary for a strut-brace, low wing.

Another structural benefit occurs if the wing box is carried over the top of the fuselage rather than passing through it. When the wing box passes through the fuselage, the fuselage must be stiffened around the cut-out area. This adds weight to the fuselage. However, passing the wing box over the fuselage will increase drag due to the increase in frontal area.

For an aircraft designed with short takeoff and landing (STOL) requirements, a high wing offers several advantages. The high position allows room for the very large wing flaps needed for a high lift coefficient. The height of the wing above the ground tends to prevent "floating," where the ground effect increases lift as the aircraft approaches the ground. A floating tendency makes it difficult to touch down on the desired spot. Finally, most STOL designs are also intended to operate from unimproved fields. A high wing places the engines and propellers away from flying rocks and debris.

There are several disadvantages to the high-wing arrangement. While landing-gear weight tends to be lower than other arrangements, the fuselage weight is usually increased because it must be strengthened to support the landing-gear loads. In many cases an external blister is used to house the gear in the retracted position. This adds weight and drag. The fuselage is also usually flattened at the bottom to provide the desired cargo-floor height above ground. This flattened bottom is heavier than the optimal circular fuselage. If the top of the fuselage is circular, as shown in Fig. 4.24, a fairing is required at the wing-fuselage junction.

For small aircraft, the high wing arrangement can block the pilot's visibility in a turn, obscuring the direction toward which the aircraft is turning. Also, the high wing can block upward visibility in a climb. (A classic mid-air collision features a high-wing aircraft climbing into a low-wing one descend-

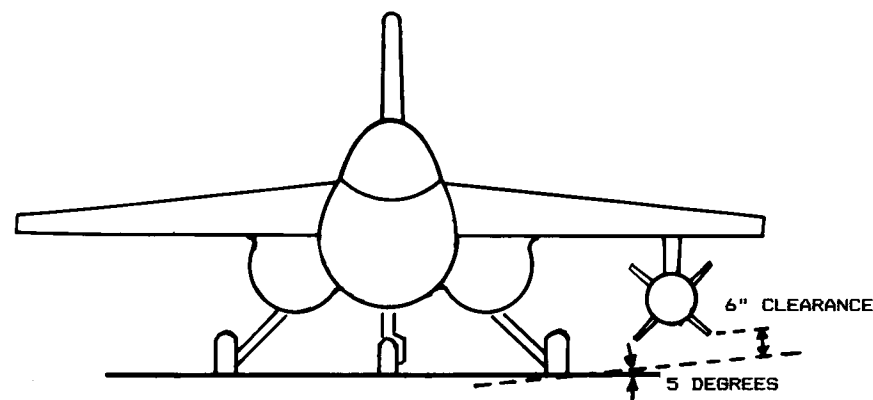


Fig. 4.25 Mid wing.

ing!) Many high-winged light aircraft have transparent panels in the roof to help the pilot see.

If the fuselage is roughly circular and fairings are not used, the mid-wing arrangement (Fig. 4.25) provides the lowest drag. High- and low-wing arrangements must use fairings to attain acceptable interference drag with a circular fuselage.

The mid wing offers some of the ground clearance benefits of the high wing. Many fighter aircraft are mid-winged to allow bombs and missiles to be carried under the wing. A high-wing arrangement would restrict the pilot's visibility to the rear—the key to survival of a fighter in combat.

The mid-wing arrangement is probably superior for aerobatic maneuverability. The dihedral usually required for adequate handling qualities in a low-wing design in normal flight will act in the wrong direction during inverted flight, making smooth aerobatic maneuvers difficult. Also, the effective-dihedral contribution of either high or low wings will make it more difficult to perform high-sideslip maneuvers such as the knife-edge pass.

Structural carrythrough presents the major problem with the mid wing. As will be discussed in Chapter 8, the bending moment produced by the lift on the wing must be carried across the fuselage either by an extension of the wing box ("wing carrythrough box") or by a set of massive ring frames built into the fuselage.

The carrythrough box often proves lighter, but cannot be used in a mid-wing design that must carry cargo or passengers. (One exception to this, the German Hansa executive jet, uses a mild forward sweep to place the carrythrough box behind the passenger compartment.) A carrythrough box is also difficult to incorporate in a mid-wing fighter, in which most of the fuselage will be occupied by the jet engines and inlet ducts.

The major advantage of the low-wing approach (Fig. 4.26) comes in landing-gear stowage. With a low wing, the trunnion about which the gear is retracted can be attached directly to the wing box which, being strong already, will not need much extra strengthening to absorb the gear loads. When retracted, the gear can be stowed in the wing itself, in the wing-fuselage fairing, or in the nacelle. This eliminates the external blister usually used with the high-wing approach.

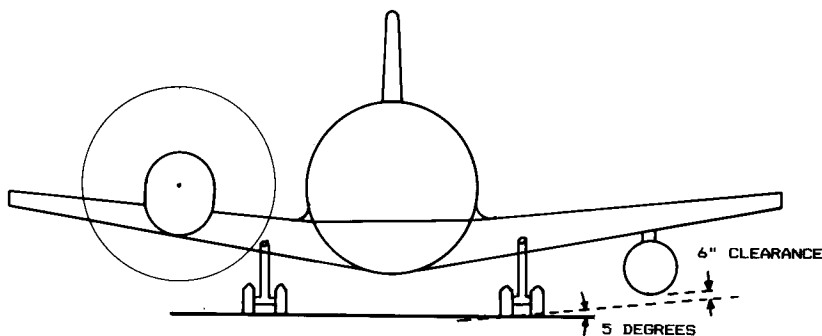


Fig. 4.26 Low wing.

To provide adequate engine and propeller clearance, the fuselage must be placed farther off the ground than for a high-wing aircraft. While this adds to the landing-gear weight, it also provides greater fuselage ground clearance. This reduces the aft-fuselage upsweep needed to attain the required takeoff angle of attack. The lesser aft-fuselage upsweep reduces drag.

While it is true that the low-wing arrangement requires special ground equipment for loading and unloading large airplanes, the high-speed commercial transports are only operated out of established airfields with a full complement of equipment. This is the main reason why military and commercial transports are so different.

Large transports have a fuselage diameter on the order of 20 ft, which allows an uninterrupted passenger compartment above the wing carrythrough box. The wing carrythrough box usually passes through the fuselage for reduced drag, and splits the lower cargo compartment into two compartments. This efficient internal fuselage layout is virtually standard for commercial transports.

If the center wing-panel of a low-wing aircraft lacks dihedral, a one-piece flap which passes under the fuselage can be used. This reduces complexity as well as reducing the risk of asymmetric lift caused by the failure of one flap to extend. Also, the continuous flap will produce more lift and drag than an equal-area flap that is broken at the fuselage.

Several disadvantages of the low-wing approach have already been mentioned, including ground-clearance difficulties. Frequently low-wing aircraft will have dihedral angle set not by aerodynamics, but by the angle required to avoid striking the wing tip on the ground during a bad landing. As was mentioned before, it may require an increase in vertical-tail size to avoid dutch roll with an excessive dihedral angle.

Clearance also affects propellers. To minimize the landing-gear length, many low-wing aircraft have the propellers mounted substantially above the plane of the wing. This will usually increase the interference effects between the wing and propeller, and result in an increase in fuel consumption during cruise.

### Wing Tips

Wing-tip shape has two effects upon subsonic aerodynamic performance. The tip shape affects the aircraft wetted area, but only to a small extent. A far more important effect is the influence the tip shape has upon the lateral spacing of the tip vortices. This is largely determined by the ease with which the higher-pressure air on the bottom of the wing can "escape" around the tip to the top of the wing.

A smoothly-rounded tip (when seen nose-on) easily permits the air to flow around the tip. A tip with a sharp edge (when seen nose-on) makes it more difficult, thus reducing the induced drag. Most of the new low-drag wing tips use some form of sharp edge. In fact, even a simple cut-off tip offers less drag than a rounded-off tip, due to the sharp edges where the upper and lower surfaces end. (Fig. 4.27).

The most widely used low-drag wing tip is the Hoerner wingtip (developed by S. Hoerner, Ref. 8). This is a sharp-edged wing tip with the upper surface continuing the upper surface of the wing. The lower surface is

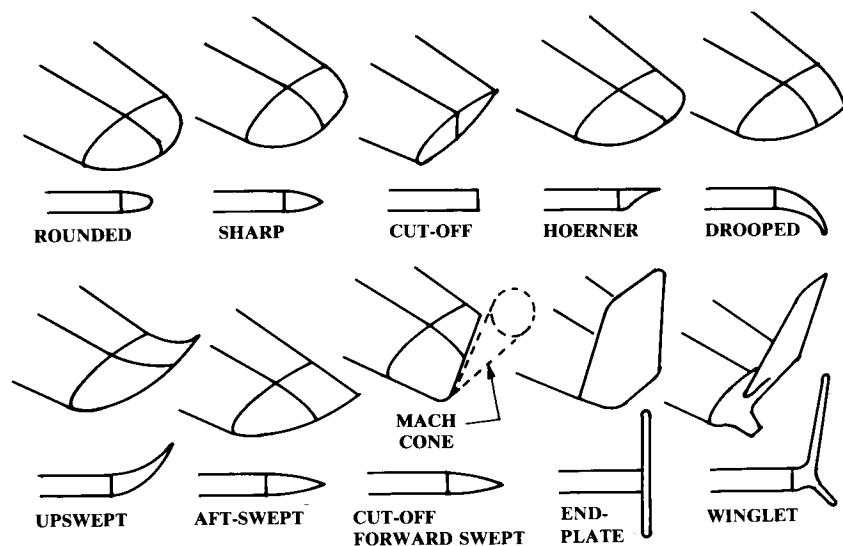


Fig. 4.27 Wing tips.

“undercut” and canted approximately 30 deg to the horizontal. The lower surface may also be “undercambered” (i.e., concave).

The “drooped” and “upswept” wing tips are similar to the Hoerner wing tip except that the tip is curved upwards or downwards to increase the effective span without increasing the actual span. This effect is similar to that employed by endplates, as discussed below.

The sweep of the wing tip also affects the drag. The tip vortex tends to be located approximately at the trailing-edge of the wing tip, so an aft-swept wing tip, with a greater trailing edge span, tends to have lower drag. However, the aft-swept wing tip tends to increase the wing torsional loads.

A cut-off, forward-swept wing tip is sometimes used for supersonic aircraft. The tip is cut off at an angle equal to the supersonic Mach-cone angle, because the area of the wing within the shock cone formed at the wing tip will contribute little to the lift. Also, this tip shape will reduce the torsional loads applied to the wing. The F-15 fighter uses such a cut-off tip for both wings and horizontal tails.

Induced drag is caused by the higher-pressure air at the bottom of the wing escaping around the wing tip to the top of the wing. An obvious way to prevent this would be to mount a vertical plate at the wing tip.

The endplate effect has been known almost since the dawn of flight, but has been seen rarely. The wetted area of the endplate itself creates drag. Also, an endplated wing has an effective span increase of only about 80% of the actual span increase caused by adding the endplates' height to the wing span. However, endplates can be useful when span must be limited.

An advanced version of the endplate can offer lower drag than an equal-area increase in wing span. The “winglet,” designed by NASA's R. Whit-

comb, gets an additional drag reduction by using the energy available in the tip vortex.

The winglet is cambered and twisted so that the rotating vortex flow at the wing tip creates a lift force on the winglet that has a forward component. This forward lift component acts as a “negative” drag, reducing the total wing drag.

A properly designed winglet can potentially provide an effective span increase up to double that bought by adding the winglets' height to the wing span. Winglets provide the greatest benefit when the wing tip vortex is strong, so a low-aspect-ratio wing will see more advantage from the use of winglets than an already-efficient high-aspect-ratio wing.

One problem with winglets is that they add weight behind the elastic axis of the wing, which can aggravate flutter tendencies. Also, the twist and camber of a winglet must be optimized for one velocity. At other than design speed, the winglet will provide less benefit.

For these and other reasons, winglets tend to be used more as add-on devices for existing wings requiring a little more efficiency without major redesign. When an all-new wing is being designed it is usually better to rely upon increased aspect ratio to improve aerodynamic efficiency. This is not always true so a trade study should be conducted sometime during the conceptual design effort.

#### 4.4 BIPLANE WINGS

Biplanes dominated aviation for the first thirty years. The Wright Brothers were influenced by Octave Chanute, a noted architect and civil engineer who applied a structural concept used in bridge building to create light-weight biplane gliders. The early airfoils were thin and birdlike, requiring external bracing, and the biplane arrangement provided more structural efficiency than an externally-braced monoplane.

With the thicker airfoils now in use, the biplane arrangement is mainly reserved for recreational purposes. However, it should be considered whenever low structural weight is more important to the design than aerodynamic efficiency, or when low speed is required without complicated high-lift devices or excessive wing span.

A biplane should theoretically produce exactly half the induced drag of a monoplane with equal span. Induced drag, or drag-due-to-lift, is a function of the square of the lift being generated. If that lift is split evenly between two wings, each wing should have only one-fourth of the drag of the original wing. Therefore, the total induced drag of a biplane should be two-fourths, or one-half of the value obtained with a monoplane of equal span.

Unfortunately, mutual-interference effects prevent the full benefit from being attained. Good design can yield on the order of a 30% reduction in drag-due-to-lift for a biplane when compared to a monoplane of equal span. However, if the total wing area is held constant to provide the same wing loading for biplane and monoplane, and the monoplane has the same wing span as the biplane, then the aspect ratio of the two wings of the biplane must each be double the aspect ratio of the monoplane.

For a typical monoplane aspect ratio of seven, a biplane would need each wing to have an aspect ratio of fourteen to maintain the same total wing area (and wetted area) while attaining the approximately 30% reduction in induced drag claimed above. Also, if the total wing area and span of a biplane and monoplane are identical, the biplane will have chord lengths half as long as the monoplane. Due to the Reynolds number effect upon airfoil drag, an additional penalty will befall the biplane.

If a monoplane were designed with the same total wing area as the biplane but with an aspect ratio the same as each of the wings of the biplane, it would have a span 41% greater (square root of two, minus one) than the biplane. This would provide a net reduction in drag due to lift of about 31% when compared to the biplane of equal wing area ( $1 - 0.5/0.7$ ). Thus, a biplane will actually provide a reduction in induced drag only if the aircraft's total span is limited for some reason to a value less than that desired for a monoplane.

Span can be limited for a number of reasons. For an aerobatic aircraft, a reduced span will increase the roll rate. For an aircraft flying at very low speeds, the wing area required to support the aircraft may require a wing span larger than practical from a structural viewpoint. Span can also be limited by the available hangar width. All of these reasons contributed to the prevalence of the biplane during World War I.

Biplane aerodynamic analysis using Prandtl's interference factor is described in Chapter 12. For initial design purposes, several key concepts should be considered. These are the "gap," "span ratio," "stagger," and "decalage."

Gap is the vertical distance between the two wings. If the gap were infinite, the theoretical result of a halving of the biplane induced drag when compared to an equal-span monoplane would be attained. However, structural weight and the drag of connecting struts generally limit the gap to a value approximately equal to the average chord length. A shorter gap will produce increasing interference between the two wings, raising the overall drag.

Span ratio is the ratio between the shorter wing and the longer wing. If both wings are the same length, the span ratio is one. When span is limited, the minimum induced drag is obtained from equal-length wings. As described, the only technical reason for using the biplane arrangement is the case where span is limited, so the biplane with wings of unequal length should be rarely seen. However, a shorter lower wing has been used in the past to provide better ground clearance.

Stagger is the longitudinal offset of the two wings relative to each other. Positive stagger places the upper wing closer to the nose than the lower wing. Stagger has little or no effect upon drag, and is usually used to improve the visibility upward from a rear-located cockpit. Negative stagger was used in the beautiful Beech D-17 Staggerwing to improve visibility from an enclosed cabin cockpit and to reduce the pitching moment of the large flaps on the lower wing.

Decalage is the relative angle of incidence between the two wings of a biplane. Decalage is positive when the upper wing is set at a larger angle than the lower. In early years much attention was paid to the selection of decalage

to minimize induced drag while encouraging the forward wing to stall before the aft one, thus providing natural stall recovery. Most biplanes since World War I have been designed with zero decalage, although the Pitts Special, holder of numerous world aerobatic championships, has a positive decalage of 1.5 deg.

Much of the discussions above concerning the initial selection of wing geometry can be applied to biplane wings. Most biplanes have wing aspect ratios comparable to monoplanes of similar class (six to eight). As discussed, this yields induced drag levels much higher than obtained from a monoplane with similar wing loading. Taper ratios for biplanes can be selected as for a monoplane, although many biplanes have untapered wings for ease of manufacture.

One or both biplane wings can be swept to enhance stability, improve pilot visibility, or provide room for retractable landing gear. Biplanes typically have dihedral of about 2 deg. Aerobatic biplanes may apply dihedral only to the lower wing.

The mean aerodynamic chord of a biplane can be found as the weighted average of the mean chords of the two wings, weighted by the relative areas of the wings. The biplane aerodynamic center is at approximately 23% of the mean aerodynamic chord, rather than 25% as for a monoplane, due to the wing interference effects.

## 4.5 TAIL GEOMETRY AND ARRANGEMENT

### Tail Functions

Tails are little wings. Much of the previous discussion concerning wings can also be applied to tail surfaces. The major difference between a wing and a tail is that, while the wing is designed routinely to carry a substantial amount of lift, a tail is designed to operate normally at only a fraction of its lift potential. Any time in flight that a tail comes close to its maximum lift potential, and hence its stall angle, something is very wrong!

Tails provide for trim, stability, and control. Trim refers to the generation of a lift force that, by acting through some tail moment arm about the center of gravity, balances some other moment produced by the aircraft.

For the horizontal tail, trim primarily refers to the balancing of the moment created by the wing. An aft horizontal tail typically has a negative incidence angle of about 2–3 deg to balance the wing pitching moment. As the wing pitching moment varies under different flight conditions, the horizontal tail incidence is usually adjustable through a range of about 3 deg up and down.

For the vertical tail, the generation of a trim force is normally not required because the aircraft is usually left-right symmetric and does not create any unbalanced yawing moment. The vertical tail of a multi-engined aircraft must be capable of providing a sufficient trim force in the event of an engine failure.

A single-engine propeller airplane will experience a yawing moment caused by the tail itself. The propeller tends to "drag" the air into a rotational motion in the same direction that the propeller spins. Since the verti-

cal tail is above the fuselage, it will be pushed on by the rotating propwash, causing a nose-left motion for the normal direction of engine rotation. To counter this, some single-engine propeller airplanes have the vertical tail offset several degrees.

The tails are also a key element of stability, acting much like the fins on an arrow. While it is possible to design a stable aircraft without tails, such a design is usually penalized in some other area, such as a compromised airfoil shape, excessive wing area or sweep, or narrow center-of-gravity range.

The other major function of the tail is control. The tail must be sized to provide adequate control power at all critical conditions. These critical conditions for the horizontal tail or canard typically include nosewheel liftoff, low-speed flight with flaps down, and transonic maneuvering. For the vertical tail, critical conditions typically include engine-out flight at low speeds, maximum roll rate, and spin recovery.

Note that control power depends upon the size and type of the movable surface as well as the overall size of the tail itself. For example, several airliners use double-hinged rudders to provide more engine-out control power without increasing the size of the vertical tail beyond what is required for dutch-roll damping. Several fighters, including the YF-12 and the F-107, have used all-moving vertical tails instead of separate rudders to increase control power.

### Tail Arrangement

Figure 4.28 illustrates some of the possible variations in aft-tail arrangement. The first shown has become "conventional" for the simple reason

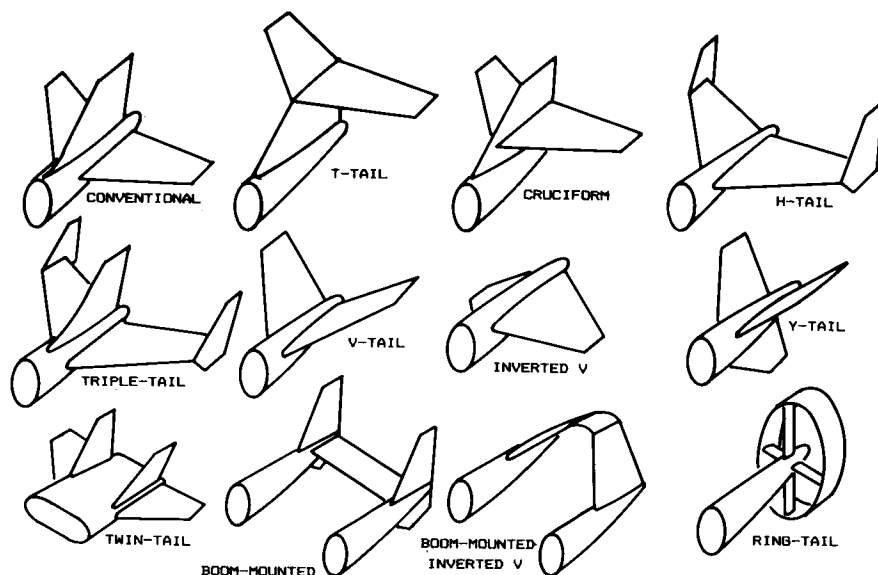


Fig. 4.28 Aft tail variations.

that it works. For most aircraft designs, the conventional tail will usually provide adequate stability and control at the lightest weight. Probably 70% or more of the aircraft in service have such a tail arrangement. However, there are many reasons for considering others.

The "T-tail" is also widely used. A T-tail is inherently heavier than a conventional tail because the vertical tail must be strengthened to support the horizontal tail, but the T-tail provides compensating advantages in many cases.

Due to end-plate effect, the T-tail allows a smaller vertical tail. The T-tail lifts the horizontal tail clear of the wing wake and propwash, which makes it more efficient and hence allows reducing its size. This also reduces buffet on the horizontal tail, which reduces fatigue for both the structure and the pilot.

In jet transport aircraft such as the DC-9 and B-727, the T-tail allows the use of engines mounted in pods on the aft fuselage. Finally, the T-tail is considered stylish, which is not a trivial consideration.

The cruciform tail, a compromise between the conventional and T-tail arrangements, lifts the horizontal tail to avoid proximity to a jet exhaust (as on the B-1B), or to expose the lower part of the rudder to undisturbed air during high angle-of-attack conditions and spins. These goals can be accomplished with a T-tail, but the cruciform tail will impose less of a weight penalty. However, the cruciform tail will not provide a tail-area reduction due to endplate effect as will a T-tail.

The "H-tail" is used primarily to position the vertical tails in undisturbed air during high angle-of-attack conditions (as on the T-46) or to position the rudders in the propwash on a multiengine aircraft to enhance engine-out control. The H-tail is heavier than the conventional tail, but its endplate effect allows a smaller horizontal tail.

On the A-10, the H-tail serves to hide the hot engine nozzles from heat-seeking missiles when viewed from an angle off the rear of the aircraft. H-tails and the related triple-tails have also been used to lower the tail height to allow an aircraft such as the Lockheed Constellation to fit into existing hangars.

The "V-tail" is intended to reduce wetted area. With a V-tail, the horizontal and vertical tail forces are the result of horizontal and vertical projections of the force exerted upon the "V" surfaces. For some required horizontal and vertical tail area, the required  $V$  surface area would theoretically be found from the Pythagorean theorem, and the tail dihedral angle would be found as the arctangent of the ratio of required vertical and horizontal areas. The resulting wetted area of the  $V$  surfaces would clearly be less than for separate horizontal and vertical surfaces.

However, extensive NACA research (Ref. 3) has concluded that to obtain satisfactory stability and control, the  $V$  surfaces must be upsized to about the same total area as would be required for separate horizontal and vertical surfaces. Even without the advantage of reduced wetted area, V-tails offer reduced interference drag but at some penalty in control-actuation complexity, as the rudder and elevator control inputs must be blended in a "mixer" to provide the proper movement of the V-tail "ruddervators."

When the right rudder pedal of a V-tail aircraft is pressed, the right ruddervator deflects downward, and the left ruddervator deflects upward. The combined forces push the tail to the left, so the nose goes to the right as desired. However, the ruddervators also produce a rolling moment toward the left—in opposition to the desired direction of turn, an action called “adverse roll-yaw coupling.”

The inverted V-tail shown in Fig. 4.28 avoids this problem, and instead produces a desirable “proverse roll-yaw coupling.” The inverted V-tail is also said to reduce spiraling tendencies. This tail arrangement can cause difficulties in providing adequate ground clearance.

The “Y-tail” is similar to the V-tail, except that the dihedral angle is reduced and a third surface is mounted vertically beneath the *V*. This third surface contains the rudder, whereas the *V* surfaces provide only pitch control. This tail arrangement avoids the complexity of the ruddervators while reducing interference drag when compared to a conventional tail. An inverted Y-tail is used on the F-4, primarily to keep the horizontal surfaces out of the wing wake at high angles of attack.

Twin tails on the fuselage can position the rudders away from the aircraft centerline, which may become blanketed by the wing or forward fuselage at high angles of attack. Also, twin tails have been used simply to reduce the height required with a single tail. Twin tails are usually heavier than an equal-area centerline-mounted single tail, but are often more effective. Twin tails are seen on most large modern fighters such as the F-14, F-15, F-18, and MiG-25.

Boom-mounted tails have been used to allow pusher propellers or to allow location of a heavy jet engine near the center of gravity. Tailbooms are typically heavier than a conventional fuselage construction, but can be desirable in some applications.

Boom-mounted tails can have a mid-mounted horizontal tail or a high horizontal, as on the Cessna Skymaster. Also, the inverted V-tail arrangement can be used with tail booms. The unmanned NASA HiMat research aircraft used boom-mounted verticals with no connecting horizontal tail, instead relying on a canard for pitch control.

The “ring-tail” concept attempts to provide all tail contributions via an airfoil-sectioned ring attached to the aft fuselage, usually doubling as a propeller shroud. While conceptually appealing, the ring-tail has proven inadequate in application. The only recent ring-tail aircraft, the JM-2 raceplane, was ultimately converted to a T-tail.

The location of an aft horizontal tail with respect to the wing is critical to the stall characteristics of the aircraft. If the tail enters the wing wake during the stall, control will be lost and pitchup may be encountered. Several T-tailed aircraft encountered “deep stall” from which they could not be extricated.

Figure 4.29 illustrates the boundaries of the acceptable locations for a horizontal tail to avoid this problem. Note that low tails are best for stall recovery. Also notice that a tail approximately in line with the wing is acceptable for a subsonic aircraft, but may cause problems at supersonic speeds due to the wake of the wing.

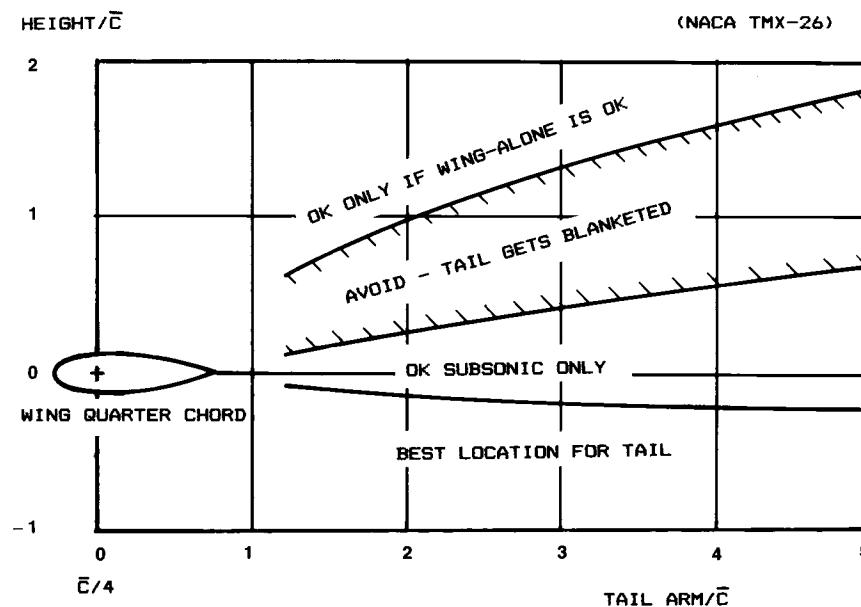


Fig. 4.29 Aft tail positioning.

A T-tail requires a wing designed to avoid pitchup without a horizontal tail, as described by Fig. 4.20. This requires an aircraft stable enough to recover from a stall even when the tail is blanketed by the wing wake. Several general aviation aircraft use this approach, which has the added benefit of a positive warning to the pilot of impending stall caused by buffeting on the tail as it enters the wing wake at high angle of attack.

Other possible tail arrangements are depicted in Fig. 4.30. Canards were used by the Wright brothers as a way of ensuring adequate control power, but fell out of favor due to the difficulty of providing sufficient stability. The early Wright airplanes were, in fact, quite unstable, and required a well-trained pilot with quick reflexes. Movie footage taken by passengers shows the Wright canards being continuously manipulated from almost full-up to full-down as the pilot responded to gusts.

There are actually two distinct classes of canard: the control-canard and the lifting-canard. In the control-canard, the wing carries most of the lift, and the canard is used primarily for control (as is an aft tail). Both the Wright Flyer and the Grumman X-29 are of this type.

The X-29 configuration is highly unstable in pitch with the canard included but is actually about neutral in stability with the canard off. This implies that the canard normally operates at nearly zero angle of attack, and thus carries little of the aircraft's weight. This is accomplished by a sophisticated, computerized flight control system that changes the angle of the canard in response to gusts, much as the pilot of an early Wright aircraft was forced to do manually.



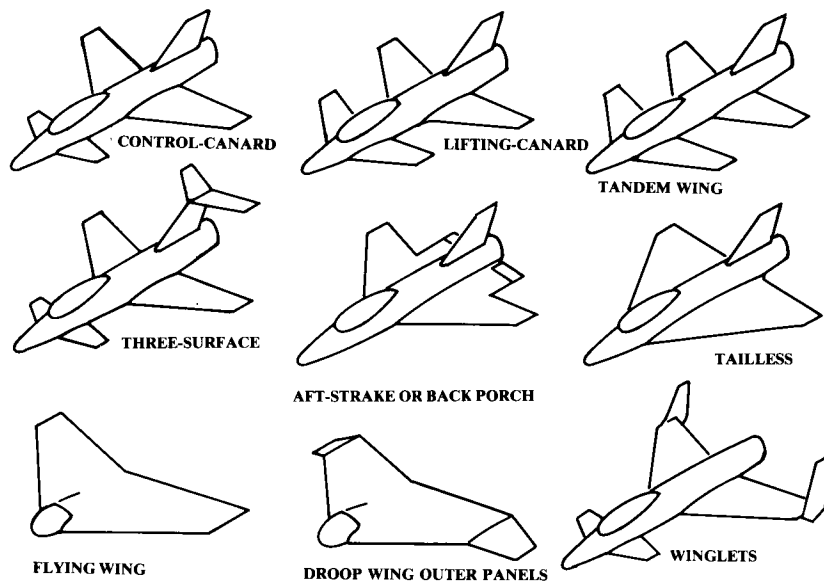


Fig. 4.30 Other tail configurations.

On the X-29 and similar control-canard aircraft, the canard is used to control the angle of attack of the wing and to balance out the pitching moment produced by deflection of the wing flaps.

In contrast, a lifting-canard aircraft uses both the wing and the canard to provide lift under normal flight conditions. This requires that the aircraft center of gravity be well forward of the normal location with respect to the wing when compared to an aft-tailed aircraft. A lifting-canard will usually have a higher aspect ratio and greater airfoil camber than a control-canard, to reduce the canard's drag-due-to-lift.

The lifting-canard arrangement is theoretically more efficient than an aft-tailed aircraft because the canard's lift reduces the lift that must be produced by the wing, which permits a smaller wing and also reduces total drag-due-to-lift. An aft-tail design frequently flies with a download on the tail to produce stability, which actually increases the amount of lift that the wing must produce.

However, the lifting-canard suffers from several drawbacks that reduce the net benefit. First, the use of a lifting-canard has the effect of locating the wing further aft on the aircraft than would be the case with an aft tail. This increases the pitching moment caused by the use of wing flaps.

The pitching moment from the flaps must be balanced during slow flight by a large increase in canard lift. For this reason most aircraft with lifting canards cannot use sophisticated wing flaps. Instead, the wing must be increased in area to provide the same total maximum lift as is provided by the aft-tailed configuration, in which more-powerful flaps may be used. To get around this problem some designs have resorted to the use of slotted canard flaps or even a canard with variable sweep (as on the Beech Starship).

Another drawback is that the canard flap, which is usually used for pitch control, is much closer to the center of gravity than an aft tail elevator would be. This reduces the trim and control effectiveness of the canard flap, requiring a larger surface and producing more trim drag when operating at fairly large deflections such as in slow flight or at an extremely forward center-of-gravity condition. On the other hand, at such conditions an aft tail is producing a download that requires the wing to generate a lift greater than the weight of the aircraft.

One additional benefit obtainable from canards is the avoidance of pitchup. An all-moving canard capable of downward deflections on the order of 45 deg can be used to escape from pitchup situations. This permits optimizing the aspect ratio and sweep without compromising for pitchup avoidance, as suggested by Fig. 4.20.

The tandem-wing is an extension of the lifting-canard concept in which the forward surface produces approximately as much lift as the aft surface. The major benefit of the tandem-wing is a theoretical 50% reduction in the drag-due-to-lift.

The drag-due-to-lift, or induced drag, is a function of the square of the lift being produced. If the weight of the aircraft is evenly distributed to two wings, each wing would have only one-fourth of the induced drag of a single wing. Thus, the sum of the induced drags of the two wings should be half of the drag of a single wing.

As was shown for biplane wings, this theoretical result is not seen in practice because of the interference between the two wings. The second wing must fly in the downwash of the first wing, which requires a higher angle of attack on the second wing. Also, the wake of the first wing tends to create turbulence on the second wing. Finally, to attain stability with a tandem-wing it is usually necessary to move the center of gravity somewhat forward of the location for an even weight split, which may prevent the aft wing from attaining its full lift capability.

To maximize efficiency of a tandem-wing design it is desirable to separate the two wings as far apart as possible, both horizontally and vertically. To attain maximum total lift, it is common to use high-lift devices on the front wing.

A three-surface arrangement provides both aft-tail and lifting-canard surfaces. This allows the use of the lifting-canard for reduction of wing drag-due-to-lift without the difficulty of incorporating wing flaps as seen on a canard-only configuration.

The three-surface aircraft theoretically offers minimum trim drag. A canard or aft-tail, when generating lift for trim purposes, will change the aircraft total lift distribution, which increases total induced drag. On a three-surface configuration the canard and aft-tail can act in opposite directions, thus cancelling out each other's effect upon the total lift distribution. (For example, to generate a nose-up trim the canard can generate an upward lift force while the tail generates an equal downward lift force. The combined effect upon total lift distribution would then be zero.)

However, this reduction in trim drag is a theoretical farfield effect and may not be fully realized in an actual design. The drawback of the three-sur-

face arrangement is the additional weight, complexity, and interference drag associated with the extra surfaces.

The “back-porch” or “aft-strake” is a horizontal control surface that is incorporated into a faired extension of the wing or fuselage. This device, seen on the X-29, is mostly used to prevent pitchup but can also serve as a primary pitch control surface in some cases.

The tailless configuration offers the lowest weight and drag of any tail configuration, if it can be made to work. For a stable aircraft, the wing of a tailless aircraft must be reflexed or twisted to provide natural stability. This reduces the efficiency of the wing.

For an unstable aircraft with a computerized flight control system, this need not be done. In fact, an unstable, tailless aircraft can be designed to be “self-trimming,” meaning that the wing trailing-edge flap angles required to balance the aircraft at different speeds and angles of attack can be designed to be almost exactly the optimal flap angles for maximum  $L/D$ .

This is very difficult to accomplish, and is very sensitive to the location of the center of gravity. In fact, all tailless designs are sensitive to center-of-gravity location, and are most successful in designs in which the expendable fuel and payload are located very close to the empty center of gravity.

The vertical tail can also be eliminated for reduced weight and drag. However, the fully tailless (flying-wing) design is probably the most difficult configuration to stabilize, either naturally or by computer. Fully-tailless designs must rely exclusively upon wing control surfaces for control, unless vectored thrust is provided. Rudder control is usually provided by wingtip-mounted drag devices.

Some fully-tailless designs utilize drooped outer wing panels for stability and control enhancement. These act somewhat like an inverted V-tail and provide the desirable proverse roll-yaw coupling with rudder deflection.

Winglets or endplates mounted at the wing tips can be used in place of a vertical tail. This may provide the required vertical tail surface for free, since the effective increase in wing aspect ratio may more than compensate for the wetted area of the tail. To place these tip surfaces far enough aft to act like vertical tails requires either extreme wing sweep or a canard arrangement, or both.

### Tail Arrangement for Spin Recovery

The vertical tail plays a key role in spin recovery. An aircraft in a spin is essentially falling vertically and rotating about a vertical axis, with the wing fully stalled. The aircraft is also typically at a large sideslip angle. To recover from the spin requires that the wing be unstalled, so the angle of attack must be reduced. However, first the rotation must be stopped and the sideslip angle reduced, or the aircraft will immediately enter another spin. This requires adequate rudder control even at the high angles of attack seen in the spin.

Figure 4.31 illustrates the effect of tail arrangement upon rudder control at high angles of attack. At high angles of attack the horizontal tail is stalled, producing a turbulent wake extending upward at approximately a 45-deg angle.

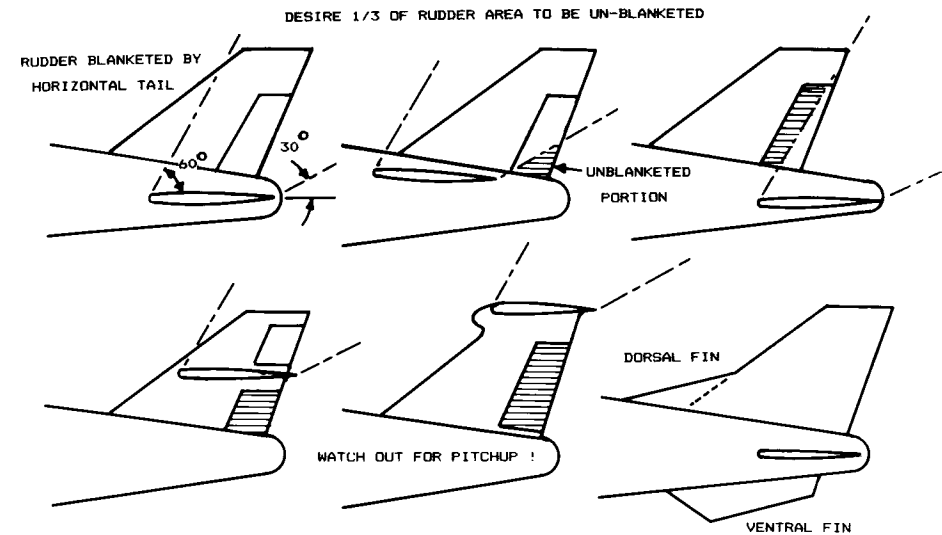


Fig. 4.31 Tail geometry for spin recovery.

In the first example, the rudder lies entirely within the wake of the horizontal tail, so little rudder control is available. The second example shows the effect of moving the horizontal tail forward with respect to the vertical tail. This “uncovers” part of the rudder, improving rudder control. The next example moves the horizontal tail aft with respect to the vertical tail, with the same result. As a rule of thumb, at least a third of the rudder should be out of the wake.

The next two examples show the effect of moving the horizontal tail upward. The T-tail arrangement completely uncovers the rudder, but can result in pitchup.

The last illustration in Fig. 4.31 shows the use of dorsal and ventral fins. The dorsal fin improves tail effectiveness at high angles of sideslip by creating a vortex that attaches to the vertical tail. This tends to prevent the high angles of sideslip seen in spins, and augments rudder control in the spin. The ventral tail also tends to prevent high sideslip, and has the extra advantage of being where it cannot be blanketed by the wing wake. Ventral tails are also used to avoid lateral instability in high-speed flight.

### Tail Geometry

The surface areas required for all types of tails are directly proportional to the aircraft’s wing area, so the tail areas cannot be selected until the initial estimate of aircraft takeoff gross weight has been made. The initial estimation of tail area is made using the “tail volume coefficient” method, which will be discussed in Chapter 6.

Other geometric parameters for the tails can be selected at this time. Tail aspect ratio and taper ratio show little variation over a wide range of aircraft types. Table 4.3 provides guidance for selection of tail aspect ratio and

Table 4.3 Tail aspect ratio and taper ratio

	Horizontal tail		Vertical tail	
	$A$	$\lambda$	$A$	$\lambda$
Fighter	3-4	0.2-0.4	0.6-1.4	0.2-0.4
Sail plane	6-10	0.3-0.5	1.5-2.0	0.4-0.6
Others	3-5	0.3-0.6	1.3-2.0	0.3-0.6
T-Tail	—	—	0.7-1.2	0.6-1.0

taper ratio. Note that T-tail aircraft have lower vertical-tail aspect ratios to reduce the weight impact of the horizontal tail's location on top of the vertical tail. Also, some general-aviation aircraft use untapered horizontal tails ( $\lambda = 1.0$ ) to reduce manufacturing costs.

Leading-edge sweep of the horizontal tail is usually set to about 5 deg more than the wing sweep. This tends to make the tail stall after the wing, and also provides the tail with a higher Critical Mach Number than the wing, which avoids loss of elevator effectiveness due to shock formation. For low-speed aircraft, the horizontal tail sweep is frequently set to provide a straight hinge line for the elevator, which usually has the left and right sides connected to reduce flutter tendencies.

Vertical-tail sweep varies between about 35 and 55 deg. For a low-speed aircraft, there is little reason for vertical-tail sweep beyond about 20 deg other than aesthetics. For a high-speed aircraft, vertical-tail sweep is used primarily to insure that the tail's Critical Mach Number is higher than the wing's.

The exact planform of the tail surfaces is actually not very critical in the early stages of the design process. The tail geometries are revised during later analytical and wind-tunnel studies. For conceptual design, it is usually acceptable simply to draw tail surfaces that "look right," based upon prior experience and similar designs.

Tail thickness ratio is usually similar to the wing thickness ratio, as determined by the historical guidelines provided in the wing-geometry section. For a high-speed aircraft, the horizontal tail is frequently about 10% thinner than the wing to ensure that the tail has a higher Critical Mach Number.

Note that a lifting canard or tandem wing should be designed using the guidelines and procedures given for initial wing design, instead of the tail-design guidelines described above.

## THRUST-TO-WEIGHT RATIO AND WING LOADING

### 5.1 INTRODUCTION

The thrust-to-weight ratio ( $T/W$ ) and the wing loading ( $W/S$ ) are the two most important parameters affecting aircraft performance. Optimization of these parameters forms a major part of the analytical design activities conducted after an initial design layout. The methods used for this optimization are described in Chapter 19.

However, it is essential that a credible estimate of the wing loading and thrust-to-weight ratio be made before the initial design layout is begun. Otherwise, the optimized aircraft may be so unlike the as-drawn aircraft that the design must be completely redone.

For example, if the wing loading used for the initial layout is very low, implying a large wing, the designer will have no trouble finding room for the landing gear and fuel tanks. If later optimization indicates the need for a much higher wing loading, the resulting smaller wing may no longer hold the landing gear and fuel. While they could be put in the fuselage, this would increase the wetted area and therefore the drag, so the optimization results would probably be no good.

Wing loading and thrust-to-weight ratio are interconnected for a number of performance calculations, such as takeoff distance, which is frequently a critical design driver. A requirement for short takeoff can be met by using a large wing (low  $W/S$ ) with a relatively small engine (low  $T/W$ ). While the small engine will cause the aircraft to accelerate slowly, it only needs to reach a moderate speed to lift off the ground.

On the other hand, the same takeoff distance could be met with a small wing (high  $W/S$ ) provided that a large engine (high  $T/W$ ) is also used. In this case, the aircraft must reach a high speed to lift off, but the large engine can rapidly accelerate the aircraft to that speed.

Due to this interconnection, it is frequently difficult to use historical data to independently select initial values for wing loading and thrust-to-weight ratio. Instead, the designer must guess at one of the parameters and use that guess to calculate the other parameter from the critical design requirements.

In many cases, the critical requirement for wing loading will be the stall speed during the approach for landing. Approach stall speed is independent of engine size, so the wing loading can be estimated based upon stall speed alone. The estimated wing loading can then be used to calculate the  $T/W$  required to attain other performance drivers such as the single-engine rate of climb.

For less obvious cases, the designer must guess one parameter, calculate the other parameter to meet various performance requirements, then recheck the first parameter. In this book, the thrust-to-weight ratio appears as the first guess because that parameter better lends itself to a statistical approach, and also because it shows less variation within a given class of aircraft.

However, for certain aircraft the designer may wish to begin instead with the wing loading. In such cases, those equations presented below for calculating the wing loading can be solved for thrust-to-weight ratio instead.

## 5.2 THRUST-TO-WEIGHT RATIO

### Thrust-to-Weight Definitions

$T/W$  directly affects the performance of the aircraft. An aircraft with a higher  $T/W$  will accelerate more quickly, climb more rapidly, reach a higher maximum speed, and sustain higher turn rates. On the other hand, the larger engines will consume more fuel throughout the mission, which will drive up the aircraft's takeoff gross weight to perform the design mission.

$T/W$  is not a constant. The weight of the aircraft varies during flight as fuel is burned. Also, the engine's thrust varies with altitude and velocity (as does the horsepower and propeller efficiency,  $\eta_p$ ).

When designers speak of an aircraft's thrust-to-weight ratio they generally refer to the  $T/W$  during sea-level static (zero-velocity), standard-day conditions at design takeoff weight and maximum throttle setting. Another commonly referred-to  $T/W$  concerns combat conditions.

You can also calculate  $T/W$  at a partial-power setting. For example, during the approach to landing the throttle setting is near idle. The operating  $T/W$  at that point in the mission is probably less than 0.05.

It is very important to avoid confusing the takeoff  $T/W$  with the  $T/W$  at other conditions in the calculations below. If a required  $T/W$  is calculated at some other condition, it must be adjusted back to takeoff conditions for use in selecting the number and size of the engines. These  $T/W$  adjustments will be discussed later.

### Power Loading and Horsepower-to-Weight

The term "thrust-to-weight" is associated with jet-engined aircraft. For propeller-powered aircraft, the equivalent term has classically been the "power loading," expressed as the weight of the aircraft divided by its horsepower ( $W/\text{hp}$ ).

Power loading has an opposite connotation from  $T/W$  because a high power loading indicates a smaller engine. Power loadings typically range from 10–15 for most aircraft. An aerobatic aircraft may have a power loading of about six. A few aircraft have been built with power loadings as low as three or four. One such over-powered airplane was the Pitts Sampson, a one-of-a-kind airshow airplane.

A propeller-powered aircraft produces thrust via the propeller, which has an efficiency  $\eta_p$  defined as the thrust output per horsepower provided by the

engine. Using Eq. (3.9), an equivalent  $T/W$  for propellered aircraft can therefore be expressed as follows:

$$\frac{T}{W} = \left( \frac{550 \eta_p}{V} \right) \left( \frac{\text{hp}}{W} \right) \quad (5.1)$$

Note that this equation includes the term  $\text{hp}/W$ , the horsepower-to-weight ratio. This is simply the inverse of the classical power loading ( $W/\text{hp}$ ). To avoid confusion when discussing requirements affecting both jet- and propeller-powered aircraft, this book refers to the horsepower-to-weight ratio rather than the classical power loading. The reader should remember that the power loading can be determined simply by inverting the horsepower-to-weight ratio.

Also, to avoid excessive verbiage in the discussions below, the term "thrust-to-weight ratio" should be understood to include the horsepower-to-weight ratio for propeller aircraft.

### Statistical Estimation of $T/W$

Tables 5.1 and 5.2 provide typical values for  $T/W$  and  $\text{hp}/W$  for different classes of aircraft. Table 5.2 also provides reciprocal values, i.e., power loadings, for propellered aircraft. These values are all at maximum power settings at sea level and zero velocity ("static").

Table 5.1 Thrust-to-weight ratio ( $T/W$ )

Aircraft type	Typical installed $T/W$
Jet trainer	0.4
Jet fighter (dogfighter)	0.9
Jet fighter (other)	0.6
Military cargo/bomber	0.25
Jet transport	0.25

Table 5.2 Horsepower-to-weight ratio

Aircraft type	Typical $\text{hp}/W$	Typical power loading ( $W/\text{hp}$ )
Powered sailplane	0.04	25
Homebuilt	0.08	12
General aviation—single engine	0.07	14
General aviation—twin engine	0.17	6
Agricultural	0.09	11
Twin turboprop	0.20	5
Flying boat	0.10	10

Note that the current generation of dogfighters approaches a  $T/W$  of 1.0, implying that the thrust is nearly equal to the weight. At combat conditions when some fuel has been burned off, these aircraft have  $T/W$  values exceeding 1, and are capable of accelerating while going straight up! The jet dogfighter  $T/W$  values are with afterburning engines, whereas the other jets typically do not have afterburning.

Thrust-to-weight ratio is closely related to maximum speed. Later in the design process, aerodynamic calculations of drag at the design maximum speed will be used, with other criteria, to establish the required  $T/W$ .

For now, Tables 5.3 and 5.4 provide curve-fit equations based upon maximum Mach number or velocity for different classes of aircraft. These can be used as a first estimate for  $T/W$  or  $hp/W$ . The equations were developed by the author using data from Ref. 1, and should be considered valid only within the normal range of maximum speeds for each aircraft class.

### Thrust Matching

For aircraft designed primarily for efficiency during cruise, a better initial estimate of the required  $T/W$  can be obtained by "thrust matching." This refers to the comparison of the selected engine's thrust available during cruise to the estimated aircraft drag.

In level unaccelerating flight, the thrust must equal the drag. Likewise, the weight must equal the lift (assuming that the thrust is aligned with the

Table 5.3  $T/W_0$  vs  $M_{\max}$

$T/W_0 = a M_{\max}^C$	$a$	$C$
Jet trainer	0.488	0.728
Jet fighter (dogfighter)	0.648	0.594
Jet fighter (other)	0.514	0.141
Military cargo/bomber	0.244	0.341
Jet transport	0.267	0.363

Table 5.4  $hp/W_0$  vs  $V_{\max}$  (mph)

$hp/W_0 = a V_{\max}^C$	$a$	$C$
Sailplane—powered	0.043	0
Homebuilt—metal/wood	0.005	0.57
Homebuilt—composite	0.004	0.57
General aviation—single engine	0.024	0.22
General aviation—twin engine	0.034	0.32
Agricultural aircraft	0.008	0.50
Twin turboprop	0.012	0.50
Flying boat	0.029	0.23

flight path). Thus,  $T/W$  must equal the inverse of  $L/D$  [Eq. (5.2)]:

$$\left(\frac{T}{W}\right)_{\text{cruise}} = \frac{1}{(L/D)_{\text{cruise}}} \quad (5.2)$$

$L/D$  can be estimated in a variety of ways. Chapter 12 will discuss the detailed drag-buildup approach. For the first estimation of  $T/W$  the method for  $L/D$  estimation presented in Chapter 3 is adequate.

Recall that this procedure for  $L/D$  estimation uses the selected aspect ratio and an estimated wetted-area ratio (Fig. 3.5) to determine the wetted aspect ratio. Figure 3.6 is then used to estimate the maximum  $L/D$ . For propeller aircraft, the cruise  $L/D$  is the same as the maximum  $L/D$ . For jet aircraft, the cruise  $L/D$  is 86.6% of the maximum  $L/D$ .

Note that this method assumes that the aircraft is cruising at approximately the optimum altitude for the as-yet-unknown wing loading. The method would be invalid if the aircraft were forced by the mission requirements to cruise at some other altitude, such as sea level.

When the wing loading has been selected, as described later in this chapter, the  $L/D$  at the actual cruise conditions should be calculated and used to recheck the initial estimate for  $T/W$ .

The thrust-to-weight ratio estimated using Eq. (5.2) is at cruise conditions, not takeoff. The aircraft will have burned off part of its fuel before beginning the cruise, and will burn off more as the cruise progresses.

Also, the thrust of the selected engine will be different at the cruise conditions than at sea-level, static conditions. These factors must be considered to arrive at the required takeoff  $T/W$ , used to size the engine.

The highest weight during cruise occurs at the beginning of the cruise. The weight of the aircraft at the beginning of the cruise is the takeoff weight less the fuel burned during takeoff and climb to cruise altitude. From Table 3.2, the typical mission weight fractions for these mission legs are 0.970 and 0.985, or 0.956 when multiplied together.

A typical aircraft will therefore have a weight at the beginning of cruise of about 0.956 times the takeoff weight. This value is used below to adjust the cruise  $T/W$  back to takeoff conditions.

Thrust during cruise is different from the takeoff value. Jet aircraft are normally designed to cruise at approximately the altitude at which the selected engine has the best (lowest) specific fuel consumption, typically 30,000–40,000 ft. While SFC is improved at these altitudes, the thrust decreases. Also, the engine is sized using the thrust setting that produces the best SFC. This is usually 70–100% of the maximum continuous, nonafterburning thrust.

The cruise thrust at altitude is therefore less than the maximum takeoff thrust at sea-level, so the required cruise  $T/W$  must be adjusted to obtain the equivalent takeoff  $T/W$ .

Typically, a subsonic, high-bypass-ratio turbofan for a transport aircraft will have a cruise thrust of 20–25% of the takeoff thrust, while a low-bypass afterburning turbofan or turbojet will have a cruise thrust of 40–70% of the

takeoff maximum value (see Fig. 5.1). Appendix A.4 provides thrust and fuel-consumption data for several representative engines.

For a piston-powered, propeller-driven aircraft, the power available varies with the density of the air provided to the intake manifold. If the engine is not supercharged, then the power falls off with increasing altitude according to the density ratio,  $\sigma$ . For example, a nonsupercharged engine at 10,000 ft will have about 73% of its sea-level power.

To prevent this power decrease, many piston engines use a supercharger to maintain the air provided to the manifold at essentially sea-level density up to the compression limit of the supercharger. Above this altitude, the power begins to drop off (see Fig. 5.2). Piston-powered aircraft typically cruise at about 75% of takeoff power.

For a turbine-powered, propeller-driven (turboprop) aircraft, the horsepower available increases somewhat with increasing speed, but the thrust drops off anyway due to the velocity effect on the propeller [Eq. (5.1)].

With a turboprop, there is an additional, residual thrust contribution from the turbine exhaust. It is customary to convert this thrust to its horsepower equivalent and add it to the actual horsepower, creating an "equivalent shaft horsepower (eshp)." For a typical turboprop engine installation, the cruise eshp is about 60–80% of the takeoff value.

The takeoff  $T/W$  required for cruise matching can now be approximated using Eq. (5.3). The ratio between initial cruise weight and takeoff weight was shown to be about 0.956. If a better estimate of this ratio is available, it should be used.

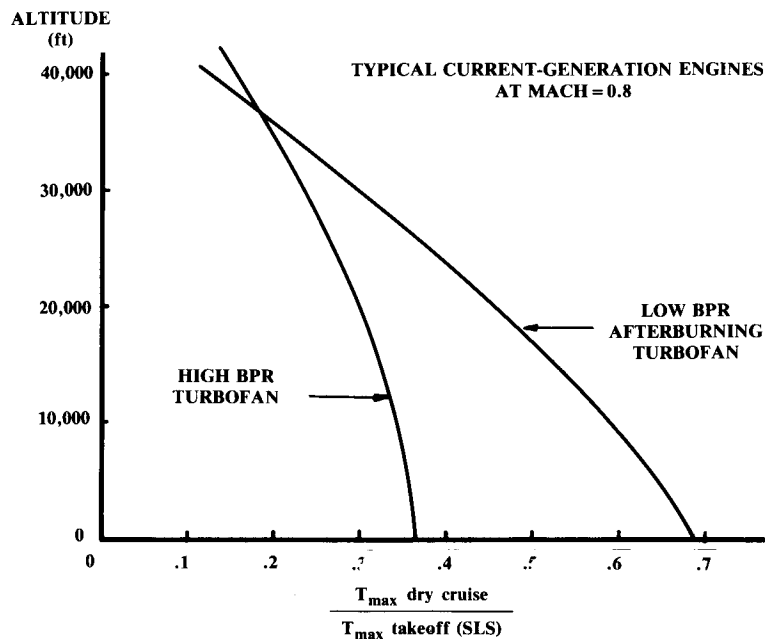


Fig. 5.1 Thrust lapse at cruise.

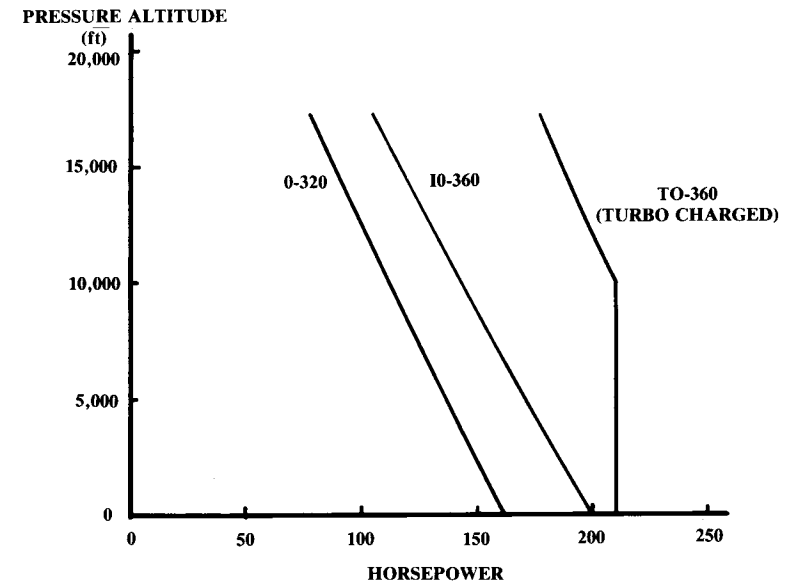


Fig. 5.2 Piston engine power variation with altitude.

$$\left(\frac{T}{W}\right)_{\text{takeoff}} = \left(\frac{T}{W}\right)_{\text{cruise}} \left(\frac{W_{\text{cruise}}}{W_{\text{takeoff}}}\right) \left(\frac{T_{\text{takeoff}}}{T_{\text{cruise}}}\right) \quad (5.3)$$

The thrust ratio between takeoff and cruise conditions should be obtained from actual engine data if possible. Otherwise, data for a similar engine from Appendix A.4 or some other source should be used.

For a propeller aircraft, the required takeoff hp/ $W$  can be found by combining Eqs. (5.1) and (5.2):

$$\left(\frac{\text{hp}}{W}\right)_{\text{takeoff}} = \left(\frac{V_{\text{cruise}}}{550 \eta_p}\right) \left(\frac{1}{(L/D)_{\text{cruise}}}\right) \left(\frac{W_{\text{cruise}}}{W_{\text{takeoff}}}\right) \left(\frac{\text{hp}_{\text{takeoff}}}{\text{hp}_{\text{cruise}}}\right) \quad (5.4)$$

where typically  $\eta_p = 0.8$ .

After an initial layout has been completed, actual aerodynamic calculations are made to compare the drag during cruise with the thrust available.

There are many other criteria which can set the thrust-to-weight ratio, such as climb rate, takeoff distance, and turning performance. These other criteria also involve the wing loading and are described in the next section.

For the first-pass estimate, the  $T/W$  (or hp/ $W$ ) should be selected as the higher of either the statistical value obtained from the appropriate equation in Tables 5.3 and 5.4, or the value obtained from the cruise matching as described above. After selection of the wing loading as described below, the selected  $T/W$  should be rechecked against all requirements.

Table 5.5 Wing loading

Historical trends	Typical takeoff $W/S$ (lb/ft <sup>2</sup> )
Sailplane	6
Homebuilt	11
General aviation—single engine	17
General aviation—twin engine	26
Twin turboprop	40
Jet trainer	50
Jet fighter	70
Jet transport/bomber	120

### 5.3 WING LOADING

The wing loading is the weight of the aircraft divided by the area of the reference (not exposed) wing. As with the thrust-to-weight ratio, the term “wing loading” normally refers to the takeoff wing loading, but can also refer to combat and other flight conditions.

Wing loading affects stall speed, climb rate, takeoff and landing distances, and turn performance. The wing loading determines the design lift coefficient, and impacts drag through its effect upon wetted area and wing span.

Wing loading has a strong effect upon sized aircraft takeoff gross weight. If the wing loading is reduced, the wing is larger. This may improve performance, but the additional drag and empty weight due to the larger wing will increase takeoff gross weight to perform the mission. The leverage effect of the sizing equation will require a more-than-proportional weight increase when factors such as drag and empty weight are increased.

Table 5.5 provides representative wing loadings.

Wing loading and thrust-to-weight ratio must be optimized together. Such optimization methods are presented in Chapter 19 using aerodynamic, weight, and propulsion data calculated from the initial design layout. The remainder of this chapter provides methods for initially estimating the wing loading to meet various requirements. These allow the designer to begin the layout with some assurance that the design will not require a complete revision after the aircraft is analyzed and sized.

This material generally assumes that an initial estimate of  $T/W$  has been made using the methods presented in the last section. However, most of the equations could also be used to solve for  $T/W$  if the wing loading is defined by some unique requirement (such as stall speed).

These methods estimate the wing loading required for various performance conditions. To ensure that the wing provides enough lift in all circumstances, the designer should select the lowest of the estimated wing loadings. However, if an unreasonably low wing loading value is driven by only one of these performance conditions, the designer should consider another way to meet that condition.

For example, if the wing loading required to meet a stall speed requirement is well below all other requirements, it may be better to equip the aircraft with a high-lift flap system. If takeoff distance or rate of climb require a very low wing loading, perhaps the thrust-to-weight ratio should be increased.

#### Stall Speed

The stall speed of an aircraft is directly determined by the wing loading and the maximum lift coefficient. Stall speed is a major contributor to flying safety, with a substantial number of fatal accidents each year due to “failure to maintain flying speed.” Also, the approach speed, which is the most important factor in landing distance and also contributes to post-touchdown accidents, is defined by the stall speed.

Civil and military design specifications establish maximum allowable stall speeds for various classes of aircraft. In some cases the stall speed is explicitly stated. FAR 23 certified aircraft (under 12,500-lb TOGW) must stall at no more than 61 knots, unless they are multiengine and meet certain climb requirements (see Appendix A.5). While not stated in any design specifications, a stall speed of about 50 knots would be considered the upper limit for a civilian trainer or other aircraft to be operated by low-time pilots.

The approach speed is required to be a certain multiple of the stall speed. For civil applications, the approach speed must be at least 1.3 times the stall speed. For military applications, the multiple must be at least 1.2 (1.15 for carrier-based aircraft). Approach speed may be explicitly stated in the design requirements or will be selected based upon prior, similar aircraft. Then the required stall speed is found by division by 1.3, 1.2, or 1.15.

Equation (5.5) states that lift equals weight in level flight, and that at stall speed, the aircraft is at maximum lift coefficient. Equation (5.6) solves for the required wing loading to attain a given stall speed with a certain maximum lift coefficient. The air density,  $\rho$ , is typically the sea-level standard value (0.00238 slugs/cubic ft) or sometimes the 5000-ft-altitude, hot-day value (0.00189) to ensure that the airplane can be flown into Denver during summer.

$$W = L = q_{\text{stall}} S C_{L_{\text{max}}} = \frac{1}{2} \rho V_{\text{stall}}^2 S C_{L_{\text{max}}} \quad (5.5)$$

$$W/S = \frac{1}{2} \rho V_{\text{stall}}^2 C_{L_{\text{max}}} \quad (5.6)$$

The remaining unknown, the maximum lift coefficient, can be very difficult to estimate. Values range from about 1.2 to 1.5 for a plain wing with no flaps to as much as 5.0 for a wing with large flaps immersed in the propwash or jetwash.

The maximum lift coefficient for an aircraft designed for short takeoff and landing (STOL) applications will typically be about 3.0. For a regular transport aircraft with flaps and slats (leading-edge flaps with slots to improve airflow), the maximum lift coefficient is about 2.4. Other aircraft, with flaps on the inner part of the wing, will reach a lift coefficient of about 1.6–2.0.

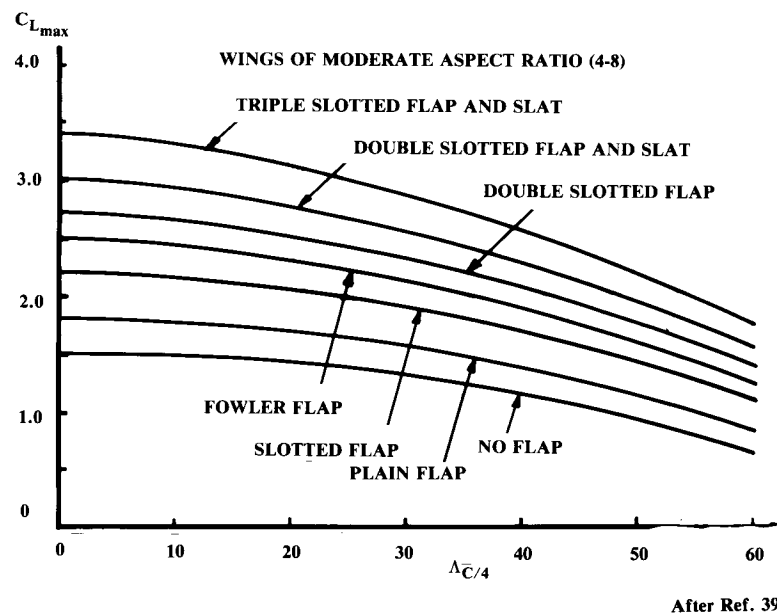


Fig. 5.3 Maximum lift coefficient.

Maximum lift coefficient depends upon the wing geometry, airfoil shape, flap geometry and span, leading-edge slot or slat geometry, Reynolds number, surface texture, and interference from other parts of the aircraft such as the fuselage, nacelles, or pylons. The trim force provided by the horizontal tail will increase or reduce the maximum lift, depending upon the direction of the trim force. If the propwash or jetwash impinges upon the wing or the flaps, it will also have a major influence upon maximum lift during power-on conditions.

Most aircraft use a different flap setting for takeoff and landing. During landing, the flaps will be deployed the maximum amount to provide the greatest lift and drag. However, for takeoff the maximum flap angle will probably cause more drag than desirable for rapid acceleration and climb, so the flaps will be deployed to about half the maximum angle. Therefore, the maximum lift coefficient for landing will be greater than for takeoff. Typically, the takeoff maximum lift coefficient is about 80% that of the landing value.

For a wing of fairly high aspect ratio (over about 5), the maximum lift coefficient will be approximately 90% of the airfoil maximum lift coefficient at the same Reynolds number, provided that the lift distribution is nearly elliptical. However, if partial-span flaps are used, their deflection will introduce a large, discontinuous twist into the wing geometry that changes the lift distribution, and thus the induced downwash, causing the effective angle of attack to vary at different span stations.

As a crude approximation, the designer can ignore this effect. Then the maximum lift can be estimated by determining the maximum angle of attack before some part of the wing stalls. Typically, the part of the wing with the flap deflected will stall first. Then, for that angle of attack the lift contributions of the flapped and unflapped sections can be summed, weighted by their areas (see Fig. 12.19 for definitions of flapped and unflapped areas). This crude approximation for wings of a fairly high aspect ratio is given in Eq. (5.7).

$$C_{L_{\max}} \cong 0.9 \left\{ (C_{l_{\max}})_{\text{flapped}} \frac{S_{\text{flapped}}}{S_{\text{ref}}} + (C_l)_{\text{unflapped}} \frac{S_{\text{unflapped}}}{S_{\text{ref}}} \right\} \quad (5.7)$$

where  $C_{l_{\text{unflapped}}}$  is the lift coefficient of the unflapped airfoil at the angle of attack at which the flapped airfoil stalls.

For a better initial estimate of maximum lift, it is necessary to resort to test results and historical data. Figure 5.3 provides maximum-lift trends vs sweep angle for several classes of aircraft. Remember that the maximum lift using the takeoff flap setting will typically be about 80% of these landing maximum values. Maximum lift is discussed in more detail in Chapter 12.

### Takeoff Distance

A number of different values are referred to as “takeoff distance.” The “ground roll” is the actual distance traveled before the wheels leave the ground. The liftoff speed for a normal takeoff is 1.1 times the stall speed.

The “obstacle clearance distance” is the distance required from brake release until the aircraft has reached some specified altitude. This is usually 50 ft for military or small civil aircraft and 35 ft for commercial aircraft.

The “balanced field length” is the length of the field required for safety in the event of an engine failure at the worst possible time in a multiengine aircraft. When the aircraft has just begun its ground roll, the pilot would have no trouble stopping it safely if one engine were to fail. As the speed increases, more distance would be required to stop after an engine failure. If the aircraft is nearly at liftoff speed and an engine fails, the pilot would be unable to stop safely and instead would continue the takeoff on the remaining engines.

The speed at which the distance to stop after an engine failure exactly equals the distance to continue the takeoff on the remaining engines is called the “decision speed.” The balanced field length is the length required to takeoff and clear the specified obstacle when one engine fails exactly at decision speed. Note that use of reversed thrust is not permitted for calculation of balanced field length.

Balanced field length is sometimes called the “FAR takeoff field length” when applied to FAR 25 aircraft (which have a 35-ft obstacle clearance requirement). For military aircraft the balanced field length has a 50-ft obstacle clearance requirement.

Both the wing loading and the thrust-to-weight ratio contribute to the takeoff distance. The equations below assume that the thrust-to-weight ratio has been selected and can be used to determine the required wing loading to attain some required takeoff distance. However, the equations could be solved for  $T/W$  if the wing loading is known.

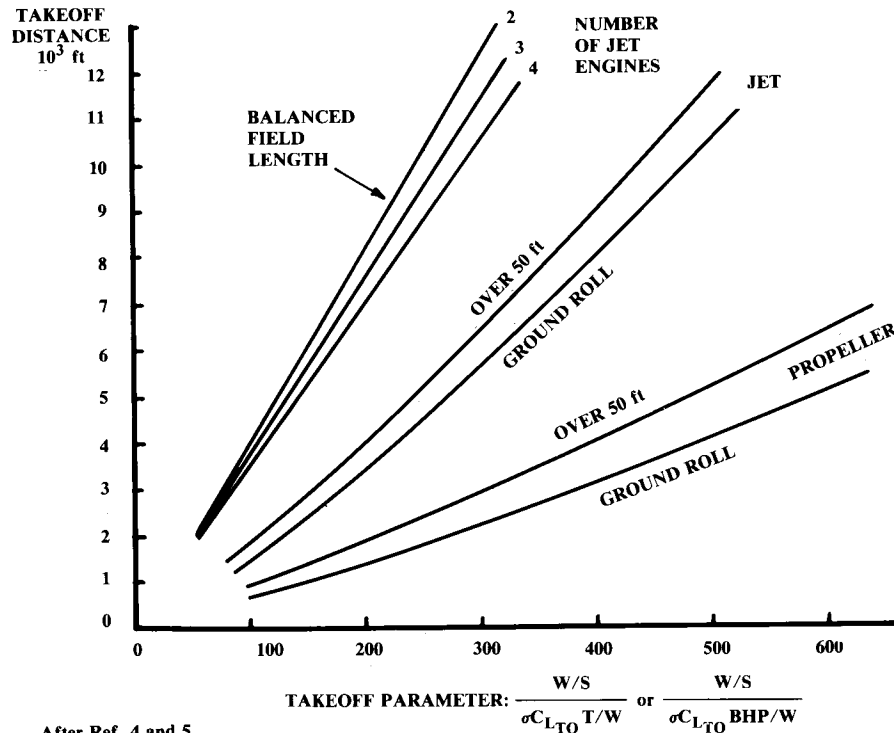


Other factors contributing to the takeoff distance are the aircraft's aerodynamic drag and rolling resistance. Aerodynamic drag on the ground depends largely upon pilot technique. For example, if the pilot rotates (lifts the nose) too early, the extra drag may prevent the aircraft from accelerating to takeoff speed. This was a frequent cause of accidents in early jets, which were underpowered by today's standards.

The aircraft's rolling resistance,  $\mu$ , is determined by the type of runway surface and by the type, number, inflation pressure, and arrangement of the tires. A thin, high-pressure tire operated over a soft dirt runway will have so much rolling resistance that the aircraft may be unable to move. A large, low pressure tire can operate over a softer runway surface but will have more aerodynamic drag if not retracted, or will take up more room if retracted. Values of  $\mu$  for different runway surfaces are provided in the detailed takeoff analysis in Chapter 17.

In later stages of analysis the takeoff distance will be calculated by integrating the accelerations throughout the takeoff, considering the variations in thrust, rolling resistance, weight, drag, and lift. For initial estimation of the required wing loading, a statistical approach for estimation of takeoff distance can be used.

Figure 5.4, based upon data from Refs. 4 and 5, permits estimation of the takeoff ground roll, takeoff distance to clear a 50-ft obstacle, and FAR



After Ref. 4 and 5

Fig. 5.4 Takeoff distance estimation.

balanced field length over a 35-ft obstacle. For a military multiengine aircraft, the balanced field length over a 50-ft obstacle is approximately 5% greater than the FAR (35-ft) balanced field value.

Note that a twin-engine aircraft has a greater FAR balanced field length than a three- or four-engine aircraft with the same total thrust. This occurs because the twin-engine aircraft loses half its thrust from a single engine failure, whereas the three- and four-engine aircraft lose a smaller percentage of their total thrust from a single engine failure.

The takeoff parameter (TOP) of Fig. 5.4 is the takeoff wing loading divided by the product of the density ratio ( $\sigma$ ), takeoff lift coefficient, and takeoff thrust-to-weight (or horsepower-to-weight) ratio. The density ratio is simply the air density ( $\rho$ ) at the takeoff altitude divided by the sea level density (0.00238 slugs/cubic ft).

The takeoff lift coefficient is the actual lift coefficient at takeoff, not the maximum lift coefficient at takeoff conditions as used for stall calculation. The aircraft takes off at about 1.1 times the stall speed so the takeoff lift coefficient is the maximum takeoff lift coefficient divided by 1.21 (1.1 squared). However, takeoff (and landing) lift coefficient may also be limited by the maximum tail down angle permitted by the landing gear (typically not more than 15 deg).

To determine the required wing loading to meet a given takeoff distance requirement, the takeoff parameter is obtained from Fig. 5.4. Then the following expressions give the maximum allowable wing loading for the given takeoff distance:

$$\text{Prop: } (W/S) = (\text{TOP}) \sigma C_{L_{TO}} (\text{hp}/W) \quad (5.8)$$

$$\text{Jet: } (W/S) = (\text{TOP}) \sigma C_{L_{TO}} (T/W) \quad (5.9)$$

### Catapult Takeoff

Most Naval aircraft must be capable of operation from an aircraft carrier. For takeoff from a carrier, a catapult accelerates the aircraft to flying speed in a very short distance.

Catapults are steam-operated, and can produce a maximum force on the aircraft depending on the steam pressure used. Therefore, a light aircraft can be accelerated to a higher speed by the catapult than a heavy one. Figure 5.5 depicts the velocities attainable as a function of aircraft weight for three catapults in use by the U.S. Navy. Note that a rough guess of takeoff weight is required.

For a catapult takeoff, the airspeed as the aircraft leaves the catapult must exceed the stall speed by 10%. Airspeed is the sum of the catapult end speed ( $V_{\text{end}}$ ) and the wind-over-deck of the carrier ( $V_{\text{wod}}$ ).

For aircraft launch operations the carrier will be turned into the wind which will produce a wind-over-deck on the order of 20–40 kt. However, the design specifications for a Navy aircraft frequently require launch capabilities with zero wind-over-deck or even a negative value, to enable aircraft launch while at anchor. Once the end speed is known, the maximum wing loading is defined by:

$$\left(\frac{W}{S}\right)_{\text{landing}} = \frac{1}{2} \rho (V_{\text{end}} + V_{\text{wod}})^2 \frac{(C_{L_{\text{max}}})_{\text{takeoff}}}{1.21} \quad (5.10)$$

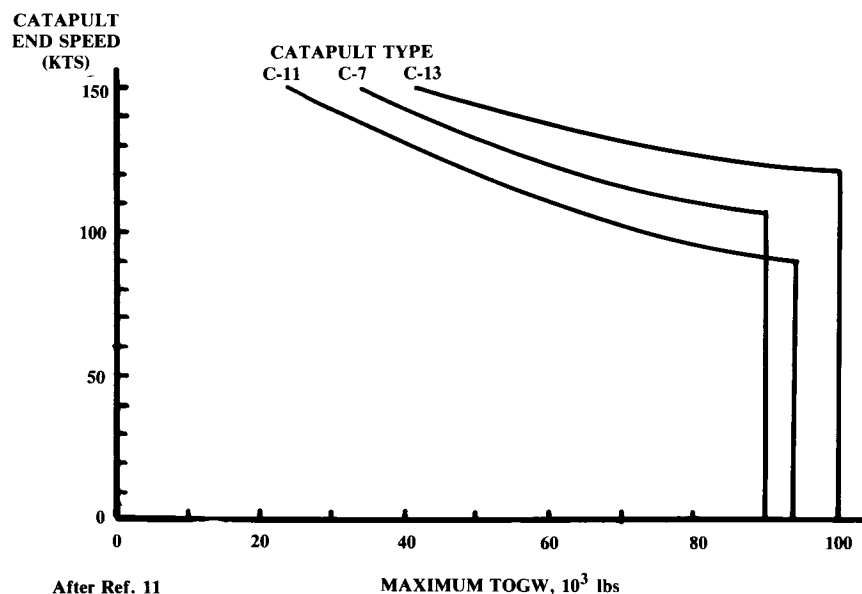


Fig. 5.5 Catapult end speeds.

### Landing Distance

There are a number of different values referred to as the "landing distance." "Landing ground roll" is the actual distance the aircraft travels from the time the wheels first touch to the time the aircraft comes to a complete stop.

The "FAR 23 landing field length" includes clearing a 50-ft obstacle while the aircraft is still at approach speed and on the approach glidepath (normally 3 deg). After crossing the obstacle, the pilot slows the aircraft to the touchdown speed of typically 1.15 times the stall speed. The obstacle-clearance distance roughly doubles the ground-roll distance alone.

The "FAR 25 landing field length" includes the 50-ft obstacle clearance at approach speed, and also adds an arbitrary two-thirds to the total distance to allow a safety margin. The landing distance definition for military aircraft is normally specified in a request for proposals (RFP), but typically resembles the FAR 23 definition.

Landing distance is largely determined by wing loading. Wing loading affects the approach speed, which must be a certain multiple of stall speed (1.3 for civil aircraft, 1.2 for military aircraft). Approach speed determines the touchdown speed, which in turn defines the kinetic energy which must be dissipated to bring the aircraft to a halt. The kinetic energy, and hence the stopping distance, varies as the square of the touchdown speed.

In fact, a reasonable first-guess of the total landing distance in feet, including obstacle clearance, is approximately 0.3 times the square of the

approach speed in knots (Ref. 5). This is approximately true for FAR 23 and military aircraft without thrust reversers, and FAR 25 aircraft with thrust reversers. While the FAR 25 aircraft have the additional requirement of a two-thirds distance increase, the thrust reversers used on most FAR 25 aircraft shorten the landing distance by about the same amount.

Equation (5.11) provides a better approximation of the landing distance, which can be used to estimate the maximum landing wing loading. The first term represents the ground roll to absorb the kinetic energy at touchdown speed. The constant term,  $S_a$ , represents the obstacle-clearance distance.

$$S_{\text{landing}} = 80 \left( \frac{W}{S} \right) \left( \frac{1}{\sigma C_{L_{\text{max}}}} \right) + S_a \quad (5.11)$$

where

$$\begin{aligned} S_a &= 1000 \text{ (airliner-type, 3-deg glideslope)} \\ &= 600 \text{ (general aviation-type power-off approach)} \\ &= 450 \text{ (STOL, 7-deg glideslope)} \end{aligned}$$

For aircraft equipped with thrust reversers or reversible-pitch propellers, multiply the ground portion of the landing [first term in Eq. (5.11)] by 0.66.

For commercial (FAR 25) aircraft, multiply the total landing distance calculated with Eq. (5.11) by 1.67 to provide the required safety margin.

The landing wing loading must be converted to takeoff conditions by dividing by the ratio of landing weight to takeoff weight. This ratio is usually not based upon the calculated end-of-mission weight, but is instead based upon some arbitrary landing weight as specified in the design requirements.

For most propeller-powered aircraft and jet trainers, the aircraft must meet its landing requirement at or near the design takeoff weight, so the ratio is about 1.0. For most jet aircraft, the landing is typically calculated at a weight of about 0.85 times the takeoff weight. Military design requirements will frequently specify full payload and some percent of fuel remaining (usually 50%) for the landing.

### Arrested Landing

Aircraft which land on Navy aircraft carriers are stopped by a cable-and-brake arrangement called "arresting gear." One of several cables strung across the flight deck is caught by a hook attached to the rear of the aircraft. The cable is attached at both ends to drum mechanisms which exert a drag upon the cable as it is pulled by the aircraft, thus stopping it in a very short distance.

For carrier-based aircraft, the approach speed (1.15 times the stall speed) is the same as the touchdown speed. Carrier pilots do not flare and slow down for landing. Instead, they are taught to fly the aircraft right into the deck, relying upon the arresting gear to make the landing. By using this technique, the aircraft has enough speed to go around if the cables are missed.

The landing weight limits for three standard arresting gears are depicted in Fig. 5.6. This figure can be used to determine the allowable approach speed based upon a first-guess of the landing weight. The approach speed divided by 1.15 defines the stall speed, which can then be used to estimate the wing loading.

### Wing Loading for Cruise

At this point we must bring in the use of two aerodynamic coefficients,  $C_{D_0}$  and “ $e$ .”  $C_{D_0}$  is the zero lift drag coefficient, and equals approximately 0.015 for a jet aircraft, 0.02 for a clean propeller aircraft, and 0.03 for a dirty, fixed-gear propeller aircraft. The Oswald efficiency factor  $e$  is a measure of drag due to lift efficiency, and equals approximately 0.6 for a fighter and 0.8 for other aircraft. These coefficients are extensively discussed in Chapter 12. Chapter 12 also contains methods for estimation of  $C_{D_0}$  and  $e$ .

To maximize range during cruise, the wing loading should be selected to provide a high  $L/D$  at the cruise conditions. The following discussion provides methods for selecting wing loading to optimize cruise range.

A propeller aircraft, which loses thrust efficiency as speed goes up, gets the maximum range when flying at the speed for best  $L/D$ , while a jet aircraft maximizes range at a somewhat higher speed where the  $L/D$  is slightly reduced. The speed for best  $L/D$  can be shown to result in parasite drag equaling the induced drag (see Chapter 17). Therefore, to maximize

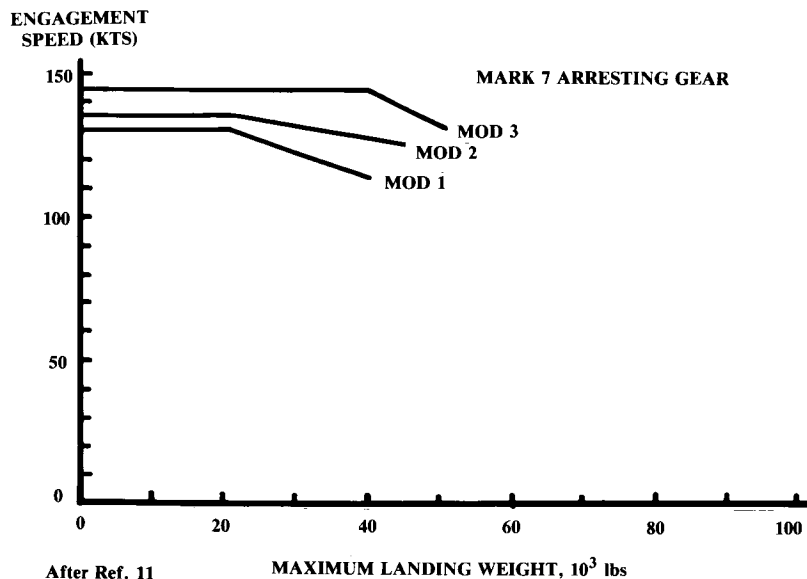


Fig. 5.6 Arresting gear weight limits.

range a propeller aircraft should fly such that:

$$qSC_{D_0} = qS \frac{C_L^2}{\pi A e} \quad (5.12)$$

During cruise, the lift equals the weight, so the lift coefficient equals the wing loading divided by the dynamic pressure. Substitution into Eq. (5.12) allows solution for the required wing loading to maximize  $L/D$  for a given flight condition. This result [Eq. (5.13)] is the wing loading for maximum range for a propeller aircraft.

$$\text{Maximum Prop Range: } W/S = q\sqrt{\pi A e C_{D_0}} \quad (5.13)$$

As the aircraft cruises, its weight reduces due to the fuel burned, so the wing loading also reduces during cruise. Optimizing the cruise efficiency while the wing loading is steadily declining requires reducing the dynamic pressure by the same percent [see Eq. (5.13)]. This can be done by reducing velocity, which is undesirable, or by climbing to obtain a lower air density. This range optimizing technique is known as a “cruise-climb.”

A jet aircraft flying a cruise-climb will obtain maximum range by flying at a wing loading such that the parasite drag is three times the induced drag (see Chapter 12 for the derivation of this relationship). This yields the following formula for wing-loading selection for range optimization of jet aircraft.

$$\text{Maximum Jet Range: } W/S = q\sqrt{\pi A e C_{D_0}/3} \quad (5.14)$$

Frequently an aircraft will not be allowed to use the cruise-climb technique to maximize range. Air Traffic Controllers prefer that aircraft maintain a single assigned altitude until given permission to climb or descend to another altitude. The pilot will attempt to obtain permission from the Air Traffic Controllers to climb several times during the flight, thus forming the characteristic “stairstep climb schedule.” This allows the thrust setting to be maintained approximately at the setting that minimizes fuel consumption.

### Wing Loading for Loiter Endurance

Most aircraft will have some loiter requirement during the mission, typically 20 min of loiter before landing. Unless the loiter requirement is a substantial fraction of the total mission duration, it is better to optimize the wing loading for cruise.

Patrol aircraft such as the ASW design example of Chapter 3 are sometimes more concerned with time on station than with cruise efficiency. Other aircraft which may be concerned with loiter endurance are airborne command posts and intelligence-gathering aircraft.

For an aircraft which must be optimized for loiter, the wing loading should be selected to provide a high  $L/D$ . For jet aircraft, the best loiter occurs at maximum  $L/D$  so Eq. (5.12) [repeated below as Eq. (5.15)] should be used. For a propeller aircraft, loiter is optimized when the induced drag is three times the parasite drag, which yields Eq. (5.16). This also provides the wing loading for minimum power required.

$$\text{Maximum Jet Loiter: } W/S = q\sqrt{\pi A e C_{D_0}} \quad (5.15)$$

$$\text{Maximum Prop Loiter: } W/S = q\sqrt{3\pi A e C_{D_0}} \quad (5.16)$$

These equations assume that the loiter velocity and altitude are known. If the loiter altitude is not specified, it should be selected for best specific fuel consumption at the loiter power setting. This is typically 30,000–40,000 ft for a jet, and the limit altitude for the turbocharger for a piston-propeller aircraft. For a nonturbocharged engine, best loiter occurs at sea level.

Usually, the loiter velocity is not specified. Instead the designer must determine the best loiter velocity and select the wing loading accordingly. This requires cross plotting of wing loadings with the resulting  $L/D$  and specific fuel consumption for various velocities and altitudes. Such a procedure is too complex for initial design purposes.

For initial design purposes, it can be assumed that the best loiter velocity will be about 150–200 knots for turboprops and jets, and about 80–120 knots for piston-props. If altitude is not specified, the altitude for best fuel consumption should be selected.

The wing loading estimated from Eqs. (5.15) or (5.16) is the average during the loiter. This must be converted to takeoff conditions by dividing the loiter wing loading by the ratio of the average loiter weight to the takeoff weight. In the absence of better information, this ratio can be assumed to be about 0.85.

Remember that Eqs. (5.15) and (5.16) are to be used for designing an aircraft optimized solely for loiter. Optimizing for loiter alone is very rare in aircraft design. For most aircraft, the wing loading will be selected for best cruise and the loiter capabilities will be a “fallout.”

### Instantaneous Turn

An aircraft designed for air-to-air dogfighting must be capable of high turn rate. This parameter,  $d\psi/dt$  or  $\dot{\psi}$ , will determine the outcome of a dogfight if the aircraft and pilots are evenly matched otherwise. When air-to-air missiles are in use, the first aircraft to turn towards the other aircraft enough to launch a missile will probably win. In a guns-only dogfight, the aircraft with the higher turn rate will be able to maneuver behind the other. A turn rate superiority of 2 deg/s is considered significant.

There are two important turn rates. The “sustained” turn rate for some flight condition is the turn rate at which the thrust of the aircraft is just sufficient to maintain velocity and altitude in the turn. If the thrust acts approximately opposite to the flight direction, then the thrust must equal the drag for a sustained turn.

If the aircraft turns at a quicker rate, the drag becomes greater than the available thrust, so the aircraft begins to slow down or lose altitude. The “instantaneous” turn rate is the highest turn rate possible, ignoring the fact that the aircraft will slow down or lose altitude.

The “load factor,” or “ $g$ -loading,” during a turn is the acceleration due to lift expressed as a multiple of the standard acceleration due to gravity ( $g = 32.2 \text{ ft/s}^2$ ). Load factor (“ $n$ ”) is equal to the lift divided by the aircraft’s weight.

Level, unturning flight implies a load factor of one ( $n = 1$ ). In a level turn, the wing must provide 1- $g$  lift in the vertical direction to hold up the aircraft, so the remaining “ $g$ ’s” available to turn the aircraft in the horizontal direction are equal to the square root of  $n$  squared minus 1 (see Fig. 17.4). Thus the radial acceleration in a level turn is  $g$  times the square root of ( $n^2 - 1$ ).

Turn rate is equal to the radial acceleration divided by the velocity. For a level turn, this results in Eq. (5.17). Note that this equation provides turn rate in radians per second, which must be multiplied by 57.3 to obtain degrees per second.

$$\dot{\psi} = \frac{g\sqrt{n^2 - 1}}{V} \quad (5.17)$$

where

$$n = \frac{qC_L}{W/S} \quad (5.18)$$

Instantaneous turn rate is limited only by the usable maximum lift, up to the speed at which the maximum lift exceeds the load-carrying capability of the wing structure. Typically, a fighter aircraft will be designed to an operational maximum load factor of 7.33  $g$ , although newer fighters are being designed to 8- or 9- $g$ . This  $g$  limit must be met at some specified combat weight.

The speed at which the maximum lift available exactly equals the allowable load factor is called the “corner speed,” and provides the maximum turn rate for that aircraft at that altitude. In a dogfight, pilots try to get to corner speed as quickly as possible as it provides the best turn rate. Typically, a modern fighter has a corner speed of about 300–350 knots indicated airspeed (i.e., dynamic pressure) regardless of altitude.

Design specifications will usually require some maximum turn rate at some flight condition. Equation (5.17) can be solved for the load factor at the specified turn rate as follows:

$$n = \sqrt{\left(\frac{\dot{\psi}V}{g}\right)^2 + 1} \quad (5.19)$$

If this value of load factor is greater than the ultimate load factor specified in the design requirements, somebody has made a mistake. The required wing loading can be solved for in Eq. (5.18) as follows:

$$\frac{W}{S} = \frac{qC_{L_{\max}}}{n} \quad (5.20)$$

The only unknown is the maximum lift coefficient at combat conditions. This is not the same as the maximum lift coefficient for landing. During combat, use of full flap settings is not usually possible. Also, there is a Mach-number effect which reduces maximum lift at higher speeds. Fre-

quently the combat maximum usable lift will be limited by buffeting or controllability considerations.

For initial design purposes, a combat maximum lift coefficient of about 0.6–0.8 should be assumed for a fighter with only a simple trailing-edge flap for combat. For a fighter with a complex system of leading- and trailing-edge flaps which can be deployed during combat, a maximum usable lift coefficient of about 1.0–1.5 is attainable. Chapter 12 provides better methods of estimating the maximum lift coefficient.

Again, the resulting wing loading must be divided by the ratio of combat weight to takeoff weight to obtain the required takeoff wing loading. Usually the combat weight is specified as the aircraft design takeoff weight with any external fuel tanks dropped and 50% of the internal fuel gone. This is approximately 0.85 times the takeoff weight for most fighters.

The resulting wing loading is the maximum which will allow the required instantaneous turn.

### Sustained Turn

The sustained turn rate is also important for success in combat. If two aircraft pass each other in opposite directions, it will take them about 10 seconds to complete 180-deg turns back towards the other. The aircraft will probably not be able to maintain speed while turning at the maximum instantaneous rate. If one of the aircraft slows down below corner speed during this time it will be at a turn rate disadvantage to the other, which could prove fatal.

Sustained turn rate is usually expressed in terms of the maximum load factor at some flight condition that the aircraft can sustain without slowing or losing altitude. For example, the ability for sustaining 4- or 5-g at 0.9 Mach number at 30,000 ft is frequently specified. Equations (5.17) or (5.19) can be used to relate turn rate to load factor.

If speed is to be maintained, the thrust must equal the drag (assuming that the thrust axis is approximately aligned with the flight direction). The lift must equal the weight times the load factor, so we can write:

$$n = (T/W) (L/D) \quad (5.21)$$

Sustained—turn load factor is maximized by maximizing the  $T/W$  and  $L/D$ . The highest  $L/D$  occurs when the induced drag equals the parasite drag, as expressed by Eq. (5.12). During a turn, the lift equals the weight times  $n$ , so the lift coefficient equals the wing loading times  $n$  divided by the dynamic pressure. Substitution into Eq. (5.12) yields:

$$W/S = \frac{q}{n} \sqrt{\pi A e C_{D0}} \quad (5.22)$$

This equation gives the wing loading that maximizes the sustained turn rate at a given flight condition. Note that if  $n$  equals one, Eq. (5.22) is the same as Eq. (5.13), the wing loading for best  $L/D$  in level flight.

Equation (5.22) estimates the wing loading that maximizes the sustained turn rate regardless of thrust available. This equation will frequently give

ridiculously low values of wing loading that will provide the required sustained turn rate using only a fraction of the available thrust.

The wing loading to exactly attain a required sustained load factor  $n$  using all of the available thrust can be determined by equating the thrust and drag, and using the fact that since lift equals weight times  $n$ , the lift coefficient during maneuver equals the wing loading times  $n$ , divided by the dynamic pressure. This yields Eq. (5.23).

$$T = q S C_{D0} + q S \left( \frac{C_L^2}{\pi A e} \right) = q S C_{D0} + \frac{n^2 W^2}{q S \pi A e} \quad (5.23)$$

or

$$\frac{T}{W} = \frac{q C_{D0}}{W/S} + \frac{W}{S} \left( \frac{n^2}{q \pi A e} \right) \quad (5.24)$$

Equation (5.24) can be solved for  $W/S$  to yield the wing loading that exactly attains a required sustained load factor  $n$  [Eq. (5.25)]. Also, Eq. (5.24) can be used later to recheck the  $T/W$  after the wing loading is selected.

$$\frac{W}{S} = \frac{(T/W) \pm \sqrt{(T/W)^2 - (4n^2 C_{D0}/\pi A e)}}{2n^2/q \pi A e} \quad (5.25)$$

The thrust-to-weight ratio for this calculation is at combat conditions, so the takeoff  $T/W$  must be adjusted to combat conditions by dividing by the ratio between combat and takeoff weight, and by multiplying by the ratio between combat thrust and takeoff thrust.

If the term within the square root in Eq. (5.25) becomes negative, there is no solution. This implies that, at a given load factor, the following must be satisfied regardless of the wing loading:

$$\frac{T}{W} \geq 2n \sqrt{\frac{C_{D0}}{\pi A e}} \quad (5.26)$$

It is very important to realize in these calculations that the efficiency factor  $e$ , is itself a function of the lift coefficient at which the aircraft is operating. This is due to the separation effects at higher lift coefficients that increase drag above the parabolic drag polar values. At high angles of attack the  $e$  value may be reduced by 30% or more.

Unfortunately, the above equations for turning flight are very sensitive to the  $e$  value. If these equations yield  $W/S$  values far from historical values, the  $e$  value is probably unrealistic and the calculated  $W/S$  values should be ignored. Methods in Chapter 12 will better account for the separation effects.

### Climb and Glide

Appendix A.5 cites numerous climb requirements for FAR or military aircraft. These specify rate of climb for various combinations of factors

such as engine-out, landing-gear position, and flap settings. While the details may vary, the method for selecting a wing loading to satisfy such requirements is the same.

Rate of climb is a vertical velocity, typically expressed in feet-per-minute (which must be converted to feet-per-second for the following calculations). Climb gradient, “ $G$ ,” is the ratio between vertical and horizontal distance traveled. As will be shown in Chapter 17, at normal climb angles the climb gradient equals the excess thrust divided by the weight, i.e.—

$$G = (T - D)/W \quad (5.27)$$

or

$$\frac{D}{W} = \frac{T}{W} - G \quad (5.28)$$

$D/W$  can also be expressed as in Eq. (5.29), where in the final expression the lift coefficient is replaced by  $(W/qS)$ .

$$\frac{D}{W} = \frac{qSC_{D0} + qS(C_L^2/\pi Ae)}{W} = \frac{qC_{D0}}{W/S} + \frac{W}{S} \frac{1}{q\pi Ae} \quad (5.29)$$

Equating Eqs. (5.28) with (5.29) and solving for wing loading yields:

$$\frac{W}{S} = \frac{[(T/W) - G] \pm \sqrt{[(T/W) - G]^2 - (4C_{D0}/\pi Ae)}}{2/q\pi Ae} \quad (5.30)$$

Note the similarity to Eq. (5.25). Equation (5.30) is merely Eq. (5.25) for a load factor of 1.0, with the  $(T/W)$  term replaced by  $[(T/W) - G]$ . As before,  $T/W$  must be ratioed to the flight conditions and weight under consideration. The resulting  $W/S$  must then be ratioed to a takeoff-weight value.

The term within the square root symbol in Eq. (5.30) cannot go below zero, so the following must be true regardless of the wing loading:

$$\frac{T}{W} \geq G + 2 \sqrt{\frac{C_{D0}}{\pi Ae}} \quad (5.31)$$

This equation says that no matter how “clean” your design is, the  $T/W$  must be greater than the desired climb gradient! [ $T/W$  for a propeller aircraft was defined in Eq. (5.1).]

Another implication of this equation is that a very “clean” aircraft that cruises at a high speed despite a very low  $T/W$  will probably climb poorly. A 200-mph airplane that flies on 20 hp can’t be expected to climb as well as an airplane that requires 200 hp to reach 200 mph (unless the latter weighs ten times as much).

$C_{D0}$  and  $e$  values for some of the climb conditions specified in Appendix A.5 must include the effects of flaps and landing gear. Chapter 12 will

provide methods for estimating these effects; but for now, approximations can be used.

For takeoff flap settings,  $C_{D0}$  will increase by about 0.02 and  $e$  will decrease about 5%. For landing flap settings,  $C_{D0}$  will increase by about 0.07 and  $e$  will decrease by about 10% relative to the no-flap value. Retractable landing gear in the down position will increase  $C_{D0}$  by about 0.02 (Ref. 7).

Sometimes the rate of climb must also be calculated with one engine windmilling or stopped. The thrust loss due to a “dead” engine can be accounted for in the  $T/W$ . For example, if a three-engined aircraft loses one engine, the  $T/W$  becomes two-thirds of the original  $T/W$ .

The drag increase due to a windmilling or stopped engine will further reduce the climb rate. Chapter 12 provides methods for estimating this drag. For rough initial analysis, however, it can probably be ignored.

Equation (5.30) can also be used to establish the wing loading required to attain some specified glide angle, by setting  $T/W$  to zero and using a negative value of  $G$  (i.e., a glide in the negative direction). If a particular sink rate must be attained, the value of  $G$  to use is the sink rate divided by the forward velocity. Make sure that both are in the same units.

### Maximum Ceiling

Equation (5.30) can be used to calculate the wing loading to attain some maximum ceiling, given the  $T/W$  at those conditions. The climb gradient  $G$  can be set to zero to represent level flight at the desired altitude. Frequently a small residual climb capability, such as 100 ft/min, is required at maximum ceiling. This can be included in Eq. (5.30) by first solving for the climb gradient  $G$  (climb rate divided by forward velocity).

For a high-altitude aircraft such as an atmospheric research or reconnaissance plane, the low dynamic pressure available may determine the minimum possible wing loading. For example, at 100,000 ft and 0.8 Mach number, the dynamic pressure is only 10 psi. Equation (5.13) [repeated below as Eq. (5.32)] can be used to determine the wing loading for minimum power.

$$W/S = q\sqrt{\pi AeC_{D0}} \quad (5.32)$$

This may suggest a wing loading so low as to be impractical, and so should be compared with the wing loading required to fly at a given lift coefficient, i.e.:

$$W/S = qC_L \quad (5.33)$$

For efficiency during high-altitude cruise, the lift coefficient should be near the airfoil design lift coefficient. For a typical airfoil, this is about 0.5. For a high-altitude aircraft, new high-lift airfoils with design lift coefficients on the order of 1.0–1.4 can be used.

### 5.4 SELECTION OF THRUST-TO-WEIGHT AND WING LOADING

An initial estimate of the thrust-to-weight (or horsepower-to-weight) ratio was previously made. From the wing loadings estimated above, the lowest

value should be selected to ensure that the wing is large enough for all flight conditions. Don't forget to convert all wing loadings to takeoff conditions prior to comparisons.

A low wing-loading will always increase aircraft weight and cost. If a very low wing-loading is driven by only one of the requirements, a change in design assumptions (such as a better high-lift system) may allow a higher wing-loading.

Also, keep in mind that the wing loadings calculated by Eqs. (5.13–5.16), and Eqs. (5.22) and (5.32) are aerodynamic optimizations for only a portion of the mission. If these give wing loadings far lower than those in Table 5.5, they may be ignored.

When the best compromise for wing loading has been selected, the thrust-to-weight ratio should be rechecked to ensure that all requirements are still met. The equations in the last section which use  $T/W$  should be recalculated with the selected  $W/S$  and  $T/W$ . Only then can the next step of design, initial sizing, be initiated.

### 6.1 INTRODUCTION

Aircraft sizing is the process of determining the takeoff gross weight and fuel weight required for an aircraft concept to perform its design mission. Sizing was introduced in Chapter 3, in which a quick method based upon minimal information about the design was used to estimate the sizing parameters. That sizing method was limited to fairly simple design missions. This chapter presents a more refined method capable of dealing with most types of aircraft-sizing problems.

An aircraft can be sized using some existing engine or a new design engine. The existing engine is fixed in size and thrust, and is referred to as a “fixed-engine” (“fixed” refers to engine size).

The new design engine can be built in any size and thrust required, and is called a “rubber engine” because it can be “stretched” during the sizing process to provide any required amount of thrust.

Rubber-engine sizing is used during the early stages of an aircraft development program that is sufficiently important to warrant the development of an all-new engine. This is generally the case for a major military fighter or bomber program, and is sometimes the case for a transport-aircraft project such as the SST.

In these cases, the designer will use a rubber engine in the early stages of design, and then, with the customer, tell the engine company what characteristics the new engine should have. When the engine company finalizes the design for the new engine, it becomes fixed in size and thrust. The aircraft concept will then be finalized around this now-fixed engine.

Developing a new jet engine costs on the order of a billion dollars. Developing and certifying a new piston engine is also very expensive. Most aircraft projects do not rate development of a new engine, and so must rely on selecting the best of the existing engines. However, even projects which must use an existing engine may begin with a rubber-engine design study to determine what characteristics to look for in the selection of an existing engine.

The rubber engine can be scaled to any thrust so the thrust-to-weight ratio can be held to some desired value even as the aircraft weight is varied. The rubber-engine sizing approach allows the designer to size the aircraft to meet both performance and range goals, by solving for takeoff gross weight while holding the thrust-to-weight ratio required to meet the performance objectives. As the weight varies, the rubber-engine is scaled up or down as required.

This is not possible for fixed-engine aircraft sizing. When a fixed size engine is used, either the mission range or the performance of the aircraft must become a fallout parameter.

For example, if a certain rate of climb must be attained, then the thrust-to-weight ratio cannot be allowed to fall to an extremely low value. If the calculation of the takeoff gross weight required for the desired range indicates that the weight is much higher than expected, then either the range must be reduced or the rate of climb must be relaxed.

A typical example of this is the would-be homebuilder who got a good buy on a Lycoming O-320, and is designing an aircraft around that 150-hp engine. If the sizing results say that a bigger engine is required, the homebuilder will change the sizing requirements!

## 6.2 RUBBER-ENGINE SIZING

### Review of Sizing

Chapter 3 presented a quick method of sizing an aircraft using a configuration sketch and the selected aspect ratio. From this information a crude estimate of the maximum  $L/D$  was obtained. Using approximations of the specific fuel consumption, the changes in weight due to the fuel burned during cruise and loiter mission segments were estimated, expressed as the mission-segment weight fraction ( $W_{i+1}/W_i$ ). Using these fractions and the approximate fractions for takeoff, climb, and landing which were provided in Table 3.2, the total mission weight fraction ( $W_x/W_0$ ) was estimated.

For different classes of aircraft, statistical equations for the aircraft empty-weight fraction were provided in Table 3.1. Then, the takeoff weight was calculated using Eq. (3.4), repeated below as Eq. (6.1).

Since the empty weight was calculated using a guess of the takeoff weight, it was necessary to iterate towards a solution. This was done by calculating the empty-weight fraction from an initial guess of the takeoff weight and using Eq. (6.1) to calculate the resulting takeoff weight. If the calculated takeoff weight did not equal the initial guess, a new guess was made somewhere between the two.

$$W_0 = \frac{W_{\text{crew}} + W_{\text{payload}}}{1 - (W_f/W_0) - (W_e/W_0)} \quad (6.1)$$

where

$$\frac{W_f}{W_0} = 1.06 \left( 1 - \frac{W_x}{W_0} \right) \quad (6.2)$$

Equation (6.1) is limited in use to missions which do not have a sudden weight change, such as a payload drop. Also, in many cases Eq. (6.1) cannot be used for fixed-engine sizing.

### Refined Sizing Equation

For missions with a payload drop or other sudden weight change, a slightly different sizing equation must be used. The takeoff weight is calcu-

Table 6.1 Empty weight fraction vs  $W_0$ ,  $A$ ,  $T/W_0$ ,  $W_0/S$ , and  $M_{\text{max}}$

	$W_e/W_0 = (a + bW_0^{C1}A^{C2}(T/W_0)^{C3}(W_0/S)^{C4}M_{\text{max}}^{C5})K_{VS}$						
	$a$	$b$	$C1$	$C2$	$C3$	$C4$	$C5$
Jet trainer	0	4.28	-0.10	0.10	0.20	-0.24	0.11
Jet fighter	-0.02	2.16	-0.10	0.20	0.04	-0.10	0.08
Military cargo/bomber	0.07	1.71	-0.10	0.10	0.06	-0.10	0.05
Jet transport	0.32	0.66	-0.13	0.30	0.06	-0.05	0.05

$K_{VS}$  = variable sweep constant = 1.04 if variable sweep

= 1.00 if fixed sweep

lated by summing the crew weight, payload weight, fuel weight, and empty weight. This is shown in Eq. (6.2), which resembles Eq. (3.1) except that the payload now includes a fixed payload and a dropped payload. The empty weight is again expressed as an empty-weight fraction, but the fuel weight is determined directly.

$$W_0 = W_{\text{crew}} + W_{\text{fixed payload}} + W_{\text{dropped payload}} + W_{\text{fuel}} + W_{\text{empty}} \quad (6.3)$$

or

$$W_0 = W_{\text{crew}} + W_{\text{fixed payload}} + W_{\text{dropped payload}} + W_{\text{fuel}} + \left( \frac{W_e}{W_0} \right) W_0 \quad (6.4)$$

As before, an initial guess of the takeoff weight is used to determine a calculated takeoff weight, and the solution is iterated until the two are approximately equal to within a few percent. Refined methods for determining the empty-weight fraction and fuel used are discussed below.

### Empty-Weight Fraction

The empty-weight fraction is estimated using improved statistical equations. Tables 6.1 and 6.2 were prepared using data from Ref. 1 to provide

Table 6.2 Empty weight fraction vs  $W_0$ ,  $A$ ,  $\text{hp}/W_0$ ,  $W_0/S$ , and  $V_{\text{max}}$  (mph)

	$W_e/W_0 = a + bW_0^{C1}A^{C2}(\text{hp}/W_0)^{C3}(W_0/S)^{C4}V_{\text{max}}^{C5}$						
	$a$	$b$	$C1$	$C2$	$C3$	$C4$	$C5$
Sailplane—unpowered	0	0.75	-0.05	0.14	0	-0.30	0.06
Sailplane—powered	0	1.20	-0.04	0.14	0.19	-0.20	0.05
Homebuilt—metal/wood	0	0.69	-0.10	0.05	0.10	-0.05	0.17
Homebuilt—composite	0	0.59	-0.10	0.05	0.10	-0.05	0.17
General aviation—single engine	-0.25	1.14	-0.20	0.08	0.05	-0.05	0.27
General aviation—twin engine	-0.90	1.32	-0.10	0.08	0.05	-0.05	0.20
Agricultural aircraft	0	1.64	-0.14	0.07	0.10	-0.10	0.11
Twin turboprop	0.37	0.08	-0.06	0.08	0.08	-0.05	0.30
Flying boat	0	0.41	-0.01	0.10	0.05	-0.12	0.18



empty-weight equations which better reflect the weight impact of the major design variables. These are the aspect ratio, thrust-to-weight (or horsepower-to-weight) ratio, wing loading, and maximum speed.

The equations of Tables 6.1 and 6.2 result in a much better statistical fit, with only about half the standard deviation of the equations in Table 3.1. However, these equations should not be used to conduct design trade studies for one particular aircraft. That must be done using the component weight buildup methods in Chapter 15.

### Fuel Weight

The remaining unknown in Eq. (6.4) is the fuel weight. Previously this was estimated as a fuel fraction by determining the ratio between the weight at the end of the mission and the takeoff weight ( $W_x/W_0$ ). As the only weight loss during the mission was due to fuel usage, the fuel fraction was found simply as  $(1 - W_x/W_0)$ . This cannot be assumed if the mission includes a weight drop.

If the mission includes a weight drop, it is necessary to actually calculate the weight of the fuel burned during every mission leg, and sum for the total mission fuel. The mission segment weight fractions ( $W_i/W_{i-1}$ ) are calculated as before for all mission segments other than those which are weight drops. For each mission segment, the fuel burned is then equal to:

$$W_{fi} = \left(1 - \frac{W_i}{W_{i-1}}\right) W_i \quad (6.5)$$

The total mission fuel,  $W_{fm}$ , then is equal to:

$$W_{fm} = \sum_1^x W_{fi} \quad (6.6)$$

The total aircraft fuel includes the mission fuel as well as an allowance for reserve and trapped fuel. This reserve fuel allowance is usually 5%, and accounts for an engine with poorer-than-normal fuel consumption. An additional allowance of 1% for trapped (i.e., unusable) fuel is typical. Thus, the total aircraft fuel is:

$$W_f = 1.06 \left( \sum_1^x W_{fi} \right) \quad (6.7)$$

The methods used for estimating the mission segment weight fractions are presented below. These are a combination of analytical and statistical methods, similar to the methods used in Chapter 3.

### Engine Start, Taxi, and Takeoff

As before, the mission segment weight fraction for engine start, taxi, and takeoff is estimated historically. A reasonable estimate is:

$$W_1/W_0 = 0.97-0.99 \quad (6.8)$$

### Climb and Accelerate

From data in Ref. 10, the weight fraction for an aircraft climbing and accelerating to cruise altitude and Mach number " $M$ ," (starting at Mach 0.1), will be approximately as follows:

$$\text{Subsonic: } W_i/W_{i-1} = 1.0065 - 0.0325M \quad (6.9)$$

$$\text{Supersonic: } W_i/W_{i-1} = 0.991 - 0.007M - 0.01M^2 \quad (6.10)$$

For an acceleration beginning at other than Mach 0.1, the weight fraction calculated by Eqs. (6.9) or (6.10) for the given ending Mach number should be divided by the weight fraction calculated for the beginning Mach number using Eqs. (6.9) or (6.10).

For example, acceleration from Mach 0.1–0.8 requires a weight fraction of about 0.9805, whereas acceleration from Mach 0.1–2.0 requires a weight fraction of 0.937. To accelerate from Mach 0.8–2.0 would require a weight fraction of  $(0.937/0.9805)$ , or 0.956.

### Cruise

Equation (3.6), repeated below as Eq. (6.11), is derived from the Breguet range equation for cruise as derived in Chapter 17. For propeller aircraft, the specific fuel consumption " $C$ " is calculated from the propeller specific fuel consumption ( $C_p$  or  $C_{bhp}$ ) using Eq. (3.10). Substitution of Eq. (3.10) into Eq. (6.11) yields Eq. (6.12).

$$\text{Jet: } \frac{W_i}{W_{i-1}} = \exp \frac{-RC}{V(L/D)} \quad (6.11)$$

where

- $R$  = range
- $C$  = specific fuel consumption
- $V$  = velocity
- $L/D$  = lift-to-drag ratio

$$\text{Prop: } \frac{W_i}{W_{i-1}} = \exp \left[ \frac{-RC_{bhp}}{550 \eta_p (L/D)} \right] \quad (6.12)$$

where  $\eta_p$  = propeller efficiency.

During cruise and loiter, the lift equals the weight, so the  $L/D$  can be expressed as the inverse of the drag divided by the weight:

$$\frac{L}{D} = \frac{1}{\frac{qC_{D0}}{W/S} + \frac{W}{S} \frac{1}{q\pi Ae}} \quad (6.13)$$

Note that the wing loading used in Eq. (6.13) and subsequent weight fraction equations is the actual wing loading at the condition being evaluated, not the takeoff wing loading.

### Loiter

Repeating Eq. (3.8), the weight fraction for a loiter mission segment is:

$$\text{Jet: } \frac{W_i}{W_{i-1}} = \exp \frac{-EC}{L/D} \quad (6.14)$$

where  $E$  = endurance or loiter time.

(Note—watch the units!) Substitution of Eq. (3.10) into Eq. (6.14) yields:

$$\text{Prop: } \frac{W_i}{W_{i-1}} = \exp \frac{-EVC_{bhp}}{550 \eta_p (L/D)} \quad (6.15)$$

### Combat

The combat mission leg is normally specified as either a time duration (“ $d$ ”) at maximum power (typically  $d = 3$  min), or as a certain number of combat turns at maximum power at some altitude and Mach number. The weight of the fuel burned is equal to the product of thrust, specific fuel consumption, and duration of the combat, so the mission segment weight fraction is:

$$W_i/W_{i-1} = 1 - C(T/W)(d) \quad (6.16)$$

Note that the  $T/W$  is defined at combat weight and thrust, not at takeoff conditions. Again, watch the units, especially the time units.

If the combat is defined by some number of turns, the duration of combat ( $d$ ) must be calculated. The time to complete “ $x$ ” turns is the total number of radians to turn divided by the turn rate. When combined with Eq. (5.17), this yields:

$$d = \frac{2\pi x}{\dot{\psi}} = \frac{2\pi Vx}{g\sqrt{n^2 - 1}} \quad (6.17)$$

The load factor “ $n$ ” for a sustained combat turn is found by assuming that the thrust angle is approximately aligned with the flight direction, so the thrust must equal the drag. The lift must equal the weight times the load factor  $n$ , which yields:

$$n = (T/W)(L/D) \quad (6.18)$$

This is subject to the constraints of maximum structural load factor [Eq. (6.19)] and maximum available lift [Eq. (6.20)].

$$n \leq n_{\max} \quad (6.19)$$

$$n \leq \frac{qC_{L\max}}{W/S} \quad (6.20)$$

The lift-to-drag ratio is found by including the load factor term into Eq. (6.13), which results in Eq. (6.21). The changes to  $C_{D0}$  and  $e$  at combat conditions which were discussed in the last chapter should be used in Eq. (6.21).

$$\frac{L}{D} = \frac{1}{q \frac{C_{D0}}{n(W/S)} + \frac{n(W/S)}{q\pi Ae}} \quad (6.21)$$

### Descent for Landing

Descent is estimated historically:

$$W_i/W_{i-1} = 0.990 \text{ to } 0.995 \quad (6.22)$$

### Landing and Taxi Back

Again, a historical approximation is used.

$$W_i/W_{i-1} = 0.992 \text{ to } 0.997 \quad (6.23)$$

### Summary of Refined Sizing Method

The design and sizing method presented above, as summarized in Fig. 6.1, resembles in many respects the first-order method presented as Fig. 3.7,

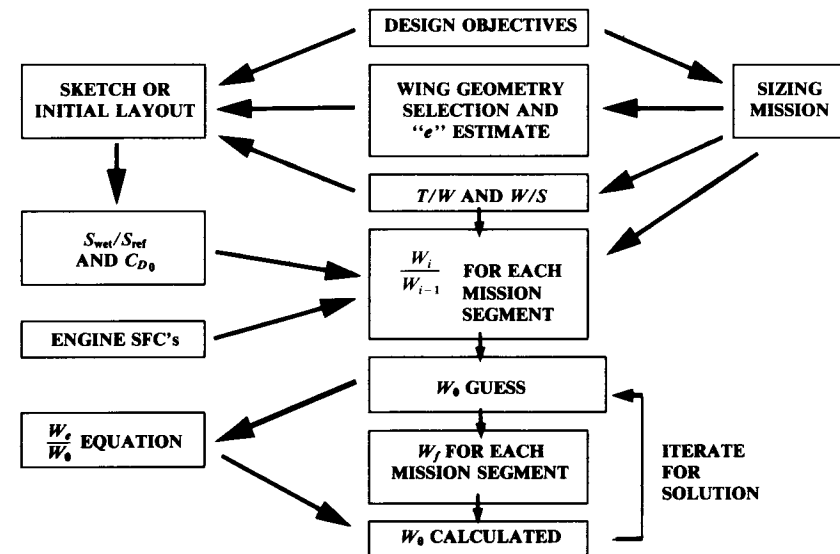


Fig. 6.1 Refined sizing method.

but makes use of more sophisticated analytical techniques and also permits sizing to missions which include weight drops.

From the design objectives and sizing mission, the wing geometry can be selected and an estimate of  $e$  obtained. A conceptual sketch or initial layout is used to estimate the wetted-area ratio, from which  $C_{D_0}$  is estimated. (Remember that  $e$  and  $C_{D_0}$  will be reduced during high-lift, combat conditions).

The methods of the previous chapter are used to select initial values for thrust-to-weight (or horsepower-to-weight) ratio and wing loading. Then the methods of this chapter are used along with engine data to determine the mission-segment weight fractions for each leg of the design mission.

The iteration for takeoff gross weight (" $W_0$ ") begins with an initial guess as to  $W_0$ , and then the aircraft weight is calculated throughout the mission. For each mission leg, the aircraft weight will be reduced by either the weight of fuel burned or the payload weight dropped. Also, the total fuel burned is summed throughout the mission. Equations (6.7) and (6.4) are then used, along with a statistical empty weight fraction estimation, to arrive at a calculated  $W_0$ .

If this does not equal the guessed value for  $W_0$ , a new guess for  $W_0$  is selected between the two values. Experience indicates that the solution will converge most rapidly if the new guess for  $W_0$  is about three-fourths of the way from the initial guess to the calculated  $W_0$  value.

This procedure is less complicated than it sounds. Examples can be found in Chapter 21.

(An alternative sizing method starts with a  $W_0$  guess, and then subtracts the payload weight, crew weight, and calculated fuel weight to arrive at the "empty weight required" to perform the mission. This is compared to the statistical "empty weight available." If the empty weight required exceeds the empty weight available, then  $W_0$  must be increased for the next iteration. This method is mathematically identical to the method presented above, but provides less-obvious guidance as to the next value of  $W_0$  to use for iteration.)

### 6.3 FIXED-ENGINE SIZING

The sizing procedure for the fixed-size engine is similar to the rubber-engine sizing, with several exceptions. These result from the fact that either the mission range or the performance must be considered a fallout parameter, and allowed to vary as the aircraft is sized.

If the range is allowed to vary, the sizing problem is very simple. The required thrust-to-weight ratio ( $T/W$ ) is determined as in the last section to provide all required performance capabilities, using the known characteristics of the selected engine. Then the takeoff gross weight is determined as the total engine takeoff thrust divided by the required takeoff thrust-to-weight ratio.

$$W_0 = \frac{NT_{\text{per engine}}}{(T/W)} \quad (6.24)$$

where  $N$  = number of engines.

With the takeoff weight known, the range capability can be determined from Eq. (6.4) using a modified iteration technique. The known takeoff weight is repeatedly used as the "guess"  $W_0$ , and the range for one or more cruise legs is varied until the calculated  $W_0$  equals the known  $W_0$ .

This technique can also be used to vary mission parameters other than range. For example, a research aircraft may be sized for a certain radius (range out and back) with the number of minutes of test time as the variable parameter.

If some range requirement must be satisfied, then performance must be the fallout. The takeoff gross weight will be set by fuel requirements, and the fixed-size engine may not necessarily provide the thrust-to-weight ratio desired for performance considerations.

In this case the takeoff gross weight can be solved by iteration of Eq. (6.4) as for the rubber-engine case, with one major exception. The thrust-to-weight ratio is now permitted to vary during the sizing iterations. Equation (6.16) cannot be used for determining a weight fraction for combat mission legs as it assumes a known  $T/W$ .

Instead, the fuel burned during combat by a fixed-size engine is treated as a weight drop. For a given engine, the fuel burned during a combat leg of duration  $d$  is simply the thrust times the specific fuel consumption times the duration:

$$W_f = CTd \quad (6.25)$$

The weight of fuel calculated by Eq. (6.25) is treated as a weight drop in the iterations to solve Eq. (6.4). Once the takeoff gross weight is determined, the resulting thrust-to-weight ratio must be used to determine the actual aircraft performance for the requirements evaluated in the last chapter. If the requirements are not met, then either your aircraft design is not very good or the requirements are too tough!

### 6.4 GEOMETRY SIZING

#### Fuselage

Once the takeoff gross weight has been estimated, the fuselage, wing, and tails can be sized. Many methods exist to initially estimate the required fuselage size.

For certain types of aircraft, the fuselage size is determined strictly by "real-world constraints." For example, a large passenger aircraft devotes most of its length to the passenger compartment. Once the number of passengers is known and the number of seats across is selected, the fuselage length and diameter are essentially determined.

For initial guidance during fuselage layout and tail sizing, Table 6.3 provides statistical equations for fuselage length developed from data provided in Ref. 1. These are based solely upon takeoff gross weight, and give remarkably good correlations to most existing aircraft.

Fuselage fineness ratio is the ratio between the fuselage length and its maximum diameter. If the fuselage cross section is not a circle, an equivalent diameter is calculated from the cross-sectional area.

Table 6.3 Fuselage length vs  $W_0$ 

Length = $aW_0^C$	$a$	$C$
Sailplane—unpowered	0.86	0.48
Sailplane—powered	0.71	0.48
Homebuilt—metal/wood	3.68	0.23
Homebuilt—composite	3.50	0.23
General aviation—single engine	4.37	0.23
General aviation—twin engine	0.86	0.42
Agricultural aircraft	4.04	0.23
Twin turboprop	0.37	0.51
Flying boat	1.05	0.40
Jet trainer	0.79	0.41
Jet fighter	0.93	0.39
Military cargo/bomber	0.23	0.50
Jet transport	0.67	0.43

Theoretically, for a fixed internal volume the subsonic drag is minimized by a fineness ratio of about 3.0 while supersonic drag is minimized by a fineness ratio of about 14. Most aircraft fall between these values.

A historically-derived fuselage fineness ratio can be used, along with the length estimate, to develop the initial fuselage layout. However, “real-world constraints” such as payload envelope must take priority. For most design efforts the realities of packaging the internal components will establish the fuselage length and diameter.

### Wing

The actual wing size can now be determined simply as the takeoff gross weight divided by the takeoff wing loading. Remember that this is the reference area of the theoretical, trapezoidal wing, and includes the area extending into the aircraft centerline.

### Tail Volume Coefficient

For the initial layout, a historical approach is used for the estimation of tail size. The effectiveness of a tail in generating a moment about the center of gravity is proportional to the force (i.e., lift) produced by the tail and to the tail moment arm.

The primary purpose of a tail is to counter the moments produced by the wing. Thus, it would be expected that the tail size would be in some way related to the wing size. In fact, there is a directly proportional relationship between the two, as can be determined by examining the moment equations presented in Chapter 16. Therefore, the tail area divided by the wing area should show some consistent relationship for different aircraft, if the effects of tail moment arm could be accounted for.

The force due to tail lift is proportional to the tail area. Thus, the tail effectiveness is proportional to the tail area times the tail moment arm. This

product has units of volume, which leads to the “tail volume coefficient” method for initial estimation of tail size.

Rendering this parameter nondimensional requires dividing by some quantity with units of length. For a vertical tail, the wing yawing moments which must be countered are most directly related to the wing span  $b_w$ . This leads to the “vertical tail volume coefficient,” as defined by Eq. (6.26). For a horizontal tail or canard, the pitching moments which must be countered are most directly related to the wing mean chord ( $\bar{C}_w$ ). This leads to the “horizontal tail volume coefficient,” as shown by Eq. (6.27).

$$c_{VT} = \frac{L_{VT}S_{VT}}{b_w S_w} \quad (6.26)$$

$$c_{HT} = \frac{L_{HT}S_{HT}}{\bar{C}_w S_w} \quad (6.27)$$

Note that the moment arm ( $L$ ) is commonly approximated as the distance from the tail quarter-chord (i.e., 25% of the mean chord length measured back from the leading edge of the mean chord) to the wing quarter-chord.

The definition of tail moment arm is shown in Fig. 6.2, along with the definitions of tail area. Observe that the horizontal tail area is commonly measured to the aircraft centerline, while a canard's area is commonly considered to include only the exposed area. If twin vertical tails are used, the vertical tail area is the sum of the two.

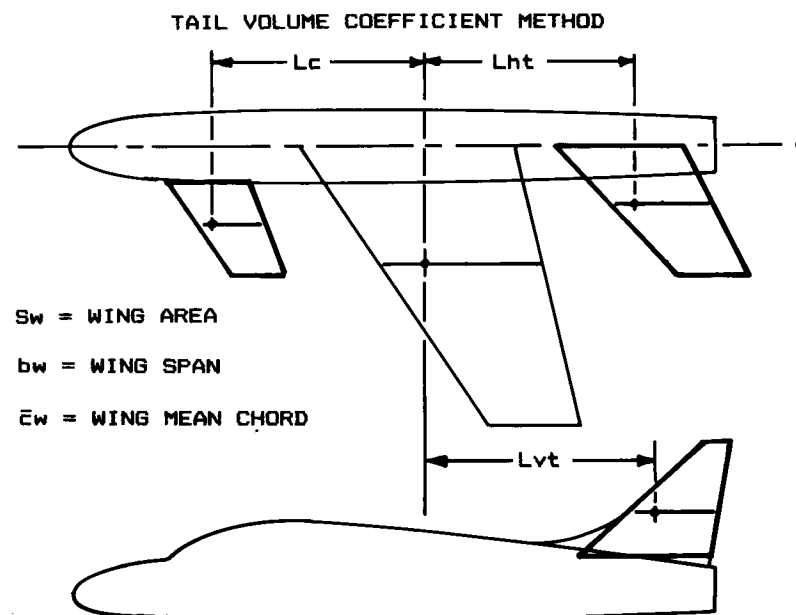


Fig. 6.2 Initial tail sizing.

Table 6.4 Tail volume coefficient

	Typical values	
	Horizontal $c_{HT}$	Vertical $c_{VT}$
Sailplane	0.50	0.02
Homebuilt	0.50	0.04
General aviation—single engine	0.70	0.04
General aviation—twin engine	0.80	0.07
Agricultural	0.50	0.04
Twin turboprop	0.90	0.08
Flying boat	0.70	0.06
Jet trainer	0.70	0.06
Jet fighter	0.40	0.07
Military cargo/bomber	1.00	0.08
Jet transport	1.00	0.09

Table 6.4 provides typical values for volume coefficients for different classes of aircraft. These values (conservative averages based upon data in Refs. 1 and 11), are used in Eqs. (6.28) or (6.29) to calculate tail area.

(Incidentally, Ref. 11 compiles a tremendous amount of aircraft data and is highly recommended for every designer's library.)

$$S_{VT} = c_{VT} b_W S_W / L_{VT} \quad (6.28)$$

$$S_{HT} = c_{HT} \bar{C}_W S_W / L_{HT} \quad (6.29)$$

To calculate tail size, the moment arm must be estimated. This can be approximated at this stage of design by a percent of the fuselage length as previously estimated.

For an aircraft with a front-mounted propeller engine, the tail arm is about 60% of the fuselage length. For an aircraft with the engines on the wings, the tail arm is about 50–55% of the fuselage length. For aft-mounted engines the tail arm is about 45–50% of the fuselage length. A sailplane has a tail moment arm of about 65% of the fuselage length.

For an all-moving tail, the volume coefficient can be reduced by about 10–15%. For a “T-tail,” the vertical-tail volume coefficient can be reduced by approximately 5% due to the end-plate effect, and the horizontal tail volume coefficient can be reduced by about 5% due to the clean air seen by the horizontal. Similarly, the horizontal tail volume coefficient for an “H-tail” can be reduced by about 5%.

For an aircraft which uses a “V-tail,” the required horizontal and vertical tail sizes should be estimated as above. Then the V surfaces should be sized to provide the same total surface area (Ref. 3) as required for conventional tails. The tail dihedral angle should be set to the arctangent of the square root of the ratio between the required vertical and horizontal tail areas. This should be near 45 deg.

The horizontal tail volume coefficient for an aircraft with a control-type canard is approximately 0.1, based upon the relatively few aircraft of this type that have flown. For canard aircraft there is a much wider variation in the tail moment arm. Typically, the canarded aircraft will have a moment arm of about 30–50% of the fuselage length.

For a lifting-canard aircraft, the volume coefficient method isn't applicable. Instead, an area split must be selected by the designer. The required total wing area is then allocated accordingly. Typically, the area split allocates about 25% to the canard and 75% to the wing, although there can be wide variation. A 50-50 split produces a tandem-wing aircraft.

For an airplane with a computerized “active” flight control system, the statistically estimated tail areas may be reduced by approximately 10% provided that trim, engine-out, and nosewheel liftoff requirements can be met. These are discussed in Chapter 16.

## 6.5 CONTROL-SURFACE SIZING

The primary control surfaces are the ailerons (roll), elevator (pitch), and rudder (yaw). Final sizing of these surfaces is based upon dynamic analysis of control effectiveness, including structural bending and control-system effects. For initial design, the following guidelines are offered.

The required aileron area can be estimated from Fig. 6.3, an updated version of a figure from Ref. 12. In span, the ailerons typically extend from

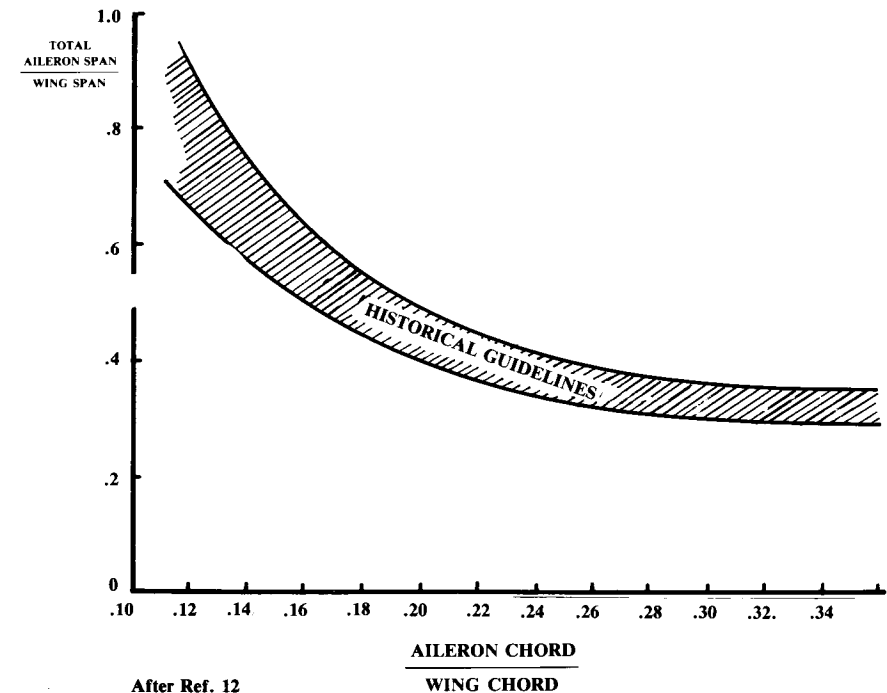


Fig. 6.3 Aileron guidelines.

about 50% to about 90% of the span. In some aircraft, the ailerons extend all the way out to the wing tips. This extra 10% provides little control effectiveness due to the vortex flow at the wingtips, but can provide a location for an aileron mass balance (see below).

Wing flaps occupy the part of the wing span inboard of the ailerons. If a large maximum lift coefficient is required, the flap span should be as large as possible. One way of accomplishing this is through the use of spoilers rather than ailerons. Spoilers are plates located forward of the flaps on the top of the wing, typically aft of the maximum thickness point. Spoilers are deflected upward into the slipstream to reduce the wing's lift. Deploying the spoiler on one wing will cause a large rolling moment.

Spoilers are commonly used on jet transports to augment roll control at low speed, and can also be used to reduce lift and add drag during the landing rollout. However, because spoilers have very nonlinear response characteristics they are difficult to implement for roll control when using a manual flight control system.

High-speed aircraft can experience a phenomena known as "aileron reversal" in which the air loads placed upon a deflected aileron are so great that the wing itself is twisted. At some speed, the wing may twist so much that the rolling moment produced by the twist will exceed the rolling moment produced by the aileron, causing the aircraft to roll the wrong way.

To avoid this, many transport jets use an auxiliary, inboard aileron for high-speed roll control. Spoilers can also be used for this purpose. Several military fighters rely upon "rolling tails" (horizontal tails capable of being deflected nonsymmetrically) to achieve the same result.

Elevators and rudders generally begin at the side of the fuselage and extend to the tip of the tail or to about 90% of the tail span. High-speed

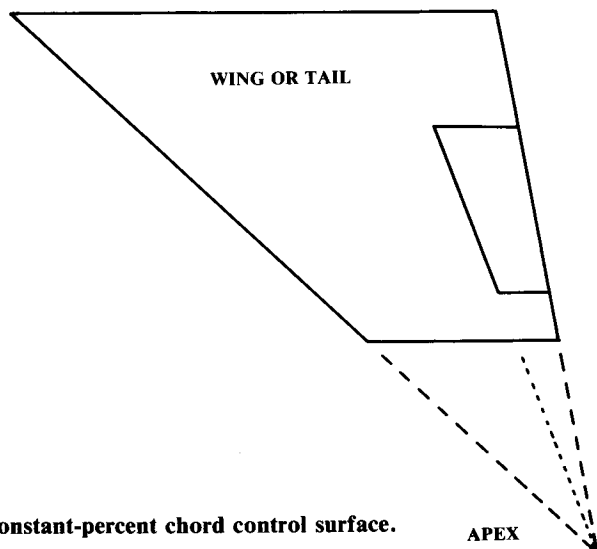


Fig. 6.4 Constant-percent chord control surface.

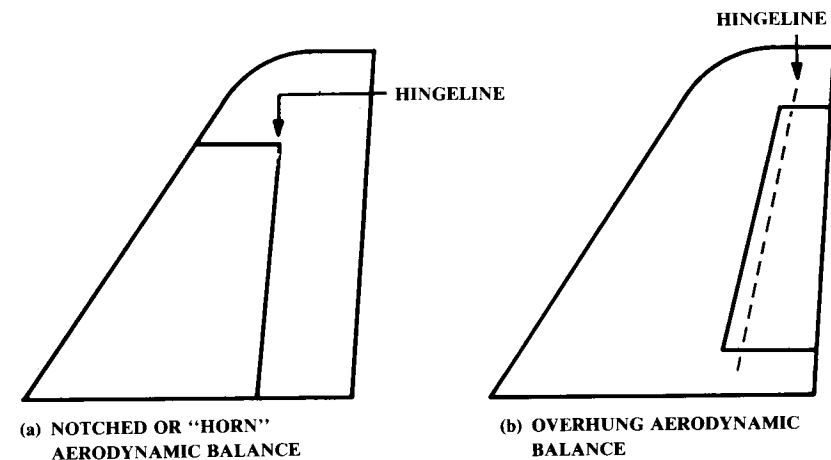


Fig. 6.5 Aerodynamic balance.

aircraft sometimes use rudders of large chord which only extend to about 50% of the span. This avoids a rudder effectiveness problem similar to aileron reversal.

Control surfaces are usually tapered in chord by the same ratio as the wing or tail surface so that the control surface maintains a constant percent chord (Fig. 6.4). This allows spars to be straight-tapered rather than curved. Ailerons and flaps are typically about 15–25% of the wing chord. Rudders and elevators are typically about 25–50% of the tail chord.

Control-surface "flutter," a rapid oscillation of the surface caused by the airloads, can tear off the control surface or even the whole wing. Flutter tendencies are minimized by using mass balancing and aerodynamic balancing.

Mass balancing refers to the addition of weight forward of the control-surface hingeline to counterbalance the weight of the control surface aft of the hingeline. This greatly reduces flutter tendencies. To minimize the weight penalty, the balance weight should be located as far forward as possible. Some aircraft mount the balance weight on a boom flush to the wing tip. Others bury the mass balance within the wing, mounted on a boom attached to the control surface.

An aerodynamic balance is a portion of the control surface in front of the hinge line. This lessens the control force required to deflect the surface, and helps to reduce flutter tendencies.

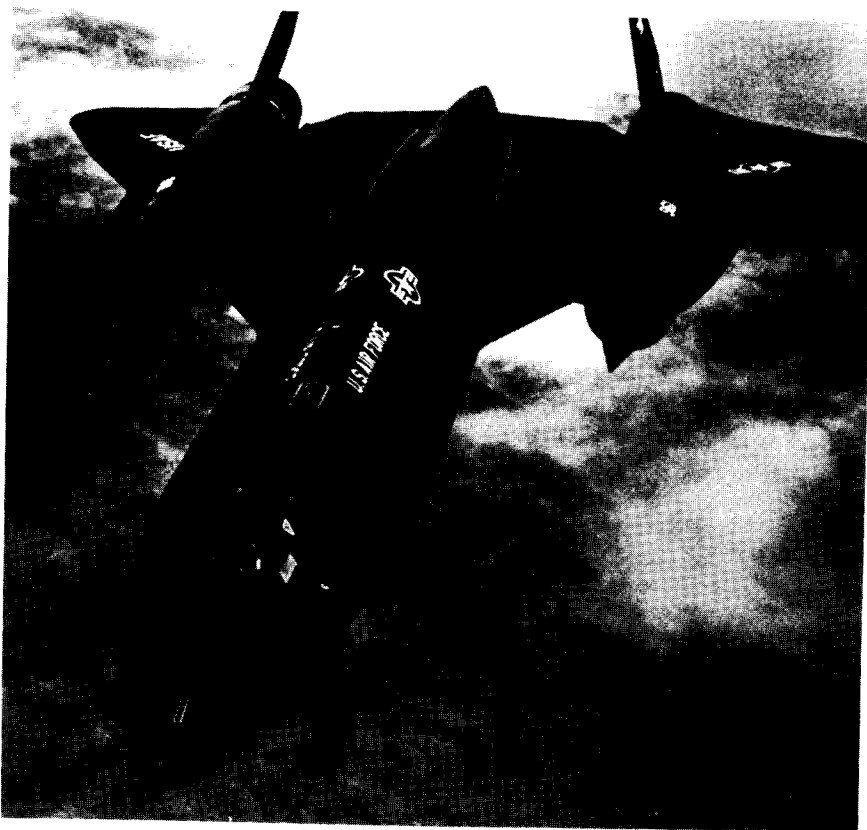
The aerodynamic balance can be a notched part of the control surface (Fig. 6.5a), an overhung portion of the control surface (Fig. 6.5b), or a combination of the two. The notched balance is not suitable for ailerons or for any surface in high-speed flight. The hinge axis should be no farther aft than about 20% of the average chord of the control surface.

The horizontal tail for a manually-controlled aircraft is almost always configured such that the elevator will have a hinge line perpendicular to the

aircraft centerline. This permits connecting the left- and right-hand elevator surfaces with a torque tube, which reduces elevator flutter tendencies.

Some aircraft have no separate elevator. Instead, the entire horizontal tail is mounted on a spindle to provide variable tail incidence. This provides outstanding "elevator" effectiveness but is somewhat heavy. Some general-aviation aircraft use such an all-moving tail, but it is most common for supersonic aircraft, where it can be used to trim the rearward shift in aerodynamic center that occurs at supersonic speeds.

A few aircraft such as the SR-71 have used all-moving vertical tails to increase control authority.



Lockheed SR-71

## CONFIGURATION LAYOUT AND LOFT

### 7.1 INTRODUCTION

The process of aircraft conceptual design includes numerous statistical estimations, analytical predictions, and numerical optimizations. However, the product of aircraft design is a drawing. While the analytical tasks are vitally important, the designer must remember that these tasks serve only to influence the drawing, for it is the drawing alone that ultimately will be used to fabricate the aircraft.

All of the analysis efforts to date were performed to guide the designer in the layout of the initial drawing. Once that is completed, a detailed analysis can be conducted to resize the aircraft and determine its actual performance. This is discussed in Chapters 12-19.

This detailed analysis is time-consuming and costly, so it is essential that the initial drawing be credible. Otherwise, substantial effort will be wasted upon analyzing an unrealistic aircraft.

This chapter and Chapters 8-11 discuss the key concepts required to develop a credible initial drawing of a conceptual aircraft design. These concepts include the development of a smooth, producible, and aerodynamically acceptable external geometry, the installation of the internal features such as the crew station, payload, landing gear, and fuel system, and the integration of the propulsion system.

Real-world considerations which must be met by the design include the correct relationship between the aerodynamic center and the center of gravity, the proper amount of pilot outside visibility, and sufficient internal access for production and maintenance.

### 7.2 END PRODUCTS OF CONFIGURATION LAYOUT

The outputs of the configuration layout task will be design drawings of several types as well as the geometric information required for further analysis.

The design layout process generally begins with a number of conceptual sketches. Figure 7.1 illustrates an actual, unretouched sketch from a fighter conceptual design study (Ref. 13). As can be seen, these sketches are crude and quickly done, but depict the major ideas which the designer intends to incorporate into the actual design layout.

A good sketch will show the overall aerodynamic concept and indicate the locations of the major internal components. These should include the landing gear, crew station, payload or passenger compartment, propulsion sys-

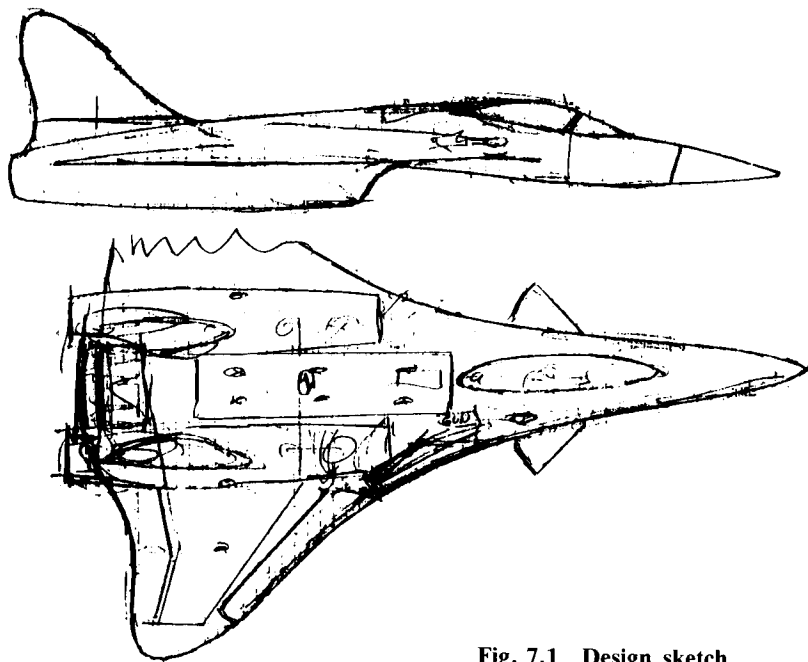


Fig. 7.1 Design sketch.

tem, fuel tanks, and any unique internal components such as a large radar. Conceptual sketches are not usually shown to anybody after the actual layout is developed, but may be used among the design engineers to discuss novel ideas before they begin the layout.

The actual design layout is developed using the techniques to be discussed in the following chapters. Figure 7.2 shows such a design layout, Rockwell's entry in the competition to build the X-29 Forward Sweep Demonstrator. This drawing typifies initial design layouts developed by major airframe companies during design studies.

Figure 7.3 is the initial design developed from the sketch shown as Fig. 7.1. In this case a computer-aided conceptual design system was used to develop a three-dimensional geometric model of the aircraft concept (Ref. 14). The design techniques are similar whether a computer or a drafting board is used for the initial design.

A design layout such as those shown in Figs. 7.2 and 7.3 represents the primary input into the analysis and optimization tasks discussed in Chapters 12–19. Three other inputs must be prepared by the designer: the wetted-area plot (Fig. 7.4), volume distribution plot (Fig. 7.5), and fuel-volume plots for the fuel tanks. Preparation of the wetted-area and volume plots is discussed later in this chapter; the fuel-volume determination is discussed in Chapter 10.

Once the design has been analyzed, optimized, and redrawn for a number of iterations of the conceptual design process, a more detailed drawing can be prepared. Called the "inboard profile" drawing, this depicts in much

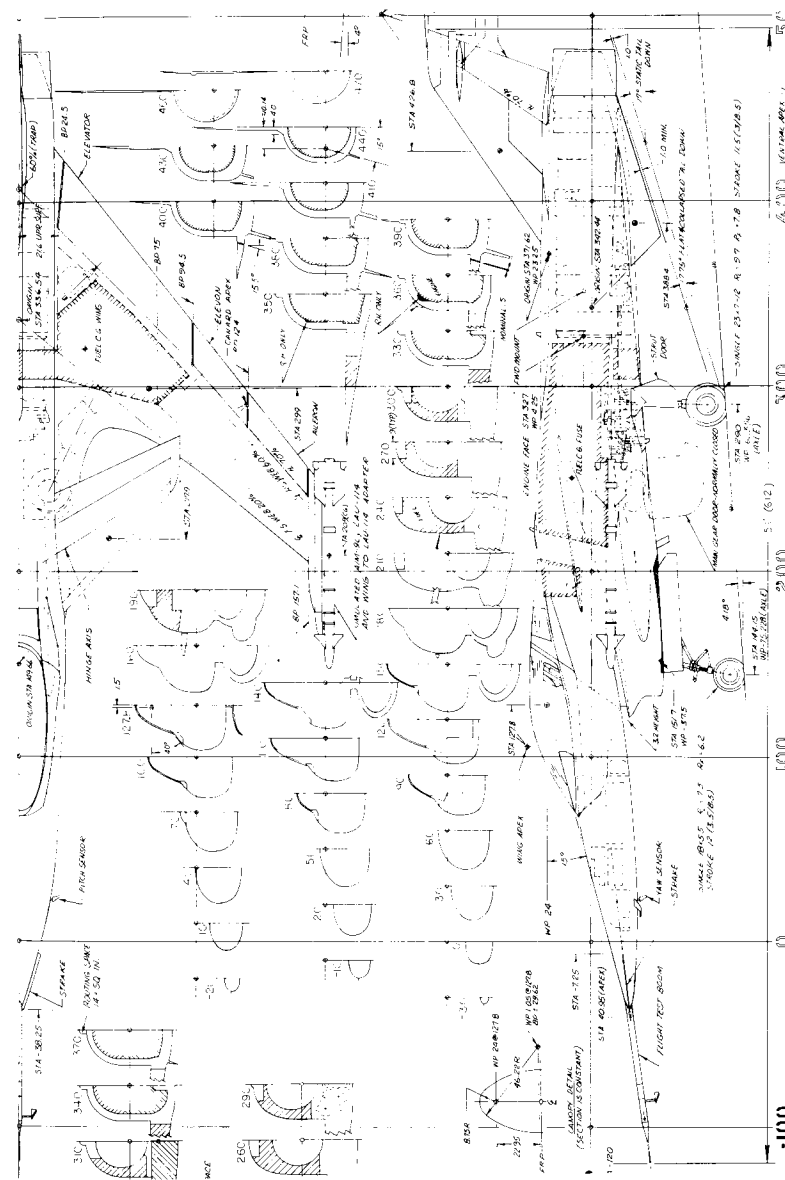


Fig. 7.2 FSW design layout.



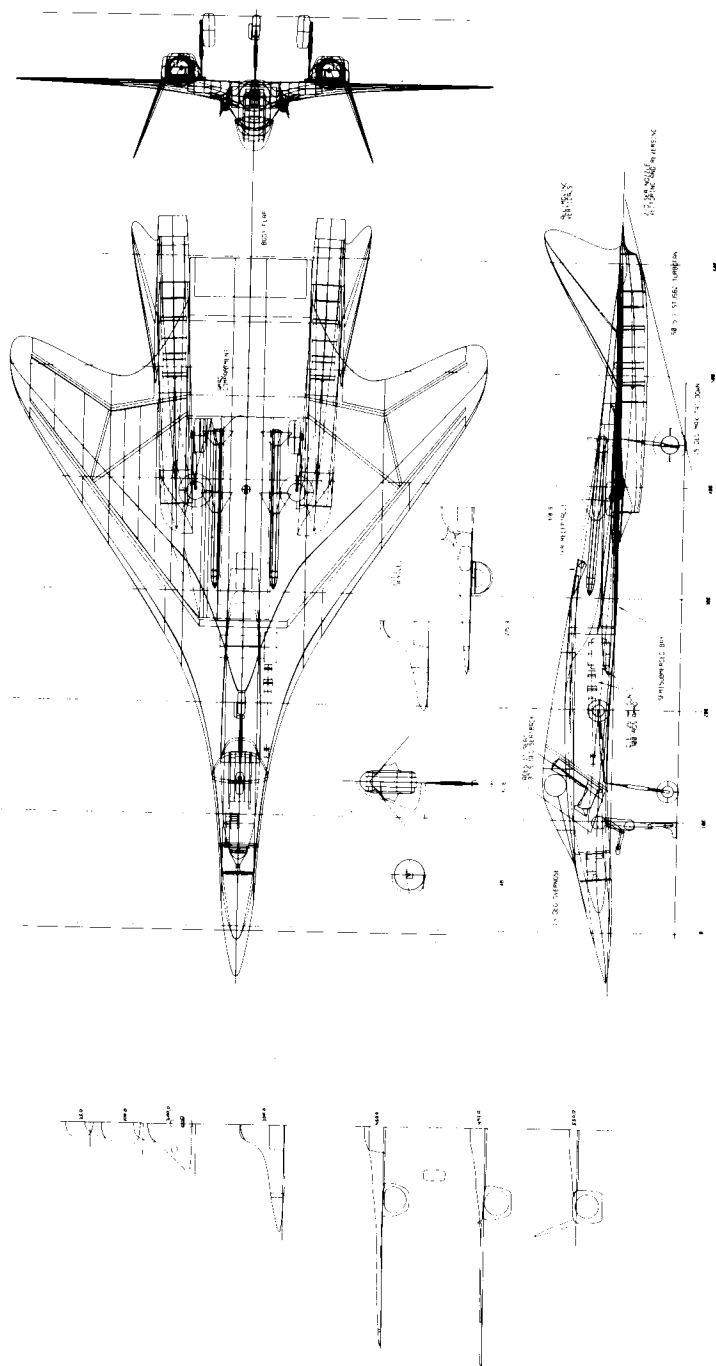


Fig. 7.3 Design layout on a CAD system.

COMPONENT	SURFACE
FUSELAGE	70344.8
VERT TAIL	26165.3
WING	102636.7
CIRCULAR ARC CANOPY	9071.4
NACELLE	25462.9
<b>TOTAL</b>	<b>233681.0</b>

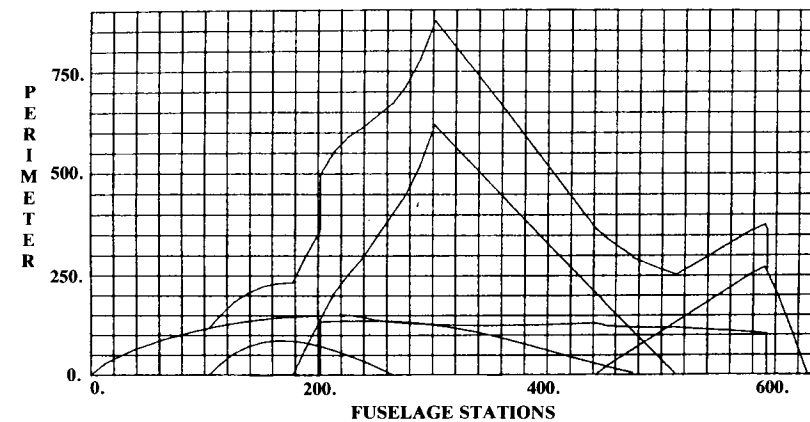


Fig. 7.4 Wetted area plot.

COMPONENT	VOLUME
FUSELAGE	847124.4
VERT TAIL	42903.5
WING	287005.5
CIRCULAR ARC CANOPY	46014.0
NACELLE	95149.8
<b>TOTAL</b>	<b>1318196.8</b>

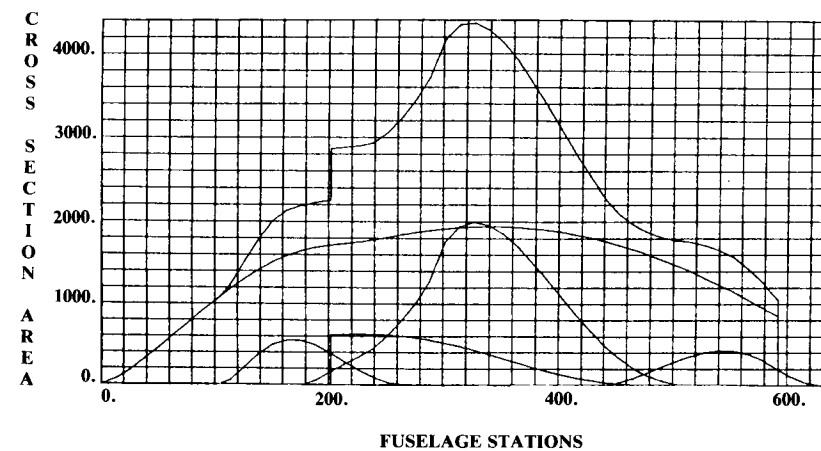


Fig. 7.5 Volume distribution plot.

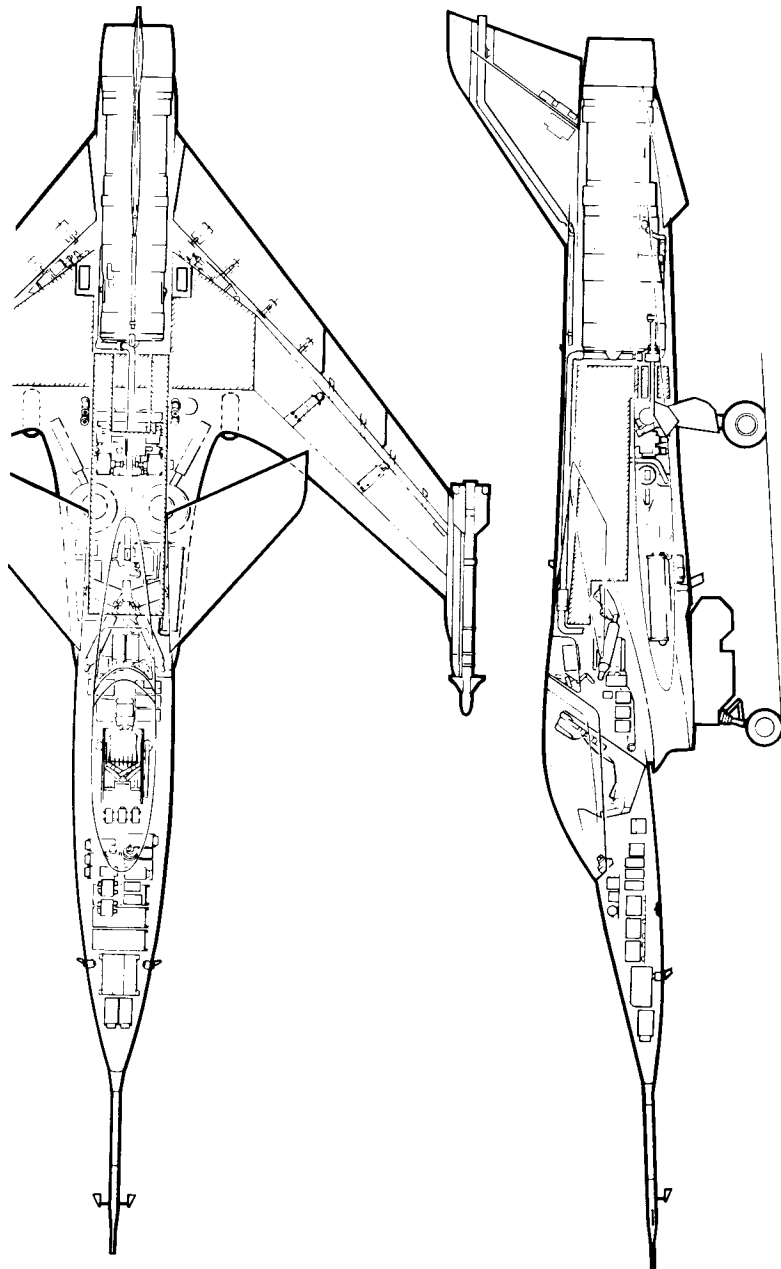


Fig. 7.6 FSW Inboard profile.

greater detail the internal arrangement of the subsystems. Figure 7.6 illustrates the inboard profile prepared for the design of Fig. 7.2. A companion drawing, not shown, would depict the internal arrangement at 20–50 cross-sectional locations.

The inboard profile is far more detailed than the initial layout. For example, while the initial layout may merely indicate an avionics bay based upon a statistical estimate of the required avionics volume, the inboard profile drawing will depict the actual location of every piece of avionics (i.e., “black boxes”) as well as the required wire bundles and cooling ducts.

The inboard profile is generally a team project, and takes many weeks. During the preparation of the inboard profile it is not uncommon to find that the initial layout must be changed to provide enough room for everything. As this can result in weeks of lost effort, it is imperative that the initial layout be as well thought-out as possible.

Figure 7.7 shows a side-view inboard profile prepared in 1942 for an early variant of the P-51. This detailed drawing shows virtually every internal system, including control bellcranks, radio boxes, and fuel lines. Preparation of such a detailed drawing goes beyond the scope of this book, but aspiring designers should be aware of them.

At about the same time that the inboard profile drawing is being prepared, a “lines control” drawing may be prepared that refines and details the external geometry definition provided on the initial layout. Again, such a detailed drawing goes beyond the scope of this book. Also, most major companies now use computer-aided lofting systems that do not require a lines control drawing.

After the inboard profile drawing has been prepared, an “inboard isometric” drawing (Fig. 7.8) may be prepared. It will usually be prepared by the art group for the purpose of illustration only, and be used in briefings and proposals. Such a drawing is frequently prepared and published by aviation magazines for existing aircraft. (In fact, the magazine illustrations are usually better than those prepared by the aircraft companies!)

### 7.3 CONIC LOFTING

“Lofting” is the process of defining the external geometry of the aircraft. “Production lofting,” the most detailed form of lofting, provides an exact, mathematical definition of the entire aircraft including such minor details as the intake and exhaust ducts for the air conditioning.

A production-loft definition is expected to be accurate to within a few hundredths of an inch (or less) over the entire aircraft. This allows the different parts of the aircraft to be designed and fabricated at different plant sites yet fit together perfectly during final assembly. Most aircraft companies now use computer-aided loft systems that incorporate methods discussed in Ref. 80.

For an initial layout it is not necessary to go into as much detail. However, the overall lofting of the fuselage, wing, tails, and nacelles must be defined sufficiently to show that these major components will properly enclose the required internal components and fuel tanks while providing a smooth aerodynamic contour.

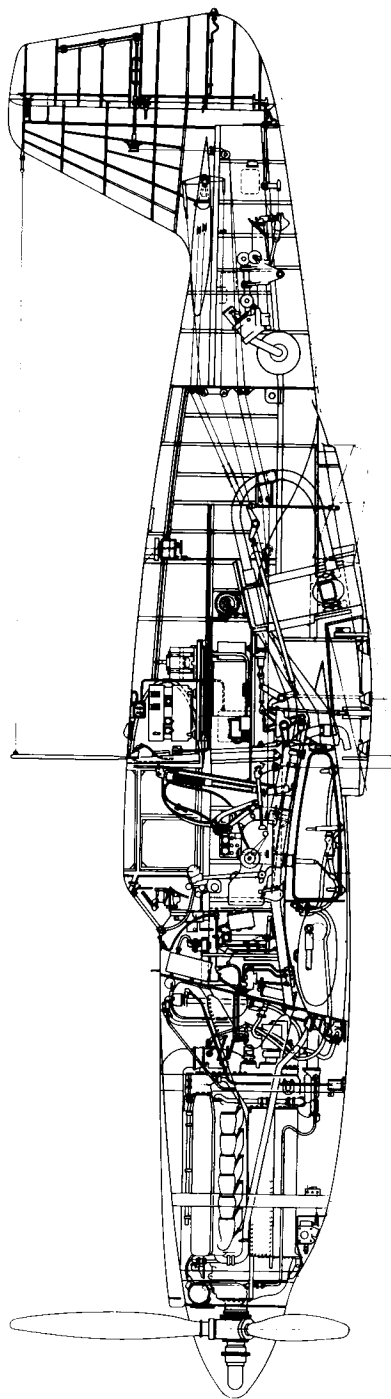


Fig. 7.7 P-51 variant inboard profile.

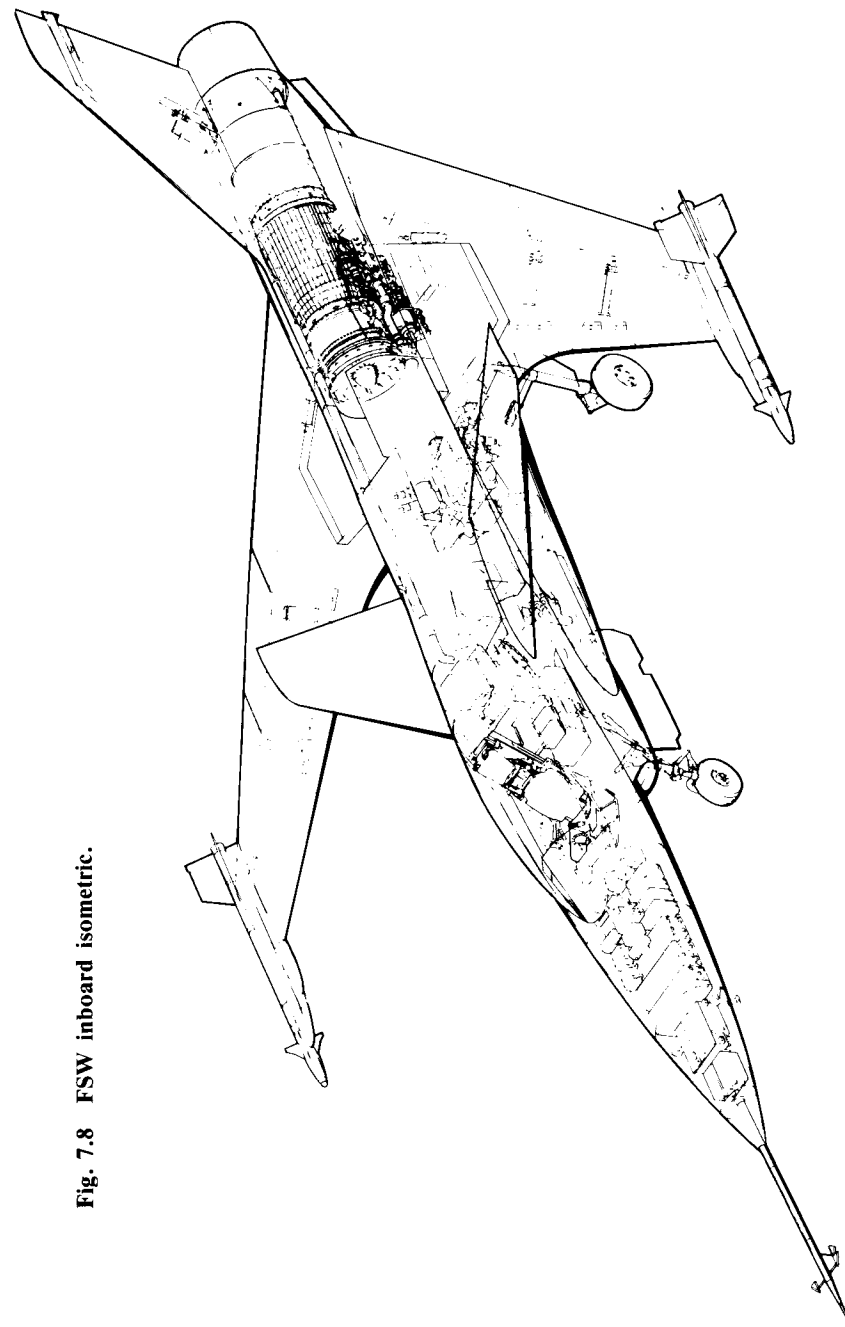


Fig. 7.8 FSW inboard isometric.

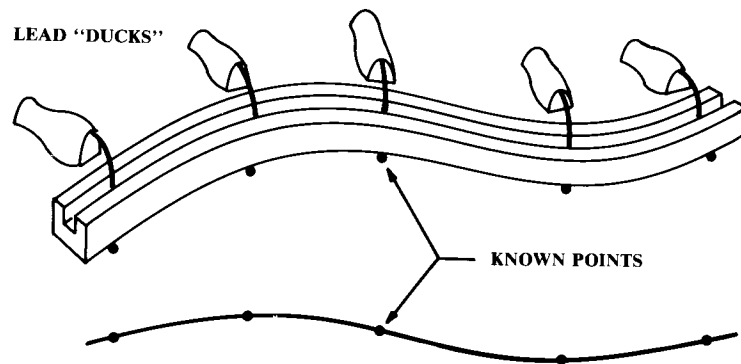


Fig. 7.9 Spline lofting.

Lofting gets its name from shipbuilding. The definition of the hull shape was done in the loft over the shipyard, using enormous drawings. To provide a smooth longitudinal contour, points taken from the desired cross sections were connected longitudinally on the drawing by flexible "splines," long, thin wood or plastic rulers held down at certain points by lead "ducks" (pointed weights—see Fig. 7.9).

This technique was used for early aircraft lofting, but suffers from two disadvantages. First, it requires a lot of trial and error to achieve a smooth surface both in cross section and longitudinally.

Second, and perhaps more important, this method does not provide a unique mathematical definition of the surface. To create a new cross section requires a tremendous amount of drafting effort, especially for a canted cross section (i.e., a cross-sectional cut at some angle other than perpendicular to the centerline of the aircraft). In addition to the time involved, this method is prone to mismatch errors.

A new method of lofting was used for the first time on the P-51 Mustang (Ref. 15). This method, now considered traditional, is based upon a mathematical curve form known as the "conic."

The great advantage of the conic is the wide variety of curves that it can represent, and the ease with which it can be constructed on the drafting table.

While many other forms of lofting are in use, conic lofting has been the most widely used. Also, an understanding of conic lofting provides the necessary foundation to learn the other forms of lofting, including computer-aided lofting.

A conic is a second-degree curve whose family includes the circle, ellipse, parabola, and hyperbola. The generalized form of the conic is given in Eq. (7.1). The conic is best visualized as a slanted cut through a right circular cone (Fig. 7.10). A number of specialized conic equations are provided in Ref. 80.

$$C_1X^2 + C_2XY + C_3Y^2 + C_4X + C_5Y + C_6 = 0 \quad (7.1)$$

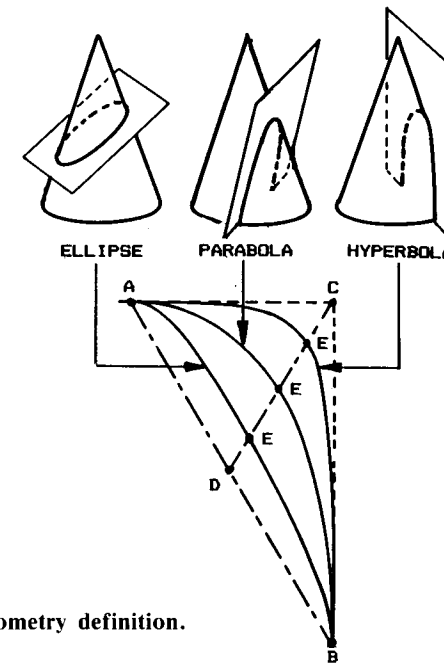


Fig. 7.10 Conic geometry definition.

The shape of the conic depends upon the angle of the cut through the cone. If the cut is flat (i.e., perpendicular to the axis of the cone), then the resulting curve will be a circle; if somewhat slanted, an ellipse; if exactly parallel to the opposite side, a parabola. A greater cut angle yields a hyperbola.

A conic curve is constructed from the desired start and end points ("A" and "B"), and the desired tangent angles at those points. These tangent angles intersect at point "C." The shape of the conic between the points A and B is defined by some shoulder point "S." (The points labeled "E" in Fig. 7.10 are a special type of shoulder point, discussed later.) Figure 7.11 illustrates the rapid graphical layout of a conic curve.

The first illustration in Fig. 7.11 shows the given points A, B, C, and S. In the second illustration, lines have been drawn from A and B, passing through S.

The remaining illustrations show the generation of one point on the conic. In the third illustration a line is drawn from point C at an arbitrary angle. Note the points where this line intersects the A-S and B-S lines.

Lines are now drawn from A and B through the points found in the last step. The intersection of these lines is a point "P" which is on the desired conic curve.

To generate additional points, the last two steps are repeated. Another line is drawn from point C at another arbitrary angle, and then the lines from A and B are drawn and their intersection is found. When enough points have been generated, a French curve is used to draw the conic.

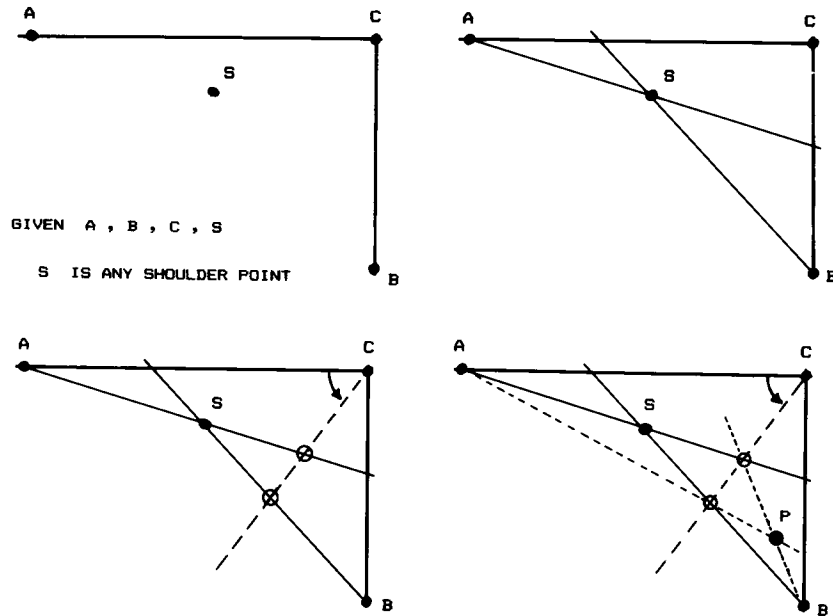
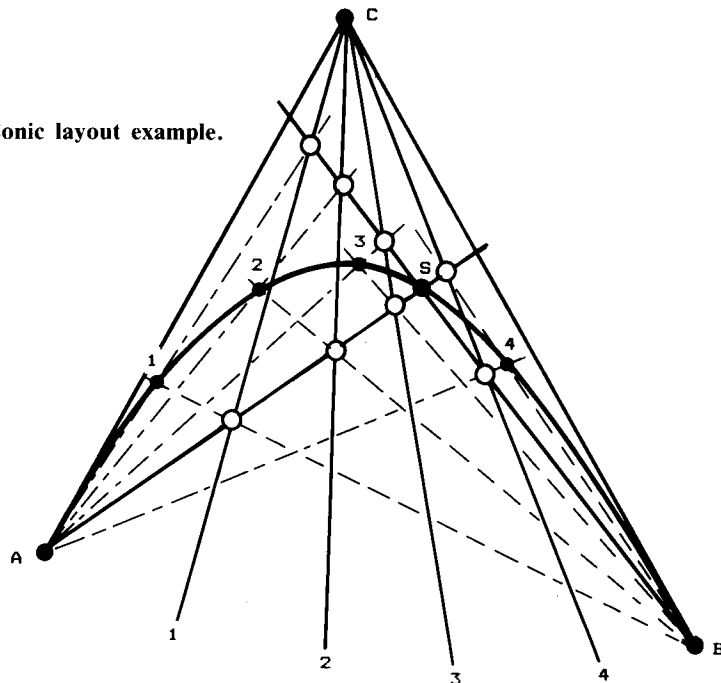


Fig. 7.11 Conic layout.

Fig. 7.12 Conic layout example.



While this procedure seems complicated at first, with a little practice a good designer can construct an accurate conic in less than a minute. Figure 7.12 illustrates a conic curve generated in this manner. Note that it is not necessary to draw completely the various lines, as it is only their intersections which are of interest.

## 7.4 CONIC FUSELAGE DEVELOPMENT

### Longitudinal Control Lines

To create a smoothly-lofted fuselage using conics, it is necessary only to ensure that the points  $A, B, C$ , and  $S$  in each of the various cross sections can be connected longitudinally by a smooth line. Figure 7.13 shows the upper half of a simple fuselage, in which the  $A, B, C$ , and  $S$  points in three cross sections are connected by smooth longitudinal lines. These are called "longitudinal control lines" because they control the shapes of the conic cross sections.

Figure 7.14 shows the side and top views of these longitudinal control lines. Since the cross sections are tangent to horizontal at the top of the fuselage, the  $A$  and  $C$  lines are identical in side view. Similarly, the cross sections are tangent to vertical at the side of the fuselage, so the  $B$  and  $C$  lines are identical in top view. This is common, but not required.

In Fig. 7.14, the longitudinal control lines are used to create a new cross section, in between the second and third cross sections previously defined. This new cross section is created by measuring, from the longitudinal control lines, the positions of the  $A, B, C$ , and  $S$  points at the desired location of the new cross section.

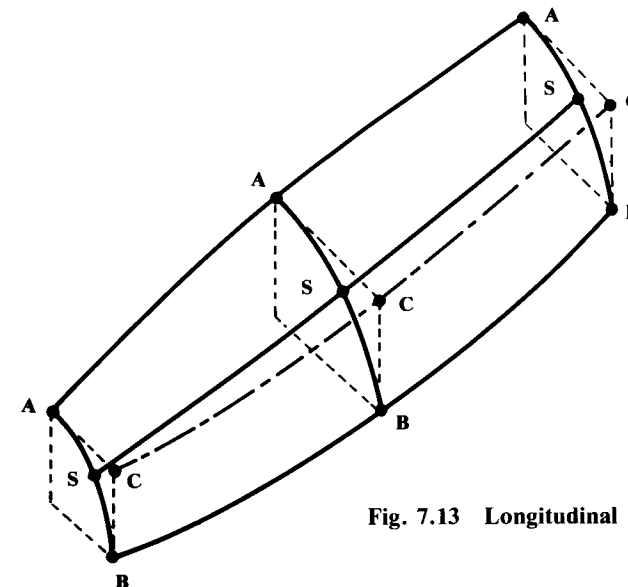


Fig. 7.13 Longitudinal control lines.

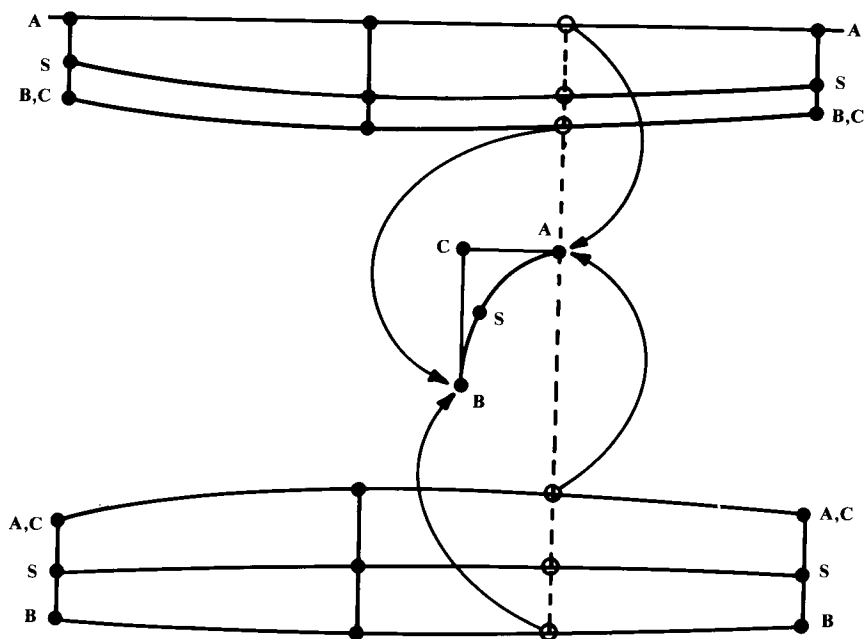


Fig. 7.14 Cross section development from longitudinal control lines.

As is shown for point *A*, each point is defined by two measurements, one from side view and one from top view. From these points the new cross section can be drawn using the conic layout procedure illustrated in Fig. 7.11.

The original cross sections that are used to develop the longitudinal control lines are called the “control cross sections,” or “control stations.” These cross sections are drawn to enclose the various internal components, such as the cockpit or engine.

Control stations can also be drawn to match some required shape. For example, the last cross section of a single-engined jet fighter with a conventional round nozzle would have to be a circle of the diameter of the nozzle.

Typically, some five to ten control stations will be required to develop a fuselage that meets all geometric requirements. The remaining cross sections of the fuselage can then be drawn from the longitudinal control lines developed from these control stations.

### Fuselage Lofting Example

Figure 7.15 illustrates a common application of conic lofting to define a fighter fuselage for an initial layout. Five control stations are required for this example. Station 0 is the nose, which is a single point. All the longitudinal control lines must originate there.

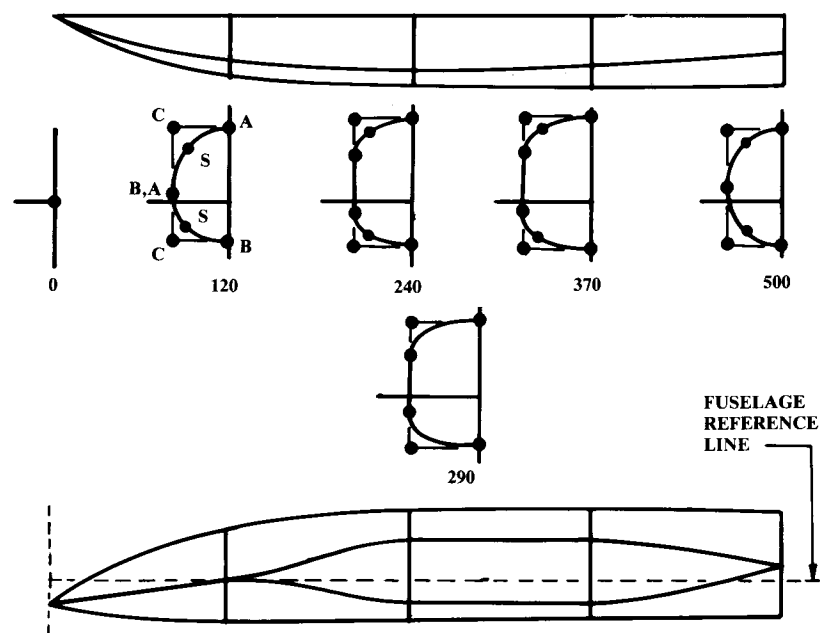


Fig. 7.15 Typical fuselage lofting.

Station 120 is established for this example by the requirements for the cockpit (Chapter 9). This station is approximately circular in shape, and is defined using two conics (upper and lower). Each conic has its own *A*, *B*, *C*, and *S* points. Note that the *B* (end) point of the upper conic is identical to the *A* (start) point of the lower conic.

Station 240 has a flat side to provide for a side-mounted inlet as can be seen on the F-4, the MiG-23, and many other aircraft. At this station, the end points of the upper and lower conics are moved apart vertically, with the area between them defined as a straight line. Note in side view that the longitudinal control lines separate smoothly, not suddenly. This is to ensure a smooth longitudinal contour.

Station 370 is similar to station 240, with a relatively square cross-sectional shape. This could allow room for the landing gear or perhaps to attach a low wing to the side of the fuselage, without a drag-producing acute angle.

Station 500 is a circular cross section, to allow for a connection with a round exhaust nozzle. The longitudinal control lines come back together in a smooth fashion, as shown.

These five control stations are then used to create the longitudinal control lines. From those lines, additional cross sections can be created as desired. Section 290 was created in such a fashion, by measuring the conic control points from the longitudinal control lines and then drawing the conics as previously described.

Figure 7.15 shows only the fuselage lofting. The canopy, inlet duct, and inlet duct fairing would be lofted in a similar fashion, using longitudinal control lines through a few control stations.

### Conic Shape Parameter

One problem arises with this method of initial lofting. The locations of the shoulder points (*S*) can be difficult to control, creating conics either too square (shoulder point too close to point *C*) or too flat (shoulder point too far away from point *C*). An alternate technique using conics involves a parameter which directly controls the shoulder point's distance from the point *C*.

The points labeled *E* in Fig. 7.10 are conic shoulder points which happen to lie upon the line *D-C*. “*D*” is the point exactly midway between *A* and *B*. Such a shoulder point *E* determines the “conic shape parameter ( $\rho$ ),” as defined in the following equation:

$$\rho = |\overline{DE}| / |\overline{DC}| \quad (7.2)$$

where

$$|\overline{AD}| = |\overline{BD}| \quad (7.3)$$

Referring to Fig. 7.10, the shoulder points labeled *E* are based upon the  $\rho$  values required to obtain the ellipse, parabola, or hyperbola forms of the conic. These are given below, along with the  $\rho$  value that defines a circle (a special form of the ellipse):

$$\begin{aligned} \text{Hyperbola: } & \rho > 0.5 \\ \text{Parabola: } & \rho = 0.5 \\ \text{Ellipse: } & \rho < 0.5 \\ \text{Circle: } & \rho = 0.4142 \quad \text{and} \quad |\overline{AC}| = |\overline{BC}| \end{aligned} \quad (7.4)$$

The conic shape parameter allows the designer to specify the conic curve's distance from the point *C*. A conic with a large  $\rho$  value (approaching 1.0) will be nearly square, with the shoulder point almost touching the point *C*. A conic with a small  $\rho$  value (approaching 0.0) will nearly resemble the straight line from *A-B*. The parameter  $\rho$  can be used to control more easily the longitudinal fairing of a fuselage.

Figure 7.16 shows the use of the conic shape parameter ( $\rho$ ) to lay out a conic. Points *A*, *B*, and *C* are known, but the shoulder point *S* is not known. However, the value of  $\rho$  is given.

In the illustration on the right side of Fig. 7.16, the line *A-B* has been drawn and bisected to find the point *D*. The shoulder point *S* is found by measuring along line *D-C*, starting at *D*, by a distance equal to  $\rho$  times the total length of line *D-C*. Once the shoulder point is found, the conic can be drawn as illustrated in Fig. 7.11.

By using this approach, a fuselage can be lofted without the use of a longitudinal control line to control the location of the shoulder points. If  $\rho$  is specified to be some constant value for all of the cross sections, then the

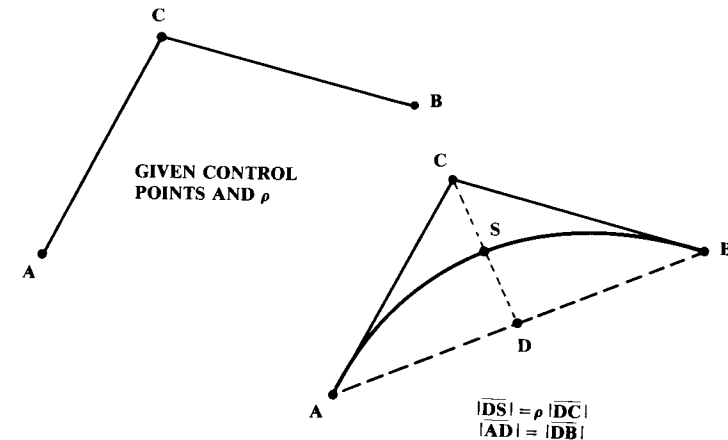


Fig. 7.16 Conic layout using  $\rho$ .

designer need only control the conic endpoints and tangent intersection points. To permit the fuselage ends to be circular in shape, the value of  $\rho$  would be fixed at 0.4142.

Greater flexibility can be attained by allowing  $\rho$  to vary longitudinally. For example, the fuselage of Fig. 7.15 requires a  $\rho$  value of 0.4142 at both ends to allow a circular shape, but the values of  $\rho$  at the middle of the fuselage are higher, perhaps around 0.7.

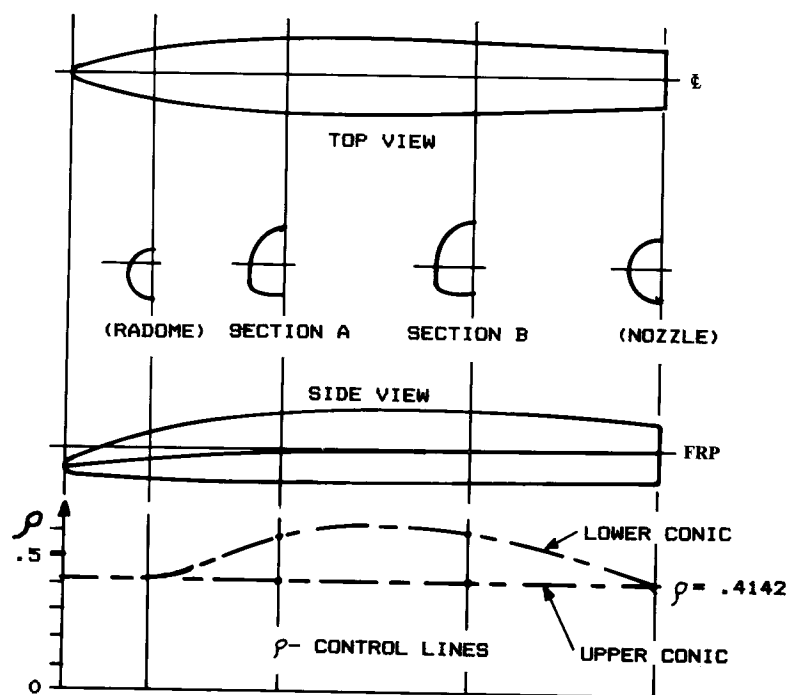
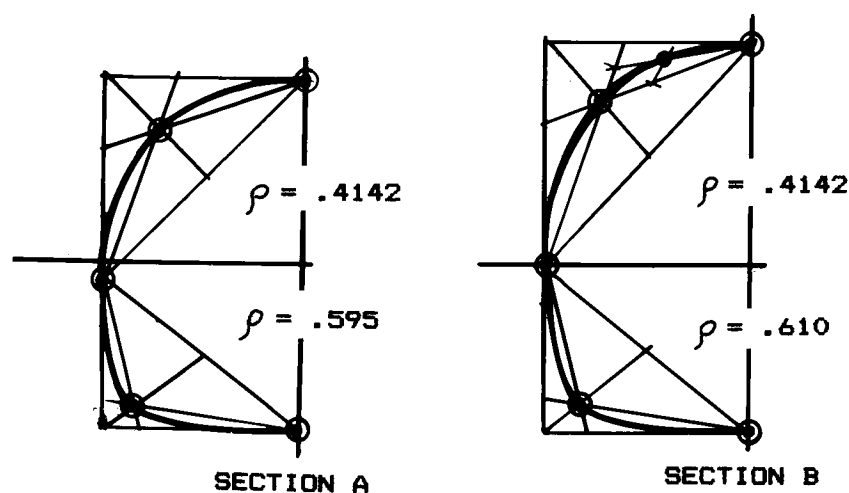
An “auxiliary control line” can be used to control graphically the value of  $\rho$ , as shown in Fig. 7.17. Note the auxiliary control line for  $\rho$  at the bottom. If the value of  $\rho$  varies smoothly from nose to tail, and the conic endpoints and tangent intersection point are controlled with smooth longitudinal lines, then the resulting fuselage surface will be smooth.

In Fig. 7.17 the upper conic has a constant  $\rho$  value of 0.4142, while the lower conic has a  $\rho$  value varying from 0.4142 at the nose and tail to about 0.6 at the middle of the fuselage. This has the effect of “squaring” the lower fuselage to provide more room for the landing gear.

Figure 7.18 shows the use of  $\rho$  to develop the cross sections labeled *A* and *B*. Observe the development of the upper and lower conics by the method shown previously in Fig. 7.16, and the use of different  $\rho$  values for the upper and lower conics.

Thus far, no mention has been made of the method for developing the longitudinal control lines and auxiliary control lines. During production lofting, these control lines would be defined mathematically, using conics or some form of polynomial.

For initial layouts, sufficient accuracy can be obtained graphically through the use of the flexible splines discussed earlier. Points are taken from the control cross sections and plotted in side and top view, then connected longitudinally using a spline to draft a smooth line. In fact, a designer with a “good eye” can obtain sufficient smoothness using a French curve if spline and ducks are not available.

Fig. 7.17 Conic fuselage development using  $\rho$ .Fig. 7.18 Cross section development using  $\rho$ .

## 7.5 FLAT-WRAP FUSELAGE LOFTING

An important cost driver for aircraft fabrication is the amount of compound-curvature used in lofting the aircraft. Compound-curvature implies the existence of surface curvature in all directions for some point on the surface.

For example, a ball is entirely composed of compound-curvature surfaces. A flat sheet has no curvature, compound or otherwise. A cylinder is curved, but only in one direction, so it does not have any compound curvature. Instead, a cylinder or any other surface with curvature in only one direction is said to be "flat-wrapped".

If a surface is flat-wrapped, it can be constructed by "wrapping" a flat sheet around its cross sections. For aircraft fabrication, this allows the skins to be cut from flat sheets and bent to the desired skin contours.

This is far cheaper than the construction technique for a surface with compound curvature. Compound curvature requires that the skins be shaped by a stretching or stamping operation, which entails expensive tools and extra fabrication steps.

Aircraft applications of flat-wrap lofting must be defined in the initial loft definition used for the conceptual layout. There are several ways of lofting a surface so that it is flat-wrapped. The simplest technique uses a constant cross section. For example, a commercial airliner usually has the identical circular-cross-sectional shape over most of its length. In fact, any cross section shape will produce a flat-wrap surface if it is held constant in the longitudinal direction.

Often an identical cross-sectional shape will not be desired, yet a flat-wrap lofting may be attained. If the same cross-sectional shape is maintained but linearly scaled in size, a flat-wrap contour is produced. For example, a cone is a flat-wrap surface produced by linearly scaling a circular cross section.

Many aircraft have a tailcone which, although not circular in cross section, is linearly scaled to produce a flat-wrap surface. This can be accomplished with conics by maintaining identical tangent angles and  $\rho$  value, using straight longitudinal control lines, and maintaining the lengths  $AC$  and  $BC$  in constant proportion.

Sometimes it is necessary to vary the shape of the cross sections other than by scaling. Flat wrap cannot be exactly maintained in such cases using conics. A more sophisticated technique (beyond the scope of this book) must be used.

However, flat wrap can be closely approximated in most such cases on two conditions. First, the longitudinal control lines must be straight. This includes the line controlling the shoulder point ( $S$ ). If the conic shape parameter ( $\rho$ ) is used instead of a shoulder-point control line, then the  $\rho$  value must be either constant or linearly varied.

Second, the tangent angles of the conics must not change longitudinally. If the tangent angles are all either horizontal or vertical, as in Figs. 7.15 and 7.17, this condition can easily be met.

Figure 7.19 shows such a complex flat-wrapped surface. The fuselage is defined by five conics plus a straight-line, flat underside. The "bump" on top could represent the back of the canopy, and grows smaller towards the



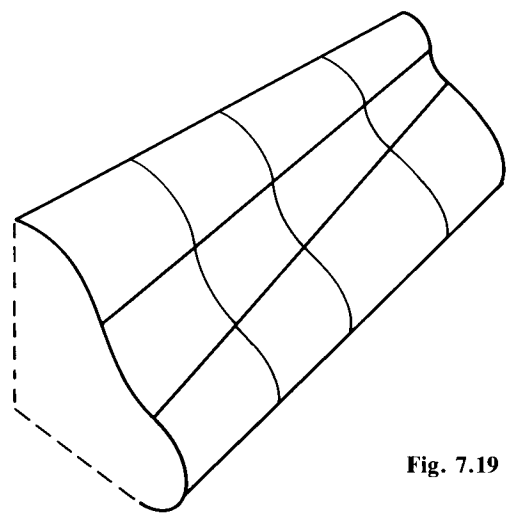


Fig. 7.19 Complex flat-wrapped surface.

rear of the fuselage. While the conics change shape and size, their endpoints hold the same tangent angles.

It is important to realize that the use of flat-wrap lofting for a fuselage represents a compromise. While flat-wrap surfaces are easier and cheaper to fabricate, they are less desirable from an aerodynamic viewpoint. For example, a smoothly contoured teardrop shape will have less drag than a flat-wrap cylinder with a nosecone and tailcone.

## 7.6 CIRCLE-TO-SQUARE ADAPTER

A common problem in lofting is the “circle-to-square adapter.” For example, the inlet duct of many supersonic jet aircraft is approximately square at the air inlet, yet must attain a circular shape at the engine front-face. Modern, two-dimensional nozzles also require a circle-to-square adapter.

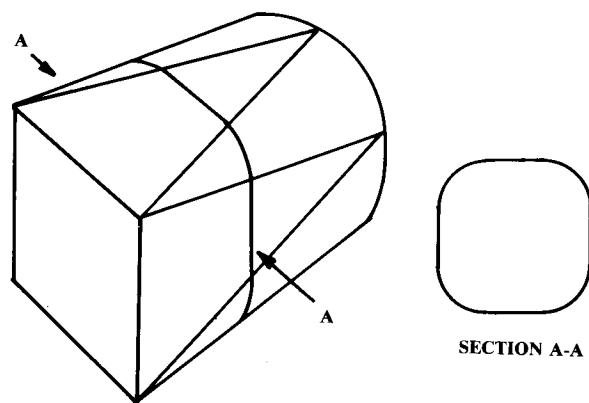


Fig. 7.20 Circle-to-square adapter.

Flat-wrap can be attained for a circle-to-square adapter by constructing the adapter of interlocking, V-shaped segments, each of which is itself flat-wrapped (Fig. 7.20).

The flat sides of the square section taper to points that just touch the circular section. Similarly, the cone-shaped sides of the circular section taper to points that touch the corners of the square section. Note the “rounded-off square” shape of the intermediate sections. The connecting surfaces must be straight longitudinally for a flat-wrap surface to be maintained.

## 7.7 FUSELAGE LOFT VERIFICATION

The use of smooth longitudinal control lines defining conic cross sections assures a smooth fuselage; but sometimes it is necessary to deviate from this type of definition. For example, if a part of the fuselage is to be flat-wrapped, it may be difficult to smoothly connect the straight control lines for the flat-wrap part of the fuselage with the curved control lines for the rest of the fuselage.

Also, it may be desirable to have two different flat-wrap parts of the fuselage that are directly connected, resulting in an unavoidable break in the smoothness of the longitudinal control lines. In such cases the designer should evaluate the resulting contours to ensure that any breaks in the longitudinal smoothness are not too extreme.

Sometimes a designer will be asked to evaluate a design created by someone else. This is common practice at government agencies such as the Air Force Aeronautical Systems Division and the Naval Air Systems Command. In addition to the analytical evaluations for performance and range, the designer should evaluate the design layout to ensure that the cross sections shown are in fact smooth longitudinally.

These smoothness evaluations are performed using a technique borrowed from shipbuilding. Hull contours are evaluated for smoothness by laying out the “waterlines.” If a ship is floating in the water, the line around the hull where the surface of the water intersects the hull is a waterline. For good ship performance, this waterline should be smooth in the longitudinal direction.

If the hull is raised partly out of the water some arbitrary distance, a new waterline is formed. Hull designers check for hull smoothness by laying out a large number of these waterlines, each separated in height by some arbitrary distance. If all the waterlines have smooth contours, then the hull is smooth.

Such horizontal waterline cuts can be used for evaluation of the smoothness of an aircraft fuselage; but it is more common to use vertically-oriented cuts known as “butt-plane cuts” (Fig. 7.21).

Butt-plane (“butt-plane”) cuts form the intersection of the aircraft with vertical planes defined by their distance from the aircraft centerline. For example, “butt-plane 30” is the contour created by intersecting a vertical plane with the fuselage at a distance of 30 in. from the centerline.

Note in Fig. 7.21 that the butt-plane cuts are oriented such that the airfoil is a butt-plane cut of the wing. It is for this reason that butt-plane cuts are more commonly used for aircraft than waterlines.

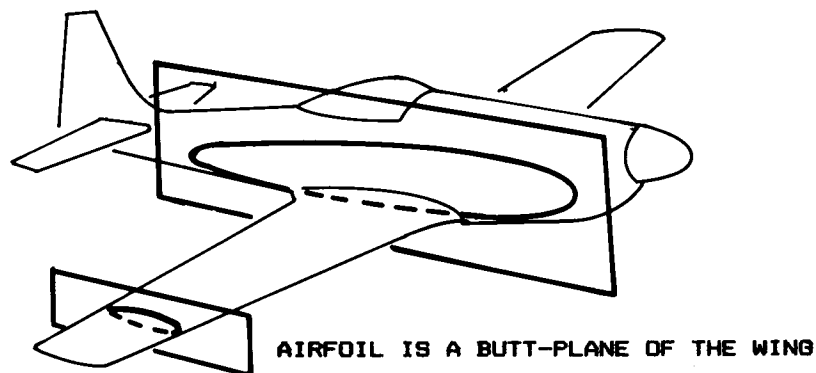


Fig. 7.21 Butt-plate cut.

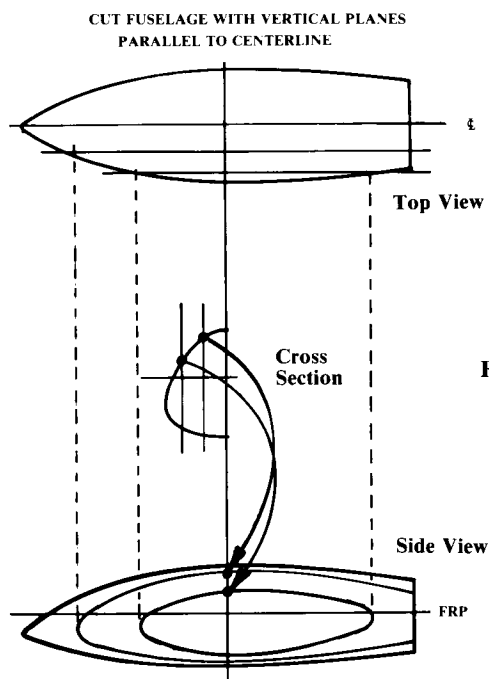


Fig. 7.22 Butt-plate cut layout.

Figure 7.22 illustrates the development of butt-plane cuts. Vertical lines are drawn on each cross section, indicating the locations of the arbitrarily-selected butt-planes. The points where these vertical lines intersect the cross sections are transferred to the side-view drawing and connected longitudinally. If the fuselage surface is smooth, then these longitudinal lines for the different butt-planes will all be smooth.

Buttock-plane cuts can also be used to generate new cross sections. Once the butt-plane cuts are developed as in Fig. 7.22, a new cross section can be

developed by transferring the vertical locations of the butt-plane cuts to the cross section desired, and then drawing a smooth cross-sectional contour using those points.

Sometimes this method is easier than developing the longitudinal control lines for conic fuselage lofting. This is most likely when the surface is highly irregular, such as the forebody of a blended wing-body aircraft like the B-1B.

## 7.8 WING/TAIL LAYOUT AND LOFT

### Reference Wing/Tail Layout

Chapter 4 described the selection of the basic geometric parameters for the wing and tails. These parameters include the aspect ratio ( $A$ ), taper ratio ( $\lambda$ ), sweep, dihedral, and thickness. Also, the selection of an appropriate airfoil was considered. In Chapter 6, the actual sizes for the wing, tails, and fuselage were defined, based upon an initial estimate for the takeoff gross weight.

From these parameters, the geometric dimensions necessary for layout of the reference (trapezoidal) wing or tail can be obtained, as shown in Fig. 7.23 and defined by the following equations:

$$b = \sqrt{AS} \quad (7.5)$$

$$C_{\text{root}} = \frac{2S}{b(1 + \lambda)} \quad (7.6)$$

$$C_{\text{tip}} = \lambda C_{\text{root}} \quad (7.7)$$

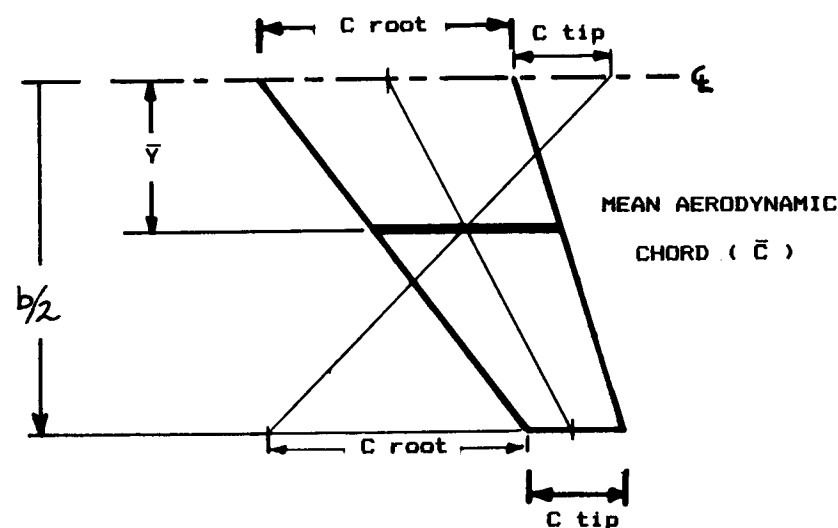


Fig. 7.23 Reference (trapezoidal) wing/tail.

$$\bar{C} = \left(\frac{2}{3}\right) C_{\text{root}} \frac{1 + \lambda + \lambda^2}{1 + \lambda} \quad (7.8)$$

$$\bar{Y} = \left(\frac{b}{6}\right) \left(\frac{1 + 2\lambda}{1 + \lambda}\right) \quad (7.9)$$

For a vertical tail,  $\bar{Y}$  is twice the value calculated in Eq. (7.9).

Figure 7.23 also shows a quick graphical method of determining the spanwise ( $Y$ ) location of the mean aerodynamic chord (MAC or  $\bar{C}$ ), which is mathematically obtained by Eq. (7.9). The location of the mean chord is obtained graphically as the intersection of the 50%-chord line and a line drawn from a point located at the tip chord length behind the root chord to a point at the root chord length ahead of the tip chord.

### Wing Location with Respect to the Fuselage

The location and length of the MAC is important because the wing is located on the aircraft so that some selected percent of the MAC is aligned with the aircraft center of gravity. This provides a first estimate of the wing position to attain the required stability characteristics.

For a stable aircraft with an aft tail, the wing should be initially located such that the aircraft center of gravity is at about 30% of the mean aerodynamic chord. When the effects of the fuselage and tail are considered, this will cause the center of gravity to be at about 25% of the total subsonic aerodynamic center of the aircraft.

For an unstable aircraft with an aft tail, the location of the wing depends upon the selected level of instability, but will usually be such that the center of gravity is at about 40% of the mean aerodynamic chord.

For a canard aircraft, such rules of thumb are far less reliable due to the canard downwash and its influence upon the wing. For a control-type canard with a computerized flight control system (i.e., unstable aircraft), the wing can be initially placed such that the aircraft center of gravity is at about 15–25% of the wing's mean aerodynamic chord.

For a lifting-type canard, the mean aerodynamic chords of the wing and canard should both be determined, and the appropriate percent MAC for each should be identified. Then the combined MAC location can be determined as the weighted average of the percent MAC locations for the wing and canard (weighted by their respective areas). Note that this is a very crude estimate!

Chapter 15 provides a quick method of approximating the aircraft center of gravity once the locations of the major internal components are known.

After the initial layout is completed and analyzed using the methods of Chapters 12–19, the wing will probably be moved and the tails resized to meet all required stability and control characteristics. Hopefully the initial estimates will be close enough so that major changes will not be needed.

### Wing/Tail Lofting

The reference (trapezoidal) wing and tails are positioned with respect to the fuselage using the methods discussed above. During the layout process the actual, exposed wing and tails will be drawn.

The reference wing is defined to the aircraft centerline, and is based upon the projected area (i.e., dihedral does not affect the top view of the reference wing). The actual, exposed wing begins at the side of the fuselage and includes the effect of the dihedral upon the true-view area. The dihedral angle increases the actual wing area equivalent to dividing by the cosine of the dihedral angle.

Also, the actual wing planform may not be trapezoidal. Figure 7.24 illustrates several of the many nontrapezoidal wing variations. A typical rounded wing tip is shown in Fig. 7.24a. This and other wing-tip shapes have already been discussed. The straightened-out trailing edge shown in Fig. 7.24b increases the flap chord and provides increased wing thickness for the landing gear.

Figure 7.24c illustrates a “Leading-Edge Extension (LEX),” which increases lift for combat maneuvering (see Chapter 12). A highly-blended wing/body is shown in Fig. 7.24d, in which the actual wing looks very little like the reference wing. This type of wing is used to minimize the transonic and supersonic shocks.

Once the designer has settled upon the actual wing and tail planforms, their surfaces must be lofted to provide accurate cross sections. These are required to verify that there is sufficient room for the fuel tanks, landing gear, spars, and other internal components. During production design this lofting would be done using conics or some other mathematical surface definition.

For initial design, simpler methods of wing and tail lofting can be used. These rely upon the assumption that the airfoil coordinates themselves are smoothly lofted. This is an excellent assumption, as otherwise the airfoil performance would be poor.

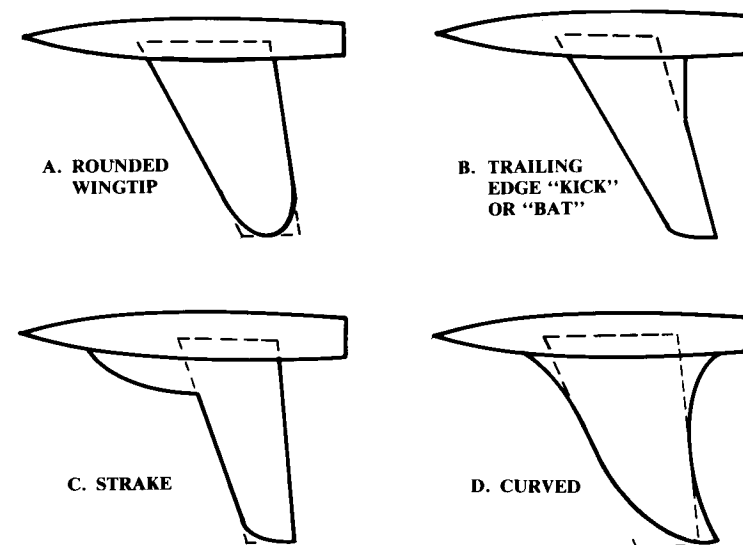


Fig. 7.24 Nontrapezoidal wings.

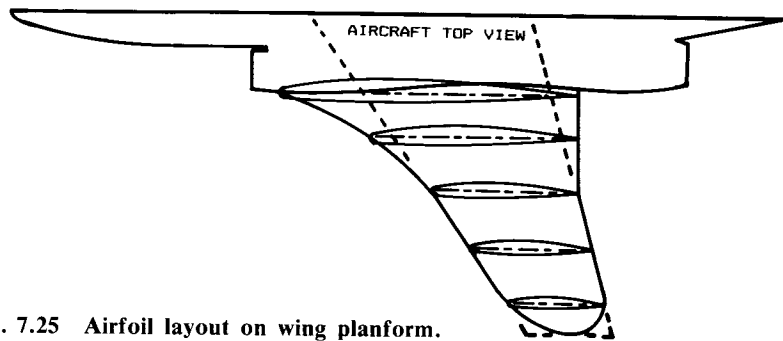


Fig. 7.25 Airfoil layout on wing planform.

If the wing or tail uses the identical airfoil section and thickness ratio at all span stations, and is without twist, the airfoils can be drawn simply by scaling the airfoil coordinates to fit the chord lengths of the selected spanwise locations.

It is customary to lightly draw the airfoils on the top view of the wing, superimposing them on their chordline (Fig. 7.25). This layout procedure simplifies the generation of cross sections, as will be discussed later. For initial design purposes the airfoils can be quickly drawn using only a few scaled coordinate points for the top and bottom surfaces.

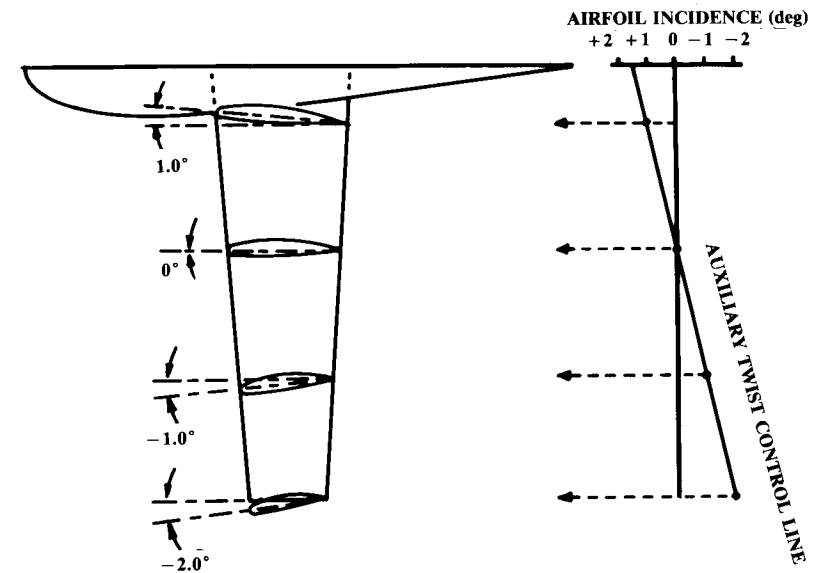
If twist is incorporated, the incidence at each span station must be determined and the chord line rotated accordingly before the airfoil is drawn. Since the chord length is defined in top view, the chord length at each spanwise station must be increased equivalent to dividing by the cosine of the appropriate incidence angle.

Instead of calculating the twist, an auxiliary twist control line may be constructed behind the wing. The airfoil incidence at each span station can then be read from the control line (Fig. 7.26).

A wing with a complicated aerodynamic design may have the twist, camber, and thickness all varying from root to tip. These spanwise variations can be lofted by using a separate auxiliary control line for each, as shown in Fig. 7.27. The airfoil coordinate points must be calculated by separating the airfoil into its camber line and thickness distribution, scaling them as indicated by the auxiliary control lines, and recombining them. Such a complicated wing design is not normally accomplished until much later in the design process.

For a wing such as shown in Fig. 7.27, the complex curvatures of the wing surface may present difficulties. A spar running from root to tip may very well be so curved that it is structurally undesirable. Even worse, the hinge lines for the ailerons and flaps may not lie in a straight line. As curved hinge lines are impossible, the ailerons and flaps may have to be broken into a number of surfaces unless the wing surface can be modified to straighten the hingeline.

This is done by "wing rigging" (not to be confused with the rigging of a biplane wing)—the process of vertically shifting the airfoil sections until some desired spanwise line is straight.



ANGLES ARE EXAGGERATED FOR ILLUSTRATION

Fig. 7.26 Airfoil layout with twist.

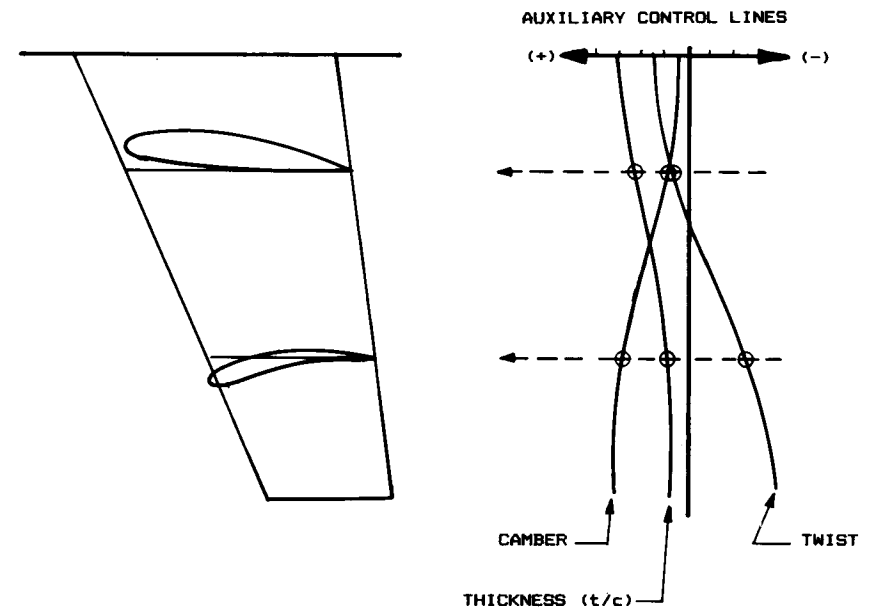


Fig. 7.27 Wing airfoil layout—nonlinear variations.

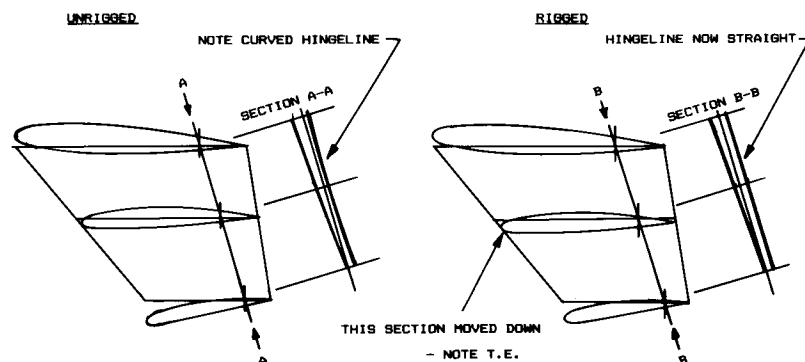


Fig. 7.28 Wing airfoil rigging.

Figure 7.28 illustrates a complex wing in which the aileron hingeline, Section A-A, is curved. On the right side of the figure is the same wing with the midspan airfoil moved downward a few inches. This provides a straight hingeline shown as Section B-B.

### Airfoil Linear Interpolation

Most wings are initially defined by a root airfoil and a tip airfoil, which may be different, and their incidence angles or relative twist. Frequently the tip airfoil will be selected for gentle stall characteristics while the root airfoil is selected for best performance. The resulting wing has good overall performance, with good stall characteristics because the tip will stall after the root. The airfoils between the root and tip can be quickly developed by one of two methods.

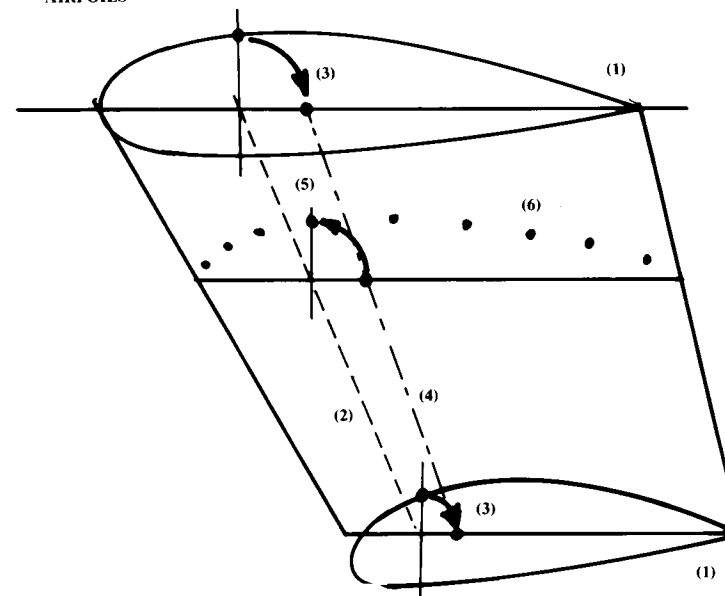
Linear interpolation, the easiest method, is depicted in Fig. 7.29. Here the new airfoils are created as “weighted averages” of the root and tip airfoils. Linearly interpolated airfoils have section properties that are approximately the interpolation of the section properties of the root and tip airfoils.

(Some modern laminar airfoils will not provide interpolated section characteristics. Instead, the interpolated airfoils must each be separately analyzed.)

The intermediate airfoils are linearly interpolated by a five-step process. The root and tip airfoils are drawn (step 1). A constant percent-chord line is drawn connecting the root and tip airfoil, and vertical lines are drawn from the intersection of that line with the chordlines (step 2). The airfoil points found at those vertical lines are “swung down” to the chord line, using an arc centered at the intersection of the chord line and the vertical line (step 3). These “swung down” points for the root and tip airfoils are then connected by a straight line (step 4).

At the desired location of an interpolated airfoil, a chord line is drawn. The intersection of that chord line with the line drawn in step 4 defines the chordwise location of a point on the interpolated airfoil. In step 5 this point is “swung up” to its thickness location by an arc centered at the intersection of the chord line and the spanwise percent-chord line from step 2.

GRAPHIC INTERPOLATION BETWEEN DIFFERING ROOT AND TIP AIRFOILS



- 1 - SUPERIMPOSE ROOT AND TIP AIRFOILS ON PLANFORM
- 2 - DRAW LINE AT SOME CONSTANT PERCENT OF CHORD
- 3 - SWING AIRFOIL POINT DOWN ONTO CHORD REFERENCE LINE
- 4 - CONNECT ROOT AND TIP POINTS FROM 3
- 5 - SWING POINT UP TO NEW AIRFOIL LOCATION
- 6 - REPEAT FOR OTHER PERCENT CHORD LINES

Fig. 7.29 Wing airfoil layout—linear interpolation.

This process is repeated for as many points as are needed to draw the new airfoil. Then the process is repeated to draw other airfoils. While it seems complicated, a wing can be developed using this method in about fifteen minutes by an experienced designer. (However, a computer does this in seconds!)

### Airfoil Flat-Wrap Interpolation

The linear-interpolation method doesn't necessarily provide a flat-wrap surface. In laying out a fuselage for flat-wrap, it was necessary to hold the same tangent angle for the conics in the different cross sections. The same is true for wings.

To provide a flat-wrap wing, it is necessary to interpolate between airfoil coordinates with the same slope (i.e., tangent angle). The linear interpolation method connects points based upon their percent of chord. If the wing is twisted or the airfoils are dissimilar, the surface slopes may be different for airfoil points that are at the same percent of chord. This requires a modification to the method described above.

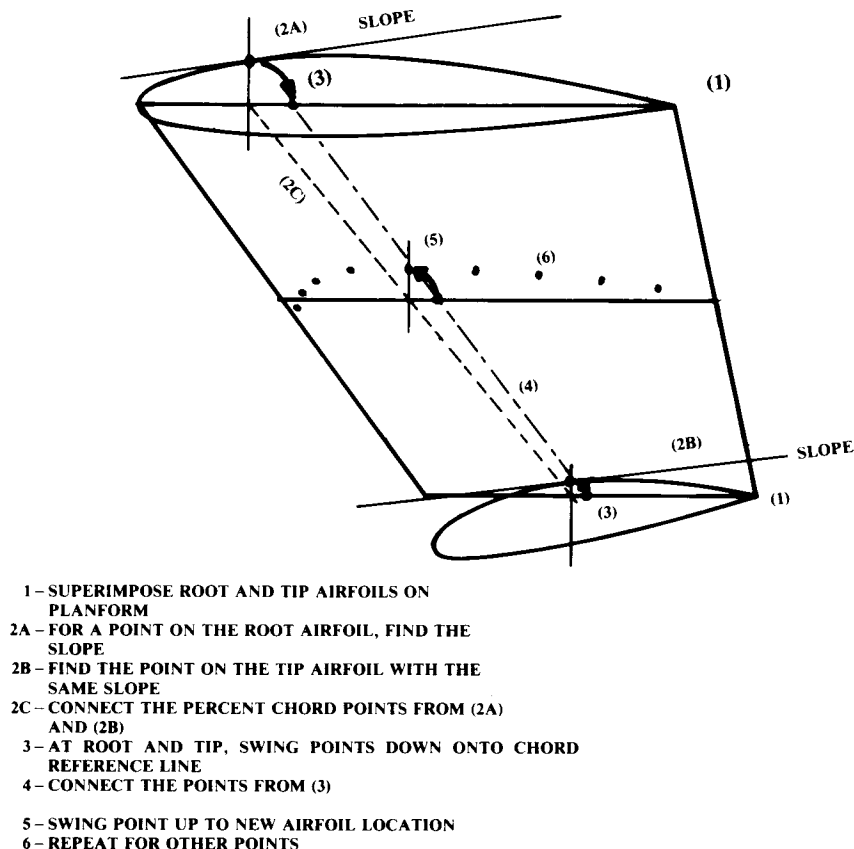


Fig. 7.30 Wing airfoil layout—flat-wrap.

Figure 7.30 illustrates this modification. The only difference is in step 2. Previously a spanwise line was drawn connecting constant percent chord locations on the chordline. To obtain a flat-wrap surface this spanwise line must be drawn connecting locations on the chordline that have the same surface slope. Note in the figure how the tip chord has the indicated slope at a more-aft percent location of the chord than does the root chord.

A number of composite homebuilts are being fabricated by a method long used for model airplanes. A large block of urethane foam is cut directly to the desired wing shape using a hot-wire cutter which is guided by root and tip airfoil templates attached to the foam block. The templates have tic-marks that are numbered. The wire is guided around the templates by two homebuilders, one of whom calls out the numbers of the tic-marks.

If the tic-marks are at constant percent-chord locations, and the wing has dissimilar airfoils or appreciable twist, this method will produce a linearly-interpolated instead of a flat-wrap surface. If the wing is to be covered by

fiberglass, this will pose no problem as the fiberglass cloth will easily conform to the slight amount of compound-curvature present.

However, if the wing is to be covered by sheet metal or plywood, the linearly-interpolated foam surface will be depressed relative to the flat-wrapped skin. This could reduce the strength of the skin bonding. It is conceivable that such a wing could fail in flight for this simple reason. Who said lofting isn't important?

### Wing/Tail Cross-Section Layout

Wing lofting during initial design permits verification that the fuel and other internal components will fit within the wing. This requires the development of wing and tail cross sections oriented perpendicular to the aircraft centerline.

Such cross sections can be easily developed once the airfoils are drawn onto the top view of the wing. Figure 7.31 illustrates the development of one such cross section.

To develop a wing (or tail) cross section, vertical lines are drawn on the cross section at the spanwise locations of the airfoils shown on the wing top view. Also, the wing reference plane is shown at the appropriate wing dihedral angle. Then the airfoil upper and lower points are measured relative to the plane of the wing, and drawn accordingly on the cross section. The cross-section shape can then be drawn using French curves.

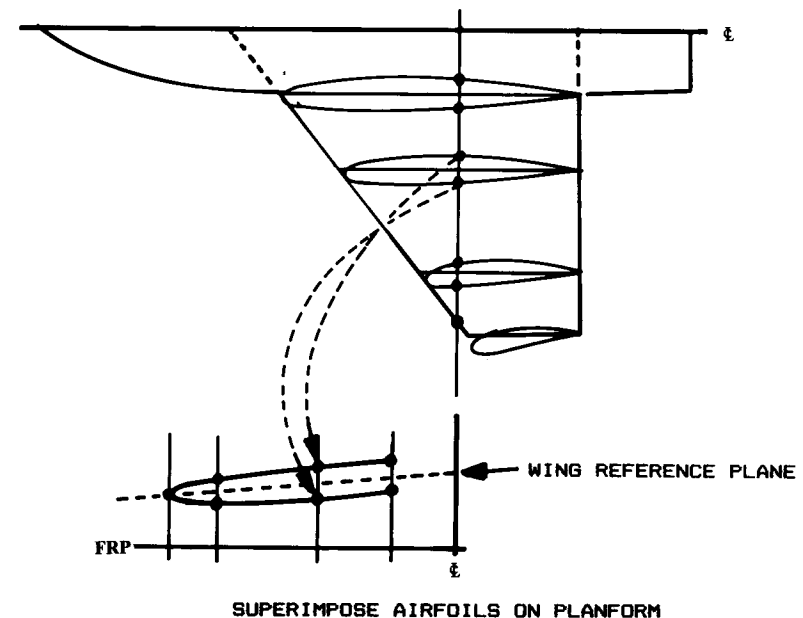


Fig. 7.31 Wing/tail cross section layout.

The same procedure can be used to develop section cuts at angles other than perpendicular to the aircraft centerline. The sections of Fig. 7.28 labeled A-A and B-B were developed in this manner.

### Wing Fillets

For improved aerodynamic efficiency, the wing-fuselage connection of most aircraft is smoothly blended using a "wing fillet" (Fig. 7.32). A wing fillet is generally defined by a circular arc of varying radius, tangent to both the wing and fuselage. Typically a wing fillet has a radius of about 10% of the root-chord length.

The fillet circular arc is perpendicular to the wing surface, so the arc is in a purely vertical plane only at the maximum thickness point of the wing. At the leading edge, the arc is in a horizontal plane.

The fillet arc radius may be constant, or may be varied using an auxiliary radius control line, as shown in Fig. 7.32. Note that the starting radius must be equal to the fillet radius shown in the wing top view. Also, the fillet radius is usually increasing towards the rear of the aircraft, to minimize airflow separation.

Some aircraft have a fillet only on the rear part of the wing. In this case the fillet starts, with zero radius, at the wing's maximum thickness point.

For initial layout purposes the fillet is frequently "eyeballed." Only a few of the 10 or 15 aircraft cross sections developed for an initial layout will show the wing fillet, so a fillet radius that "looks good" can be used. If better accuracy is desired, a fillet radius control line can be used with the simplifying assumption that the fillet arc is approximately vertical over most

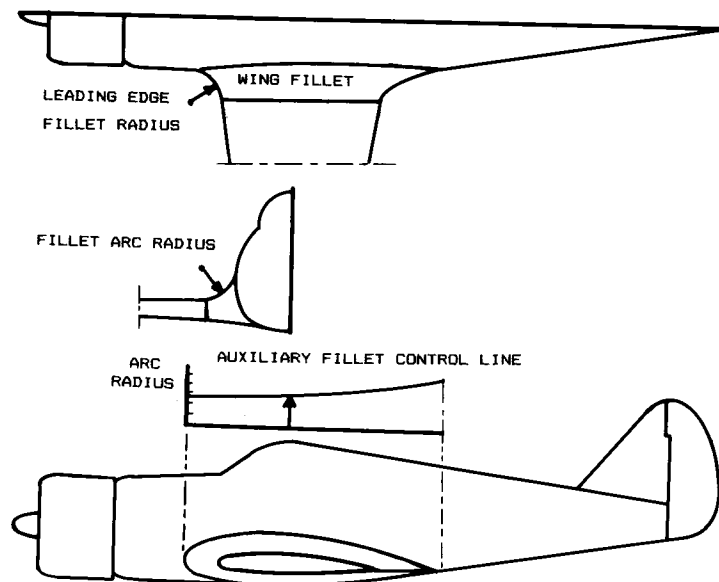


Fig. 7.32 Wing fillet layout.

of the wing. This avoids the necessity of constructing auxiliary views perpendicular to the wing surface to accurately develop each fillet radius.

### 7.9 AIRCRAFT LAYOUT PROCEDURES

There are really no standard procedures for aircraft layout. Every aircraft demands its own procedure. The designer must develop the aircraft drawing while simultaneously considering a wide variety of requirements, design drivers, and good design practices. This process can only be learned through practice and a high level of desire.

Nevertheless, certain generalities can be made. First, the initial design should be "roughed-out" before a quality drawing is begun. This is best done in the desired scale of the finished drawing. Common drawing scales are 1/10, 1/20, 1/40, and 1/100, depending upon the size of the aircraft. Computer-aided design systems usually work in "full scale" on the scope, and any desired scale can be selected if a paper copy is required.

This "roughed-out" design is based upon the conceptual sketch and should identify the locations of the major internal components such as the crew station, payload, passengers, fuel tanks, landing gear, and engines. The fuselage length should be based upon prior aircraft or the statistical approach presented earlier, and should be modified as necessary to contain the internal components.

The completed roughed-out layout is used to define the initial lofting approach. The designer must determine the number of longitudinal control lines to use as well as selecting the control stations. A minimum number of control stations should be selected to insure that all of the large internal components can be properly enclosed by the aircraft surface. Remember that the more control stations selected, the greater the difficulty in insuring smooth longitudinal contours.

At this point the actual layout is begun, using the roughed-out layout as an "underlay" (i.e., the actual layout is done on transparent paper or mylar placed over the roughed-out layout). The fuselage is developed using the selected lofting approach, and the internal components are drawn.

The wing and tail trapezoidal geometries should be drawn on separate pieces of paper. The mean aerodynamic chord should be shown, including the desired initial location of the wing with respect to the center of gravity.

The wing drawing can then be slid under the actual drawing and moved to the desired position with respect to the estimated center of gravity location on the fuselage. The trapezoidal wing geometry is traced on to the layout, and the actual wing geometry is drawn. This includes desired planform modifications as well as fillets and wing tips.

Tails are usually drawn after the fuselage is defined on the drawing. If the actual tail moment arm is different from that assumed in sizing the tail, the tail area should be recalculated at this time.

The wing and tail geometric parameters should be tabulated somewhere on the drawing, along with the estimated takeoff gross weight, fuel weight and volume, engine type and size (if not 100%), inlet capture area, propeller geometry, etc. This information will greatly aid those who later attempt to analyze the drawing.

### 7.10 WETTED AREA DETERMINATION

Aircraft wetted area ( $S_{wet}$ ), the total exposed surface area, can be visualized as the area of the external parts of the aircraft that would get wet if it were dipped into water. The wetted area must be calculated for drag estimation, as it is the major contributor to friction drag.

The wing and tail wetted areas can be approximated from their planforms, as shown in Fig. 7.33. The wetted area is estimated by multiplying the true-view exposed planform area ( $S_{exposed}$ ) times a factor based upon the wing or tail thickness ratio.

If a wing or tail were paper-thin, the wetted area would be exactly twice the true planform area (i.e., top and bottom). The effect of finite thickness is to increase the wetted area, as approximated by Eqs. (7.10) or (7.11). Note that the true exposed planform area is the projected (top-view) area divided by the cosine of the dihedral angle.

If  $t/c < .05$

$$S_{wet} = 2.003 S_{exposed} \quad (7.10)$$

If  $t/c > .05$

$$S_{wet} = S_{exposed} [1.977 + 0.52(t/c)] \quad (7.11)$$

The exposed area shown in Fig. 7.33 can be measured from the drawing in several ways. A professional designer will have access to a "planimeter," a mechanical device for measuring areas. Use of the planimeter is a dying art as the computer replaces the drafting board. Alternatively, the area can be measured by tracing onto graph paper and "counting squares."

The wetted area of the fuselage can be initially estimated using just the side and top views of the aircraft by the method shown in Fig. 7.34. The side- and top-view projected areas of the fuselage are measured from the drawing, and the values are averaged.

For a long, thin body circular in cross section, this average projected area times  $\pi$  will yield the surface wetted area. If the body is rectangular in cross section, the wetted area will be four times the average projected area. For typical aircraft, Eq. (7.12) provides a reasonable approximation.

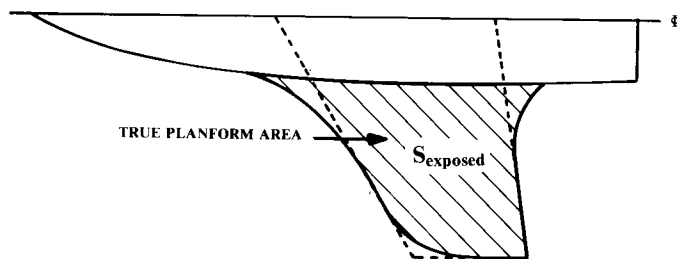


Fig. 7.33 Wing/tail wetted area estimate.

$$S_{wet} = K (A_{top} + A_{side})/2$$

$$K = \pi \text{ FOR ELLIPTIC CROSS SECTION}$$

$$K = 4 \text{ FOR SQUARE CROSS SECTION}$$

TYPICALLY USE  $K = 3.4$

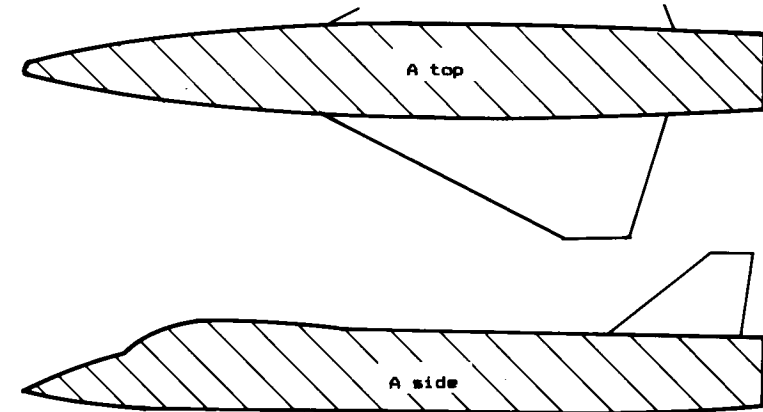


Fig. 7.34 Quick fuselage wetted area estimate.

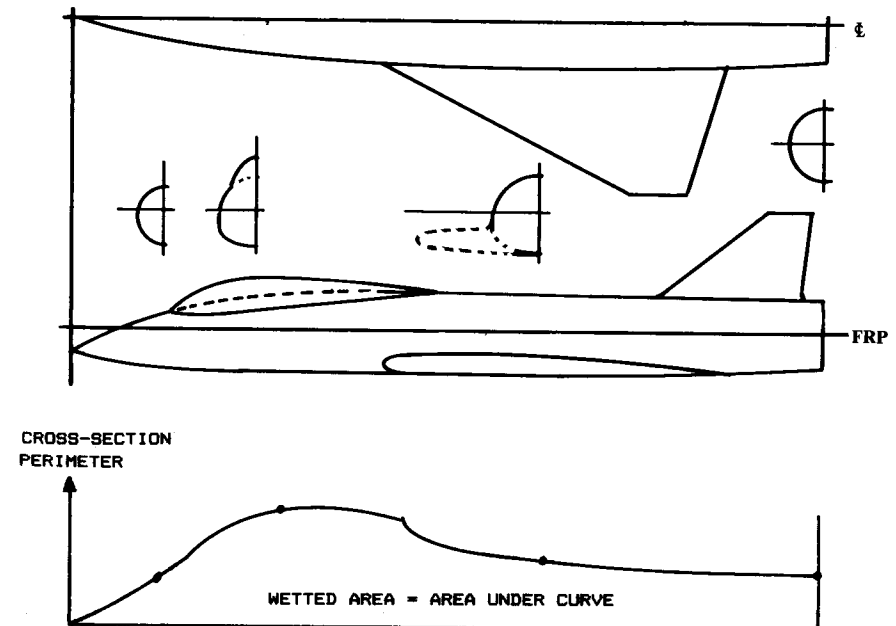


Fig. 7.35 Fuselage wetted area plot.



$$S_{\text{wet}} \cong 3.4 \left( \frac{A_{\text{top}} + A_{\text{side}}}{2} \right) \quad (7.12)$$

A more accurate estimation of wetted area can be obtained by graphical integration using a number of fuselage cross sections. If the perimeters of the cross sections are measured and plotted vs longitudinal location, using the same units on the graph, then the integrated area under the resulting curve gives the wetted area (Fig. 7.35).

Perimeters can be measured using a professional's "map-measure," or approximated using a piece of scrap paper. Simply follow around the perimeter of the cross section making tic marks on the paper, and then measure the total length using a ruler.

Note that the cross-sectional perimeter measurements should not include the portions where components join, such as at the wing-fuselage intersection. These areas are not "wetted."

### 7.11 VOLUME DETERMINATION

The aircraft internal volume can be used as a measure of the reasonableness of a new design, by comparing the volume to existing aircraft of similar weight and type. This is frequently done by customer engineering groups, using statistical data bases which correlate internal volume with takeoff gross weight for different classes of aircraft. An aircraft with a less-than-typical internal volume will probably be tightly packed, which makes for poor maintainability.

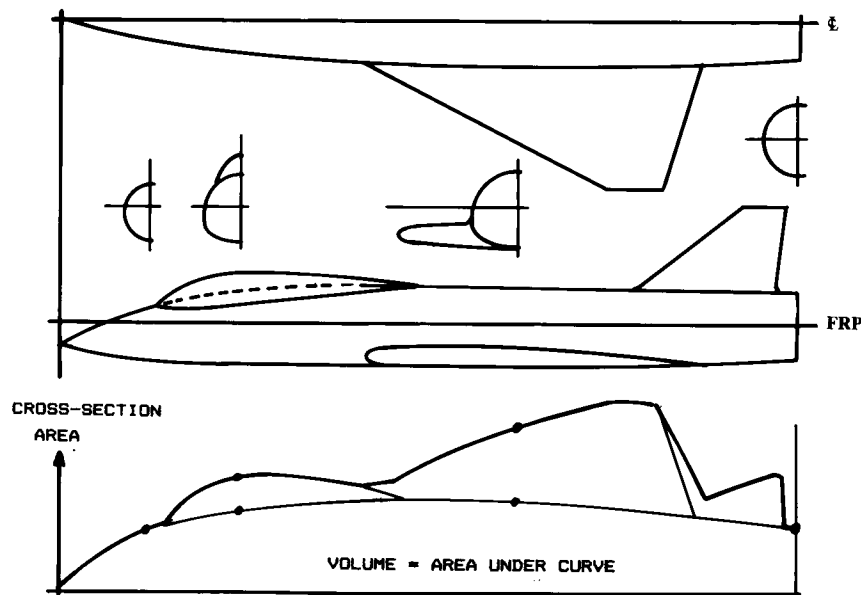


Fig. 7.36 Aircraft volume plot.

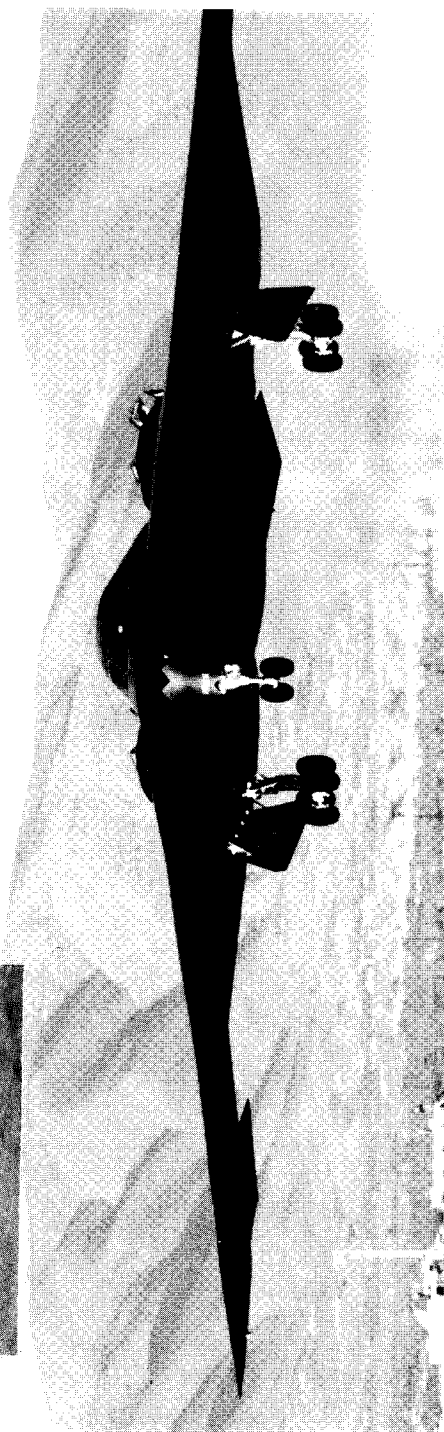
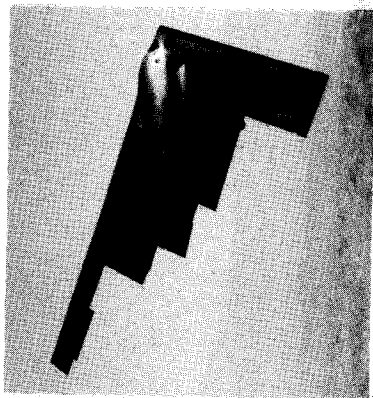
Aircraft internal volume can be estimated in a similar fashion to the wetted-area estimation. A crude estimate of the fuselage internal volume can be made using Eq. (7.13), which uses the side and top view projected areas as used in Eq. (7.12). "L" in Eq. (7.13) is the fuselage length.

$$\text{Vol} \cong 3.4 \frac{(A_{\text{top}})(A_{\text{side}})}{4L} \quad (7.13)$$

A more accurate estimate of internal volume can be found by a graphical integration process much like that used for wetted area determination. The cross-section areas of a number of cross sections are measured and plotted vs longitudinal location, using consistent units (typically inches horizontally and square inches vertically on the graph). The area under the resulting curve is the volume, as shown in Fig. 7.36.

To obtain reasonable accuracy, cross sections should be plotted and measured anywhere that the cross-sectional area changes substantially. This typically includes the start of an inlet duct, the start and end of a canopy, and where a wing or tail begins and ends.

Another use of the "volume distribution plot" is to predict and minimize supersonic wave drag and transonic drag rise. This will be discussed in Chapter 12.



Northrop B-2 Stealth Bomber

## SPECIAL CONSIDERATIONS IN CONFIGURATION LAYOUT

### 8.1 INTRODUCTION

The previous chapter discussed the mechanics of configuration layout. Later chapters will focus on the required provisions for specific internal components, such as the crew station and landing gear. This chapter discusses a number of important intangible considerations, such as aerodynamics, structures, detectability, vulnerability, producibility, and maintainability. All of these are numerically analyzed in later stages of the design process. During configuration layout the designer must consider their impact in a qualitative sense.

### 8.2 AERODYNAMIC CONSIDERATIONS

The overall arrangement and smoothness of the fuselage can have a major effect upon aerodynamic efficiency. A poorly designed aircraft can have excessive flow separation, transonic drag rise, and supersonic wave drag. Also, a poor wing-fuselage arrangement can cause lift losses or disruption of the desired elliptical lift distribution.

Aerodynamic analysis will be discussed in Chapter 12 and a variety of first-order estimation methods will be presented. During concept layout, the designer must consider the requirements for aerodynamics based upon experience and a "good eye."

Minimization of wetted area is the most powerful aerodynamic consideration for virtually all aircraft. Wetted area directly affects the friction drag. Fuselage wetted area is minimized by tight internal packaging and a low fineness ratio (i.e., a short, fat fuselage). However, excessively tight packaging should be avoided for maintainability considerations. Also, a short, fat fuselage will have a short tail moment arm which increases the required tail areas. The short, fat fuselage will also have high supersonic wave drag.

Another major driver for good aerodynamic design during fuselage layout is the maintenance of smooth longitudinal contours. These can be provided by the use of smooth longitudinal control lines. Generally, longitudinal breaks in contour should follow a radius at least equal to the fuselage diameter at that point.

To prevent separation of the airflow, the aft-fuselage deviation from the freestream direction should not exceed 10–12 deg (Fig. 8.1). However, the air inflow induced by a pusher-propeller will prevent separation despite contour angles of up to 30 deg or more.

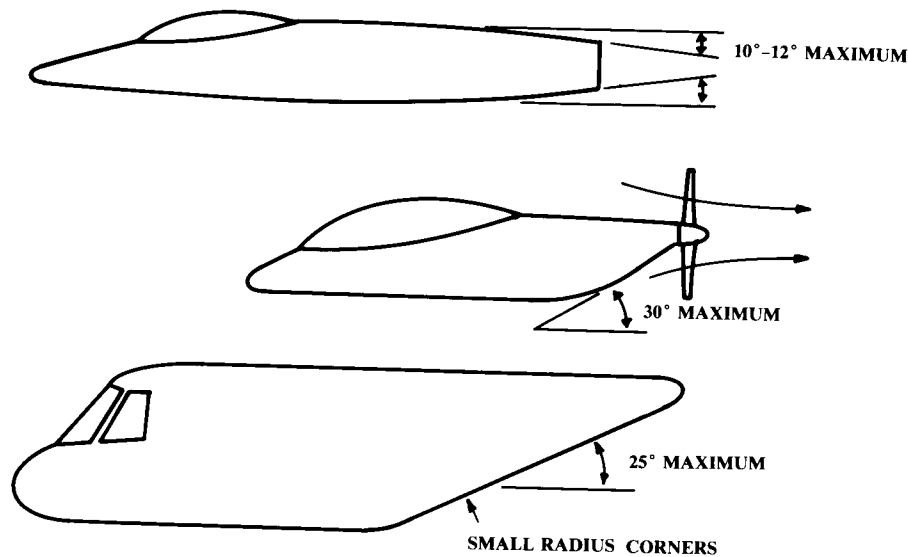


Fig. 8.1 Longitudinal contour guidelines.

A lower-surface upsweep of about 25 deg can be tolerated for a rear-loading transport aircraft provided that the fuselage lower corners are fairly sharp. This causes a vortex-flow pattern that reduces the drag penalty. In general, aft-fuselage upsweep should be minimized as much as possible, especially for high-speed aircraft.

The importance of well-designed wing fillets has already been discussed. Fillets are especially important for low-wing, high-speed aircraft such as jet transports.

These aircraft will frequently have a modified wing-root airfoil to further minimize fuselage interference and shock-induced drag increases. This modification takes the form of an uncambered or even negatively-cambered airfoil set at a high positive angle of incidence. Design of such a wing modification is beyond the scope of this book, but for layout purposes can be approximated by examining the wing of an existing, similar speed-class aircraft.

“Base area” is any unfaired, rearward-facing blunt surface. Base area causes extremely high drag due to the low pressure experienced by the rearward-facing surface (see Chapter 12).

However, a base area between or very near to the jet exhausts may be “filled-in” by the pressure field of the exhaust, partially alleviating the drag penalty. The T-38 has such a base area between its nozzles. A base area fill-in effect is difficult to predict.

The aerodynamic interaction between different components should be visualized in designing the aircraft. For example, a canard should not be located such that its wake might enter the engine inlets at any possible angle of attack. Wake ingestion can stall or even destroy a jet engine.

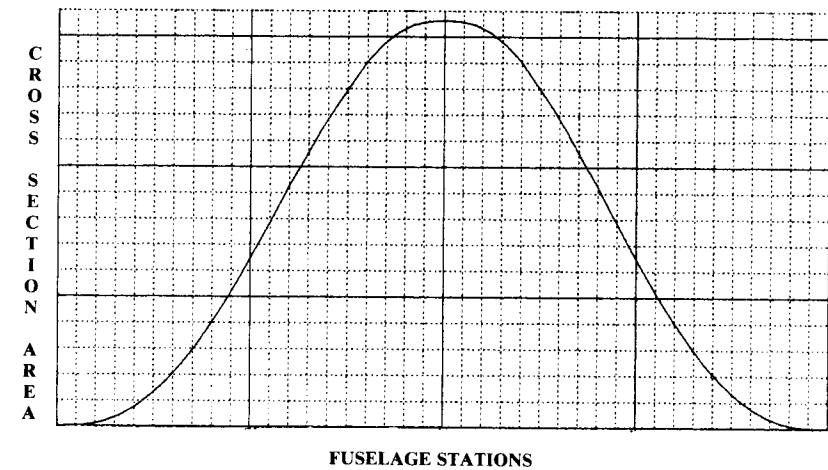


Fig. 8.2 Sears-Haack volume distribution.

If an aircraft’s forebody has sharp lower corners, a separated vortex can be expected at high angle of attack. This could also be ingested by the inlets, with bad results. Also, such a vortex could unpredictably affect the wing or tail surfaces.

For supersonic aircraft, the greatest aerodynamic impact upon the configuration layout results from the desire to minimize supersonic wave drag, a pressure drag due to the formation of shocks. This is analytically related to the longitudinal change in the aircraft’s total cross-sectional area. In fact, wave drag is calculated using the second derivative (i.e., curvature) of the volume-distribution plot as shown in Fig. 7.36.

Thus, a “good” volume distribution from a wave-drag viewpoint has the required total internal volume distributed longitudinally in a fashion that minimizes curvature in the volume-distribution plot. Several mathematical solutions to this problem have been found for simple bodies-of-revolution, with the “Sears-Haack” body (Fig. 8.2—see Ref. 16) having the lowest wave drag.

If an aircraft could be designed with a volume plot shaped like the Sears-Haack volume distribution it would have the minimum wave drag at Mach 1.0 for a given length and total internal volume. (What happens at higher Mach numbers is discussed in Chapter 12, but for initial layout purposes the minimization of wave drag at Mach 1.0 is a suitable goal in most cases.)

However, it is usually impossible to exactly or even approximately match the Sears-Haack shape for a real aircraft. Fortunately, major drag reductions can be obtained simply by smoothing the volume distribution shape.

As shown in Fig. 8.3, the main contributors to the cross-sectional area are the wing and the fuselage. A typical fuselage with a trapezoidal wing will have an irregularly-shaped volume distribution with the maximum cross-sectional area located near the center of the wing. By “squeezing” the

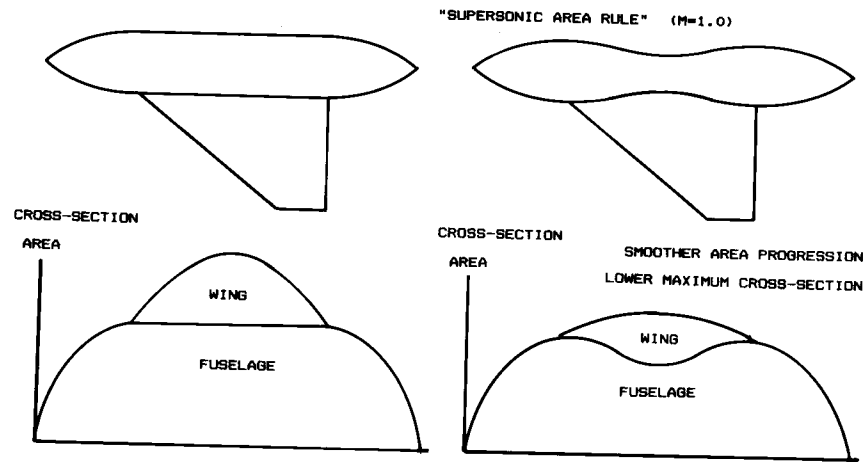


Fig. 8.3 Design for low wave drag.

fuselage at that point, the volume-distribution shape can be smoothed and the maximum cross-sectional area reduced.

This design technique, developed by R. Whitcomb of the NACA (Ref. 17), is referred to as "area-ruling" or "coke-bottling" and can reduce the wave drag by as much as 50%. Note that the volume removed at the center of the fuselage must be provided elsewhere, either by lengthening the fuselage or by increasing its cross-sectional area in other places.

While area-ruling was developed for minimization of supersonic drag, there is reason to believe that even low-speed aircraft can benefit from it to some extent. The airflow over the wing tends to separate toward the trailing edge. If an aircraft is designed such that the fuselage is increasing in cross-sectional area towards the wing trailing edge, this may "push" air onto the wing, thus reducing the tendency to separate. The Wittman Tailwind, which is remarkably efficient, uses this approach.

### 8.3 STRUCTURAL CONSIDERATIONS

In most larger companies, the configuration designer is not ultimately responsible for the structural arrangement of the aircraft. That is the responsibility of the structural design group. However, a good configuration designer will consider the structural impacts of the general arrangement of the aircraft, and will in fact have at least an initial idea as to a workable structural arrangement.

The primary concern in the development of a good structural arrangement is the provision of efficient "load paths"—the structural elements by which opposing forces are connected. The primary forces to be resolved are the lift of the wing and the opposing weight of the major parts of the aircraft, such as the engines and payload. The size and weight of the structural members will be minimized by locating these opposing forces near to each other.

Carried to the extreme, this leads to the Flying Wing concept. In a flying wing the lift and weight forces can be located at virtually the same place. In the ideal case, the weight of the aircraft would be distributed along the span of the wing exactly as the lift is distributed (Fig. 8.4). This is referred to as "spanloading," and eliminates the need for a heavy wing structure to carry the weight of the fuselage to the opposing lift force exerted by the wing. The structure can then be sized by lesser requirements such as the landing-gear loads.

While ideal span-loading is rarely possible, the span-loading concept can be applied to more-conventional aircraft by spreading some of the heavy items such as engines out along the wing. This will yield noticeable weight savings, but must be balanced against the possible drag increase.

If the opposing lift and weight forces cannot be located at the same place, then some structural path will be required to carry the load. The weight of structural members can be reduced by providing the shortest, straightest load path possible.

Figure 8.5 illustrates a structural arrangement for a small fighter. The major fuselage loads are carried to the wing by "longerons," which are typically I- or H-shaped extrusions running fore and aft and attached to the

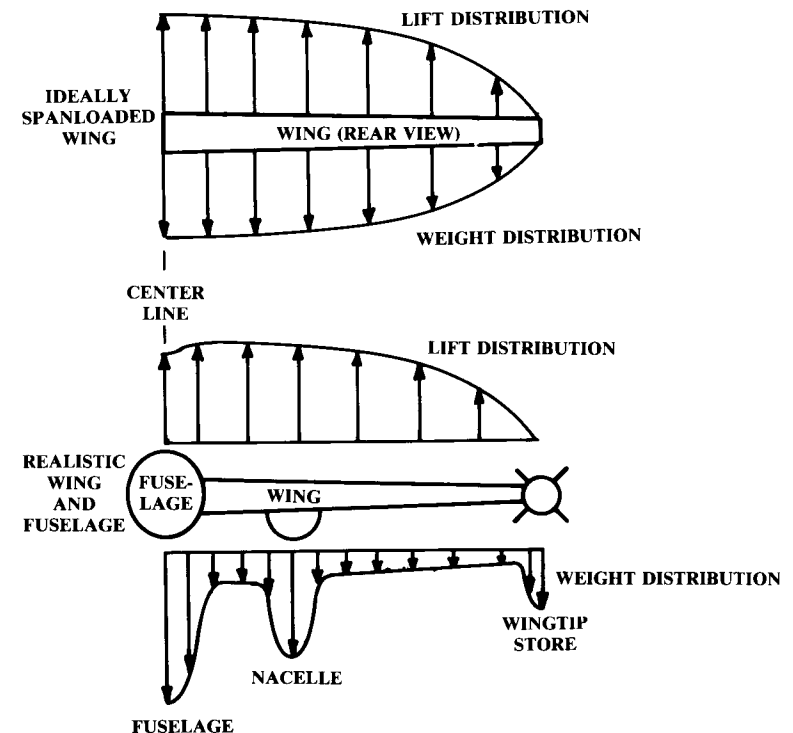


Fig. 8.4 Spanloading for weight reduction.

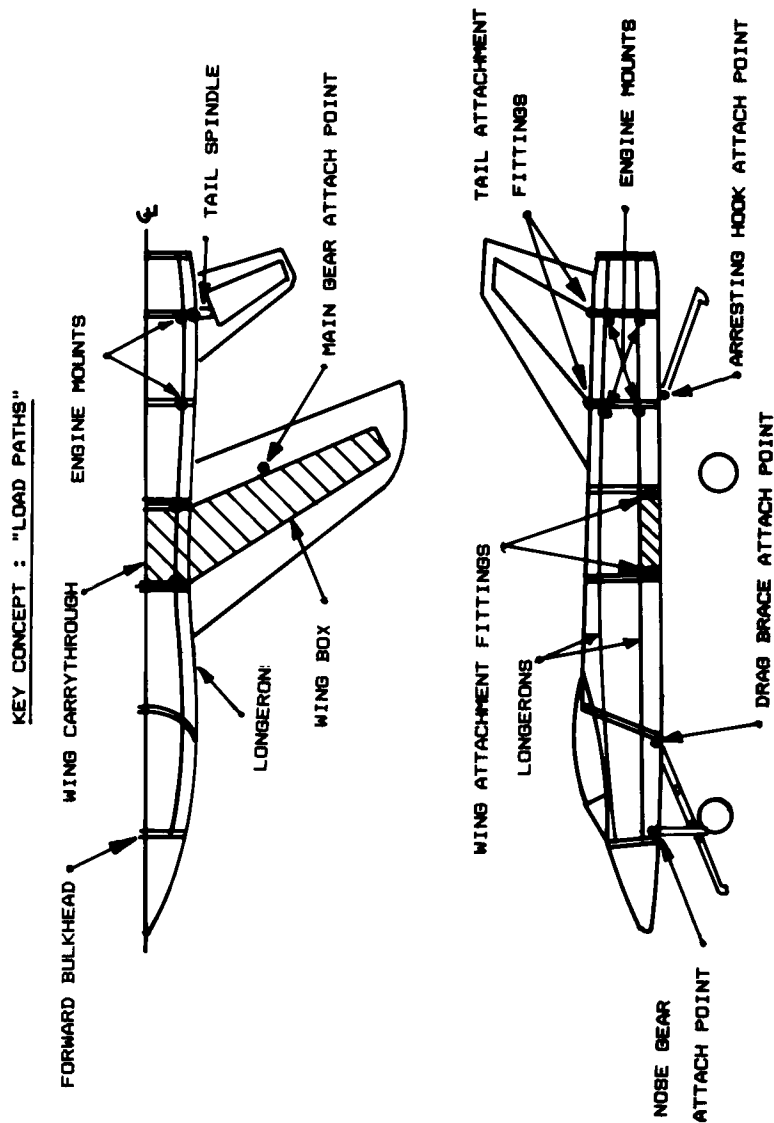


Fig. 8.5 Structural arrangement.

skin. Longerons are heavy, and their weight should be minimized by designing the aircraft so that they are as straight as possible.

For example, the lower longerons in Fig. 8.5 are high enough that they pass over the wing-carrythrough box. Had the longerons been placed lower, they would have required a kink to pass over the box.

On the other hand, the purpose of the longeron is to prevent fuselage bending. This implies that the lightest longeron structure occurs when the upper and lower longerons are as far apart vertically as possible. In Fig. 8.6 the longerons are farther apart, but this requires a kink to pass over the box. Only a trade study can ultimately determine which approach is lighter for any particular aircraft.

In some designs similar to Fig. 8.5 the lower longerons are placed near the bottom of the aircraft. A kink over the wing box is avoided by passing the longeron under or through the wing box. This minimizes weight but complicates both fabrication and repair of the aircraft.

For aircraft such as transports, which have fewer cutouts and concentrated loads than a fighter, the fuselage will be constructed with a large number of "stringers" which are distributed around the circumference of the fuselage (Fig. 8.7). Weight is minimized when the stringers are all straight and uninterrupted.

Another major structural element used to carry fuselage bending loads is the "keelson." This is like the keel on a boat, and is a large beam placed at the bottom of the fuselage as shown in Fig. 8.7. A keelson is frequently used to carry the fuselage bending loads through the portion of the lower fuselage which is cut up by the wheel wells.

As the wing provides the lift force, load-path distances can be reduced by locating the heavy weight items as near to the wing as possible. Similarly, weight can be reduced by locating structural cutouts away from the wing. Required structural cutouts include the cockpit area and a variety of doors (passenger, weapons bay, landing gear, engine access, etc.).

An especially poor arrangement (seen on some older fighter aircraft) has the main landing gear retracting into the wing-box area, which requires a large cutout where the loads are the greatest.

When possible, structural cutouts should be avoided altogether. For example, a jet engine that is buried in the fuselage requires a cutout for the inlet, a cutout for the exhaust, and in most cases another cutout for removal

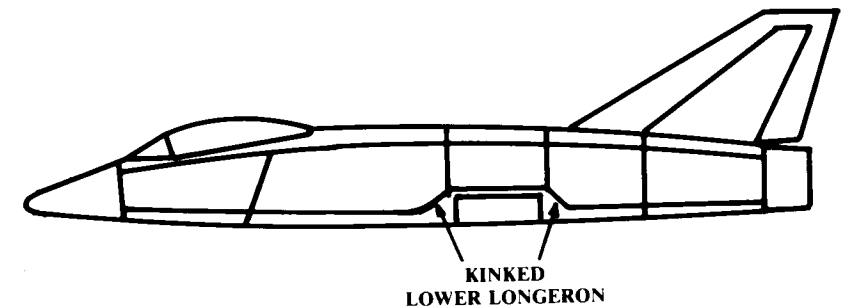


Fig. 8.6 Kinked lower longeron.

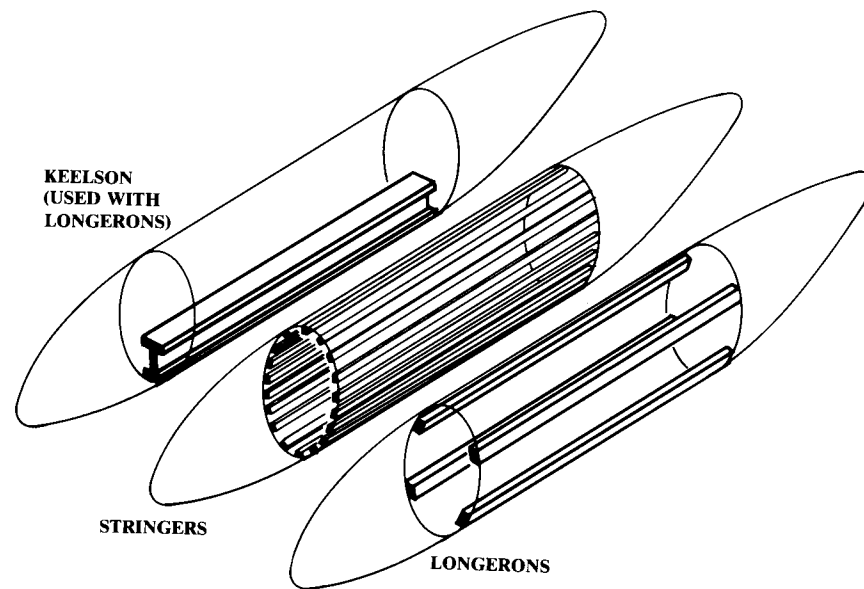


Fig. 8.7 Structural concepts for fuselage loads.

of the engine. The resulting weight penalty compared to a podded engine must be balanced against the reduced drag of a buried engine installation.

Figure 8.5 illustrates another important concept in structural arrangement. Large concentrated loads such as the wing and landing gear attachments must be carried by a strong, heavy structural member such as a major fuselage bulkhead. The number of such heavy bulkheads can be minimized by arranging the aircraft so that the bulkheads each carry a number of concentrated loads, rather than requiring a separate bulkhead for each concentrated load.

In Fig. 8.5 the two bulkheads in the aft fuselage carry the loads for the engines, tails, and arresting hook. Had the tails and engine been located without this in mind, the structural designer would have had to provide four or five heavy bulkheads rather than the two shown.

The lift force on the wing produces a tremendous bending moment where the wing attaches to the fuselage. The means by which this bending moment is carried across the fuselage is a key parameter in the structural arrangement, and will greatly influence both the structural weight and the aerodynamic drag of the aircraft.

Figure 8.8 illustrates the four major types of wing carrythrough structure. The “box carrythrough” is virtually standard for high-speed transports and general-aviation aircraft. The box carrythrough simply continues the wing box through the fuselage. The fuselage itself is not subjected to any of the bending moment of the wing, which minimizes fuselage weight.

However, the box carrythrough occupies a substantial amount of fuselage volume, and tends to add cross-sectional area at the worst possible place for

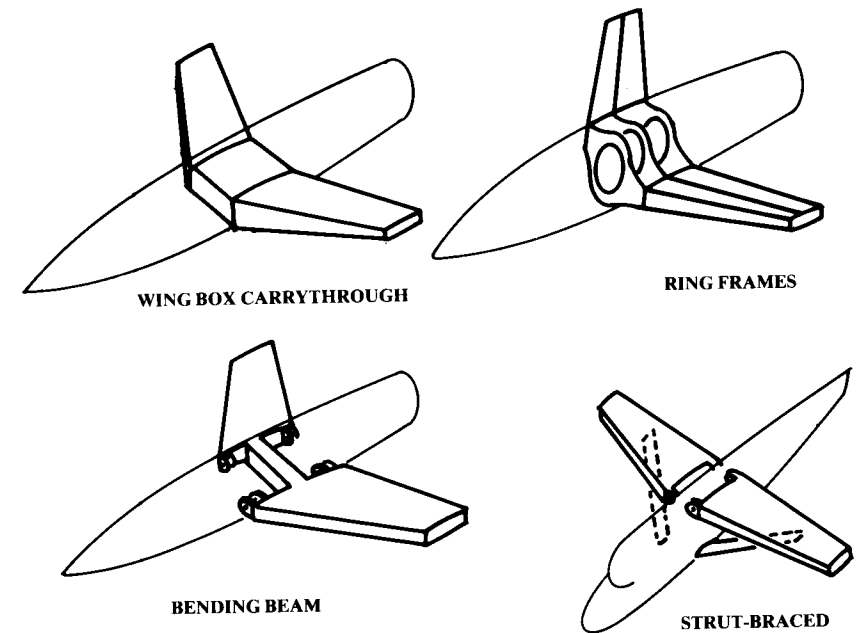


Fig. 8.8 Wing carrythrough structure.

wave drag, as discussed above. Also, the box carrythrough interferes with the longeron load-paths.

The “ring-frame” approach relies upon large, heavy bulkheads to carry the bending moment through the fuselage. The wing panels are attached to fittings on the side of these fuselage bulkheads. While this approach is usually heavier from a structural viewpoint, the resulting drag reduction at high speeds has led to the use of this approach for most modern fighters.

The “bending beam” carrythrough can be viewed as a compromise between these two approaches. Like the ring-frame approach, the wing panels are attached to the side of the fuselage to carry the lift forces. However, the bending moment is carried through the fuselage by one or several beams that connect the two wing panels. This approach has less of a fuselage volume increase than does the box-carrythrough approach.

Many light aircraft and slower transport aircraft use an external strut to carry the bending moments. While this approach is probably the lightest of all, it obviously has a substantial drag penalty at higher speeds.

Aircraft wings usually have the front spar at about 20–30% of the chord back from the leading edge. The rear spar is usually at about the 60–75% chord location. Additional spars may be located between the front and rear spars forming a “multispar” structure. Multispar structure is typical for large or high-speed aircraft.

If the wing skin over the spars is an integral part of the wing structure, a “wing box” is formed which in most cases provides the minimum weight.

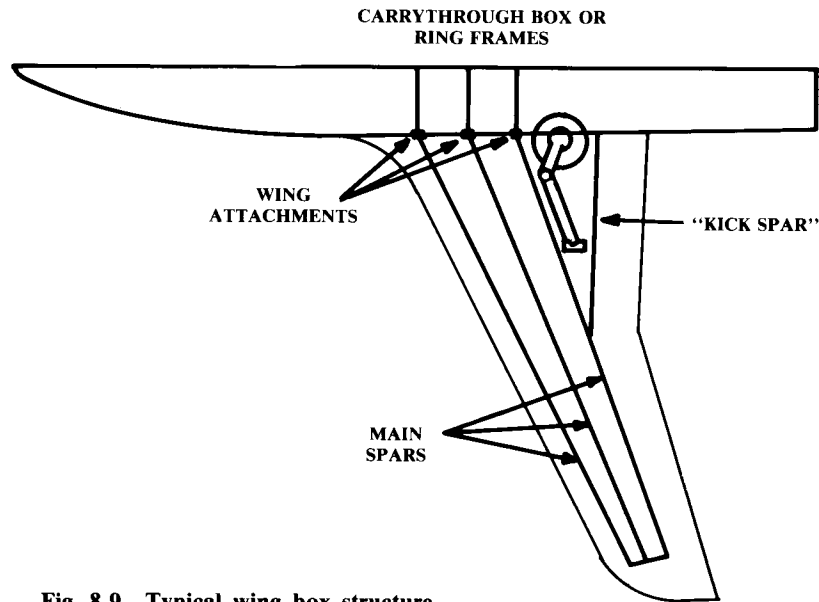


Fig. 8.9 Typical wing box structure.

Aircraft with the landing gear in the wing will usually have the gear located aft of the wing box, with a single trailing-edge spar behind the gear to carry the flap loads, as shown in Fig. 8.9.

Ribs carry the loads from the control surfaces, store stations, and landing gear to the spars and skins. A multispar wing box will have comparatively few ribs, located only where major loads occur.

Another form of wing structure, the "multirib" or "stringer panel" box, has only two spars, plus a large number of spanwise stringers attached to the wing skins. Numerous ribs are used to maintain the shape of the box under bending.

Variable sweep and folding capability add considerably to the wing structural weight. On the other hand, use of a delta wing will reduce the structural weight. These are further discussed in Chapter 15.

First-order structural sizing will be discussed in Chapter 14. For initial layout purposes the designer must guess at the amount of clearance required for structure around the internal components. A good designer with a "calibrated eyeball" can prevent a lot of lost effort, for the aircraft may require substantial redesign if later structural analysis determines that more room is required for the structural members.

A large airliner will typically require about 4 in. of clearance from the inner wall of the passenger compartment to the outer skin ("moldline"). The structure of a conventional fighter fuselage will typically require about 2 in. of offset from the moldline for internal components. For a small general aviation aircraft, 1 in. clearance or less may be acceptable.

The type of internal component will affect the required clearance. A jet engine contained within an aluminum or composite fuselage will require

perhaps an additional inch of clearance to allow for a heat shield. The heat shield may be constructed of titanium, steel, or a heat-proof matting. On the other hand, an "integral" fuel tank in which the existing structure is simply sealed and filled with fuel will require no clearance other than the thickness of the skin.

There is no easy formula for the estimation of structural clearance. The designer must use judgement acquired through experience. The best way to gain this judgement other than actual design experience is by looking at existing designs.

#### 8.4 RADAR DETECTABILITY

Ever since the dawn of military aviation attempts have been made to reduce the detectability of aircraft. During World War I, the only "sensor" in use was the human eyeball. Camouflage paint in mottled patterns was used on both sides to reduce the chance of detection.

Radar (acronym for Radio Detection And Ranging), the primary sensor used against aircraft today, consists of a transmitter antenna that broadcasts a directed beam of electromagnetic radio waves and a receiver antenna which picks up the faint radio waves that bounce off objects "illuminated" by the radio beam. Usually the transmitter and receiver antennas are collocated ("monostatic radar"), although some systems have them in different locations ("bistatic radar").

Detectability to radar has been a concern since radar was first used in World War II. "Chaff" was the first radar "stealth" technology. Chaff, also called "window," consists of bits of metal foil or metallized fibers dropped by an aircraft to create many radar echos that hide its actual echo return. Chaff is still useful against less-sophisticated radars.

Chaff obscures the actual location of the aircraft, but does not allow the aircraft to pass unnoticed. To avoid detection, the aircraft must return such a low amount of the transmitted radio beam that the receiver antenna cannot distinguish between it and the background radio static.

The extent to which an object returns electromagnetic energy is the object's "Radar Cross Section" (RCS). RCS is usually measured in square meters or in decibel square meters, with "zero dBsm" equal to ten to the zero power, or one square meter. "Twenty dBsm" equals ten to the second power, or 100 square meters. Because radar signal strength is an inverse function of the fourth power of the distance to the target, it takes a very substantial reduction in RCS to obtain a meaningful operational benefit.

Actually, the RCS of an aircraft is not a single number. The RCS is different for each "look-angle" (i.e., direction from the threat radar). Also, the RCS varies depending upon the frequency and polarization of the threat radar (see Ref. 21). The following comments relate to typical threat radars seen by military aircraft.

There are many electromagnetic phenomena that contribute to the RCS of an aircraft. These require different design approaches for RCS reduction, and can produce conflicting design requirements. Figure 8.10 illustrates the major RCS contributors for a typical, untreated fighter aircraft.

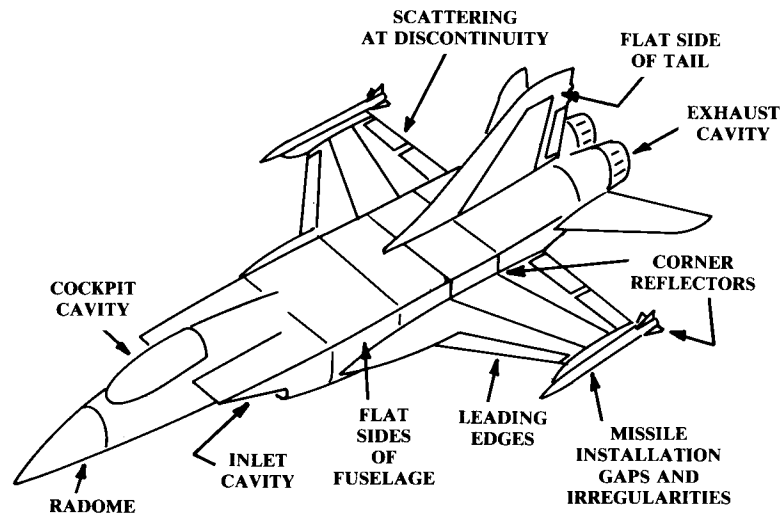


Fig. 8.10 Major RCS contributors.

One of the largest contributions to airframe RCS occurs any time a relatively flat surface of the aircraft is perpendicular to the incoming radar beam. Imagine shining a flashlight at a shiny aircraft in a dark hanger. Any spots where the beam is reflected directly back at you will have an enormous RCS contribution.

Typically this “specular return” occurs on the flat sides of the aircraft fuselage and along an upright vertical tail (when the radar is abeam the aircraft). To prevent these RCS “spikes,” the designer may slope the fuselage sides, angle the vertical tails, and so on, so that there are no flat surfaces presented towards the radar (Fig. 8.11).

Note that this RCS reduction approach assumes that the designer knows where the threat radar will be located relative to the aircraft. This information is usually provided by the operations-analysis department as a design driver. Also, this assumes a monostatic radar.

Another area of the aircraft which can present a perpendicular bounce for the radar is the round leading edge of the wing and tail surfaces. If the aircraft is primarily designed for low detectability by a nose-on threat radar, the wings and tails can be highly swept to reduce their contribution to RCS. Note that this and many other approaches to reducing the RCS will produce a penalty in aerodynamic efficiency.

It is also important to avoid any “corner reflectors,” i.e., intersecting surfaces that form approximately a right angle, as shown in Fig. 8.10 at the wing-fuselage junction.

Another contributor to airframe RCS occurs due to the electromagnetic currents that build up on the skin when illuminated by a radar. These currents flow across the skin until they hit a discontinuity such as at a sharp

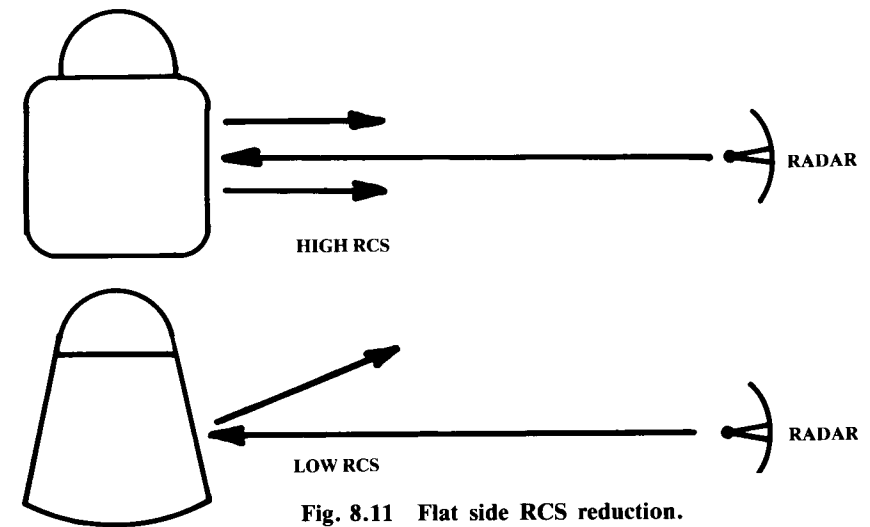


Fig. 8.11 Flat side RCS reduction.

trailing edge, a wing tip, a control surface, or a crack around a removable panel or door. At a discontinuity, the currents “scatter,” or radiate electromagnetic energy, some of which is transmitted back to the radar (Fig. 8.12).

This effect is much lower in intensity than the specular return, but is still sufficient for detection. The effect is strongest when the discontinuity is straight and perpendicular to the radar beam. Thus, the discontinuities such as at the wing and tail trailing edges can be swept to minimize the detectability from the front. Carried to the extreme, this leads to diamond- or sawtooth-shaped edges on every door, access plate, and other discontinuity on the aircraft, as seen on the B-2 and F-117.

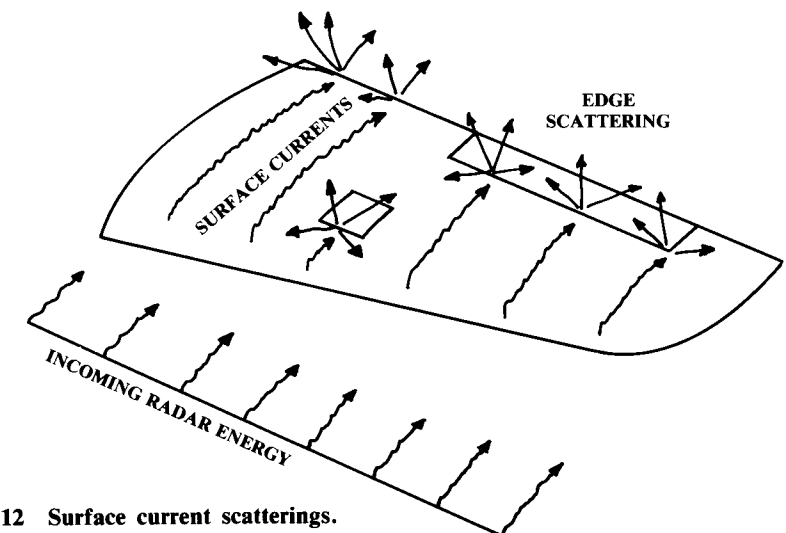


Fig. 8.12 Surface current scatterings.



First-generation stealth designs such as the Lockheed F-117 and the never-constructed North American Rockwell "Surprise Fighter" relied upon faceted shaping in which the aircraft shape is constructed of interlocking flat triangles and trapezoids. This has advantages in ease of construction and signature analysis, but offers a large number of sharp edges to create diffraction returns, and so is no longer in favor (Ref. 92).

Current stealth design begins by configuring the aircraft such that all "big" returns, such as from perpendicular bounces, are "aimed" in just a few directions. For example, if the leading edges of the wings and tails are all straight and set at the same angle, there would be a huge radar return from that angle direction, but little return from other directions. This would presumably offer a small probability that the aircraft and threat radar would be mutually oriented in exactly the angle of high return, and the aircraft would be undetectable from all other angles.

It is also common practice to "aim" the wing leading-edge return in the same direction as the edge diffraction return from the trailing edge. This is done either by using identical sweep angles at the leading and trailing edges (thus, a wing with no taper, as on the B-2), or by aligning the left wing leading edge at the same sweep angle as the right wing trailing edge (and vice versa). This creates a diamond wing as on the F-23 and an early Mikoyan research aircraft.

Once all wing and tail returns are "aimed" in the same direction, the returns from doors, access panels, and other discontinuities can be "aimed" in the same direction by alignment of their edges. This is clearly seen on the B-2, where virtually every feature on the aircraft, including weapons, bay doors, gear doors, inlets, nozzles, and access panels, is constructed using only lines which are parallel to a wing leading edge.

This design approach leads to an aircraft planform composed entirely of straight, highly swept lines, much like the first-generation stealth designs. However, the desire to eliminate the edge diffractions caused by the facets of first-generation stealth now produces designs in which cross-sectional shapes are smooth, not sharp-edged. The steep angles on the fuselage sides as shown in Fig. 8.11 are employed to prevent broadside perpendicular bounce returns, but these angled sides flow smoothly over the top and bottom of the fuselage. Such shaping can be seen on the B-2, F-22, and F-23.

RCS can also be reduced simply by eliminating parts of the aircraft. A horizontal tail that isn't there cannot contribute to the radar return! Modern computerized flight controls combined with the use of vectored-thrust engines can solve many of the difficulties of the tailless configuration.

Similarly, RCS can be reduced if the nacelles can be eliminated through the use of buried engines, or better yet, by eliminating the entire fuselage through the use of the flying-wing concept. This approach is used in the Northrop B-2.

In addition to reshaping the aircraft, detectability can be reduced through the use of skin materials that absorb radar energy. Such materials, called "radar absorbing materials" (RAM), are typically composites such as fiber-glass embedded with carbon or ferrite particles.

These particles are heated by the radar electromagnetic waves, thus absorbing some of the energy. This will reduce (not eliminate!) the radar

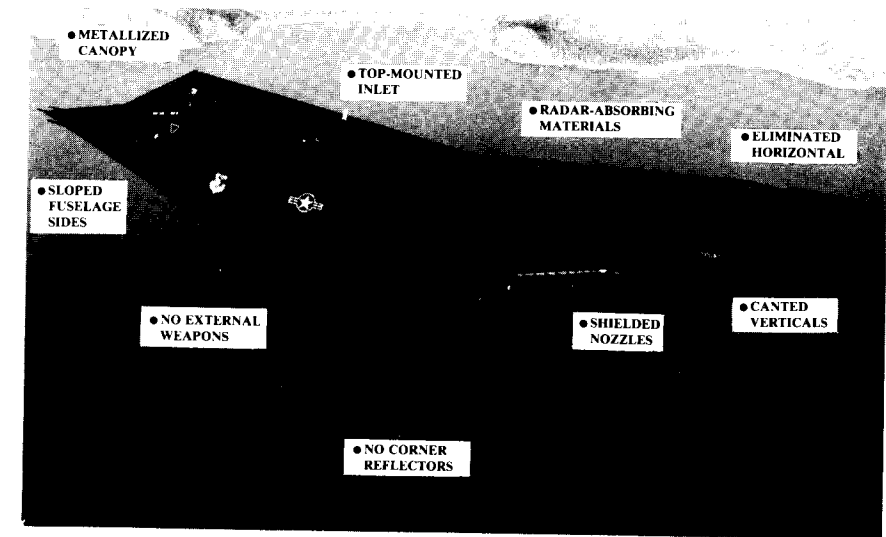


Fig. 8.13 Detectability reduction approaches.

return due to perpendicular bounce, and can also reduce the surface currents and thus reduce the RCS due to scattering at sharp edges.

As there are many types of RAM and similar treatments, no quick estimate for the weight impact of their use can be provided here. However, one can probably assume that such use will reduce or eliminate any weight savings otherwise assumed for the use of composite materials.

For most existing aircraft, the airframe is not the largest contributor to RCS, especially nose-on. A conventional radome, covering the aircraft's own radar, is transparent to radar for obvious reasons. Therefore, it is also transparent to the threat radar, allowing the threat radar's beam to bounce off the forward bulkhead and electronic equipment within the radome.

Even worse, the aircraft's own radar antenna, when illuminated by a threat radar, can produce a radar magnification effect much like a cat's eye. These effects can be reduced with a "bandpass" radome, which is transparent to only one radar frequency (that of the aircraft's radar).

Other huge contributors to the RCS for a conventional aircraft are the inlet and exhaust cavities. Radar energy gets into these cavities, bounces off the engine parts, and sprays back out the cavity towards the threat radar. Also, these cavities represent additional surface discontinuities.

The best solution for reducing these RCS contributions is to hide them from the expected threat locations. For example, inlets can be hidden from ground-based radars by locating them on top of the aircraft (Fig. 8.13). Exhausts can be hidden through the use of two-dimensional nozzles.

Cockpits provide a radar return for a similar reason. The radar energy enters the cockpit, bounces around off the equipment inside, and then reradiates back outside. One solution for this is to thinly coat the canopy with some conductive metal such as gold, causing the canopy to reflect the radar energy away.

Finally, the aircraft's weapons can have a major impact on RCS. Missiles and bombs have fins that form natural corner reflectors. The carriage and release mechanisms have numerous corner reflectors, cavities, and surface discontinuities. Gun ports present yet another kind of cavity. The only real solution for these problems is to put all the weapons inside, behind closed doors. However, the weight, volume, and complexity penalties of this approach must be carefully considered.

Electronic countermeasures (ECM)—devices to trick the threat radar—usually consist of some sort of radar receiver that picks up the threat radar emissions, and some sort of transmit antenna to send a deceiving signal back to the threat radar. The many techniques for tricking radar (and ECM) go beyond the scope of this book. However, designers should be aware that there is a tradeoff between the aircraft's RCS level and the required amount of ECM.

### 8.5 INFRARED DETECTABILITY

Infrared (IR) detectability also concerns the aircraft designer. Many short-range air-to-air and ground-to-air missiles rely upon IR seekers. Modern IR sensors are sensitive enough to detect not only the radiation emitted by the engine exhaust and hot parts, but also that emitted by the whole aircraft skin due to aerodynamic heating at transonic and supersonic speeds. Also, sensors can detect the solar IR radiation that reflects off the skin and cockpit transparencies (windows).

Of several approaches for reduction of IR detectability, one of the most potent reduces engine exhaust temperatures through the use of a high-bypass-ratio engine. This reduces both exhaust and hot-part temperatures. However, depending upon such an engine for IR reduction may result in selecting one that is less than optimal for aircraft sizing, which increases aircraft weight and cost.

Emissions from the exposed engine hot-parts (primarily the inside of the nozzle) can be reduced by cooling them with air bled off the engine compressor. This will also increase fuel consumption slightly. Another approach hides the nozzles from the expected location of the threat IR sensor. For example, the H-tails of the A-10 hide the nozzles from some angles. Unfortunately, the worst-case threat location is from the rear, and it is difficult to shield the nozzles from that direction!

Plume emissions are reduced by quickly mixing the exhaust with the outside air. As mentioned, a high-bypass engine is the best way of accomplishing this. Mixing can also be enhanced by the use of a wide, thin nozzle rather than a circular one. Another technique is to angle the exhaust upward or downward relative to the freestream. This will have an obvious thrust penalty, however.

Sun glint in the IR frequencies can be somewhat reduced by the use of special paints that have low IR reflectivity. Cockpit transparencies (which can't be painted!) can be shaped with all flat sides to prevent continuous tracking by an IR sensor.

Emissions due to aerodynamic heat are best controlled by slowing the aircraft down.

IR missiles can sometimes be tricked by throwing out a flare which burns to produce approximately the same IR frequencies as the aircraft. However, modern IR seekers are getting better at identifying which hot source is the actual aircraft.

IR fundamentals are more thoroughly discussed in Ref. 18.

### 8.6 VISUAL DETECTABILITY

The human eyeball is still a potent aircraft-detection sensor. On a clear day, an aircraft or its contrail may be spotted visually before detection by the on-board radar of a typical fighter. Also, fighter aircraft usually have radar only in front, which leaves the eyeball as the primary detector for spotting threat aircraft which are abeam or above.

Visual detection depends upon the size of aircraft and its color and intensity contrast with the background. In simulated combat, pilots of the small F-5 can frequently spot the much-larger F-15s well before the F-5s are seen. However, aircraft size is determined by the mission requirements and cannot be arbitrarily reduced.

Background contrast is reduced primarily with camouflage paints, using colors and surface textures that cause the aircraft to reflect light at an intensity and color equal to that of the background. This requires assumptions as to the appropriate background as well as the lighting conditions.

Frequently aircraft will have a lighter paint on the bottom, because the background for look-up angles is the sky. Current camouflage paint schemes are dirty blue-grey for sky backgrounds and dull, mottled grey-greens and grey-browns for ground backgrounds.

Different parts of the aircraft can contrast against each other, which increases detectability. To counter this, paint colors can be varied to lighten the dark areas, such as where one part of the aircraft casts a shadow on another. Also, small lights can sometimes be used to fill in a shadow spot.

Canopy glint is also a problem for visual detection. The use of flat transparencies can be applied as previously discussed, but will tend to detract from the pilot's outside viewing.

At night, aircraft are visually detected mostly by engine and exhaust glow and by glint off the transparencies. These can be reduced by techniques previously discussed for IR and glint suppression.

There are also psychological aspects to visual detection. If the aircraft does not look like an aircraft, the human mind may ignore it. The irregular mottled patterns used for camouflage paints exploit this tendency.

In air-to-air combat, seconds are precious. If a pilot is confused as to the opponent's orientation, the opponent may obtain favorable positioning. To this end, some aircraft have even had fake canopies painted on the underside. Forward-swept and oblique wings may also provide momentary disorientation.

### 8.7 AURAL SIGNATURE

Aural signature (noise) is important for civilian as well as military aircraft. Commercial airports frequently have antinoise ordinances that restrict some aircraft. Aircraft noise is largely caused by airflow shear layers, primarily due to the engine exhaust.

A small-diameter, high-velocity jet exhaust produces the greatest noise, while a large-diameter propeller with a low tip-speed produces the least noise. A turbofan falls somewhere in between. Blade shaping and internal duct shaping can somewhat reduce noise.

Piston exhaust stacks are also a source of noise. This noise can be controlled with mufflers, and by aiming the exhaust stacks away from the ground and possibly over the wings.

Within the aircraft, noise is primarily caused by the engines. Well-designed engine mounts, mufflers, and insulation materials can be used to reduce the noise. Internal noise will be created if the exhaust from a piston engine impinges upon any part of the aircraft, especially the cabin.

Wing-mounted propellers can have a tremendous effect on internal noise. All propellers should have a minimum clearance to the fuselage of about 1 ft, and should preferably have a minimum clearance of about one-half of the propeller radius.

However, the greater the propeller clearance, the larger the vertical tail must be to counter the engine-out yaw.

Jet engines mounted on the aft fuselage (DC-9, B727, etc.) should be located as far away from the fuselage as structurally permitted to reduce cabin noise.

## 8.8 VULNERABILITY CONSIDERATIONS

Vulnerability concerns the ability of the aircraft to sustain battle damage, continue flying, and return to base. An aircraft can be “killed” in many ways. A single bullet through a non-redundant elevator actuator is as bad as a big missile up the tailpipe!

“Vulnerable area” is a key concept. This refers to the product of the projected area (square feet or meters) of the aircraft components, times the probability that each component will, if struck, cause the aircraft to be lost. Vulnerable area is different for each threat direction. Typical components with a high aircraft kill probability (near 1.0) are the crew compartment, engine (if single-engined), fuel tanks (unless self-sealing), and weapons. Figure 8.14 shows a typical vulnerable area calculation.

When assessing the vulnerability of an aircraft, the first step is to determine the ways in which it can be “killed.” Referred to as a “failure modes and effects analysis (FMEA),” this step will typically be performed during the later stages of conceptual design. The FMEA considers both the ways in which battle damage can affect individual aircraft components, and the ways in which damage to each component will affect the other components.

During initial configuration layout, the designer should strive to avoid certain features known to cause vulnerability problems. Fire is the greatest danger to a battle-damaged aircraft. Not only is the fuel highly flammable, but so is the hydraulic fluid. Also, combat aircraft carry gun ammo, bombs, and missiles. An aircraft may survive a burst of cannon shells only to explode from a fire in the ammo box.

If at all possible, fuel should not be located over or around the engines and inlet ducts. While tanks can be made self-sealing to a small puncture, a large hole will allow fuel to ignite on the hot engine. The pylon-mounted engines on the A-10 insure that leaking fuel cannot ignite on the engines.

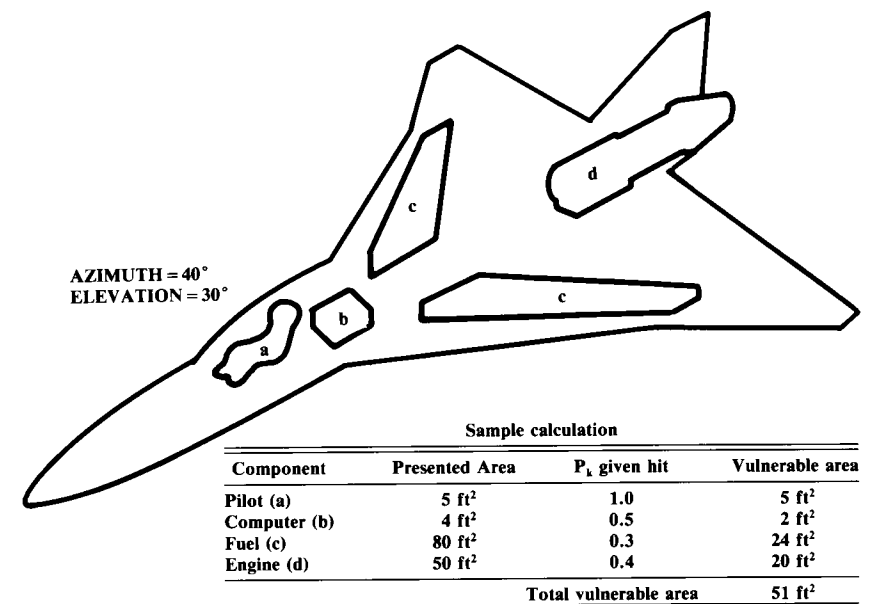


Fig. 8.14 Vulnerable area calculation.

Similarly, hydraulic lines and reservoirs should be located away from the engines.

Firewalls should be used to prevent the spread of flames beyond a burning engine bay. Engine bays, fuel bays, and weapon bays should have a fire-suppression system.

When an engine is struck, turbine and compressor blades can fly off at high speeds. Avoid placing critical components such as hydraulic lines or weapons anywhere where they could be damaged by an exploding engine. Also, a twin-engine aircraft should have enough separation between engines to prevent damage to the good engine. If twin engines are together in the fuselage, a combined firewall and containment shield should separate them. This requires at least 1 foot of clearance between engines.

Propeller blades can fly off either from battle damage or during a wheels-up landing. Critical components, especially the crew and passenger compartments, shouldn't be placed within a 5-deg arc of the propeller disk.

Avoid placing guns, bombs, or fuel near the crew compartment. Fuel should not be placed in the fuselage of a passenger plane.

Redundancy of critical components can be used to allow the survival of the aircraft when a critical component is hit. Typical components that could be redundant include the hydraulic system, electrical system, flight control system, and fuel system. Note that while redundancy improves the survivability and reliability, it worsens the maintenance requirements because there are more components to fail.

For more information on vulnerability, Ref. 18 is again suggested.

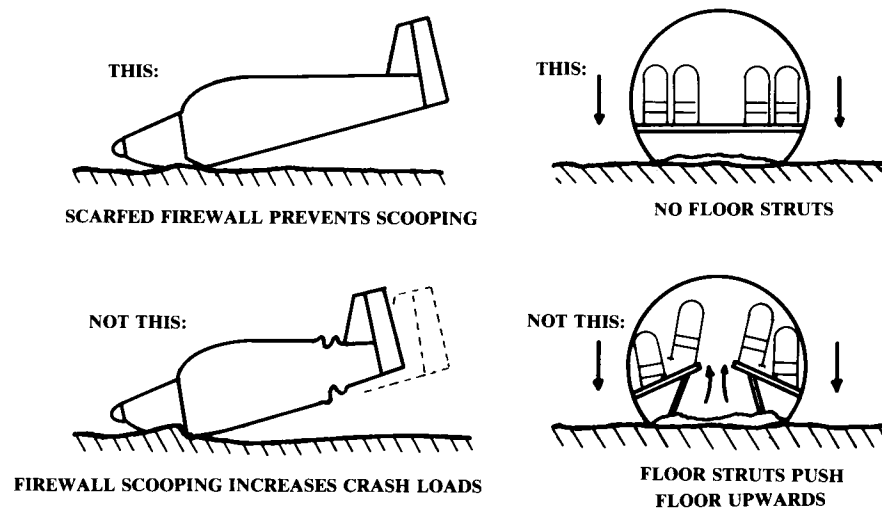


Fig. 8.15 Crashworthiness design.

## 8.9 CRASHWORTHINESS CONSIDERATIONS

Airplanes crash. Careful design can reduce the probability of injury in a moderate crash. Several suggestions have been mentioned above, including positioning the propellers so that the blades will not strike anyone if they fly off during a crash. Also mentioned was the desire to avoid placing fuel tanks in the fuselage of a passenger airplane (although fuel in the wing box carrythrough structure is usually acceptable).

Figure 8.15 shows several other design suggestions which were learned the hard way. A normal, vertical firewall in a propeller aircraft has a sharp lower corner which tends to dig into the ground, stopping the aircraft dangerously fast. Sloping the lower part of the firewall back as shown will prevent digging in, therefore reducing the deceleration.

For a large passenger aircraft, the floor should not be supported by braces from the lower part of the fuselage. As shown, these braces may push upward through the floor in the event of a crash.

Common sense will avoid many crashworthiness problems. For example, things will break loose and fly forward during a crash. Therefore, don't put heavy items behind and/or above people. This sounds obvious, but there are some aircraft with the engine in a pod above and behind the cockpit.

There are also some military jets with large fuel tanks directly behind the cockpit, offering the opportunity to be bathed in jet fuel during a crash. However, the pilot would probably try to eject rather than ride out a crash bad enough to rupture the fuel tanks.

One should also consider secondary damage. For example, landing gear and engine nacelles will frequently be ripped away during a crash. If possible, they should be located so that they do not rip open fuel tanks in the process.

Some form of protection should be provided in the not-unlikely event that the aircraft flips over during a crash. This is lacking in several small homebuilt designs.

## 8.10 PRODUCIBILITY CONSIDERATIONS

It is often said that aircraft are bought "by the pound." While it is true that aircraft cost is most directly related to weight, there is also a strong cost impact due to the materials selected, the fabrication processes and tooling required (forging, stamping, molding, etc.), and the assembly manhours.

The configuration designer does not usually determine the materials used or exactly how the aircraft will be fabricated. However, the ease of producing the aircraft can be greatly facilitated by the overall design layout.

The greatest impact the configuration designer has upon producibility is the extent to which flat-wrap structure is incorporated. This has a major impact upon the tooling costs and fabrication manhours, as discussed in the last chapter.

Part commonality can also reduce production costs. If possible, the left and right main landing gear should be identical (left-right common). It may be desirable to use uncambered horizontal tails to allow left-right commonality even if a slight aerodynamic penalty results. In some cases the wing airfoil can be slightly reshaped to allow left-right common ailerons.

Forgings are the most expensive type of structure in common usage, and are also usually the longest-lead-time items for production tooling. Forgings may be required whenever a high load passes through a small area. Forgings are used for landing-gear struts, wing-sweep pivots, and all-moving tail pivots (trunnions). The designer should avoid, if possible, such highly-loaded structure.

Installation of internal components and routing of hydraulic lines, electrical wiring, and cooling ducts comprises another major production cost due to the large amount of manual labor required. To ease installation of components and routing, avoid the tight internal packaging so desirable for reduced wetted area and wave drag. When evaluating proposed designs, government design boards will compare the overall aircraft density (weight divided by volume) with historical data for similar aircraft to insure packaging realism.

Routing can be simplified through provision of a clearly defined "routing tunnel." This can be internal or, as shown in Fig. 8.16, an external and nonstructural fairing that typically runs along the spine of the aircraft. However, if all routing is concentrated in one area the aircraft vulnerability will be drastically worsened.

Routing can be reduced by careful placement of the internal components. For example, the avionics and the crew station will both require cooling air ("environmental control"). If the avionics, crew station, and environmental control system (ECS) can be located near to each other, the routing distances will be minimized.

Sometimes clever design can reduce routing. The Rutan Defiant, a "push-pull" twin-engined design, uses completely separate electrical systems for the front and rear engines, including separate batteries. This requires an extra battery, but a trade study determined that the extra battery weighs less

than the otherwise-required electrical cable, and eliminates the front-to-rear routing requirement.

Another factor for producibility concerns manufacturing breaks. Aircraft are built in subassemblies. Typically, a large aircraft will be built up from a cockpit, an aft-fuselage, and a number of mid-fuselage subassemblies. A small aircraft may be built from only two or three subassemblies.

It is important that the designer consider where the subassembly breaks will occur, and avoid placing components across the convenient break locations. Figure 8.17 shows a typical fighter with a fuselage production break located just aft of the cockpit. This is very common because the cockpit pressure vessel should not be broken for fabrication.

In the upper design, the nose wheel well is divided by the production break, which prevents fully assembling the nose-wheel linkages before the two subassemblies are connected. The lower illustration shows a better arrangement.

Design for producibility requires experience that no book can provide. A good understanding of structural design and fabrication and the basic principles of operation for the major subsystems provides the background for developing producible designs. The following material provides a brief introduction to aircraft fabrication.

While there have been tremendous advances in aircraft production in recent years, much of the modern factory would be recognizable to a manufacturing engineer from the Wright Brothers' days. Aircraft production, then and now, involves the application of the mechanical arts of machining, forming, finishing, joining, assembly, and testing.

Machining involves the removal of a carefully-controlled amount of material from a part, typically by the application of a cutting tool via relative motion between the part and the tool. The cutting tool is generally based upon the inclined wedge, and acts to peel away a thin shaving of the part (a drill bit can be seen as a set of inclined wedges positioned radially around an axis). The relative motion between tool and part can be rotational, as with the drill, lathe, and mill, or it can be translational, as with the broach and planer.

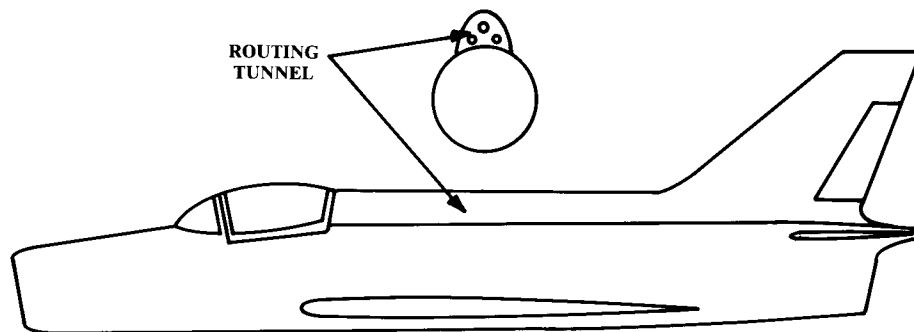


Fig. 8.16 External routing tunnel.

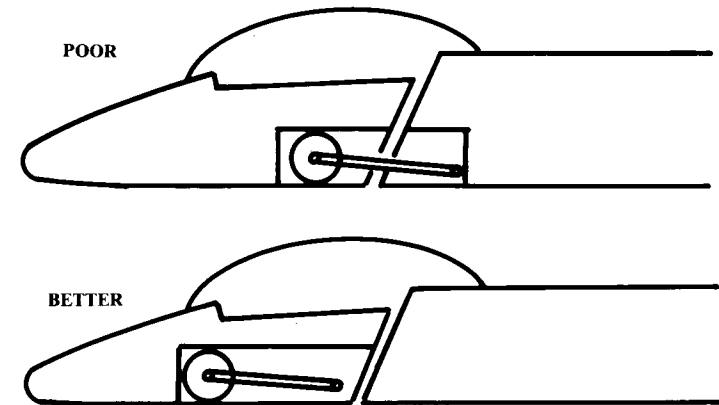


Fig. 8.17 Production breaks.

Forming refers to the numerous ways in which materials, especially metals, are changed in shape other than by machining. Forming includes casting, forging, extruding, stamping, punching, bending, and drawing. In casting, the metal is brought up to its melting temperature then poured into a mold. Forging involves forcing nonmolten metal into a mold through pressure or impact. Extrusion is the process of forcing metal to flow out a hole with the desired cross-sectional area, creating shaped bar stock. Stamping and punching are used to cut out shapes and holes in sheet metal. Bending is self-explanatory, and drawing is the process of forcing sheet metal into a form creating cup-like geometries.

Finishing encompasses a number of processes applied to formed and/or machined parts. Some finish processes include further material removal to create a smoother surface, such as deburring, lapping, and finish grinding. Other finish processes, such as painting, anodization, and plating, involve application of a surface coating.

Composite fabrication is sufficiently unlike metal fabrication that it deserves special mention. In thermoset composite production, a liquid or pliable semisolid plastic material undergoes a chemical change into a new, solid material, usually accompanied by the application of heat and/or pressure. For aircraft applications the plastic "matrix" material is reinforced by a fiber, typically of graphite material. Thermoset composite manufacture is unique in that the material itself is produced at the same time and place as the part. A second class of composites, the thermoplastics, involves a plastic matrix which is heated in a mold until it deforms readily, assuming the shape of the mold. Composite fabrication is further described in Chapter 14.

Joining is simply the attachment of parts together, by processes including brazing, soldering, welding, bonding, riveting, and bolting. All these processes historically have a high manual-labor content, and all are being automated to various extents in modern factories. For example, modern car factories have long lines of robotic spot-welders attaching body panels.

Automatic riveting machines, applicable for simple geometries such as rivets in a row down a wing spar, can be found in the modern aircraft factory.

Assembly is the process of combining parts and subassemblies into the final product. Assembly usually involves joining operations such as riveting or bolting, but is distinguished from joining by the greater level of completeness of the subassemblies. For example, when you attach a wing skin to the wing ribs it is "joining," but when you attach the wing to the fuselage, it is "assembly."

Testing is a key part of the manufacturing process. In traditional factories, testing was generally done by random selection of finished product and was frequently of a destructive nature. While helping to keep average quality up, such random destructive testing did not insure that any given part was acceptable because the only parts known by testing to be acceptable were destroyed in the process!

Today's factories are tending toward nondestructive testing techniques such as magnaflux, ultrasonic, and nuclear magnetic resonance, and are also applying advanced statistical techniques to better select samples to test and to determine the corrective action required.

CAD/CAM, or Computer-Aided Design/Computer-Aided Manufacture, is a generic term for the many different ways in which computers are being used in design and manufacture. Typically CAD/CAM refers specifically to the use of computers for two- and three-dimensional component design, and the use of the resulting CAD data base as the input for the programming of numerically-controlled machinery and robots (as described below). The benefits of CAD/CAM are well-established and include improved design quality, reduction in design time and/or increase in the number of design iterations possible, earlier discovery of errors, integration of design, analysis, and manufacturing engineering, and facilitation of training.

Automation refers to almost any use of computerized equipment during manufacture. However, the generic term "automation" is most frequently applied to tasks such as riveting, parts retrieval, and process control (such as autoclave cycling), whereas the more specific terms "numerical control" and "robotics" are used as described below.

Numerical control (NC) programming refers to the creation of digital instructions which command a computer-controlled machine tool such as a mill or lathe. This area is probably one of the highest leverage in terms of reducing cost and improving quality. While machine tools themselves have experienced little fundamental change in this century (this author knows of a company making high-tech wind turbines on a 100-year-old lathe!), the application of numerical control replacing the skilled but bored machinist has had a tremendous effect on productivity and quality.

The most sophisticated subset of automation is robotics, in which a computer-controlled machine performs tasks involving highly complex motions which previously might have been performed by a human. Note that it is the ability to physically manipulate objects in response to programming which distinguishes the robot from other forms of automation or mechanism. Robotics examples include part pickup and positioning, painting,

composite-ply laydown, material handling, simple assembly, and welding, and are usually limited to "semi-skilled" jobs, at least to date.

A key robotics technology for composites is in the labor-intensive tape lay-up process. Programmable robot arms with tape dispenser end effectors are widely used to place the prepreg. Also, autoclave cycle control is widely automated.

Rapid prototyping of parts without tools is being performed using a new technique known as Stereolithography (SLA), which can produce plastic prototype parts in a day or less. SLA works by mathematically slicing CAD designs into thin cross sections, which are traced one at a time by an ultraviolet laser beam on a vat of photosensitive chemicals that solidify as they are irradiated. After each layer is completed, an "elevator" holding the part moves down slightly and the next layer is solidified on top of it. While to date only certain types of relatively fragile plastics may be used by SLA devices, the plastic prototypes can then be used to create molds for strong epoxy or aluminum parts.

## 8.11 MAINTAINABILITY CONSIDERATIONS

Maintainability means simply the ease with which the aircraft can be fixed. "Reliability and Maintainability" (R&M) are frequently bundled together and measured in "Maintenance Manhours Per Flighthour" (MMH/FH). MMH/FH's range from less than one for a small private aircraft to well over a hundred for a sophisticated supersonic bomber or interceptor.

Reliability is usually out of the hands of the conceptual designer. Reliability depends largely upon the detail design of the avionics, engines, and other subsystems. The configuration designer can only negatively impact reliability by placing delicate components, such as avionics, too near to vibration and heat sources such as the engines.

Anybody who has attempted to repair a car will already know what the major driver is for maintainability. Getting at the internal components frequently takes longer than fixing them! Accessibility depends upon the packaging density, number and location of doors, and number of components that must be removed to get at the broken component.

Packaging density has already been discussed. The number and location of doors on modern fighters have greatly improved over prior-generation designs. Frequently the ratio between the total area of the access doors and the total wetted area of the aircraft's fuselage is used as a measure of merit, with modern fighters approaching a value of one-half.

A structural weight penalty must be paid for such access. This leads to the temptation to use "structural doors" that carry skin loads via heavy hinges and latches. These are always more difficult to open than nonload-bearing doors because the airframe's deflection from its own weight will bind the latches and hinges. In extreme cases, the aircraft must be supported on jacks or a cradle to open these structural doors.

As a general rule, the best access should be provided to the components that break the most often or require the most routine maintenance. Engine access doors should definitely be provided that allow most of the engine to be exposed. Also, large doors should be provided for the avionics compart-

ment, hydraulic pumps, actuators, electrical generators, environmental control system, auxiliary power unit, and gun bay.

The worst feature an aircraft can have for maintainability is a requirement for major structural disassembly to access or remove a component. For example, the V/STOL AV-8B Harrier requires that the entire wing be removed before removing the engine. Several aircraft require removal of a part of the longeron to remove the wing.

Similarly, the designer should avoid placing internal components such that one must be removed to get to another. In the F-4 Phantom, an ejection seat must be removed to get to the radio (a high-break-rate item). It is not uncommon for the ejection seat to be damaged during this process. "One-deep" design will avoid such problems.

## CREW STATION, PASSENGERS, AND PAYLOAD

### 9.1 INTRODUCTION

At the conceptual design level it is not necessary to go into the details of crew-station design, such as the actual design and location of controls and instruments, or the details of passenger and payload provisions. However, the basic geometry of the crew station and payload/passenger compartment must be considered so that the subsequent detailed cockpit design and payload integration efforts will not require revision of the overall aircraft.

This chapter presents dimensions and "rule-of-thumb" design guidance for conceptual layout of aircraft crew stations, passenger compartments, payload compartments, and weapons installations. Information for more detailed design efforts is contained in the various civilian and military specifications and in subsystem vendors' design data packages.

### 9.2 CREW STATION

The crew station will affect the conceptual design primarily in the vision requirements. Requirements for unobstructed outside vision for the pilot can determine both the location of the cockpit and the fuselage shape in the vicinity of the cockpit.

For example, the pilot must be able to see the runway while on final approach, so the nose of the aircraft must slope away from the pilot's eye at some specified angle. While this may produce greater drag than a more-streamlined nose, the need for safety overrides drag considerations. Similarly, the need for over-side vision may prevent locating the cockpit directly above the wing.

When laying out an aircraft's cockpit, it is first necessary to decide what range of pilot sizes to accommodate. For most military aircraft, the design requirements include accommodation of the 5th to the 95th percentile of male pilots, (i.e., a pilot height range of 65.2–73.1 in.). Due to the expense of designing aircraft that will accommodate smaller or larger pilots, the services exclude such people from pilot training.

Women are only now entering the military flying profession in substantial numbers, and a standard percentile range for the accommodation of female pilots had not yet been established as this was written. Future military aircraft might require the accommodation of approximately the 20th percentile female and larger. This may affect the detailed layout of cockpit controls and displays, but should have little impact upon conceptual cockpit layout.

General-aviation cockpits are designed to whatever range of pilot sizes the marketing department feels is needed for customer appeal, but typically are comfortable only for those under about 72 in. Commercial-airliner cockpits are designed to accommodate pilot sizes similar to those of military aircraft.

Figure 9.1 shows a typical pilot figure useful for conceptual design layout. This 95th percentile pilot, based upon dimensions from Ref. 22, includes allowances for boots and a helmet. A cockpit designed for this size of pilot will usually provide sufficient cockpit space for adjustable seats and controls to accommodate down to the 5th percentile of pilots.

Designers sometimes copy such a figure onto cardboard in a standard design scale such as twenty-to-one, cut out the pieces, and connect them with pins to produce a movable manikin. This is placed on the drawing, positioned as desired, and traced onto the layout. A computer-aided aircraft design system can incorporate a built-in pilot manikin (see Ref. 14).

Dimensions for a typical cockpit sized to fit the 95th-percentile pilot are shown in Fig. 9.2. The two key reference points for cockpit layout are shown. The seat reference point, where the seat pan meets the back, is the reference for the floor height and the legroom requirement. The pilot's eye point is used for defining the overnose angle, transparency grazing angle, and pilot's head clearance (10-in. radius).

This cockpit layout uses a typical 13-deg seatback angle, but seatback angles of 30 deg are in use (F-16), and angles of up to 70 deg have been considered for advanced fighter studies. This entails a substantial penalty in

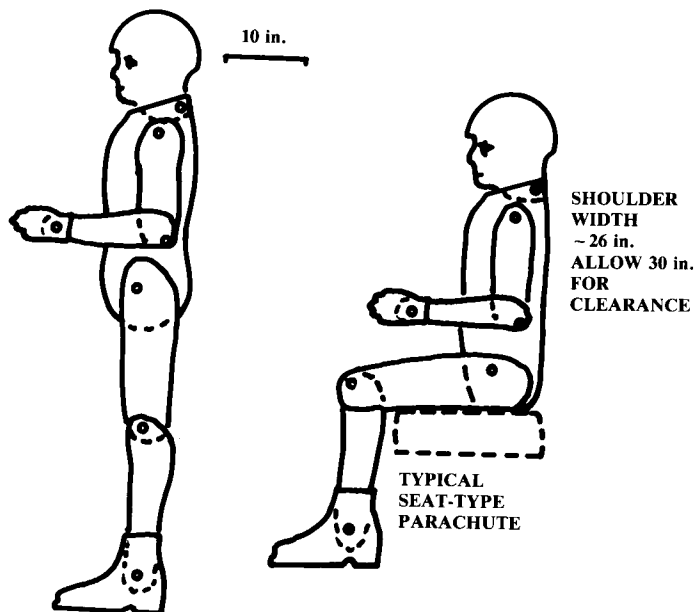


Fig. 9.1 Average 95th percentile pilot.

outside vision for the pilot, but can improve his ability to withstand high-g turns and also can reduce drag because of a reduction in the cockpit height.

When designing a reclined-seat cockpit, rotate both the seat and the pilot's eye point about the seat reference point, and then use the new position of the pilot's eye to check overnose vision.

Overnose vision is critical for safety especially during landing, and is also important for air-to-air combat. Military specifications typically require 17-deg overnose vision for transports and bombers, and 11–15 deg for fighter and attack aircraft. Military trainer aircraft in which the instructor pilot sits behind the student require 5-deg vision from the back seat over the top of the front seat.

Various military specifications and design handbooks provide detailed requirements for the layout of the cockpit of fighters, transports, bombers, and other military aircraft.

General-aviation aircraft land in a fairly level attitude, and so have overnose vision angles of only about 5–10 deg. Many of the older designs have such a small overnose vision angle that the pilot loses sight of the runway from the time of flare until the aircraft is on the ground and the nose is lowered.

Civilian transports frequently have a much greater overnose vision angle, such as the Lockheed L-1011 with an overnose vision angle of 21 deg. Civilian overnose vision angles must be calculated for each aircraft based upon the ability of the pilot to see and react to the approach lights at decision height (100 ft) during minimum weather conditions (1200-ft runway visual range). The higher the approach speed, the greater the overnose vision angle must be.

Reference 23 details a graphical technique for determining the required overnose angle, but it can only be applied after the initial aircraft layout is complete and the exact location of the pilot's eye and the main landing gear is known. For initial layout, Eq. (9.1) is a close approximation, based upon the aircraft angle of attack during approach and the approach speed.

$$\alpha_{\text{overnose}} \cong \alpha_{\text{approach}} + 0.07 V_{\text{approach}} \quad (9.1)$$

where  $V_{\text{approach}}$  is in knots.

Figure 9.2 shows an over-the-side vision requirement of 40 deg, measured from the pilot's eye location on centerline. This is typical for fighters and attack aircraft. For bombers and transports, it is desirable that the pilot be able to look down at a 35-deg angle without head movement, and at a 70-deg angle when the pilot's head is pressed against the cockpit glass. This would also be reasonable for general-aviation aircraft, but many general-aviation aircraft have a low wing blocking the downward view.

The vision angle looking upward is also important. Transport and bomber aircraft should have unobstructed vision forwards and upwards to at least 20 deg above the horizon. Fighters should have completely unobstructed vision above and all the way to the tail of the aircraft. Any canopy structure should be no more than 2 in. wide to avoid blocking vision.



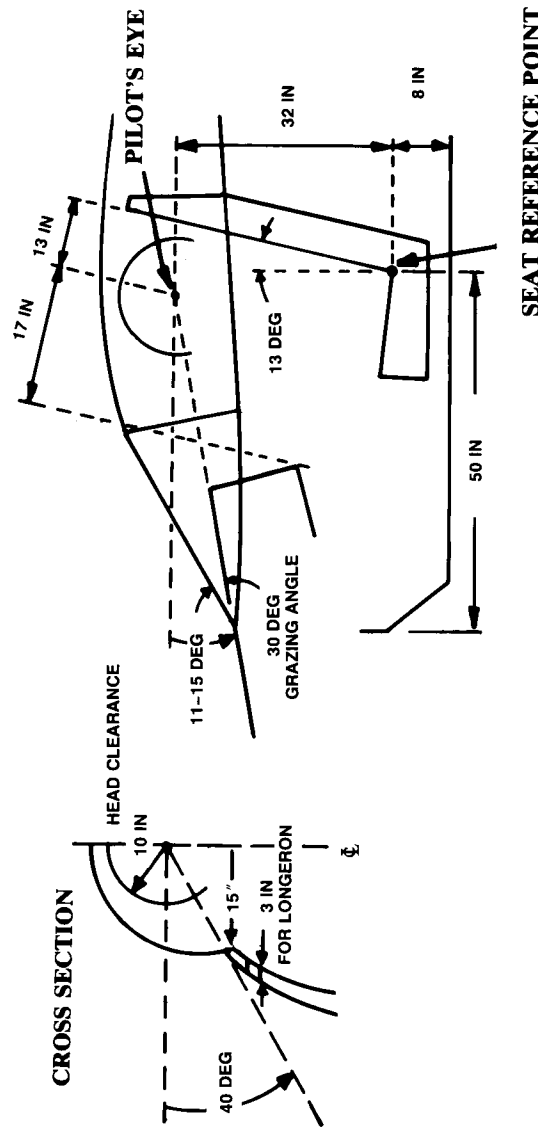


Fig. 9.2 Typical fighter cockpit.

The transparency grazing angle shown in Fig. 9.2 is the smallest angle between the pilot's line of vision and the cockpit windscreen. If this angle becomes too small, the transparency of the glass or plexiglass will become substantially reduced, and under adverse lighting conditions the pilot may only see a reflection of the top of the instrument panel instead of whatever is in front of the aircraft! For this reason, a minimum grazing angle of 30 deg is recommended.

The cockpit of a transport aircraft must contain anywhere from two to four crew members as well as provisions for radios, instruments, and stowage of map cases and overnight bags. Reference 23 suggests an overall length of about 150 in. for a four-crewmember cockpit, 130 in. for three crewmembers, and 100 in. for a two-crewmember cockpit.

The cockpit dimensions shown in Fig. 9.2 will provide enough room for most military ejection seats. An ejection seat is required for safe escape when flying at a speed which gives a dynamic pressure above about 230 psf (equal to 260 knots at sea level).

At speeds approaching Mach 1 at sea level (dynamic pressure above 1200), even an ejection seat is unsafe and an encapsulated seat or separable crew capsule must be used. These are heavy and complex. A separable crew capsule is seen on the FB-111 and the prototype B-1A. The latter, including seats for four crew members, instruments, and some avionics, weighed about 9000 lb.

### 9.3 PASSENGER COMPARTMENT

The actual cabin arrangement for a commercial aircraft is determined more by marketing than by regulations. Figure 9.3 defines the dimensions of interest. "Pitch" of the seats is defined as the distance from the back of one seat to the back of the next. Pitch includes fore and aft seat length as well as leg room. "Headroom" is the height from the floor to the roof over the seats. For many smaller aircraft the sidewall of the fuselage cuts off a portion of the outer seat's headroom, as shown. In such a case it is important to assure that the outer passenger has a 10-in. clearance radius about the eye position.

Table 9.1 provides typical dimensions and data for passenger compartments with first-class, economy, or high-density seating. This information (based upon Refs. 23, 24, and others) can be used to lay out a cabin floor plan.

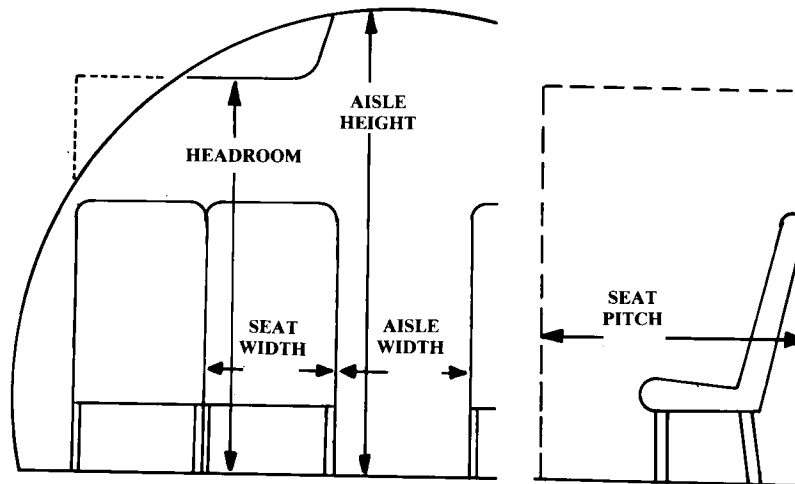
There should be no more than three seats accessed from one aisle, so an aircraft with more than six seats abreast will require two aisles. Also, doors and entry aisles are required for approximately every 10-20 rows of seats. These usually include closet space, and occupy 40-60 in. of cabin length each.

Passengers can be assumed to weigh an average of 180 lb (dressed and with carry-on bags), and to bring about 40-60 lb of checked luggage. A current trend towards more carry-on luggage and less checked luggage has been overflowing the current aircrafts' capacity for overhead stowage of bags.

The cabin cross section and cargo bay dimensions (see below) are used to determine the internal diameter of the fuselage. The fuselage external di-

**Table 9.1 Typical passenger compartment data**

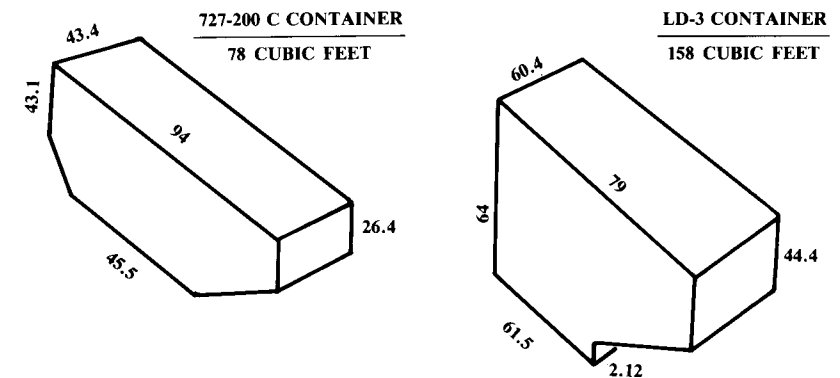
	First class	Economy	High density/ small aircraft
Seat pitch (in.)	38–40	34–36	30–32
Seat width (in.)	20–28	17–22	16–18
Headroom (in.)	> 65	> 65	–
Aisle width (in.)	20–28	18–20	≥ 12
Aisle height (in.)	> 76	> 76	> 60
Passengers per cabin staff (international-domestic)	16–20	31–36	≤ 50
Passengers per lavatory (40" × 40")	10–20	40–60	40–60
Galley volume per passenger (ft <sup>3</sup> /pass)	5–8	1–2	0–1

**Fig. 9.3 Commercial passenger allowances.**

ameter is then determined by estimating the required structural thickness. This ranges from 1 in. for a small business or utility transport to about 4 in. for a jumbo jet.

## 9.4 CARGO PROVISIONS

Cargo must be carried in a secure fashion to prevent shifting while in flight. Larger civilian transports use standard cargo containers that are pre-loaded with cargo and luggage and then placed into the belly of the aircraft. During conceptual design it is best to attempt to use an existing container rather than requiring purchase of a large inventory of new containers.

**Fig. 9.4 Cargo containers.**

Two of the more widely used cargo containers are shown in Fig. 9.4. Of the smaller transports, the Boeing 727 is the most widely used, and the 727 container shown is available at virtually every commercial airport.

The LD-3 container is used by all of the widebody transports. The B-747 carries 30 LD-3's plus 1000 ft<sup>3</sup> of bulk cargo volume (non-containerized). The L-1011 carries 16 LD-3's plus 700 ft<sup>3</sup> of bulk cargo volume, and the DC-10 and Airbus each carry 14 LD-3's (plus 805 and 565 ft<sup>3</sup>, respectively, of bulk cargo volume).

To accommodate these containers, the belly cargo compartments require doors measuring approximately 70 in. on a side. As was discussed in the section on wing vertical placement, low-wing transports usually have two belly cargo compartments, one forward of the wing box and one aft.

The cargo volume per passenger of a civilian transport ranges from about 8.6–15.6 ft<sup>3</sup> per passenger (Ref. 24). The smaller number represents a small short-haul jet (DC-9). The larger number represents a transcontinental jet (B-747). The DC-10, L-1011, Airbus, and B-767 all have about 11 ft<sup>3</sup> per passenger. Note that these volumes provide room for paid cargo as well as passenger luggage.

Smaller transports don't use cargo containers, but instead rely upon hand-loading of the cargo compartment. For such aircraft a cargo provision of 6–8 ft<sup>3</sup> per passenger is reasonable.

Military transports use flat pallets to pre-load cargo. Cargo is placed upon these pallets, tied down, and covered with a tarp. The most common pallet measures 88 by 108 in.

Military transports must have their cargo compartment floor approximately 4–5 ft off the ground to allow direct loading and unloading of cargo from a truck bed at air bases without cargo-handling facilities. However, the military does use some commercial aircraft for cargo transport and has pallet loaders capable of raising to a floor height of 13 ft at the major Military Airlift Command bases.

The cross section of the cargo compartment is extremely important for a military transport aircraft. The C-5, largest of the U.S. military transports,

is sized to carry so-called “outsized” cargo, which includes M-60 tanks, helicopters, and large trucks. The C-5 cargo bay is 19 ft wide, 13½ ft high, and 121 ft long.

The C-130 is used for troop and supply delivery to the front lines, and cannot carry outsized cargo. Its cargo bay measures 10'3" wide, 9'2" high, and 41'5" long.

### 9.5 WEAPONS CARRIAGE

Carriage of weapons is the purpose of most military aircraft. Traditional weapons include guns, bombs, and missiles. Lasers and other exotic technologies may someday become feasible as airborne weapons, but will not be discussed here.

The weapons are a substantial portion of the aircraft's total weight. This requires that the weapons be located near the aircraft's center of gravity. Otherwise the aircraft would pitch up or down when the weapons are released.

Missiles differ from bombs primarily in that missiles are powered. Today, virtually all missiles are also guided in some fashion. Most bombs are “dumb,” or unguided, and are placed upon a target by some bombsight mechanism or computer which releases them at the proper position and velocity so that they free-fall to the desired target. However, “smart-bombs,” which have some guidance mechanism, are also in use.

Missiles are launched from the aircraft in one of two ways. Most of the smaller missiles such as the AIM-9 are rail-launched. A rail-launcher is mounted to the aircraft, usually at the wingtip or on a pylon under the wing. Attached to the missile are several mounting lugs, which slide onto the rail as shown on Fig. 9.5. For launch, the missile motor powers the missile down the rail and free of the aircraft.

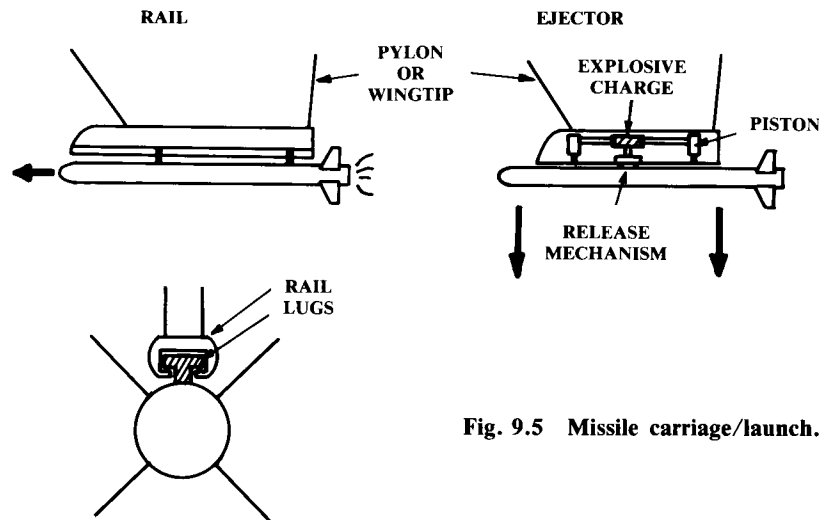


Fig. 9.5 Missile carriage/launch.

Ejection-launch is used mainly for larger missiles. The missile is attached to the aircraft through hooks which are capable of quick-release, powered by an explosive charge. This explosive charge also powers two pistons that shove the missile away from the aircraft at an extremely high acceleration. The missile motor is lit after it clears the aircraft by some specified distance.

Bombs can also be ejected, or can simply be released and allowed to fall free of the aircraft.

There are four options for weapons carriage. Each has pros and cons, depending upon the application. External carriage is the lightest and simplest, and offers the most flexibility for carrying alternate weapon stores.

While most fighter aircraft are designed to an air-to-air role, the ability to perform an additional air-to-ground role is often imposed. To avoid penalizing the aircraft's performance when “clean” (i.e., set up for dogfighting), most fighter aircraft have “hardpoints” under the wing and fuselage to which weapon pylons can be attached, as shown in Fig. 9.6. These are used to carry additional external weapons, and are removed for maximum dog-fighting performance.

Most fighter aircraft can also carry external fuel tanks on the weapons pylons. These can be dropped when entering a dogfight, but are not dropped during long overwater ferry flights. Standard external fuel tanks include 150 and 600 gal sizes.

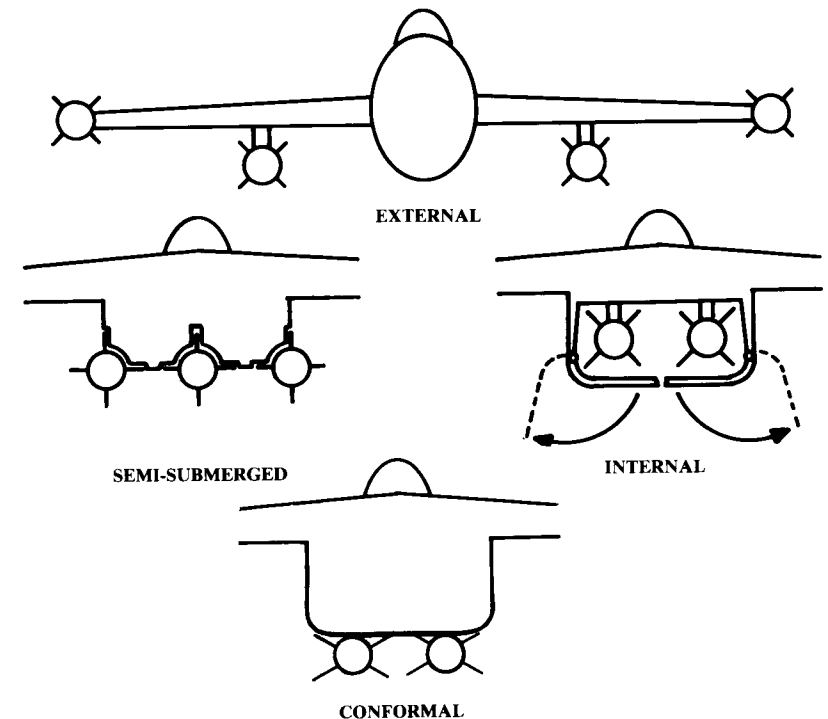


Fig. 9.6 Weapon carriage options.

Externally-carried weapons have extremely high drag. At near-sonic speeds, a load of external bombs can have more drag than the entire rest of the aircraft. Supersonic flight is virtually impossible with pylon-mounted external weapons, due to drag and buffeting. (Wing tip-mounted missiles are small, and have fairly low drag.)

To avoid these problems, semisubmerged or conformally-carried weapons may be used. Conformal weapons mount flush to the bottom of the wing or fuselage. Semisubmerged weapons are half-submerged in an indentation on the aircraft. This is seen on the F-4 for air-to-air missiles.

Semisubmerged carriage offers a substantial reduction in drag, but reduces flexibility for carrying different weapons. Also, the indentations produce a structural weight penalty on the airplane. Conformal carriage doesn't intrude into the aircraft structure, but has slightly higher drag than the semisubmerged carriage.

The lowest-drag option for weapons carriage is internal. An internal weapons bay has been a standard feature of bombers for over fifty years, but has been seen on only a few fighters and fighter-bombers, such as the F-106 and FB-111. This is partly due to the weight penalty imposed by an internal weapons bay and its required doors, but is also due to the prevalent desire to maximize dogfighting performance at the expense of alternate mission performance. However, only an internal weapons bay can completely eliminate the weapons' contribution to radar cross section, so the internal weapons bay may become common for fighters as well as bombers.

During conceptual layout, there are several aspects of weapons carriage that must be considered once the type of carriage is selected. Foremost is the need to remember the loading crew. They will be handling large, heavy, and extremely dangerous missiles and bombs. They may be working at night, in a snowstorm, on a rolling carrier deck, and under attack. Missiles must be physically attached to the mounting hooks or slid down the rail, then secured by a locking mechanism. Electrical connections must be made to the guidance mechanism, and the safety wire must be removed from the fusing mechanism. For an ejector-type launcher, the explosive charge must be inserted. All of this cannot be done if the designer, to reduce drag, has provided only a few inches of clearance around the missile. The loading crew absolutely must have sufficient room in which to work.

Clearance around the missiles and bombs is also important for safety. To insure that the weapons never strike the ground, the designer should provide

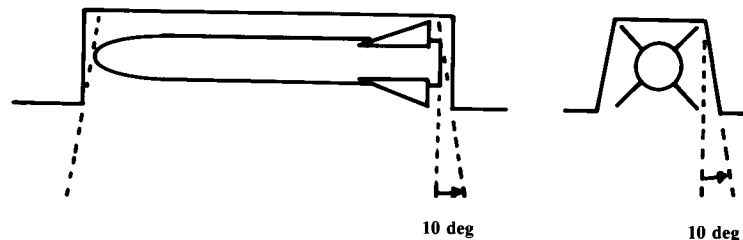


Fig. 9.7 Weapon release clearance.

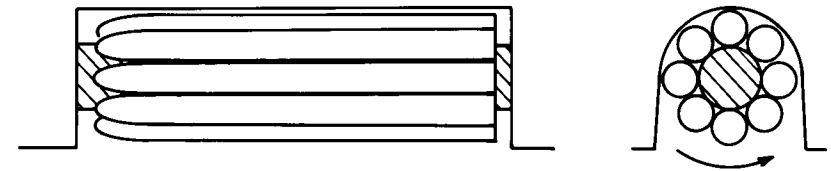


Fig. 9.8 Rotary weapons bay.

at least a 3-in. clearance to the ground in all aircraft attitudes. This includes the worst-case bad landing in which one tire and shock-strut are completely flat, the aircraft is at its maximum tail-down attitude (usually 15 deg or more) and the aircraft is in a 5-deg roll. The minimum clearance should be doubled if the airplane is to operate from rough runways.

If weapons are mounted near each other, there should be a clearance on the order of 3 in. between them. There should also be a foot or more clearance between weapons and a propeller disk.

The path taken by missiles or bombs when launched must be considered. For rail-launched missiles, there should be at least a 10-deg cone of clearance between any part of the aircraft and the launch direction of the missile. Also, the designer must consider the effects of the missile exhaust blast on the aircraft's structure.

For an ejector-launched or free-fall released weapon, there should be a fall line clearance of 10 deg off the vertical down from any part of the missile to any part of the aircraft or other weapons as shown in Fig. 9.7.

A special type of internal weapons carriage is the rotary weapons bay, as shown in Fig. 9.8. This allows launching all of the weapons through a single, smaller door. At supersonic speeds it can be difficult or impossible to launch weapons out of a bay due to buffeting and airloads which tend to push the weapon back into the bay. A single smaller door reduces these tendencies. Also, the rotary launcher simplifies installation of multiple weapons into a single bay. In fact, it is possible to design a rotary launcher that can be pre-loaded with weapons and loaded full into the aircraft.

## 9.6 GUN INSTALLATION

The gun has been the primary weapon of the air-to-air fighter since the first World War I scout pilot took a shot at an opposing scout pilot with a handgun. For a time during the 1950's it was felt that the then—new air-to-air missiles would replace the gun, and in fact several fighters such as the F-4 and F-104 were originally designed without guns. History proved that missiles cannot be solely relied upon, and all new fighters are being designed with guns.

The standard U.S. air-to-air gun today is the M61A1 "Vulcan" six-barrel gatling gun, shown in Fig. 9.9. This is used in the F-15, F-16, F-18, and others. Note the ammunition container. This must be located near the aft end of the gun. Rounds of ammo are fed out of the container ("drum") through feed chutes and into the gun. Ammo is loaded into the drum by attaching an ammo loading cart to the feed chute shown. The door to this loading chute must be accessible from the ground.

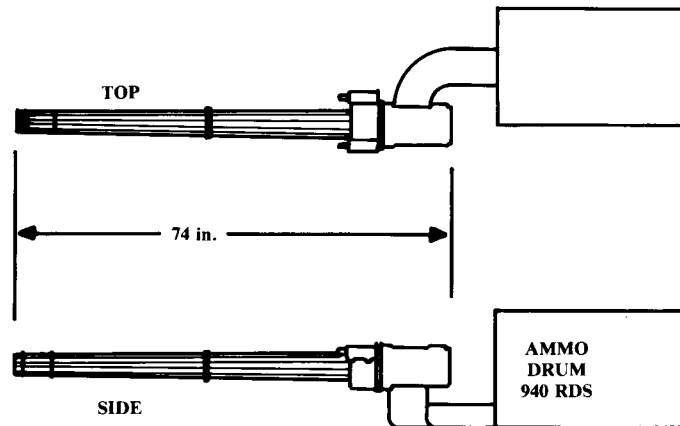


Fig. 9.9 M61 "VULCAN" gun.

An air-to-air gun such as the M61A1 can produce a recoil force on the order of two tons. A large anti-tank gun such as the GAU-8 used in the A-10 can produce a recoil force five times greater. To avoid a sudden yawing motion from firing, guns should be located as near as possible to the centerline of the aircraft. On the A-10, the nose landing gear is offset to one side to allow the gun to be exactly on the centerline. This extreme is not necessary for the smaller air-to-air guns.

When a gun is fired, it produces a bright flash and a large cloud of smoke. The gun muzzle should be located so that these do not obscure the pilot's vision. Also, being very noisy, a gun should be located away from the cockpit.

The cloud of smoke produced by a gun can easily stall a jet engine if sucked into the inlet. This should also be considered when locating a gun.

## 10

# PROPULSION AND FUEL SYSTEM INTEGRATION

## 10.1 INTRODUCTION

This section treats the integration and layout of the propulsion system into the overall vehicle design, not the calculation of installed propulsion performance. Propulsion analysis methods are covered in Chapter 13.

To develop the propulsion system layout it is necessary to know the actual dimensions and installation requirements of the engine as well as its supporting equipment such as inlet ducts, nozzles, or propellers. Also, the fuel system including the fuel tanks must be defined.

## 10.2 PROPULSION SELECTION

Figure 10.1 illustrates the major options for aircraft propulsion. All aircraft engines operate by compressing outside air, mixing it with fuel, burning the mixture, and extracting energy from the resulting high-pressure hot gases. In a piston-prop, these steps are done intermittently in the cylinders via the reciprocating pistons. In a turbine engine, these steps are done continuously, but in three distinct parts of the engine.

The piston-prop was the first form of aircraft propulsion. By the dawn of the jet era, a 5500-hp piston-prop engine was in development. Today piston-props are mainly limited to light airplanes and some agricultural aircraft.

Piston-prop engines have two advantages. They are cheap, and they have the lowest fuel consumption. However, they are heavy and produce a lot of noise and vibration. Also, the propeller loses efficiency as the velocity increases.

The turbine engine consists of a "compressor," a "burner," and a "turbine." These separately perform the three functions of the reciprocating piston in a piston engine.

The compressor takes the air delivered by the inlet system and compresses it to many times atmospheric pressure. This compressed air passes to the burner, where fuel is injected and mixed with the air and the resulting mixture ignited.

The hot gases could be immediately expelled out the rear to provide thrust, but are first passed through a turbine to extract enough mechanical power to drive the compressor. It is interesting to note that one early jet engine used a separate piston engine to drive the compressor.

There are two types of compressors. The centrifugal compressor relies upon centrifugal force to "fling" the air into an increasingly narrow chan-

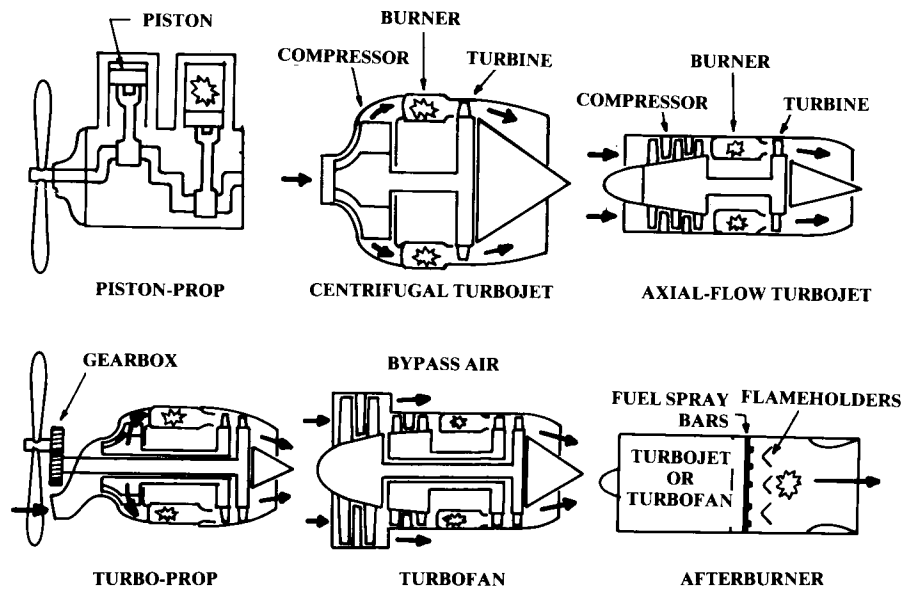


Fig. 10.1 Propulsion system options.

nel, which raises the pressure. In contrast, an axial compressor relies upon blade aerodynamics to force the air into an increasingly narrow channel. An axial compressor typically has about six to ten “stages,” each of which consists of a “rotor” (i.e., rotating) disk of blades and a “stator” (i.e., stationary) disk of blades. The rotors tend to swirl the air, so the stators are used to remove the swirl.

The axial compressor, relying upon blade aerodynamics, is intolerant to distortions in the incoming air such as swirl or pressure variations. These distortions can stall the blades, causing a loss of compression and a possible engine flame-out.

The centrifugal compressor is much more forgiving of inlet distortion, but causes the engine to have a substantially higher frontal area, which increases aircraft drag. Also, a centrifugal compressor cannot provide as great a pressure increase (pressure ratio) as an axial compressor. Several smaller turbine engines use a centrifugal compressor behind an axial compressor to attempt to get the best of both types.

The turboprop and turbofan engines both use a turbine to extract mechanical power from the exhaust gases. This mechanical power is used to accelerate a larger mass of outside air, which increases efficiency at lower speeds.

For the turboprop engine, the outside air is accelerated by a conventional propeller. The “prop-fan” or “unducted fan” is essentially a turboprop with an advanced aerodynamics propeller capable of near-sonic speeds.

For the turbofan engine, the air is accelerated with a ducted fan of one or several stages. This accelerated air is then split, with part remaining in the

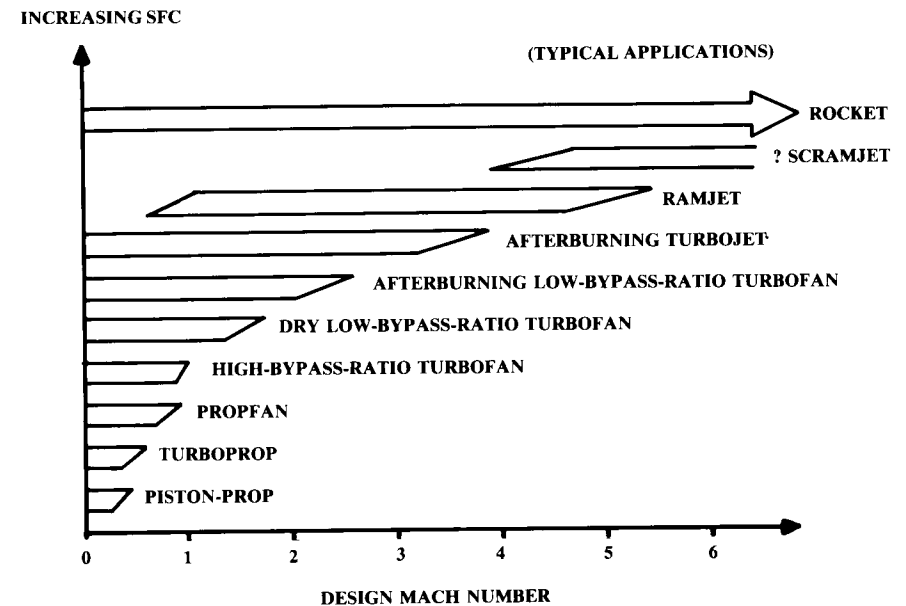


Fig. 10.2 Propulsion system speed limits.

engine for further compression and burning, and the remainder being “bypassed” around the engine to exit unburned.

The “bypass ratio” is the mass-flow ratio of the bypassed air to the air that goes into the core of the engine. Bypass ratio ranges from as high as 6 to as low as 0.25 (the so-called “leaky turbojet”).

The ideal turbine engine would inject enough fuel to completely combust all of the compressed air, producing maximum thrust for a given engine size. Unfortunately, this “stoichiometric” air/fuel mixture ratio of about 15 to 1 produces temperatures far greater than the capabilities of known materials, and would therefore burn up the turbine blades.

To lower the temperature seen by the turbine blades, excess air is used. Currently engines are limited to a turbine temperature of about 2000–2500°F, which requires an air/fuel mixture ratio of about 60 to 1. Thus, only about a quarter of the captured and compressed air is actually used for combustion. The exhaust is 75% unused hot air.

If fuel is injected into this largely-uncombusted hot air, it will mix and burn. This will raise the thrust as much as a factor of two, and is known as “afterburning.” Unfortunately, afterburning is inefficient in terms of fuel usage. The fuel flow required to produce a pound of thrust in afterburner is approximately double that used to produce a pound of thrust during normal engine operations.

Due to the high temperatures produced, afterburning must be done downstream of the turbine. Also, it is usually necessary to divert part of the compressor air to cool the walls of the afterburner and nozzles. Addition of

an afterburner will approximately double the length of a turbojet or turbofan engine.

If the aircraft is traveling fast enough, the inlet duct alone will compress the air enough to burn if fuel is added. This is the principle of a "ramjet." Ramjets must be traveling at above Mach 3 to become competitive with a turbojet in terms of efficiency.

A "scramjet" is a ramjet that can operate with supersonic internal flow and combustion. Scramjets are largely unproven as of this writing, and are probably suitable only for operation above Mach 5 or 6. Ramjets and scramjets require some other form of propulsion for takeoff and acceleration to the high Mach numbers they require for operation.

The selection of the type of propulsion system—piston-prop, turboprop, turbofan, turbojet, ramjet—will usually be obvious from the design requirements. Aircraft maximum speed limits the choices, as shown in Fig. 10.2. In most cases there is no reason to select a propulsion system other than the lowest on the chart for the design Mach number. Fuel-consumption trends have been shown in Fig. 3.3.

The choice between a piston-prop and a turboprop can depend upon several additional factors. The turboprop uses more fuel than a piston prop of the same horsepower, but is substantially lighter and more reliable. Also, turboprops are usually quieter. For these reasons turbine engines have largely replaced piston engines for most helicopters, business twins, and short-range commuter airplanes regardless of design speed. However, piston-props are substantially cheaper and will likely remain the only choice for light aircraft for a long time.

### 10.3 JET-ENGINE INTEGRATION

#### Engine Dimensions

If the aircraft is designed using an existing, off-the-shelf engine, the dimensions are obtained from the manufacturer. If a "rubber" engine is being used, the dimensions for the engine must be obtained by scaling from some nominal engine size by whatever scale factor is required to provide the desired thrust. The nominal engine can be obtained by several methods.

In the major aircraft companies, designers can obtain estimated data for hypothetical "rubber" engines from the engine companies. This data is presented for a nominal engine size, and precise scaling laws are provided. Appendix A.4 provides data for several hypothetical advanced engines.

Better yet, engine companies sometimes provide a "parametric deck," a computer program that will provide performance and dimensional data for an arbitrary advanced-technology engine based upon inputs such as bypass ratio, overall pressure ratio, and turbine-inlet temperature. This kind of program, which provides great flexibility for early trade studies, goes beyond the scope of this book.

Another method for defining a nominal engine assumes that the new engine will be a scaled version of an existing one, perhaps with some performance improvement due to the use of newer technologies. For example, in designing a new fighter one could start with the dimensions and performance charts of the P&W F-100 turbofan, which powers the F-15 and F-16.

To approximate the improvements due to advanced technologies, one could assume, say, a 10 or 20% reduction in fuel consumption and a similar reduction in weight. This would reflect the better materials, higher operating temperatures, and more efficient compressors and turbines that could be built today.

Figure 10.3 illustrates the dimensions that must be scaled from the nominal engine. The scale factor "SF" is the ratio between the required thrust and the actual thrust of the nominal engine. Equations (10.1–10.3) show how length, diameter, and weight vary with the scale factor for the typical jet engine.

$$L = L_{\text{actual}}(\text{SF})^{0.4} \quad (10.1)$$

$$D = D_{\text{actual}}(\text{SF})^{0.5} \quad (10.2)$$

$$W = W_{\text{actual}}(\text{SF})^{1.1} \quad (10.3)$$

Although statistically derived, these equations make intuitive sense. Thrust is roughly proportional to the mass flow of air used by the engine, which is related to the cross-sectional area of the engine. Since area is proportional to the square of the diameter, it follows that the diameter should be proportional to the square root of the thrust scale-factor.

Note the engine-accessories package beneath the engine. The accessories include fuel pumps, oil pumps, power-takeoff gearboxes, and engine control boxes. The location and size of the accessory package varies widely for different types of engines. In the absence of a drawing, the accessory package can be assumed to extend below the engine to a radius of about 20–40% greater than the engine radius. On some engines these accessories have been located in the compressor spinner or other places.

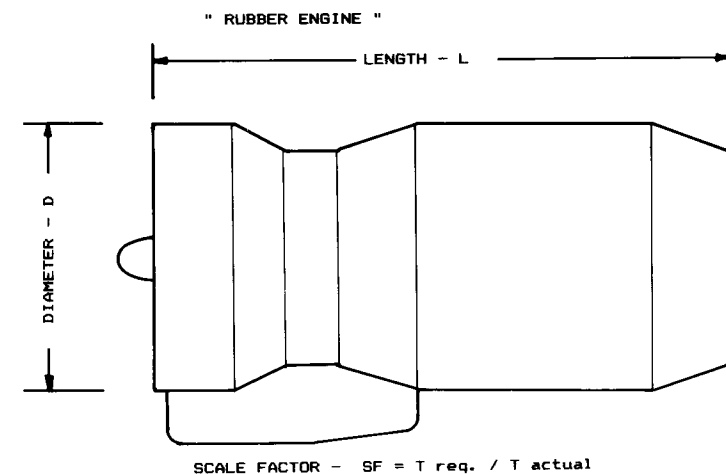


Fig. 10.3 Engine scaling.

If a parametric deck is unavailable, and no existing engines come close enough to the desired characteristics to be rubberized and updated as described above, then a parametric statistical approach can be used to define the nominal engine.

Equations (10.4–10.15) define two first-order statistical jet-engine models based upon data from Ref. 1. One model is for subsonic nonafterburning engines such as found on commercial transports, and covers a bypass-ratio range from zero to about 6. The other model is for afterburning engines for supersonic fighters and bombers ( $M < 2.5$ ), and includes bypass ratios from zero to just under 1.

Nonafterburning engines:

$$W = 0.084T^{1.1}e^{(-0.045 \text{ BPR})} \quad (10.4)$$

$$L = 2.22T^{0.4}M^{0.2} \quad (10.5)$$

$$D = 0.393T^{0.5}e^{(0.04 \text{ BPR})} \quad (10.6)$$

$$\text{SFC}_{\max T} = 0.67e^{(-0.12 \text{ BPR})} \quad (10.7)$$

$$T_{\text{cruise}} = 0.60T^{0.9}e^{(0.02 \text{ BPR})} \quad (10.8)$$

$$\text{SFC}_{\text{cruise}} = 0.88e^{(-0.05 \text{ BPR})} \quad (10.9)$$

Afterburning engines:

$$W = 0.063T^{1.1}M^{0.25}e^{(-0.81 \text{ BPR})} \quad (10.10)$$

$$L = 3.06T^{0.4}M^{0.2} \quad (10.11)$$

$$D = 0.288T^{0.5}e^{(0.04 \text{ BPR})} \quad (10.12)$$

$$\text{SFC}_{\max T} = 2.1e^{(-0.12 \text{ BPR})} \quad (10.13)$$

$$T_{\text{cruise}} = 1.6T^{0.74}e^{(0.023 \text{ BPR})} \quad (10.14)$$

$$\text{SFC}_{\text{cruise}} = 1.04e^{(-0.186 \text{ BPR})} \quad (10.15)$$

where

$W$  = weight  
 $T$  = takeoff thrust  
 BPR = bypass ratio  
 $M$  = max Mach number  
 Cruise is at 36,000 ft and  $0.9M$ .

These equations represent a very unsophisticated model for initial estimation of engine dimensions. They should not be applied beyond the given bypass-ratio and speed ranges. Also, these equations represent today's state of the art. Improvement factors should be applied to approximate future

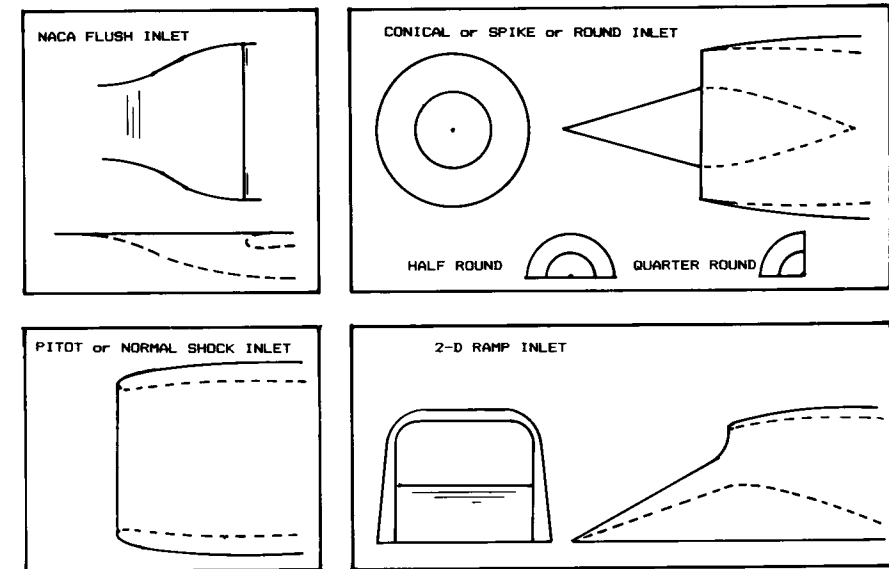


Fig. 10.4 Inlet types.

engines. For a post-1995 engine this author recommends, as a crude approximation, a 20% reduction in SFC, weight, and length for a given maximum thrust.

Reference 46 is recommended for the theory and practice of jet-engine design.

### Inlet Geometry

Turbojet and turbofan engines are incapable of efficient operation unless the air entering them is slowed to a speed of about Mach 0.4–0.5. This is to keep the tip speed of the compressor blades below sonic speed relative to the incoming air. Slowing down the incoming air is the primary purpose of an inlet system.

The installed performance of a jet engine greatly depends upon the air-inlet system. The type and geometry of the inlet and inlet duct will determine the pressure loss and distortion of the air supplied to the engine, which will affect the installed thrust and fuel consumption. Roughly speaking, a 1% reduction in inlet pressure recovery (total pressure delivered to the engine divided by freestream total pressure) will reduce thrust by about 1.3%.

Also, the inlet's external geometry including the cowl and boundary-layer diverter will greatly influence the aircraft drag. As discussed in Chapter 13, this drag due to propulsion is counted as a reduction in the installed thrust.

There are four basic types of inlet, as shown in Fig. 10.4. The NACA flush inlet was used by several early jet aircraft but is rarely seen today for aircraft propulsion systems due to its poor pressure recovery (i.e., large losses). At the subsonic speeds for which the NACA inlet is suitable, a



pitot-type inlet will have virtually 100% pressure recovery vs about 90% for a well-designed NACA inlet. However, the NACA inlet tends to reduce aircraft wetted area and weight if the engine is in the fuselage.

The NACA inlet is regularly used for applications in which pressure recovery is less important, such as the intakes for cooling air or for turbine-powered auxiliary power units. The BD-5J, a jet version of the BD-5 homebuilt, used the NACA inlet, probably to minimize the redesign effort.

Figure 10.5 and Table 10.1 provide dimensions for laying out a good NACA flush inlet. This inlet will provide as high as 92% pressure recovery when operating at a mass flow ratio of 0.5 (i.e., air mass flow through inlet is 0.5 times the mass flow through the same cross-sectional area in the freestream).

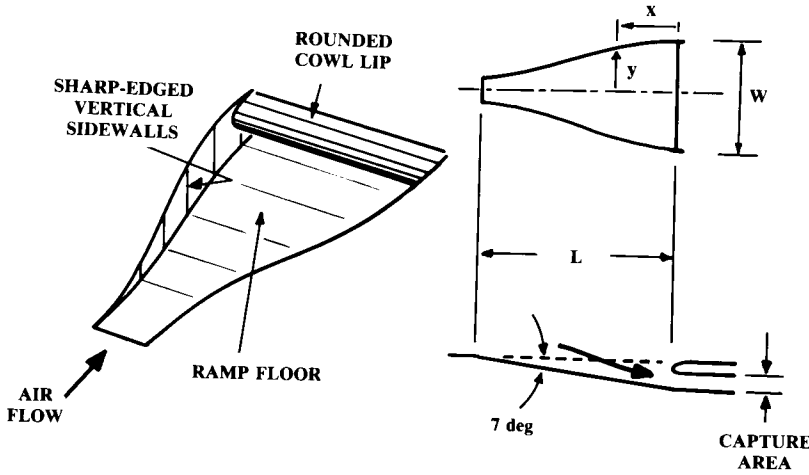


Fig. 10.5 Flush inlet geometry.

Table 10.1 Flush inlet wall geometry

$x/L$	$\frac{y}{W/2}$
1.0	0.083
0.9	0.160
0.8	0.236
0.7	0.313
0.6	0.389
0.5	0.466
0.4	0.614
0.3	0.766
0.2	0.916
0.1	0.996
0.0	1.000

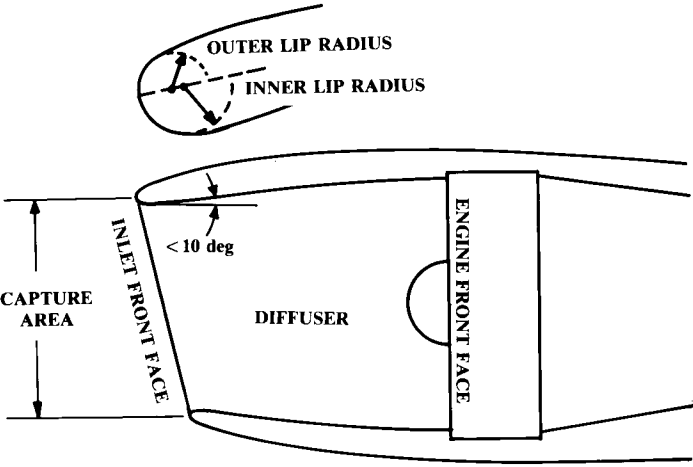


Fig. 10.6 Pitot (normal shock) inlet layout.

The pitot inlet is simply a forward-facing hole. It works very well subsonically and fairly well at low supersonic speeds. It is also called a “normal shock inlet” when used for supersonic flight (“normal” meaning perpendicular in this case). Figure 10.6 gives design guidance for pitot inlets.

The cowl lip radius has a major influence upon engine performance and aircraft drag. A large lip radius tends to minimize distortion, especially at high angles of attack and sideslip. Also, a large lip radius will readily accommodate the additional air required for takeoff thrust, when the ram air effect is small. However, a large lip radius will produce shock-separated flow on the outside of the inlet as the speed of sound is approached, and that greatly increases the drag.

For supersonic jets, the cowl lip should be nearly sharp. Typically the lip radius will be about 3–5% of the inlet front face radius. For subsonic jets, the lip radius ranges from 6–10% of the inlet radius.

To minimize distortion the lip radius on a subsonic inlet is frequently greater on the inside than the outside, with perhaps an 8% inner radius and a 4% outer radius. Also, a number of aircraft have a lip radius on the lower part of the inlet up to 50% greater than that on the upper lip. This reduces the effects of angle of attack during takeoff and landing.

Note that the inlet front face may not be perpendicular to the engine axis. The desired front-face orientation depends upon the location of the inlet and the aircraft’s angle-of-attack range. Normally the inlet should be about perpendicular to the local flow direction during cruise. If the aircraft is to operate at large angles of attack, it may be desirable to compromise between these angles and the angle at cruise.

The remaining inlet types shown in Fig. 10.4 are for supersonic aircraft, and offer improvements over the performance of the normal shock inlet at higher supersonic speeds. The conical inlet (also called a spike, round, or axisymmetric inlet) exploits the shock patterns created by supersonic flow

over a cone. Similarly, the two-dimensional ramp inlet (also called a “*D*-inlet”) uses the flow over a wedge.

The spike inlet is typically lighter and has slighter better pressure recovery (1.5%), but has higher cowl drag and involves much more complicated mechanisms to produce variable geometry. The ramp inlet tends to be used more for speeds up to about Mach 2, while the spike inlet tends to be used above that speed.

Any inlet must slow the air to about half the speed of sound before it reaches the engine. The final transition from supersonic to subsonic speed always occurs through a normal shock. The pressure recovery through a shock depends upon the strength of the shock, which is related to the speed reduction through the shock.

In other words, a normal shock used to slow air from Mach 2 down to subsonic speeds will have a far worse pressure recovery than a normal shock used to slow the air from Mach 1.1 to subsonic speeds (72% vs 99.9%). For this reason a normal-shock inlet is rarely used for prolonged operation above Mach 1.4.

An oblique shock, however, does not reduce the air speed all the way to subsonic. The speed reduction and pressure recovery through an oblique shock depends upon the angle of the wedge or cone used to establish the shock. For example, a 10-deg wedge in Mach 2 flow creates an oblique shock at 39 deg that reduces the flow speed to Mach 1.66 (see Appendix A.2). This gives a pressure loss of only 1.4% (i.e., pressure recovery of 98.6%).

If the Mach 1.66 air downstream of this oblique shock is then run into a normal shock inlet, it will slow to Mach 0.65, with a pressure recovery of 87.2%. The total pressure recovery from Mach 2 to subsonic speed is 98.6 times 87.2, or 86%. Thus, use of an oblique shock before the normal shock has improved pressure recovery for this example Mach 2 inlet from 72% to 86%. (Note that this is far from optimal. A well-designed Mach 2 inlet with one oblique shock will approach a 95% pressure recovery.)

This illustrates the principle of the external-compression inlet shown in Fig. 10.7. The above example is a two-shock system, one external and one normal. The greater the number of oblique shocks employed, the better the pressure recovery.

The theoretical optimal is the isentropic ramp inlet, which corresponds to infinitely-many oblique shocks and produces a pressure recovery of 100% (ignoring friction losses). The pure isentropic ramp inlet works properly at only its design Mach number, and is seen only rarely. However, isentropic ramps are frequently used in combination with flat wedge ramps, such as on the Concorde SST.

Figure 10.8 illustrates a typical three-shock external-compression inlet. This illustration could be a side view of a 2-D inlet or a section view through a spike inlet. Note that the second ramp has a variable angle, and can collapse to open a larger duct opening for subsonic flight.

Some form of boundary-layer bleed is required on the ramp to prevent shock-induced separation on the ramp. The bled air is usually dumped overboard out a rearward-facing hole above the inlet duct.

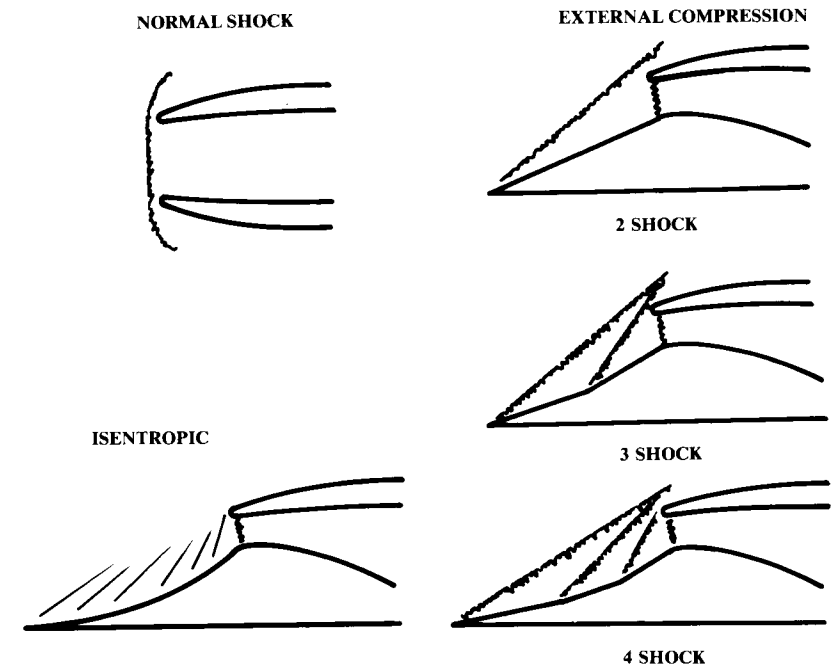


Fig. 10.7 Supersonic inlets—external shocks.

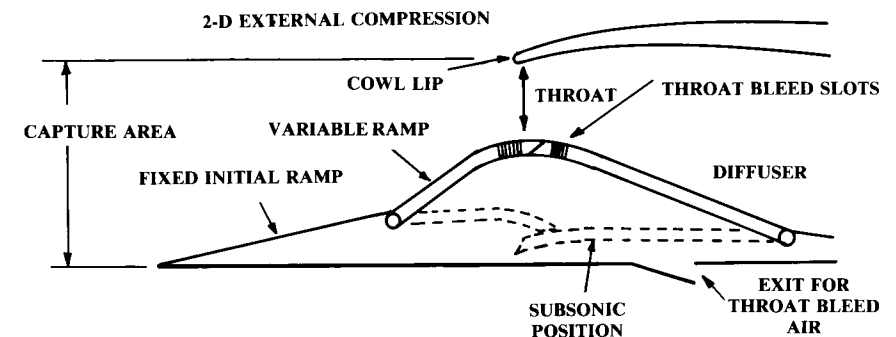


Fig. 10.8 Variable inlet geometry.

Not shown are “suck-in” or “bypass” doors in the diffuser section that may be required to provide extra air to the engine for takeoff or get rid of excess air during high-speed operation.

For initial layout, the overall length of the external portion of the inlet can be estimated by assuming an initial ramp angle (10–20 deg) and determining the shock angle for the design Mach number using standard shock charts such as in Appendix A.2. The cowl lip should be placed just aft of the shock.

The throat area should be about 70–80% of the engine front-face area. The speed limitation on external compression inlets is due to the flow turning angle introduced by the shocks. A wedge turns the flow parallel to the wedge angle, while a cone turns the flow to an angle slightly less than the cone angle.

At speeds approaching Mach 3, the required oblique shocks to obtain good pressure recovery will introduce a total flow turning of about 40 deg. This air must be turned by the outside cowl lip back to the freestream direction, which may not be possible without either separation or an excessively large lip radius that will increase aircraft drag.

One form of inlet system introduces no outside flow turning: the internal compression inlet, as shown in Fig. 10.9. In this inlet a pair of inward-facing ramps produce oblique shocks that cross upstream of the final normal shock.

This form of shock system can be very efficient when operating properly at its design Mach number. However, this inlet must be “started.” If it is simply placed into supersonic flow, a normal shock will form across its front. To start the inlet and produce the efficient shock structure shown in Fig. 10.9, it is necessary to “suck” the normal shock down to the throat by opening doors downstream. Once formed, the desired shock structure is unstable. Any deviation in flow condition, such as temperature, pressure, or angle of attack can cause an “unstart” in which the normal shock pops out of the duct. This can stall the engine.

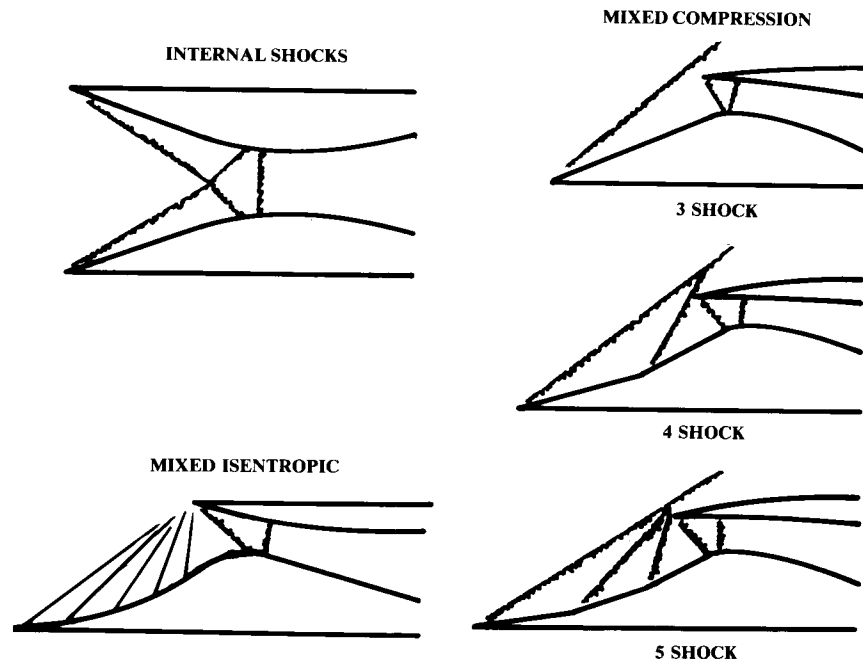


Fig. 10.9 Supersonic inlets—internal and mixed.

The “mixed compression inlet” as shown in Fig. 10.9 uses both external and internal compression to provide high efficiency over a wide Mach number range, with an acceptable amount of external flow turning. Typically one or more external oblique shocks will feed a single internal oblique shock, followed by a final normal shock.

Such an inlet has been used for most aircraft designed to fly above Mach 2.5, including the B-70, which has a 2-D inlet, and the SR-71, which has an axisymmetric inlet. Unstart remains a problem for this type of inlet. Automatically opening doors are used to control unstart.

Mixed-compression inlets are complex, and can be defined only by detailed propulsion analysis beyond the scope of this book. Reference 25 is recommended. The rules of thumb provided above for the dimensions of external-compression inlets give a reasonable first approximation for mixed-compression inlets.

The “diffuser” is the interior portion of an inlet where the subsonic flow is further slowed down to the speed required by the engine. Thus, a diffuser is increasing in cross-sectional area from front to back.

The required length of a diffuser depends upon the application. For a subsonic aircraft such as a commercial transport, the diffuser should be as short as possible without exceeding an internal angle of about 10 deg. Typically, this produces a pitot inlet with a length about equal to its front-face diameter.

For a supersonic application, the theoretical diffuser length for maximum efficiency is about eight times the diameter. Lengths longer than eight times the diameter are permissible but have internal friction losses as well as an additional weight penalty.

A supersonic diffuser shorter than about four times the diameter may produce some internal flow separation, but the weight savings can exceed the engine performance penalty. Diffusers as short as two times the diameter have been used with axisymmetric spike inlets.

For a long diffuser it is important to verify that the cross-sectional area of the flow path is smoothly increasing from the inlet front face back to the engine. This verification is done with a volume-distribution plot of the inlet duct, constructed in the same fashion as the aircraft volume plot shown in Fig. 7.36.

To reduce distortion, some aircraft use a diffuser oversized about 5% that “pinches” the flow down to the engine front-face diameter in a very short distance just before the engine.

Figure 10.10 summarizes the selection criteria for different inlets, based upon design Mach number. Note that these are approximate criteria, and may be overruled by special considerations. Estimated pressure recoveries of these inlets is provided in Chapter 13.

### Inlet Location

The inlet location can have almost as great an effect on engine performance as the inlet geometry. If the inlet is located where it can ingest a vortex off the fuselage or a separated wake from a wing, the resulting

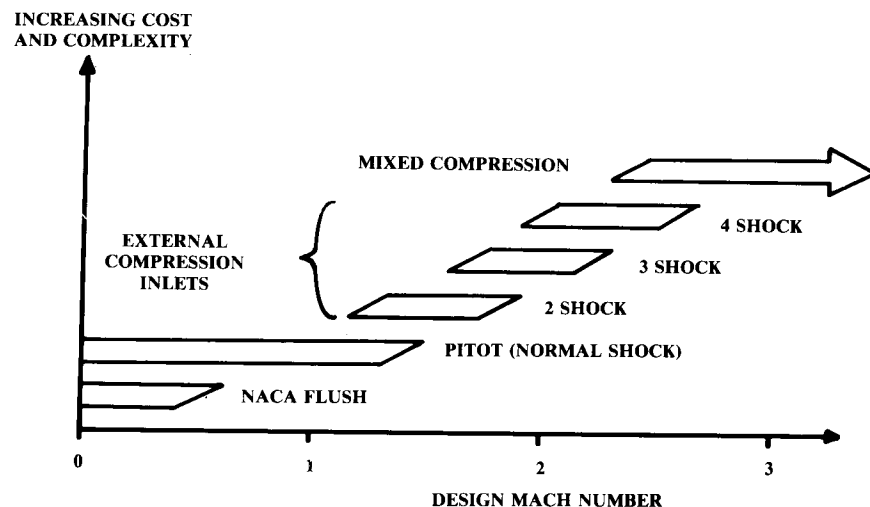


Fig. 10.10 Inlet applicability.

inlet-flow distortion can stall the engine. The F-111 had tremendous problems with its inlets, which were tucked up under the intersection of the wing and fuselage. The A-10 required a fixed slot on the inboard wing leading edge to cure a wake-ingestion problem.

Figures 10.11 and 10.12 illustrate the various options for inlet location. The nose location offers the inlet a completely clean airflow, and was used in most early fighters including the F-86 and MiG 21 as a way of insuring that the fuselage would not cause distortion problems. However, the nose inlet requires a very long internal duct, which is heavy, has high losses, and occupies much of the fuselage volume.

The chin inlet as seen on the F-16 has most of the advantages of the nose inlet but a shorter duct length. The chin inlet is especially good at high angle of attack because the fuselage forebody helps to turn the flow into it.

The location of the nose landing gear is a problem. It cannot be placed forward of the inlet because it would block and distort the flow, and also the nose wheel would tend to throw water and rocks into the inlet. Instead, it is usually placed immediately behind the inlet, which requires that the cowl be deep enough to hold the retracted gear, which can increase cowl drag. Also, the cowl must be strong enough to carry the nose-gear loads.

If two engines are used, twin inlets can be placed in the chin position with the nose wheel located between them. This was used on the North American Rockwell proposal for the F-15, and is seen on the Sukhoi Su-27.

Another problem with the chin inlet is foreign-object ingestion by suction. As a rule of thumb, all inlets should be located a height above the runway equal to at least 80% of the inlet's height if using a low bypass ratio engine, and at least 50% of the inlet's height for a high-bypass-ratio engine.

Side-mounted inlets are now virtually standard for aircraft with twin engines in the fuselage. Side inlets provide short ducts and relatively clean air. Side-mounted inlets can have problems at high angles of attack due to

the vortex shed off the lower corner of the forebody. This is especially severe if the forward fuselage has a fairly square shape.

If side-mounted inlets are used with a single engine, a split duct must be used. Split ducts are prone to a pressure instability that can stall the engine. To minimize this risk, it is best to keep the two halves of the duct separate all the way to the engine front face, although several aircraft have flown with the duct halves rejoined well forward of the engine.

A side inlet at the intersection of the fuselage and a high wing is called an "armpit" inlet. It is risky! The combined boundary layers of the forebody and wing can produce a boundary layer in the wing-fuselage corner that is too thick to remove (boundary-layer removal is discussed later). This type of inlet is especially prone to distortion at angle of attack and sideslip. In many cases however, the armpit inlet does offer a very short internal duct.

An over-fuselage inlet is much like an inverted chin inlet, and has a short duct length but without the problems of nose-wheel location. This was used on the unusual F-107. The upper-fuselage inlet is poor at high angle of attack because the forebody blanks the airflow. Also, many pilots fear that they may be sucked down the inlet if forced to bail out manually.

Placed over the wing and near the fuselage, an inlet encounters problems similar to those of an inverted-armpit inlet. It also suffers at angle of attack.

An inlet above the aft fuselage for a buried engine is used on the L-1011 and B-727, with the inlet located at the root of the vertical tail. This arrangement allows the engine exhaust to be placed at the rear of the fuselage, which tends to reduce fuselage separation and drag. The buried engine with a tail inlet must use an "S-duct." This requires careful design to avoid internal separation. Also, the inlet should be well above the fuselage to avoid ingesting the thick boundary layer.

Inlets set into the wing leading edge can reduce the total aircraft wetted area by eliminating the need for a separate inlet cowl. However, these inlets can disturb the flow over the wing and increase its weight. The wing-root position may also ingest disturbed air off the fuselage.

A podded engine has higher wetted area than a buried engine, but offers substantial advantages that have made it standard for commercial and business jets. Podded engines place the inlet away from the fuselage, providing undisturbed air with a very short inlet duct. Podded engines produce less noise in the cabin because the engine and exhaust are away from the fuselage. Podded engines are usually easier to get to for maintenance. Most are mounted on pylons, but they can also be mounted conformal to the wing or fuselage.

The wing-mounted podded engine is the most commonly used engine installation for jet transports. The engines are accessible from the ground and well away from the cabin. The weight of the engines out along the wing provides a "span-loading" effect, which helps reduce wing weight. The jet exhaust can be directed downward by flaps which greatly increases lift for short takeoff.

On the negative side, the presence of pods and pylons can disturb the airflow on the wing, increasing drag and reducing lift. To minimize this, the pylons should not extend above and around the wing leading edge, as was seen on one early jet transport.

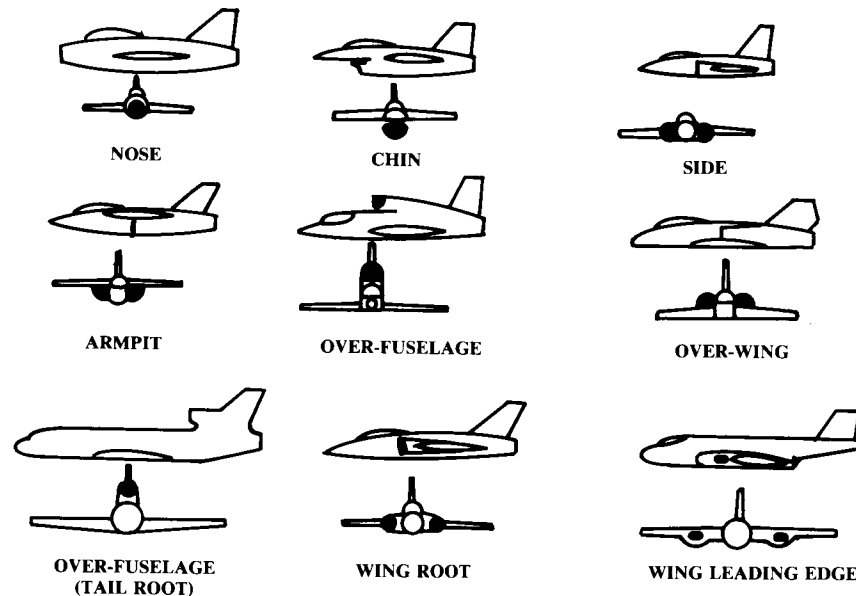


Fig. 10.11 Inlet locations—buried engines.

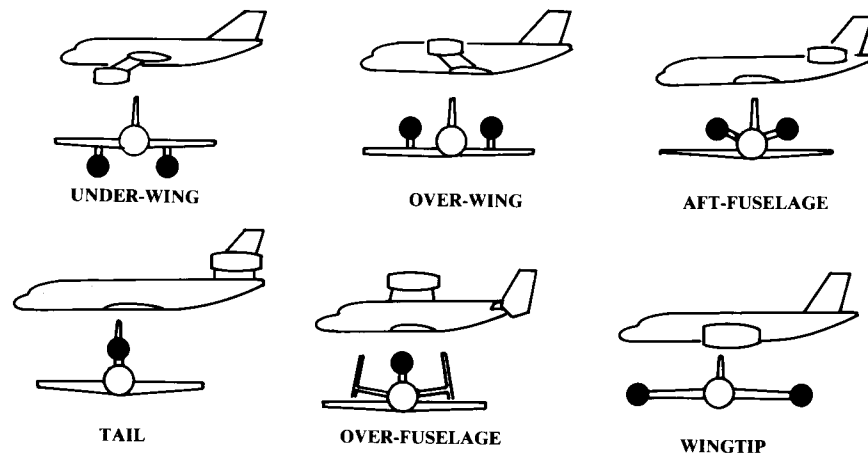


Fig. 10.12 Inlet locations—podded engines.

On the basis of years of wind-tunnel study, design charts for pylon-mounted engines have been prepared that minimize the interference effects of the nacelle pod on the wing. As a classical rule-of-thumb, the inlet for a wing-mounted podded engine should be located approximately two inlet diameters forward and one inlet diameter below the wing leading edge. However, modern computational fluid dynamic (CFD) methods now allow

designing a wing-mounted nacelle much closer to the wing, or even conformal to the wing, without incurring substantial drag increase due to interference. This will be further discussed in Chapter 12.

The wing-mounted nacelle should be angled nose down by about 2–4 deg, and canted nose inward about 2 deg to align it to the local flow under the wing.

To reduce foreign-object ingestion by suction, the inlet of a high-bypass engine should be located about half a diameter above the ground. This requirement increases the required landing-gear height of the under-wing arrangement.

The over-wing podded nacelle reduces the landing-gear height and reduces noise on the ground, but is difficult to get to for maintenance. The inlets can be forward of the wing to minimize distortion, or above it. If an over-wing nacelle is conformal to the wing, the exhaust can be directed over the top of flaps, which, through Coanda effect, turn the flow downward for increased lift.

The other standard engine installation for jet transports is the aft-fuselage mount, usually with a T-tail. This eliminates the wing-interference effects of wing-mounted engines, and allows a short landing gear. However, it increases the cabin noise at the rear of the aircraft.

Also, aft-mounting of the engines tends to move the center of gravity aft, which requires shifting the entire fuselage forward relative to the wing. This shortens the tail moment arm and increases the amount of fuselage forward of the wing, and that necessitates a larger vertical and horizontal tail.

To align the aft nacelle with the local flow, a nose-up pitch of 2–4 deg and a nose outward cant of 2 deg are recommended.

The Illyushin Il-76 uses four aft-podded engines in two twin-engine pods. The L-1011, B-727, and Hawker-Siddeley Trident combine aft-fuselage podded engines with a buried engine using an inlet over the tail.

The DC-10 combines aft-fuselage side pods with a tail-mounted podded engine. This is similar to the tail-mounted inlet for a buried engine, but eliminates the need for an S-duct. However, this arrangement increases the tail weight and doesn't have the fuselage drag-reduction effect. All told, the two installations are probably equivalent.

The supersonic Tupolev Tu-22 ("Blinder") uses twin engines, pod-mounted on the tail, but this arrangement has not been seen on later Soviet supersonic designs.

The over-fuselage podded engine has been used only rarely. Most recently it was used to add a jet engine to the turboprop Rockwell OV-10. Access and cabin noise are undesirable for this installation.

The wing tip-mounted engine has an obvious engine-out controllability problem. It was used on the Soviet supersonic Myasishchev M-52 ("Bouncer"), which also had under-wing engine pods.

### Capture-Area Calculation

Figure 10.13 provides a quick method of estimating the required inlet capture area. This statistical method is based upon the design Mach number and the engine mass flow in pounds per second.

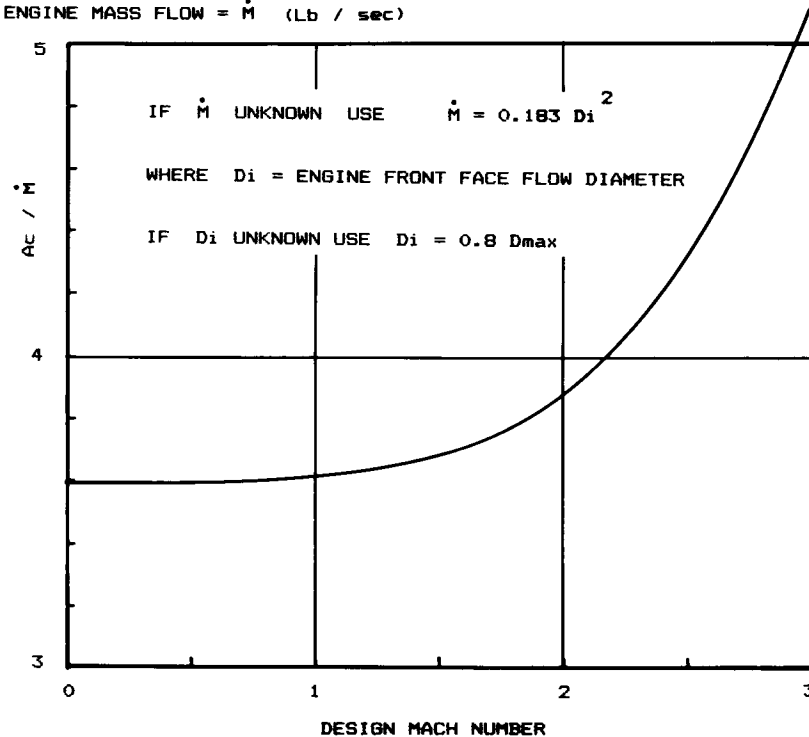
INLET CAPTURE AREA =  $A_c$  (square inches)ENGINE MASS FLOW =  $\dot{M}$  (Lb / sec)

Fig. 10.13 Preliminary capture area sizing.

If mass flow is not known, it may be estimated as 0.18 times the square of the engine front-face diameter in inches, or as 0.12 times the square of the maximum engine diameter. To determine the required capture area, the mass flow is multiplied by the value from Fig. 10.13.

This capture-area estimation is adequate for initial layout and rough analysis, but not accurate enough for a good configuration layout. A better estimate of capture area should be made during configuration layout based upon the actual mass flow of the engine, as described below.

In a jet propulsion system, the engine is the boss. It takes the amount of air it wants, not what the inlet wants to give it. If the inlet is providing more air than the engine wants, the inlet must spill the excess out the front. If the inlet is not providing what the engine needs, it will attempt to suck in the extra air required.

The inlet capture area must be sized to provide sufficient air to the engine at all aircraft speeds. For many aircraft the capture area must also provide "secondary air" for cooling and environmental control, and also provide for the air bled off the inlet ramps to prevent boundary-layer buildup.

Figure 10.14 defines the capture area for a subsonic inlet. A typical subsonic jet inlet is sized for cruise at about Mach 0.8–0.9, and the inlet must

slow the air to about Mach 0.4 for most engines. Since this is subsonic flow, the inlet does not need to do all the work itself. As shown in Fig. 10.14, the expansion associated with slowing the flow from its freestream velocity at "infinity" takes place about half within and half outside the inlet duct.

The area at the inlet front face is both the capture area and the throat area. It can be calculated from the following isentropic compressible flow relationship:

$$\frac{A_{throat}}{A_{engine}} = \frac{(A/A^*)_{throat}}{(A/A^*)_{engine}} \quad (10.16)$$

$$\frac{A}{A^*} = \frac{1}{M} \left( \frac{1 + 0.2M^2}{1.2} \right)^3 \quad (10.17)$$

where  $A^*$  is the area of the same flow at sonic speed.

For a typical inlet designed to a cruise speed of Mach 0.8, the inlet must slow the air from about Mach 0.6 down to Mach 0.4. The air is slowed from Mach 0.8–0.6 outside the inlet.

Equations (10.16) and (10.17) give the ratio between throat area and engine front-face area as 1.188/1.59, or 0.75 (for this example). Taking the square root gives a diameter ratio of about 0.88, which is reasonable. Note that a subsonic inlet generally does not require bleed air, since secondary air is obtained from separate, small NACA flush inlets in most subsonic aircraft.

Equations (10.16) and (10.17) may be used to determine the capture area for a supersonic pitot inlet with negligible bleed or secondary airflow by finding the Mach number behind the normal shock from Appendix A.2. For other supersonic inlets the required capture area must be determined by considering the air-flow requirements for the engine, bleed, and secondary

In sizing a supersonic inlet, a variety of flight conditions must be considered to find the largest required capture area. Typically this will be at the aircraft maximum Mach number, but may also occur during takeoff or subsonic cruise. If the maximum required capture-area occurs during take-

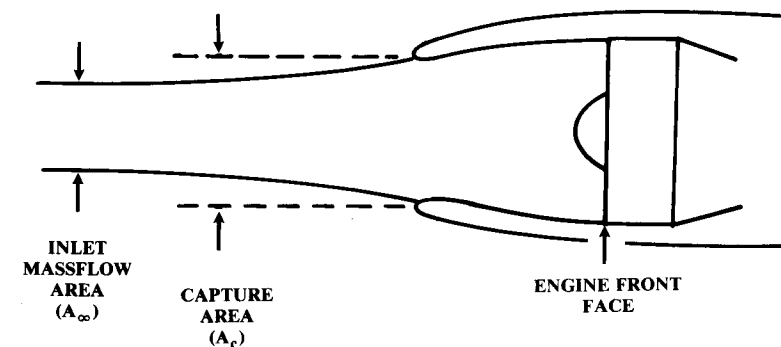


Fig. 10.14 Subsonic inlet capture area.

off, consider using auxiliary “suck-in” doors during takeoff. This allows the inlet to be sized to another, lesser capture area requirement.

To avoid the confusion of differing velocities and densities, the airflow is defined by mass flow in pounds mass per second. Mass flow is related to flow conditions by Eq. (10.18), where  $g$  is 32.2 ft/s<sup>2</sup>.

$$\dot{m} = g \rho V A, \text{ lb/s}$$

(10.18)

Figure 10.15 defines the capture area geometry for a supersonic ramp or cone inlet. This inlet is shown at the design case, which is known as “shock-on-cowl.” At this Mach number and ramp angle, the initial oblique shock is almost touching the cowl lip. If the auxiliary doors are shut and the shock is on cowl, the geometric capture area is providing exactly the right amount of air for the engine, bleed, and secondary flow.

Usually the inlet ramp geometry provides shock-on-cowl at about Mach 0.1–0.2 above the aircraft’s maximum speed, giving a safety margin for speed overshoot and engine mass-flow fluctuations.

If the total mass flow required by the engine, bleed, and secondary flow is known, then Eq. (10.18) can be solved for the required cross-sectional area upstream of the inlet (at “infinity”) using the freestream values for density and velocity. This calculated area is identical to the capture area in the design case (shock-on-cowl) since all of the air in the capture area is going into the inlet.

The required engine mass flow is provided by the engine manufacturer, and is a function of the Mach number, altitude, and throttle setting (percent power). Usually the manufacturer’s data should be increased by 3% to allow for manufacturing tolerances.

The secondary airflow requirements are accurately determined by an evaluation of the aircraft’s subsystems such as environmental control. For initial capture-area estimation, Table 10.2 (from Ref. 26) provides secondary airflow as a fraction of engine mass flow.

Table 10.2 Secondary airflow (typical)<sup>26</sup>

	$\dot{m}_s/\dot{m}_e$
Engine	
Nacelle cooling	0–0.04
Oil cooling	0–0.01
Ejector nozzle air	0.04–0.20
Hydraulic system cooling	0–0.01
Environmental control system cooling air (if taken from inlet)	0.02–0.05
Typical totals	
Fighter	0.20
Transport	0.03

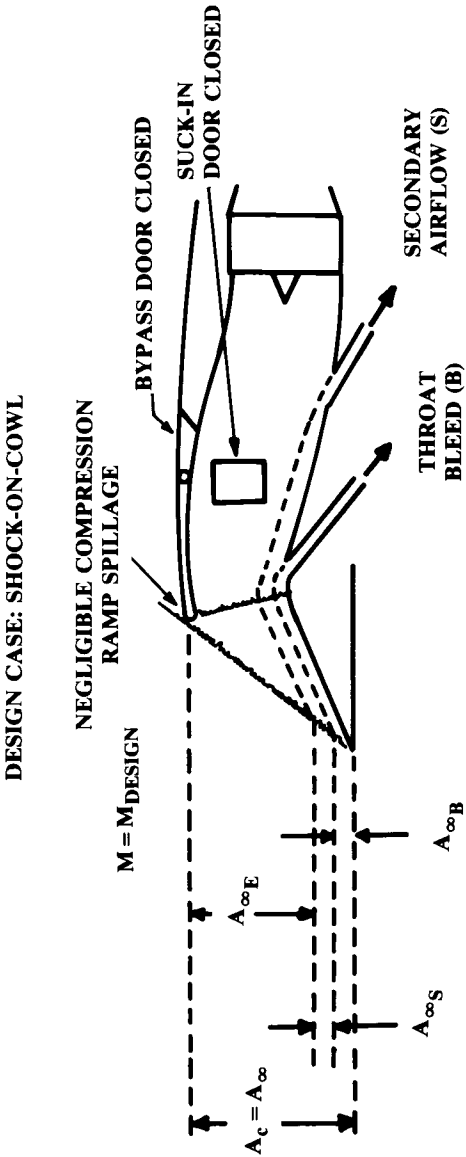


Fig. 10.15 Supersonic inlet capture area—on design.

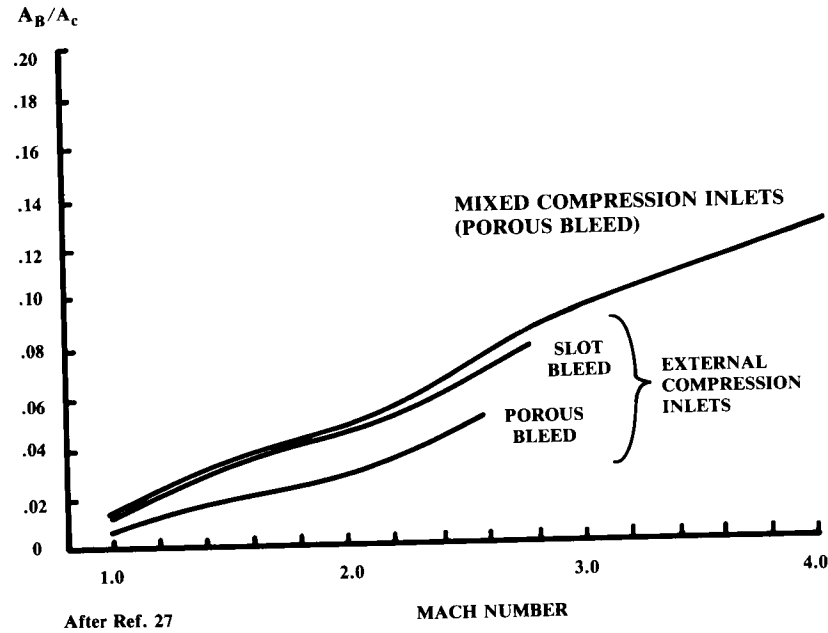


Fig. 10.16 Typical boundary layer bleed area.

Inlet boundary layer bleed should also be determined analytically, but can be approximated using Fig. 10.16, taken from Ref. 27. This estimates the required extra capture area for bleed as a percent of the capture area required for the engine and secondary airflow.

The capture area is therefore determined as in Eq. (10.19), using Table 10.2 and Fig. 10.16.

$$A_{\text{capture}} = \left[ \frac{\dot{m}_E(1 + \dot{m}_S/\dot{m}_E)}{g\rho_\infty V_\infty} \right] \left( 1 + \frac{A_B}{A_c} \right) \quad (10.19)$$

Figure 10.15 shows the inlet operating at its design condition, shock-on-cowl, where the geometric capture area equals the freestream area of the air actually taken into the inlet and used. If the freestream Mach number is reduced, the oblique shock angle drops, which moves the oblique shock in front of the cowl, as shown in Fig. 10.17a.

Since the airflow is parallel to the ramp, it can be seen that the freestream cross-sectional area of the air that actually goes into the inlet has been reduced. Part of the air defined by the geometric capture area is now spilled after being compressed. This represents wasted work and increased drag compared to the case of shock-on-cowl.

If the mass-flow demand exactly equals the mass flow shown going into the inlet in Fig. 10.17a (i.e., capture area less compression-ramp spillage), then the engine and inlet duct are still “matched” and the normal shock will be at the cowl lip, as shown in Fig. 10.17a.

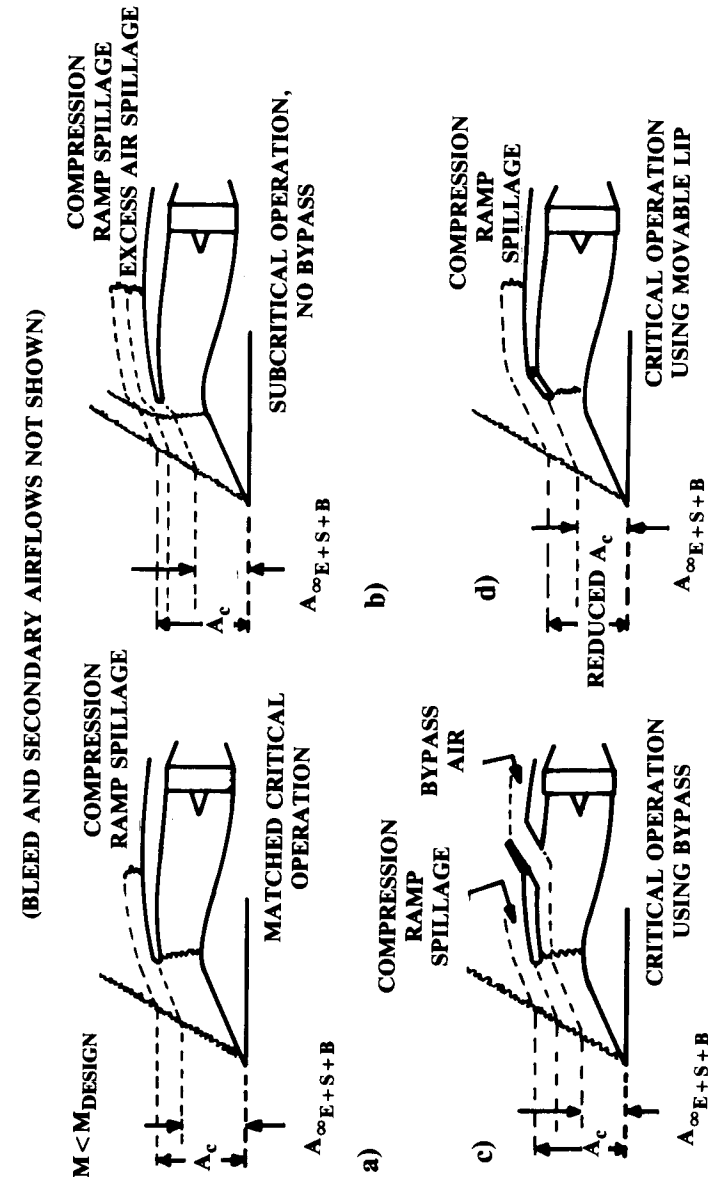


Fig. 10.17 Off-design inlet operation.



However, the engine demand is usually reduced at a slower speed. The excess air is simply rejected by the inlet, as shown in Fig. 10.17b. (Remember, the engine is the boss!) This pushes the normal shock forward of the inlet and creates a much larger spillage drag than for the matched condition.

Two approaches to move the normal shock back to the cowl lip are shown in Figs. 10.17c and 10.17d. By opening a bypass door in the diffuser section, the excess air can be taken into the inlet and thrown away before reaching the engine. While an inlet bypass will create some additional drag, the total is reduced compared with the case in Fig. 10.17b.

(Do not confuse inlet bypass air with the engine bypass air. Inlet bypass air is dumped out of the inlet before it reaches the engine, and is therefore not a contributor to thrust. Engine bypass air is exited after being accelerated by the compressor, and does contribute to thrust.)

Another approach for returning the normal shock to the inlet lip is to move the cowl lip down, reducing the capture area as shown in Fig. 10.17d. This is complex and heavy to mechanize, and virtually impossible for an axisymmetric inlet.

It is also possible to translate the ramp or spike fore and aft to maintain shock-on-cowl at different Mach numbers. This is often employed with high-speed spike inlets.

The ratio between the air flow actually going into the inlet and the total possible air flow (i.e., the airflow of the capture area) is called the “capture area ratio,” or “inlet mass flow ratio.” The total mass flow actually going into the inlet is the mass flow required for the engine plus secondary airflow plus bleed airflow plus inlet bypass air, if any.

Capture-area ratio is calculated by determining the required mass flow and dividing by the mass flow through the capture area far upstream (Eq. (10.20). Note that capture-area ratio is generally critical for conditions in which the inlet bypass doors are closed (no bypass mass flow).

$$\frac{A_\infty}{A_c} = \frac{\dot{m}_E + \dot{m}_S + \dot{m}_{BL} + \dot{m}_{bypass}}{g \rho_\infty V_\infty A_c} \quad (10.20)$$

The capture-area ratio in subsonic flow can be greater than, equal to, or less than 1. In supersonic flow, it can only be equal to or less than 1.

### Boundary-Layer Diverter

Any object moving through air will build up a boundary layer on its surface. In the last section, boundary-layer bleed was included in the capture-area calculation. This boundary-layer bleed was used to remove the low-energy boundary layer air from the compression ramps, to prevent shock-induced separation.

The aircraft's forebody builds up its own boundary layer. If this low-energy, turbulent air is allowed to enter the engine, it can reduce engine performance subsonically and prevent proper inlet operation supersonically. Unless the aircraft's inlets are very near the nose (within two to four inlet diameters), some form of boundary-layer removal should be used just in front of the inlet.

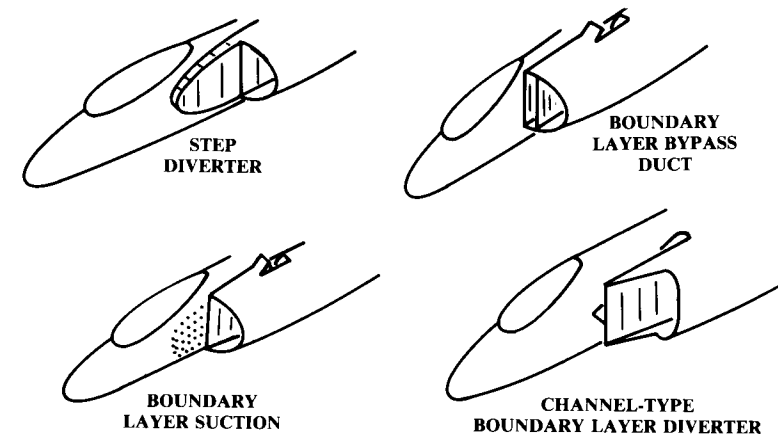


Fig. 10.18 Boundary layer removal.

The four major varieties of boundary-layer diverter are shown in Fig. 10.18. The step diverter is suitable only for subsonic aircraft, and relies upon the boundary layer itself for operation. The boundary layer consists of low-energy air, compared to the air outside of the boundary layer.

The step diverter works by forcing the boundary-layer air to either climb the step, pushing aside high-energy air outside the boundary layer, or to follow the step, pushing aside other boundary-layer air which is of lower energy. If the step diverter is properly shaped, the latter option prevails.

The step diverter should have an airfoil-like shape that is faired smoothly to the nacelle. The diverter should extend about one inlet diameter forward of the inlet, and should be have a depth equal to roughly 2–4% of the forebody length ahead of the inlet.

The boundary-layer bypass duct (simply a separate inlet duct) admits the boundary-layer air and ducts it to an aft-facing hole. The internal duct shape should expand roughly 30% from intake to exit to compensate for the internal friction losses.

The suction form of boundary-layer diverter is similar. The boundary-layer air is removed by suction through holes or slots just forward of the inlet and ducted to an aft-facing hole. This type of diverter does not benefit from the ram impact of the boundary-layer air, and therefore does not work as well.

The channel diverter (Fig. 10.19) is the most common boundary-layer diverter for supersonic aircraft. It provides the best performance and the least weight in most cases. The inlet front face is located some distance away from the fuselage, with a “splitter plate” to insure that the boundary-layer air does not get into the inlet. The boundary-layer air is caught between the splitter plate and the fuselage, and pushed out of the resulting channel by the diverter ramps. The diverter ramps should have an angle of no more than about 30 deg.

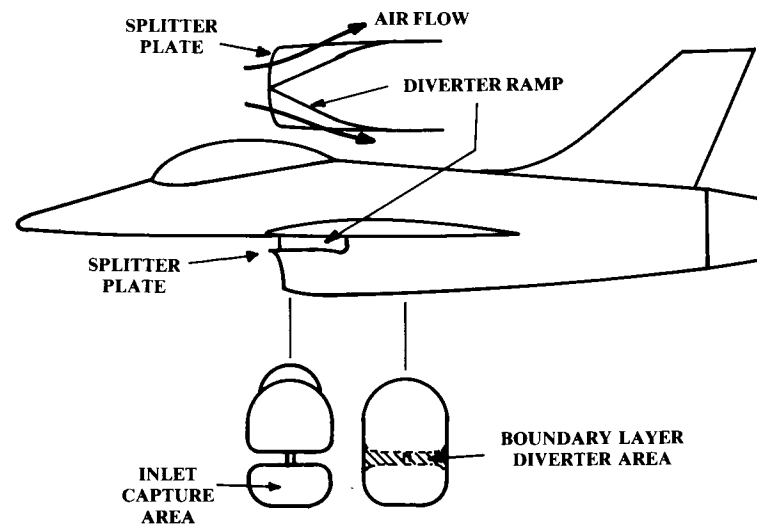


Fig. 10.19 Boundary layer diverter.

The required depth of a boundary-layer diverter depends on the depth of the boundary layer itself. This cannot be simply calculated. The classic boundary-layer equations assume a flat plate, which is unlike a fuselage forebody. The 3-D effects of a real forebody tend to reduce boundary-layer buildup compared to a flat plate.

A very good rule of thumb for the required thickness of a boundary-layer diverter is that it should be between 1 and 3% of the fuselage length in front of the inlet, with the larger number for fighters which go to high angle of attack.

As will be discussed in Chapter 12, the drag of a boundary-layer diverter depends upon its frontal area. During conceptual layout, the fuselage and inlet should be designed to minimize this area, shown shaded in Fig. 10.19.

### Nozzle Integration

The fundamental problem in jet engine nozzle design is the mismatch in desired exit areas at different speeds, altitudes, and thrust settings. The engine can be viewed as a producer of high-pressure subsonic gases. The nozzle accelerates those gases to the desired exit speed, which is controlled by the exit area.

The nozzle must converge to accelerate the exhaust gases to a high subsonic exit speed. If the desired exit speed is supersonic, a converging-diverging nozzle is required.

The exit area to obtain a desired exhaust velocity depends upon the engine mass flow (i.e., percent power). This is especially a problem with afterburning engines, in which the desired exit area for supersonic afterburning operation can be three times the desired area for subsonic, part-thrust operation.

Typical nozzles are shown in Fig. 10.20. In the past, the nozzle of a jet engine was considered an integral part of the engine, to be installed on the aircraft without question or change. This is still the case for subsonic commercial aircraft, but is changing for supersonic military aircraft due to the emergence of 2-D and other advanced nozzles.

The fixed convergent nozzle is almost universally used for subsonic commercial turbojet and turbofan engines. The nozzle exit area is selected for cruise efficiency, resulting in a loss of theoretical performance at lower speeds. However, the gain in simplicity and weight reduction of the fixed nozzle more than makes up for the performance loss in most subsonic applications.

For an aircraft which occasionally flies at high-subsonic to low-supersonic speeds, a variable-area convergent nozzle allows a better match between low-speed, part-thrust operation and the maximum speed and thrust conditions. The nozzle shown has a fixed outer surface, which causes a “base” area when the nozzle inside is in the closed position.

Such a nozzle was used on many early transonic fighters, but is not typically used today. Instead, the convergent-iris nozzle is used to vary the area of a convergent nozzle without introducing a base area.

Another means to vary the exit area of a convergent nozzle is the translating plug. This was used on the engine for the Me-262, the first jet to be employed in combat in substantial numbers. The plug slides aft to decrease exit area.

The ejector nozzle takes engine bypass air that has been used to cool the afterburner and ejects it into the exhaust air, thus cooling the nozzle as well. The variable-geometry convergent-divergent ejector nozzle is most commonly applied to supersonic jet aircraft. It allows varying the throat and

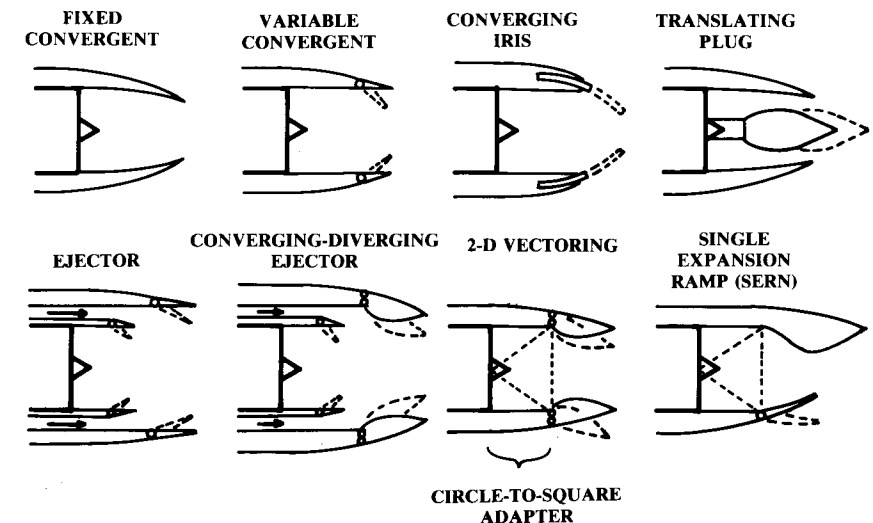


Fig. 10.20 Types of nozzles.

exit areas separately for maximum engine performance throughout the flight envelope.

If an existing engine is used in the design, or if a hypothetical engine data package has been obtained from an engine company, the nozzle areas will be provided for the design flight regime. If not, the nozzle areas must be estimated because they have a substantial effect upon the calculated aircraft wave drag and boattail drag.

For initial design layout, a reasonable approximation can be made based upon the estimated capture area. For a subsonic convergent nozzle or a convergent-divergent nozzle in the closed position, the required exit area is approximately 0.5–0.7 times the capture area. For maximum supersonic afterburning operation, the required exit area is about 1.2–1.6 times the capture area.

As mentioned, nozzle arrangement can have a substantial effect on boat-tail drag. This is the drag due to separation on the outside of the nozzle and aft fuselage. To reduce boattail drag to acceptable levels, the closure angles on the aft fuselage should be kept below 15 deg, and the angles outside of the nozzle should be kept below 20 deg in the nozzle-closed position.

Jet engines mounted next to each other produce an interference effect that reduces net thrust. To minimize this, the nozzles should be separated by about one to two times their maximum exit diameter. The area between them should taper down like the back of an airfoil, terminating just before the nozzles. However, this arrangement increases weight and wetted area so many fighters have twin engines mounted right next to each other despite the increased interference.

## 10.4 PROPELLER-ENGINE INTEGRATION

### Propeller Sizing

The actual details of the propeller design such as the blade shape and twist are not required to lay out a propeller-engine aircraft. But the diameter of the propeller, the dimensions of the engine, and the required inlets and exhausts must be determined.

Generally speaking, the larger the propeller diameter, the more efficient the propeller will be. The old rule of thumb was “keep it as long as possible, as long as possible.” The limitation on length is the propeller tip speed, which should be kept below sonic speed.

The tip of a propeller follows a helical path through the air. Tip speed is the vector sum of the rotational speed [Eq. (10.21)] and the aircraft’s forward speed as defined in Eq. (10.22).

$$(V_{\text{tip}})_{\text{static}} = \pi n d / 60 \quad (\text{ft/s}) \quad (10.21)$$

where

$n$  = rotational rate (rpm) obtained from engine data

$d$  = diameter

$$(V_{\text{tip}})_{\text{helical}} = \sqrt{V_{\text{tip}}^2 + V^2} \quad (10.22)$$

Note: watch the units!

At sea level the helical tip speed of a metal propeller should not exceed 950 fps. A wooden propeller, which must be thicker, should be kept below 850 fps. If noise is of concern, the upper limit for metal or wood should be about 700 fps during takeoff.

Equations (10.23–10.25) provide an estimate of the propeller diameter as a function of horsepower (Ref. 28). The propeller diameters obtained from these equations should be compared to the maximum diameters obtained from tip-speed considerations, and the smaller of the two values used for initial layout.

$$\text{Two blade: } d = 22 \sqrt[4]{\text{Hp}} \quad (10.23)$$

$$\text{Three blade: } d = 18 \sqrt[4]{\text{Hp}} \quad (10.24)$$

$$\text{Three blade (agricultural): } d = 20 \sqrt[4]{\text{Hp}} \quad (10.25)$$

As forward velocity increases the angle of attack seen by the blades of a fixed-pitch propeller will decrease. This limits the thrust obtained at higher speeds. If the fixed pitch is increased, the blades will tend to stall at low speeds, which reduces low-speed thrust. A fixed-pitch propeller is called a “cruise prop” or “climb prop” depending upon the flight regime the designer has decided to emphasize.

A variable-pitch propeller can be used to improve thrust across a broad speed range. A “controllable-pitch” propeller has its pitch directly controlled by the pilot through a lever alongside the throttle. A “constant-speed” propeller is automatically controlled in pitch to maintain the engine at its optimal RPM.

Most aircraft propellers have a “spinner,” a cone- or bullet-shaped fairing at the hub. The inner part of the propeller contributes very little to the thrust. A spinner pushes the air out to where the propeller is more efficient. Also, a spinner streamlines the nacelle. Ideally, the spinner should cover the propeller out to about 25% of the radius, although most spinners are not that large.

To further streamline the nacelle, some aircraft designers use a “prop extension,” a short shaft which locates the propeller 2–4 in. farther forward (or aft) of the engine. If the propeller is located much farther away from the engine, a complicated drive shaft with a separate bearing support for the propeller must be used. This type of installation was used in the P-39, which had a piston engine behind the cockpit and a drive shaft to the forward-mounted propeller. Similarly, the BD-5 had a drive shaft to a rear-mounted pusher propeller.

### Propeller Location

A matrix of possible propeller locations is shown in Fig. 10.21. A tractor installation has the propeller in front of its attachment point (usually the motor). A pusher location has the propeller behind the attachment point.

The Wright Flyer was a pusher. However, the tractor location has been standard for most of the history of aviation. The conventional tractor loca-

tion puts the heavy engine up front, which tends to shorten the forebody, allowing a smaller tail area and improved stability. The tractor location also provides a ready source of cooling air, and places the propeller in undisturbed air.

The pusher location is now seeing wider use because of its advantages. Most importantly, it can reduce aircraft skin friction drag because the pusher location allows the aircraft to fly in undisturbed air. With a tractor propeller the aircraft flies in the turbulence from the propeller wake.

The fuselage-mounted pusher propeller can allow a reduction in aircraft wetted area by shortening the fuselage. The inflow caused by the propeller allows a much steeper fuselage closure angle without flow separation than otherwise possible. The canard-pusher combination is especially favorable because the canard requires a shorter tail arm than the aft tail.

The pusher propeller reduces cabin noise because the engine exhaust is pointed away from the cabin, and because the windscreen isn't buffeted by propwash. Also, the pusher arrangement usually improves the pilot's outside vision.

The pusher propeller may require longer landing gear because the aft location causes the propeller to dip closer to the runway as the nose is lifted for takeoff. The propeller should have at least 9 in. of clearance in all attitudes.

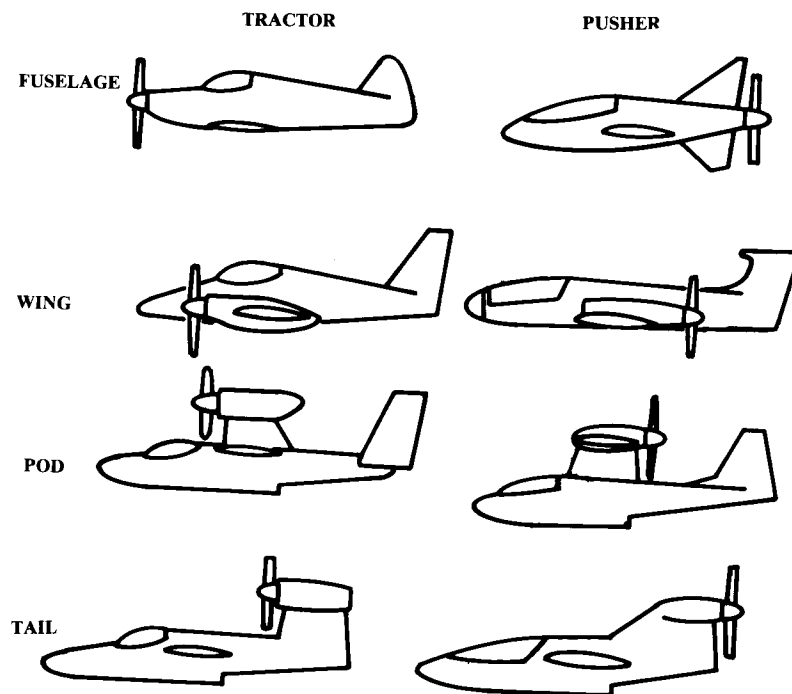


Fig. 10.21 Propeller location matrix.

The pusher-propeller is also more likely to be damaged by rocks thrown up by the wheels. A pusher location for a turboprop propeller can create problems due to the engine exhaust impinging upon the propeller.

The Cessna Skymaster and Rutan Defiant use a combination of pusher and tractor engines on the fuselage.

Wing mounting of the engines is normally used for multiengine designs. Wing mounting of engines reduces wing structural weight through a span-loading effect, and reduces fuselage drag by removing the fuselage from the propeller wake.

Wing mounting of engines introduces engine-out controllability problems that force an increase in the size of the rudder and vertical tail. Also, care must be taken to insure that the crew compartment is not located within plus or minus 5 deg of the propeller disk, in case a blade is thrown through the fuselage.

Most twin-engine aircraft are of low-wing design. For these, the location of the engine and propeller on the wing requires a longer landing gear. Frequently the propeller will be raised above the plane of the wing to reduce landing-gear height. This causes additional interference between the wing and propeller.

The wing-mounted pusher arrangement has been seen on the Beech Starship and B-36. This arrangement tends to lengthen the forebody and require a very long landing gear.

Also, the propeller is half in the wake from under the wing and half in the wake from over the wing. The pressure differences between these two wakes can cause the propeller to lose efficiency and produce vibrations. This is minimized by locating the propeller as far as possible behind the wing.

Upper fuselage pods and tail-mounted pods tend to be used only for seaplane and amphibian designs, which need a huge clearance between the water and the propeller (minimum of 18 in., preferably one propeller diameter). The high thrust line can cause undesirable control characteristics in which application of power for an emergency go-around produces a nose-down pitching moment.

### Engine-Size Estimation

The required horsepower has previously been calculated. The dimensions of an engine producing this power must now be determined. In propeller aircraft design it is far more common to size the aircraft to a known, fixed-size engine as opposed to the rubber-engine aircraft sizing more common in jet-aircraft design.

In fact, most propeller-aircraft designs are based around some production engine, probably because very few new piston or turboprop engines have been designed and certified. Most piston engines in production were designed three decades ago. The high cost of developing and certifying a new engine, and the relatively small market, prevent new engines from appearing.

However, rubber-engine trade studies can point to the optimal existing engine. Also, the use of rubber-engine trade studies for comparison of alternate technologies (such as composite vs aluminum structure) can prevent a bias in the results due to the use of a fixed engine size.

**Table 10.3 Scaling laws for piston and turboprop engines**

$$X_{\text{scaled}} = X_{\text{actual}} SF^b; b \text{ from table values}$$

$$SF = \text{bhp}_{\text{scaled}} / \text{bhp}_{\text{actual}}$$

X	Piston engines			Turboprop
	Opposed	In-line	Radial	
Weight	0.78	0.78	0.809	0.803
Length	0.424	4.24	0.310	3.730
Diameter	*	*	0.130	0.120

\*Width and height vary insignificantly within  $\pm 50\%$  horsepower.

**Table 10.4 Piston and turboprop statistical models**

$$X = a(\text{bhp})^b \text{ (lb or in.)}$$

X	Piston engines						Turboprop	
	Opposed		In-line		Radial		a	b
	a	b	a	b	a	b		
Weight	5.47	0.780	5.22	0.780	4.90	0.809	1.67	0.803
Length	3.86	0.424	5.83	0.424	6.27	0.310	4.14	0.373
Diameter	Width 32–34 in. Height 22–25 in.		Width 17–19 in. Height 24–26 in.		20.2	0.130	9.48	0.120
Typical propeller rpm	2770		2770		2300			
Applicable bhp range	60–500		100–300		200–2000		400–5000	

If a production engine is to be used, dimensional and installation data can be obtained from the manufacturer. If a rubber-engine is to be used, an existing engine can be scaled using the scaling equations defined in Table 10.3. Alternatively, the statistical models defined in Table 10.4 can be used to define a nominal engine. The equations in Tables 10.3 and 10.4 were developed by the author from data taken from Ref. 1.

Tables 10.3 and 10.4 include equations for four different types of propeller powerplant. The horizontally-opposed piston engine sees most use today. In-line and radial engines were common up to the 1950's, but are rare today in the Western countries. In Soviet-block countries large radial engines are still in production for agricultural and utility aircraft. The radial arrangement provides better piston cooling for a high-horsepower piston engine.

### Piston-Engine Installation

Piston engines have special installation requirements that can greatly affect the configuration layout. These are illustrated in Fig. 10.22.

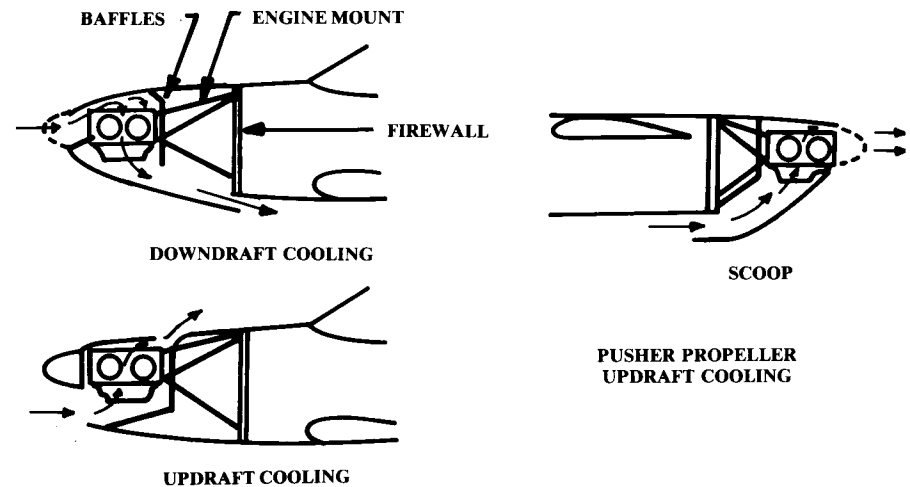
Cooling is a major concern. Up to 10% of the engine's horsepower can be wasted by the drag associated with taking in cooling air, passing it over the engine, and exiting it.

To minimize this cooling drag, the cooling-air mass flow should be kept as small as possible and used as efficiently as possible. As a rough rule of thumb, the cooling-air intake should be about 30–50% of the engine frontal area. The exit should be about 30% larger, and may be variable in area ("cowl flaps") to better control cooling airflow.

For tractor engines, the cooling-air intake is usually located directly in front of the engine cylinders. The air is diverted over the top of the engine by "baffles," which are flat sheets of metal that direct the airflow within the engine compartment. The air then flows down through and around the cylinders into the area beneath the engine, and then exits through an aft-facing hole below the fuselage. This is referred to as "down-draft" cooling.

Down-draft cooling exits the air beneath the fuselage, which is a high-pressure area and therefore a poor place to exit air. "Up-draft" cooling flows the cooling air upwards through the cylinders and exits it into low-pressure air above the fuselage, creating more efficient cooling flow due to a suction effect.

However, updraft cooling dumps hot air in front of the windscreen; this can heat up the cabin. An engine oil leak can coat the windscreen with black oil. Aircraft engines have the exhaust pipes below the cylinders, so updraft cooling causes the cooling air to be heated by the exhaust pipes before reaching the cylinders.

**Fig. 10.22 Piston engine installation.**

For pusher engines cooling is much more difficult. On the ground a front-mounted propeller blows air into the cooling intakes. This is not the case for a pusher engine. Also, the cooling-air intakes for a pusher engine are at the rear of the fuselage where the boundary layer is thick and slow-moving. For these reasons virtually all piston-pushers use updraft cooling with a large scoop mounted below the fuselage. Also, internal fans are sometimes used to improve cooling on pusher configurations.

Figure 10.22 also shows the motor mount and firewall. The motor mount—usually fabricated from welded steel tubing—transfers the engine loads to the corners of the fuselage or the longerons. Typically the motor mount extends the engine forward of the firewall by about half the length of the engine. This extra space is used for location of the battery and nosewheel steering linkages.

The firewall is typically a 0.015-in. steel sheet (stainless or galvanized) attached to the first structural bulkhead of the fuselage or nacelle. Its purpose is to prevent a fire in the engine compartment from damaging the aircraft structure or spreading into the rest of the aircraft.

The firewall should not be broken with cutouts (such as for a retractable nose wheel). All controls, hoses, and wires that pass through the firewall have to be sealed with fireproof fittings.

Piston-engine installation is covered in depth in Ref. 29.

## 10.5 FUEL SYSTEM

An aircraft fuel system includes the fuel tanks, fuel lines, fuel pumps, vents, and fuel-management controls. Usually the tanks themselves are the only components that impact the overall aircraft layout, although the winglets on the round-the-world Rutan Voyager were added solely to raise the fuel vents above the wing tanks when the wing tips bent down to the runway on takeoff.

There are three types of fuel tank: discrete, bladder, and integral. Discrete tanks are fuel containers which are separately fabricated and mounted in the aircraft by bolts or straps. Discrete tanks are normally used only for small general aviation and homebuilt aircraft. Discrete tanks are usually shaped like the front of an airfoil and placed at the inboard wing leading edge, or are placed in the fuselage directly behind the engine and above the pilot's feet.

Bladder tanks are made by stuffing a shaped rubber bag into a cavity in the structure. The rubber bag is thick, causing the loss of about 10% of the available fuel volume. However, bladders are widely used because they can be made "self-sealing." If a bullet passes through a self-sealing tank, the rubber will fill in the hole preventing a large fuel loss and fire hazard. This offers a major improvement in aircraft survivability as approximately a third of combat losses are attributed to hits in the fuel tanks.

Integral tanks are cavities within the airframe structure that are sealed to form a fuel tank. Ideally, an integral tank would be created simply by sealing existing structure such as wing boxes and cavities created between two fuselage bulkheads.

Despite years of research, integral tanks are still prone to leaks as witnessed upon the introduction of the B-1B into service. Due to the fire hazard in the event of a leak or battle damage, integral tanks should not be used near personnel compartments, inlet ducts, gun bays, or engines.

The fire hazard of an integral tank can be reduced by filling the tank with a porous foam material, but some fuel volume is lost. Approximately 2½% of the fuel volume is displaced by the foam. In addition, another 2½% of the volume is lost because the foam tends to absorb fuel. This increases the unusable fuel weight. Furthermore, the foam itself weighs roughly 1.3 lb per cubic ft.

The required volume of the fuel tanks is based upon the total required fuel, as calculated during the mission sizing. Densities for various fuels are provided in Table 10.5. The lower values represent hot-day densities. The higher densities are the 32°F values. The actual fuel volume required can be calculated using the fact that one gallon occupies 231 cubic in.

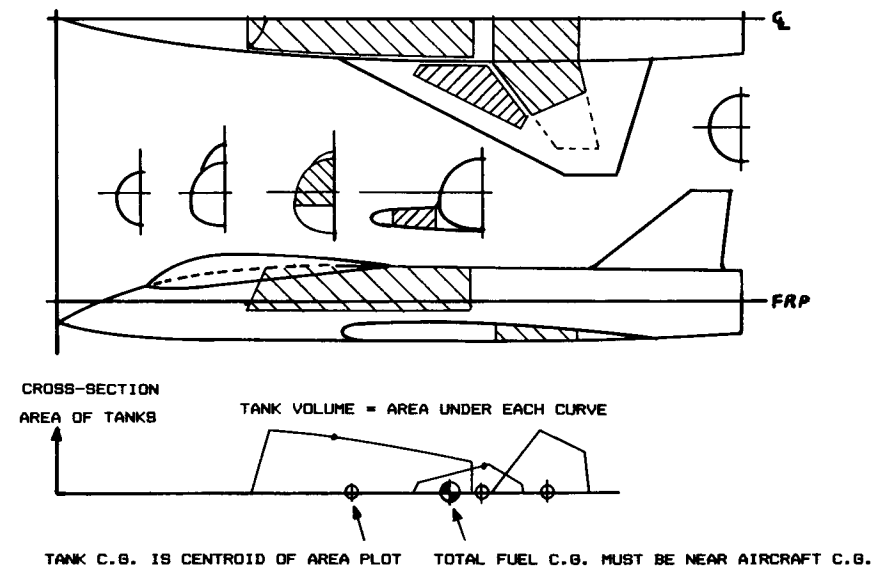


Fig. 10.23 Fuel tank volume plotting.

Table 10.5 Fuel densities (lb/gal)

	Average actual density		Mil-spec density
	0°F	100°F	
Aviation gasoline	6.1	5.7	6.0
JP-4	6.7	6.4	6.5
JP-5	7.2	6.8	6.8
JP-8	—	—	6.7

If fuel tanks of simple geometry are used, the tank volume can be calculated directly. Wing-box fuel volume can be approximated by assuming a tapered box shape. For complex integral and bladder tanks, the tank volume is determined using a fuel-volume plot as shown in Fig. 10.23. This is constructed by measuring the cross-sectional area of the tanks at various fuselage locations, then plotting those cross-sectional areas on a volume plot similar to the aircraft volume plot previously discussed.

If a discrete tank is used, the actually available internal volume can be calculated by subtracting the wall thickness from the external dimensions. For integral and bladder tanks, the available tank volume must be reduced from the measured value to allow for wall thickness, internal structure, and bladder thickness.

A rule of thumb is to assume that 85% of the volume measured to the external skin surface is usable for integral wing tanks, and 92% is usable for integral fuselage tanks. If bladder tanks are used, the values become 77% for wing tanks and 83% for fuselage tanks.

Note in Fig. 10.23 that the fuel volume plot allows the estimation of the center of gravity (c.g.) for each fuel tank, which is the centroid of the area plotted for the tank. The total fuel c.g. is simply the weighted average of the individual tank c.g.'s, and should be close to the aircraft c.g.

## LANDING GEAR AND SUBSYSTEMS

### 11.1 INTRODUCTION

Of the many internal components that must be defined in an aircraft layout, the landing gear will usually cause the most trouble. Landing gear must be placed in the correct down position for landing, and must somehow retract into the aircraft without chopping up the structure, obliterating the fuel tanks, or bulging out into the slipstream. This chapter covers landing-gear design as well as installation of other subsystems.

### 11.2 LANDING GEAR ARRANGEMENTS

The common options for landing-gear arrangement are shown in Fig. 11.1. The single main gear is used for many sailplanes because of its simplicity. The wheel can be forward of the center of gravity (c.g.), as shown here, or can be aft of the c.g. with a skid under the cockpit.

“Bicycle” gear has two main wheels, fore and aft of the c.g., with small “outrigger” wheels on the wings to prevent the aircraft from tipping sideways. The bicycle landing gear has the aft wheel so far behind the c.g. that the aircraft must takeoff and land in a flat attitude, which limits this type of gear to aircraft with high lift at low angles of attack (i.e., high-aspect-ratio wings with large camber and/or flaps). Bicycle gear has been used mainly on aircraft with narrow fuselage and wide wing span such as the B-47.

The “taildragger” landing gear has two main wheels forward of the c.g. and an auxiliary wheel at the tail. Taildragger gear is also called “conventional” landing gear, because it was the most widely used arrangement during the first 40 years of aviation. Taildragger gear provides more propeller clearance, has less drag and weight, and allows the wing to generate more lift for rough-field operation than does tricycle gear.

However, taildragger landing gear is inherently unstable. If the aircraft starts to turn, the location of the c.g. behind the main gear causes the turn to get tighter until a “ground loop” is encountered, and the aircraft either drags a wingtip, collapses the landing gear, or runs off the side of the runway. To prevent this the pilot of a taildragger aircraft must align the aircraft almost perfectly with the runway at touchdown, and “dance” on the rudder pedals until the aircraft stops.

The most commonly used arrangement today is the “tricycle” gear, with two main wheels aft of the c.g. and an auxiliary wheel forward of the c.g.. With a tricycle landing gear, the c.g. is ahead of the main wheels so the aircraft is stable on the ground and can be landed at a fairly large “crab”

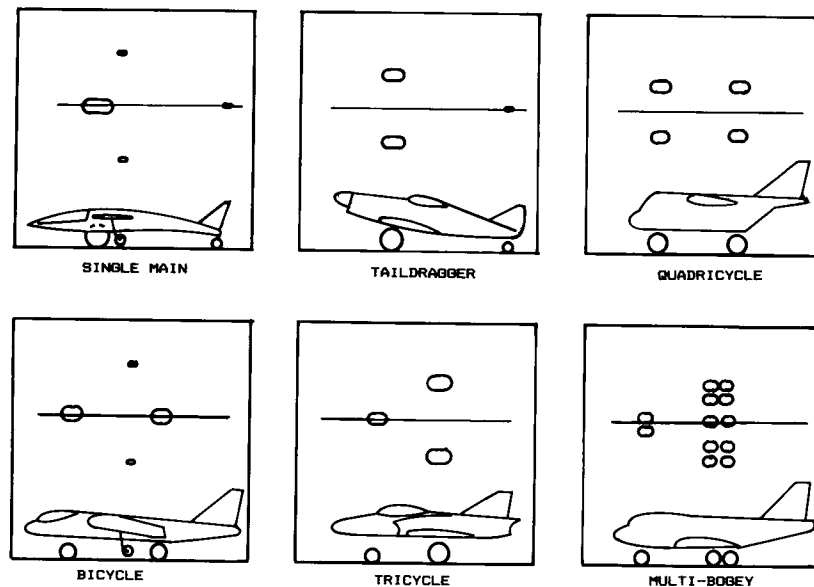


Fig. 11.1 Landing gear arrangements.

angle (i.e., nose not aligned with the runway). Also, tricycle landing gear improves forward visibility on the ground and permits a flat cabin floor for passenger and cargo loading.

Quadricycle gear is much like bicycle gear but with wheels at the sides of the fuselage. Quadricycle gear also requires a flat takeoff and landing attitude. It is used on the B-52 and several cargo planes where it has the advantage of permitting a cargo floor very low to the ground.

The gear arrangements described above are also seen with two, four, or more wheels in place of the single wheels shown in Fig. 11.1. As aircraft weights become larger, the required wheel size for a single wheel capable of holding the aircraft's weight becomes too large. Then multiple wheels are used to share the load between reasonably-sized tires.

Also, it is very common to use twin nose-wheels to retain some control in the event of a nose-wheel flat tire. Similarly, multiple main wheels (i.e., total of four or more) are desirable for safety. When multiple wheels are used in tandem, they are attached to a structural element called a "bogey," or "truck," which is attached to the end of the shock-absorber strut.

Typically an aircraft weighing under about 50,000 lb will use a single main wheel per strut, although for safety in the event of a flat tire it is always better to use two wheels per strut. Between 50,000 and 150,000 lb, two wheels per strut are typical. Two wheels per strut are sometimes used for aircraft weighing up to about 250,000 lb.

Between aircraft weights of about 200,000 and 400,000 lb the four-wheel bogey is usually employed; for aircraft over 400,000 lb, four bogeys, each with four or six wheels, spread the total aircraft load across the runway pavement.

Except for light aircraft and a few fighters, most aircraft use twin nose-wheels to retain control in the event of a flat nose tire. Carrier-based aircraft must use twin nose-wheels at least 19 inches in diam to straddle the catapult-launching mechanism. The massive C-5 employs four nose-wheels to spread the tire load, permitting operation off of relatively soft fields.

Guidelines for layout of a bicycle landing gear are shown in Fig. 11.2. The c.g. should be aft of the midpoint between the two wheels.

The requirements for taildragger gear are shown in Fig. 11.3. The tail-down angle should be about 10–15 deg with the gear in the static position (i.e., tires and shock absorbers compressed the amount seen when the aircraft is stationary on the ground at takeoff gross weight).

The c.g. (most forward and most aft) should fall between 16–25 deg back from vertical measured from the main wheel location. If the c.g. is too far forward the aircraft will tend to nose over, and if it is too far back it will tend to groundloop.

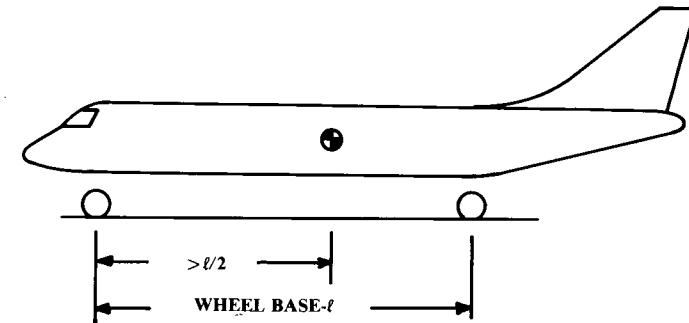


Fig. 11.2 Bicycle landing gear.

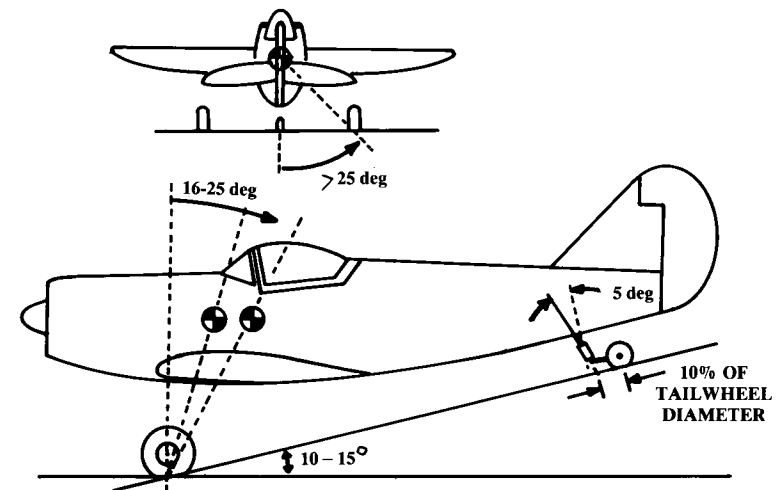


Fig. 11.3 Taildragger landing gear.



To prevent the aircraft from overturning the main wheels should be laterally separated beyond a 25 deg angle off the c.g., as measured from the rear in a tail-down attitude.

The layout of tricycle landing gear as shown in Fig. 11.4 is even more complex. The length of the landing gear must be set so that the tail doesn't hit the ground on landing. This is measured from the wheel in the static position assuming an aircraft angle of attack for landing which gives 90% of the maximum lift. This ranges from about 10–15 deg for most types of aircraft.

The “tipback angle” is the maximum aircraft nose-up attitude with the tail touching the ground and the strut fully extended. To prevent the aircraft from tipping back on its tail, the angle off the vertical from the main wheel position to the c.g. should be greater than the tipback angle or 15 deg, whichever is larger.

For carrier-based aircraft this angle frequently exceeds 25 deg, implying that the c.g. for carrier-based aircraft is well forward of the main wheels. This insures that the rolling of the deck will not cause an aircraft to tip back on its tail.

However, this also makes it difficult to lift the nose for a runway takeoff. If the nose wheel is carrying over 20% of the aircraft's weight, the main gear is probably too far aft relative to the c.g.

On the other hand, if the nose wheel is carrying less than 5% of the aircraft's weight, there will not be enough nose-wheel traction to steer the aircraft. The optimum range for the percent of the aircraft's weight which

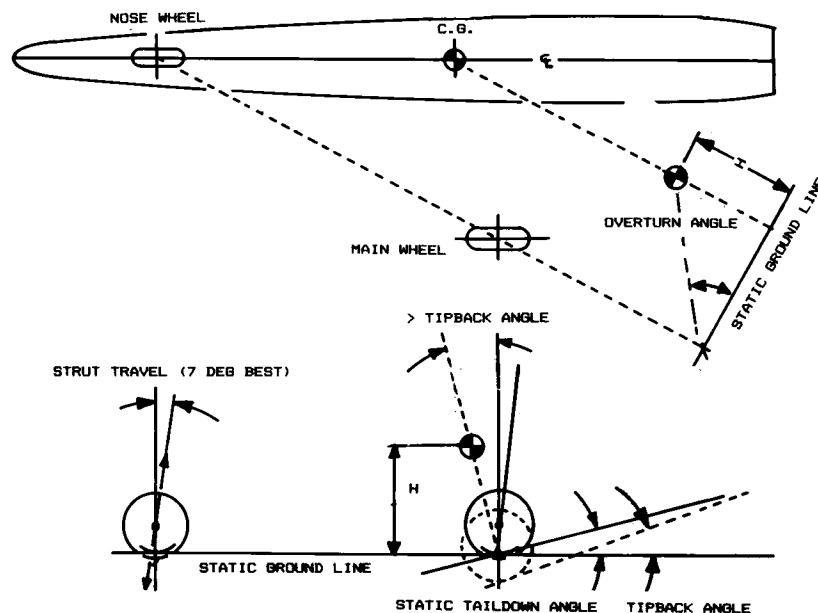


Fig. 11.4 Tricycle landing gear geometry.

is carried by the nose wheel is about 8–15%, for the most-aft and most-forward c.g. positions.

The “overturn angle” is a measure of the aircraft's tendency to overturn when taxied around a sharp corner. This is measured as the angle from the c.g. to the main wheel, seen from the rear at a location where the main wheel is aligned with the nose wheel. For most aircraft this angle should be no greater than 63 deg (54 deg for carrier-based aircraft).

Figure 11.4 also shows the desired strut-travel angle as about 7 deg. This optimal angle allows the tire to move upwards and backwards when a large bump is encountered, thus tending to smooth out the ride. However, any strut-travel angle from purely vertical to about 10 deg aft of vertical is acceptable. Strut geometry in which the tire must move forward as it moves up is undesirable.

### 11.3 TIRE SIZING

Strictly speaking, the “wheel” is the circular metal object upon which the rubber “tire” is mounted. The “brake” inside the wheel slows the aircraft by increasing the rolling friction. However, the term “wheel” is frequently used to mean the entire wheel/brake/tire assembly.

The tires are sized to carry the weight of the aircraft. Typically the main tires carry about 90% of the total aircraft weight. Nose tires carry only about 10% of the static load but experience higher dynamic loads during landing.

For early conceptual design, the engineer can copy the tire sizes of a similar design or use a statistical approach. Table 11.1 provides equations developed from data in Ref. 1 for rapidly estimating main tire sizes (assuming that the main tires carry about 90% of the aircraft weight).

These calculated values for diameter and width should be increased about 30% if the aircraft is to operate from rough unpaved runways.

Nose tires can be assumed to be about 60–100% the size of the main tires. The front tires of a bicycle or quadricycle-gear aircraft are usually the same size as the main tires. Taildragger aft tires are about a quarter to a third the size of the main tires.

For a finished design layout, the actual tires to be used must be selected from a manufacturer's catalog. This selection is usually based upon the smallest tire rated to carry the calculated static and dynamic loads.

Table 11.1 Statistical tire sizing

Main wheels diameter or width (in.) = $A W_W^B$	Diameter		Width	
	A	B	A	B
General aviation	1.51	0.349	0.7150	0.312
Business twin	2.69	0.251	1.170	0.216
Transport/bomber	1.63	0.315	0.1043	0.480
Jet fighter/trainer	1.59	0.302	0.0980	0.467

$W_W$  = Weight on Wheel

Calculation of the static loads on the tires is illustrated in Fig. 11.5 and Eqs. (11.1–11.3). The additional dynamic load on the nose tires under a 10 fps per second braking deceleration is given in Eq. (11.4). Note that these loads are divided by the total number of main or nose tires to get the load per tire (wheel) “ $W_w$ ,” which is used for tire selection.

$$(\text{Max Static Load}) = W \frac{N_a}{B}$$

(11.1)

$$(\text{Max Static Load})_{\text{nose}} = W \frac{M_f}{B}$$

(11.2)

$$(\text{Min Static Load})_{\text{nose}} = W \frac{M_a}{B}$$

(11.3)

$$(\text{Dynamic Braking Load})_{\text{nose}} = \frac{10HW}{gB}$$

(11.4)

Equation (11.4) assumes a braking coefficient ( $\mu$ ) of 0.3, which is typical for hard runways. This results in a deceleration of 10 ft/s<sup>2</sup>.

To insure that the nose gear is not carrying too much or too little of the load, the parameter ( $M_a/B$ ) should be greater than 0.05, and the parameter ( $M_f/B$ ) should be less than 0.20 (0.08 and 0.15 preferred).

If an airplane is to be operated under FAR 25 provisions, a 7% margin should be added to all calculated wheel loads. Also, it is common to add an additional 25% to the loads to allow for later growth of the aircraft design.

Table 11.2 summarizes design data for typical tires (Ref. 30), including maximum load ratings, inflation pressures at that load, maximum landing

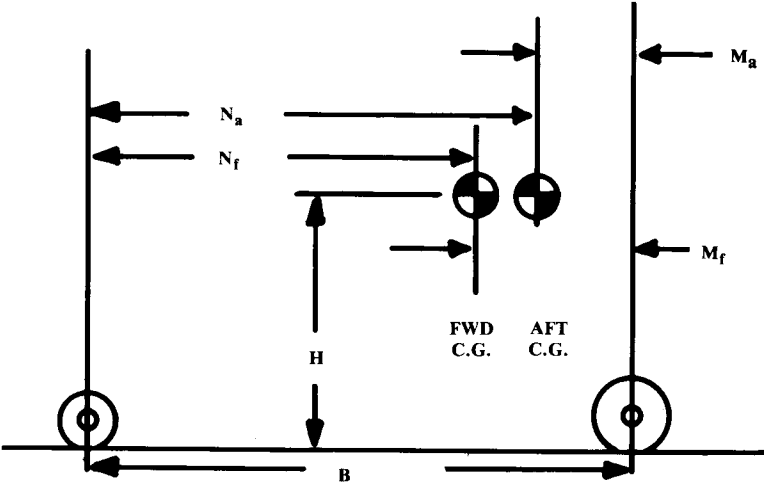


Fig. 11.5 Wheel load geometry.

Table 11.2 Tire data

Size	Speed, mph	Max load, lb	Infi, psi	Max width, in.	Max diam, in.	Rolling radius	Wheel diam	Number of plies
Type III								
5.00-4	120	1,200	55	5.05	13.25	5.2	4.0	6
5.00-4	120	2,200	95	5.05	13.25	5.2	4.0	12
7.00-8	120	2,400	46	7.30	20.85	8.3	8.0	6
8.50-10	120	3,250	41	9.05	26.30	10.4	10.0	6
8.50-10	120	4,400	55	8.70	25.65	10.2	10.0	8
9.50-16	160	9,250	90	9.70	33.35	13.9	16.0	10
12.50-16	160	12,800	75	12.75	38.45	15.6	16.0	12
20.00-20	174kt	46,500	125	20.10	56.00	22.1	20.0	26
Type VII								
16×4.4	210	1,100	55	4.45	16.00	6.9	8.0	4
18×4.4	174kt	2,100	100	4.45	17.90	7.9	10.0	6
18×4.4	217kt	4,350	225	4.45	17.90	7.9	10.0	12
24×5.5	174kt	11,500	355	5.75	24.15	10.6	14.0	16
30×7.7	230	16,500	270	7.85	29.40	12.7	16.0	18
36×11	217kt	26,000	235	11.50	35.10	14.7	16.0	24
40×14	174kt	33,500	200	14.00	39.80	16.5	16.0	28
46×16	225	48,000	245	16.00	45.25	19.0	20.0	32
50×18	225	41,770	155	17.50	49.50	20.4	20.0	26
Three Part Name								
18×4.25-10	210	2,300	100	4.70	18.25	7.9	10.0	6
21×7.25-10	210	5,150	135	7.20	21.25	9.0	10.0	10
28×9.00-12	156kt	16,650	235	8.85	27.60	11.6	12.0	22
37×14.0-14	225	25,000	160	14.0	37.0	15.1	14.0	24
47×18-18	195kt	43,700	175	17.9	46.9	19.2	18.0	30
52×20.5-23	235	63,700	195	20.5	52.0	21.3	23.0	30

speed, tire width, diameter, and “rolling radius” (i.e., radius when under load, typically two-thirds of tire radius). For a complete listing of available tires, a “tire book” can be obtained from the tire manufacturers.

The data in Table 11.2 is organized by tire type. A Type III tire, used for most piston-engined aircraft, has a wide tread and low internal pressure. The identifying numbers for a Type III tire, such as 8.50-10, refer to the approximate tire width (8.2–8.7 in.) and wheel rim diameter (10 in.). The tire outside diameter must be obtained from a tire book such as Ref. 30.

Type VII tires, used by most jet aircraft, operate under higher internal pressures, which reduces their size. Also, the Type VII tires are designed for higher landing speeds. They are identified by their approximate external

dimensions. For example, an  $18 \times 5.7$  tire has an outside diameter of 17.25–17.8 in. and a width of 5.25–5.6 in. These actual numbers are obtained from a tire book.

For a while, the newest and highest-pressure tires were called “Type VIII,” but are now simply referred to as “new design” or “three-part name” tires. Designed for specific requirements, they are identified by outside diameter, width, and rim diameter. For example, a  $36 \times 10.00-18$  tire has diameter ranging from 35.75–36.6 in., width from 9.75–10.3 in., and rim diameter of 18 in.

Tires are selected by finding the smallest tire that will carry the calculated maximum loads ( $W_w$ ). For the nose tire the total dynamic load must be carried as well as the maximum static load.

However, a tire is permitted to carry more dynamic load than the rated static value found in Table 11.2 or a tire book. A Type III tire is permitted a dynamic load of 1.4 times the static value. A Type VII or a “new design” tire is allowed to carry 1.3 times the static value.

The total dynamic nosewheel load (static plus dynamic) should therefore be divided by 1.4 or 1.3, and then used to pick the nose tire size for dynamic load. Both static and dynamic loadings should be used to determine a minimum size of nose-wheel tire. Then the larger of the two should be selected.

As a tire ages it loses ability to withstand its own internal pressure. This causes it to swell in size by about 2 or 3% in diameter and 4% in width. This swelling should be allowed for in designing the wheel wells and retraction geometry, or the wheel pants for a fixed-gear aircraft.

A tire supports a load almost entirely by its internal pressure. The load-carrying ability of the sidewalls and tread can be ignored. The weight carried by the tire ( $W_w$ ) is simply the inflation pressure ( $P$ ) times the tire's contact area with the pavement ( $A_p$ , also called “footprint area”), as shown in Fig. 11.6 and defined in Eq. (11.5).

$$W_w = PA_p \quad (11.5)$$

$$A_p = 2.3 \sqrt{wd} \left( \frac{d}{2} - R_r \right) \quad (11.6)$$

Equation (11.6), from Ref. 31, relates the pavement contact area ( $A_p$ ) to the tire width ( $w$ ), diameter ( $d$ ), and rolling radius ( $R_r$ ). [Note: do not confuse tire width ( $w$ ) with weight on the wheel ( $W_w$ )].

Usually a tire is kept at about the same rolling radius as given in the tire book even when being used for a lower-than-maximum load. From Eq. (11.5), the internal pressure must therefore be proportionally reduced when a tire is operated at a lower than maximum load.

Operating a tire at a lower internal pressure will greatly improve tire life. Roughly speaking, operating a tire at half of its maximum rated load (hence pressure) will increase the number of landings obtained from the tire by a factor of six. However, this requires a larger tire causing greater drag, weight, and wheel-well size.

Tire pressure should also be reduced (i.e., larger tires used) if the aircraft will operate from soft or rough runways. Actual determination of the tire

size for a particular soft-field landing requirement is very complex (see Ref. 32). As a rough estimate, tires should be sized to keep internal pressures below the values in Table 11.3 (Ref. 33) for the desired application.

Sometimes the diameter of the tires is set by the braking requirements. Aircraft brakes are similar to automobile disk brakes, and are usually placed inside the wheels in all but the smallest aircraft. The wheel typically has a rim diameter of about half the total diameter of the tire mounted on it. Wheel rim diameters are provided in Table 11.2 or a tire book.

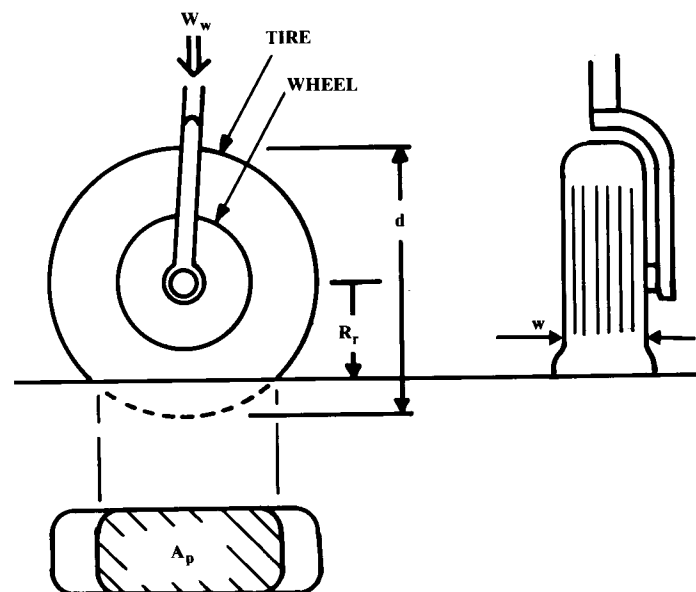


Fig. 11.6 Tire contact area.

Table 11.3 Recommended tire pressures

Surface	Maximum pressure, psi
Aircraft carrier	200 +
Major military airfield	200
Major civil airfield	120
Tarmac runway, good foundation	70–90
Tarmac runway, poor foundation	50–70
Temporary metal runway	50–70
Dry grass on hard soil	45–60
Wet grass on soft soil	30–45
Hard packed sand	40–60
Soft sand	25–35

The brakes must absorb the kinetic energy of the aircraft at touchdown, less the energy absorbed by aerodynamic drag and thrust reversing. These can be ignored by assuming that the brakes are applied when the aircraft has slowed to stall speed. This yields Eq. (11.7), which must be divided by the number of wheels with brakes to get the kinetic energy that must be absorbed by each brake. Note that while Western design practice puts brakes only on the main wheels, several Soviet designs also put brakes on the nose wheels.

$$KE_{\text{braking}} = \frac{1}{2} \frac{W_{\text{landing}}}{g} V_{\text{stall}}^2 \quad (11.7)$$

where  $g = 32.2 \text{ ft/s}^2$ .

The landing weight in Eq. (11.7) is not the same as the weight at the end of the design mission. To allow an emergency landing shortly after takeoff, the landing weight should be approximated as 80–100% of the takeoff weight.

A brake absorbs kinetic energy by turning it into heat. There is insufficient time during landing for much heat energy to be radiated to the air, so

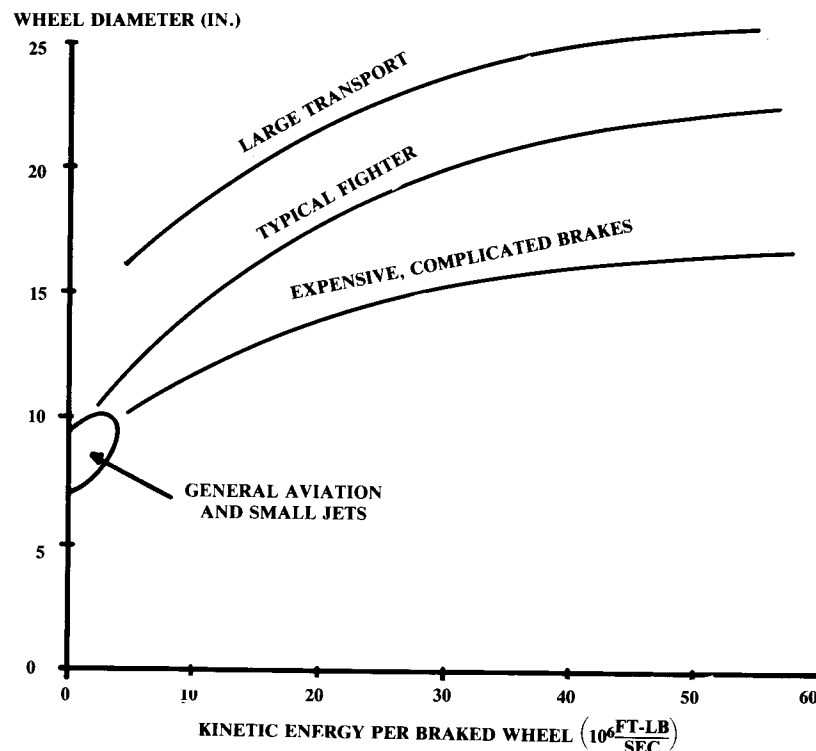


Fig. 11.7 Wheel diameter for braking.

it must be absorbed in the mass of the brake material. The amount of heat a brake can tolerate depends upon its size.

Figure 11.7 provides a statistical estimate of the required wheel rim diameter to provide a brake that can absorb a given amount of kinetic energy. Note that if an aircraft is initially designed with inadequate brakes, additional braking ability can be obtained in the same-sized wheels but only at a much higher cost by using exotic materials and complex design.

If the wheel rim diameter as estimated from Fig. 11.7 is larger than the rim diameter of the selected tire, a larger tire must be used. Alternatively, a brake which protrudes laterally from the tire can be used but will require a larger wheel well.

## 11.4 SHOCK ABSORBERS

### Shock-Absorber Types

The landing gear must absorb the shock of a bad landing and smooth out the ride when taxiing. The more common forms of shock absorber are shown in Fig. 11.8.

The tires themselves provide some shock-absorbing ability by deflecting when a bump is encountered. Sailplanes and a few homebuilt aircraft have been built with rigid axles, relying solely upon the tires for shock absorbing.

Many World War I fighters used a rigid axle mounted with some vertical movement. The axle was attached to the aircraft with strong rubber chords

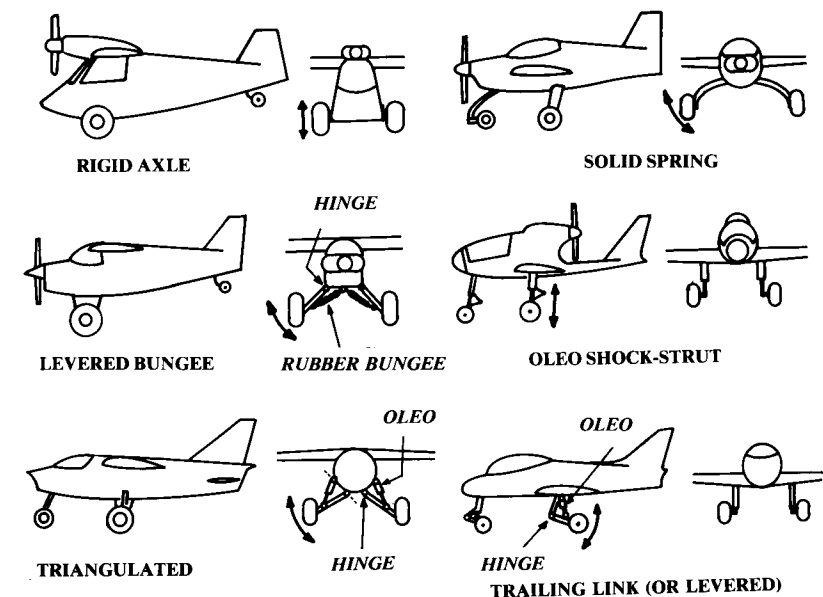


Fig. 11.8 Gear/shock arrangements.

("bungees") that stretched as the axle moved upward. This is rarely seen today.

The solid spring gear is used in many general-aviation aircraft (especially Cessna products). The solid spring is as simple as possible, but is slightly heavier than other types of gear.

Note that the solid-spring gear deflects with some lateral motion instead of straight up and down. This lateral motion tends to scrub the tires sideways against the runway, wearing them out. The solid spring has no damping other than this scrubbing action. The aircraft thus tends to bounce a lot, much like a car with bad shock-absorbers.

The levered bungee-chord gear was very common in early light aircraft such as the Piper Cub. The gear leg is pivoted at the fuselage. Rubber bungee chords underneath the gear are stretched as the gear deflects upward and outwards. This gear is light in weight but is high in drag. This gear also causes lateral scrubbing of the tires.

The oleopneumatic shock strut, or "oleo," is the most common type of shock-absorbing gear in use today (Fig. 11.9). The oleo concept was patented in 1915 as a recoil device for large cannons. The oleo combines a spring effect using compressed air with a damping effect using a piston which forces oil through a small hole (orifice). For maximum efficiency, many oleos have a mechanism for varying the size of the orifice as the oleo compresses ("metered orifice").

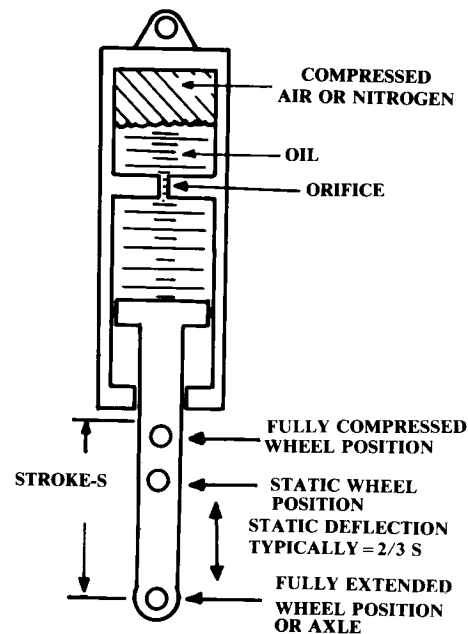


Fig. 11.9 Oleo shock absorber (most simple type).

When used as a shock-strut, the oleo itself must provide the full required amount of wheel deflection, which can lengthen the total landing-gear height. Also, the oleo strut must be strong enough to handle the lateral and braking loads of the wheels. To repair or replace the oleo strut, the entire wheel assembly must be removed because it is attached to the bottom of the strut.

The triangulated gear is similar to the levered bungee gear. When the triangulated gear is deflected, an oleopneumatic shock absorber is compressed. This provides a leveraged effect in which the oleo can be shorter than the required wheel travel. This is especially useful for carrier-based aircraft such as the A-7 that require large amounts of wheel travel to absorb the carrier-landing impact loads.

On a triangulated gear, the oleo can be replaced without removing the wheel assembly. The wheel lateral and braking loads are carried by the solid gear legs, which reduces the oleo weight. However, the complete triangulated gear is usually a little heavier than the oleo shock-strut gear. Also, there is a tire-scrubbing effect that shortens tire life.

The triangulated gear is sometimes seen on smaller aircraft using rubber blocks or springs in compression instead of an oleopneumatic shock absorber. The rubber blocks or springs can be inside the fuselage which streamlines the exposed part of the gear but requires the gear leg to support the aircraft's weight in a cantilevered fashion. This increases the gear weight.

The trailing-link, or levered, gear resembles the triangulated gear, but with the solid gear leg running aft rather than laterally. This gear is common for carrier-based aircraft such as the F-18 where it provides the large amounts of gear travel required for carrier landings. Typically the pivot point of the lower gear leg is slightly in front of the tire, less than one tire radius in front of the tire.

The levered gear allows the wheel to travel aft as it deflects. This is very desirable for operations on rough fields. If a large rock or other obstacle is encountered, the aft motion of the wheel gives it more time to ride over the obstacle. For this reason the levered gear was used on the North American Rockwell OV-10.

The triangulated gear and levered gear provide a mechanical lever effect that reduces the deflection of the shock-absorber oleo. However, this also increases the forces on the shock-absorber oleo, which increases its required diameter. The mechanical advantage of the triangulated or levered gear is determined from the actual dimensions of the gear layout, and is used to size the shock absorber.

### Stroke Determination

The required deflection of the shock-absorbing system (the "stroke") depends upon the vertical velocity at touchdown, the shock-absorbing material, and the amount of wing lift still available after touchdown. As a rough rule-of-thumb, the stroke in inches approximately equals the vertical velocity at touchdown in (ft/s).

Table 11.4 Shock absorber efficiency

Type	Efficiency $\eta$
Steel leaf spring	0.50
Steel coil spring	0.62
Air spring	0.45
Rubber block	0.60
Rubber bungee	0.58
Oleopneumatic	
– Fixed orifice	0.65–0.80
– Metered orifice	0.75–0.90
Tire	0.47

The vertical velocity (or “sink speed”) at touchdown is established in various specifications for different types of aircraft. Most aircraft require 10 ft/s vertical velocity capability. This is substantially above the 4–5 ft/s that most passengers would consider a “bad” landing.

While most Air Force aircraft require only 10 ft/s, Air Force trainer aircraft require 13 ft/s. Due to steeper descent angles, Ref. 32 suggests 15 ft/s for short takeoff and landing (“STOL”) aircraft.

Carrier-based naval aircraft require 20 or more ft/s vertical velocity, which is much like a controlled crash! This is the reason that carrier-based aircraft tend to use triangulated or levered gear, which provide longer strokes than shock-strut gear.

In most cases it may be assumed that the wing is still creating lift equal to the aircraft’s weight during the time that the shock absorber is deflecting. The detailed shock-absorber calculations for FAR-23 aircraft must assume that only two-thirds of the aircraft’s weight is supported by the wing during touchdown. However, this can be ignored for initial stroke calculations.

The vertical energy of the aircraft, which must be absorbed during the landing, is defined in Eq. (11.8). This kinetic energy is absorbed by the work of deflecting the shock absorber and tire.

$$KE_{\text{vertical}} = \left(\frac{1}{2}\right) \left(\frac{W_{\text{landing}}}{g}\right) V_{\text{vertical}}^2 \quad (11.8)$$

where

$W$  = total aircraft weight

$g$  = 32.2 ft/s<sup>2</sup>

If the shock absorber were perfectly efficient, the energy absorbed by deflection would be simply the load times the deflection. Actual efficiencies of shock absorbers range from 0.5–0.9, as provided in Table 11.4. The actual energy absorbed by deflection is defined in Eq. (11.9).

$$KE_{\text{absorbed}} = \eta LS \quad (11.9)$$

where

$\eta$  = shock-absorbing efficiency

$L$  = average total load during deflection (not lift!)

$S$  = stroke

For tires it is assumed that the tire deflects only to its rolling radius, so the “stroke” ( $S_T$ ) of a tire is equal to half the diameter minus the rolling radius.

Combining Eqs. (11.8) and (11.9) and assuming that the shock absorber and tire both deflect to absorb the vertical kinetic energy yields:

$$\left(\frac{1}{2}\right) \left(\frac{W_{\text{landing}}}{g}\right) V_{\text{vertical}}^2 = (\eta LS)_{\text{shock absorber}} + (\eta_T L S_T)_{\text{tire}} \quad (11.10)$$

Note in Eq. (11.10) that the number of shock absorbers doesn’t enter into the equation. Remember that “ $L$ ” is the average total load on the shock absorbers during deflection. The number of shock absorbers affects the diameter of the shock absorbers but not the required stroke.

The shock absorbers and tires act together to decelerate the aircraft from the landing vertical velocity to zero vertical velocity. The vertical deceleration rate is called the “gear load factor” ( $N_{\text{gear}}$ ). Gear load factor is the average total load summed for all of the shock absorbers divided by the landing weight, and is assumed to be constant during touchdown.  $N_{\text{gear}}$  is defined in Eq. (11.11) and typically equals three.

$$N_{\text{gear}} = L/W_{\text{landing}} \quad (11.11)$$

The gear load factor determines how much load the gear passes to the airframe, which affects the airframe structural weight as well as crew and passenger comfort during the landing. Table 11.5 provides typical gear load factors permitted for various types of aircraft.

Substituting Eq. (11.11) into Eq. (11.10) yields Eq. (11.12) for shock-absorber stroke. Note that the equation for stroke does not include any terms containing the aircraft weight. For the same required landing vertical velocity and gear load-factor, an airliner and an ultralight would require the same stroke!

$$S = \frac{V_{\text{vertical}}^2}{2g \eta N_{\text{gear}}} - \frac{\eta_T}{\eta} S_T \quad (11.12)$$

Table 11.5 Gear load factors

Aircraft type	$N_{\text{gear}}$
Large bomber	2.0–3
Commercial	2.7–3
General aviation	3
Air Force fighter	3.0–4
Navy fighter	5.0–6

The stroke calculated by Eq. (11.12) should be increased by about 1 in. as a safety margin. Also, a stroke of 8 in. is usually considered a minimum, and at least 10–12 in. is desirable for most aircraft.

Nosewheel stroke is generally set equal to or slightly larger than main-wheel stroke to provide a smooth ride while taxiing.

Note that the stroke defined by Eq. (11.12) is a vertical distance. If a type of gear is used which produces some lateral motion of the wheel, the total distance the wheel moves must provide the required stroke in a vertical direction.

Equation (11.12) defines the total stroke required. If a levered or triangulated gear is used, the required stroke of the oleo, bungee, or rubber block is reduced and is determined by dividing the total stroke by the mechanical advantage. The actual load on the shock absorber is increased (multiplied) by the mechanical advantage.

### Oleo Sizing

The actual dimensions of an oleo shock absorber or shock strut can now be estimated. The total oleo stroke is known. For most types of aircraft the static position is approximately 66% of the distance from the fully extended to the fully compressed position (see Fig. 11.9). For large transport aircraft, the static position is about 84% of stroke above the fully extended position. For a general-aviation aircraft the static position is typically about 60% of stroke above the extended position.

The total length of the oleo including the stroke distance and the fixed portion of the oleo will be approximately 2.5 times the stroke. For an aircraft with the desired gear attachment point close to the ground, this minimum oleo length may require going to a levered gear.

Oleo diameter is determined by the load carried by the oleo. The main wheel oleo load is the static load found from Eq. (11.1) divided by the number of main-wheel oleos (usually two). The nose-wheel oleo load is the sum of the static and dynamic loads [Eqs. (11.2) and (11.4)]. These loads must be increased by the mechanical advantage if levered or triangulated gear is used.

The oleo carries its load by the internal pressure of compressed air, applied across a piston. Typically an oleo has an internal pressure (“ $P$ ”) of 1800 psi. Internal diameter is determined from the relationship which states that force equals pressure times area. The external diameter is typically 30% greater than the piston diameter, so the external oleo diameter can be approximated by Eq. (11.13).

$$D_{\text{oleo}} = 1.3 \sqrt{\frac{4L_{\text{oleo}}}{P\pi}} \cong 0.04 \sqrt{L_{\text{oleo}}} \quad (11.13)$$

where  $L_{\text{oleo}}$  = load on the oleo in pounds.

### Solid-Spring Gear Sizing

Figure 11.10 illustrates the deflection geometry for a solid-spring gear leg. The total stroke as determined by Eq. (11.12) is the vertical component of

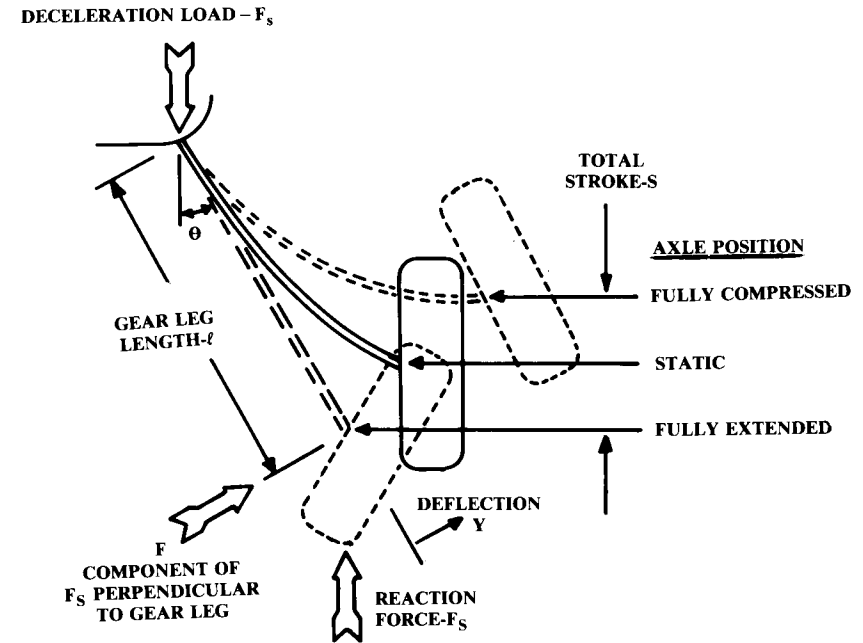


Fig. 11.10 Solid spring gear deflection.

the deflection of the gear leg. Note that the wheel is mounted so that it is vertical when the gear leg is deflected under the static load. This provides even tire wear.

If the gear leg is not excessively tapered, it may be approximated as a constant-cross-section bending beam using the average values of beam width ( $w$ ) and thickness ( $t$ ).

The load on the gear leg in the fully deflected position is the force required to produce the gear load factor,  $N_{\text{gear}}$ . Assuming there are two gear legs yields Eq. (11.14). The component of the load on the gear that is perpendicular to the gear leg is defined by Eq. (11.15).

$$F_s = WN_{\text{gear}}/2 \quad (11.14)$$

$$F = F_s(\sin\theta) \quad (11.15)$$

The deflection “ $y$ ” perpendicular to the gear leg is related to the stroke by Eq. (11.16), and is calculated by the structural bending-beam equation [Eq. (11.17)—see Chapter 14]. Substituting Eqs. (11.14)–(11.16) into Eq. (11.17) yields the equation for the stroke “ $S$ ” of a solid-spring gear leg:

$$S = y \sin\theta \quad (11.16)$$

$$y = Fl^3/3EI \quad (11.17)$$

$$S = F_s (\sin^2 \theta) \frac{l^3}{3EI} \quad (11.18)$$

where

$I$  = beam's moment of inertia

$E$  = material modulus of elasticity (psi)

(approximately 30 million for steel; 10 million for aluminum)

For a rectangular-cross-section gear leg, the moment of inertia is defined by Eq. (11.19).

$$I = \frac{wt^3}{12} \quad (11.19)$$

The static deflection is also determined using Eq. (11.18), but from the static wheel-load for the force ( $F_s$ ).

### 11.5 CASTORING-WHEEL GEOMETRY

For ground steering, a nosewheel or tailwheel must be capable of being castored (turned). The castoring can introduce static and dynamic stability problems causing "wheel shimmy," a rapid side-to-side motion of the wheel that can tear the landing gear off the airplane.

Prevention of shimmy is accomplished by selection of the "rake angle" and "trail," as shown in Fig. 11.11. In some cases a frictional shimmy damper is also used to prevent shimmy. This can be a separate hydraulic plunger or simply a pivot with a lot of friction.

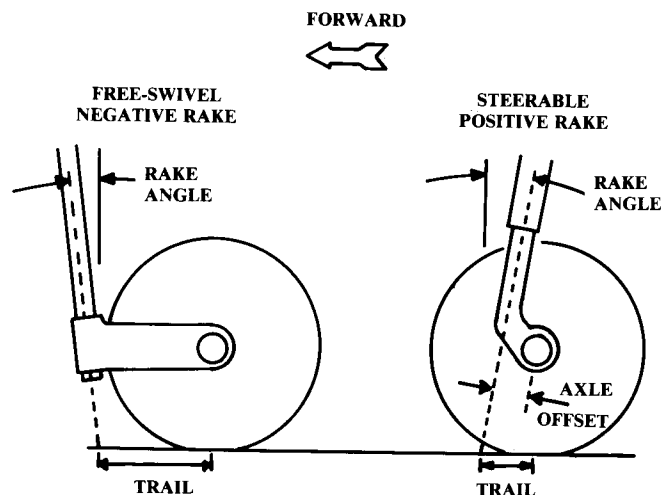


Fig. 11.11 Castoring wheel geometry.

If the castoring wheel is free to swivel, shimmy can be prevented by using a small negative angle of rake (4–6 deg), and trail equal to 0.2–1.2 times the tire radius (0.2 is typical for tailwheels). If the trail is less than the tire radius, a shimmy damper may be required.

If the nosewheel is free to swivel, the pilot must steer the aircraft on the ground using only the brakes. This increases brake wear and presents a great danger if one brake fails during takeoff or landing.

Note that tailwheels are always designed as if they are free to swivel. Steerable tailwheels are connected to the rudder pedals by soft springs that don't affect the wheel dynamics. Most larger tailwheel aircraft have provisions for locking the tailwheel during takeoff and landing.

For most tricycle-gear aircraft, a steering linkage is connected to the rudder pedals or a separate steering wheel, providing positive control of the turning angle. A key objective in the design of a steerable nosewheel is to reduce the required control forces while retaining dynamic stability.

This is done by minimizing the trail through use of a positive rake angle. Note that the weight of the aircraft tends to cause this gear to "flop over," i.e., the gear is statically unstable. This is prevented by the control linkages.

For a large aircraft with a steerable nose-wheel, the rake angle should be about 7 deg positive, and the trail should be at least 16% of the tire radius. For smaller aircraft, rake angles up to 15 deg and trail of about 20% are used.

### 11.6 GEAR-RETRACTION GEOMETRY

At this point, the required sizes for the wheels, tires, and shock absorbers are known, along with the required down locations of the wheels. The one remaining task is to find a "home for the gear" in the retracted position.

A poor location for the retracted gear can ruin an otherwise good design concept! A bad choice for the retracted position can chop up the aircraft structure (increasing weight), reduce the internal fuel volume, or create additional aerodynamic drag.

Figure 11.12 shows the options for main-landing-gear retracted positions. Locating the gear in the wing, in the fuselage, or in the wing-fuselage junction produces the smallest aerodynamic penalty but tends to chop up the structure. Gear in the wing reduces the size of the wing box, which increases weight and may reduce fuel volume. Gear in the fuselage or wing-fuselage junction may interfere with the longerons. However, the aerodynamic benefits of these arrangements outweigh the drawbacks for higher-speed aircraft.

Virtually all civilian jet transports retract the gear into the wing-fuselage junction. Most low-wing fighters retract the gear into the wing or wing-fuselage junction, while mid- and high-wing fighters retract the gear into the fuselage.

While some slower aircraft retract the gear into the wing, fuselage, or wing-fuselage junction, many retract the gear into the nacelles or a separate gear pod. This reduces weight significantly because the wing and fuselage structure is uninterrupted.

The wing-podded arrangement is rarely seen in Western aircraft designs (A-10), but is used in Soviet designs even for jet transports and bombers.



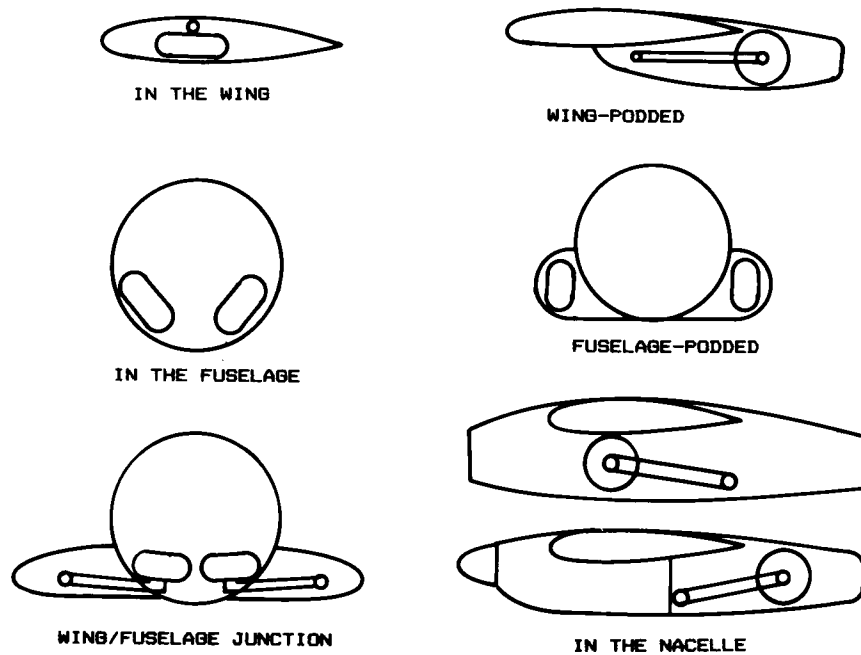


Fig. 11.12 "A home for the gear."

The aerodynamic penalty is minimized by placing the pods at the trailing edge of the wing, where some "area-ruling" benefit is obtained.

The fuselage-podded arrangement is common for high-winged military transports where the fuselage must remain open for cargo. The drag penalty of the pods can be substantial.

Retraction of the gear into the nacelles behind the engine is typical for propeller-driven aircraft. For jet-engined aircraft, nacelle-mounted landing gear must go alongside the engine, which widens the nacelle, increasing the drag.

Most mechanisms for landing-gear retraction are based upon the "four-bar linkage." This uses three members (the fourth bar being the aircraft structure) connected by pivots. The four-bar linkage provides a simple and lightweight gear because the loads pass through rigid members and simple pivots.

Several variations of four-bar linkage landing gear are shown in Fig. 11.13. The oldest form of four-bar linkage for landing gear retraction is shown in front view (Fig. 11.13a), where the wheel is at the bottom of a vertical gear member attached to parallel arms, which in turn attach to the fuselage. The gear retracts by pivoting the arms upward and inward. This was widely used during the 1930's, and is seen today in modified form on the MiG-23.

Figure 11.13b shows the typical retraction arrangement for nose wheels. The diagonal arm is called a "drag brace" because it withstands the aerody-

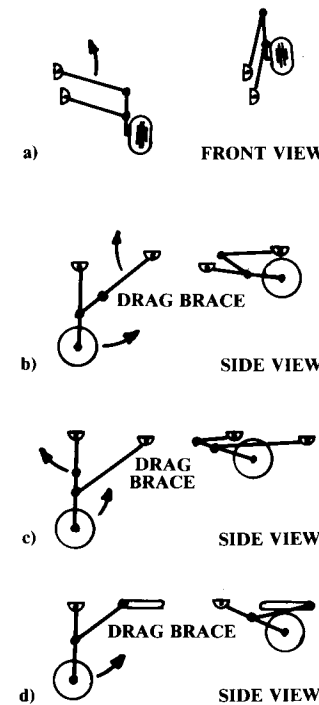


Fig. 11.13 Landing gear retraction.

amic loads (as well as braking loads). The drag brace breaks at the middle for retraction.

The drag brace may be behind the wheel with the gear retracting rearward or it may be in front of the wheel with the gear retracting forward. The latter is preferable because the air loads will blow the gear down in the event of a hydraulic failure.

In Fig. 11.13c the vertical gear member breaks for retraction instead of the drag brace. This has the advantage of reducing the length of the retracted gear, but is usually heavier. This gear was used on the DC-3 and several World War II bombers.

Figure 11.13d shows the use of a sliding pivot rather than a four-bar linkage. The sliding motion is frequently provided by a wormscrew mechanism that is rotated to retract the gear. This is usually heavier than a four-bar linkage because the entire length of the wormscrew must be strong enough for the landing-gear loads. However, this gear is very simple and compact.

The retraction concepts as shown in Fig. 11.13 are for nose or main wheels that retract in a fore or aft direction. However, the same basic concepts can be used for main wheels that retract inwards or outwards. These illustrations then become front views, and the tires are redrawn accordingly. The gear members labeled "drag brace" become "sway braces" because they provide lateral support for the gear in this arrangement.

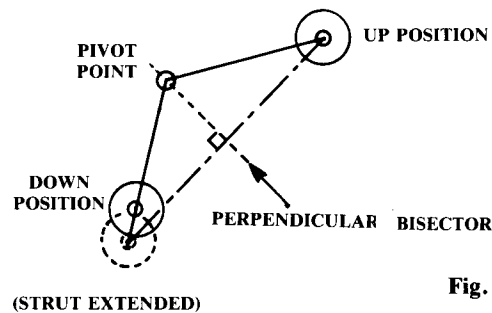


Fig. 11.14 Pivot point determination.

There are dozens of additional geometries for gear retraction based upon the four-bar linkage and other concepts. For these, see Ref. 32 or 33.

The landing-gear leg is attached to the aircraft at the “pivot point.” This is determined as shown in Fig. 11.14. The pivot point can lie anywhere along the perpendicular bisector to the line connecting the up and down positions of the wheel.

Normally the gear strut is allowed to extend fully before retraction, as shown in Fig. 11.14, although it is possible to install a “strut compressor” that causes the gear to be retracted with the strut in the compressed position. This should be used only when internal space is absolutely unavailable for the fully extended strut.

It is also possible to provide a “rotator” mechanism or “planing link” that will change the angle between the gear leg and the wheel axis when the gear is retracted. This is sometimes required to permit the wheel to lie flat inside the wheel well when retracted. This is fairly simple and is seen on many military aircraft such as the F-16. However, all such mechanisms should be avoided if possible due to the increased weight, complexity, and maintenance.

### 11.7 SEAPLANES

Seaplanes were important during the early days of aviation because of the limited number of good airports. Early commercial over-water flights were made exclusively by seaplanes, for safety. Most early speed records were held by seaplanes (or floatplanes) because the use of water for takeoff allowed long takeoff runs and hence high wing-loadings.

Today the seaplane concept is largely restricted to sportplanes, bush planes, and search-and-rescue aircraft. However, the notion of a “sea-sitter” strategic bomber which “loiters” for weeks at an unknown ocean location is revived every few years.

The hull of a seaplane and the pontoon of a float plane are based on the planing-hull concept. The bottom is fairly flat, allowing the aircraft to skim (plane) on top of the water at high speeds. A step breaks the suction on the after body. A vertical discontinuity, as shown in Fig. 11.15, the step can be straight in planview, or it can have an elliptical shape in planview to reduce aerodynamic drag.

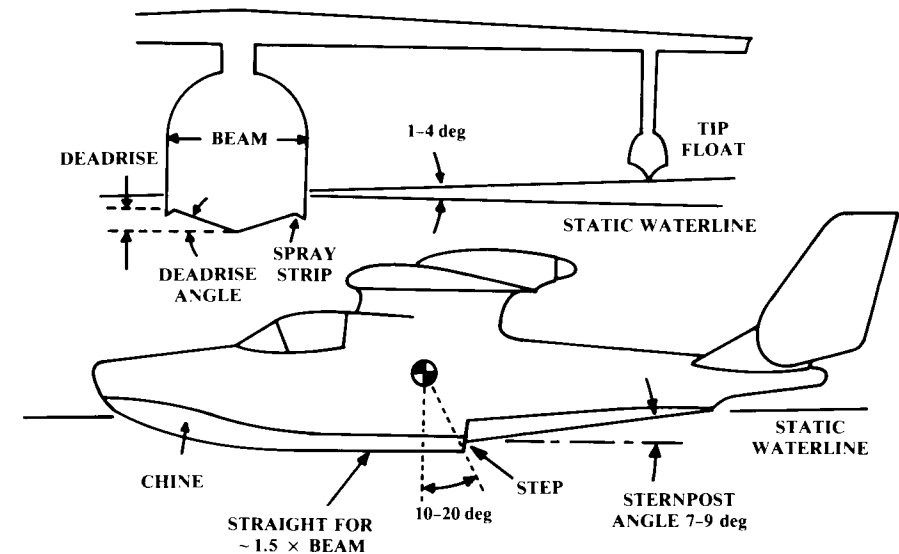


Fig. 11.15 Seaplane geometry.

While a few small seaplanes have been built with flat bottoms, most use a V-shaped bottom to reduce the water-impact loads. The height of the V is called the “deadrise,” and the angle is the “deadrise angle.” Deadrise angle must be increased for higher landing speeds, and should roughly follow Eq. (11.20). Deadrise angle is increased toward the nose to about 30–40 deg to better cut through waves.

$$\alpha_{\text{deadrise}} \cong \frac{V - 20}{2}, \text{ deg} \quad (11.20)$$

where  $V$  = stall speed in miles per hour.

To reduce water spray, spray strips can be attached to the edges of the bottom, as shown. These are angled about 30 deg below the horizon.

The ratio between the waterline length and “beam” (width) has a strong effect upon water resistance and landing impact. A wider hull has a lower water resistance due to its better planing ability but suffers a higher landing impact. Length-to-beam ratios vary from about six for a small seaplane to about 15 for a large one.

The step height should be about 5% of the beam. The step should be located on an angle about 10–20 deg behind the c.g. The bottom of the hull forward of the step should not be curved for a distance about equal to 1.5 times the beam. This is to reduce porpoising tendencies. Also, the hull bottom aft of the step (the “sternpost”) should angle upward about 8 deg.

For a true “flying boat” (i.e., seaplane with a boat-like fuselage), lateral stability on the water is usually provided by wing-mounted pontoons. These

should be located such that they contact the water when the aircraft tips sideways about 1 deg.

Determination of the static waterline is done using a modification of the fuselage-volume plotting technique previously described. First, a static waterline is assumed and drawn on the configuration layout. Then a volume plot is prepared from the cross-sectional areas of only those parts of the fuselage which are below the assumed waterline.

The area under the curve on the volume plot defines the fuselage submerged volume (i.e., below the waterline). This is multiplied by the density of water ( $62.4 \text{ lb/ft}^3$ ) to determine the weight of aircraft which can be supported by that amount of displaced water.

The centroid of the area on the volume plot is the center of buoyancy, which should coincide with the c.g.. If either the weight of aircraft supported or the center of buoyancy are incorrect, another waterline must be assumed and a new volume plot prepared.

Water-resistance drag is very difficult to estimate. It depends upon the mechanics of wave production, and can vary widely for similar hull shapes. Also, water-resistance drag varies with speed. A seaplane hull can have a maximum water resistance at "hump speed" equal to 20% or more of the aircraft's weight.

Seaplane design and analysis should be based upon some published set of test results for a known hull shape. These can be found in early NACA reports. The major U.S. facility for testing seaplane and ship hulls is the Naval Ship Research and Development Center (NSRDC) near Washington, D.C.

For a rough estimate of a seaplane's takeoff distance, it can be assumed that the water-resistance drag will average about 10–15% of the waterborne weight. This is analogous to a rolling-friction coefficient ( $\mu$ ) of 0.10–0.15 in the takeoff calculations provided in Chapter 17.

## 11.8 SUBSYSTEMS

Aircraft subsystems include the hydraulic, electrical, pneumatic, and auxiliary/emergency power systems. Also, the avionics can be considered a subsystem (although to the avionics engineers, the airframe is merely the "mobility subsystem" of their avionics package!)

In general, the subsystems do not have a major impact on the initial design layout. However, later in the design cycle the configuration designer will have to accommodate the needs of the various subsystems, so a brief introduction is provided below. No attempt is made to provide examples or rules of thumb because the subsystems hardware varies widely between different classes of aircraft. Reference 11 provides additional information on subsystems.

### Hydraulics

A simplified hydraulic system is shown in Fig. 11.16. Hydraulic fluid, a light oil-like liquid, is pumped up to some specified pressure and stored in an "accumulator" (simply a holding tank).

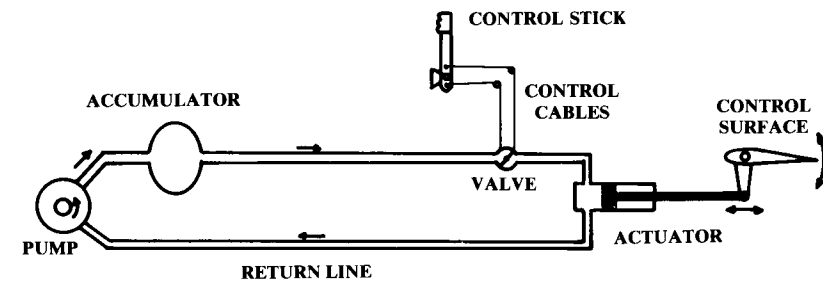


Fig. 11.16 Simplified hydraulic system.

When the valve is opened, the hydraulic fluid flows into the actuator where it presses against the piston, causing it to move and in turn moving the control surface. To move the control surface the other direction, an additional valve (not shown) admits hydraulic fluid to the back side of the piston. The hydraulic fluid returns to the pump by a return line.

To obtain rapid response, the valve must be very close to the actuator. The valve therefore cannot be in or near the cockpit, and instead is usually attached to the actuator.

In most current designs the pilot's control inputs are mechanically carried to the actuator by steel cables strung from the control wheel or rudder pedals to the valves on the actuators. In many new aircraft the pilot's inputs are carried electronically to electromechanical valves ("fly-by-wire").

Hydraulics are used for aircraft flight control as well as actuation of the flaps, landing gear, spoilers, speed brakes, and weapon bays. Flight-control hydraulic systems must also include some means of providing the proper control "feel" to the pilot. For example, the controls should become stiffer at higher speeds, and should become heavier in a tight, high-g turn. Such "feel" is provided by a combination of springs, bobweights, and air bellows.

In most cases the hydraulic system will impact the aircraft conceptual design only in the provision of space for the hydraulic pumps, which are usually attached to the engines. These should be copied from a similar aircraft if better information is not available.

### Electrical System

An aircraft electrical system provides electrical power to the avionics, hydraulics, environmental-control, lighting, and other subsystems. The electrical system consists of batteries, generators, transformer-rectifiers ("TR's"), electrical controls, circuit breakers, and cables.

Aircraft generators usually produce alternating current (AC) and are located on or near the engines. TR's are used to convert the alternating current to direct current (DC). Aircraft batteries can be large and heavy if they are used as the only power source for starting.

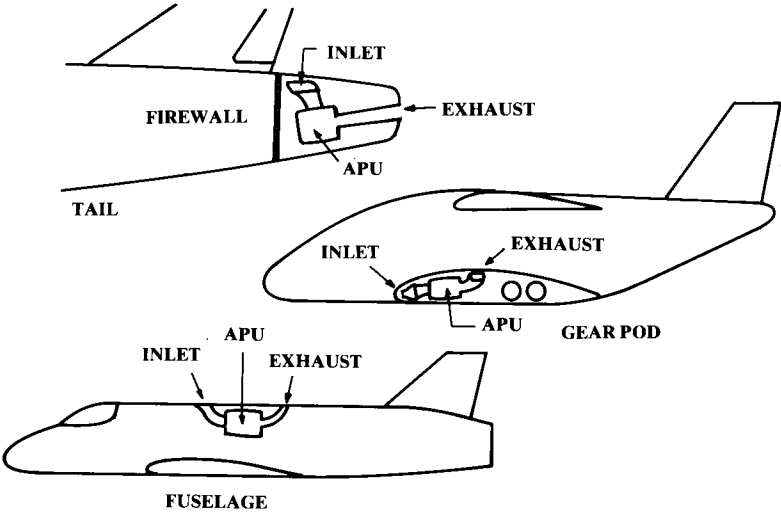


Fig. 11.17 APU installation.

**Pneumatic System**

The pneumatic system provides compressed air for pressurization, environmental control, anti-icing, and in some cases engine starting. Typically the pneumatic system uses pressurized air bled from the engine compressor.

This compressed air is cooled through a heat exchanger using outside air. This cooling air is taken from a flush inlet inside the inlet duct (i.e., inlet secondary airflow) or from a separate inlet usually located on the fuselage or at the front of the inlet boundary-layer diverter.

The cooled compressor air is then used for cockpit pressurization and avionics cooling. For anti-icing, the compressor bleed air goes uncooled through ducts to the wing leading edge, inlet cowls, and windshield.

Compressed air is sometimes used for starting other engines after one engine has been started by battery. Also, some military aircraft use a ground power cart that provides compressed air through a hose to start the engine.

**Auxiliary/Emergency Power**

Large or high-speed aircraft are completely dependent upon the hydraulic system for flight control. If the hydraulic pumps stop producing pressure for any reason, the aircraft will be uncontrollable. If the pumps are driven off the engines, an engine flame-out will cause an immediate loss of control.

For this reason, some form of emergency hydraulic power is required. Also, electrical power must be retained until the engines can be restarted. The three major forms of emergency power are the ram-air turbine (RAT), monopropellant emergency power unit (EPU), and jet-fuel EPU.

The ram-air turbine is a windmill extended into the slipstream. Alternatively, a small inlet duct can open to admit air into a turbine.

The monopropellant EPU uses a monopropellant fuel such as hydrazine to drive a turbine. The available monopropellants are all toxic and caustic, so monopropellant EPU's are undesirable for operational considerations.

However, they have the advantage of not requiring any inlet ducts and can be relied upon to provide immediate power regardless of aircraft altitude, velocity, or attitude. Monopropellant EPU's must be located such that a small fuel leak will not allow the caustic fuel to puddle in the aircraft structure, possibly dissolving it!

Jet-fuel EPU's are small jet engines that drive a turbine to produce emergency power. These may also be used to start the main engines ("jet-fuel starter"). While they do not require a separate and dangerous fuel, the jet-fuel EPU's require their own inlet duct.

Most commercial transports and an increasing number of military aircraft use a jet-fuel auxiliary power unit ("APU"). An APU is much like an EPU but is designed and installed to allow continuous operation.

Usually an APU is designed to provide ground power for air conditioning, cabin lighting, and engine starting. This frees the aircraft from any dependence upon ground power carts. The APU is also used for in-flight emergency power, and in some cases is run continuously in-flight for additional hydraulic and/or electrical power.

The APU is actually another jet engine, and its installation must receive attention in the earliest design layout. The APU requires its own inlet and exhaust ducts, and must be contained in a firewalled structure. APU's have fairly high maintenance requirements so access is important.

To avoid high levels of noise, the inlet and exhaust of an APU should be directed upward. For in-flight operation of the APU, the inlet should ideally be in a high-pressure area and the exhaust in a low-pressure area. Also, the inlet should not be located where the exhaust of the jet engines or APU can be ingested. The exhaust of an APU is hot and noisy, and should not impinge upon aircraft structure or ground personnel.

Transport aircraft usually have the APU in the tail, as shown in Fig. 11.17. This removes the APU from the vicinity of the passenger compart

Table 11.6 Avionics weights

	Typical values
	$\frac{W_{\text{avionics}}}{W_{\text{empty}}}$
General aviation—single engine	.01–.03
Light twin	.02–.04
Turboprop transport	.02–.04
Business jet	.04–.05
Jet transport	.01–.02
Fighters	.03–.08
Bombers	.06–.08
Jet trainers	.03–.04

ment to reduce noise. The APU firewall is of minimum size, and the APU is easily accessible from a workstand.

Military transports with the landing gear in fuselage-mounted pods can place the APU in the pod. This provides ground-level access to the APU, but requires increased firewall area.

Fighters usually have the APU in the fuselage, near the hydraulic pumps and generators. This requires a firewall that completely encloses the APU.

APU installation is discussed in detail in Ref. 34.

### Avionics

Avionics (a contraction of “aviation electronics”) includes radios, flight instruments, navigational aids, flight control computers, radar, and other aircraft sensors such as infrared detectors. For initial layout, it is necessary to provide sufficient volume in the avionics bays. Also, the nose of the aircraft should be designed to hold the radar.

On the average, avionics has a density of about 30–45 lb/ft<sup>3</sup>. The required avionics weight can be estimated from the aircraft empty weight ( $W_e$ ), which is known at this point. Table 11.6 provides ratios between avionics weight and aircraft empty weight.

Estimation of radar size is very complex, and depends upon the desired detection range, radar cross section of the threat aircraft, and radar frequency. For initial design, the radar from a similar design should be used until the avionics group provides a definition of the required radar.

In the absence of better information, it can be assumed that a bomber will use a 40-in. radar, a large fighter will use a 35-in. radar, and a small fighter will use a 22-in. radar. Transport-aircraft radars are only for weather avoidance. They are small relative to the size of the aircraft nose and can be initially ignored.

### 12.1 INTRODUCTION

The previous chapters have presented methods for the design layout of a credible aircraft configuration. Initial sizing, wing geometry, engine installation, tail geometry, fuselage internal arrangement, and numerous other design topics have been discussed.

The initial sizing was based upon rough estimates of the aircraft’s aerodynamics, weights, and propulsion characteristics. At that time we could not calculate the actual characteristics of the design because the aircraft had not been designed yet!

Now the aircraft design can be analyzed “as-drawn” to see if it actually meets the required mission range. If not, we will resize the aircraft until it does.

Also, a variety of trade studies can now be performed to determine the best combination of design parameters ( $T/W$ ,  $W/S$ , aspect ratio, etc.) to meet the given mission and performance requirements at the minimum weight and cost.

Additional analysis on the as-drawn aircraft is also required at this time to insure that stability and control requirements are met. In previous chapters, an approximate tail volume coefficient method was used for tail sizing. Now that the aircraft is drawn, we can analytically determine if the selected tail sizes are adequate.

These methods will be presented in Chapters 12–19. The overall objective of these chapters is the understanding of the sizing optimization and trade study process, not the presentation of particular theories and analysis methods. Presumably the student has spent several years studying aerodynamics, controls, structures, and propulsion.

The analysis techniques presented in these chapters, all approximate methods, illustrate the major parameters to be determined and provide realistic trends for trade studies. In many cases these are not the methods employed by the major aircraft companies, whose methods are highly computerized and cannot be presented in any single textbook. Also, each company uses many proprietary methods that are simply unavailable to students.

By using the simplified methods provided in this book, the student designer will experience the interaction of the major design variables but will not devote excessive time to the analytical tasks. This should leave more time for learning the basic principles of sizing optimization and trade studies, which are the same regardless of analytical techniques.

12.2 AERODYNAMIC FORCES

Figure 12.1 shows the only two ways that the airmass and the airplane can act upon each other. As the aircraft moves forward, the air molecules slide over its skin. The molecules closest to the skin act as if they are stuck to it, moving with the aircraft (“no-slip condition”).

If the air molecules closest to the aircraft skin are moving with it, there must be slippage (or “shear”) between these molecules and the nonmoving molecules away from the aircraft. “Viscosity” is the honey-like tendency of air to resist shear deformation, which causes additional air near the aircraft skin to be dragged along with the aircraft. The force required to accelerate this “boundary-layer” air in the direction the aircraft is travelling produces skin-friction drag.

If the air molecules slide over each other (shear) in an orderly fashion, the flow is said to be “laminar.” If the molecules shear in a disorderly fashion the flow is “turbulent.” This produces a thicker boundary layer, indicating that more air molecules are dragged along with the aircraft, generating more skin-friction drag.

Airflow along a smooth plate becomes turbulent when the local Reynolds number reaches about one-half million, but can become turbulent at a lower Reynolds number if there is substantial skin roughness. Also, the curvature of the surface can either prevent or encourage the transition from laminar to turbulent flow.

As the aircraft moves forward, the air molecules are pushed aside. This causes the relative velocity of the air to vary about the aircraft. In some places, mostly toward the nose, the air is slowed down. In other places the air is speeded up relative to the freestream velocity.

According to Bernoulli’s equation, the total pressure (static plus dynamic) along a subsonic streamline remains constant. If the local air velocity increases, the dynamic pressure has increased so the static pressure must decrease. Similarly, a reduction in local air velocity leads to an increase in static pressure.

Thus, the passage of the aircraft creates varying pressures around it, which push on the skin as shown in Fig. 12.1.

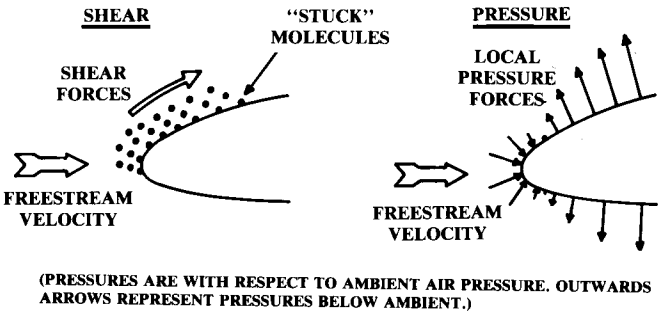


Fig. 12.1 Origin of aerodynamic forces.

In fact, lift is created by forcing the air that travels over the top of the wing to travel faster than the air which passes under it. This is accomplished by the wing’s angle of attack and/or wing camber. The resulting difference in air velocity creates a pressure differential between the upper and lower surfaces of the wing, which produces the lift that supports the aircraft.

If the aircraft is traveling near or above the speed of sound, additional pressure forces are produced by the shock waves around the aircraft. Shock waves result whenever supersonic flow is being slowed down.

All aerodynamic lift and drag forces result from the combination of shear and pressure forces. However, the dozens of classification schemes for aerodynamic forces can create considerable confusion because of overlapping terminology.

For example, the drag on a wing includes forces variously called airfoil profile drag, skin-friction drag, separation drag, parasite drag, camber drag, drag-due-to-lift, wave drag, wave-drag-due-to-lift, interference drag—and so forth.

Figure 12.2 presents the various drag terminologies using a matrix that defines the drag type based upon the origin of the drag force (shear or pressure) and whether or not the drag is strongly related to the lift force being developed.

Drag forces not strongly related to lift are usually known as parasite drag or zero-lift drag. In subsonic cruising flight of a well-designed aircraft, the

	SHEAR FORCES	PRESSURE FORCES		
		SEPARATION	SHOCK	CIRCULATION
PARASITE DRAG	SKIN FRICTION	VISCOUS SEPARATION	WAVE DRAG	
	SCRUBBING DRAG	SHOCK-INDUCED SEPARATION “DRAG RISE”		
	INTERFERENCE DRAG			
INDUCED DRAG (f(Lift))	PROFILE DRAG			
		CAMBER DRAG		
	SUPERVELOCITY EFFECT ON SKIN FRICTION	SUPERVELOCITY EFFECT ON PROFILE DRAG—i.e., LANDING GEAR, ETC.		DRAG DUE TO LIFT
REFERENCE AREA:			WAVE DRAG DUE TO LIFT	TRIM DRAG
	$S_{wetted}$	Max. Cross Section	(Volume Distribution)	$S_{ref}$

Fig. 12.2 Drag terminology matrix.

parasite drag consists mostly of skin-friction drag, which depends mostly upon the wetted area.

The skin-friction drag of a flat plate of the same wetted area as the aircraft can be determined for various Reynolds numbers and skin roughnesses using equations provided below. However, the actual parasite drag will be somewhat larger than this value, as will be shown later.

“Scrubbing drag” is an increase in the skin-friction drag due to the propwash or jet exhaust impinging upon the aircraft skin. This produces a higher effective air velocity and assures turbulent flow, both of which increase drag. It is for this reason that pusher-propellers are desirable, and that few modern jets have conformal nacelles in which the exhaust rubs along the aft fuselage.

There are three separate origins of the drag-producing pressure forces. The first, viscous separation, was the source of considerable difficulty during the early theoretical development of aerodynamics.

If the theoretical pressure forces in a perfect fluid are integrated over a streamlined body without flow separation, it is found that the pressures around the body which yield a drag force in the flight direction are exactly matched by the pressures around the body which yield a forward force. Thus, if skin friction is ignored the net drag is zero.

This was known to be false, and was called d'Alembert's paradox. The paradox was finally resolved by Prandtl who determined that the boundary layer, which is produced by viscosity, causes the flow to separate somewhere on the back half of the body. This prevents the full attainment of the forward-acting force, leaving a net drag force due to viscous separation. (See Ref. 35 for a more detailed discussion.)

Viscous separation drag, also called “form drag,” depends upon the location of the separation point on the body. If the flow separates nearer to the front of the body the drag is much higher than if it separates more towards the rear.

The location of the separation point depends largely upon the curvature of the body. Also, the separation point is affected by the amount of energy in the flow. Turbulent air has more energy than laminar air, so a turbulent boundary layer actually tends to delay separation.

If a body is small and flying at low speed, the Reynolds number will be so low that the flow will remain laminar resulting in separated flow. For this reason a small body may actually have a lower total drag when its skin is rough. This produces turbulent flow, which will remain attached longer than would laminar flow. The dimples on a golf ball are an example of this.

For a very long body such as the fuselage of an airliner, the turbulent boundary layer will become so thick that the air near the skin loses most of its energy. This causes separation near the tail of the aircraft, resulting in high “boattail drag.”

To prevent this, small vanes perpendicular to the skin and angled to the airflow are placed just upstream of the separation point. These vanes produce vortices off their ends, which mix the boundary layer with higher-energy air from outside the boundary layer. This delays separation and reduces boattail drag. Such “vortex generators” are also used on wing and tail surfaces.

Viscous separation is largely responsible for the drag of irregular bodies such as landing gear and boundary-layer diverters. It also produces base drag, the pressure drag created by a “cut-off” aft fuselage.

The subsonic drag of a streamlined, nonlifting body consists solely of skin friction and viscous separation drag and is frequently called the “profile drag.” Profile drag is usually referenced to the maximum cross-sectional area of the body.

Note that the terms “profile drag” and “form drag” are frequently intermixed, although strictly speaking the profile drag is the sum of the form drag and the skin-friction drag. Also note that the term “profile drag” is sometimes used for the zero-lift drag of an airfoil.

Interference drag is the increase in the drag of the various aircraft components due to the change in the airflow caused by other components. For example, the fuselage generally causes an increase in the wing's drag by encouraging airflow separation at the wing root.

Interference drag usually results from an increase in viscous separation, although the skin-friction drag can also be increased if one component causes the airflow over another component to become turbulent or to increase in velocity.

“Wave drag” is the drag caused by the formation of shocks at supersonic and high subsonic speeds. At high subsonic speeds, the shocks form first on the upper surface of the wings because the airflow is accelerated as it passes over the wing.

Drag forces that are a strong function of lift are known as “induced drag” or “drag-due-to-lift.” The induced drag is caused by the circulation about the airfoil that, for a three-dimensional wing, produces vortices in the airflow behind the wing. The energy required to produce these vortices is extracted from the wing as a drag force, and is proportional to the square of the lift.

Another way of looking at induced drag is that the higher-pressure air under the wing escapes around the wingtip to the wing upper surface, reducing the lift and causing the outer part of the wing to fly in an effective downwash. In other words, the wing is always flying uphill! This rotates the lift force vector toward the rear, so that a component of the lift is now in the drag direction.

To counter the pitching moment of the wing, the tail surfaces produce a lift force generally in the downward direction. The induced drag of the tail is called “trim drag.” Trim drag also includes the additional lift required of the wing to counter any download produced by the tail.

When aircraft total drag vs lift is presented, the drag can be calculated with some fixed elevator deflection or it can be calculated using the varying elevator deflections required to trim the aircraft at each lift coefficient. This “trimmed” drag provides the correct data for use in performance calculations.

In supersonic flight there is a component of wave drag that changes as the lift changes. The creation of lift results from changes in the pressure around the aircraft. Wave drag is a pressure drag due to shock formation, and any changes in the pressures around the aircraft will change the location and

strength of the shocks around it resulting in “wave-drag-due-to-lift.” This drag is fairly small and is usually ignored in early conceptual design.

Two-dimensional (2-D) airfoil drag, or profile drag, is a combination of skin-friction drag and viscous separation drag. There is no drag-due-to-lift for the 2-D airfoil because the lift force is perpendicular to the freestream direction. However, the profile drag increases as the angle of attack is increased, leading to some confusion.

This increase in 2-D airfoil drag is due to an increase in viscous separation caused by a greater pressure drop on the upper surface of the airfoil as the angle of attack is increased. This increase in profile drag with increasing angle of attack is not technically caused by the generation of lift, but does vary as the lift is varied.

Most preliminary drag-estimation methods do not actually use the airfoil profile drag data to determine total wing drag. Instead, the drag for an idealized wing with no camber or twist is determined, and then a separate “camber drag” is estimated. Often the camber drag term is included statistically in the drag-due-to-lift calculation even though it is not technically caused by the generation of lift!

Changing the lift on the wing changes the velocities above and below it. This change in local airflow velocity causes a small change in skin-friction drag. Sometimes called a “supervelocity” effect, this is minor and is usually ignored.

### 12.3 AERODYNAMIC COEFFICIENTS

Lift and drag forces are usually treated as nondimensional coefficients as defined in Eqs. (12.1) and (12.2). The wing reference area,  $S_{ref}$  or simply  $S$ , is the full trapezoidal area extending to the aircraft centerline. The dynamic pressure of the freestream air is called “ $q$ ,” as defined in Eq. (12.3).

$$L = qSC_L \quad (12.1)$$

$$D = qSC_D \quad (12.2)$$

where

$$q = \frac{1}{2}\rho V^2 \quad (12.3)$$

By definition, the lift force is perpendicular to the flight direction while the drag is parallel to the flight direction. Remember that the 2-D airfoil characteristics are denoted by lowercase subscripts (i.e.,  $C_D$ ) whereas the 3-D wing characteristics are denoted by uppercase subscripts (i.e.,  $C_L$ ).

Drag is normally spoken of as so many “counts” of drag, meaning the four digits to the right of the decimal place. For example, 38 counts of drag mean a drag coefficient of 0.0038.

Figure 12.3 illustrates the drag polar, which is the standard presentation format for aerodynamic data used in performance calculations. The drag polar is simply a plot of the coefficient of lift vs the coefficient of drag.

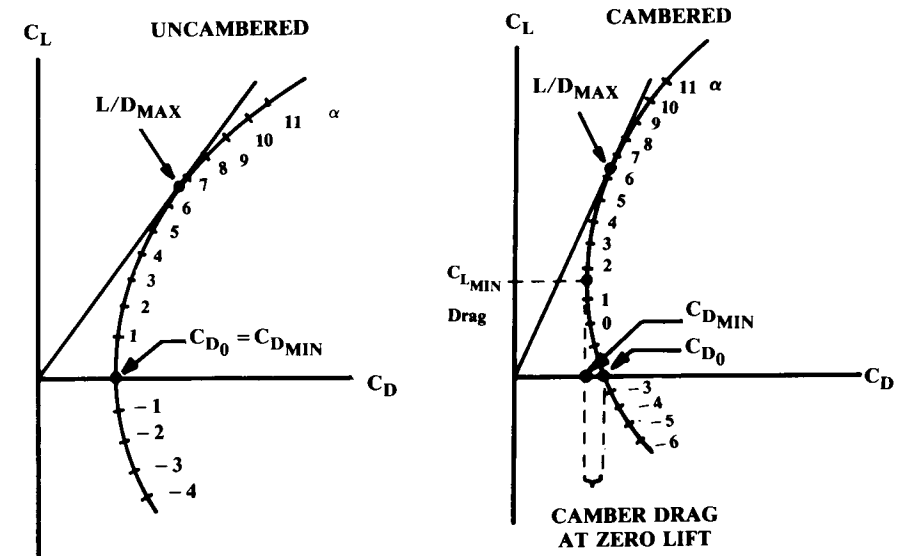


Fig. 12.3 Drag polar.

Note that the angle of attack ( $\alpha$ ) is indicated here by tic marks along the polar curve. This is not standard practice, but is useful for understanding the relationship between lift, drag, and angle of attack.

$$\text{Uncambered: } C_D = C_{D_0} + KC_L^2 \quad (12.4)$$

$$\text{Cambered: } C_D = C_{D_{\min}} + K(C_L - C_{L_{\min \text{ drag}}})^2 \quad (12.5)$$

For an uncambered wing, the minimum drag (“ $C_{D_0}$ ”) occurs when the lift is zero. The drag polar has an approximately parabolic shape, as defined by Eq. (12.4). The value of “ $K$ ” will be discussed later.

For a cambered wing, the minimum drag (“ $C_{D_{\min}}$ ”) occurs at some positive lift (“ $C_{L_{\min \text{ drag}}}$ ”). The drag polar also has a parabolic shape, but is offset vertically as defined by Eq. (12.5). For wings of moderate camber this offset is usually small, which implies that  $C_{D_0}$  approximately equals  $C_{D_{\min}}$  and that Eq. (12.4) may be used.

The point at which a line from the origin is just tangent to the drag polar curve is the point of maximum lift-to-drag ratio. Note that this is not the point of minimum drag!

### 12.4 LIFT

Figure 12.4 shows typical wing lift curves. The uncambered wing has no lift at zero angle of attack, while the cambered wing has a positive lift at zero angle of attack. A negative angle of attack is required to obtain zero lift with a cambered wing.



An old rule-of-thumb is that the negative angle of attack for zero lift in degree equals the airfoil's percent camber (the maximum vertical displacement of the camber line divided by the chord).

Maximum lift is obtained at the "stall" angle of attack, beyond which the lift rapidly reduces. When a wing is stalled, most of the flow over the top has separated.

The slope of the lift curve is essentially linear except near the stall angle, allowing the lift coefficient below stall to be calculated simply as the lift-curve slope times the angle of attack (relative to the zero-lift angle). At the stall, the lift curve has become nonlinear such that the angle for maximum lift is greater than the linear value by an amount shown as  $\Delta\alpha$  at  $C_{L_{max}}$  in the figure.

Figure 12.4 also shows the effect of aspect ratio on lift. For an infinite-aspect-ratio wing (the 2-D airfoil case) the theoretical low-speed lift-curve slope is two times  $\pi$  (per radian).

Actual airfoils have lift-curve slopes between about 90 and 100% of the theoretical value. This percentage of the theoretical value is sometimes called the "airfoil efficiency ( $\eta$ )."

Reduction of aspect ratio reduces the lift-curve slope, as shown. At very low aspect ratios, the ability of the air to escape around the wing tips tends to prevent stalling even at very high angles of attack. Also note that the lift curve becomes nonlinear for very low aspect ratios.

Increasing the wing sweep has an effect similar to reducing the aspect ratio. A highly-swept wing has a lift-curve slope much like the aspect-ratio-three curve shown.

The effect of Mach number on the lift-curve slope is shown in Fig. 12.5. The 2-D airfoil lines represent upper boundaries for the no-sweep, infinite aspect-ratio wing. Real wings fall below these curves as shown.

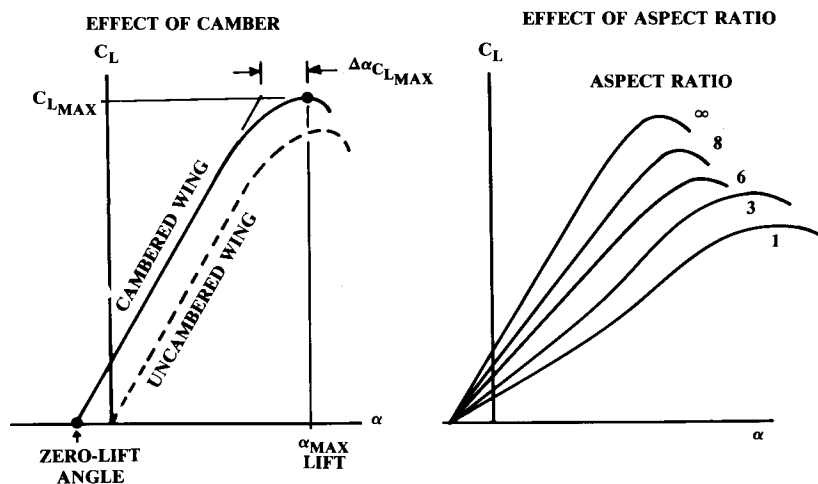


Fig. 12.4 Wing lift curve.

Note that real wings follow a transition curve in the transonic regime between the upward-trending subsonic curve and the downward-trending supersonic curve. Also, note that a fat and unswept wing loses lift in the transonic regime whereas a thinner, swept wing does not.

The lift-curve slope is needed during conceptual design for three reasons. First, it is used to properly set the wing incidence angle. This can be especially important for a transport aircraft, in which the floor must be level during cruise. Also, the wing incidence angle influences the required fuselage angle of attack during takeoff and landing, which affects the aft-fuselage upsweep and/or landing-gear length.

Secondly, the methodology for calculating drag-due-to-lift for high-performance aircraft uses the slope of the lift curve, as will be seen.

The third use of the lift curve slope in conceptual design is for longitudinal-stability analysis, as discussed in Chapter 16.

### Subsonic Lift-Curve Slope

Equation (12.6) is a semi-empirical formula from Ref. 36 for the complete wing lift curve slope (per radian). This is accurate up to the drag-divergent Mach number, and reasonably accurate almost to Mach one for a swept wing.

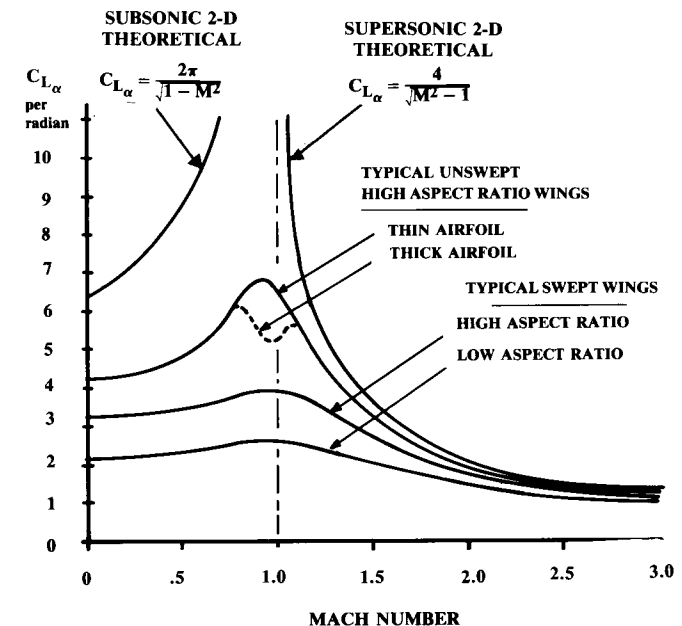


Fig. 12.5 Lift curve slope vs Mach number.

$$C_{L\alpha} = \frac{2\pi A}{2 + \sqrt{4 + \frac{A^2 \beta^2}{\eta^2} \left(1 + \frac{\tan^2 \Lambda_{\max t}}{\beta^2}\right)}} \left(\frac{S_{\text{exposed}}}{S_{\text{ref}}}\right) (F) \quad (12.6)$$

where

$$\beta^2 = 1 - M^2 \quad (12.7)$$

$$\eta = \frac{C_{l\alpha}}{2\pi/\beta} \quad (12.8)$$

$\Lambda_{\max t}$  is the sweep of the wing at the chord location where the airfoil is thickest.

If the airfoil lift-curve slope as a function of Mach number is not known, the airfoil efficiency  $\eta$  can be approximated as about 0.95. (In several textbooks this term is dropped by assuming that  $\eta$  equals 1.0 at all Mach numbers.)

“ $S_{\text{exposed}}$ ” is the exposed wing planform, i.e., the wing reference area less the part of the wing covered by the fuselage. “ $F$ ” is the fuselage lift factor [Eq. (12.9)] that accounts for the fact that the fuselage of diameter “ $d$ ” creates some lift due to the “spill-over” of lift from the wing.

$$F = 1.07(1 + d/b)^2 \quad (12.9)$$

The wing aspect ratio “ $A$ ” is the geometric aspect ratio of the complete reference planform. The effective aspect ratio will be increased by wing endplates or winglets.

$$\text{Endplate: } A_{\text{effective}} = A(1 + 1.9 h/b) \quad (12.10)$$

where  $h$  = endplate height.

$$\text{Winglet: } A_{\text{effective}} \cong 1.2A \quad (12.11)$$

These effective aspect ratios should also be used in the induced drag calculations below. Note that Eq. (12.11) for winglets is a crude approximation based upon limited data for wings of moderate aspect ratio.

The actual increase in effective aspect ratio due to the use of winglets is a function of velocity and lift coefficient and depends upon the selected airfoils and the relative location, geometry, and twist of the wing and winglet. Typically, a wing with higher aspect ratio will obtain less improvement by the use of winglets.

### Supersonic Lift-Curve Slope

For a wing in purely supersonic flow, the lift-curve slope is ideally defined by Eq. (12.12), as shown in Fig. 12.5. A wing is considered to be in purely supersonic flow when the leading edge is “supersonic,” i.e., when the Mach cone angle is greater than the leading-edge sweep [see Eq. (12.14)].

$$C_{L\alpha} = 4/\beta \quad (12.12)$$

where

$$\beta = \sqrt{M^2 - 1} \quad (12.13)$$

when

$$M > 1/\cos \Lambda_{\text{LE}} \quad (12.14)$$

The actual lift-curve slope of a wing in supersonic flight is difficult to predict without use of a sophisticated computer program. The charts in Fig. 12.6 are probably the best approximate method available. They were defined in Ref. 37 and have been used in a number of textbooks.

These charts actually estimate the slope of the “normal force” coefficient ( $C_n$ ), i.e., the lift curve slope in a direction perpendicular to the surface of the wing. For low angles of attack, this is approximately equal to the lift-curve slope.

To use these charts, the wing aspect ratio, taper ratio, and leading-edge sweep are employed. The six charts each represent data for wings of a different taper ratio. If a chart for the actual taper ratio of a wing is not provided, interpolation must be used.

The term  $\beta$  [Eq. (12.13)] divided by the tangent of the leading-edge sweep is calculated and found on the horizontal axis of the chart. If this ratio is greater than 1.0, it is inverted and the right side of the chart must be used. Then the appropriate line is selected by calculating the wing aspect ratio times the tangent of the leading-edge sweep, and the vertical-axis value is read.

To obtain the approximate slope of the lift curve, this value is then divided by the tangent of the leading-edge sweep, if on the left side of the chart, or by  $\beta$  if on the right side of the chart.

As this value is referenced to the exposed planform of the wing, it must be multiplied by ( $S_{\text{exposed}}/S_{\text{ref}}$ ) as in Eq. (12.6). Also, the value must be multiplied by  $F$  from Eq. (12.9) to account for the fuselage lift effect.

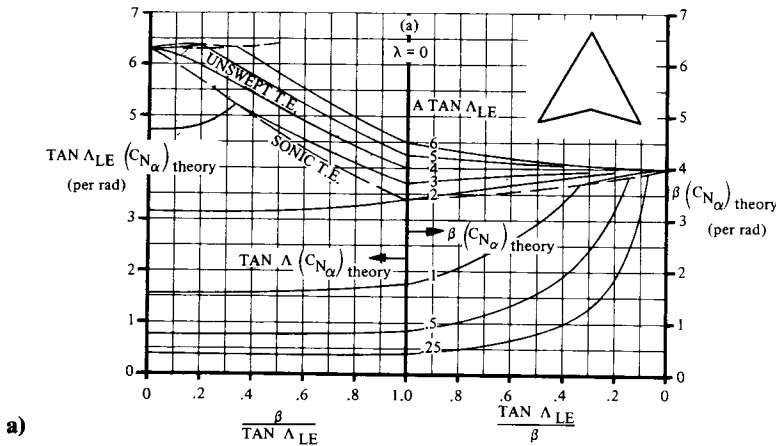
Note that these charts give best results only for trapezoidal wings without kinks or strakes. For highly nontrapezoidal planforms, Ref. 37 contains additional estimation procedures. However, these charts are rarely used in industry where computerized “panel methods” are available. These are discussed later.

### Transonic Lift-Curve Slope

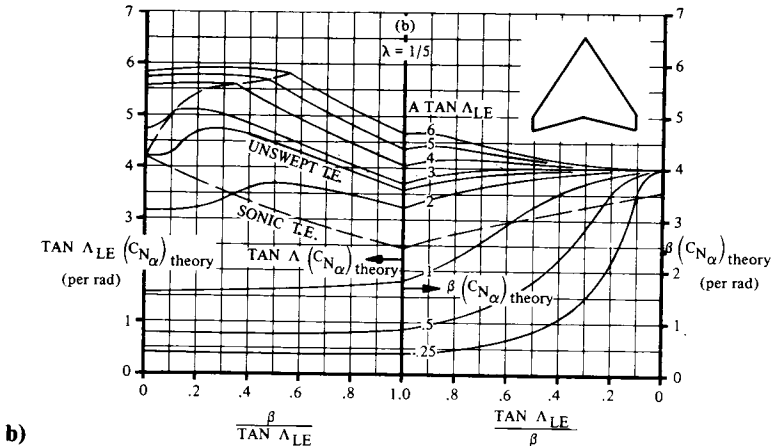
In the transonic regime (roughly Mach 0.85–1.2 for a swept wing) there are no good initial-estimation methods for slope of the lift curve. It is suggested that the subsonic and supersonic values be plotted vs Mach number, and that a smooth curve be faired between the subsonic and supersonic values similar to the curves shown in Fig. 12.5.

### Nonlinear Lift Effects

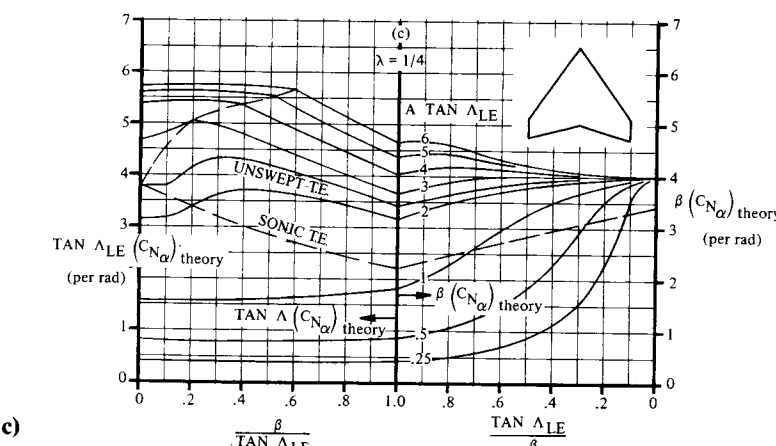
For a wing of very high sweep or very low aspect ratio (under two or three), the air escaping around the swept leading edge or wing tip will form



a)

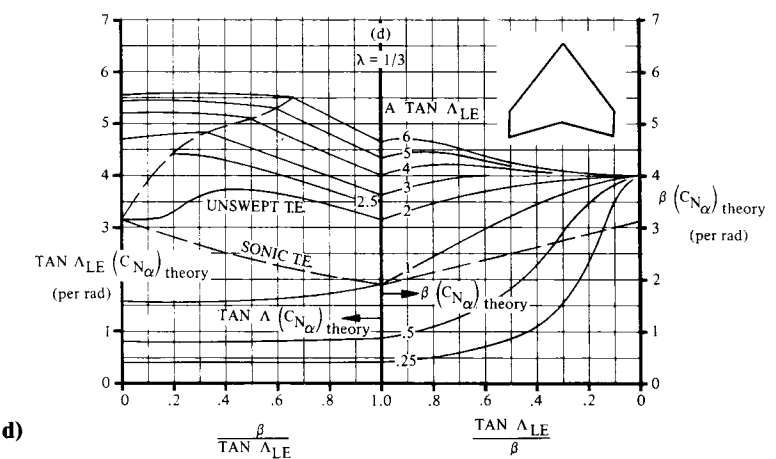


b)

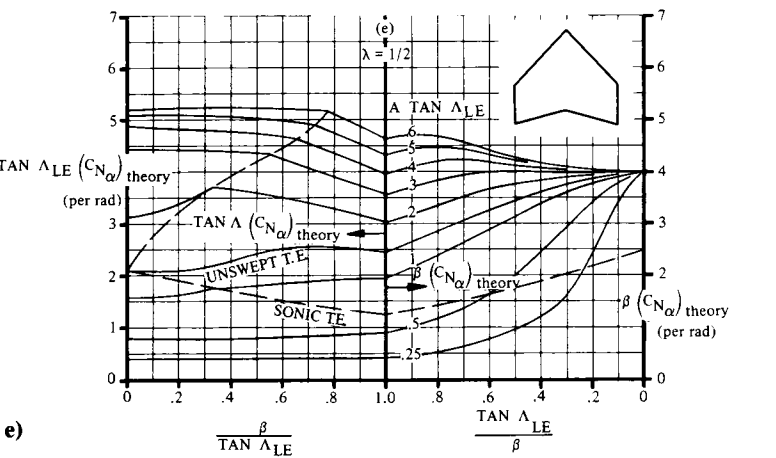


c)

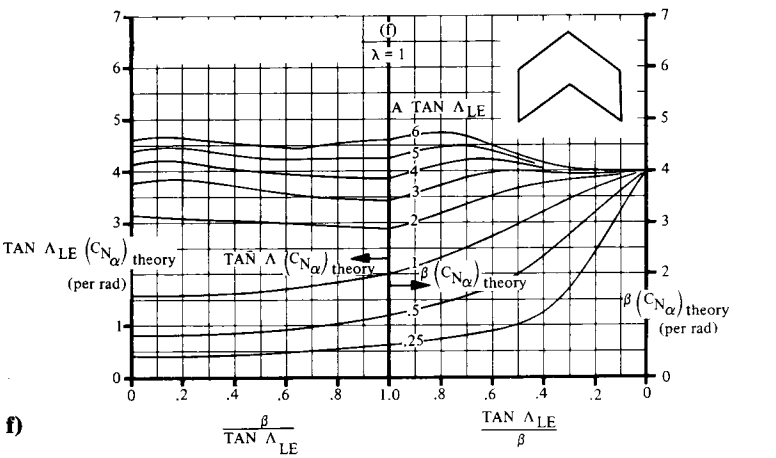
Fig. 12.6 Wing supersonic normal-force-curve slope. (Ref. 37)



d)



e)



f)

Fig. 12.6 (cont'd.) Wing supersonic normal-force-curve slope. (Ref. 37)

a strong vortex that creates additional lift at a given angle of attack. This additional lift varies approximately by the square of the angle of attack. This nonlinear increase in the slope of the lift curve is difficult to estimate and can conservatively be ignored during early conceptual design.

(However, the increase in maximum lift due to vortex formation is very important. It will be discussed in the next section.)

**Maximum Lift (Clean)**

The maximum lift coefficient of the wing will usually determine the wing area. This in turn will have a great influence upon the cruise drag. This strongly affects the aircraft takeoff weight to perform the design mission.

Thus, the maximum lift coefficient is critical in determining the aircraft weight; yet the estimation of maximum lift is probably the least reliable of all of the calculations used in aircraft conceptual design. Even refined wind-tunnel tests cannot predict maximum lift with great accuracy. Frequently an aircraft must be modified during flight test to achieve the estimated maximum lift.

For high-aspect-ratio wings with moderate sweep and a large airfoil leading edge radius, the maximum lift depends mostly upon the airfoil characteristics. The maximum lift coefficient of the “clean” wing (i.e., without the use of flaps and other high-lift devices) will usually be about 90% of the airfoil’s maximum lift as determined from the 2-D airfoil data at a similar Reynolds number.

Sweeping the wing reduces the maximum lift, which can be found by multiplying the unswept maximum lift value by the cosine of the quarter-chord sweep [Eq. (12.15)]. This equation is reasonably valid for most subsonic aircraft of moderate sweep.

$$C_{L_{max}} = 0.9 C_{\ell_{max}} \cos \Lambda_{0.25c} \tag{12.15}$$

If a wing has a low aspect ratio or has substantial sweep and a relatively sharp leading edge, the maximum lift will be increased due to the formation of leading-edge vortices. This vortex formation is strongly affected by the shape of the upper surface of the leading edge.

Leading-edge shape could be defined by the airfoil nose radius. However, the nose radius alone doesn’t take into account the effect of airfoil camber on the shape of the upper surface of the airfoil leading edge.

Instead, an arbitrary “leading-edge sharpness parameter” has been defined as the vertical separation between the points on the upper surface, which are 0.15% and 6% of the airfoil chord back from the leading edge (Fig. 12.7). The leading-edge sharpness parameter (or “ $\Delta y$ ”) as a function of thickness ratio for various airfoils is provided in Table 12.1.

The leading-edge sharpness parameter has been used in Ref. 37 to develop methods for the construction of the lift curve up to the stall, for low- or high-aspect-ratio wings. For high-aspect-ratio wings, Eq. (12.16) is used along with Figs. 12.8 and 12.9. The first term of Eq. (12.16) represents the maximum lift at Mach 0.2, and the second term represents the correction to a higher Mach number.

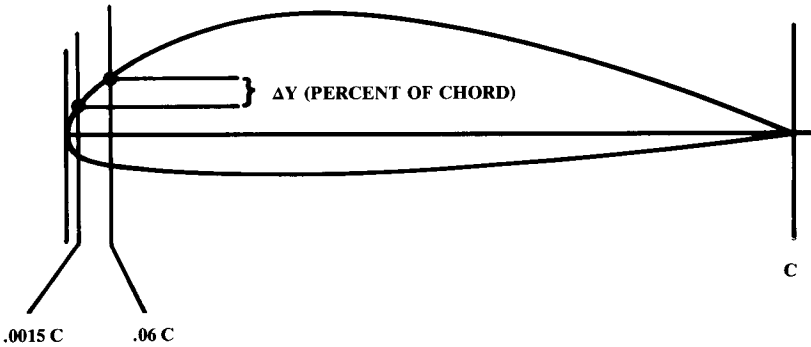


Fig. 12.7 Airfoil leading edge sharpness parameter.

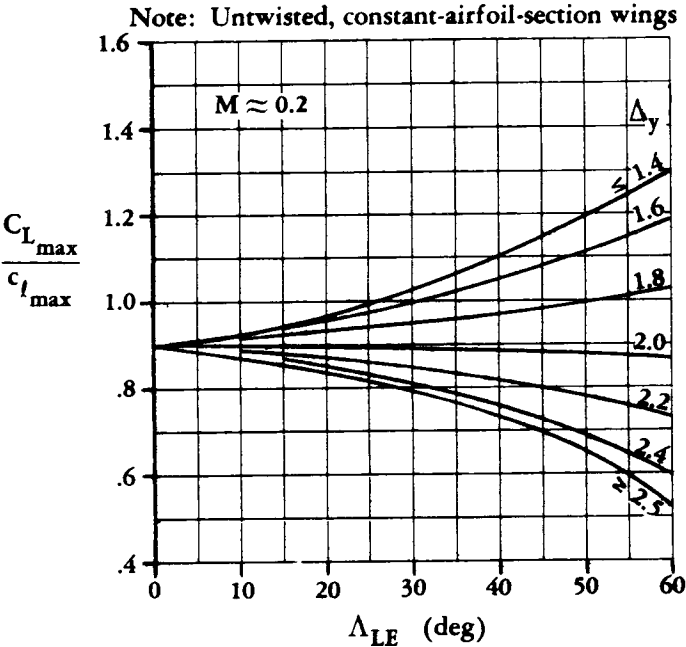


Fig. 12.8 Subsonic maximum lift of high-aspect-ratio wings. (Ref. 37)

Table 12.1  $\Delta Y$  for common airfoils

Airfoil type	$\Delta Y$
NACA 4 digit	26 t/c
NACA 5 digit	26 t/c
NACA 64 series	21.3 t/c
NACA 65 series	19.3 t/c
Biconvex	11.8 t/c

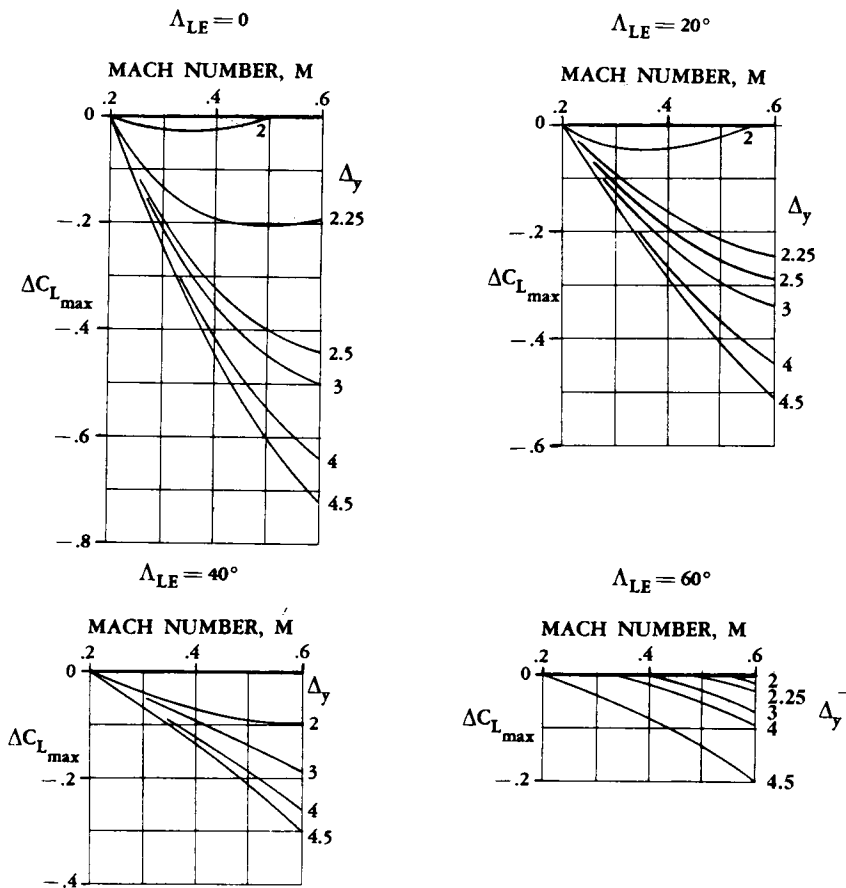


Fig. 12.9 Mach-number correction for subsonic maximum lift of high-aspect-ratio wings. (Ref. 37)

$$\text{High Aspect Ratio: } C_{L_{\max}} = C_{l_{\max}} \left( \frac{C_{L_{\max}}}{C_{l_{\max}}} \right) + \Delta C_{L_{\max}} \quad (12.16)$$

where  $C_{l_{\max}}$  is the airfoil maximum lift coefficient at  $M = 0.2$ .

The angle of attack for maximum lift is defined in Eq. (12.17) with the help of Fig. 12.10. Note that the first and second terms represent the angle of attack if the lift curve slope were linear all the way up to stall. The second term may be approximated by the airfoil zero-lift angle, which is negative for a cambered airfoil. If the wing is twisted, the zero-lift angle is approximately the zero lift angle at the mean chord location. The third term in Eq. (12.17) is a correction for the nonlinear effects of vortex flow.

$$\text{High Aspect Ratio: } \alpha_{C_{L_{\max}}} = \frac{C_{L_{\max}}}{C_{L_{\alpha}}} + \alpha_{0L} + \Delta\alpha_{C_{L_{\max}}} \quad (12.17)$$

A different set of charts is used for a low-aspect-ratio wing, where vortex flow dominates the aerodynamics. For use of these charts, low aspect ratio is defined by Eq. (12.18), which uses the parameter  $C_1$  from Fig. 12.11. Maximum lift of a low-aspect-ratio wing is defined by Eq. (12.19) using Figs. 12.12 and 12.13. The angle of attack at maximum lift is defined by Eq. (12.20) using Figs. 12.14 and 12.15.

$$\text{Low Aspect Ratio if: } A \leq \frac{3}{(C_1 + 1) (\cos \Lambda_{LE})} \quad (12.18)$$

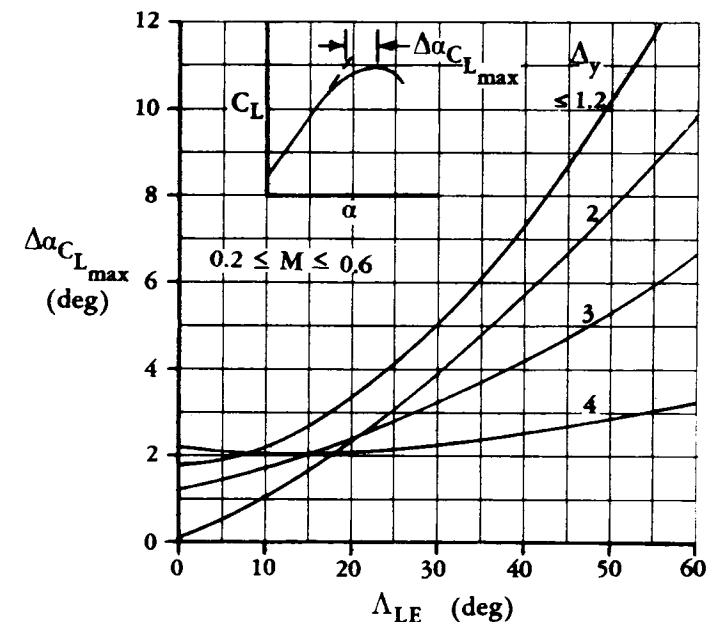


Fig. 12.10 Angle-of-attack increment for subsonic maximum lift of high-aspect-ratio wings. (Ref. 37)

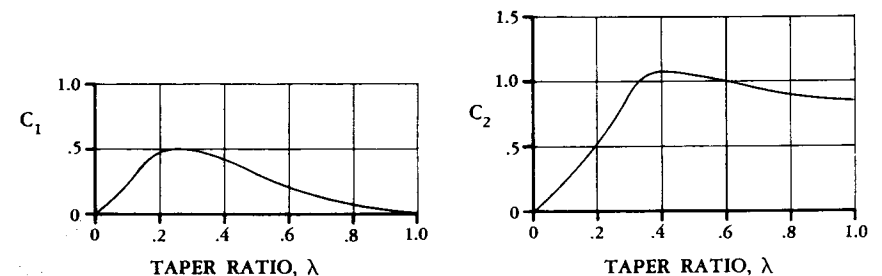


Fig. 12.11 Taper-ratio correction factors for low-aspect-ratio wings. (Ref. 37)

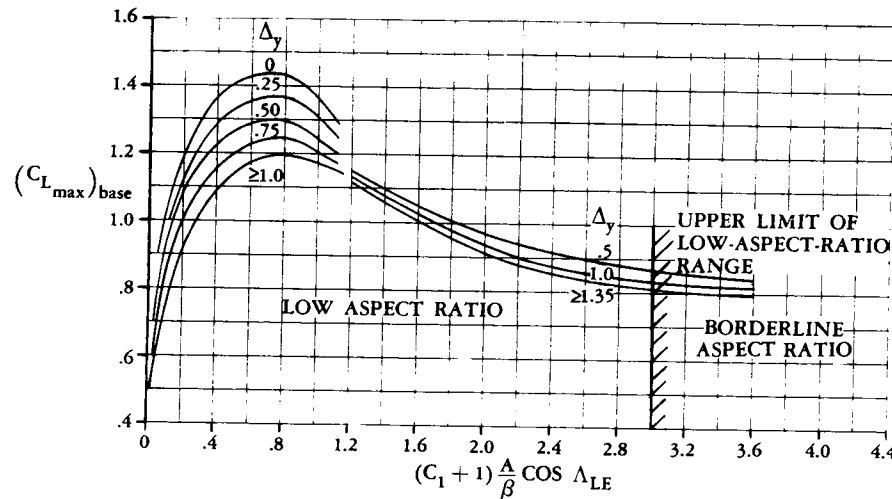


Fig. 12.12 Maximum subsonic lift of low-aspect-ratio wings. (Ref. 37)

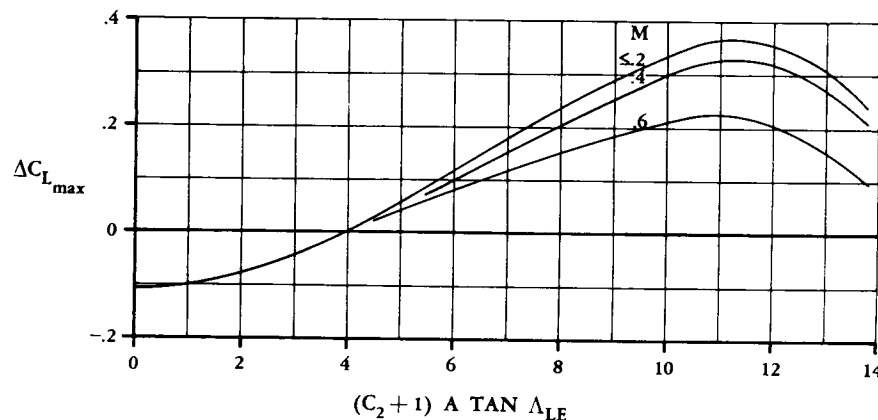


Fig. 12.13 Maximum-lift increment for low-aspect-ratio wings. (Ref. 37)

$$\text{Low Aspect Ratio: } C_{L_{\max}} = (C_{L_{\max}})_{\text{base}} + \Delta C_{L_{\max}} \quad (12.19)$$

$$\alpha_{C_{L_{\max}}} = (\alpha_{C_{L_{\max}}})_{\text{base}} + \Delta \alpha_{C_{L_{\max}}} \quad (12.20)$$

At transonic and supersonic speeds, the maximum lift a wing can achieve is usually limited by structural considerations rather than aerodynamics. Unless the aircraft is flying at a very high altitude, the available maximum lift at Mach 1 is usually enough to break the wings off!

As a conservative assumption, it can be assumed that the maximum lift available at Mach 0.6 will remain constant at higher Mach numbers. Actually, the maximum lift will usually increase through the transonic regime, and then fall again at supersonic speeds.

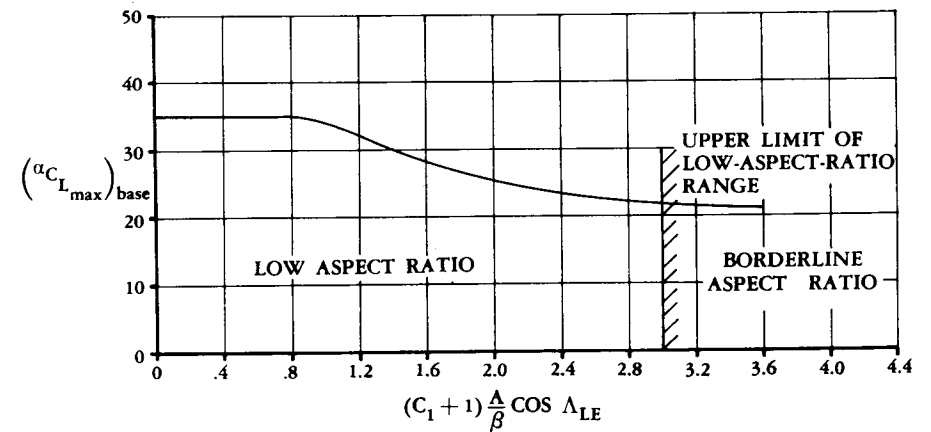


Fig. 12.14 Angle of attack for subsonic maximum lift of low-aspect-ratio wings. (Ref. 37)

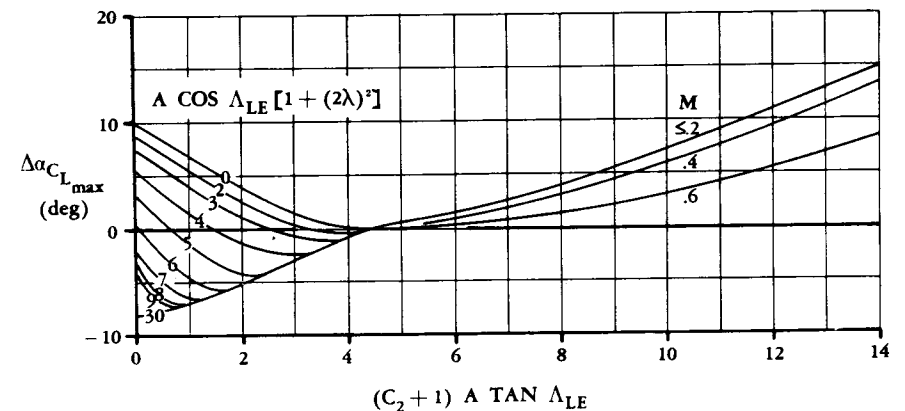


Fig. 12.15 Angle-of-attack increment for subsonic maximum lift of low-aspect-ratio wings. (Ref. 37)

### Maximum Lift with High-Lift Devices

There is always a basic incompatibility in aircraft wing design. For cruise efficiency a wing should have little camber and should operate at a high wing-loading. For takeoff and landing a wing should have lots of lift, which means a lot of camber and a low wing-loading.

In the history of aviation almost every imaginable device for varying the wing camber and wing area has been attempted, including a wing with a telescoping outer panel, a fabric membrane which unfurls behind the wing, a device which pivots out from the fuselage forming an extended flap, and even something called a "mutable" wing having variable span, camber, and sweep (Ref. 38).

Figure 12.16 illustrates the commonly used high lift flaps. The plain flap is simply a hinged portion of the airfoil, typically with a flap chord " $C_f$ "

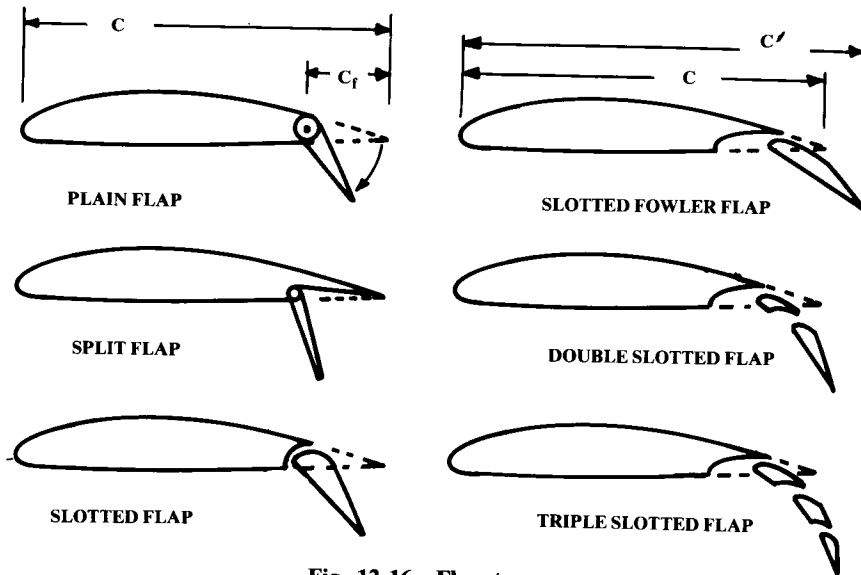


Fig. 12.16 Flap types.

of 30% of the airfoil chord. The plain flap increases lift by increasing camber. For a typical airfoil, the maximum lift occurs with a flap deflection angle of about 40–45 deg. Note that ailerons and other control surfaces are a form of plain flap.

The split flap is like the plain flap except that only the bottom surface of the airfoil is hinged. This produces virtually the same increase in lift as the plain flap. However, the split flap produces more drag and much less change in pitching moment, which may be useful in some designs. Split flaps are rarely used now but were common during World War II.

The slotted flap is a plain flap with a slot between the wing and the flap. This permits high-pressure air from beneath the wing to exit over the top of the flap, which tends to reduce separation. This increases lift and reduces drag.

The “Fowler-type” flap is like a slotted flap, but mechanized to slide rearward as it is deflected. This increases the wing area as well as the camber. Fowler flaps can be mechanized by a simple hinge located below the wing, or by some form of track arrangement contained within it.

To further improve the airflow over the Fowler flap, double- and even triple-slotted flaps are used on some airliners. These increase lift but at a considerable increase in cost and complexity.

Aft flaps do not increase the angle of stall. In fact, they tend to reduce the stall angle by increasing the pressure drop over the top of the airfoil, which promotes flow separation. To increase the stall angle, some form of leading-edge device is required, as shown in Fig. 12.17.

The leading-edge slot is simply a hole which permits high-pressure air from under the wing to blow over the top of the wing, delaying separation and stall. Usually such a slot is fixed, but may have closing doors to reduce drag at high speeds.

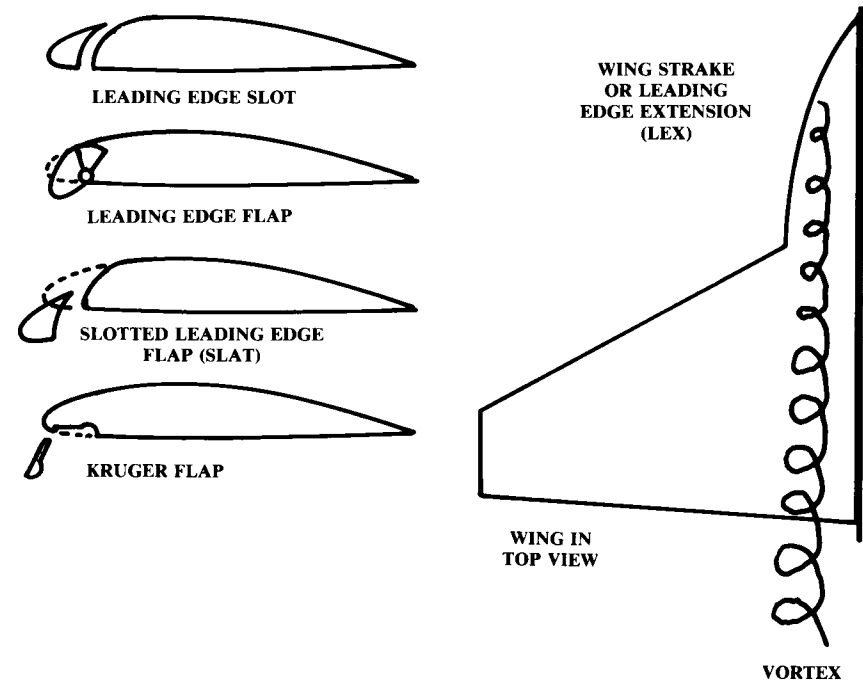


Fig. 12.17 Leading edge devices.

A leading-edge flap is a hinged portion of the leading edge that droops down to increase camber. This has the effect of increasing the curvature on the upper surface. The increase has been shown to be a major factor in determining maximum lift. Leading-edge flaps are usually used for improving the transonic maneuvering performance of high-speed fighters, which need a thin wing for supersonic flight.

A slotted leading-edge flap (“slat”) provides increased camber, a slot, and an increase in wing area. Slat is the most widely used leading-edge device for both low-speed and transonic maneuvering. At transonic speeds, slats are also useful for reducing the buffeting tendency which may limit the usable lift. At Mach 0.9 the use of slats improved the usable lift of the F-4 by over 50%.

The Kruger flap is used mostly by large airliners. It works as an air dam, forcing air up and over the top of the wing. Kruger flaps are lighter in weight than slats but produce higher drag at the lower angles of attack.

The wing strake, or “Leading Edge Extension” (LEX), is similar to the dorsal fin used on vertical tails. Like dorsal fins, the LEX at high angle of attack produces a vortex that delays separation and stall. Unfortunately, a LEX tends to promote pitch-up tendencies and so must be used with care.

Figure 12.18 illustrates the effects these high-lift devices have upon the lift curve of the wing. The nonextending flaps such as the plain, split, or slotted flaps act as an increase in camber, which moves the angle of zero-lift

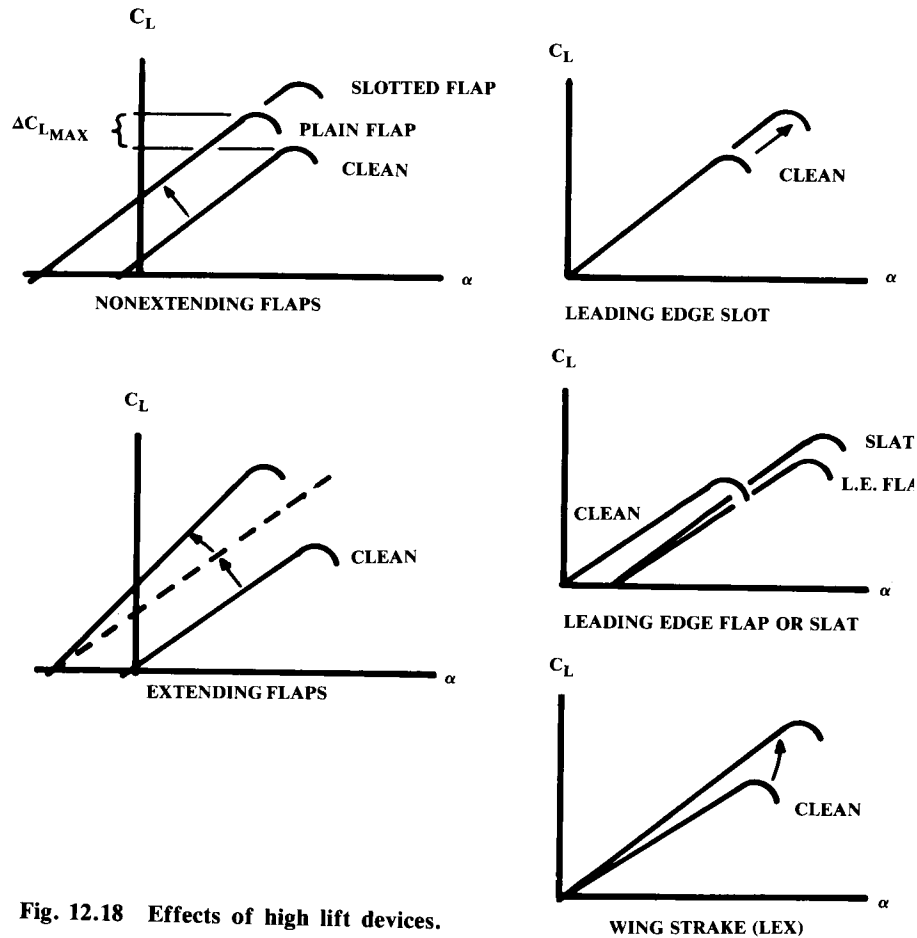


Fig. 12.18 Effects of high lift devices.

to the left and increases the maximum lift. The slope of the lift curve remains unchanged, and the angle of stall is somewhat reduced.

An extending flap such as the Fowler type acts much like the other flaps as far as zero lift angle and stall angle. However, the wing area is increased as the flap deflects, so the wing generates more lift at any given angle of attack compared to the nonextending flap.

Since the lift coefficient is referenced to the original wing area, not the extended wing area, the effective slope of the lift curve for an extending flap is increased by approximately the ratio of the total extended wing area to the original wing area.

Double- and triple-slotted flaps act much like single-slotted Fowler flaps, but the maximum lift is increased.

A leading-edge slot acts only to delay stall. A leading-edge flap or slat delays the stall, but also has the effect of reducing the lift at a given angle of attack (i.e., the lift curve moves to the right). This is because the droop

in the leading edge acts as a reduction in the effective angle of attack as measured from the leading edge to the trailing edge. Note that a leading edge slot, which increases wing area, also increases the slope of the lift curve much as does a Fowler flap.

Leading-edge devices alone do little to improve lift for takeoff and landing, because they are effective only at fairly high angles of attack. However, they are very useful when used in combination with trailing-edge flaps because they prevent premature airflow separation caused by the flaps.

The wing strake, or LEX, delays the stall at high angles of attack (over 20 deg). Also, the area of the LEX provides additional lift, thus increasing the slope of the lift curve. However, the LEX does little to increase lift at the angles of attack seen during takeoff and landing. The LEX does not delay the premature stall associated with trailing-edge flaps.

There are many complex methods for estimating the effects of high-lift devices, some of which are detailed in Ref. 37. For initial design, Eqs. (12.21) and (12.22) provide a reasonable estimate of the increase in maximum lift and the change in the zero-lift angle for flaps and leading-edge devices when deployed at the optimum angle for high lift during landing.

$\Delta C_{L_{\max}}$  values should be obtained from test data for the selected airfoil, or may be approximated from Table 12.2. For takeoff flap settings, lift increments of about 60–80% of these values should be used. The change in zero-lift angle for flaps in the 2-D case is approximately  $-15^\circ$  at the landing setting, and  $-10^\circ$  at the takeoff setting.

$$\Delta C_{L_{\max}} = \Delta C_{L_{\max}} \left( \frac{S_{\text{flapped}}}{S_{\text{ref}}} \right) \cos \Lambda_{H.L.} \quad (12.21)$$

$$\Delta \alpha_{OL} = (\Delta \alpha_{OL})_{\text{airfoil}} \left( \frac{S_{\text{flapped}}}{S_{\text{ref}}} \right) \cos \Lambda_{H.L.} \quad (12.22)$$

Table 12.2 Approximate lift contributions of high-lift devices

High-lift device	$\Delta C_{L_{\max}}$
<b>Flaps</b>	
Plain and split	0.9
Slotted	1.3
Fowler	1.3 c'/c
Double slotted	1.6 c'/c
Triple slotted	1.9 c'/c
<b>Leading edge devices</b>	
Fixed slot	0.2
Leading edge flap	0.3
Kruger flap	0.3
Slat	0.4 c'/c



In Eqs. (12.21) and (12.22), “H.L.” refers to the hinge line of the high-lift surface. “ $S_{\text{flapped}}$ ” is defined in Fig. 12.19. The lift increment for a leading-edge extension may be crudely estimated as 0.4 at high angles of attack.

Other methods for increasing the lift coefficient involve active flow control using either suction or blowing. Suction uses mechanical air pumps to suck the thickening boundary layer off the wing before it causes separation. This increases the stall angle of attack, and therefore increases maximum lift in a manner similar to leading-edge flaps.

Blowing uses compressor bleed air or compressed air provided by a mechanical air pump to prevent flow separation and increase the freestream-flow turning. Typically, the compressed air is exited through rearward-facing slots over the flaps or leading-edge flaps.

## 12.5 PARASITE (ZERO-LIFT) DRAG

### Equivalent Skin-Friction Method

Two methods for the estimation of the parasite drag (“ $C_{D0}$ ”) are presented below. The first is based upon the fact that a well-designed aircraft in subsonic cruise will have parasite drag that is mostly skin-friction drag plus a small separation pressure drag. The latter is a fairly consistent percentage of the skin-friction drag for different classes of aircraft. This leads to the concept of an “equivalent skin friction coefficient” ( $C_{fe}$ ), which includes both skin-friction and separation drag.

$C_{fe}$  is multiplied by the aircraft’s wetted area to obtain an initial estimate of parasite drag. This estimate [Eq. (12.23) and Table 12.3] is suitable for initial subsonic analysis and for checking the results of the more detailed method described in the next section.

$$C_{D0} = C_{fe} \frac{S_{\text{wet}}}{S_{\text{ref}}} \quad (12.23)$$

Table 12.3 Equivalent skin friction coefficients

$C_{D0} = C_{fe} \frac{S_{\text{wet}}}{S_{\text{ref}}}$	$C_{fe}$ -subsonic
Bomber and civil transport	0.0030
Military cargo (high upsweep fuselage)	0.0035
Air Force fighter	0.0035
Navy fighter	0.0040
Clean supersonic cruise aircraft	0.0025
Light aircraft – single engine	0.0055
Light aircraft – twin engine	0.0045
Prop seaplane	0.0065
Jet seaplane	0.0040

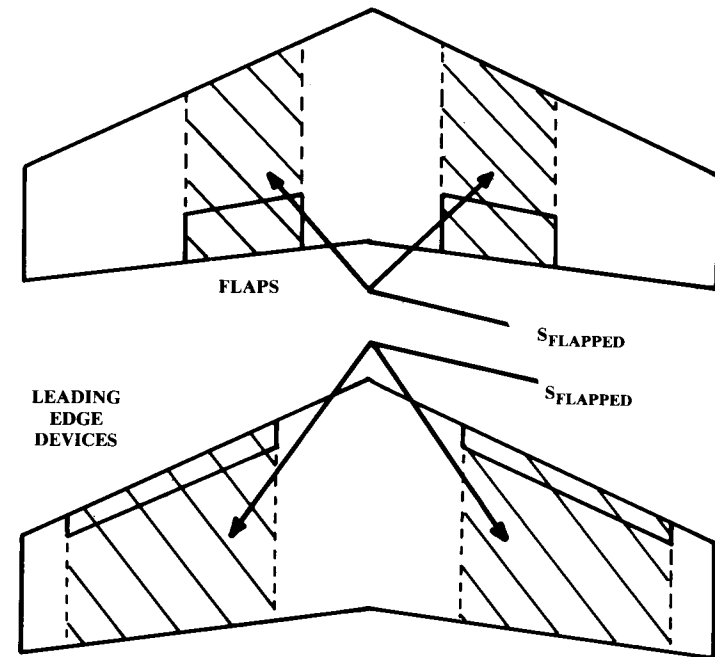


Fig. 12.19 “Flapped” wing area.

### Component Buildup Method

The component buildup method estimates the subsonic parasite drag of each component of the aircraft using a calculated flat-plate skin-friction drag coefficient ( $C_f$ ) and a component “form factor” ( $FF$ ) that estimates the pressure drag due to viscous separation. Then the interference effects on the component drag are estimated as a factor “ $Q$ ” and the total component drag is determined as the product of the wetted area,  $C_f$ ,  $FF$ , and  $Q$ .

(Note that the interference factor  $Q$  should not be confused with dynamic pressure  $q$ .)

Miscellaneous drags ( $C_{D_{\text{misc}}}$ ) for special features of an aircraft such as flaps, unretracted landing gear, an upswept aft fuselage, and base area are then estimated and added to the total, along with estimated contributions for leakages and protuberances ( $C_{D_{\text{L\&P}}}$ ). Subsonic parasite-drag buildup is shown in Eq. (12.24), where the subscript “ $c$ ” indicates that those values are different for each component.

$$(C_{D0})_{\text{subsonic}} = \frac{\sum (C_{fe} FF_c Q_c S_{\text{wet}_c})}{S_{\text{ref}}} + C_{D_{\text{misc}}} + C_{D_{\text{L\&P}}} \quad (12.24)$$

For supersonic flight, the skin-friction contribution is simply the flat-plate skin friction coefficient times the wetted area. All supersonic pressure drag contributions (except base drag) are included in the wave-drag term, which is determined from the total aircraft volume distribution.

For transonic flight, a graphical interpolation between subsonic and supersonic values is used. Supersonic and transonic drag calculations are discussed later.

### Flat-Plate Skin Friction Coefficient

The flat-plate skin friction coefficient  $C_f$  depends upon the Reynolds number, Mach number, and skin roughness. The most important factor affecting skin-friction drag is the extent to which the aircraft has laminar flow over its surfaces.

At a local Reynolds number of one million, a surface with turbulent flow will have a friction drag coefficient as much as three times the drag coefficient of a surface with laminar flow. Laminar flow may be maintained if the local Reynolds number is below roughly half a million, and only if the skin is very smooth (molded composite or polished aluminum without rivets).

Most current aircraft have turbulent flow over virtually the entire wetted surface, although some laminar flow may be seen towards the front of the wings and tails. A typical current aircraft may have laminar flow over perhaps 10–20% of the wings and tails, and virtually no laminar flow over the fuselage.

A carefully designed modern composite aircraft such as the Piaggio GP180 can have laminar flow over as much as 50% of the wings and tails, and about 20–35% of the fuselage.

For the portion of the aircraft that has laminar flow, the flat-plate skin friction coefficient is expressed by Eq. (12.25). Note that laminar flow is unlikely at transonic or supersonic speeds, unless great attention is paid to shaping and surface smoothness.

$$\text{Laminar: } C_f = 1.328/\sqrt{R} \quad (12.25)$$

where Reynolds number is:

$$R = \rho V \ell / \mu \quad (12.26)$$

The “ $\ell$ ” in Eq. (12.26) is the characteristic length. For a fuselage,  $\ell$  is the total length. For a wing or tail,  $\ell$  is the mean aerodynamic chord length.

For turbulent flow, which in most cases covers the whole aircraft, the flat-plate skin friction coefficient is determined by Eq. (12.27). Note that the second term in the denominator, the Mach number correction, goes to 1.0 for low-subsonic flight.

$$\text{Turbulent: } C_f = \frac{0.455}{(\log_{10} R)^{2.58} (1 + 0.144 M^2)^{0.65}} \quad (12.27)$$

If the surface is relatively rough, the friction coefficient will be higher than indicated by this equation. This is accounted for by the use of a “cut-off Reynolds number,” which is determined from Eq. (12.28) or (12.29) using the characteristic length  $\ell$  (feet) and a skin-roughness value “ $k$ ” based upon Table 12.4. The lower of the actual Reynolds number and the cut-off Reynolds number should be used in Eq. (12.27).

$$\text{Subsonic: } R_{\text{cutoff}} = 38.21(\ell/k)^{1.053} \quad (12.28)$$

$$\text{Transonic or Supersonic: } R_{\text{cutoff}} = 44.62(\ell/k)^{1.053} M^{1.16} \quad (12.29)$$

Once laminar and turbulent flat-plate skin friction coefficients have been calculated, an “average” coefficient can be calculated as the weighted average of the two. This requires estimation of the percentage of laminar flow which can be attained. This estimation is a judgment call based on past experience as discussed above, and one must review the current literature to determine how much laminar flow can be attained with current state of the art.

### Component Form Factors

Form factors for subsonic-drag estimation are presented in Eqs. (12.30–12.32). These are considered valid up to the drag-divergent Mach number. In Eq. (12.30), the term “ $(x/c)_m$ ” is the chordwise location of the airfoil maximum thickness point. For most low-speed airfoils, this is at about 0.3 of the chord. For high-speed airfoils this is at about 0.5 of the chord.  $\Lambda_m$  refers to the sweep of the maximum-thickness line.

Wing, Tail, Strut, and Pylon:

$$FF = \left[ 1 + \frac{0.6}{(x/c)_m} \left( \frac{t}{c} \right) + 100 \left( \frac{t}{c} \right)^4 \right] \left[ 1.34 M^{0.18} (\cos \Lambda_m)^{0.28} \right] \quad (12.30)$$

Fuselage and Smooth Canopy:

$$FF = \left( 1 + \frac{60}{f^3} + \frac{f}{400} \right) \quad (12.31)$$

Nacelle and Smooth External Store:

$$FF = 1 + (0.35/f) \quad (12.32)$$

where

$$f = \frac{\ell}{d} = \frac{\ell}{\sqrt{(4/\pi) A_{\text{max}}}} \quad (12.33)$$

A tail surface with a hinged rudder or elevator will have a form factor about 10% higher than predicted by Eq. (12.30) due to the extra drag of the gap between the tail surface and its control surface.

Table 12.4 Skin roughness value ( $k$ )

Surface	$k$ (ft)
Camouflage paint on aluminum	$3.33 \times 10^{-5}$
Smooth paint	$2.08 \times 10^{-5}$
Production sheet metal	$1.33 \times 10^{-5}$
Polished sheet metal	$0.50 \times 10^{-5}$
Smooth molded composite	$0.17 \times 10^{-5}$

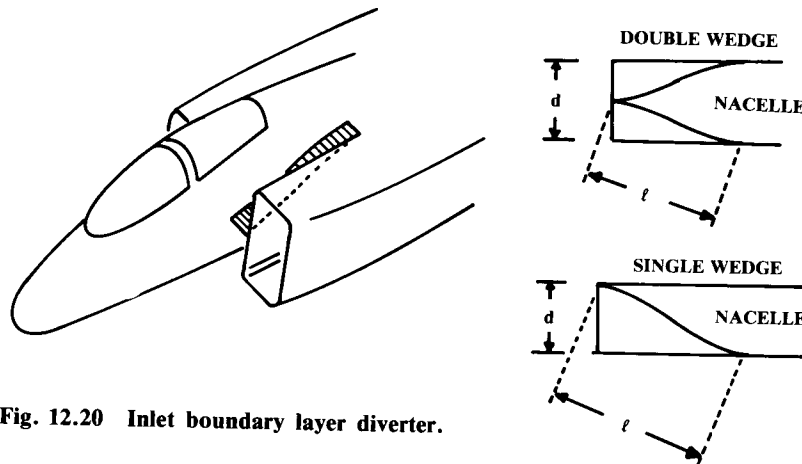


Fig. 12.20 Inlet boundary layer diverter.

Equation (12.31) is mainly used for estimation of the fuselage form factor, but can also be used for a blister or fairing such as a pod used for landing-gear stowage.

For a fuselage with a steep aft-fuselage closure angle in front of a pusher propeller, the separation drag will be lower than predicted using this form-factor equation.

A square-sided fuselage has a form factor about 40% higher than the value estimated with Eq. (12.31) due to additional separation caused by the corners. This can be somewhat reduced by rounding the corners. A flying-boat hull has a form factor about 50% higher, and a float has a form factor about three times the estimated value.

Equation (12.31) will predict the form factor for a smooth, one-piece fighter canopy such as seen on the F-16. For a typical two-piece canopy with a fixed but streamlined windscreen (i.e., F-15), the form factor calculated with Eq. (12.31) should be increased by about 40%. A canopy with a flat-sided windscreen has a form factor about three times the value estimated with Eq. (12.31).

The external boundary-layer diverter for an inlet mounted on the fuselage can have a large drag contribution. Equations (12.34) and (12.35) estimate the form factors to use for a double-wedge and single-wedge diverter, where the Reynolds number is determined using  $l$  and the wetted area is defined as shown in Fig. 12.20. Remember to double the drag if there are two inlets.

$$\text{Double Wedge: } FF = 1 + (d/l) \quad (12.34)$$

$$\text{Single Wedge: } FF = 1 + (2d/l) \quad (12.35)$$

### Component Interference Factors

Parasite drag is increased due to the mutual interference between components. For a nacelle or external store mounted directly on the fuselage or wing, the interference factor  $Q$  is about 1.5. If the nacelle or store is mounted less than about one diameter away, the  $Q$  factor is about 1.3. If it

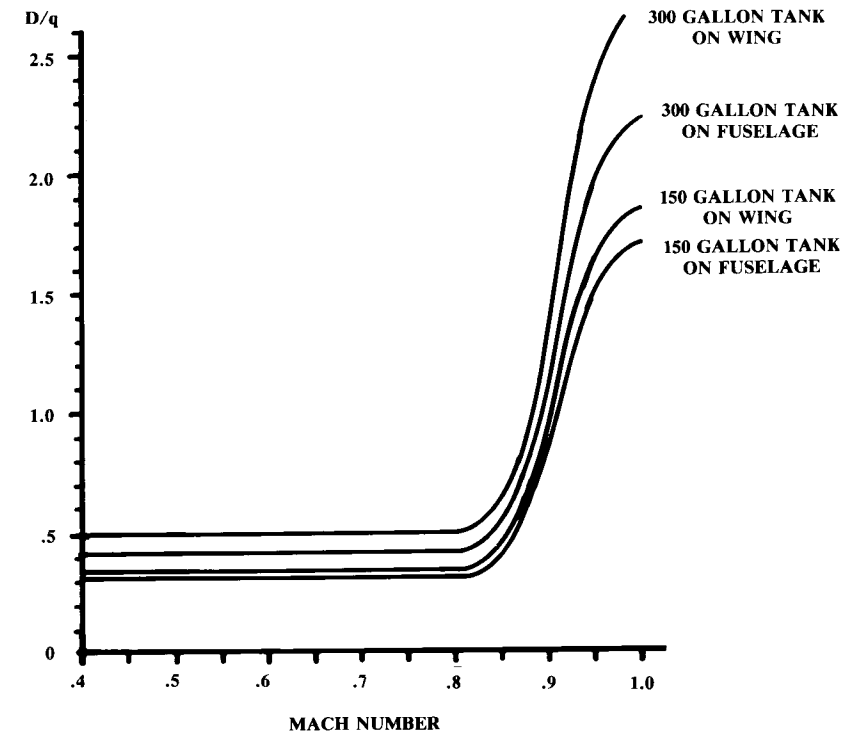


Fig. 12.21 External stores drag-fuel tanks.

is mounted much beyond one diameter, the  $Q$  factor approaches 1.0. Wing tip-mounted missiles have a  $Q$  factor of about 1.25.

For a high-wing, a mid-wing, or a well-filletted low wing, the interference will be negligible so the  $Q$  factor will be about 1.0. An unfilletted low wing can have a  $Q$  factor from about 1.1–1.4.

The fuselage has a negligible interference factor ( $Q = 1.0$ ) in most cases. Also,  $Q = 1.0$  for a boundary-layer diverter. For tail surfaces, interference ranges from about three percent ( $Q = 1.03$ ) for a clean V-tail to about eight percent for an H-tail. For a conventional tail, four to five percent may be assumed (Ref. 8).

Component parasite drags can now be determined using Eq. (12.24) and the skin-friction coefficients, form factors, and interference factors.

### Miscellaneous Drags

The drag of miscellaneous items can be determined separately using a variety of empirical graphs and equations, and then adding the results to the parasite drags determined above.

While the drag of smooth external stores can be estimated using Eq. (12.31), the majority of external stores are in fact not very smooth. Figures 12.21 and 12.22 provide drag estimates for external fuel tanks and weapons, presented as drag divided by dynamic pressure ( $D$ -over- $q$  or  $D/q$ ).

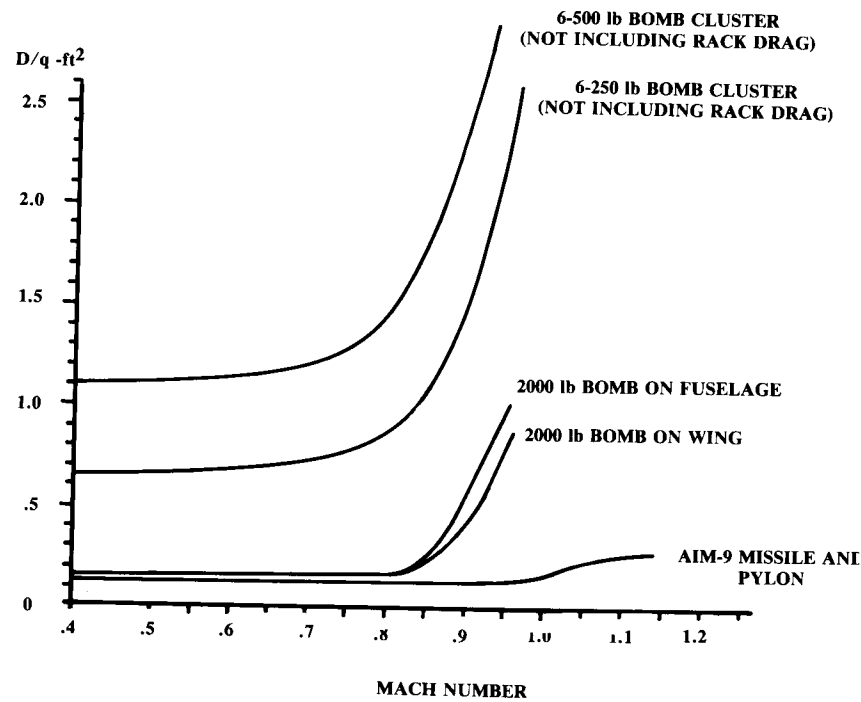


Fig. 12.22 Bomb and missile drag.

$D/q$  has units of square feet, and so is sometimes called the “drag area.”  $D/q$  divided by the wing reference area yields the miscellaneous parasite drag coefficient. Note that pylon and bomb-rack drag as estimated using Fig. 12.23 must be added to the store drag.

Most transport and cargo aircraft have a pronounced upsweep to the aft fuselage (Fig. 12.24). This increases the drag beyond the value calculated using Eq. (12.31). This extra drag is a complicated function of the fuselage cross-sectional shape and the aircraft angle of attack, but can be approximated using Eq. (12.36) where “ $u$ ” is the upsweep angle (radians) of the fuselage centerline and  $A_{\max}$  is the maximum cross-sectional area of the fuselage.

$$D/q_{\text{upsweep}} = 3.83u^{2.5}A_{\max} \quad (12.36)$$

The landing-gear drag is best estimated by comparison to test data for a similar gear arrangement. Such data for a variety of aircraft is available in Refs. 7, 8, 28, and others. If such data is not available, the gear drag can be estimated as the summation of the drags of the wheels, struts, and other gear components using the data in Table 12.5 (largely from Ref. 8).

These values times the frontal area of the indicated component yield  $D/q$  values, which must be divided by the wing reference area to obtain parasite-drag coefficients. To account for mutual interference it is suggested that the sum of the gear component drags be multiplied by 1.2. Also, the total gear drag should be increased by about 7% for a retractable landing gear in which the gear wells are left open when the gear is down.

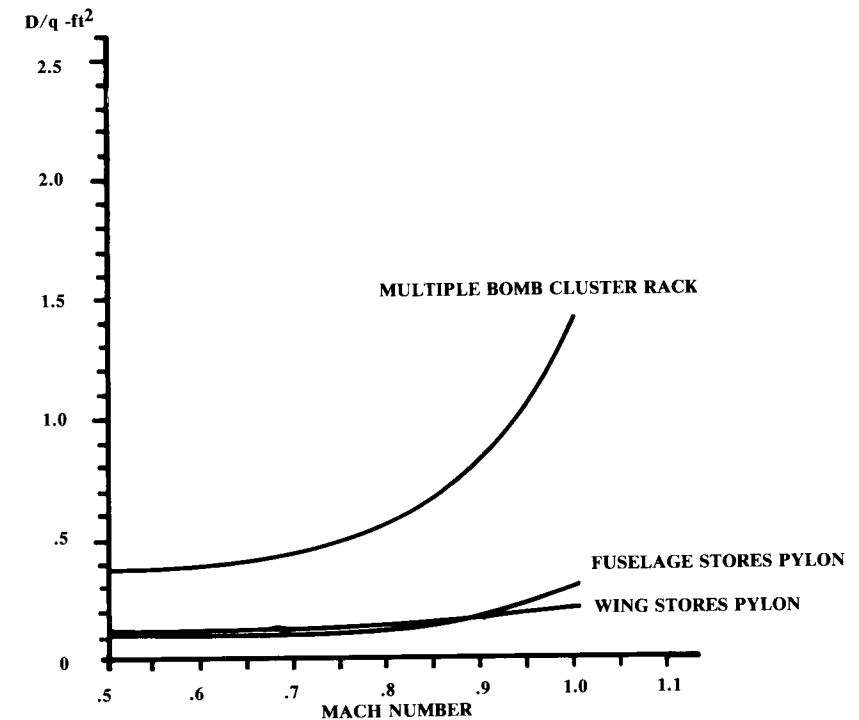


Fig. 12.23 Pylon and bomb rack drag.



Fig. 12.24 Fuselage upsweep.

Table 12.5 Landing gear component drags

	$D/q$ Frontal area (Ft <sup>2</sup> )
Regular wheel and tire	0.25
Second wheel and tire in tandem	0.15
Streamlined wheel and tire	0.18
Wheel and tire with fairing	0.13
Streamline strut ( $1/6 < t/c < 1/3$ )	0.05
Round strut or wire	0.30
Flat spring gear leg	1.40
Fork, bogey, irregular fitting	1.0–1.4

Note that landing-gear drag is actually a function of lift. The more lift the aircraft wing is producing, the greater the velocity of the airflow over the top of the wing and, conversely, the lesser the airflow velocity underneath the wing where the gear is located. Hence, at higher lift coefficients the gear drag is reduced. This can be ignored for initial analysis.

Strut, wire, and fitting data in Table 12.4 may also be used to estimate the extra drag for a braced wing or biplane. The optimal thickness ratio considering both aerodynamic and structural efficiency is about 0.19 for a strut in tension and about 0.23 for a strut in compression.

Flaps affect both the parasite and induced drag. The induced effect is due to the change in the lift distribution, but is relatively small and can be ignored for initial analysis.

The flap contribution to parasite drag is caused by the separated flow above the flap, and can be estimated using Eq. (12.37) for most types of flap. Note that this is referenced to wing area. Typically the flap deflection is about 60–70 deg for landing and about 20–40 deg for takeoff. Light aircraft usually take off with no flaps.

$$\Delta C_{D_{0\text{flap}}} = 0.0023 \frac{\text{flap span}}{\text{wing span}} \delta_{\text{flap}} \quad (12.37)$$

where  $\delta_{\text{flap}}$  is in deg. Note that this is a very rough estimate!

Many aircraft have some form of speed brake. Typically these are plates which extend from the fuselage or wing. Fuselage-mounted speed brakes have a  $D/q$  of about 1.0 times the speed-brake frontal area, while wing-mounted speed brakes have a  $D/q$  of about 1.6 times their frontal area if mounted at about the 60% of chord location.

Speed brakes mounted on top of the wing will also disturb the airflow and spoil the lift, and so are called “spoilers.” These further reduce landing distance by transferring more of the aircraft’s weight to the landing-gear which increases the braking action.

Base area produces a drag according to Eqs. (12.38) and (12.39) (Ref. 40). “ $A_{\text{base}}$ ” includes any aft-facing flat surfaces as well as the projected aft-facing area for any portions of the aft fuselage that experience highly-separated airflow. Roughly speaking, this should be expected any place where the aft fuselage angle to the freestream exceeds about 20 deg. As previously mentioned, a pusher propeller may prevent aft-fuselage separation despite an aft fuselage angle of 30 deg or more.

$$\text{Subsonic: } (D/q)_{\text{base}} = [0.139 + 0.419(M - 0.161)^2] A_{\text{base}} \quad (12.38)$$

$$\text{Supersonic: } (D/q)_{\text{base}} = [0.064 + 0.042(M - 3.84)^2] A_{\text{base}} \quad (12.39)$$

Fighter-type canopies have been discussed above. For transport and light-aircraft windshields that smoothly fair into the fuselage, an additional  $D/q$  of about 0.07 times the windshield frontal area is suggested. A sharp-edged, poorly-faired windshield has an additional  $D/q$  of about 0.15 times its frontal area.

An open cockpit has a  $D/q$  of about 0.50 times the windshield frontal area. For an aircraft with an unenclosed cockpit, such as a hang-glider or ultralight, a seated person has a  $D/q$  of about 6 ft<sup>2</sup>. This reduces to a  $D/q$  of 1.2 ft<sup>2</sup> in the prone position.

An arresting hook for carrier operation adds a  $D/q$  of about 0.15 ft<sup>2</sup>. The smaller emergency arresting hook for Air Force aircraft adds a  $D/q$  of about 0.10 ft<sup>2</sup>. Machine-gun ports add a  $D/q$  of about 0.02 ft<sup>2</sup> per gun. A cannon port such as for the M61 adds a  $D/q$  of about 0.2 ft<sup>2</sup>.

### Leakage and Protuberance Drag

Leaks and protuberances add drag that is difficult to predict by any method. Leakage drag is due to the tendency of an aircraft to “inhale” through holes and gaps in high-pressure zones, and “exhale” into the low-pressure zones. The momentum loss of the air “inhaled” contributes directly to drag, and the air “exhaled” tends to produce additional airflow separation.

Protuberances include antennas, lights, and such manufacturing defects as protruding rivets and rough or misaligned skin panels. Typically these drag increments are estimated as a percent of the total parasite drag.

For a normal production aircraft, leaks and protuberance drags can be estimated as about 2–5% of the parasite drag for jet transports or bombers, 5–10% for propeller aircraft, and 10–15% for current-design fighters (5–10% for new-design fighters). If special care is taken during design and manufacturing, these drag increments can be reduced to near zero but at a considerable expense.

An aircraft with variable-sweep wings will have an additional protuberance drag of about 3% due to the gaps and steps of the wing pivot area.

### Stopped-Propeller and Windmilling Engine Drags

The specifications for civilian and military aircraft require takeoff and climb capabilities following an engine failure. Not only does this reduce the available thrust, but the drag of the stopped propeller or windmilling engine must be considered.

Data on the drag of a stopped or windmilling propeller are normally obtained from the manufacturer. For a jet engine, detailed knowledge of the characteristics of the engine, inlet, and nozzle are required to estimate the drag from a stopped or windmilling engine. In the absence of such data, the following rough approximations can be used.

For a stopped propeller, Ref. 8 indicates that the subsonic drag coefficient will be about 0.1 based upon the total blade area if the propeller is feathered (turned so that the blades align with the airflow). If the propeller has fixed pitch and cannot be feathered, the drag coefficient is about 0.8.

To determine the total blade area it is necessary to know or to estimate the propeller “solidity” ( $\sigma$ ), the ratio between the total blade area and the propeller disk area. This can be shown to equal the number of blades divided by the blade aspect ratio and  $\pi$ .

For a typical blade aspect ratio of 8, the solidity will be 0.04 times the number of blades. A small piston-prop engine will generally use a two-

bladed propeller. A fast piston-prop or a small turboprop will use a three-bladed propeller, while a large turboprop may use a four-bladed propeller. Drag of a feathered propeller can be roughly estimated by Eq. (12.40). For an unfeathered, stopped propeller, the 0.1 term is replaced by 0.8.

$$(D/q)_{\text{feathered prop}} = 0.1 \sigma A_{\text{propeller disk}} \quad (12.40)$$

For jet engines, Ref. 9 indicates that the subsonic drag coefficient of a windmilling turbojet engine will be about 0.3, referenced to the flow area at the engine's front face. Thus, the drag of a windmilling turbojet will be approximately:

$$(D/q)_{\text{windmilling jet}} = 0.3 A_{\text{engine front face}} \quad (12.41)$$

### Supersonic Parasite Drag

The supersonic parasite drag is calculated in a similar fashion to the subsonic drag, with two exceptions. First, the supersonic skin-friction drag does not include adjustments for form factors or interference effects (i.e.,  $FF = Q = 1.0$ ). Second, a new term, wave drag, is added. This accounts for the pressure drag due to shock formation. Supersonic parasite-drag buildup is defined in Eq. (12.42).

$$C_{D0\text{supersonic}} = \frac{\Sigma(C_{fc} S_{wet_c})}{S_{\text{ref}}} + C_{D\text{misc}} + C_{D_{L\&P}} + C_{D\text{wave}} \quad (12.42)$$

The supersonic turbulent skin friction coefficient was previously presented in Eq. (12.27), using the cutoff Reynolds number from Eq. (12.29).

Miscellaneous drag calculations for supersonic flight have been presented above, where appropriate. Many of the items that produce miscellaneous drag will not appear on a supersonic aircraft (floats, open cockpits, etc.).

The drag due to leaks and protuberances in supersonic flight follows about the same percentages presented above, applied to the skin-friction drag only.

The wave drag in supersonic flight will often be greater than all the other drag put together. Wave drag is pressure drag due to shocks, and is a direct result of the way in which the aircraft's volume is distributed.

An ideal volume distribution is produced by the Sears-Haack body (Ref. 16), which was shown in Fig. 8.2. A Sears-Haack body, as defined by Eq. (12.43), has a wave drag as in Eq. (12.45). This is the minimum possible wave drag for any closed-end body of the same length and total volume.

$$\frac{r}{r_{\text{max}}} = \left[ 1 - \left( \frac{x}{\ell/2} \right)^2 \right]^{0.75} \quad (12.43)$$

where

$r$  = the cross-section radius  
 $\ell$  = the longitudinal dimension

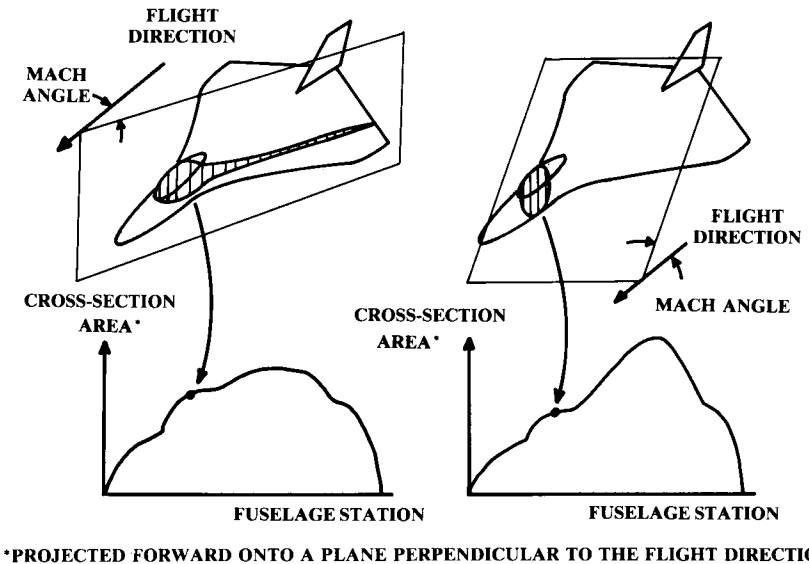


Fig. 12.25 Mach-plane cut volume distribution (two roll angles).

and

$$-\ell/2 \leq x \leq \ell/2 \quad (12.44)$$

$$(D/q)_{\text{wave}} = \frac{9\pi}{2} \left( \frac{A_{\text{max}}}{\ell} \right)^2 \quad (12.45)$$

where  $A_{\text{max}}$  is the maximum cross-sectional area.

The linear area-rule theory says that the theoretical wave drag of an aircraft at Mach 1.0 is identical to the wave drag of a body of revolution with the same volume-distribution plot. In other words, the actual cross-sectional shape at a given longitudinal location has no effect on wave drag at Mach 1.0. All that matters is the cross-sectional area at each longitudinal location and the way that the cross-sectional area varies longitudinally.

This leads to the area-rule principle for minimizing wave drag. Wave drag at Mach 1.0 is minimized when the aircraft has a volume distribution identical to that of a Sears-Haack body. Drag is reduced when the volume distribution is changed to more resemble the Sears-Haack's, which has a minimal amount of longitudinal curvature.

As was discussed in Chapter 8, the wave drag at Mach 1.0 is directly related to the second derivative (i.e., curvature) of the longitudinal volume distribution. To minimize wave drag the designer should try to arrange the configuration so that the volume distribution is smooth and bell-shaped.

For a typical aircraft, the wing tends to put a "bump" in the volume distribution. This bump can be reduced by pinching in the fuselage at the wing location, creating the characteristic "coke-bottle" area-ruled fuselage.

No realistic aircraft will have a volume distribution identical to that of a Sears-Haack body. However, a well-designed supersonic aircraft will have

a theoretical wave drag at Mach 1.0 that is less than twice the Sears-Haack value. Typical ratios of actual wave drag to the optimum Sears-Haack value will be used below as a first-order wave drag estimation method.

At Mach 1.0, shocks form at an angle of 90 deg to the freestream direction. At Mach numbers higher than 1.0, the shocks may form at an angle less than 90 deg. The "Mach angle" is the smallest angle at which a shock may form, representing a "zero-strength" shock. Mach angle is defined as arcsine  $(1/M)$ .

At Mach 1.0, the wave drag is based upon the aircraft's cross-sectional areas found by the intersection of the aircraft and an infinite plane set at an angle perpendicular (90 deg) to the freestream direction. At speeds higher than Mach 1.0, the wave drag still depends upon the volume distribution as before, but with one major exception.

At higher Mach numbers the volume distribution is based upon aircraft cross sections that are determined by intersecting the aircraft with "Mach planes," set at the appropriate Mach angle to the freestream direction.

A Mach plane may be rolled about the freestream direction to any roll angle. Figure 12.25 shows two roll angles. Note that the different Mach-plane roll angles produce entirely different volume-distribution plots. In the left illustration, the Mach-plane cut includes the fuselage and canopy plus a slice of the left wing. In the right illustration only the fuselage and canopy are cut, producing a much smaller cross-sectional area at that location.

For each Mach-plane roll angle, a volume-distribution plot can be prepared by taking Mach-plane cuts at a number of longitudinal locations. According to linear wave drag theory (Ref. 41) the supersonic wave drag at Mach numbers greater than 1.0 is determined by averaging the wave drags of the Mach-plane-cut volume distributions for different roll angles.

This is the basis of the widely-used Harris Wave Drag code (Ref. 42). A simplified computer code suitable for university use is presented in Ref. 43.

The use of canted Mach-plane cuts to determine the volume distribution at Mach numbers greater than 1.0 requires a different approach to area-ruling. Pinching the fuselage at the wing location may smooth out the volume distribution for one Mach-plane roll angle, but may make the volume distribution even less smooth at another Mach-plane roll angle.

At higher Mach numbers it is very difficult to minimize total wave drag by "eyeball" area-ruling. Instead it is more profitable to smooth the entire configuration through wing-body blending, as seen on the B-1B and in the design concept of Fig. 7.3.

For preliminary wave drag analysis at  $M \geq 1.2$ , without use of a computer, a correlation to the Sears-Haack body wave drag is presented in Eq. (12.46), where the Sears-Haack  $D/q$  is from Eq. (12.45).

The maximum cross-sectional area ( $A_{\max}$ ) is determined from the aircraft volume-distribution plot. Inlet capture area should be subtracted from  $A_{\max}$ . The length term  $\ell$  is the aircraft length except that any portion of the aircraft with a constant cross-sectional area should be subtracted from the length.

$$(D/q)_{\text{wave}} = E_{\text{WD}} \left[ 1 - 0.386(M - 1.2)^{0.57} \left( 1 - \frac{\pi \Lambda_{LE}^{0.77}}{100} \right) \right] (D/q)_{\text{Sears-Haack}} \quad (12.46)$$

" $E_{\text{WD}}$ " is an empirical wave-drag efficiency factor and is the ratio between actual wave drag and the Sears-Haack value. For a perfect Sears-Haack body,  $E_{\text{WD}} = 1.0$ .

A very clean aircraft with a smooth volume distribution, such as a blended-delta-wing design, may have an  $E_{\text{WD}}$  as low as 1.2. A more typical supersonic fighter, bomber, or SST design has an  $E_{\text{WD}}$  of about 1.4–2.0. A poor supersonic design with a very bumpy volume distribution can have an  $E_{\text{WD}}$  of 2.0–3.0. The F-15, optimized for the dogfight instead of supersonic flight, has an  $E_{\text{WD}}$  of about 2.9 (Ref. 35).

Note, however, that this efficiency factor is less important in drag determination than the fineness ratio as represented by  $(A_{\max}/\ell)$ . This term is squared, which explains why area ruling that actually reduces  $A_{\max}$  provides a far greater drag reduction than does merely smoothing the volume distribution without lowering  $A_{\max}$ .

### Transonic Parasite Drag

The transonic flow regime extends roughly from Mach 0.8–1.2. The increase in drag as an aircraft accelerates through the transonic regime, called the "drag rise," is due to the formation of shocks, and is in fact the transonic portion of wave drag.

The critical Mach number ( $M_{cr}$ ) occurs when shocks first form on the aircraft. The drag divergent Mach number ( $M_{DD}$ ) is the Mach number at

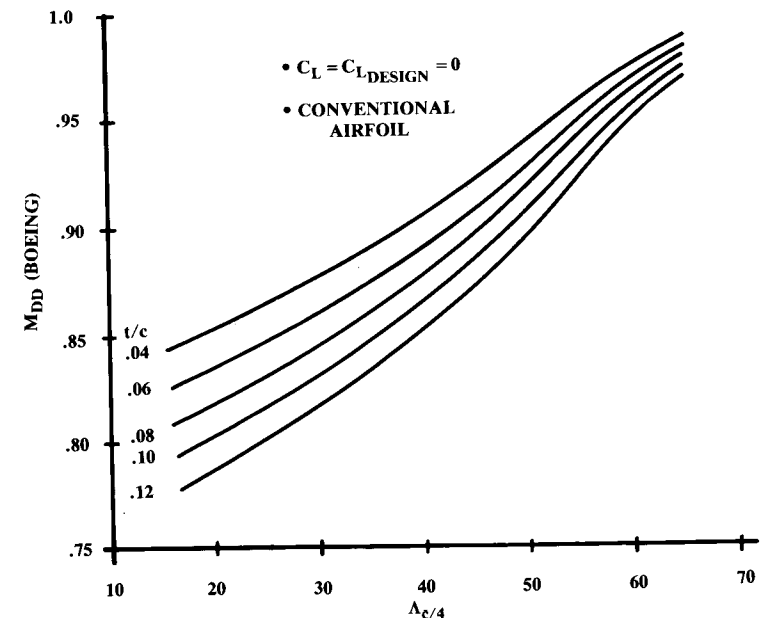


Fig. 12.26 Wing drag-divergence Mach number.

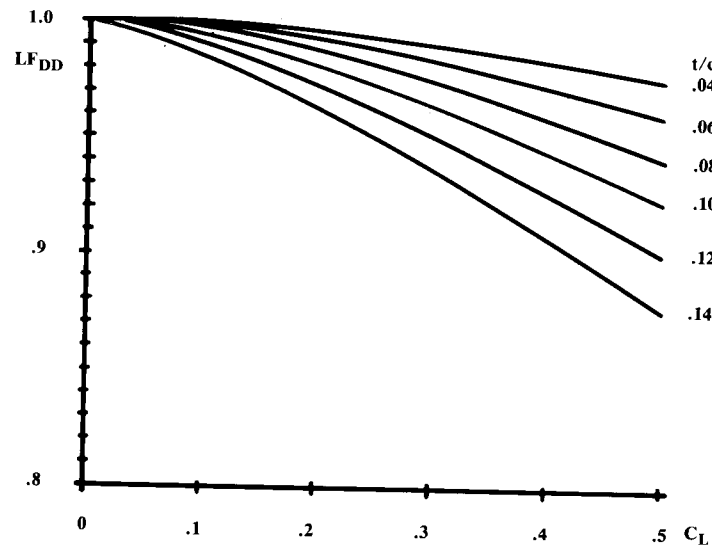


Fig. 12.27 Lift adjustment for  $M_{DD}$ .

which the formation of shocks begins to substantially affect the drag.

The definition of what speed constitutes  $M_{DD}$  is arbitrary, and several definitions are in use. The Boeing definition is that  $M_{DD}$  is where the drag rise reaches 20 counts.  $M_{DD}$  (Boeing) is usually about 0.08 Mach above the critical Mach number. The Douglas definition, also used by the Air Force in Ref. 37, is that  $M_{DD}$  is the Mach number at which the rate of change in parasite drag with Mach number ( $dC_{D_0}/dM$ ) first reaches 0.10.

The Douglas  $M_{DD}$  is typically 0.06 Mach above the Boeing  $M_{DD}$ , and represents a drag rise of perhaps 80–100 counts. Jet transports usually cruise at about  $M_{DD}$  (Boeing), and have a maximum level speed of about  $M_{DD}$  (Douglas).

Shocks are formed on the top of the wing as a result of the increased airflow velocity, so  $M_{DD}$  reduces with an increased lift coefficient. For example, the Boeing 727 has an  $M_{DD}$  of about Mach 0.86 when the lift coefficient is only 0.1, but when the lift coefficient is increased to 0.3 the  $M_{DD}$  reduces to about Mach 0.82.

A preliminary estimate of wing  $M_{DD}$  (Boeing) is provided by Eq. (12.47) using Figs. 12.26 and 12.27. Figure 12.26 provides the wing drag divergence Mach number of an uncambered wing at zero lift. Figure 12.27 adjusts  $M_{DD}$  to the actual lift coefficient.

The last term in Eq. (12.47) is an adjustment for the wing design lift coefficient (i.e., camber and twist). Initially it can be assumed that the design lift coefficient is the same as the lift coefficient at cruise.

$$M_{DD} = M_{DD_{L=0}} LF_{DD} - 0.05 C_{L_{\text{design}}} \quad (12.47)$$

If the wing uses a supercritical airfoil the actual thickness ratio should be multiplied by 0.6 before using these figures. This approximation is to account for the shock-delaying characteristics of the supercritical airfoil.

$M_{DD}$  changes with lift coefficient. Lift coefficient changes with weight and altitude, both of which may change during cruise. To be completely accurate it is necessary to calculate  $M_{DD}$  for each point in the mission. For initial analysis, however, it is acceptable to use a single  $M_{DD}$  based upon a mid-mission weight and cruise altitude.

If the fuselage is relatively blunt it will experience shock formation before the wing does. In this case,  $M_{DD}$  is set by the shape of the forebody. Body  $M_{DD}$  can be estimated using Fig. 12.28 (Ref. 44), where “ $L_n$ ” is the length from the nose to the longitudinal location at which the fuselage cross section becomes essentially constant.  $d$  is the body diameter at that location. If the fuselage is noncircular,  $d$  is an equivalent diameter based upon the fuselage cross-sectional area. Determine both wing and fuselage  $M_{DD}$ , and use the lower value.

The linear-wave-drag analysis gives completely incorrect results in the transonic regime. This analysis is called “linear” because the higher-order, nonlinear terms have been dropped from the aerodynamic equations to permit computation.

Some of these dropped nonlinear terms account for any changes in the airflow longitudinal velocity. At high supersonic speeds these terms have little effect compared to the far greater aircraft velocity.

However, the drag rise at transonic speeds is largely caused by the increase in airflow velocity over the top of the wing. Thus, drag rise below

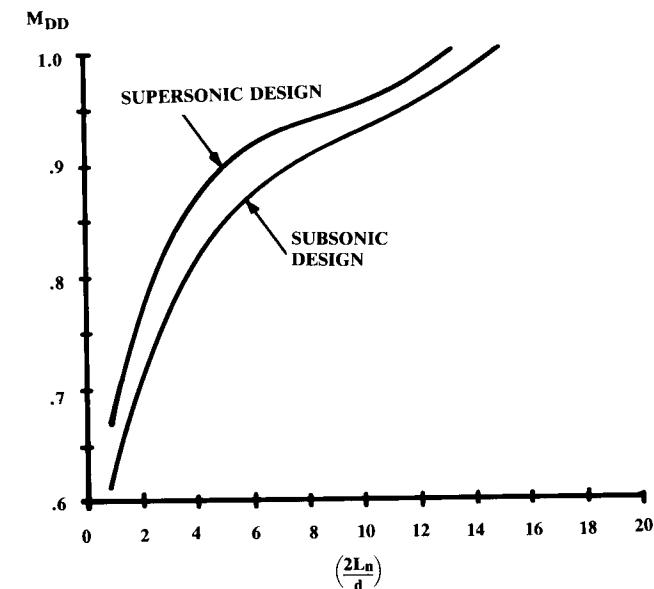


Fig. 12.28 Body drag-divergent Mach number.





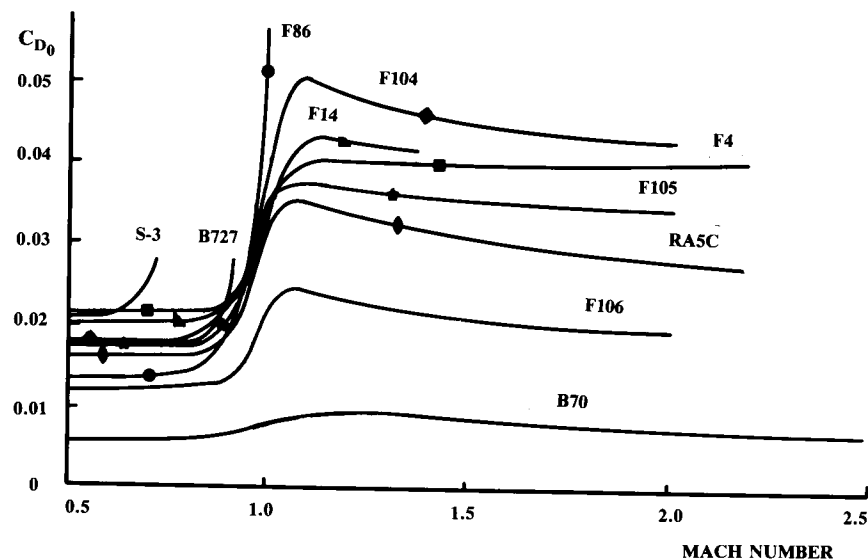


Fig. 12.31 Parasite drag and drag rise.

sented for subsonic monoplanes and biplanes along with an empirical equation for supersonic speeds.

The second method for the estimation of  $K$  is based upon the concept of leading-edge suction and provides, for high-speed designs, a better estimate of  $K$ , one that includes the effects of the change in viscous separation as lift coefficient is changed. This method also reflects the choice of the wing design lift coefficient on the drag due to lift at different lift coefficients.

#### Oswald Span Efficiency Method

According to classical wing theory, the induced-drag coefficient of a 3-D wing with an elliptical lift distribution equals the square of the lift coefficient divided by the product of aspect ratio and  $\pi$ . However, few wings actually have an elliptical lift distribution. Also, this doesn't take into account the wing separation drag.

The extra drag due to the nonelliptical lift distribution and the flow separation can be accounted for using  $e$ , the "Oswald span efficiency factor." This effectively reduces the aspect ratio, producing the following equation for  $K$ .

$$K = \frac{1}{\pi A e} \quad (12.48)$$

The Oswald efficiency factor is typically between 0.7 and 0.85. Numerous estimation methods for  $e$  have been developed over the years, such as those by Glauert and Weissinger. These tend to produce results higher than the  $e$  values of real aircraft. More realistic estimation equations based upon actual aircraft (Ref. 45) are presented below.

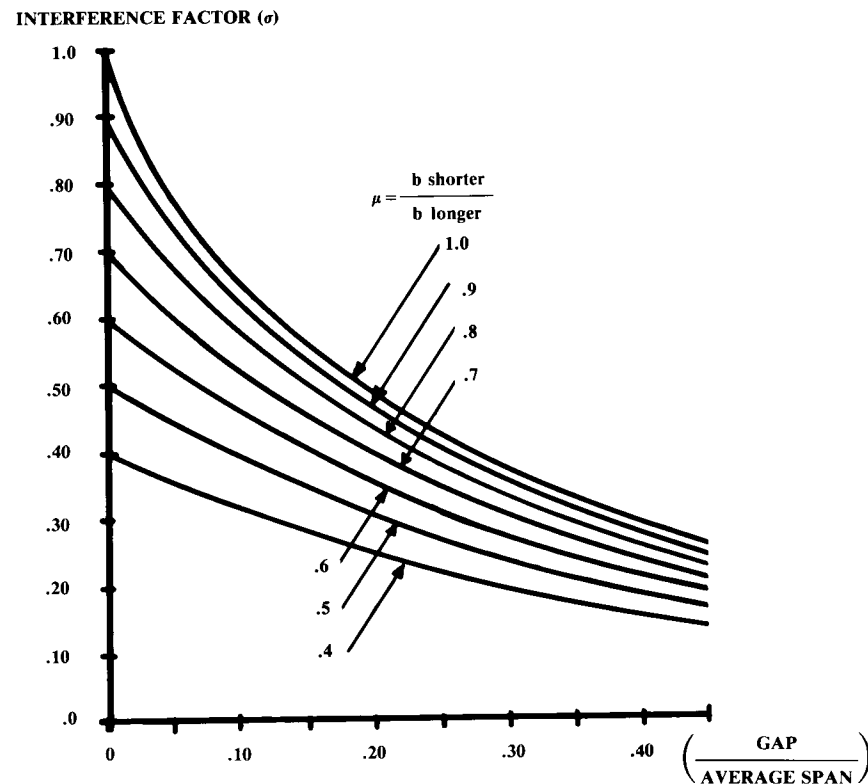


Fig. 12.32 Prandtl's biplane interference factor. (Ref. 12)

$$\text{Straight-Wing Aircraft: } e = 1.78(1 - 0.045A^{0.68}) - 0.64 \quad (12.49)$$

$$\text{Swept-Wing Aircraft: } e = 4.61(1 - 0.045A^{0.68})(\cos \Lambda_{LE})^{0.15} - 3.1 \quad (12.50)$$

$$(\Lambda_{LE} > 30 \text{ deg})$$

If the wing has end-plates or winglets, the effective aspect ratio from Eq. (12.10) or (12.11) should be used in Eq. (12.48).

Drag-due-to-lift for a biplane was first analytically determined by Max Munk in 1922, based upon the calculation of an equivalent monoplane span providing the same wing area and the same drag.

Prandtl developed an interference factor ( $\sigma$ , shown in Fig. 12.32) that is used in Eq. (12.51) to determine a biplane span efficiency factor (Ref. 12). The biplane aspect ratio is the square of the longer span divided by the total area of both wings.

$$\text{Biplane: } e = \frac{\mu^2(1 + r^2)}{\mu^2 + 2\sigma\mu r + r^2} \quad (12.51)$$

where

$\mu$  = shorter span/longer span

$r$  = lift on shorter wing/lift on longer wing

(approximately = area of shorter wing/area of longer wing)

At supersonic speeds, the drag-due-to-lift factor ( $K$ ) increases substantially. In terms of Oswald efficiency factor,  $e$  is reduced to approximately 0.3–0.5 at Mach 1.2. Equation (12.52) provides a quick estimate of  $K$  at supersonic speeds (Ref. 6), although the leading-edge suction method presented later is preferable.

$$\text{Supersonic Speeds: } K = \frac{A(M^2 - 1)}{4A\sqrt{M^2 - 1} - 2} \cos \Lambda_{LE} \quad (12.52)$$

### Leading-Edge-Suction Method

Drag at angle of attack is strongly affected by viscous separation. At high lift-coefficients the drag polar breaks away from the parabolic shape represented by a fixed value of  $K$  in Eq. (12.4). The  $e$  method ignores this variation of  $K$  with lift coefficient. For a wing with a large leading-edge radius this is acceptable, but for most supersonic aircraft it gives a poor approximation.

A semi-empirical method for estimation of  $K$  allows for the variation of  $K$  with lift coefficient and Mach number; it is based upon the concept of “leading-edge suction.” Figure 12.33 illustrates the concept. The thick airfoil on the left is at an angle of attack below that at which substantial separation occurs. The flow streamlines curve rapidly to follow the leading-edge radius over the top of the wing.

This rapid curvature creates a pressure drop on the upper part of the leading edge. The reduced pressure exerts a suction force on the leading-edge in a forward direction. This “leading-edge suction” force  $S$  is shown at the bottom of the figure in a direction perpendicular to the normal force  $N$ .

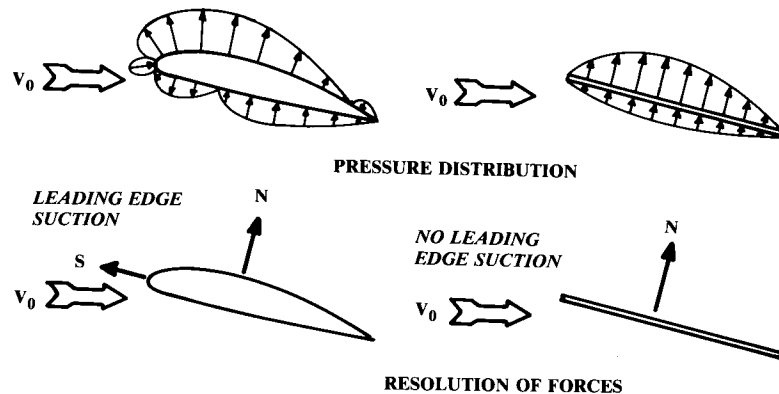


Fig. 12.33 Leading edge suction definition.

If there is no viscous separation or induced downwash, the leading-edge suction force exactly balances the rearward component of the normal force and the airfoil experiences zero drag. This is the ideal 2-D case described by d'Alembert's Paradox, and is called “100% leading-edge suction.”

A 3-D wing is considered to have 100% leading-edge section when the Oswald efficiency factor ( $e$ ) exactly equals 1.0. When  $e$  equals 1.0, the induced-drag constant  $K$  exactly equals the inverse of the aspect ratio times  $\pi$ .

On the right side of Fig. 12.33 is a zero-thickness flat plate airfoil. Even without the leading-edge separation, which will almost certainly occur, this airfoil must have higher drag because there is no forward-facing area for the leading-edge pressure forces to act against. All pressure forces for a zero-thickness flat plate must act in a direction perpendicular to the plate, shown as  $N$ . There is zero leading-edge suction, and the lift and induced drag are simply  $N$  times the cosine or sine of the angle of attack [Eqs. (12.53) and (12.54)].

$$L = N \cos \alpha \quad (12.53)$$

$$D_i = N \sin \alpha = L \tan \alpha \quad (12.54)$$

or

$$C_{D_i} = C_L \tan \alpha \quad (12.55)$$

but (assuming  $\alpha$  is small),

$$C_{D_i} = KC_L^2 \cong \alpha C_L \quad (12.56)$$

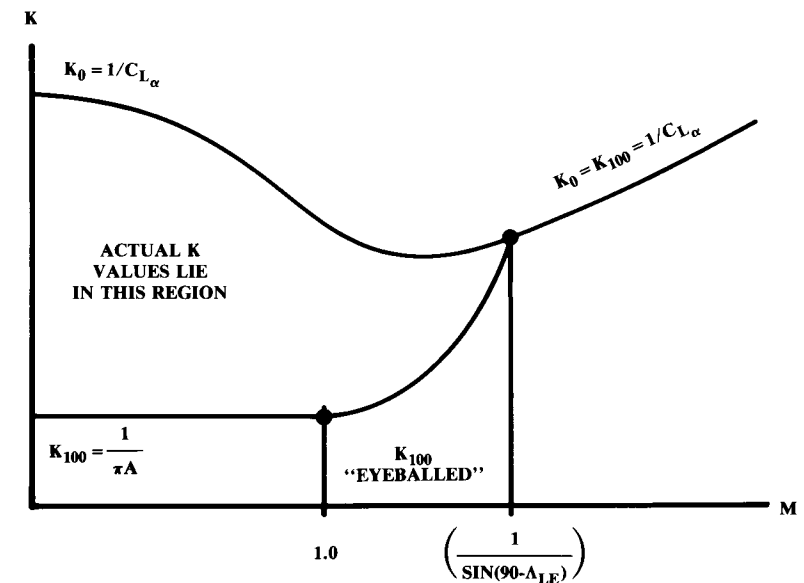


Fig. 12.34 0% and 100%  $K$  vs Mach number.

so,

$$K = \frac{\alpha C_L}{C_L^2} = \frac{\alpha}{C_L} = \frac{1}{C_{L\alpha}} \quad (12.57)$$

Thus, in the worst case of zero leading-edge suction, the drag-due-to-lift factor  $K$  is simply the inverse of the slope of the lift curve (in radians), as previously determined.

All real wings operate somewhere between 100 and 0% leading-edge suction. The percent of leading-edge suction a wing attains is called  $S$  (not to be confused with the force  $S$  in Fig. 12.33).

During subsonic cruise, a wing with moderate sweep and a large leading-edge radius will have  $S$  equal to about 0.85–0.95 (85–95% leading-edge suction). The wing of a supersonic fighter in a high- $g$  turn may have an  $S$  approaching zero.

The method below for calculating  $K$  for high-speed aircraft is based upon an empirical estimate of the actual percent of leading-edge suction attainable by a wing, which is then applied to the calculated  $K$  values for 100 and 0% leading-edge suction. The actual  $K$  is calculated as a weighted average of the 100 and 0%  $K$ , as in Eq. (12.58).

$$K = SK_{100} + (1 - S)K_0 \quad (12.58)$$

The 0%  $K$  value is the inverse of the slope of the lift curve, as determined before. The 100%  $K$  value in subsonic flight is the inverse of the aspect ratio times  $\pi$ .

In transonic flight, the shock formation interferes with leading-edge suction. This increases the  $K$  value. When the leading-edge becomes supersonic, the suction goes to zero so the  $K$  value equals the 0%  $K$  value.

This occurs at the speed at which the Mach angle ( $\arcsine 1/M$ ) equals the leading-edge sweep. Above that speed the wing has zero leading-edge suction so the  $K$  value is always the inverse of the slope of the lift curve.

For initial analysis, the supersonic behavior of the 100%  $K$  line may be approximated by a smooth curve, as shown in Fig. 12.34. This shows the typical behavior of the 100 and 0%  $K$  values vs Mach number.

The only unknown remaining is the value of  $S$ , the percent of leading-edge suction actually attained by the wing at the flight condition in question.  $S$  depends largely upon the leading-edge radius, and is also affected by the sweep and other geometric parameters.

$S$  is also a strong function of the wing design lift coefficient and the actual lift coefficient. For any wing, the value of  $S$  is at a maximum when the wing is operating at the design lift coefficient. For most wings,  $S$  equals approximately 0.9 when operating at the design lift coefficient.

For a subsonic wing with large leading-edge radius and moderate sweep, the value of  $S$  will change very little with lift coefficient until the wing is near the stall angle of attack. For this reason, the induced drag for this type of wing can reasonably be estimated using the  $e$  method.

For the thin, swept wings typical in supersonic aircraft, the value of  $S$  can change substantially with lift coefficient. A wing with an  $S$  of 0.9 at its

design lift coefficient of 0.5 may have an  $S$  value less than 0.3 at a lift coefficient of 1.0.

Proper calculation of  $S$  for an actual wing is complex. An empirical approach may be used during conceptual design. Figure 12.35 provides a first-order estimate of the percent of leading-edge suction for a typical supersonic aircraft's wing, given the actual lift coefficient and the design lift coefficient (this determines which curve to use). Note that this chart assumes a well-designed wing, and at some later date the aerodynamics department must optimize the twist and camber to attain these values.

From Fig. 12.35 the leading-edge suction at various lift coefficients can be estimated. This allows adding curves to Fig. 12.34 that represent the estimated  $K$  value for different lift coefficients as a function of Mach number, as in Fig. 12.36. These are then used for total drag estimation via Eq. (12.4).

For the sake of comparison, Eqs. (12.59) and (12.60) relate  $S$  to  $e$  and  $\Delta N$  (used in several other textbooks).

$$e = \frac{1}{(\pi A / C_{L\alpha})(1 - S) + S} \quad (12.59)$$

$$\Delta N = S \left( \frac{1}{C_{L\alpha}} - \frac{1}{\pi A} \right) \quad (12.60)$$

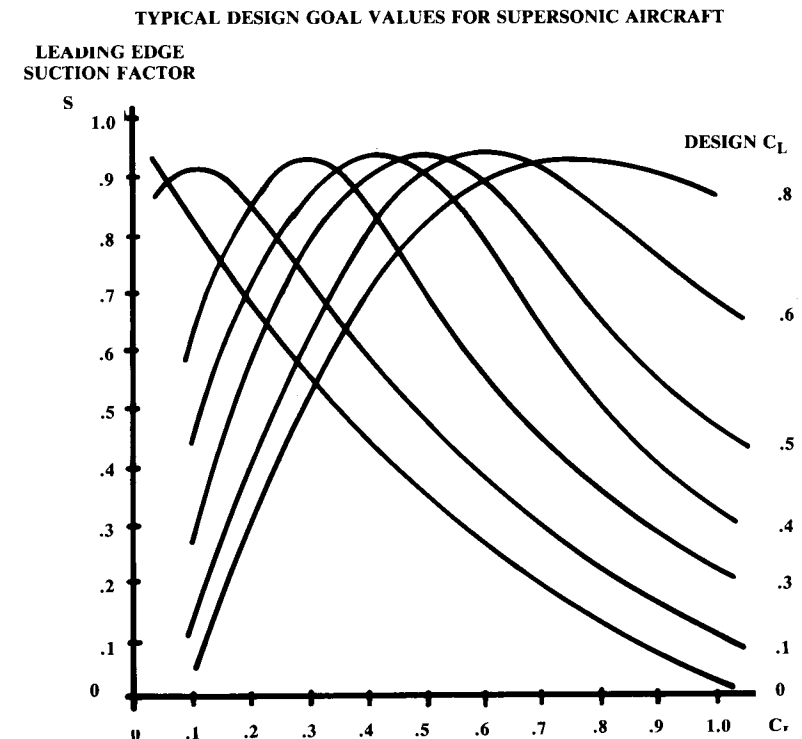


Fig. 12.35 Leading edge suction vs  $C_L$ .

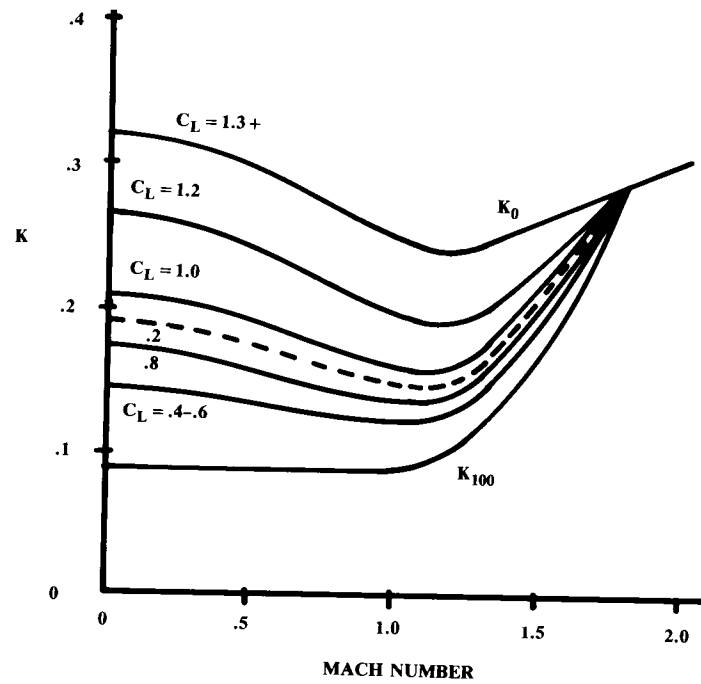


Fig. 12.36 Sample results— $K$  vs Mach and  $C_L$ .

### Ground Effect

When a wing is near the ground, say less than half the span away, the drag due to lift ( $K$ ) can be substantially reduced. This is theoretically explained as a reduction in the induced downwash angle, but can be visualized as a trapping of a “cushion of air” under the wing. This effect is accounted for by multiplying  $K$  by the factor calculated in Eq. (12.61) (Ref. 70).

$$\frac{K_{\text{effective}}}{K} = \frac{33(h/b)^{1.5}}{1 + 33(h/b)^{1.5}} \quad (12.61)$$

where  $h$  is wing height above ground.

### Trim Drag

The drag values used for performance calculations should include the trim drag. This additional induced drag is caused by the horizontal tail force required to balance (trim) the aircraft so that the total pitching moment about the aircraft c.g. will be zero for any given flight condition.

The tail usually trims the aircraft with a download that must be countered by additional lift from the wing. This produces an increase in the wing induced drag that must also be included in the trim drag.

Trim calculation is discussed in Chapter 16. The trim drag is determined using the above induced-drag methods once the tail lift force required for trim is known.

## 12.7 AERODYNAMIC CODES AND COMPUTATIONAL FLUID DYNAMICS (CFD)

### Industry Practice for Aerodynamic Estimation

The aerodynamic methods presented above do not reflect current industry practice. Aircraft companies rely upon linearized computer codes such as the Harris wave-drag code, the Sommer and Short skin-friction code, and one of several panel codes such as USSAERO for induced effects. Newer panel codes such as PANAIR and QUADPAN are used to estimate the induced effects and the wave drag simultaneously and with better accuracy than the older codes.

These linearized computer codes can provide correct results only when the airflow around the aircraft is steady, unseparated, and does not contain any strong vortices. This is typically true only during cruising flight. Lift and drag at high angles of attack are estimated empirically using correlations to flight-test and wind-tunnel data for similar configurations.

The same is true for transonic lift and drag, where some of the very terms which are thrown away to linearize the equations are the longitudinal velocity-variation terms that produce the transonic shocks. Linearized wave-drag codes tend to over estimate the wave drag from Mach 1.0 to about Mach 1.2, and incorrectly predict zero drag rise below Mach 1.0. Empirical data is therefore used for the transonic regime.

Despite these problems, the standard industry practice of combining linearized computer codes with empirical data and corrections will produce good results in most cases. Actual flight-measured values of lift and drag are usually within about 2–10% of the estimates. Also, the estimates are the most accurate for the cruise portions of the flight where the most fuel is burned.

However, the fact that we can estimate a given design's lift and drag with reasonable accuracy does not guarantee that these methods will produce the best of all possible designs. Aerodynamic design has had to rely upon a trial-and-error process of design, analyze, test, and redesign.

Wind-tunnel testing offers a powerful tool for aircraft development. Unfortunately, the costs associated with detailed wind-tunnel testing tend to preclude an exhaustive evaluation of all possible designs. At a cost of several hundred thousand dollars per model, one is not likely to try something different just to see if it is better than the baseline design. Instead, the wind-tunnel is largely used to verify that a given design is workable.

It is sometimes difficult to identify the source of a problem during a wind-tunnel investigation because the wind tunnel “solves” all the flow equations simultaneously (i.e., viscous effects, vortex flow, induced effects, etc.). An unacceptable wiggle in the pitching-moment curve may be due to one of a number of causes, and the wind tunnel may not tell you which cause to fix!

Another problem with wind-tunnel testing is the Reynolds-number effect. Most wind tunnels cannot test at anything close to full-scale Reynolds numbers, resulting in substantial errors. Even worse, the optimal solution at a lower Reynolds number may not be the optimum at full-scale Reynolds

numbers. Who would propose a full-scale test on an airfoil or complete aircraft design that is known to be less-than-optimal in the wind tunnel?

### CFD Definitions

It is for these reasons that Computational Fluid Dynamics (CFD) has rapidly become a key part of the aircraft design process. CFD is a catch-all phrase for a number of new computational techniques for aerodynamic analysis. It differs from prior aerodynamic codes by solving for the complete properties of the flowfield around the aircraft, rather than only on the surface of the aircraft.

CFD codes are based upon the Navier-Stokes (NS) equations, which were first derived in 1822. The NS equations completely describe the aerodynamics of a fluid (except for chemical-reaction effects at high temperatures).

NS includes equations based upon the existence of flow continuity, the conservation of momentum, and the conservation of energy. These are derived in many textbooks on theoretical and computational aerodynamics, and will not be repeated here.

The NS equations seem straightforward enough but cannot be analytically solved for any useful flow conditions. The author of Ref. 80 describes them as “some of the nastiest differential equations in theoretical physics.”

The history of theoretical aerodynamics to date can largely be described as the quest for solvable simplifications of the NS equations. The classical lifting-line theory is one such simplification, as are the linearized wave-drag and panel codes, the Euler Codes, and the various NS codes.

There is a complete hierarchy of aerodynamic codes depending upon how many flow phenomena are neglected from the full NS equations. No current codes attempt to actually solve the true, full NS equations, due to the difficulty in mathematically analyzing turbulence. Turbulence occurs at the molecular level, which would probably require gridding the flowfield with billions of molecule-sized grids.

The current so-called “Navier-Stokes Codes” actually use a simplification in the handling of turbulence, which is the most difficult flow phenomena to analyze mathematically. Turbulence is handled with some type of separate statistically-calibrated model apart from the NS solution.

The most sophisticated codes to date, the “Large Eddy Simulation” codes, use a statistically-based turbulence model for small-scale turbulence effects. Large Eddy codes are capable of directly analyzing the larger turbulent eddies. The Large Eddy Simulation is beyond the capabilities of current computers for a complex aircraft configuration, but has been used for simplified geometries.

The current state of the art for complex aircraft configurations, the “Reynolds-Averaged Navier-Stokes,” has both large and small eddies (turbulence) modeled statistically. Reynolds-Averaged codes can handle most of the complex flow phenomena that elude linearized codes, including vortex formation, separation, transonic effects, and unsteady effects.

Reynolds-Averaged codes are being used on the National Aerospace Plane (NASP) project to solve particular design problems where no other methods can give correct results. Unfortunately, Reynolds-Averaged codes are extremely expensive to set up and run. One recent example took 20 hours

on a Cray XMP-22 to yield results at one Mach number, altitude, angle of attack, and angle of sideslip. Because of the expense these codes are not yet useful for routine design work.

The NS simplification emerging as the workhorse for design analysis, the “Parabolized Navier-Stokes” (PNS), drops the viscous terms in the streamwise direction, which ignores streamwise separation effects. However, with a good turbulence model the PNS codes give correct and illuminating results for most design problems.

If all viscosity effects are ignored and the flow is assumed to be steady, the Euler equations are derived from the NS equations. Euler codes are much cheaper to run than even PNS codes, and are widely used at this time. The Euler codes can handle vortex formation, and with the addition of a separate boundary-layer code, can also realistically estimate viscous and separation effects.

The “Potential Flow” equations are further simplified from the Euler equations by dropping the rotational terms. This prevents the analysis of vortex flow, which is important at high angles of attack but is of lesser importance during cruise conditions. Potential Flow codes can handle transonic shock formation and are very useful for transonic design compared to the linearized methods. The Potential Flow codes are not usually considered to be true “CFD,” but are probably the most widely-used aerodynamic codes that treat the entire flowfield rather than just the surface conditions.

The “Linearized” aerodynamic codes are based upon a further simplification to the Potential Flow equations by neglecting the higher-order terms. It is assumed that, since they involve small quantities multiplied by other small quantities, they must be very small and therefore negligible. At transonic speeds, however, these terms are not so small!

The Linearized Potential Flow equations are the basis of the standard industry methods described at the beginning of this section. These include the Harris Wave Drag and the USSAERO and similar panel methods. With further simplifications, such classical methods as the lifting-line theory are derived.

To recap, only the Large Eddy, Reynolds-Averaged, and PNS codes are considered to be true “Navier-Stokes” codes. However, the Euler, Potential Flow, and Linearized aerodynamic codes are in fact successive simplifications of the NS equations. The choice of code for a given design problem depends upon the nature of the problem and the available budget (and not always in that order!).

### Applications of CFD

CFD does not replace the wind tunnel. In fact, it really doesn’t even reduce the number of wind-tunnel test hours. CFD does permit you to design a better airplane by a truer understanding of the flow field around it. Not only do the CFD codes determine the entire flowfield around the aircraft, but also, unlike the wind tunnel, the flowfield determination is done at the full-scale Reynolds number.

A perfect example of the use of CFD can be found at every major commercial airport in the country. The installation of the fuel-efficient CFM-56

engine on the Boeing 737 would not have been possible without the use of CFD, as described in Ref. 80.

The original Boeing 737 used the P&W JT8D, a low-bypass-ratio engine that was mounted in a wing-conformal nacelle. The nacelle barely cleared the ground, providing a minimum-weight landing gear.

When Boeing decided to develop an updated version of the 737, the CFM-56 engine was the logical choice as a modern fuel-efficient engine of the required thrust class. However, it has a diameter some 20% greater than the old engine. Furthermore, the CFM-56 exits its fan air up front like most modern turbofans. For this reason, a wing-conformal nacelle was not possible.

In a prior chapter, the cited rough rule of thumb for podded jet nacelles said that the inlet should be about two inlet diameters forward of the wing and about one inlet diameter below it. A more-refined empirical method of locating a turbofan engine indicated that the geometry shown in Fig. 12.37a was the closest acceptable nacelle spacing. Clearly this posed a ground clearance problem!

The empirical rules for nacelle spacing were based upon years of trial and error in the wind tunnel. Closer spacings were found to increase cruise drag, although the wind-tunnel investigations had not clearly determined just exactly what this "interference" drag consisted of. Various suspects included increased skin friction due to supersonic velocity, increased separation, shock effects, and a change in the wing's spanwise lift distribution resulting in an increase in the induced drag.

Through the use of a nonlinear potential flow panel program (CFD state of the art in the 1970's), Boeing was able to determine that it was in fact the induced drag effect that was creating the "interference drag." This important piece of information had not been determined in 20 years of wind-tunnel testing!

With this information, Boeing was then able to contour a closely-spaced podded nacelle to prevent any change in the wing's spanwise lift distribution. This was possible with CFD because the entire flowfield is solved, allowing the designers to study the streamlines and pressure fields resulting from various design changes. The designers sought to minimize the impact of the nacelle on the streamlines of the bare wing.

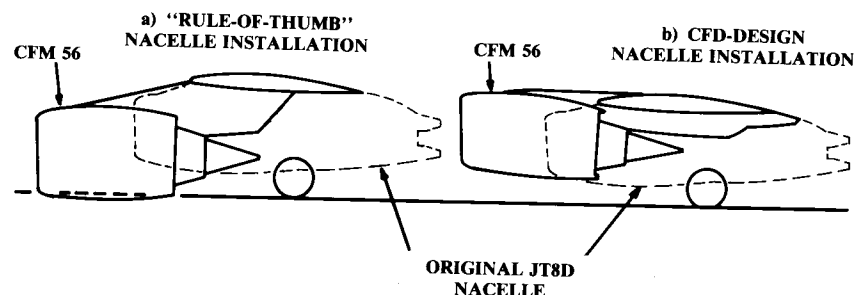


Fig. 12.37 CFD example: Boeing 737 nacelle (after R. Bengelink, AIAA Paper 88-2043).

Figure 12.37b shows the result, namely, a nacelle of extremely close spacing to the wing that, nevertheless, has acceptable drag characteristics.

The formation and effects of vortices at high angles of attack represent another area of substantial concern to the designers of fighter aircraft. These vortices produce completely different lift, drag, and pitching-moment characteristics than those which would be predicted using the linear methods.

Reference 81 details the CFD solution of a typical vortex-flow problem using a Lockheed Euler code called TEAM (Three-Dimensional Euler Aerodynamic Method). Figure 12.38 (reprinted with permission) shows the close match between the calculated and the measured pressures over the double-delta configuration used in the study. The vortex region can be seen by the diagonal pressure contours in both calculated and measured plots.

Figure 12.39 illustrates the power of CFD to fully analyze the flowfield around the aircraft rather than just at the surface. Arrows are used to depict the flowfield at four longitudinal locations on the aircraft. The length of the arrows shows the relative magnitudes of the flow velocity in the plane of the cross section. The vortex flow is clearly seen beginning inboard toward the

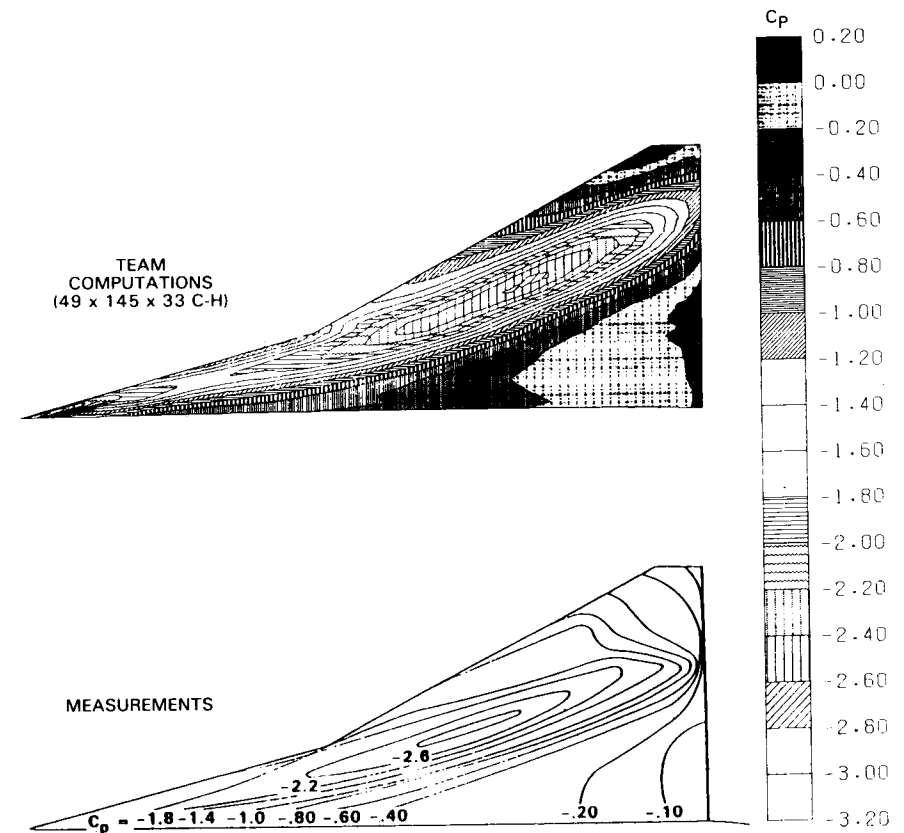


Fig. 12.38 Correlation of computed and measured surface pressure contours; 75°/62° double-Delta wing body;  $M_\infty = 0.3$ ;  $\alpha = 20^\circ$ . (Ref. 81)

front of the wing, and growing and moving outward toward the rear of the aircraft.

### CFD Issues and Challenges

We have come a long ways since 1879 when the annual proceedings of the British Royal Aeronautical Society could say, “Mathematics up to the present day has been quite useless to us in regard to flying” (quoted in Ref. 80). However, there are still many problems associated with the use of CFD

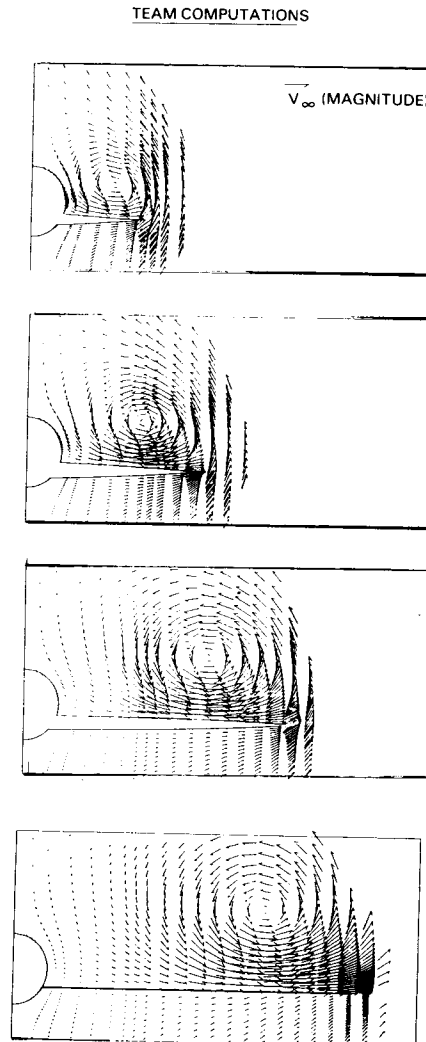


Fig. 12.39 Correlation of computed and measured cross-plate velocity fields;  $75^\circ/62^\circ$  double-Delta wing body;  $M_\infty = 0.3$ ;  $\alpha = 20^\circ$ . (Ref. 81)

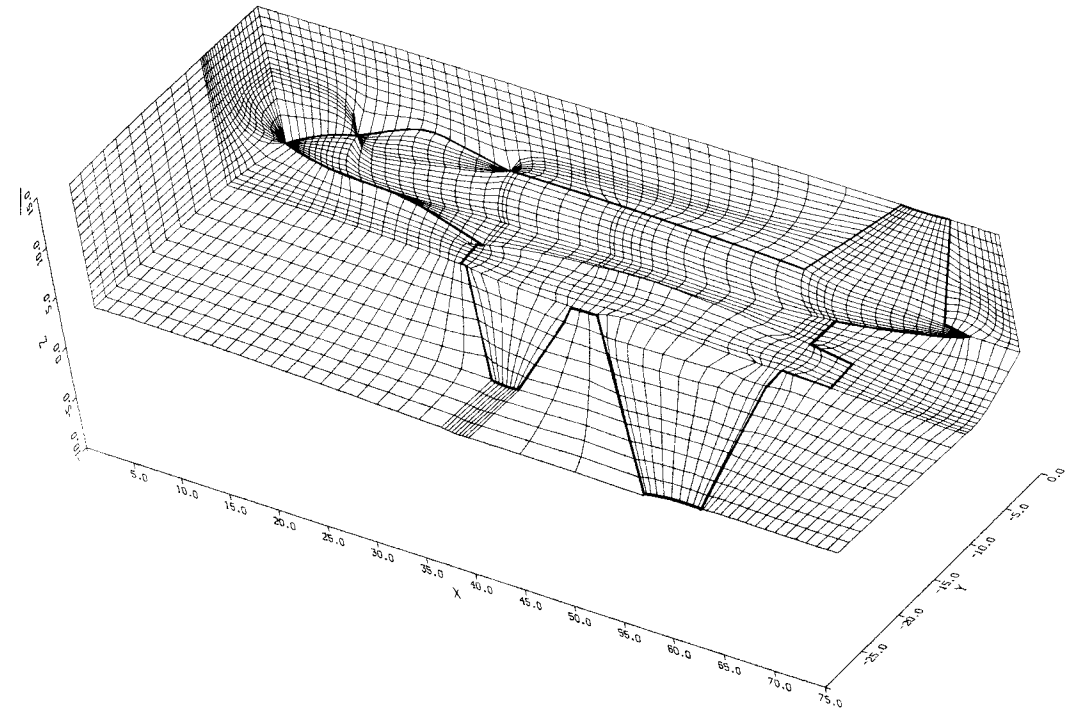


Fig. 12.40 Flowfield gridding. (Ref. 82)

for routinely solving aircraft design problems. Two problems are especially important: the influence of the turbulence model and the requirements for flow gridding.

The use of separate turbulence models for NS codes has been discussed. The results of the various NS codes are very sensitive to the turbulence model used, especially when separated flow is present.

CFD codes tend to produce reasonable-looking flowfields and pressures, but sometimes the integration of the calculated pressures yields lifts, drags, and moments which do not match experience. Reproduction of experimental data sometimes requires extensive “calibration” (i.e., fudging!) of the turbulence model. For this reason, CFD results are always somewhat suspect until the code has been checked against experimental data for a similar configuration.

The need to grid the entire flowfield around the aircraft presents another big problem for CFD users. “Gridding” refers to the breaking up of the space around the aircraft into numerous small blocks, or “cells,” usually of roughly hexahedral shape. CFD methods calculate the flow properties

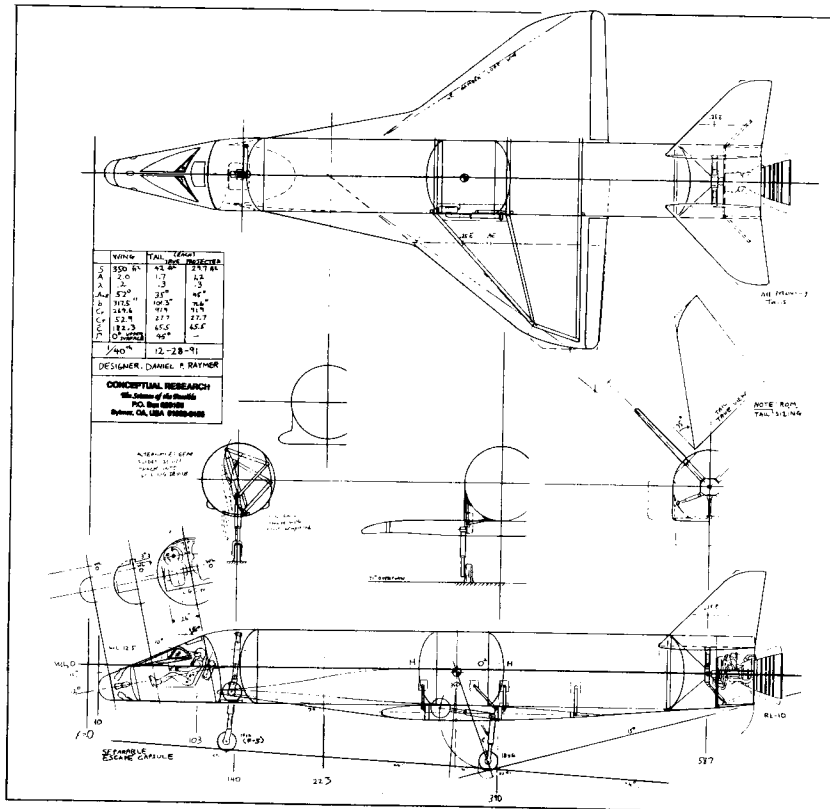


within each cell, using various convergence schemes to equate the flow properties along the boundaries connecting the cells.

While gridding the space around a simple cylinder or a lone wing can be easily automated, the gridding of the flowfield around a full aircraft must currently be done manually and can literally take months. Figure 12.40 (reprinted with permission from Ref. 82) illustrates the complexity of the flowfield gridding. Note, for example, where the canopy meets the fuselage and where the cells must fan out in the empty region between wing and canard.

Gridding is especially important because the CFD results are highly sensitive to the shaping of the cells. You can actually get different answers for the same aircraft using two different gridding schemes. According to the author of Ref. 82, “this sensitivity is more pronounced than that due to the type of mathematical model being used, e.g., NS vs Euler equations.”

To address the gridding problem, researchers are investigating artificial intelligence (AI) approaches to gridding. Another approach is the computationally-adaptive gridding in which the gridding scheme is automatically adjusted based upon the CFD results.



Skyrocket Aerospace Plane Concept

## 13 PROPULSION

### 13.1 INTRODUCTION

All forms of aircraft propulsion develop thrust by pushing air (or hot gases) backward. In a simplified case the force obtained can be determined using Newton's equation ( $F = ma$ ) by summing all the accelerations imparted to the air.

This is shown for fluid flow in Eq. (13.1), where  $s$  is the cross-sectional area of the fluid acted upon by the propulsion system,  $V$  is the fluid velocity, and the zero subscript indicates the freestream condition. The propeller or jet engine is assumed to “magically” accelerate the air from velocity  $V_0$  to  $V$ .

The rate of useful work done by the propulsion system, called the “thrust power ( $P_t$ ),” equals the product of the thrust force and the aircraft velocity [Eq. (13.2)].

The kinetic energy imparted to the fluid by the propulsion system is determined by the difference in fluid velocity, as shown in Eq. (13.3).

The “propulsion efficiency ( $\eta_{PE}$ )” is defined as the ratio of thrust power obtained to energy expended, as shown in Eq. (13.4). Note that the efficiency is maximized when there is no change in fluid velocity. Unfortunately, at this condition Eq. (13.1) shows that the thrust is zero!

$$F = ma = \dot{m}\Delta V = (\rho Vs)(V - V_0) = \rho sV(V - V_0) \quad (13.1)$$

$$P_t = FV_0 = \rho sV(V - V_0)V_0 \quad (13.2)$$

$$\Delta E = \frac{1}{2}\dot{m}V^2 - \frac{1}{2}\dot{m}V_0^2 = \frac{1}{2}\rho Vs(V^2 - V_0^2) = \frac{\rho s}{2}V(V^2 - V_0^2) \quad (13.3)$$

$$\eta_{PE} = \frac{P_t}{\Delta E} = \frac{2}{V/V_0 + 1} \quad (13.4)$$

There is an unavoidable tradeoff between thrust and efficiency as determined by the ratio between exhaust and freestream fluid velocity. For maximum thrust, this ratio must be very high. For maximum efficiency, this ratio should be unity.

If the exhaust velocity is reduced to little more than the freestream velocity for improved efficiency, the cross-sectional area of fluid affected by the

propulsion system must approach infinity to maintain constant thrust. A typical turbojet will operate with the ratio of exhaust velocity to freestream velocity at well above 3.0, whereas a typical propeller aircraft will operate with this ratio at about 1.5.

The analysis above is too simplistic for actual thrust calculation. It falsely assumes that the fluid velocity is constant throughout the exhaust and that all of the accelerations experienced by the airmass occur at the propeller plane or within the jet engine.

Actually, the exhaust of a jet engine is usually at a higher pressure than the outside air, so the flow expands after leaving the nozzle. In other words, the air is still accelerating after the aircraft has passed.

For a propeller, the airmass acceleration doesn't even occur at the propeller disk! Roughly half the airmass acceleration occurs before reaching the propeller, and the other half occurs after passing the propeller.

Propulsion force estimation is also complicated by the fact that the propeller flowfield or jet intake and exhaust will influence the whole flowfield of the aircraft. It has already been mentioned that a pusher propeller will reduce the drag of a stubby aft fuselage by "sucking" air inward and preventing flow separation. Should this reduced drag be considered a part of the propulsive force because it is controlled with the throttle? What about the increased drag due to the propeller wake on a conventional airplane?

For a propeller aircraft, most of the propulsive force is exerted directly on the aircraft by the pull (or push) of the propeller itself through the propeller shaft. The propeller shaft is usually connected to the engine so the engine mounts actually pull (or push) the rest of the aircraft through the air.

For a jet aircraft the force exerted through the engine mounts may only be a third of the total propulsive force. Figure 13.1 shows the thrust contributors for a typical Mach 2.2 nacelle. The engine itself only contributes about 8% of the total. The nozzle, which generates thrust by expanding the high-pressure engine exhaust, contributes almost 30%.

The inlet system uses a system of shocks to slow the air to a subsonic speed. This creates a substantial drag. However, the subsonic expansion inside the inlet duct contributes a positive force that more than makes up

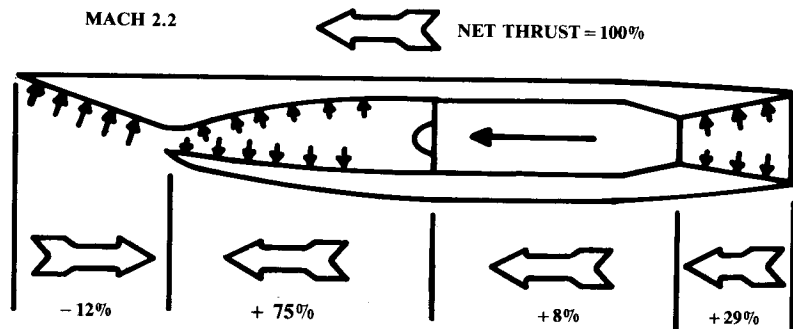


Fig. 13.1 Turbojet thrust contributors.

for the external inlet system drag. In fact, the subsonic expansion inside the inlet duct is the largest single contributor of thrust! This illustrates the difficulty of calculating thrust by any simple model.

This chapter provides methods for estimating the net thrust provided by a propeller or jet engine as a part of the overall vehicle analysis and optimization. These methods are simplified to permit experiencing the whole design process within the time devoted to the typical college design course. The chapter will also introduce the vastly more complicated process of installed-thrust estimation used at major aerospace firms. Reference 46 (highly recommended) provides a detailed treatment of jet-engine design and installation.

### 13.2 JET-ENGINE THRUST CONSIDERATIONS

Before we begin the discussion of jet-engine installed thrust, a brief introduction to jet-engine cycle analysis and its effect on design is in order. As mentioned in Chapter 10 and shown in Fig. 10.1, a jet engine develops thrust by taking in air, compressing it (via the inlet duct and the compressor), mixing in fuel, burning the mixture, and expanding and accelerating the resulting high-pressure, high-temperature gases out the rear through a nozzle.

To provide power to drive the compressor, a turbine is placed in the exhaust stream which extracts mechanical power from the high-pressure gases. If greater thrust is required for a short period of time, an afterburner can be placed downstream of the turbine permitting the unburned air in the turbine exhaust to combust with additional fuel and thereby increase the exhaust velocity.

"Gross thrust" is produced as a result of the total momentum in the high-velocity exhaust stream. "Net thrust" is calculated as the gross thrust minus the "ram drag," which is the total momentum in the inlet stream. Note that the ram drag, which results from the deceleration of the air taken into the inlet, is included in the engine cycle analysis performed by the engine manufacturer to determine net uninstalled thrust.

Jet-engine cycle analysis, as detailed in Ref. 46 and other propulsion texts, is the straightforward application of the laws of thermodynamics to this Brayton engine cycle. In an "ideal" analysis, the efficiencies of components such as compressors and turbines are assumed to be 100%, i.e., no losses, and the resulting thrust for a given fuel flow, altitude, and Mach number is calculated. While optimistic, such ideal cycle analysis produces results in the "right ballpark" and illustrates the trends produced by varying such cycle parameters as overall pressure ratio, turbine inlet temperature, bypass ratio, and flight condition. These are discussed below.

One over-riding factor in the determination of jet-engine performance is that the net thrust produced is roughly proportional to the air mass flow (velocity  $\times$  air density  $\times$  airflow cross section) entering the engine. For a modern afterburning turbojet engine, roughly 126 pounds of thrust (the "specific net thrust") is developed for each pound per second of air taken in by the engine. For a turbofan engine, a specific net thrust of roughly 40–60 can be obtained.

An increase in air density such as at low altitude or low outside air temperature would therefore increase thrust by increasing mass flow. Hot day takeoffs from a high-elevation airport such as Denver pose problems because the reduction in air density causes a reduction in mass flow, and hence, thrust.

Similarly, an increase in aircraft velocity also increases thrust due to ram effect increasing the mass flow. However, for a typical subsonic jet, the exhaust comes out the nozzle at a choked condition, and so the exit velocity equals the speed of sound regardless of aircraft velocity. As aircraft velocity approaches the speed of sound, the thrust is therefore reduced for the choked exit nozzle [see Eq. (13.1)]. When combined with the favorable ram effect, this results in a relatively constant thrust as velocity increases for the typical subsonic jet, dropping off as transonic speeds are reached.

For supersonic jet engines, a variable area, converging-diverging nozzle is typically employed which permits supersonic exhaust velocities. Therefore, the ram effect does cause the thrust to tend to increase with increasing velocity until at high Mach numbers where excessive total pressure losses occur in the inlet, resulting in thrust degradation. The Mach number at which inlet losses become excessive is determined by the number of shocks and the extent of variable geometry employed, as described in Chapter 10.

Thrust and propulsive efficiency are strongly affected by the engine's overall pressure ratio (OPR). OPR is the ratio of the pressures at the engine exhaust plane and inlet front face. This pressure ratio is a measure of the engine's ability to accelerate the exhaust, which produces thrust. OPRs usually range from about 15 to 1 to about 30 to 1.

Another key parameter which currently limits turbine engine performance is the turbine inlet temperature (TIT). As mentioned earlier, it would be desirable for maximum thrust and efficiency to combust at the stoichiometric air-fuel ratio of about 15 to 1. This produces temperatures far too high for current turbine materials, even using the best available cooling techniques. Instead, a "lean" mixture of about 60 to 1 (air to fuel) is used, with the extra air holding down the TIT to about 2000–2500°F. This results in less thrust and thermal efficiency, and so a key objective in propulsion technology development has always been the increase in allowable TIT.

To increase propulsive efficiency, the turbofan engine uses an oversized fan with some of the accelerated fan air "bypassed" around the engine, not being used for combustion. This has the effect of allowing the engine to accelerate a larger cross-sectional area of air by a smaller change in velocity, which increases efficiency as determined by Eqs. (13.1) and (13.4). The bypass ratio was defined in Chapter 10 as the ratio of the mass flows of the bypassed air and the air that goes through the core of the engine to be used for combustion.

A higher bypass ratio, which enables the engine to accelerate a larger cross section of air, produces higher efficiency and hence greater thrust for a given expenditure of fuel. However, the fan alone cannot efficiently accelerate the air to transonic or supersonic exit speeds, and so this favorable effect works only at lower speeds. As was shown in Fig. 10.2, the high-bypass turbofan is best at subsonic speeds, giving way to the low-bypass ratio turbofan at the low supersonic speeds. At higher supersonic speeds, say over about Mach 2.2, the pure turbojet is superior.

### 13.3 TURBOJET INSTALLED THRUST

Chapter 10 described statistical methods for estimating installed thrust and specific fuel consumption for jet engines. These are suitable for initial sizing and performance estimation. For a more sophisticated analysis it is necessary to estimate analytically the installed performance of an existing engine or a proposed new engine from the uninstalled engine data.

Uninstalled engine data can be obtained from the engine manufacturer. Data for several conceptual engines is summarized in the appendices. For a new-design engine, the data must be estimated using cycle-analysis equations such as in Ref. 46. Usually the designers in an aircraft company will obtain the uninstalled-engine data for a proposed engine from the engine manufacturer, and then will correct the data for installation effects.

It is common early in design studies to approximate the performance of a new-design engine by a "fudge-factor" approach. An existing engine with approximately the same bypass ratio is selected, and its size, weight, and performance data are multiplied by factors based upon the expected improvements by applying advanced technologies.

For example, it might be assumed that an engine designed ten years from now would have 25%-less specific fuel consumption, 30%-less length, and 30%-less weight compared to an existing engine. Such "fudge-factors" are based upon either historical trend analysis or an approximate cycle analysis for expected technology improvements.

It is assumed below that uninstalled-engine data is available, either from an engine manufacturer, a preliminary cycle analysis, or a fudge-factor approach based upon some given engine (such as those in the appendices).

### 13.4 THRUST-DRAG BOOKKEEPING

Bookkeeping is not normally considered an engineering subject. However, the interactions between thrust and drag are so complex that only a bookkeeping-like approach can assure that all forces have been counted once and only once. It is not at all uncommon to discover, halfway through an aircraft design project, that some minor drag item has been either included in both drag and thrust calculations or has been ignored by both departments under the assumption that it is being included by the other!

Each aircraft company develops its own system for thrust-drag bookkeeping. In fact, a different system may be developed for each design project. In most cases the guiding principle for determining whether a force is considered a part of the drag or the thrust is whether that force changes when the throttle setting is changed.

In an afterburning jet engine, for example, the nozzles open wide when the throttle is advanced to the afterburning position. This changes the aerodynamic drag on the outside of the nozzles, so the nozzle aerodynamic drag is counted as a reduction in the engine thrust in many thrust-drag bookkeeping systems.

In other thrust-drag bookkeeping systems, the nozzle drag is separated into two components: (1) the drag value at some fixed nozzle setting (usually full open), which is included in the aerodynamic drag calculation, and

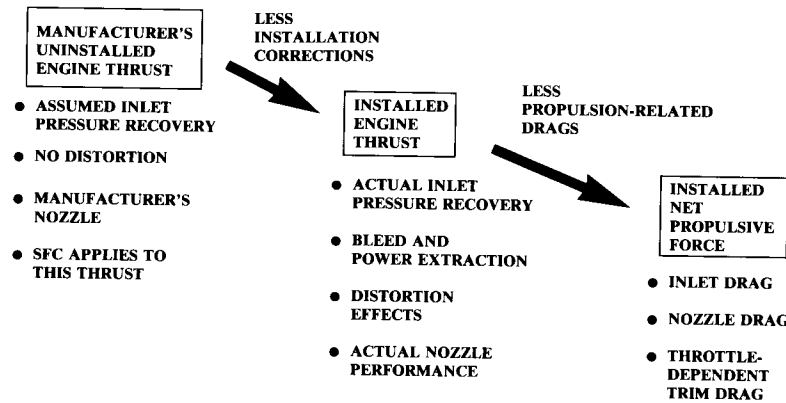


Fig. 13.2 Installed thrust methodology.

(2) the variation of drag as the nozzle setting is changed, which is included in the propulsion-installation calculations.

Either bookkeeping approach will give correct results providing that the Aerodynamics and Propulsion departments both understand it.

Thrust-drag bookkeeping becomes especially complex when sorting out the results of wind-tunnel testing. Different wind-tunnel models are used to test different thrust and drag items. The model used for determining basic aerodynamic and stability derivatives is usually unpowered, and a separate powered model is used to estimate propulsion effects. Lack of a mutually understood bookkeeping system by both the Aerodynamic and Propulsion departments will cause chaos.

The student should realize that the organization of this book assumes a thrust-drag bookkeeping system. Items presented in this chapter as reductions to thrust may be considered to be drag items in another bookkeeping system. Reference 35 contains a detailed review of the subject of thrust-drag bookkeeping.

### 13.5 INSTALLED-THRUST METHODOLOGY

The actual available thrust used in performance calculations—called the “installed net propulsive force”—is the uninstalled thrust corrected for installation effects, minus the drag contributions that are assigned to the propulsion system by the selected thrust-drag bookkeeping system. This is depicted in Fig. 13.2.

The “manufacturer’s uninstalled engine thrust” is obtained by cycle analysis and/or testing, or can be approximated using fudge-factors as described above. The manufacturer’s engine data is based upon some assumed schedule of inlet pressure recovery vs Mach number. Inlet pressure recovery ( $P_1/P_0$ ) is the total pressure at the engine front face (1) divided by the total pressure in the freestream (0).

For subsonic engines, it is frequently assumed that the inlet pressure recovery is perfect, i.e.,  $P_1/P_0 = 1.0$ . For supersonic military aircraft a Mil-Spec formula is used. Inlet distortion, engine bleed, and engine power extraction are usually assumed by the manufacturer to be zero. Also, the engine data is based upon the manufacturer’s nozzle design.

Note that the SFC values supplied with the engine are based upon this uninstalled-engine thrust, not the installed net propulsive force. When determining fuel usage, the SFC values must be ratioed up by the ratio between uninstalled-engine thrust and the net propulsive force (i.e., the thrust required for the desired performance).

The “installed-engine thrust” is the actual thrust generated by the engine when installed in the aircraft. This is obtained by correcting the thrust for the actual inlet pressure recovery and nozzle performance, and applying thrust losses to account for engine bleed and power extraction.

“Inlet distortion” refers to pressure and velocity variations in the air delivered to the engine. It primarily affects the allowable operating envelope of the engine.

The installed net propulsive force is the installed engine thrust minus the inlet, nozzle, and throttle-dependent trim drags. The steps depicted in Fig. 13.2 are detailed below.

#### Installed Engine Thrust Corrections

The manufacturer’s uninstalled engine thrust is based upon an assumed inlet pressure-recovery. For a subsonic engine, it is typically assumed that the inlet has perfect recovery, i.e., 1.0. Supersonic military aircraft engines are usually defined using an inlet pressure-recovery of 1.0 at subsonic speeds and the inlet recovery of Eq. (13.5) (MIL-E-5008B) at supersonic speeds. Added to this is the pressure recovery loss due to internal flow in the inlet duct itself. Typically this adds 2–3% to the losses.

Figure 13.3 shows this reference inlet pressure-recovery plotted vs Mach number, compared to the recovery available for a normal-shock inlet and external compression inlets with one, two, and three ramps.

$$\left(\frac{P_1}{P_0}\right)_{\text{ref}} = 1 - 0.075(M_\infty - 1)^{1.35} \quad (13.5)$$

The external compression inlets of Fig. 13.3 are of movable ramp design with a perfectly optimized schedule of ramp angles as a function of Mach number. To determine the pressure recovery of a fixed or less-than-perfect inlet, the shock tables in the appendix should be used.

The pressure losses inside the inlet duct must also be accounted for. These losses are determined by the length and diameter of the duct, the presence of bends in the duct, and the internal Mach number.

For initial evaluation of a typical inlet duct, an internal pressure recovery of 0.96 for a straight duct and 0.94 for an S duct may be used. The short

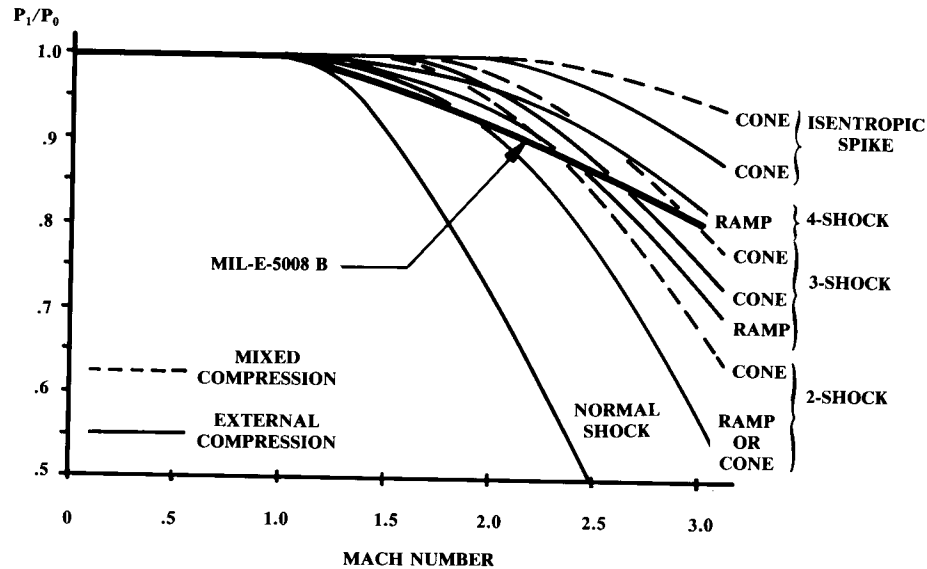


Fig. 13.3 Reference and available inlet pressure recovery.

duct of a subsonic podded nacelle will have a pressure recovery of 0.98 or better. More detailed estimation of inlet internal-pressure loss is based upon experimental data (see Ref. 27), and requires a separate evaluation at each Mach number.

Figure 13.4 provides the actual inlet pressure recoveries of some existing designs. This figure may be used for pressure-recovery estimation during early design studies.

Reducing inlet pressure recovery has a greater-than-proportional effect upon the engine thrust, as shown in Eq. (13.6). The inlet “ram recovery correction factor ( $C_{ram}$ )” is provided by the manufacturer for various altitudes, Mach numbers, air temperatures, and thrust settings. Typically,  $C_{ram}$  ranges from 1.2–1.5. If the manufacturer’s data is not available,  $C_{ram}$  may be approximated as 1.35 for subsonic flight and by Eq. (13.7) for supersonic flight.

$$\text{Percent thrust loss} = C_{ram} \left[ \left( \frac{P_1}{P_0} \right)_{ref} - \left( \frac{P_1}{P_0} \right)_{actual} \right] \times [100] \quad (13.6)$$

$$\text{Supersonic: } C_{ram} \cong 1.35 - 0.15(M_\infty - 1) \quad (13.7)$$

High-pressure air is bled from the engine compressor for cabin air, anti-icing, and other uses. This engine bleed air (not to be confused with inlet boundary-layer bleed and other forms of secondary airflow) exacts a thrust

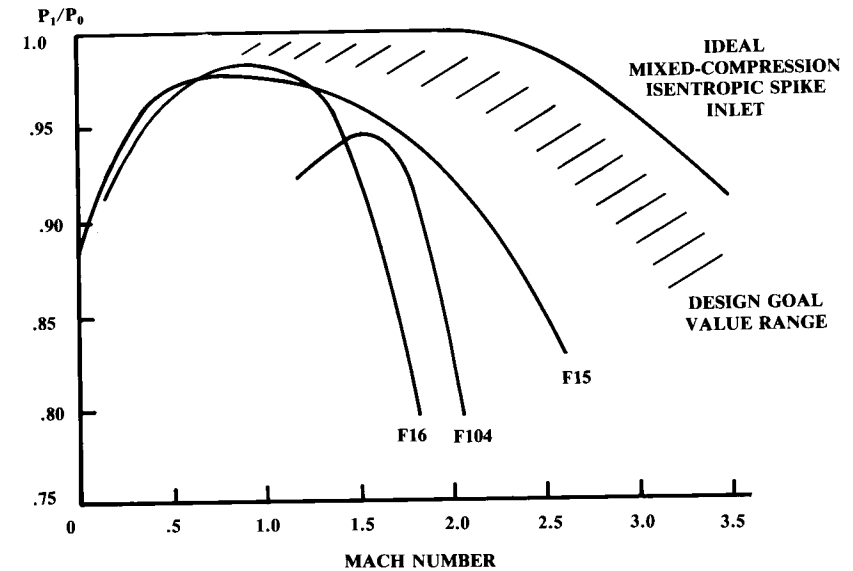


Fig. 13.4 Actual inlet pressure recoveries.

penalty that is also more-than-proportional to the percent of the total engine massflow extracted as bleed air.

Equation (13.8) illustrates this, where the “bleed correction factor ( $C_{bleed}$ )” is provided by the manufacturer for various flight conditions. For initial analysis,  $C_{bleed}$  can be approximated as 2.0. The bleed massflow typically ranges from 1–5% of the engine mass-flow.

$$\text{Percent thrust loss} = C_{bleed} \left( \frac{\text{bleed mass flow}}{\text{engine mass flow}} \right) \times [100] \quad (13.8)$$

Installed engine thrust is also affected by horsepower extraction. Jet engines are equipped with rotating mechanical shafts turned by the turbines. The electrical generators, hydraulic pumps, and other such components connect to these shafts.

This extraction is typically less than 200 hp for a 30,000-lb-thrust engine, and usually has only a small effect upon installed thrust. Horsepower extraction is included in the cycle analysis used for detailed calculation of installed-engine thrust, but can be ignored for initial analysis.

As mentioned, moderate inlet distortion usually has little effect upon installed thrust, but can restrict the engine operating envelope. The effects of distortion are calculated later in the design process. For initial design, the

guidelines previously suggested for location of inlets and for forebody shaping should avoid any later problems with inlet distortion.

Nozzle efficiency has a direct effect upon thrust. However, it is rare to use a nozzle other than that provided by the manufacturer. For cases in which a unique nozzle (such as a 2-D vectoring nozzle) is employed, the new nozzle can usually be designed to provide the same efficiency as the manufacturer's nozzle. (The drag effects of alternate nozzles are discussed later.)

### Installed Net Propulsive Force Corrections

The "installed engine thrust" is the actual thrust produced by the engine as installed in the aircraft. However, the engine creates three forms of drag that must be subtracted from the engine thrust to determine the thrust force actually available for propelling the aircraft. This propelling force, the "installed net propulsive force," is the thrust value to be used for aircraft performance calculations.

Most of the engine-related drag is produced by the inlet as a result of a mismatch between the amount of air demanded by the engine and the amount of air that the inlet can supply at a given flight condition. When the inlet is providing exactly the amount of air the engine demands (mass flow ratio equals 1.0), the inlet drag is negligible.

The inlet must be sized to provide enough air at the worst-case condition, when the engine demands a lot of air. This sets the capture area. Most of the time the engine demands less air than an inlet with this capture area would like to provide (i.e., mass flow ratio is less than 1.0).

When the mass flow ratio is less than 1.0, the excess air must either be spilled before the air enters the inlet or bypassed around the engine via a duct that dumps it overboard (Fig. 13.5) or into an ejector-type engine nozzle.

The drag from air spilled before entering the inlet is called "spillage," or "additive" drag. Additive drag represents a loss in momentum of the air which is slowed and compressed by the external part of the inlet but not used by the engine. The additive drag is determined by calculating, for each flight Mach number and engine mass-flow ratio, the Mach numbers and pressures throughout the inlet and integrating the forces in the flight direction for the part of the air which is spilled.

The spilled air will be turned back toward the freestream direction by the inlet cowl lip, producing a reduced pressure on the cowl. This provides a

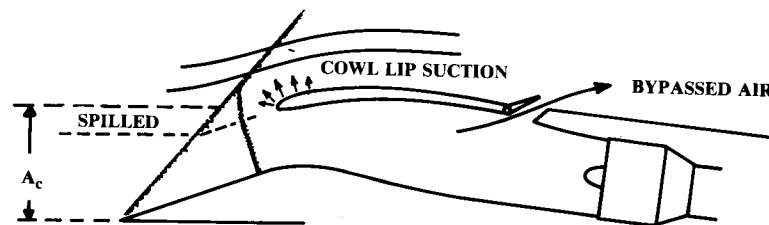


Fig. 13.5 Additive drag, cowl lip suction, and bypass subcritical operation.

suction with a component in the forward direction, i.e., a thrust (as shown in Fig. 13.5). This cowl-lip suction reduces the additive drag by as much as 30–40% in the low-supersonic regime. For a subsonic jet with well-rounded cowl lips, this suction will virtually eliminate additive drag.

Even with cowl-lip suction, the additive drag under certain flight conditions could exceed 20% of the total aircraft drag. A penalty of this magnitude is never seen because the designers resort to inlet-air bypass whenever the additive drag is too great.

Allowing the excess air to enter the inlet and be dumped overboard or into an ejector nozzle, will keep the inlet additive drag to a small value. The resulting bypass drag will be substantially less than the additive drag would have been. Bypass drag is calculated by summing the momentum loss experienced by the bypassed air.

Another form of inlet drag is the momentum loss associated with the inlet boundary-layer bleed. Air is bled through holes or slots on the inlet ramps and within the inlet to prevent shock-induced separation and to prevent the buildup of a thick turbulent boundary layer within the inlet duct. This air is dumped overboard out an aft-facing discharge exit, which is usually located a few feet behind the inlet.

(Note: don't confuse inlet boundary-layer bleed with the inlet boundary-layer diverter. The diverter prevents the fuselage boundary-layer air from entering the inlet. Diverter drag has been accounted for in the aerodynamics chapter.)

Calculation of bleed, bypass, and additive drag including cowl-lip suction is a complicated procedure combining analytical and empirical methods. The textbook methods (see Refs. 26, 27, 25, and 10) are very time-consuming and cannot account for the effects of the actual aircraft geometry, which may greatly affect both the inlet flowfield and the pressure loss through bleed and bypass ducts.

In a major aircraft company such calculations are made by propulsion specialists using complex computer programs. The results are included in the installed net propulsive force data that are provided to the sizing and performance analyst.

To permit rapid initial analysis and trade studies, Fig. 13.6 provides a "ballpark" estimate of inlet drag for a typical supersonic aircraft. This chart was prepared by the author using data from Ref. 47 and other sources, and should be used with great caution as it is merely typical data, not an estimate for any given inlet design.

This chart assumes that the engine is operating at a maximum dry or afterburning power setting, and that the inlet is operating at a corresponding mass-flow ratio. The chart does not reflect the increase in inlet drag experienced when the thrust setting is reduced (which reduces the mass-flow ratio). However, this chart should provide a reasonable approximation of inlet drag suitable for initial analysis and student design studies.

Nozzle drag varies with nozzle position as well as with the flight condition. To properly determine nozzle drag the actual nozzle geometry as a function of throttle setting and flight condition must be known, and the drag calculated by taking into account the overall aircraft flowfield. As an initial approximation, the effect of nozzle position may be ignored and the

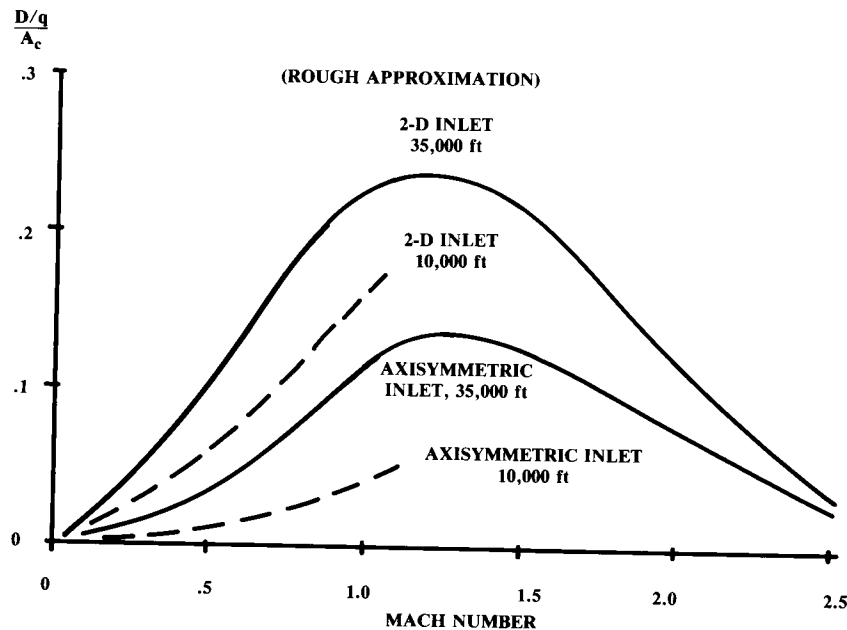


Fig. 13.6 Inlet drag trends.

nozzle drag estimated by the typical subsonic values shown in Table 13.1 (Ref. 10) for the nozzle types shown in Fig. 10.20.

The nozzle drag increases transonically and then drops off at supersonic speeds. For initial analysis the subsonic value may be assumed for all speeds. Note that these nozzle drags are referenced to the maximum cross-sectional area of the fuselage. For a subsonic, podded nacelle, the nozzle drag is negligible.

The remaining propulsion-system drag is the variation of trim drag with throttle setting. If the engine thrust axis is not through the center of gravity, any thrust change will cause a pitching moment. The trim force required to counter this moment is charged to the propulsion in most thrust-drag book-

Table 13.1 Nozzle incremental drag<sup>10</sup>

Nozzle type	Subsonic $\Delta C_{D_{Fuselage}}$ *
Convergent	.036-.042
Convergent iris	.001-.020
Ejector	.025-.035
Variable ejector	.010-.020
Translating plug	.015-.020
2-D nozzle	.005-.015

\*Referenced to fuselage maximum cross-section area.

keeping systems. For initial analysis this may be ignored unless the thrust line is substantially above or below the aircraft centerline.

### 13.6 PISTON-ENGINE PERFORMANCE

The aircraft piston engine operates on the four-stroke Otto cycle used by automobiles. The thermodynamic theory of the Otto-cycle reciprocating engine is described in Refs. 28, 48, and 49. For design purposes the most important thing to know about the piston engine is that the horsepower produced is directly proportional to the massflow of the air into the intake manifold. In fact, horsepower is approximately 620 times the air massflow (lb/s).

Mass flow into the engine is affected by the outside air density (altitude, temperature, and humidity) and intake manifold pressure. Equation (13.9) accounts for the air-density effect upon horsepower, and is attributed to Gagg and Ferrar of the Wright Aeronautical Company (1934). This equation indicates that at an altitude of 20,000 ft a piston engine has less than half of its sea-level horsepower.

$$bhp = bhp_{SL} \left( \frac{\rho}{\rho_0} - \frac{1 - \rho/\rho_0}{7.55} \right) \quad (13.9)$$

The intake manifold is usually at atmospheric pressure. A forward-facing air-intake scoop can provide some small increase in manifold pressure at higher speeds. Large increases in manifold pressure require mechanical pumping via a "supercharger" or "turbosupercharger."

The supercharger is a centrifugal air compressor mechanically driven by a shaft from the engine. The amount of air compression available is proportional to engine RPM. The turbosupercharger, or "turbocharger," is driven by a turbine placed in the exhaust pipe. This recovers energy which would otherwise be wasted, and decouples the available amount of compression from the engine RPM.

Supercharging or turbocharging is usually used to maintain sea level pressure in the intake manifold as the aircraft climbs. Typically the sea-level pressure can be maintained up to an altitude of about 15,000–20,000 ft. Above this altitude the manifold pressure, and hence the horsepower, drops. Figure 13.7 shows typical engine performance for nonsupercharged, supercharged, and turbocharged engines.

Supercharging or turbocharging may also be used to raise the intake manifold pressure above the sea-level value to provide additional horsepower from a given engine. However, the increased internal pressures require a heavier engine for structural reasons.

Piston engine performance charts are provided by the manufacturer as a function of manifold pressure, altitude, and RPM.

### Propeller Performance

A propeller is a rotating airfoil that generates thrust much as a wing generates lift. Like a wing, the propeller is designed to a particular flight

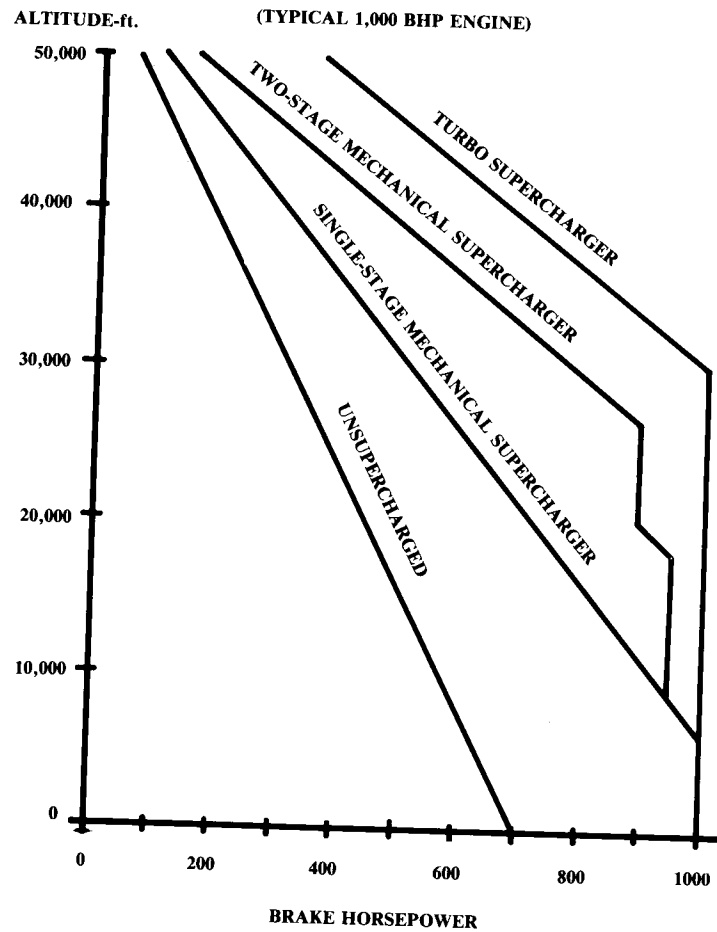


Fig. 13.7 Effects of supercharging.

condition. The propeller airfoil has a selected design lift coefficient (usually around 0.5), and the twist of the airfoil is selected to give the optimal airfoil angle of attack at the design condition.

Since the tangential velocities of the propeller airfoil sections increase with distance from the hub, the airfoils must be set at progressively reduced pitch-angles going from root to tip. The overall “pitch” of a propeller refers to the blade angle at 75% of the radius (70% in some books).

Propeller theory is well covered in many textbooks, such as Ref. 49. While theory is useful for propeller designers, the aircraft designers usually work with experimental propeller data provided by the propeller companies.

As for a wing, the properties of a propeller are expressed in coefficient form. Experimental data for design purposes are expressed using a variety of parameters and coefficients, as described below.

$$\text{Advance Ratio: } J = V/nD \quad (13.10)$$

$$\text{Power Coefficient: } c_P = \frac{P}{\rho n^3 D^5} = \frac{550 \text{ bhp}}{\rho n^3 D^5} \quad (13.11)$$

$$\text{Thrust Coefficient: } c_T = T/\rho n^2 D^4 \quad (13.12)$$

$$\text{Speed-Power Coefficient: } c_S = V \sqrt[5]{\rho/Pn^2} \quad (13.13)$$

Activity Factor:

$$AF_{\text{per blade}} = \frac{10^5}{D^5} \int_{0.15R}^R cr^3 dr = \frac{10^5 c_{\text{root}}}{16D} [0.25 - (1 - \lambda)0.2] \quad (13.14)$$

$$\text{Propeller Efficiency: } \eta_p = \frac{TV}{P} = \frac{TV}{550 \text{ bhp}} = \frac{J c_T}{c_P} \quad (13.15)$$

$$\text{Thrust: } T = \frac{550 \text{ bhp } \eta_p}{V} = \frac{c_T}{c_P} \frac{550 \text{ bhp}}{nD} \quad (13.16)$$

where

- $T$  = thrust (lb)
- $V$  = velocity (ft/s)
- $P$  = power (ft-lb/s)
- bhp = brake horsepower
- $n$  = rotation speed (rev/s)
- $D$  = propeller diameter (ft)
- $c$  = propeller airfoil chord (ft)

The advance ratio (equivalent to the wing angle of attack) is related to the distance the aircraft moves with one turn of the propeller. Advance ratio is sometimes called the “slip function” or “progression factor.”

The power and thrust coefficients are nondimensional measures of those quantities, much like the wing lift-coefficient. The speed-power coefficient is defined as the advance ratio raised to the fifth power divided by the power coefficient. The speed-power coefficient is nondimensional and does not involve the propeller diameter, which is useful for comparison between propellers of different size.

The activity factor is a measure of the amount of power being absorbed by the propeller. Activity factors range from about 90–200, with a typical light-aircraft activity factor being 100 and a typical large turboprop having an activity factor of 140. The final expression in Eq. (13.14) is the activity factor for a straight-tapered propeller blade of taper ratio  $\lambda$ .

Equation (13.15) relates the propeller efficiency, previously discussed in Chapters 3 and 10, to the advance ratio and the ratio of the thrust coefficient to the power coefficient. This ratio is used in Eq. (13.16) to determine the thrust at static conditions when the velocity is zero and the propeller-efficiency equation cannot be used for thrust determination.



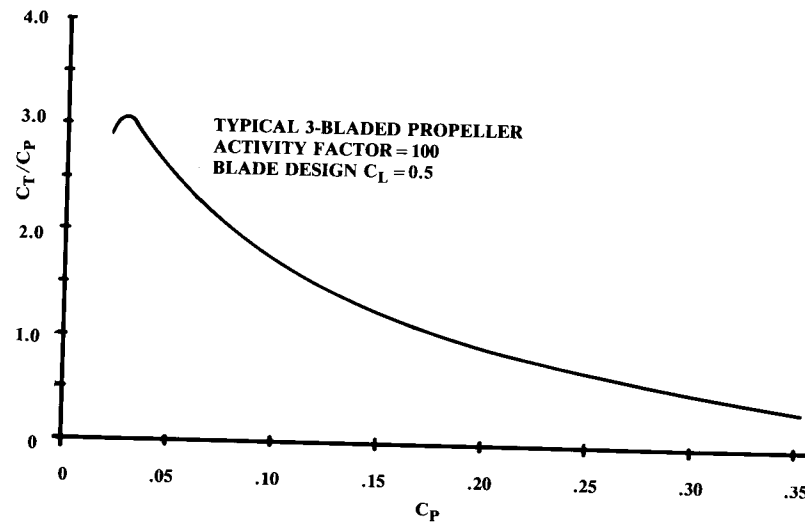


Fig. 13.8 Static propeller thrust. (after Ref. 50)

Propeller data is available from the manufacturers as well as various NASA/NACA reports. This data is provided in many different formats using different combinations of the above parameters and coefficients. Whatever the format, Eq. (13.16) is ultimately used to determine the propeller thrust at a given flight condition.

Figures 13.8 and 13.9, propeller charts for static and forward flight (Ref. 50), have been chosen as typical of propellers used for modern light and business aircraft. These charts represent a three-bladed propeller with a design lift-coefficient of 0.5 and an activity factor of 100.

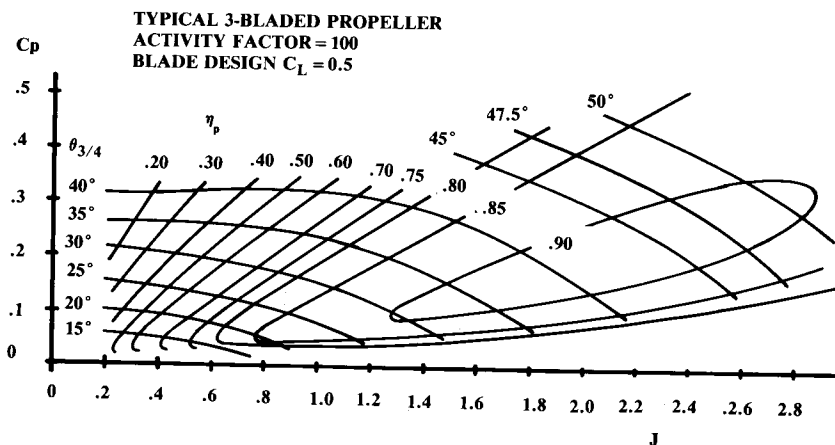


Fig. 13.9 Forward flight thrust and efficiency. (after Ref. 50)

For a two-bladed propeller, the forward-flight efficiencies are about 3% better than shown in Fig. 13.9, but the static thrust is about 5% less than shown in Fig. 13.8. The reverse trends are true for a four-bladed propeller. Also, a wooden propeller has an efficiency about 10% lower due to its greater thickness.

If Ref. 50 is unavailable, Ref. 49 contains 43 pages of propeller charts taken from Ref. 50. Reference 49 also contains a compressibility correction for a propeller with a high tip Mach number (greater than 0.9).

If the propeller is of variable-pitch design, its pitch is adjusted to the optimum blade angle at each flight condition to produce a constant engine RPM regardless of the horsepower being produced.

The advance ratio and power coefficient are then independent variables and the propeller efficiency can be read in Fig. 13.9 for any combination of advance ratio and power coefficient that may occur in flight. Blade angle for the variable-pitch propeller can be read as a fallout parameter in Fig. 13.9.

Remember that the propeller thrust in forward flight is proportional to the inverse of the velocity, which would imply infinite thrust at zero velocity. Instead, the propeller produces the static-thrust value from Fig. 13.8 at zero velocity.

In the speed range from zero to about 50 knots (such as during takeoff), the thrust varies in a fashion that can be represented by a smooth curve faired between the static-thrust value and the calculated forward-flight thrust.

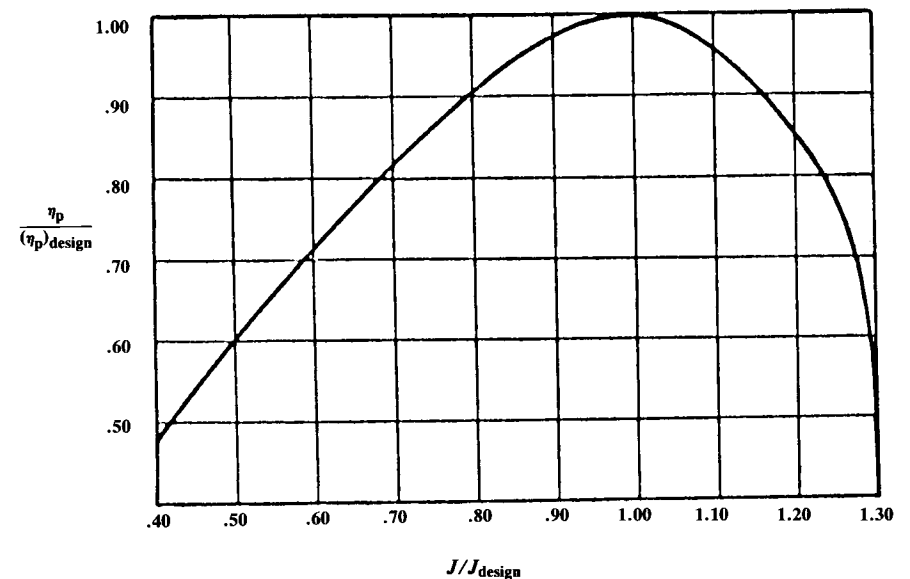


Fig. 13.10 Fixed-pitch propeller adjustment.

If a fixed-pitch propeller is used, the blade angle cannot be varied in flight to maintain engine RPM at any flight condition. Since the RPM and therefore horsepower will vary with velocity, the efficiency and hence the thrust will be reduced at any speed other than the design speed.

Figure 13.9 could be used to determine the thrust from a fixed-pitch propeller by following the appropriate line for the selected blade angle. However, it is simpler to use the approximate method of Fig. 13.10 unless actual propeller data is available.

Figure 13.10 relates the fixed-pitch propeller efficiency at an off-design velocity and RPM to the on-design efficiency, which is attained by the propeller at some selected flight condition. The on-design efficiency is obtained from Fig. 13.9, which is also used to get the required blade angle for the design condition.

The static thrust of a fixed-pitch propeller will be less than is estimated using Fig. 13.8. A fixed-pitch propeller suffers at low speeds due to the high local angles of attack of the blades at low speeds and high RPMs. As a rough approximation it can be assumed that the static thrust is about equal to the thrust at 50 knots for the fixed-pitch propeller.

These charts provide useful rough estimations of propeller performance, but actual charts for the selected propeller should be obtained from the manufacturer for any serious design effort.

### Piston-Prop Thrust Corrections

As with jet engines, there are several engine-related drag items that must be considered, namely, scrubbing drag, cooling drag, and engine miscellaneous drag.

Scrubbing drag is the increase in aircraft drag due to the higher velocity and turbulence experienced by the parts of the aircraft within the propwash. This drag could be calculated by determining, for each flight condition, the increased dynamic pressure within the propwash and using that value for the component-drag calculation.

A simpler approach, called the SBAC (Society of British Aircraft Constructors) method, adjusts the propeller efficiency as in Eq. (13.17). The subscript “washed” refers to the parts of the aircraft which lie within the propwash. If the parasite-drag coefficient for the propwashed parts of the aircraft cannot be determined, 0.004 is a reasonable estimate.

$$\eta_{p\text{effective}} = \eta_p \left[ 1 - \frac{1.558}{D^2} \frac{\rho}{\rho_0} \Sigma(C_{f_e} S_{\text{wet}})_{\text{washed}} \right] \quad (13.17)$$

where  $C_{f_e}$  is the equivalent skin-friction (parasite) drag coefficient, referenced to wetted area.

For a pusher-propeller configuration, the scrubbing drag is zero. However, the pusher propeller suffers a loss of efficiency due to the wake of the fuselage and wing. This loss is strongly affected by the actual aircraft configuration, and should equal about 2–5%.

Cooling drag represents the momentum loss of the air passed over the engine for cooling. This is highly dependent upon the detail design of the intake, baffles, and exit.

Miscellaneous engine drag includes the drag of the oil cooler, air intake, exhaust pipes, and other parts. Cooling and miscellaneous drags for a well-designed engine installation can be estimated by Eqs. (13.18) and (13.19) (Ref. 23). However, a typical light aircraft engine installation may experience cooling and miscellaneous drag levels 2–3 times the values estimated by these equations.

$$(D/q)_{\text{cooling}} = (4.9 \times 10^{-7}) \frac{\text{bhp} \cdot T^2}{\sigma V}, \text{ ft}^2 \quad (13.18)$$

$$(D/q)_{\text{misc}} = (2 \times 10^{-4}) \text{ bhp}, \text{ ft}^2 \quad (13.19)$$

where

$T$  = air temperature, deg Rankine

$V$  = velocity in ft/s

### 13.7 TURBOPROP PERFORMANCE

A turboprop is a jet engine that drives a propeller using a turbine in the exhaust. The jet exhaust retains some thrust capability, and can contribute as much as 20% of the total thrust. For this reason the horsepower rating of a turboprop engine includes the horsepower equivalent of this residual thrust.

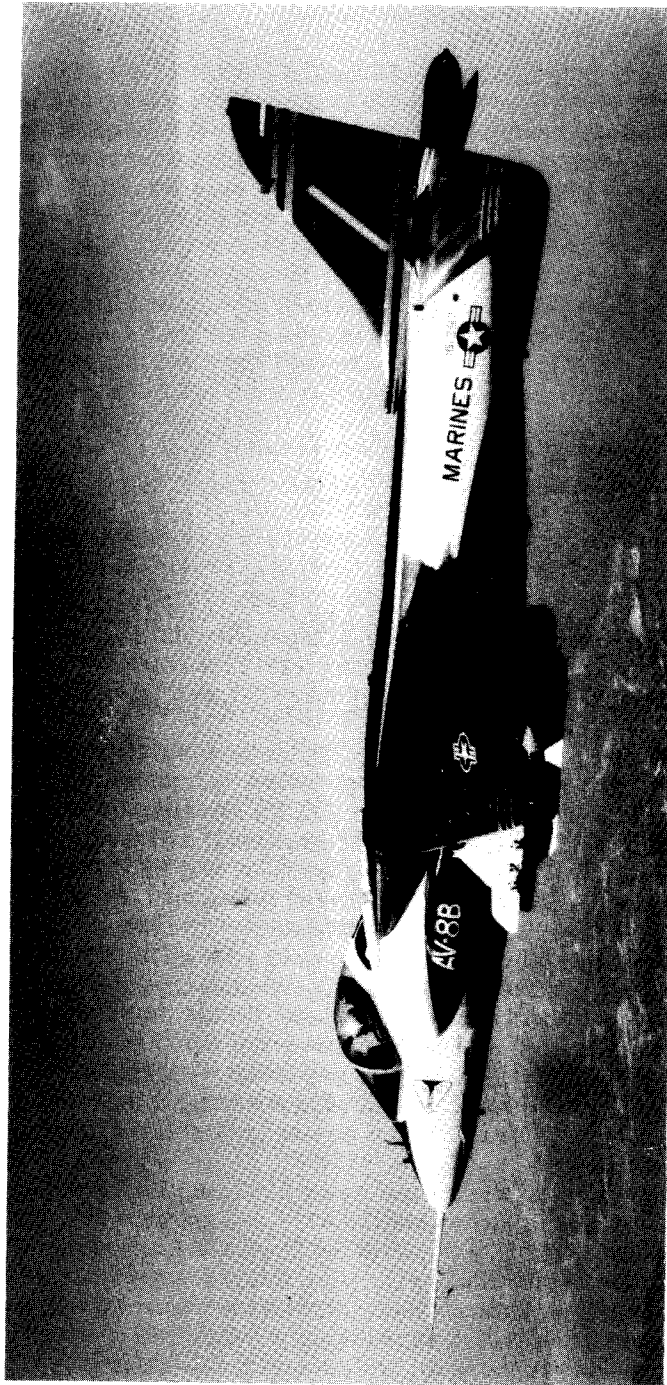
This horsepower equivalent of residual thrust is arbitrarily calculated under static conditions as the residual thrust divided by 2.5. Under forward-flight conditions it is calculated using Eq. (13.16) assuming that the propeller efficiency  $\eta_p = 0.80$ . The total of the mechanical and thrust residual horsepower is called the “equivalent shaft horsepower (ESHP).”

Analysis of the turboprop is a hybrid between the jet and the piston-prop analysis. The engine is analyzed like a jet, including the inlet effects. The residual thrust is provided by the manufacturer as a horsepower equivalent. The propeller is analyzed as described above, including the scrubbing-drag term.

The conventional turboprop, like the piston-prop, is limited by tip Mach number to about Mach 0.7. The turboprop has higher efficiency than the piston-prop at Mach numbers greater than about 0.5 due to the residual jet thrust, but the conventional turboprop is no match for a turbofan engine at the higher subsonic speeds.

Recently, a new type of advanced propeller has been developed that offers good efficiencies up to about Mach 0.85. These are known as “propfans” or “unducted fans (UDF).” They are smaller in diameter than the regular propellers and feature numerous wide, thin, and swept blades. Test programs to date indicate that a well-designed propfan can retain propeller efficiencies of over 0.8 at speeds on the order of Mach 0.85.

Up-to-date data on propfans can be found in publications such as the AIAA’s *Journal of Aircraft* and *Journal of Propulsion and Power*.



AV-8B Harrier VTOL Fighter-Bomber

## 14 STRUCTURES AND LOADS

### 14.1 INTRODUCTION

In a large aircraft company, the conceptual designer may never do any structural analysis. The conceptual designer relies upon an experienced eye to insure that sufficient space is provided for the required structural members. The only direct impact of structures during the initial stages of conceptual design is in the weights estimation. As will be shown in the next chapter the statistical weights methods usually used in conceptual design do not require any actual structural analysis.

Designers at small aircraft companies and designers of homebuilt aircraft are more likely to perform an initial structural analysis as a part of the conceptual design process. This is especially true for a novel design concept such as the Rutan Voyager. To attain a design range of 26,000 miles the Voyager needed an empty-weight fraction of about 0.20 (!) and a wing aspect ratio over 30. Clearly, the knowledge that this was structurally possible was required before the design concept could be frozen.

Before the actual structural members can be sized and analyzed, the loads they will sustain must be determined. Aircraft loads estimation, a separate discipline of aerospace engineering, combines aerodynamics, structures, and weights.

In the past, the Loads Group was one of the larger in an aircraft company. Loads were estimated for each structural member of the aircraft using a combination of handbook techniques and wind-tunnel-data reduction.

Today's computer programs have mechanized much of the time-consuming work in loads estimation. Modern aerodynamic panel programs determine the airloads as an intermediate step toward determining aerodynamic coefficients. Also, modern wind tunnels employ computerized data reduction. These have reduced the workload so much that in some companies today there is no longer a separate loads group.

However, loads estimation remains a critical area because an error or faulty assumption will make the aircraft too heavy or will result in structural failure when the real loads are encountered in flight.

This chapter introduces the concepts of loads estimation and summarizes the subjects of aircraft materials and structural analysis. This material is presented from the viewpoint of the conceptual designer, and is not intended to serve as a general introduction to structures.

Furthermore, many of the methods presented are no longer in regular usage, having been supplanted by finite-element methods, as discussed at the end of this chapter. The older methods are useful, however, for approx-

imating the correct answer to insure that the finite-element method results are in the right “ballpark.” Also, study of the classical methods is useful for learning the vocabulary of structural design.

A more thorough introduction to modern structural design will be found in Ref. 83. Reference 84 recounts in detail the theoretical development of the finite-element method.

14.2 LOADS CATEGORIES

When one thinks of aircraft loads, the airloads due to high-*g* maneuvering come immediately to mind. While important, maneuvering loads are only a part of the total loads that must be withstood by the aircraft structure.

Table 14.1 lists the major load categories experienced by aircraft. Civil and military specifications [FAR Vol. III (23 and 25) and Mil-A-8860/8870] define specific loading conditions for these categories, as discussed later.

For each structural member of the aircraft, one of the loads listed in Table 14.1 will dominate. Figures 14.1 and 14.2 show typical critical loads for a fighter and a transport. Note that the lifting surfaces are almost always critical under the high-*g* maneuver conditions.

Table 14.1 Aircraft loads

Airloads	Landing	Other
– Maneuver	– Vertical load factor	– Towing
– Gust	– Spin-up	– Jacking
– Control deflection	– Spring-back	– Pressurization
– Component interaction	– Crabbed	– Bird strike
– Buffet	– One wheel	– Actuation
	– Arrested	– Crash
	– Braking	
Inertia loads		
– Acceleration		
– Rotation	Takeoff	
– Dynamic		
– Vibration	– Catapult	
– Flutter	– Aborted	
Power plant		
– Thrust	Taxi	
– Torque		
– Gyroscopic	– Bumps	
– Vibration	– Turning	
– Duct Pressure		

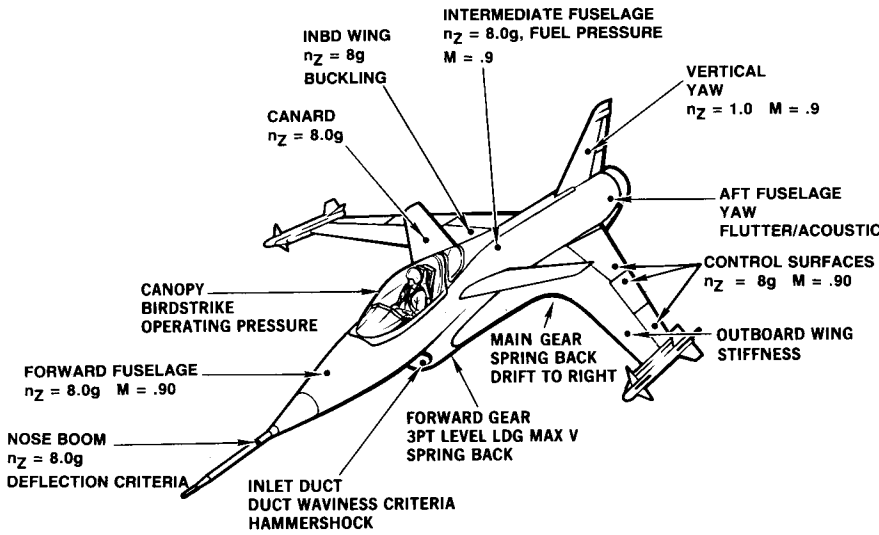


Fig. 14.1 Typical fighter limit loads.

The largest load the aircraft is actually expected to encounter is called the “limit,” or “applied,” load. For the fighter of Fig. 14.1, the limit load on the wing occurs during an 8-*g* maneuver.

To provide a margin of safety, the aircraft structure is always designed to withstand a higher load than the limit load. The highest load the structure is designed to withstand without breaking is the “design,” or “ultimate,” load.

The “factor of safety” is the multiplier used on limit load to determine the design load. Since the 1930’s the factor of safety has usually been 1.5. This was defined in an Air Corps specification based upon the ratio between the ultimate tensile load and yield load of 24ST aluminum alloy, and has proven to be suitable for other aircraft materials in most cases. For the fighter in Fig. 14.1, the design load for the wing structure would then be based upon a 12-*g* maneuver, above which the wing would break.

14.3 AIR LOADS

Maneuver Loads

The greatest air loads on an aircraft usually come from the generation of lift during high-*g* maneuvers. Even the fuselage is almost always structurally sized by the lift of the wing rather than by the air pressures produced directly on the fuselage.

Aircraft load factor (*n*) expresses the maneuvering of an aircraft as a multiple of the standard acceleration due to gravity (*g* = 32.2 ft/s-s). At lower speeds the highest load factor an aircraft may experience is limited by the maximum lift available.

At higher speeds the maximum load factor is limited to some arbitrary value based upon the expected use of the aircraft. The Wright Brothers

Table 14.2 Typical limit load factors

	$n_{\text{positive}}$	$n_{\text{negative}}$
General aviation—normal	2.5 to 3.8	-1 to -1.5
General aviation—utility	4.4	-1.8
General aviation—acrobatic	6	-3
Homebuilt	5	-2
Transport	3 to 4	-1 to -2
Strategic bomber	3	-1
Tactical bomber	4	-2
Fighter	6.5 to 9	-3 to -6

designed their Flyer to a 5-g limit load. This remains a reasonable limit load factor for many types of aircraft. Table 14.2 lists typical limit load factors. Note that the required negative load factors are usually much less in magnitude than the positive values.

The  $V$ - $n$  diagram depicts the aircraft limit load factor as a function of airspeed. The  $V$ - $n$  diagram of Fig. 14.3 is typical for a general aviation aircraft. Note that the maximum lift load factor equals 1.0 at level-flight stall speed, as would be expected. The aircraft can be stalled at a higher speed by trying to exceed the available load factor, such as in a steep turn.

The point labeled “high A.O.A.” (angle of attack) is the slowest speed at which the maximum load factor can be reached without stalling. This part of the flight envelope is important because the load on the wing is approximately perpendicular to the flight direction, not the body-axis vertical direction.

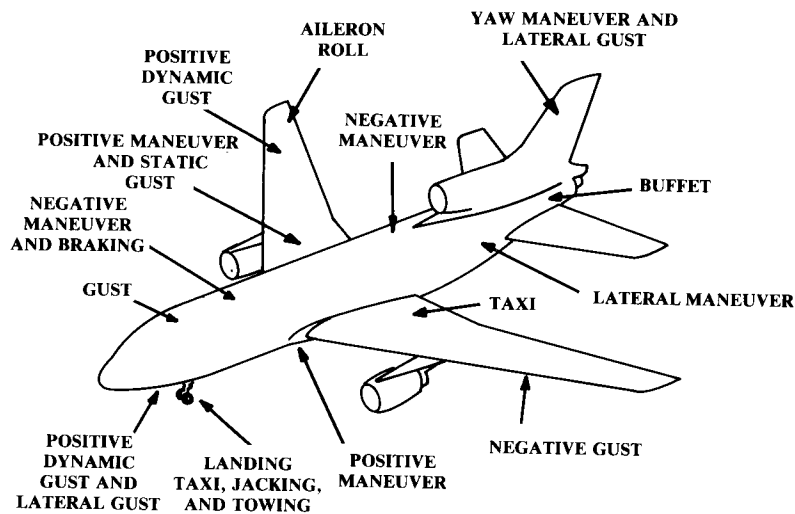


Fig. 14.2 L1011 critical loads.

At high angle of attack the load direction may actually be forward of the aircraft body-axis vertical direction, causing a forward load component on the wing structure (Fig. 14.4). During World War I, several aircraft had a problem with the wings shedding forward due to this unexpected load.

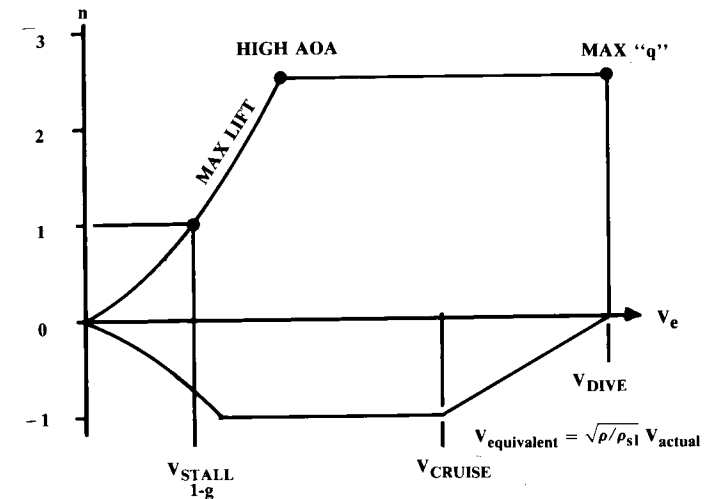
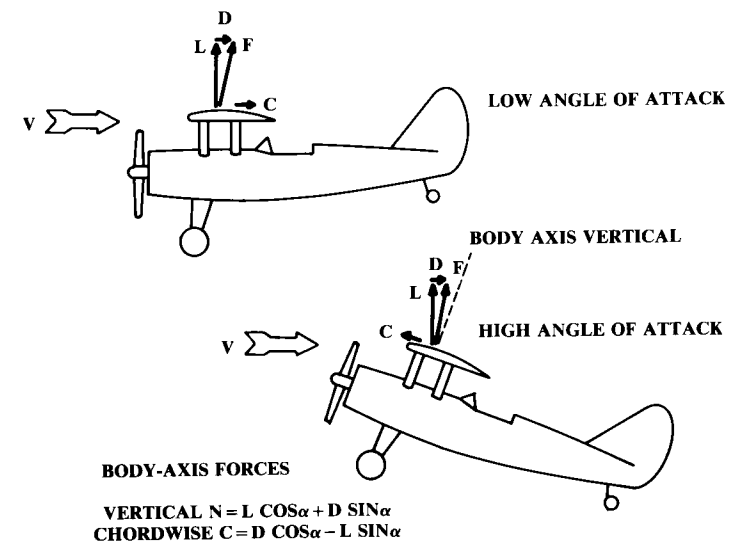
Fig. 14.3  $V$ - $n$  diagram (maneuver).

Fig. 14.4 Wing load direction at angle of attack.

The aircraft maximum speed, or dive speed, at the right of the  $V$ - $n$  diagram represents the maximum dynamic pressure  $q$ . The point representing maximum  $q$  and maximum load factor is clearly important for structural sizing. At this condition the aircraft is at a fairly low angle of attack because of the high dynamic pressure, so the load is approximately vertical in the body axis.

For a subsonic aircraft, maximum or dive speed is typically 50% higher than the level-flight cruise speed. For a supersonic aircraft the maximum speed is typically about Mach 0.2 faster than maximum level-flight speed, although many fighters have enough thrust to accelerate past their maximum structural speed.

Note that aircraft speeds for loads calculation are in “equivalent” airspeeds  $V_e$ . An aircraft airspeed indicator uses a pitot probe to determine airspeed from the dynamic pressure, so the “airspeed” as measured by a pitot probe is based upon the dynamic pressure at the aircraft’s velocity and altitude, and not the actual velocity. This dynamic pressure-based equivalent airspeed will be less than the actual airspeed at altitude due to the reduction in air density, as this expression describes:

$$V_e = \sqrt{\rho/\rho_{SL}} (V_{\text{actual}}) = \sqrt{\sigma} (V_{\text{actual}}) \quad (14.1)$$

For loads estimation,  $V_e$  is a convenient measure of velocity because it is constant with respect to dynamic pressure regardless of altitude. However, pilots must convert  $V_e$  to actual velocity to determine how fast they are really flying. Also, the dynamic pressure as measured by a pitot tube has a compressibility error at higher Mach numbers, so the “indicated” airspeed  $V_i$  as displayed to the pilot must be corrected for compressibility to produce the equivalent airspeed  $V_e$ , which can then be converted to actual airspeed.

### Gust Loads

The loads experienced when the aircraft encounters a strong gust can exceed the maneuver loads in some cases. For a transport aircraft flying near thunderstorms or encountering high-altitude “clear air turbulence,” it is not unheard of to experience load factors due to gusts ranging from a negative 1.5 to a positive 3.5  $g$  or more.

When an aircraft experiences a gust, the effect is an increase (or decrease) in angle of attack. Figure 14.5 illustrates the geometry for an upward gust of velocity  $U$ . The change in angle of attack, as shown in Eq. (14.2), is approximately  $U$  divided by  $V$ , the aircraft velocity. The change in aircraft

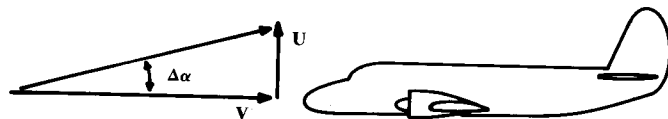


Fig. 14.5 Gust encounter.

lift is shown in Eq. (14.3) to be proportional to the gust velocity. The resulting change in load factor is derived in Eq. (14.4).

$$\Delta\alpha = \tan^{-1} \frac{U}{V} \cong \frac{U}{V} \quad (14.2)$$

$$\Delta L = \frac{1}{2}\rho V^2 S (C_{L\alpha} \Delta\alpha) = \frac{1}{2}\rho V S C_{L\alpha} U \quad (14.3)$$

$$\Delta n = \frac{\Delta L}{W} = \frac{\rho U V C_{L\alpha}}{2W/S} \quad (14.4)$$

Figure 14.5 and Eq. (14.4) assume that the aircraft instantly encounters the gust and that it instantly affects the entire aircraft. These assumptions are unrealistic.

Gusts tend to follow a cosine-like intensity increase as the aircraft flies through, allowing it more time to react to the gust. This reduces the acceleration experienced by the aircraft by as much as 40%. To account for this effect a statistical “gust alleviation factor ( $K$ )” has been devised and applied to measured gust data ( $U_{de}$ , discussed later). The gust velocity in Eq. (14.4) can be defined in the following terms (Ref. 51):

$$U = K U_{de} \quad (14.5)$$

where

$$\text{Subsonic: } K = \frac{0.88\mu}{5.3 + \mu} \quad (14.6)$$

$$\text{Supersonic: } K = \frac{\mu^{1.03}}{6.95 + \mu^{1.03}} \quad (14.7)$$

$$\text{Mass Ratio: } \mu = \frac{2(W/S)}{\rho g \bar{c} C_{L\alpha}} \quad (14.8)$$

The mass ratio term accounts for the fact that a small, light plane encounters the gust more rapidly than a larger plane.

The design requirements for gust velocities are “derived” from flight-test data and are in “equivalent” airspeed (hence  $U_{de}$ ). Actual accelerations experienced in flight have been applied to Eqs. (14.4–14.8) to determine what the vertical gust velocities must have been to produce those accelerations in the various flight-research aircraft employed.

For many years the standard vertical gust  $U_{de}$  has been 30 ft/s (positive and negative). For most aircraft this produces roughly a 3- $g$  positive load factor. This is still a suitable gust  $U_{de}$  for normal, utility, and aerobatic civil aircraft at speeds up to cruise speed. For higher speeds it may be assumed that  $U_{de}$  drops linearly to 15 ft/s at maximum dive speed.

For transport and other classes of aircraft, a more detailed requirement of  $U_{de}$  is shown in Fig. 14.6 (data from Ref. 52). Note that the expected

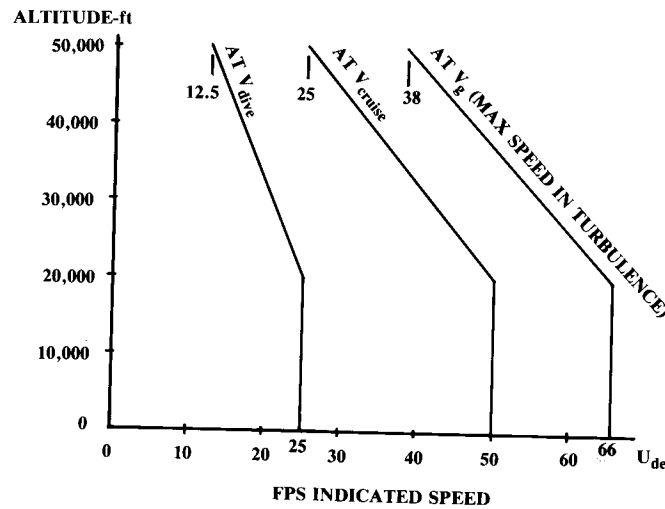


Fig. 14.6 Derived equivalent gust velocities (transport).

gusts are reduced at higher altitude. The maximum turbulence speed  $V_g$  may be specified in the design requirements or may be a fallout parameter.

One interesting point concerning gusts is that, as shown in Eq. (14.4), the load factor due to a gust increases if the aircraft is lighter. This is counter to the natural assumption that an aircraft is more likely to have a structural failure if it is heavily loaded.

In fact, the change in lift due to a gust [Eq. (14.3)] is unaffected by aircraft weight, so the change in wing stress is the same in either case. However, if the aircraft is lighter the same lift increase will cause a greater vertical acceleration (load factor) so the rest of the aircraft will experience more stress.

Aeroelastic effects can also influence the load factor due to gusts. An aft-swept wing will bend up under load, which twists the wing and reduces the outboard angle of attack. This reduces total lift and also moves the spanwise lift distribution inboard, reducing the wing bending stress. An aft-swept wing will experience roughly 15% lower load factor due to a given gust than an unswept wing.

The gust load factors as calculated with Eqs. (14.4–14.8) and using the appropriate  $U_{de}$  (positive and negative) can then be plotted on a  $V$ - $n$  diagram as shown in Fig. 14.7. It is assumed that the aircraft is in 1-g level flight when the gust is experienced. Few pilots will “pull g’s” in severe turbulence conditions. The load factor between  $V_{dive}$ ,  $V_{cruise}$ , and  $V_g$  is assumed to follow straight lines, as shown.

In Fig. 14.8, the  $V$ - $n$  diagrams of Figs. 14.3 and 14.7 are combined to determine the most critical limit load-factor at each speed. Since the gust loads are greater than the assumed limit load, it may be desirable to raise the assumed limit load at all velocities, as shown by the dotted line. Remember that the structural design load factors will be 50% higher to provide a margin of safety.

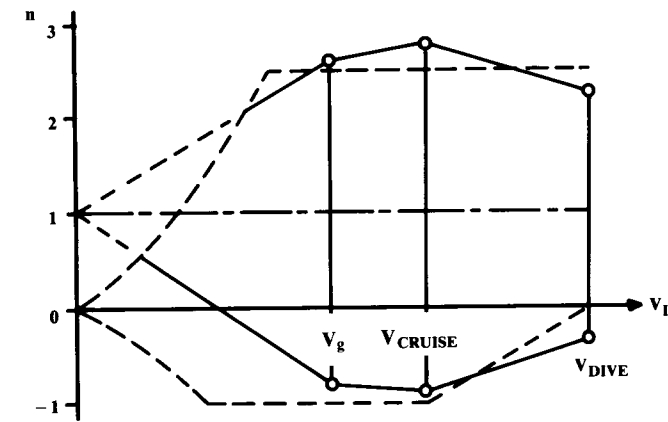


Fig. 14.7 V-n diagram (gust).

This method for estimation of gust loads is not as complete or accurate as the methods used at most large aircraft companies. The more accurate methods rely upon a power-spectral-density approach in which the gusts are included in an atmospheric transfer function and the actual aircraft dynamics are modeled. However, the methods presented above are useful for initial analysis and provide an introduction to the more detailed techniques. (See Ref. 91).

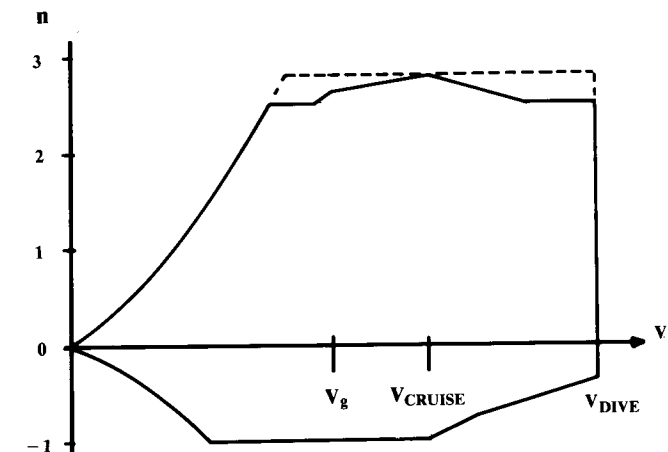


Fig. 14.8 Combined V-n diagram.

### Air Loads on Lifting Surfaces

Now that the  $V$ - $n$  diagram is complete, the actual loads and load distributions on the lifting surfaces can be determined. In most cases this needs to be done only at the “high A.O.A.” and “max  $q$ ” velocities (see Fig. 14.3) and any velocities where the gust load factor exceeds the assumed limit load factor.

The first step involves a stability-and-control calculation to determine the required lift on the horizontal tail to balance the wing pitching moment at the critical conditions. Note that the required tail lift will increase or decrease the required wing lift to attain the same load factor.

Complicated methods for estimating the lift on the trimmed tail and wing for a given load factor are presented in Chapter 16. These can be initially approximated by a simple summation of wing and tail moments about the aircraft center of gravity, ignoring the effects of downwash, thrust axis, etc.

Once the total lift on the wing and tail are known, the spanwise and chordwise load distributions can be determined (Fig. 14.9). Wind-tunnel and aerodynamic panel program data are used if available. For initial design and design of light aircraft, classical approximation methods give reasonably good results.

According to classical wing theory, the spanwise lift (or load) distribution is proportional to the circulation at each span station. A vortex lifting-line calculation will yield the spanwise lift distribution. For an elliptical planform wing, the lift and load distribution is of elliptical shape.

For a nonelliptical wing, a good semi-empirical method for spanwise load estimation is known as Schrenk's Approximation (Ref. 53). This method assumes that the load distribution on an untwisted wing or tail has a shape that is the average of the actual planform shape and an elliptic shape of the same span and area (Fig. 14.10). The total area under the lift load curve must sum to the required total lift. Equations (14.9) and (14.11) describe the chord distributions of a trapezoidal and elliptical wing.

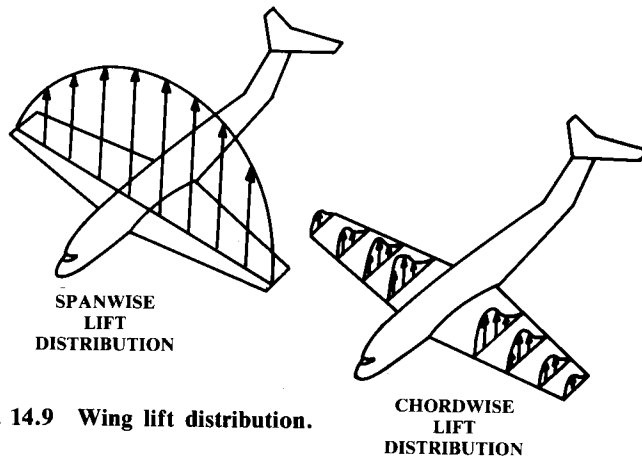


Fig. 14.9 Wing lift distribution.

$$\text{Trapezoidal Chord: } C(y) = C_r \left[ 1 - \frac{2y}{b}(1 - \lambda) \right] \quad (14.9)$$

where

$$S = \frac{b}{2} C_r (1 + \lambda) \quad (14.10)$$

$$\text{Elliptical Chord: } C(y) = \frac{4S}{\pi b} \sqrt{1 - \left( \frac{2y}{b} \right)^2} \quad (14.11)$$

Note in Fig. 14.10 that the load is assumed to continue to the centerline of the aircraft. This has proven to be a good assumption in subsonic flight. Also remember that if substantial dihedral is used, the perpendicular load on the wing is greater than the lift. Divide the lift by the cosine of the dihedral angle to get the perpendicular load.

If a wing has substantial geometric or aerodynamic twist, the effect upon spanwise lift-load distribution can be approximated by determining the load distribution when the wing is generating no net lift (the “basic load”) and adding it to the “additional” load which is determined as above for the net lift being produced (Ref. 54).

When a twisted wing has no net lift, part of the wing is generating an up-load (usually the inboard section) and the rest of the wing is generating a down-load (usually the tips). The basic load can be approximated by ignoring the induced effects and basing the load at each spanwise station on the chord and section lift. The section lift is the section lift coefficient times the section's twist angle with respect to the wing angle of attack when no lift is being generated. This no-lift angle is approximately the angle of the mean aerodynamic chord, and must be found by trial and error.

Schrenk's Approximation does not apply to highly swept planforms experiencing vortex flow. Vortex flow tends to greatly increase the loads at the wingtips. Loads for such a planform must be estimated using computers and wind tunnels.

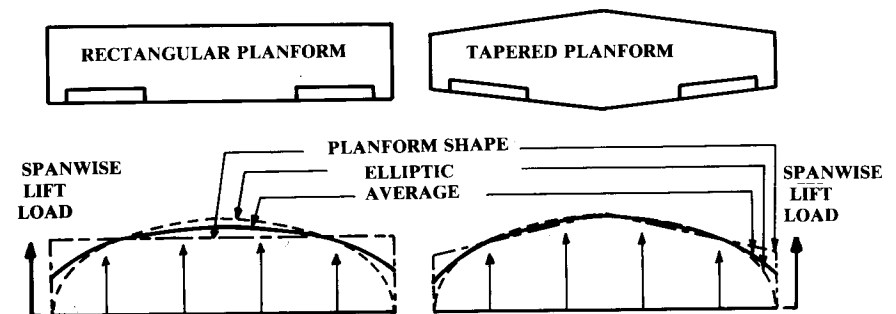


Fig. 14.10 Schrenk's approximation.



The spanwise distribution of drag loads must also be considered, especially for fabric-covered aircraft in which drag loads are carried by internal “drag wires.” Drag loads tend to be greatest near the wingtips, and should be determined from wind-tunnel or aerodynamic panel program data.

As a first approximation the spanwise distribution of drag loads can be roughly approximated as a constant 95% of the average drag loading from the root to 80% of the span, and 120% of the average loading from 80% of span to the wingtip.

The aerodynamic interaction of various aircraft components can produce additional loads. For example, the downwash from a canard will reduce the effective angle of attack of the inboard part of the wing. This moves the lift distribution of the wing outboard, producing greater wing bending stresses than expected.

A vortex from a leading-edge strake can cause vibrational stresses on any component of the aircraft it touches. The F-18 had a problem with vertical-tail fatigue for this reason. A similar problem can occur due to propeller propwash. These effects are difficult to predict, but must be considered during conceptual design.

Once the spanwise load distribution is known, the wing or tail bending stress can be determined as described in a later section. To determine torsional stresses, the airfoil moment coefficient is applied to spanwise strips and the total torsional moment is summed from tip to root. When wind-tunnel data is available, the torsional moments are summed from the chordwise pressure data.

Actual chordwise pressure distributions for a NACA 4412 airfoil at various angles of attack are shown in Fig. 14.11. Figure 14.12 shows a rough

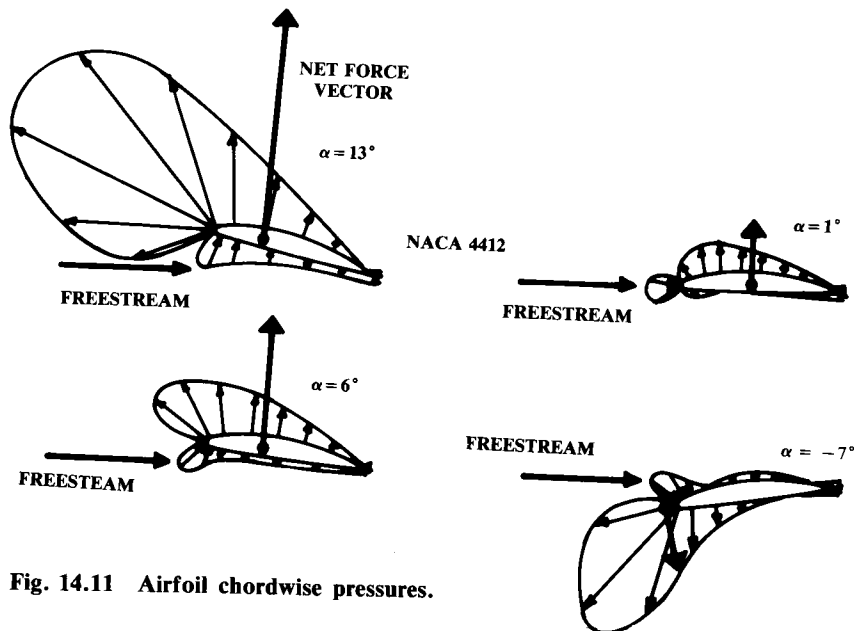


Fig. 14.11 Airfoil chordwise pressures.

approximation for the lift load distribution on a conventional airfoil if wind-tunnel data is unavailable.

### Airloads due to Control Deflection

Operation of the control surfaces produces airloads in several ways. The greatest impact is in the effect of the elevator on angle of attack and hence load factor. The rudder's effect on yaw angle can also impose large loads. Deflection of control surfaces produces additional loads directly upon the wing or tail structure.

“Maneuver speed,” or “pullup speed  $V_p$ ,” is the maximum speed at which the pilot can fully deflect the controls without damaging either the airframe or the controls themselves. For most aircraft the maneuver speed is less than the maximum level cruise speed  $V_L$ .

Maneuver speed is established in the design requirements or may be selected using an old empirical relationship, Eq. (14.12). Velocities are in feet per second, and aircraft weight  $W$  is in pounds. Stall speed  $V_s$  is with high-lift devices deployed. The factor  $K_p$  is estimated in Eq. (14.13), but should not be allowed to fall below 0.5 or above 1.0. (For general-aviation aircraft,  $K_p$  usually doesn't exceed 0.9.)

$$V_p = V_s + K_p(V_L - V_s) \quad (14.12)$$

$$K_p = 0.15 + \frac{5400}{W + 3300} \quad (14.13)$$

At the selected maneuver speed, a control analysis using the methods of Chapter 16 determines the angle of attack or sideslip obtained by maximum control deflection. The airloads imposed upon the structure can then be determined.

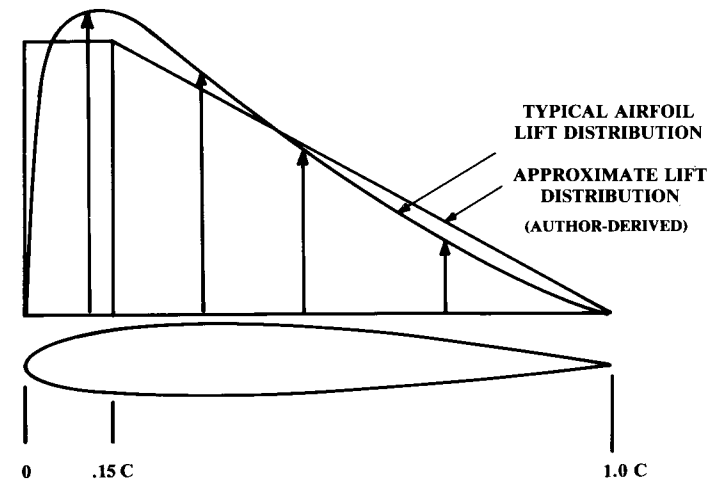


Fig. 14.12 Approximate airfoil lift distribution.

Note that the instantaneous loads imposed by maximum aileron deflection while at maximum load factor (rolling pull-up) are frequently critical to the wing structure.

The maximum speed allowed with flaps down is also needed for estimation of the maximum loads on the flaps. Flap speed  $V_f$  will usually be twice the flaps-down stall speed.

Figure 14.13 shows an approximate distribution of the additional airloads imposed directly upon a conventional airfoil (Fig. 14.12) by the deflection of a control surface. Control deflection will typically provide a change in section lift coefficient of about 0.8–1.1 at 25 deg deflection. Estimation methods are provided in Chapter 16.

In the absence of better data, the change in airfoil moment coefficient can be estimated as  $(-0.01)$  times the control deflection in degrees. Note that

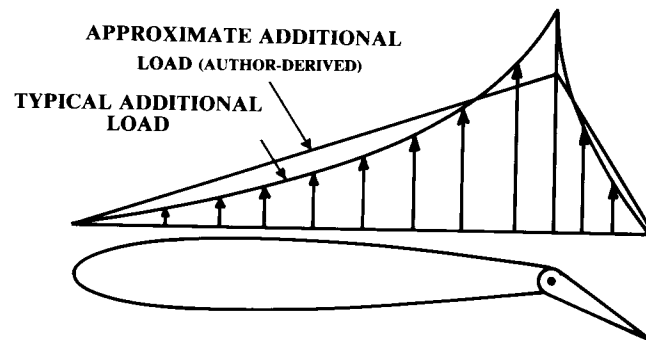


Fig. 14.13 Approximate additional load due to control deflection.

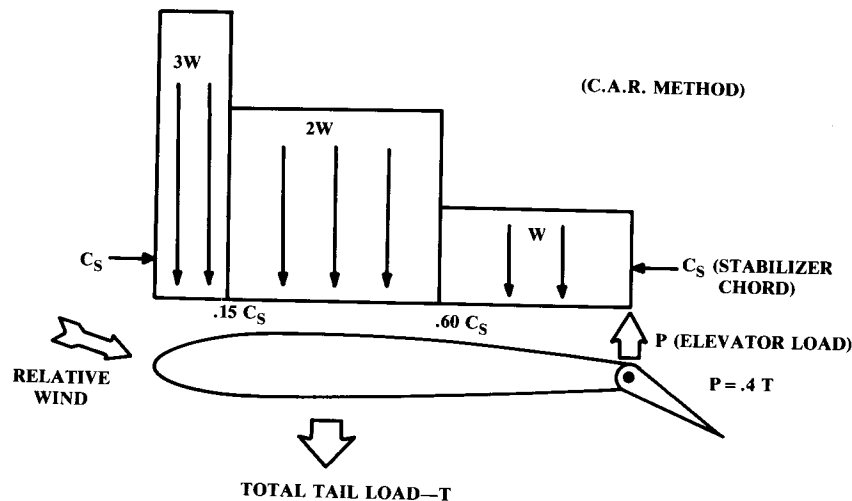


Fig. 14.14 Loads on fixed stabilizer with elevator deflection.

the deflection of a control surface increases the load on the fixed part of the airfoil as well as on the moving control surface.

Figure 14.14 shows the loading distribution used for the special case of a horizontal tail consisting of a fixed stabilizer and a moving elevator. Under some combinations of angle of attack and elevator position the stabilizer and elevator will actually have loads in opposite directions, as shown.

For design purposes, the elevator load  $P$  is assumed to equal 40% of the total required tail load  $T$ , but in the opposite direction. The distributed load shown on the stabilizer must then equal 140% of the tail load. The spanwise load distribution is usually assumed to be proportional to chord length.

For an aircraft with a manual flight-control system, the control loads may be limited by the strength of the pilot. For a stick-controlled aircraft, the pilot strength is limited to 167 lb for the elevator and to 67 lb for the ailerons. For a wheel-controlled aircraft, the pilot strength is limited to 200 lb for the elevator and to 53 (times the wheel diameter) in.-lbs for the ailerons. The rudder force is limited to 200 lb.

In addition to the maneuvering and control-surface loads determined above, the tail group of an aircraft is designed to withstand some arbitrarily determined loads at maneuver speed. These loads are based upon normal force coefficients ( $C_n$ ) assuming that the spanwise load distribution is proportional to chord length. For the horizontal tail, the required  $C_n$  values are  $(-0.55)$  downward and  $(0.35)$  upward. For the vertical tail the required  $C_n$  value is  $(0.45)$ .

#### 14.4 INERTIAL LOADS

Inertial loads reflect the resistance of mass to acceleration ( $F = ma$ ). The various accelerations due to maneuver and gust, described above, establish the stresses for the aerodynamic surfaces.

Every object in the aircraft experiences a force equal to the object's weight times the aircraft load factor. This creates additional stresses throughout the aircraft, which must be determined. Note that the weight of the wing structure will produce torsional loads on the wing in addition to the aerodynamic torsional loads.

Inertial loads due to rotation must also be considered. For example, the tip tanks of a fighter rolling at a high rate will experience an outward centrifugal force. This force produces an outward load factor equal to the distance from the aircraft c.g. times the square of the rotation rate, divided by  $g$ .

A tangential acceleration force is produced throughout the aircraft by a rotational acceleration such as is caused by a gust, a sudden elevator deflection, or by nose-wheel impact. This force is equal to the distance from the aircraft c.g. times the angular acceleration, divided by  $g$ .

The loads produced by vibration and flutter are actually acceleration forces of a special nature. Calculation of these loads goes beyond this book. Proper design should avoid flutter and reduce vibrations to a negligible level.

### 14.5 POWER-PLANT LOADS

The engine mounts must obviously be able to withstand the thrust of the engine as well as its drag when stopped or windmilling. The mounts must also vertically support the weight of the engine times the design load factor. The engine mounts are usually designed to support a lateral load equal to one-third of the vertical design load. The mounts must withstand the gyroscopic loads caused by the rotating machinery (and propeller) at the maximum pitch and yaw rates.

For a propeller-powered aircraft, the engine mounts must withstand the torque of the engine times a safety factor based upon the number of cylinders. This reflects the greater jerkiness of an engine with few cylinders when one cylinder malfunctions.

For an engine with two cylinders, the safety factor is 4.0; with three cylinders, 3.0; and with four cylinders, 2.0. An engine with five or more cylinders requires a safety factor of 1.33. These safety factors are multiplied times the maximum torque in normal operation to obtain the design torque for the engine mounts.

For a jet engine, air loads within the inlet duct must be considered as they will frequently bound a part of the flight envelope. A pressure surge known as “hammershock” is especially severe.

### 14.6 LANDING-GEAR LOADS

The landing gear's main purpose is to reduce the landing loads to a level that can be withstood by the aircraft. Chapter 11 presented calculations for landing gear stroke to yield an acceptable gear load-factor, as transmitted to the structure of the aircraft.

To analyze fully all the possible gear loads, a number of landing scenarios must be examined. These include a level landing, a tail-down landing, a one-wheel landing, and a crabbed landing. For certification the aircraft may be subjected to drop tests, in which an actual aircraft is dropped from a height of somewhere between 9.2–18.7 in. The required drop distance typically will be 3.6 times the square root of the wing loading.

When the tires contact the ground they are not rotating. During the brief fraction of a second it takes for them to spin up, they exert a large rearward force by friction with the runway. This spin-up force can be as much as half the vertical force due to landing.

When the tire is rotating at the correct speed, the rearward force is relieved and the gear strut “springs back” forward, overshooting the original position and producing a “spring-back” deflection load equal to or greater than the spin-up load.

Another landing-gear load, the braking load, can be estimated by assuming a braking coefficient of 0.8.

The load on the landing gear during retraction is usually based upon the airloads plus the assumption that the aircraft is in a 2-g turn. Other landing-gear loads such as taxiing and turning are usually of lesser importance, but must be considered during detail design of the landing gear and supporting structure.

### 14.7 STRUCTURES FUNDAMENTALS

Timoshenko's classic 1930 book “Strength of Materials” (Ref. 55) begins with this overall description of the action of structural members:

“We assume that a body consists of small particles, or molecules, between which forces are acting. These molecular forces resist the change in the form of the body which external forces tend to produce. If such external forces are applied to the body, its particles are displaced and the mutual displacements continue until equilibrium is established between the external and internal forces. It is said in such a case that the body is in a state of strain.”

Thus, a structural member responds to a load by deforming in some fashion until the structure is pushing back with a force equal to the external load. The internal forces produced in response to the external load are called “stress,” and the deformation of the structure is called “strain.”

Figure 14.15 shows the three basic types of structural loading: tension, compression, and shear. The meanings of tension and compression should be clear from the illustration. Shear may be viewed as a combination of forces tending to cause the object to deform into two parts that slide with respect to each other. Scissors cut paper by application of shear. Figure 14.15 also shows the load on a rivet, a typical example of shear.

Figure 14.16 shows three other types of structural loading. These can be considered as variations and combinations of tension, compression, and shear. Bending due to a load at the end of a beam is a combination of

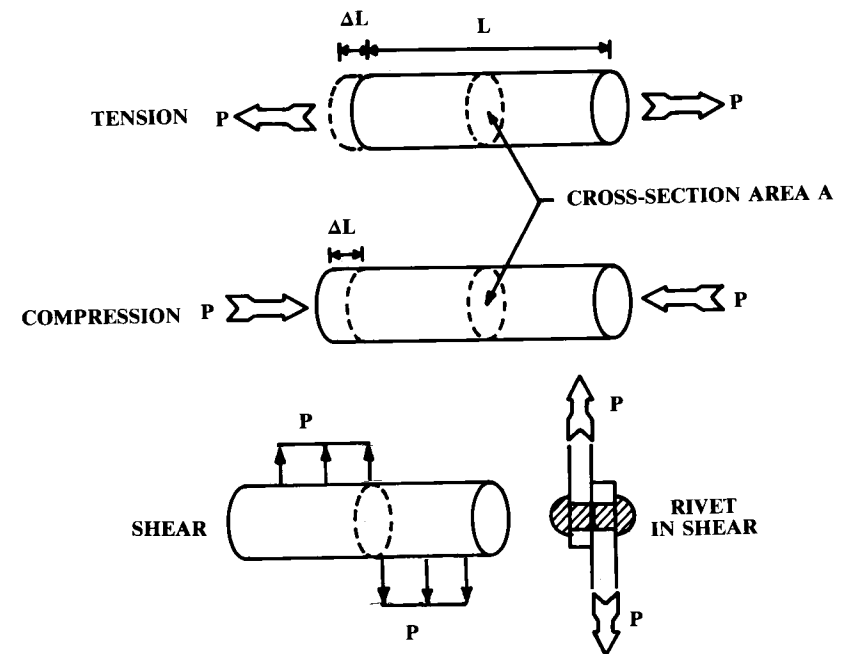


Fig. 14.15 Three basic structural loadings.

tension and compression. The top part of the beam in Fig. 14.16 is in compression, while the bottom part is in tension.

Torsion is due to a combination of forces producing a moment (torque) which tends to twist the object. Torsion produces tangential shear forces that resist the torque.

Thermal stresses are due to the expansion of materials with an increase in temperature. If a structural member is not free at one end, it will push against its supports as it is heated. This produces compression loads. Similarly, a severe reduction in material temperature will produce tension loads unless at least one end is free.

The unit stress ( $\sigma$  or  $F$ ) is the stress force ( $P$ ) per unit area [i.e., total stress divided by area—see Eq. (14.14)]. The unit strain ( $\epsilon$  or  $e$ ) is the deformation per unit length [i.e., total strain divided by length—see Eq. (14.15)].

$$\sigma = P/A \quad (14.14)$$

$$\epsilon = \Delta L/L \quad (14.15)$$

The relationship between stress (load) and strain (deformation) is critically important to the design of structure. Figure 14.17 illustrates a typical stress-strain diagram for an aluminum alloy. Over most of the stress range the strain is directly proportional to the stress (Hooke's Law), with a constant of proportionality defined as Young's Modulus, or the Modulus of Elasticity ( $E$ ) [Eq. (14.16)].

$$E = \sigma/\epsilon \quad (14.16)$$

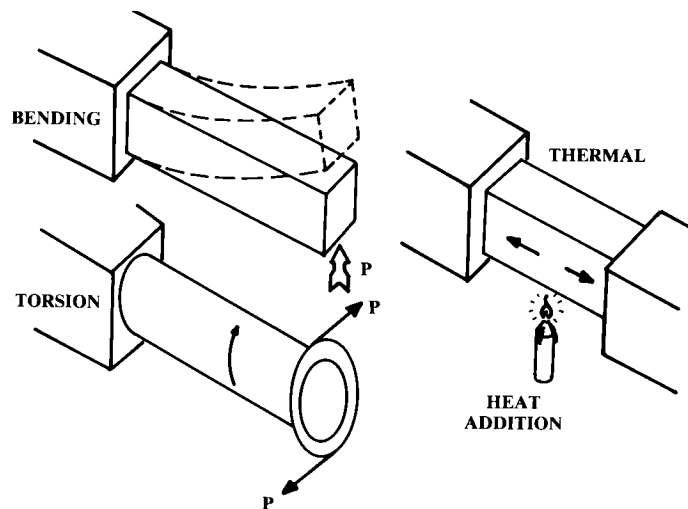


Fig. 14.16 Other structural loadings.

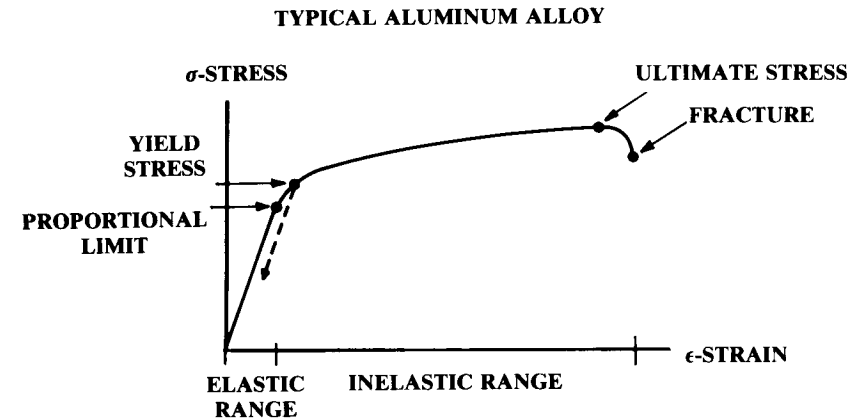


Fig. 14.17 Stress-strain diagram.

The highest stress level at which the strain is proportional to the stress is called the "proportional limit," and stresses less than this value are considered within the "elastic range." Within the elastic range a structure will return to its original shape when the load is removed.

At higher stress levels a permanent deformation ("set") remains when the load is removed, as shown by the dotted line on Fig. 14.17. The "yield stress" is the stress level at which a substantial permanent set occurs.

Yield stress is arbitrarily defined as a permanent set of 0.002 in. per inch, and is typically only slightly higher than the proportional limit. Above the yield stress is called the "inelastic range."

Within the inelastic range, Hooke's Law is no longer true and the Modulus of Elasticity can no longer be applied to Eq. (14.16) to determine the strain for a given stress. However, for some stress calculations it is useful to define an artificial modulus called the Tangent Modulus ( $E_t$ ), which is the slope of the stress-strain curve at a given point in the inelastic range. This modulus cannot be applied to Eq. (14.16). The tangent modulus varies with stress and strain, and is plotted in material-property tables such as Ref. 61.

The "ultimate stress" is the highest stress level the material can withstand. Ultimate stress goes well past the elastic range. A material subjected to its ultimate stress will suffer a large and permanent set.

For aluminum alloys, ultimate stress is about 1.5 times the yield stress. If an aircraft is designed such that the application of a limit load factor causes some aluminum structural member to attain its yield stress, then the ultimate stress will not be reached until a load factor of 1.5 times the limit load factor is applied (i.e., at the design or ultimate load factor). However, when the aircraft exceeds its limit load factor some structural elements will be permanently deformed and must be repaired after the aircraft lands.

The "specific strength" of a material is defined as the ultimate stress divided by the material density. The "specific stiffness" is defined as the modulus of elasticity  $E$  divided by the material density. These parameters are useful for comparing the suitability of various materials for a given application.

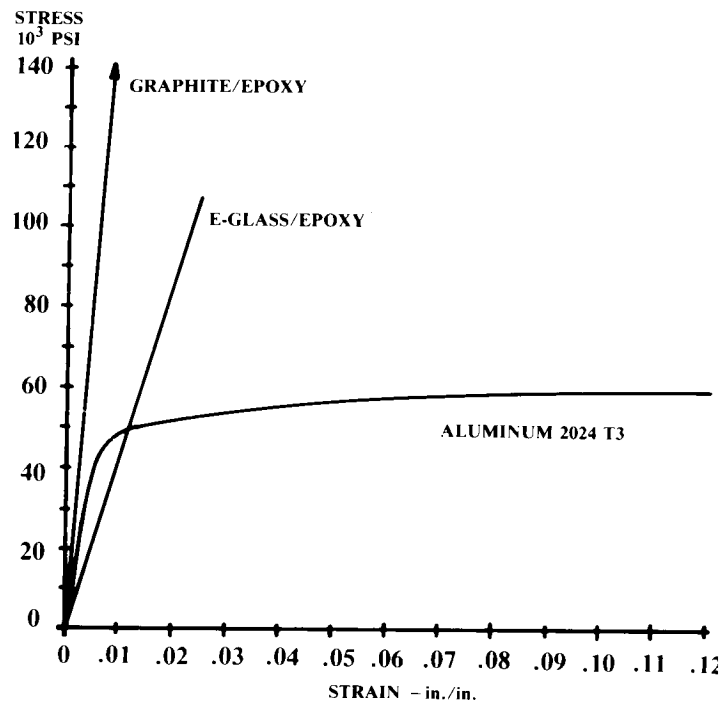


Fig. 14.18 Composite material stress-strain.

Not all materials behave like the aluminum alloy of Fig. 14.17. Composites such as fiberglass and graphite-epoxy will fracture without warning at a stress just past the proportional limit (Ref. 56), as shown in Fig. 14.18. These materials do not have a “built in” 1.5 safety factor, so a safety factor must be assumed for design purposes.

Typically a safety factor for composites is assumed by designing to a stress level that provides a strain equal to two-thirds (i.e.,  $1/1.5$ ) of the strain at the ultimate stress level. If this stress level is higher than the proportional limit, then the proportional limit stress is used for designing to limit loads.

When a material elongates due to a tension load, the cross-sectional area decreases as shown in Fig. 14.19 (much exaggerated). Experimentation has shown that the ratio of lateral to axial strain is constant within the elastic range. This ratio (Poisson's Ratio,  $\mu$  or  $\nu$ ) is approximately 0.3 for steel and 0.33 for nonferrous materials such as aluminum.

The deformation due to shear, which was not shown in Fig. 14.15, is illustrated in Fig. 14.20. At the top is a bar subjected to a shear loading typical for a rivet, with a download and an upload separated by some very small distance. These loads are assumed to be provided by loads applied to two plates (not shown) that the bar or rivet connects.

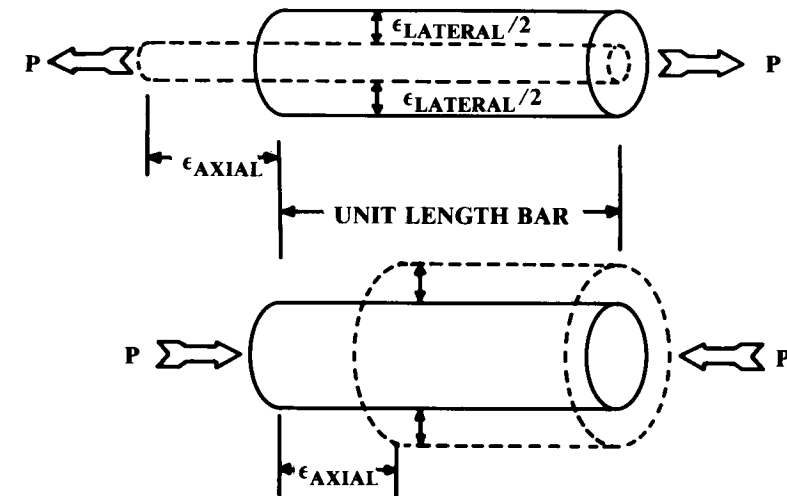


Fig. 14.19 Poisson's ratio.

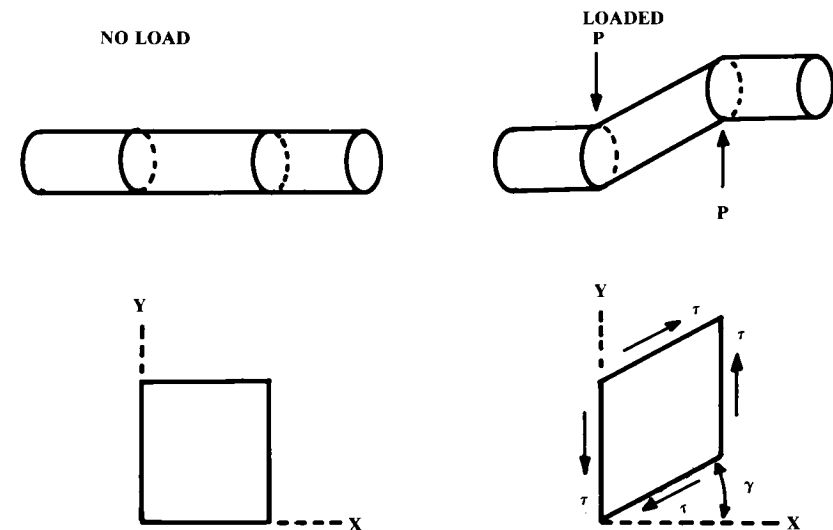


Fig. 14.20 Shear deformation.

The deformation of the bar is shown to the right. Shear introduces a kink within the material. The deformation is not a change in length, as with tension or compression, but instead is an angular deformation (shearing strain, or  $\gamma$ ).

The upper-right illustration in Fig. 14.20 cannot be a complete free-body diagram because of the unbalanced moment of the two forces. Additional forces must exist to balance this moment. The lower right figure illustrates

the total forces on a square element within the “kinked” portion of the bar. Again, the angle  $\gamma$  defines the shearing strain within the bar. The “unit shear stress ( $\tau$ )” is defined in Eq. (14.17).

These additional balancing forces, horizontal in the example in Fig. 14.20, are themselves shear forces that must be resisted by the material. For a riveted wing spar, the rivets which attach the shear web to the spar caps must be designed to resist these shear forces. Similarly, in a wood or composite wing box the glue which attaches the upper and lower covers must resist these shear forces.

Note in Fig. 14.20 that the transverse deformation (i.e.,  $Y$  direction) due to the shear stress is equal to the longitudinal distance ( $X$  direction) from the point of no shear, times the shearing strain angle ( $\gamma$ ) in radians, since  $\gamma$  is small.

As with tension or compression, there is a linear relationship between shear stress and shear strain provided that the shear force is below the proportional limit. The Shear Modulus, or Modulus of Rigidity ( $G$ ), is defined in Eq. (14.18). Also, it can be shown that the shear modulus is related to the modulus of elasticity by Poisson's Ratio (Ref. 55), as shown in Eq. (14.19).

$$\tau = P_{\text{shear}}/A \quad (14.17)$$

$$G = \tau/\gamma \quad (14.18)$$

$$G = \frac{E}{2(1 + \mu)} \quad (14.19)$$

#### 14.8 MATERIAL SELECTION

A number of properties are important to the selection of materials for an aircraft. The selection of the “best” material depends upon the application. Factors to be considered include yield and ultimate strength, stiffness, density, fracture toughness, fatigue crack resistance, creep, corrosion resistance, temperature limits, producibility, repairability, cost, and availability.

Strength, stiffness, and density have been discussed already. Fracture toughness measures the total energy per unit volume required to deflect the material to the fracture point, and is equivalent to the area under the stress-strain curve. A ductile material with a large amount of inelastic deformation prior to fracture will absorb more work energy in fracturing than a material with the same ultimate stress but with little inelastic deformation prior to fracture.

A material subjected to a repeated cyclic loading will eventually experience failure at a much lower stress than the ultimate stress. This “fatigue” effect is largely due to the formation and propagation of cracks, and is probably the single most common cause of aircraft material failure. There are many causes of fatigue, including gust loads, landing impact, and the vibrations of the engine and propeller.

Creep is the tendency of some materials to slowly and permanently deform under a low but sustained stress. For most aerospace materials, creep

is a problem only at elevated temperatures. However, some titaniums, plastics, and composites will exhibit creep at room temperatures. Creep deformation data is presented in materials handbooks as a function of time, temperature, and stress loading.

Corrosion of aircraft materials has been a major problem since the early days of aviation. Aircraft materials are exposed to atmospheric moisture, salt-water spray, aircraft fuel, oils, hydraulic fluids, battery acid, engine exhaust products, missile plumes, gun gases, and even leaking toilets.

Furthermore, electrically dissimilar materials such as aluminum and graphite-epoxy composite will experience galvanic corrosion in which an electrical current is formed that deteriorates the more anodic material, converting it into ions or an oxide.

Corrosion of materials is greatly accelerated when the materials experience a sustained stress level. The corrosion products at the surface tend to form a protective coating that delays further corrosion. When the material is subjected to a tension stress, however, cracks in the protective coating are formed that accelerate the corrosion.

Once corrosion begins, it tends to follow cracks opened in the material by the stress. This “stress corrosion” can cause fracture at a stress level one-tenth the normal ultimate stress level. For this reason it is important to avoid manufacturing processes that leave residual tension stresses.

Operating temperature can play a major role in determining material suitability. Stainless steel or some other high-temperature material must be used as a firewall around the engine. For high-speed aircraft, aerodynamic heating may determine what materials may be used. Figure 14.21 shows typical skin temperatures at speeds of Mach 2.2 and 3.0.

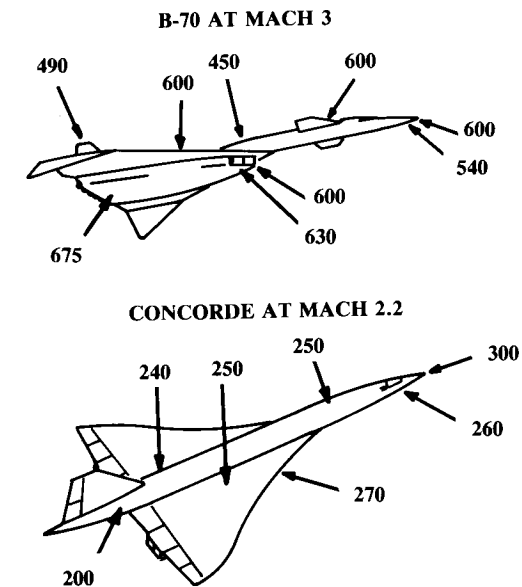


Fig. 14.21 Supersonic skin temperatures ( $^{\circ}\text{F}$ ).

The stagnation (total) temperature is the highest possible temperature due to aerodynamic heating [Eq. (14.20)]. Actual skin temperatures are difficult to calculate because they depend upon the airflow conditions, surface finish, and atmospheric conditions. Figure 14.22 provides a reasonable estimate of the expected skin temperatures over most of the airframe.

$$T_{\text{stagnation}} = T_{\text{ambient}}(1 + 0.2M^2) \quad (14.20)$$

Producibility and repairability are also important in material selection. As a rule, the better the material properties, the more difficult it is to work with.

For example, a major difficulty in the development of the SR-71 was in learning how to work with the selected titanium alloy. Similarly, composite materials offer a large reduction in weight, but pose problems both in fabrication and repair.

Cost is also important in material selection, both for raw material and fabrication. The better the material, the more it usually costs. Wood, mild steel, and standard aluminums are all relatively inexpensive. Titaniums and composites have high cost.

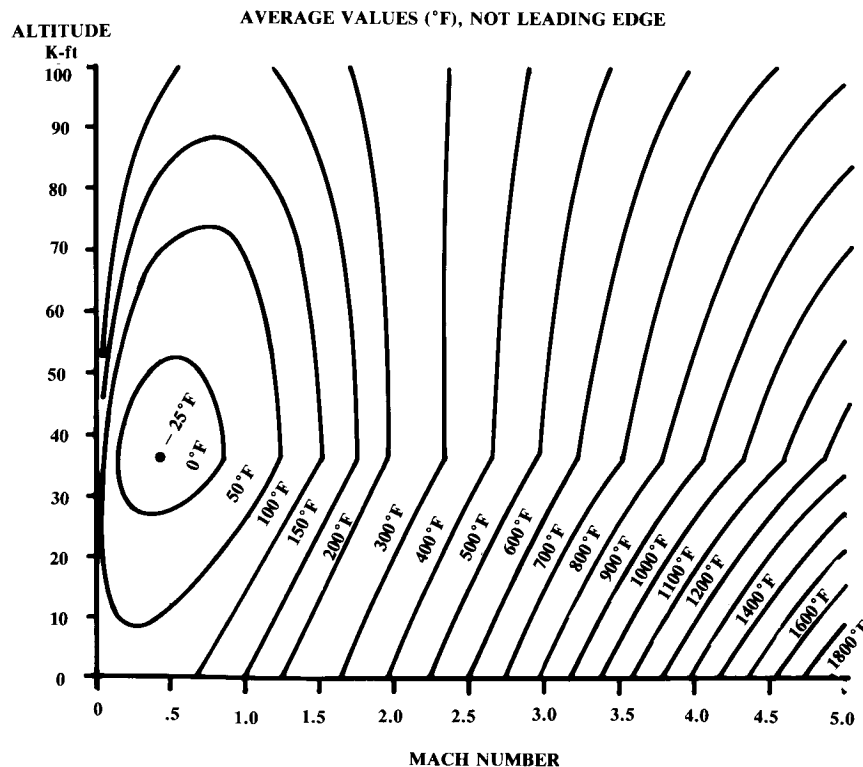


Fig. 14.22 Skin temperature estimate.

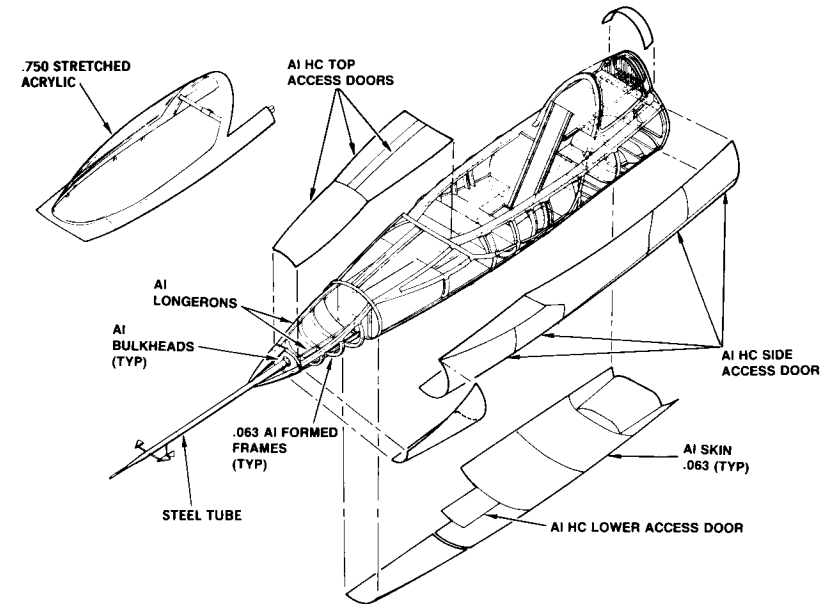


Fig. 14.23 Materials – forebody.

Another factor to consider is material availability. Titanium and some of the materials used to produce high-temperature alloys are obtained from unfriendly or unstable countries, and it is possible that the supply may someday be cut off. Also, aircraft-quality wood is in fairly short supply.

Figures 14.23, 14.24, and 14.25 illustrate the materials selected for the Rockwell proposal for the X-29. These are typical of current fighter design practice. Note the stainless-steel heat shield and nozzle interface and the aluminum-honeycomb access doors. In a production fighter, the stretched acrylic windshield would be replaced by a bulletproof material.

## 14.9 MATERIAL PROPERTIES

This section covers various commonly-used aircraft materials. Tables of representative material properties are at the back of this section.

### Wood

The Wright Brothers selected spruce as the primary structural material for their aircraft, and it remained the material of choice for many years. Wood is rarely used today in production aircraft, but it is interesting to note that the Chinese have recently selected oak for the heat shield of a re-entry vehicle!

Wood offers good strength-to-weight ratio and is easy to fabricate and repair. It is actually much like composite materials in that it has different properties in different directions. Wood makes a natural bending beam for wing spars because of the lengthwise fibers.

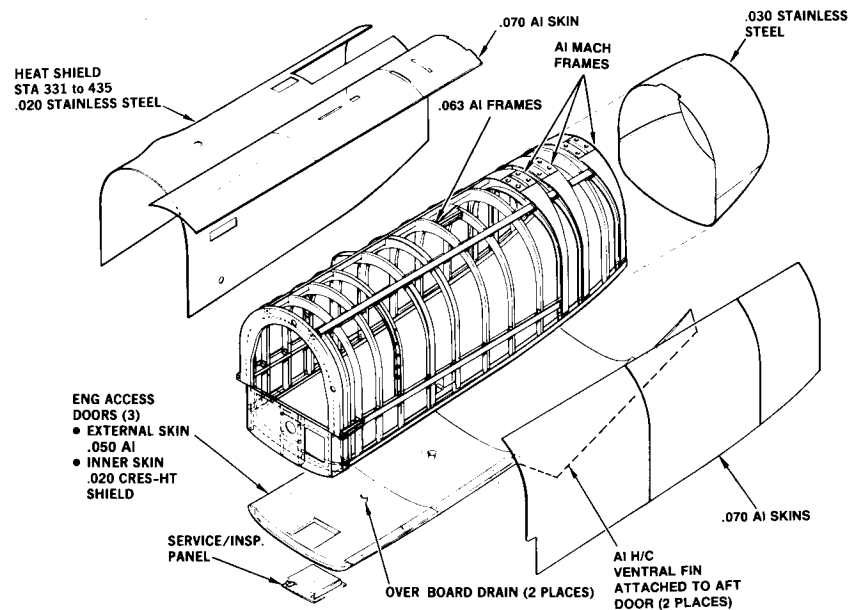


Fig. 14.24 Material selection—aft fuselage.

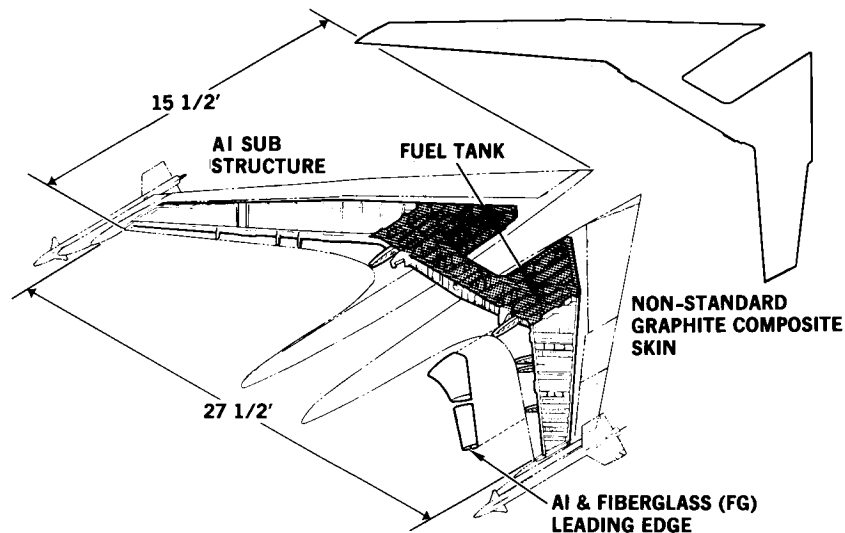


Fig. 14.25 Wing materials.

The wooden Hughes H-4 Hercules Flying Boat was built like a modern composite aircraft. Multiple thin plies of wood were placed in molds along with a resin glue and subjected to pressure during cure. Ply orientation was varied to give specific properties.

The disadvantages of wood are its sensitivity to moisture and its susceptibility to rot and insect damage. Wood must be regularly maintained and should not be left exposed to the elements. The Hughes H-4 looks virtually new today because it was kept in a climate-controlled hangar. Also, wood is produced by nature with poor quality control! Each piece of wood is unique so it requires craftsman-like skills to manufacture aircraft with wood.

Today wood is used largely in homebuilt and specialty, low-volume production aircraft. Wood has one additional advantage for homebuilders in that almost everyone knows how to saw, drill, and glue wood. However, the use of foam core and fiberglass-epoxy has largely replaced wood in homebuilt aircraft.

### Aluminum

Aluminum remains by far the most widely used aircraft material. It has an excellent strength-to-weight ratio, is readily formed, is of moderate cost, and is resistant to chemical corrosion.

Aluminum is the most abundant metal in the Earth's crust, occurring mostly as silicates in clays. Discovered in 1827, it remained an expensive novelty until an electrical extraction method was developed in 1885. In 1856 aluminum cost \$90 a pound. By 1935 the cost had dropped to 23 cents per pound. Inflation has raised this to several dollars per pound today depending upon its form.

Being relatively soft, pure aluminum is alloyed with other metals for aircraft use. The most common aluminum alloy is "2024 (or 24ST)," sometimes called "duralumin." 2024 consists of 93.5% aluminum, 4.4% copper, 1.5% manganese, and 0.6% magnesium.

For high-strength applications, the 7075 alloy is widely used. 7075 is alloyed with zinc, magnesium, and copper. Since the corrosion resistance is lessened by alloying, aluminum sheet is frequently "clad" with a thin layer of pure aluminum. Newer alloys such as 7050 and 7010 have improved corrosion resistance and strength.

The strength and stiffness properties of aluminum are affected by the form (sheet, plate, bar, extrusion, or forging) and by heat treatment and tempering. In general, the stronger the aluminum, the more brittle it is.

While composite materials are considered the latest state of the art for lightweight aircraft structures, there are new aluminum alloys such as aluminum-lithium that offer nearly the same weight savings and can be formed by standard aluminum techniques. Aluminum will remain important in aircraft design for many years to come.

### Steel

A major early advance in aircraft structures was the adoption of welded mild-steel tubing for the fuselage. Previously, aircraft such as the Sopwith



Camel had fuselages of wire-braced wood construction that required constant maintenance. The steel-tube fuselage, used extensively by Fokker, greatly improved strength and required less maintenance.

Today steel is used for applications requiring high strength and fatigue resistance, such as wing attachment fittings. Also, steel is used wherever high temperatures are encountered such as for firewalls and engine mounts. The Mach 3 XB-70 (Fig. 14.21) was constructed largely of brazed steel honeycomb. This material proved strong at high temperatures but was extremely difficult to fabricate.

Steel is primarily an alloy of iron and carbon, with the carbon adding strength to the soft iron. As carbon content increases, strength and brittleness increase. Typical steel alloys have about 1% of carbon. Other materials such as chromium, molybdenum, nickel, and cobalt are alloyed with steel to provide various characteristics. The “stainless steel” alloys are commonly used where corrosion resistance is important.

The properties of steel are strongly influenced by heat treatment and tempering. The same alloy can have moderate strength and good ductility or can have much higher strength but at the expense of brittleness, depending upon the heat treatment and tempering employed.

Heat treatment begins by raising the temperature of the steel to about 1400–1600°F, at which point the carbon goes into solid solution with the iron. The rate at which the steel is then cooled defines the grain structure, which determines strength and ductility.

If the steel is slowly cooled by steadily reducing the temperature in the furnace (“annealing”), a coarse grain structure is formed and the steel is very ductile but weak. This is sometimes done before working with steel to make it easier to cut, drill, and bend.

If the heated steel is allowed to air-cool (“normalized”) it becomes much stronger but retains good ductility. Welded steel tubing structure is usually normalized after all welding is completed to return the steel around the welds to the original strength.

If quenched with water or oil, the steel becomes “martensitic” with a needle-like grain structure, great strength, and extreme brittleness.

To regain some ductility the steel must be “tempered” by reheating it to about 1000°F for an hour or more.

Standard heat-treatment and tempering processes are defined in material handbooks along with the resulting material properties.

Steel is very cheap, costing about one-sixth what aluminum does. Steel is also easy to fabricate.

### **Titanium**

Titanium would seem to be the ideal aerospace material. It has a better strength-to-weight ratio and stiffness than aluminum, and is capable of temperatures almost as high as steel. Titanium is also corrosion-resistant.

However, titanium is extremely difficult to form for these same reasons. Most titanium alloys must be formed at temperatures over 1000°F and at very high forming stresses.

Also, titanium is seriously affected by any impurities that may be accidentally introduced during forming. One of the worst impurity elements for

“embrittling” titanium is hydrogen, followed by oxygen and nitrogen. After forming, titanium must be treated for embrittlement by chemical “pickling” or through heat treatment in a controlled environment.

Titanium is very expensive, costing about five to ten times as much as aluminum. Much of the titanium comes from the Soviet Union.

To handle the aerodynamic heating of Mach 3 + flight, the structure of the SR-71 is about 93% titanium. The XB-70 uses a substantial amount of titanium in the forebody area. Titanium is extensively used in jet-engine components, and is also used in lower-speed aircraft for such high-stress airframe components as landing-gear beams and spindles for all-moving tails. Because it does not cause galvanic corrosion with graphite-epoxy, titanium is sometimes used as the substructure to graphite-epoxy skins.

Reference 57 gives a more detailed discussion of titanium and its alloys.

### **Magnesium**

Magnesium has a good strength-to-weight ratio, tolerates high temperatures, and is easily formed, especially by casting, forging, and machining. It has been used for engine mounts, wheels, control hinges, brackets, stiffeners, fuel tanks, and even wings. However, magnesium is very prone to corrosion and must have a protective finish. Furthermore, it is flammable!

Mil Specs advise against the use of magnesium except to gain significant weight savings. Also, magnesium should not be used in areas which are difficult to inspect or where the protective finish would be eroded by rain (leading edges) or engine exhaust.

### **High-Temperature Nickel Alloys**

Inconel, Rene 41, and Hastelloy are high-temperature nickel-based alloys suitable for hypersonic aircraft and re-entry vehicles. Inconel was used extensively in the X-15, and Rene 41 was to have been used in the X-20 Dynasoar. Hastelloy is used primarily in engine parts.

These alloys are substantially heavier than aluminum or titanium, and are difficult to form. For these reasons, the Space Shuttle uses an aluminum structure with heat-protective tiles. While a substantially lighter structure was obtained, the difficulties experienced with the tiles should be noted by the designers of the next-generation shuttle.

### **Composites**

The greatest revolution in aircraft structures since the all-aluminum Northrop Alpha has been the ongoing adoption of composite materials for primary structure. In a typical aircraft part, the direct substitution of graphite-epoxy composite for aluminum yields a weight savings of 25%.

The AV-8B wing is almost entirely made of graphite-epoxy composite, and numerous military and commercial aircraft use composites for tails, flaps, and doors. The Beech Starship business turboprop is almost entirely of composite construction.

Composites consist of a reinforcing material suspended in a “matrix” material that stabilizes the reinforcing material and bonds it to adjacent

reinforcing materials. Composite parts are usually molded, and may be cured at room conditions or at elevated temperature and pressure for greater strength and quality. Figure 14.26 shows the two major composite forms, filament-reinforced and whisker-reinforced.

In the whisker-reinforced composite, short strands of the reinforcing material are randomly located throughout the matrix. The most common example of this is chopped fiberglass, which is used for low-cost fabrication of boats and fast-food restaurant seats. Whisker reinforcing is sometimes used in advanced metal matrix composites such as boron-aluminum.

Most of the advanced composites used in aircraft structure are of the filament reinforced type because of outstanding strength-to-weight ratio. Also, filament composites may have their structural properties tailored to the expected loads in different directions.

Metals and whisker-reinforced composites are isotropic, having the same material properties in all directions. Filament composites, like wood, are strongest in the direction the fibers are running. If a structural element such as a spar cap is to carry substantial load in only one direction, all the fibers can be oriented in that direction. This offers a tremendous weight savings.

Figure 14.27 shows four common arrangements for tailoring fiber orientation. In (a), all fibers are aligned with the principle axis so the composite has maximum strength in that direction, and has little strength in other directions. Arrangement (b) offers strength in the vertical direction as well.

In (c), the fibers are at 45-deg angles with the principle axis. This provides strength in those two directions, and also provides good shear strength in the principle-axis direction. For this reason, this arrangement is commonly seen in a composite-wing-box shear web. Also, the 45-deg orientation is frequently used in structure that must resist torque.

Arrangement (d) combines (b) and (c), providing alternate layers ("plies") of fibers at 0-, 45-, and 90-deg orientations. By varying the number of plies at these orientations the designer can obtain virtually any combination of tensile, compression, and shear strength in any desired directions.

Another ply-orientation scheme uses plies that are 60 deg apart. Composites are sometimes designed with completely arbitrary ply directions to provide special characteristics.

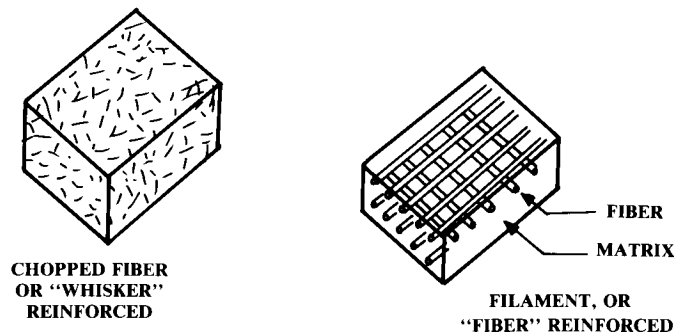


Fig. 14.26 Composite material types.

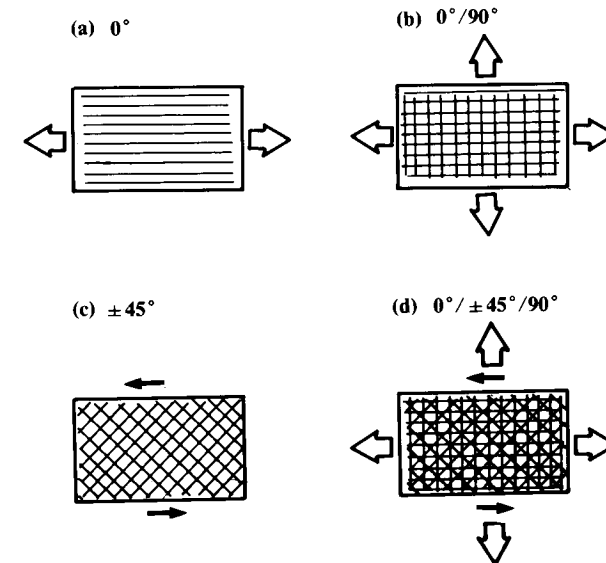


Fig. 14.27 Composite ply tailoring.

Note that an odd number of plies is commonly used. This tends to reduce warpage, as has long been known by the makers of plywood.

The common forms of fiber used in composite production are shown in Fig. 14.28. The chopped form is simply sprayed or pressed into the mold. Unidirectional tape comes on large rolls and is placed in the mold by hand or by a robotic tape-laying machine. Tape is usually pre-impregnated ("prepreg") with the matrix material.

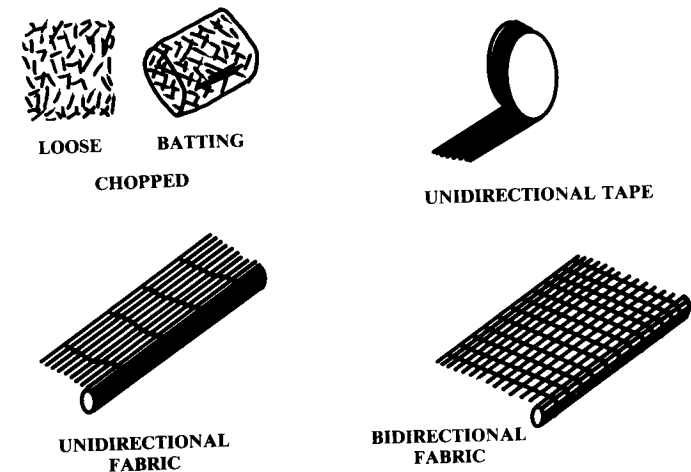


Fig. 14.28 Composite production forms.

Fabrics may be bidirectional, with fibers running at 0 and 90 deg, or unidirectional, with the fibers running in one direction. (A few fibers run at 90 deg to bind the fabric together.) Fabrics may also be prepreg. Fabrics are sometimes called “broadgoods.”

Prepreg tape and fabric is typically about 0.005–0.01 in. thick per ply.

In another form of composite, the individual filaments are wound around plugs to form shapes such as missile bodies and golf club shafts. This is called “filament-wound” construction.

There are a number of fiber and matrix materials used in composite aircraft structure. Fiberglass with an epoxy-resin matrix has been used for years for such nonstructural components as radomes and minor fairings. More recently, fiberglass-epoxy has been used by homebuilders.

While fiberglass-epoxy has good strength characteristics, its excessive flexibility (tensile E) prevents its use in highly loaded structure in commercial or military aircraft. However, it is cheap and easy to form, and is suitable for some applications.

The most commonly used advanced composite is graphite-epoxy, called “carbon-fiber composite” by the British who developed it. Graphite-epoxy composite has excellent strength-to-weight ratio and is not difficult to mold. It is substantially more expensive than aluminum at the present time (roughly 20 times), but unlike metals, little material is wasted in manufacturing operations such as milling and cutting from flat patterns.

Boron-epoxy was developed in the U.S. and initially used for complete part fabrication. An F-111 horizontal tail and F-4 rudder were built of boron-epoxy. However, boron-epoxy costs over four times as much as graphite-epoxy, so boron is used today largely to provide additional stiffness to graphite-epoxy parts, especially in compression.

Aramid, sold under the trade name “Kevlar,” is used with an epoxy matrix in lightly-loaded applications. Aramid has a low compression strength, but exhibits much more gradual failure than other composites (i.e., less brittle). A graphite-aramid-epoxy hybrid composite offers more ductility than pure graphite-epoxy. It is used in the Boeing 757 for fairings and landing-gear doors.

Composites using epoxy as the matrix are limited to maximum temperatures of about 350°F, and normally aren’t used in applications where temperatures will exceed 260°F. For higher-temperature applications, several advanced matrix materials are in development. The polyimide resins show great promise. One polyimide, bismaleimide (BMI), shows good strength at 350°F. A material called polyimide shows good strength at up to 600°F, but is difficult to process.

The matrix materials described above are all “thermoset” resins, chemical mixtures which “cure,” producing a change in the material’s chemistry at the molecular level upon the application of heat. The thermoset process is not reversible. If the composite part is heated up again the thermosetting matrix does not revert to a liquid state.

In contrast, a “thermoplastic” matrix material does not undergo a chemical change when heated. It merely “runs,” and can be heated up again and reformed. This offers a huge advantage for repairing damaged parts com-

pared to the thermoset composites. Much like the plastics used in model airplanes, thermoplastic materials can be readily formed with heat.

Thermoplastic materials under study for use as the matrix in aircraft structures include polyester, acrylic, polycarbonate, phenoxy, and polyethersulfone. Thermoplastic matrix materials can be used with the same fiber materials (graphite, boron, etc.) as the thermoset composites. Thermoplastics are still in development, but will be available for the next major aircraft development.

For higher-temperature, high-strength applications, “metal-matrix composites” are in development. These use aluminum or titanium as the matrix with boron, silicon carbide, or aramid as the fiber.

Composite materials offer impressive weight savings, but have problems too, one problem being a reluctance to accept concentrated loads. Joints and fittings must be used that smoothly spread the concentrated load out over the composite part. If a component such as a fuselage or wing has a large number of cutouts and doors, the fittings to spread out those concentrated loads may eliminate the weight savings.

The strength of a composite is affected by moisture content, cure cycle, temperature exposure, ultraviolet exposure, and the exact ratio of fiber to matrix. These are difficult to control and every composite part will probably have slightly different properties. Manufacturing voids are difficult to avoid or detect, and the scrapage rate for composite parts can be excessively high.

Furthermore, composites are difficult to repair because of the need to match strength and stiffness characteristics. A patch that is weak is obvi-

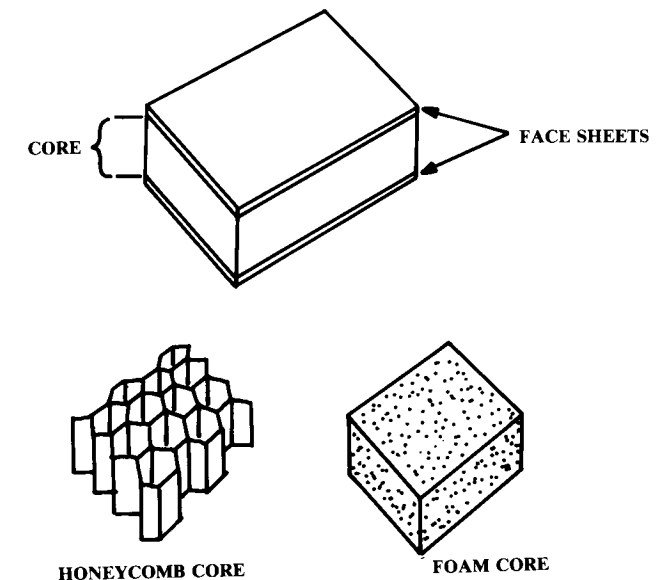


Fig. 14.29 Sandwich construction.

Table 14.3 Typical metal properties (room temperature)

Material	Density lb/in. <sup>3</sup>	Temp limit °F	$F_u$ 10 <sup>3</sup> psi	$F_{cy}$ 10 <sup>3</sup> psi	$F_{cy}$ 10 <sup>3</sup> psi	$F_{su}$ 10 <sup>3</sup> psi	$E$ 10 <sup>6</sup> psi	$G$ 10 <sup>6</sup> psi	Comments
<b>Steel</b>									
Aircraft steel (5 Cr-Mo-V)	0.281	1000	260	220	240	155	30	11	Heat treat to 1850°F
Low carbon steel (AISI 1025)	0.284	900	55	36	36	35	29	11	Shop use only today
Low alloy steel (D6AC-wrought)	0.283	1000	220	190	198	132	29	11	—
Chrom-moly steel (AISI 4130)	0.283	900	90	70	70	54	29	11	Widely used
sheet, plate, & tubing	0.283	900	180	163	173	108	29	11	—
wrought	0.282	800	185	150	158	120	29	11	Good corrosion resistance
Stainless steel (AM-350)	0.277	600	190	170	179	123	29	11	B-70 honeycomb material
Stainless (PH 15-7 Mo-sheet & plate)									
<b>Aluminum</b>									
Aluminum-2017	0.101	250	55	32	32	33	10.4	3.95	—
Clad 2024 (24 st)-(sheet & plate)	0.100	250	61	45	37	37	10.7	4.0	Widely used, weldable
extrusions	0.100	250	70	52	49	34	10.8	4.1	
Clad 7178-T6 (78 st)	0.102	250	80	71	71	48	10.3	3.9	High strength, not weldable, subject to stress corrosion
-(sheet & plate)	0.102	250	84	76	75	42	10.4	4.0	
extrusions	0.101	250	72	64	63	43	10.3	3.9	High strength, not weldable, common in high-speed aircraft
Clad 7075-T6-(sheet)	0.101	250	74	63	66	43	10.0	3.8	
(forgings)	0.101	250	81	72	72	42	10.4	4.0	
(extrusions)									
<b>Magnesium</b>									
Magnesium-HK 31A	0.0674	700	34	24	22	23	6.5	2.4	High-temperature, high strength-to-weight, subject to corrosion
-HM 21A	0.0640	800	30	21	17	19	6.5	2.4	

Table 14.3 (continued) Typical metal properties (room temperature)

Table 200 (Continued) — <i>Strength and Properties (Room Temperature)</i>									
Material	Density lb./in. <sup>3</sup>	Temp limit °F	$F_u$ 10 <sup>3</sup> psi	$F_{cy}$ 10 <sup>3</sup> psi	$F_{cy}$ 10 <sup>3</sup> psi	$F_{su}$ 10 <sup>3</sup> psi	$E$ 10 <sup>6</sup> psi	$G$ 10 <sup>6</sup> psi	Comments
Titanium									
Titanium-Ti-6Al-4V	0.160	750	160	145	154	100	16.0	6.2	Most-used titanium, including B-70 SR-71 titanium
-Ti-13V-11Cr-3Al	0.174	600- 1000	170	160	162	105	15.5	—	
High temperature nickel alloys									
Inconel X-750	0.300	1000- 1500	155	100	100	101	31.0	11.0	X-15
Rene 41	0.298	1200- 1800	168	127	135	107	31.6	12.1	X-20, very difficult to form
Hastelloy B	0.334	1400	100	45	—	—	30.8	—	Engine parts

ously undesirable, but one that is overstrong can cause excessive deflection on adjoining areas, which can lead to fracture. Proper repair of an important composite part requires running a computer program to insure that the repaired part will match the original design specifications.

The properties of a composite material are not simply the algebraic sum of the properties of the individual ply layers. Although a simple summation provides a rough approximation of the total material properties, actual material properties must be calculated using tensor calculus equations, such as are outlined in Ref. 58. Furthermore, extensive coupon testing is required to determine design allowables for the selected materials and ply orientation. Introductions to composites are provided in Refs. 59 and 83.

### Sandwich Construction

While not properly classed a “material,” sandwich construction has special characteristics and is very important to aircraft design. A structural sandwich is composed of two “face sheets” bonded to and separated by a “core” (Fig. 14.29).

The face sheets can be of any material, but are typically aluminum, fiberglass-epoxy, or graphite-epoxy. The core is usually an aluminum or phenolic honeycomb material for commercial and military aircraft, but various types of rigid foam are used as the core in some cases. Many homebuilt aircraft today are constructed of foam-core sandwich with fiberglass composite skins.

In a sandwich, the face sheets carry most of the tension and compression loads due to bending. The core carries most of the shear loads as well as the compression loads perpendicular to the skin. As with composites, joints and fittings are a problem with sandwich construction. Analysis of sandwich construction is discussed in Ref. 60.

### Material-Property Tables

Tables 14.3, 14.4, and 14.5 provide typical material properties for various metals, composites, and woods. Note that these are typical values only, and

Table 14.4 Typical composite material properties (room temperature)

Material	Fiber orientation	Fiber % volume	Density lb/in <sup>3</sup>	Temp. limit °F	$F_{tu}(L)$	$F_{tu}(T)$	$F_{cu}(L)$
					10 <sup>3</sup> psi	10 <sup>3</sup> psi	10 <sup>3</sup> psi
High-strength Graphite/epoxy	0	60	0.056	350	180.0	8.0	180.0
	±45	60	0.056	350	23.2	23.2	23.9
High-modulus Graphite/epoxy	0	60	0.056	350	110.0	4.0	100
	±45	60	0.058	350	16.9	16.9	18
Boron/epoxy	0	50	0.073	350	195	10.4	353
Graphite/polyimide	0	—	—	—	204	4.85	111
S-Fiberglass/epoxy	0	—	0.074	350	219	7.4	73.9
E-Fiberglass/epoxy	0	45	0.071	350	105	10.2	69
Aramid/epoxy	0	60	.052	350	200	4.3	40

L — Longitudinal direction; T = transverse direction;  $F_{isu}$  = interlaminar shear stress (ultimate); t = tension; c = compression.

that actual material properties for use in detail design should be obtained from the producer or from a specification document such as Ref. 61.

For example, Ref. 61 contains 68 pages of design data on 2024 aluminum alone, covering many different forms, heat treatments, tempering, gauges, etc. The values for 2024 in Table 14.3 are merely typical, suitable for rough estimates and student design projects.

### 14.10 STRUCTURAL-ANALYSIS FUNDAMENTALS

The following sections will introduce the key equations for structural analysis of aircraft components. Derivations will not be presented as they are available in many references, such as 54, 55, and 60.

#### Properties of Sections

A number of geometric properties of cross sections are repeatedly used in structural calculations. Three of the most important—centroid, moment of inertia, and radius of gyration—are discussed below. Note that the cross sections of interest in tension and compression calculations are perpendicular to the stress, while in shear calculations they are in the plane of the shearing stress.

$$X_c = \frac{\sum x_i dA_i}{A} \quad (14.21)$$

$$Y_c = \frac{\sum y_i dA_i}{A} \quad (14.22)$$

The “centroid” of a cross section is the geometric center, or the point at which a flat cutout of the cross-section shape would balance. The coordinates of the centroid ( $X_c, Y_c$ ) of an arbitrary shape (Fig. 14.30) are found from Eqs. (14.21) and (14.22). A symmetrical cross section always has its centroid on the axis of symmetry and if a cross section is symmetric in two directions, the centroid is at the intersection of the two axes of symmetry.

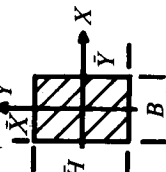
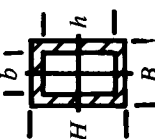
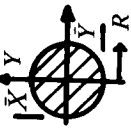
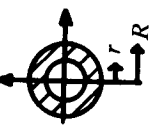
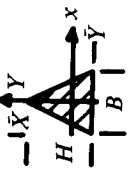
Table 14.4 (contd.) Typical composite material properties (room temperature)

$F_{cu}(T)$ 10 <sup>3</sup> psi	$F_{su}(LT)$ 10 <sup>3</sup> psi	$F_{isu}$ 10 <sup>3</sup> psi	$\epsilon_{tu}(L)$ in/in	$\epsilon_{tu}(T)$ in/in	$E_t(L)$ 10 <sup>6</sup> psi	$E_t(T)$ 10 <sup>6</sup> psi	$E_C(L)$ 10 <sup>6</sup> psi	$E_C(T)$ 10 <sup>6</sup> psi	$G(LT)$ 10 <sup>6</sup> psi
30.0	12	13	0.0087	0.0048	21.00	1.70	21.00	1.70	0.65
23.9	65.5	—	0.022	0.022	2.34	2.34	2.34	2.34	5.52
20	9.0	10	0.0046	0.0025	25.00	1.70	25.00	1.70	0.65
18	43.2	—	0.012	0.012	2.38	2.38	2.38	2.38	6.46
40	15.3	13	0.0065	0.004	30	2.7	30	2.7	0.70
18.5	8.5	—	—	0.0036	20	1.35	17.4	1.4	0.84
22.4	—	11	—	—	7.70	2.70	6.80	2.5	—
33	7.9	—	0.025	0.019	4.23	1.82	4.43	1.8	0.51
20	9	—	0.018	0.006	11	0.8	11	0.8	0.3

Table 14.5 Wood properties (ANC-5)

	Density lb/in <sup>3</sup>	$F_{cu}$ 10 <sup>3</sup> psi	Parallel to grain $F_y$ 10 <sup>3</sup> psi $F_{cy}$ 10 <sup>3</sup> psi	Perpendicular to grain $F_{cu}$ 10 <sup>3</sup> psi $F_{cy}$ 10 <sup>3</sup> psi	Parallel to grain $F_s$ 10 <sup>3</sup> psi	$E$ 10 <sup>6</sup> psi
Ash	0.024	14.8	8.9	7.0	2.3	1.46
Birch	0.026	15.5	9.5	7.3	1.6	1.78
African mahogany	0.019	10.8	7.9	5.7	1.4	1.28
Douglas fir	0.020	11.5	8.0	7.0	1.3	1.70
Western pine	0.016	9.3	6.0	5.3	0.8	1.31
Spruce	0.016	9.4	6.2	5.0	0.8	1.30

Table 14.6 Properties of simple sections

Illustrations	Area	Centroid	Mom. of inertia		Rad. of gyration	
		$\bar{X}$ $\bar{Y}$	$I_x$ $I_y$	$\rho_x$ $\rho_y$		
	$BH$	$B/2$ $H/2$	$\frac{BH^3}{12}$ $\frac{HB^3}{12}$	$\frac{H}{\sqrt{12}}$ $\frac{B}{\sqrt{12}}$		
	$BH - bh$	$B/2$ $H/2$	$\frac{BH^3 - bh^3}{12}$ $\frac{HB^3 - hb^3}{12}$	$\sqrt{\frac{BH^3 - bh^3}{12(BH - bh)}}$ $\sqrt{\frac{HB^3 - hb^3}{12(BH - bh)}}$		
	$\pi R^2$	$R$ $R$	$\frac{\pi R^4}{4}$ $\frac{\pi R^4}{4}$	$R/2$ $R/2$		
	$\pi (R^2 - r^2)$	$R$ $R$	$\frac{\pi (R^4 - r^4)}{4}$ $\frac{\pi (R^4 - r^4)}{4}$	$\frac{\sqrt{R^2 + r^2}}{2}$ $\frac{\sqrt{R^2 + r^2}}{2}$		
	$\frac{BH}{2}$	$O$ $H/3$	$\frac{BH^3}{36}$ $\frac{B^3 H}{48}$	$\frac{H}{\sqrt{18}}$ $\frac{B}{\sqrt{24}}$		

A “centroidal axis” is any axis that passes through the centroid. An axis of symmetry is always a centroidal axis.

Centroids for simple shapes are provided in Table 14.6. The centroid of a complex shape built up from simple shapes can be determined using Eqs. (14.21) and (14.22) using the centroids and areas of the simple shapes.

The moment of inertia  $I$  is a difficult-to-define parameter that appears in bending and buckling equations. Moment of inertia can be viewed as the cross section’s resistance to rotation about some axis, assuming that the cross-sectional shape has unit mass. Moment of inertia is the sum of the elemental areas times the square of the distance to the selected axis [Eqs. (14.23) and (14.24)], and has units of length to the fourth power.

The polar moment of inertia ( $J$  or  $I_p$ ) is the moment of inertia about an axis perpendicular to the cross section [Eq. (14.25)];  $J$  is important in torsion calculations.

$$I_x = \sum y_i^2 dA_i \quad (14.23)$$

$$I_y = \sum x_i^2 dA_i \quad (14.24)$$

$$I_p = J = \sum r_i^2 dA_i = I_x + I_y \quad (14.25)$$

Structural calculations usually require the moments of inertia about centroidal axes. Table 14.6 provides moments of inertia for simple shapes about their own centroidal axis. For a complex built-up shape, the combined centroid must be determined, then Eqs. (14.26) and (14.27) can be used to transfer the moments of inertia of the simple shapes to the combined centroidal axes. The “ $\ell$ ” terms are the  $x$  and  $y$  distances from the simple shapes’ centroidal axes to the new axes (see Fig. 14.30, bottom).

Once the simple shapes’ moments of inertia are transferred to the combined centroidal axes, the moments of inertia are added to determine the combined moment of inertia ( $I_x$  and  $I_y$ ). The new  $J$  is determined from the new  $I_x$  and  $I_y$  using Eq. (14.25):

$$I_x = I_{x_c} + A \ell_y^2 \quad (14.26)$$

$$I_y = I_{y_c} + A \ell_x^2 \quad (14.27)$$

The radius of gyration  $\rho$  is the distance from the centroidal axis to a point at which the same moment of inertia would be obtained if all of the cross-sectional area were concentrated at that point. By Eq. (14.23), the moment of inertia is the total cross-sectional area times  $\rho$  squared; so  $\rho$  is obtained as follows:

$$\rho = \sqrt{I/A} \quad (14.28)$$

The main use of  $\rho$  is in column-buckling analysis. Also, the  $\rho$  values in Table 14.6 can be used to approximate  $I$  for the given shapes.

Other cross-sectional properties such as the product of inertia and the principal axes will not be used in this overview of structures. See Refs. 60,

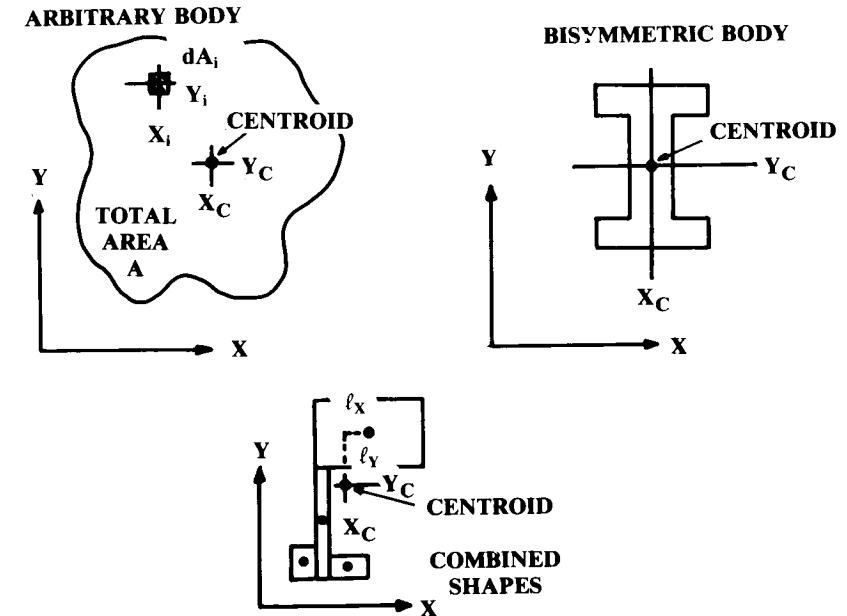


Fig. 14.30 Section property definitions.

54, or other structures textbooks for more information about section properties.

### Tension

Tension, the easiest stress to analyze, is simply the applied load divided by the cross-sectional area [Eq. (14.14), repeated below as Eq. (14.29)]. The shape of the cross section is unimportant in most cases.

The appropriate cross section is the smallest area in the loaded part. For example, if the part has rivet or bolt holes the smallest cross-sectional area will probably be where the holes are located, because the areas of the holes are not included for tensional calculations.

Usually the relevant cross section is perpendicular to the load. If a line of holes forms a natural “zipper” at an angle off the perpendicular, the part may fail there if the cross-sectional area along the “zipper” line is less than the smallest perpendicular cross section.

$$\sigma = P/A \quad (14.29)$$

Remember that the stress level at the limit load should be equal to or less than the yield stress or, for composite materials, the stress level corresponding to a strain of two-thirds of the ultimate strain.

### Compression

The compression stress is also given by Eq. (14.29) (load divided by area). For the determination of the limit stress, this equation can only be applied to parts that are very short compared to cross-sectional dimensions (such as fittings) or to parts which are laterally constrained (such as spar caps and sandwich face sheets). Long unconstrained members in compression, called “columns” or “struts,” are discussed below.

For short or laterally constrained parts in compression, the ultimate compressive strength is usually assumed to equal the tensile value. For ductile metals this is a conservative assumption as they never actually fail, but merely “squish” out and support the load by the increased area.

Rivet and bolt holes are included in the cross-sectional area calculation for compression because the rivets or bolts can carry compressive loads.

Columns in compression usually fail at a load well below that given by applying the ultimate stress to Eq. (14.29). Columns in compression fail either by “primary buckling” or by “local buckling.”

An important parameter is the column’s “slenderness ratio”: the column’s effective length  $L_e$  divided by the cross-sectional radius of gyration [Eq. (14.30)]. The effective length of a column is determined by the end connections (pinned, fixed, or free) as shown in Fig. 14.31.

$$\text{Slenderness Ratio: } \frac{L_e}{\rho} = \frac{L_e}{\sqrt{I/A}} \quad (14.30)$$

When you push down on an upright yardstick, the middle part bends outward in a direction perpendicular to the load. This bending action produces internal stresses much greater than the direct compression stress due to the applied load, and is called “primary column buckling.” If the bend-

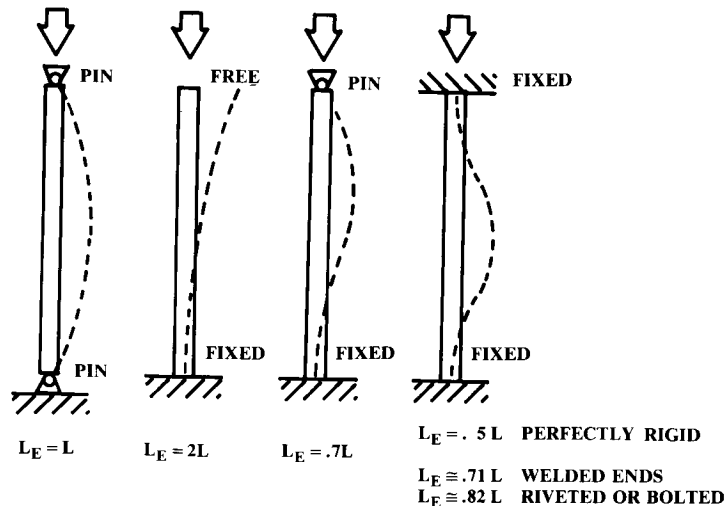


Fig. 14.31 Column effective length.

ing action after buckling involves stresses below the proportional limit, the column is said to experience “elastic buckling.”

The highest compression load that will not cause this elastic column buckling—the so-called “Euler load,” or critical load  $P_c$ —will be determined from the Euler column equation [Eq. (14.31)]. The resulting compressive stress is found from Eq. (14.32).

Note in Eq. (14.31) that the total load a column can carry without buckling does not depend upon either the cross-sectional area or the ultimate compressive stress of the material! Only the column’s effective length, its cross-sectional moment of inertia, and the material’s modulus of elasticity affect the buckling load if the column is long.

$$P_c = \frac{\pi^2 EI}{L_e^2} \quad (14.31)$$

$$F_c = \frac{\pi^2 EI}{AL_e^2} = \frac{\pi^2 E}{(L/\rho)^2} \quad (14.32)$$

The buckling stresses of Eq. (14.32) are failure stresses and do not have any margin of safety. For design purposes the limit loads should be reduced, usually to two-thirds of these values.

A column with an open or highly irregular cross section may fail at a lower load due to cross sectional twisting or deformation. Methods for analysis of such members can be found in Refs. 60 and 83.

Equation (14.31) implies that, as column length is reduced to zero, the Euler load goes to infinity. However, the compression stresses experienced due to bending in a buckled column are much greater than the applied load would directly produce. At some point as column length is reduced the internal compressive stresses produced at the onset of buckling will exceed the proportional limit and the column will no longer be experiencing elastic buckling. This has the effect of reducing the buckling load compared to the Euler load.

The “critical slenderness ratio” defines the shortest length at which elastic buckling occurs. At a lower slenderness ratio, the stresses at buckling exceed the proportional limit. The column experiences “inelastic buckling” so the Euler equation cannot be used as shown. The critical slenderness ratio depends upon the material used. It is about 77 for 2024 aluminum, 51 for 7075 aluminum, 91.5 for 4130 steel, and 59–76 for alloy steel depending upon heat treatment. Most columns used in aircraft are below these critical slenderness values, so the elastic Euler equation cannot usually be used in aircraft column analysis.

The buckling load for inelastic buckling can be determined by Eq. (14.32), with one modification. The modulus of elasticity must be replaced by the tangent modulus, described previously. As the tangent modulus is a function of the stress, iteration is required to find the buckling load for a particular column. However, handbook graphs such as Fig. 14.32 are usually used for design (see Refs. 60 and 61).



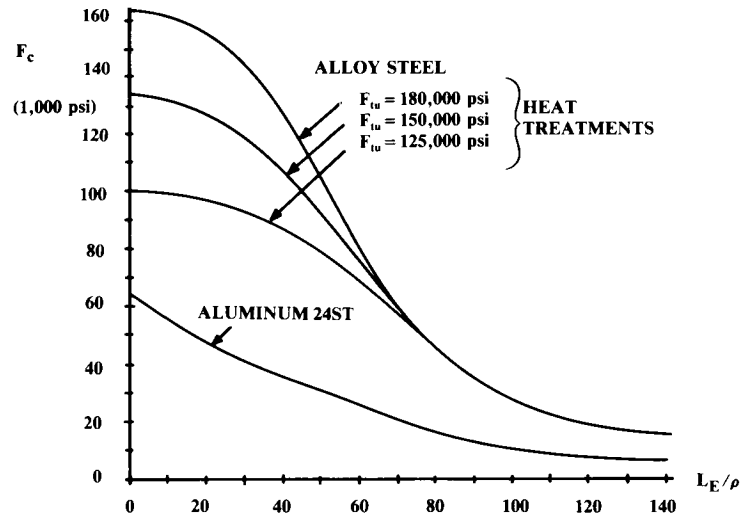


Fig. 14.32 Column buckling loads (round tubing).

As discussed at the beginning of this section, a very short “column” experiences pure compression without any danger of primary column buckling. This is sometimes called “block compression.” The compression yield value is used as the limit load, providing a cutoff value for the buckling load of a short column with either a solid cross section or with relatively thick walls (structural tubing). A column can usually be considered in block compression if the slenderness ratio is less than about 12.

When you step on an upright soda can, it fails in a form of local buckling called “crippling,” in which the walls of the cross section collapse without warning, and the load-carrying ability drops to virtually zero. This is typical for short columns with very thin walls. Methods for estimation of thin-wall crippling are found in Ref. 60. A rough estimate for the crippling stress of a thin-wall cylindrical tube is shown in Eq. (14.33), where  $t$  is the wall thickness and  $R$  is the radius.

$$F_{\text{crippling}} \cong 0.3(Et/R) \quad (14.33)$$

A flat sheet or panel under compression fails by buckling in a manner similar to a column. The buckling load [Eq. (14.34)] depends upon the length ( $a$ ) in the load direction, the width ( $b$ ), the thickness, and the manner in which the sides are constrained.

Clamped sides cannot rotate about their axis, and provide the greatest strength. Simply-supported sides are equivalent to a pinned end on a column, and can rotate about their axis but cannot bend perpendicularly. A free side can rotate and bend perpendicularly and provides the least strength.

Figure 14.33 provides the buckling coefficient  $K$  for Eq. (14.34) based upon panel length to width ratio and end constraints. Most aircraft panels

are clamped, but with some flexibility to rotate about the side axes. A  $K$  value between the clamped and simply-supported values should be used in such a case.

$$F_{\text{buckling}} = KE(t/b)^2 \quad (14.34)$$

### Truss Analysis

A truss is a structural arrangement in which the structural members (struts) carry only compression or tension loads (“columns” and “ties”). In the ideal truss, the struts are weightless and connected by frictionless pins. No loads are applied except at the pins, and no moments are applied anywhere. These ideal assumptions guarantee that the struts carry only compression or tension.

The strut loads calculated with these ideal assumptions are called “primary truss loads.” Additional loads such as those caused by the attachment of an aircraft component to the middle of a strut must be calculated separately and added to the primary load during analysis of each individual strut. The impact of rigid welded connections in a typical aircraft applica-

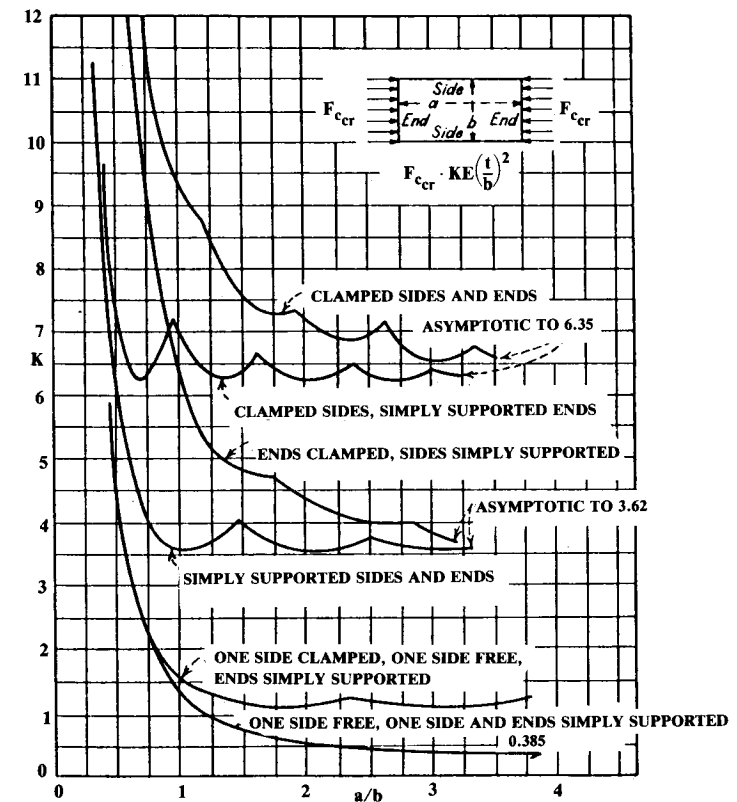


Fig. 14.33 Panel buckling coefficient. (NACA TN3781)

tion is considered only in the definition of effective length in the column-buckling equation (see Fig. 14.31).

Truss structure was used extensively in welded steel-tube fuselages. Today the truss structure is largely used in piston-engine motor mounts, the ribs of large aircraft, and landing gear.

Figure 14.34 shows a typical truss structure, a light aircraft motor mount. For illustration purposes this will be analyzed as if it were a two-dimensional truss with only the three struts shown. Analysis of three-dimensional "space structures" will be discussed later.

The bottom of Fig. 14.34 shows an equivalent truss that includes the lines of force to the c.g. of the engine, and the vertical resisting forces due to the rigid attachment of the fuselage and engine to the truss. This equivalent truss can be solved by several methods.

The most general truss solution, the "method of joints," relies upon the fact that at each joint of the truss, the sums of the vertical and horizontal forces must each total zero.

To obtain a solution from the two equations (vertical and horizontal), the solution must begin at and always proceed to a joint with only two unknown struts. The method usually begins at a free joint with an applied external load, in this case at the engine load.

Figure 14.35 shows the forces at the joints. All the forces are shown as radiating outward from the joints so that a positive force is a tension and a negative force is a compression.

When summing forces at a joint, the positive or negative force is added to the sum if it is up (when summing vertical forces) or to the right (when summing horizontal forces), and subtracted if down or to the left. Confusion about the appropriate sign is the most common error in truss analysis (the author did joint three wrong the first time!).

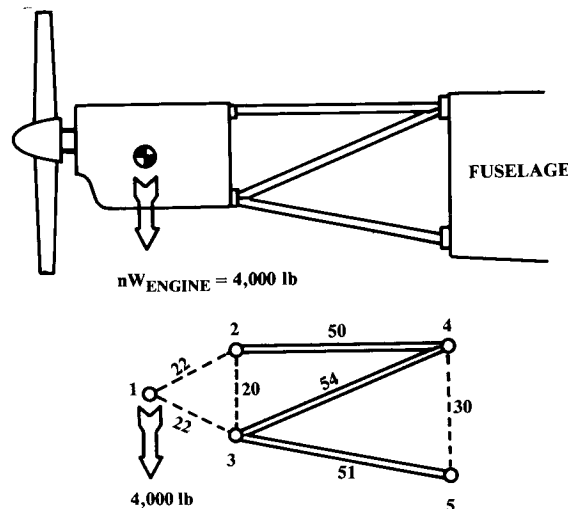


Fig. 14.34 Typical truss structure.

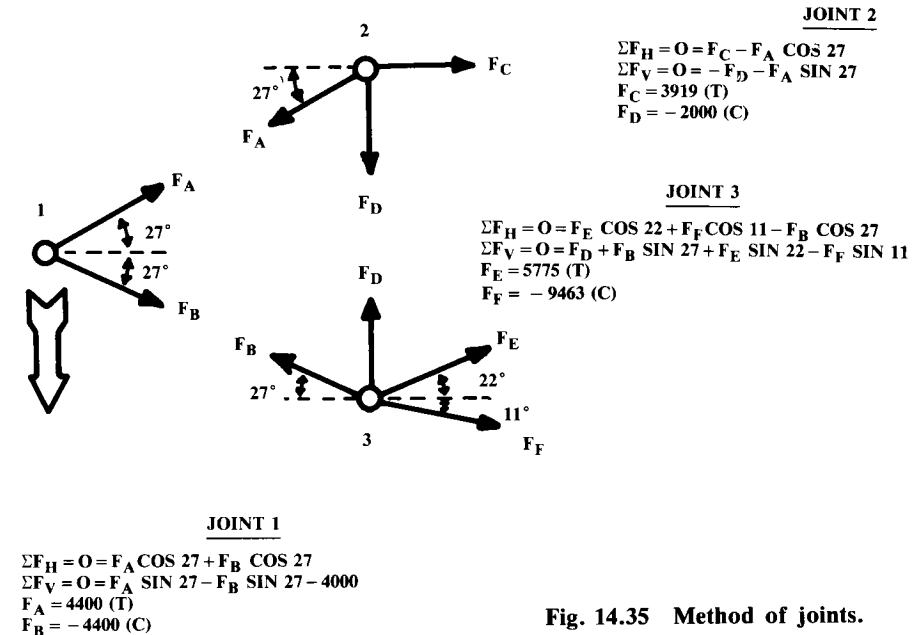


Fig. 14.35 Method of joints.

Joint one is at the engine's c.g.. The unknown forces  $F_a$  and  $F_b$  must react the engine load of 4000 lb. Solving the equations shown yields  $F_a$  of 4400 lb (tension) and  $F_b$  of -4400 lb (compression).

Selection of the next joint to analyze depends upon the number of unknown struts. At joint three, there are three unknown struts at this time, so we select joint two. Solving the equations yields  $F_c$  of 3919 lb (tension).  $F_d$  is found to be -2000 lb, a compression load on the engine due to the motor mount. If this load is in excess of what the engine can withstand, a vertical motor-mount strut should be welded between joints two and three.

At joint three there are now only two unknown strut loads. Solving the equations yields  $F_e$  of 5775 lb (tension) and  $F_f$  of -9463 lb (compression).

In some cases a quicker method can be employed to determine the forces in selected struts without having to solve the whole truss as in the method of joints. This quicker method is actually two methods, the "method of moments" for the upper and lower struts and the "method of shears" for the inner struts.

The top illustration of Fig. 14.36 shows the use of the method of moments to solve the force in the top strut of the motor mount. The whole structure is replaced by two rigid bodies connected by a pin, with rotation about the pin prevented by the unknown force in the strut under analysis. The moments about the pin are readily summed and solved for the unknown strut force, which is found to be 3919 lb.

A similar technique is shown in the middle illustration for the lower strut, which has a load of 9463 lbs. Note that this technique, where applicable, allows direct solution for the desired unknown forces.

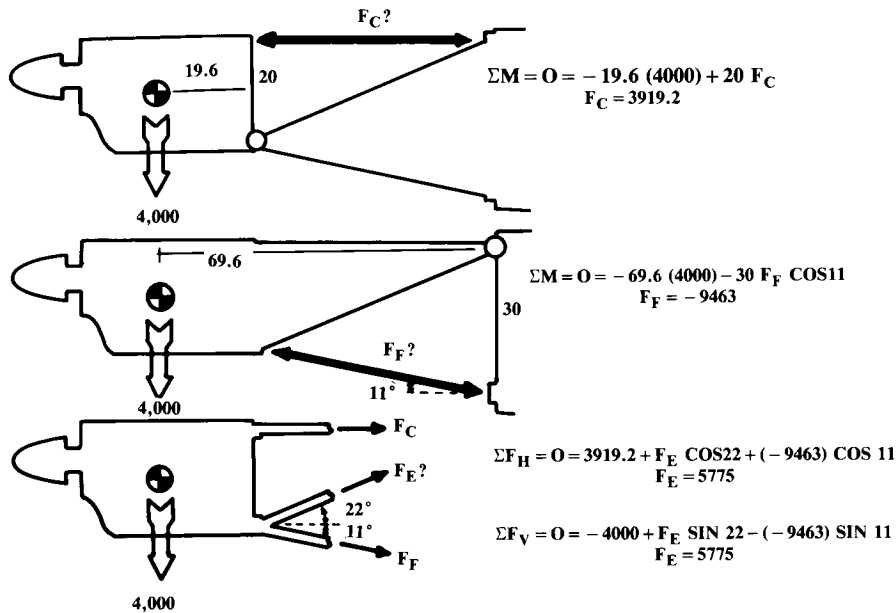


Fig. 14.36 Method of moments/method of shears.

The lower illustration of Fig. 14.36 shows the use of the method of shears to solve for the inner strut. This method involves severing the structure along a plane which cuts only three members, the upper and lower strut and the inner strut under analysis.

The severed part of the structure is analyzed as a free body, summing either the vertical and horizontal forces, which must total zero. Note that by calculating the unknown strut force both ways (vertical and horizontal summation), a check of your result can be made. This example gives a result of 5775 lb.

These methods are only applicable if the truss structure is "statically determinate." In general, a truss is statically determinate if every strut can be cut by some plane that cuts only two other struts. This insures that there is always a joint with only two unknown struts, permitting solution by the method of joints. For "indeterminate" trusses, more complicated methods based upon deflection analysis must be used (see Refs. 54 and 60).

Once the loads in each member of the truss are known, the struts can be analyzed using the equations presented above for tension or compression. Use the appropriate effective length for welded, riveted, or bolted columns from Fig. 14.31. To provide an extra margin of safety, it is customary to assume that welded steel-tube motor mounts act as though the ends were pinned ( $L_e = L$ ).

The 3-D trusses, or "space structures," are solved similarly to the 2-D truss. Square cross section 3-D trusses, such as a typical welded-tube fuselage, can sometimes be solved separately in side view and top view as 2-D

structures. The resulting strut loads are then summed for the various members. This is permitted provided that the combined loads on all struts are within the elastic range.

For more complicated 3-D trusses, the method of joints can be applied using three equations and three unknown strut loads. This involves simultaneous solution of equations, e.g., with a simple computer iteration program. In some cases the moments about some selected point can be used to obtain the solution with less effort. Space structures are discussed in detail in Ref. 54.

### Beam Shear and Bending

A common problem in aircraft design is the estimation of the shear and bending stresses in the wing spars or fuselage. This is a two-step process. First, the shear and bending moment distributions must be determined; then the resulting stresses must be found.

Figure 14.37 shows a simple beam with a distributed vertical load. The beam is shown cut to depict internal forces. The right side of the beam being a free body, the sum of the vertical forces and the sum of the moments must equal zero.

If the severed part of the beam is to remain in vertical equilibrium, the externally applied vertical forces must be opposed by a vertical shear force within the cross section of the material, as shown. Thus, for any span station the shear force is simply the sum of the vertical loads outboard of that station, or the integral of a distributed load.

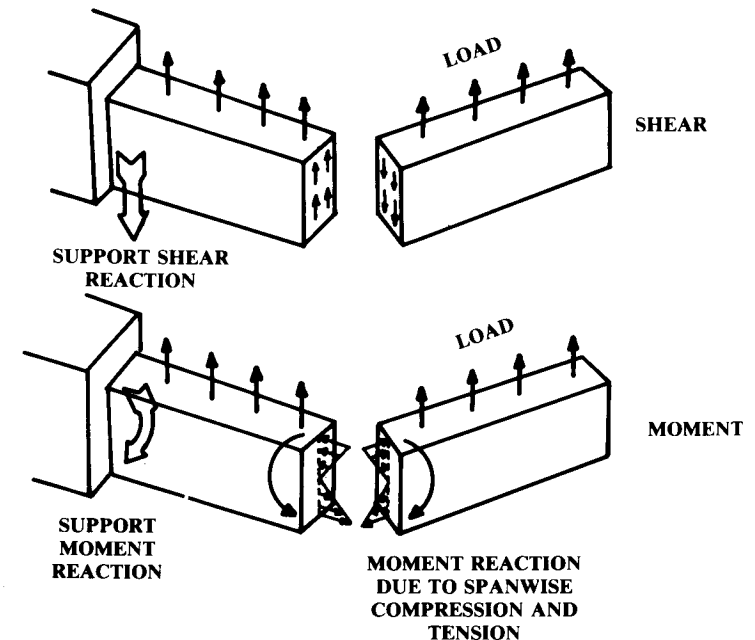


Fig. 14.37 Shear and moment in beams.